Effects of low dose-rate irradiation on human tumour cells

by

Catherine Ruth Mayes

A thesis submitted to the University of London for the degree of Doctor of Philosophy
2001

Gray Laboratory Cancer Research Trust
Mount Vernon Hospital
Northwood
Middlesex HA6 2JR

ProQuest Number: U642779

All rights reserved

INFORMATION TO ALL USERS
The quality of this reproduction is dependent upon the quality of the copy submitted.

In the unlikely event that the author did not send a complete manuscript
and there are missing pages, these will be noted. Also, if material had to be removed,
a note will indicate the deletion.

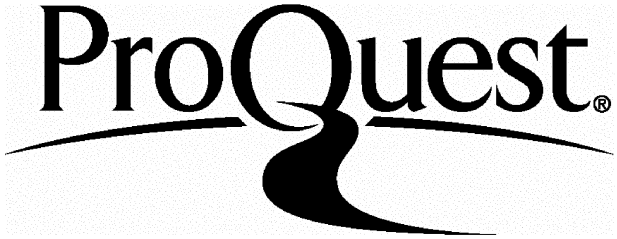

ProQuest U642779

Published by ProQuest LLC(2015). Copyright of the Dissertation is held by the Author.

All rights reserved.
This work is protected against unauthorized copying under Title 17, United States Code.
Microform Edition © ProQuest LLC.

ProQuest LLC
789 East Eisenhower Parkway
P.O. Box 1346
Ann Arbor, MI 48106-1346

Acknowledgements

I would like to thank several people, without whose help and support this thesis would not have been possible.

Firstly I would like to thank my supervisor, Professor Mike Joiner for his help and guidance throughout this project. I would also like to acknowledge Nycomed Amersham for funding this research. There are several other people I would like to mention including Professor Edwin Aird and Dr Melvyn Folkard for their considerable input into the development of irradiation techniques and for their attempts at teaching me physics! Thanks also to Graeme Bowey and Stuart Gilchrist for their wonderful dosimetry! I would also like to thank my friends, co-workers and proof-readers at the Gray Laboratory past and present who have provided me with both technical help and have put up with my complaints during the writing of this thesis! Thanks Mick, Brian, George, Chris, Frances, Kay, Jane, Peter B, Heba, Dr. Susan, Suzanne Kudmany and Emma Mayes (my tissue culturing summer students!) and Lila (cudowny druhna).

I would like to thank my parents and Kevin and Emma for keeping me positive and being there for me and finally I would especially like to thank my best friend in the whole world, Stephen, for making me laugh and keeping me calm during stressful episodes! Thanks boy!

This is for Susan and Henry Gallagher.

Abstract

The phenomenon of hyper-radiosensitivity (HRS) to very low doses of radiation has been observed in many tumour cell lines. HRS is a decrease in cell survival at low acute doses (<1 Gy) below the prediction by the Linear-Quadratic model for the response to higher doses. This increased sensitivity to low doses is surmised to be due to a failure to activate "repair processes". This thesis explores a corresponding enhanced sensitivity that occurs after clinically-relevant low dose-*rate* exposures.

Two novel low dose-rate irradiation systems were developed: (1) an ^{125}I irradiator containing nine ^{125}I brachytherapy seeds was used to irradiate cells at dose rates from 3 to 40 cGy h^{-1}; (2) a ^{60}Co γ-source and an attenuating water tank were used to carry out simultaneous irradiations over a wide range of dose rates (1 to 100 cGy h^{-1}). Three asynchronously growing human tumour cell lines (PC3, T98G, A7), which demonstrated HRS to acute single doses, were irradiated with low dose-rate ^{60}Co γ-rays. These cell lines showed a strong inverse dose-rate effect on cell survival at dose rates below 100 cGy h^{-1}. Analysis of the cell cycle using propidium iodide staining indicated that this inverse dose-rate effect was not due to pre-mitotic accumulation or other cell-cycle perturbations. T98G cells can be put into a reversible G1 arrest upon reaching confluence. Confluent T98G cells also show an inverse dose-rate effect at low dose rates (5 and 10 cGy h^{-1}) and a sparing effect at higher dose rates (30 and 60 cGy h^{-1}). The HRS-negative cell line investigated, U373MG, did not demonstrate an inverse dose-rate effect.

Experiments were carried out to determine combinations of dose and dose rate that enhanced survival. T98G cells were irradiated at low-dose rate and then at acute doses to determine the presence of HRS with varying time intervals. Asynchronous T98G cells showed HRS when previously irradiated with dose rates ranging from 5 to 60 cGy h^{-1} to total doses of 2 and 5 Gy, suggesting repair mechanisms are not switched on during the LDR irradiation. In confluent cells irradiated at dose rates of 60 and 30 cGy h^{-1} to a total dose of 5 Gy and then immediately with acute-dose X-rays, no HRS was seen. However, HRS was observed if an interval of 4 h was left between irradiations. HRS was present at dose rates of 60 and 30 cGy h^{-1} at a total dose of 2 Gy with both a 0 h and 4 h interval between irradiations, suggesting that at 30 and 60 cGy h^{-1} repair is triggered between a total dose of 2 and 5 Gy. These data indicate that the inverse dose-rate effect and HRS may be mechanistically related and this effect may contribute to the clinical efficacy of ^{125}I brachytherapy.

Contents Page

Acknowledgements **2**
Abstract **3**
Contents **4**
Index of figures **10**
Index of tables **16**
Abbreviations **19**

1. Introduction **21**
1.1 Introduction 21

1.2 Cellular effects of ionising radiation 21
1.2.1 DNA damage 22
1.2.2 Cell killing 22
1.2.3 DNA repair 23
1.2.3.1 Excision repair 24
1.2.3.2 DSB repair 24

1.3 Survival at acute doses of radiation 25
1.3.1 Low-dose hyper-radiosensitivity 25
1.3.2 LET 27
1.3.3 Hypoxia 27
1.3.4 Prevalence of HRS *in vitro* 27

1.4 The adaptive response 29

1.5 Possible mechanisms of HRS/IRR 30
1.5.1 Apoptosis 30
1.5.2 Cell cycle 31
1.5.3 DNA repair 31

1.6 Low dose-rate irradiation 32
1.6.1 Low dose-rate sparing 33
1.6.2 Mechanisms 34
1.6.3 Discrimination of cell radioresponsiveness 39
1.6.4 Inverse dose-rate effect and cell survival 41
1.6.4.1 Cell cycle 43
1.6.4.2 Hypoxia 45
1.6.4.3 IRR 45

1.6.5 Inverse dose-rate effect on mutation induction 46

1.7 Cell survival curves 50
1.7.1 Early models 50
1.7.2 Linear-Quadratic (LQ) model 51
1.7.3 Induced Repair (IR) model 51
1.7.4 Two-population model 52
1.7.5 Low dose-rate modelling 52

1.8 Prostate cancer 55

1.9 Brachytherapy 57
1.9.1 Comparison between treatments 60
1.9.1.1 High dose-rate vs. low dose-rate brachytherapy 60
1.9.1.2 Pulsed dose-rate vs. low dose-rate brachytherapy 61

1.10 Aims 67

2. Materials and methods **68**

2.1 Introduction 68

2.2 Cell lines 68

2.3 Cell culture 68
2.3.1 Media 68
2.3.1.1 Monolayer culture 68
2.3.1.2 Suspension culture 70
2.3.2 Sub culture 70
2.3.2.1 Monolayer culture 70
2.3.2.2 Suspension culture 70
2.3.3 Frozen stocks 71
2.3.4 Mycoplasma testing 71

2.4 Cell growth experiments 71
2.4.1 Assessment of cell growth 71
2.4.1.1 Cell number 71
2.4.1.2 Plating efficiency 72
2.4.1.3 Confluent cells 72
2.4.1.4 Supernatant 72

2.4.1.5 Suspension culture 73

2.5 Irradiations 73
2.5.1 X-ray irradiations 73
2.5.2 ^{60}Cobalt irradiations 73
2.5.3 ^{125}Iodine irradiations 73
2.5.4 Fricke dosimetry 73

2.6 Cell-survival assays 79
2.6.1 Dynamic microscope image processing scanner (DMIPS) 79
2.6.1.1 Introduction 79
2.6.1.2 Cell culture, irradiation and assessment of cell survival 80
2.6.2 FACS Vantage cell sorter 82
2.6.2.1 Introduction 82
2.6.2.2 Cell culture, irradiation and assessment of cell survival 82

2.7 Cell-cycle analysis 85
2.7.1 Flow cytometry: The FACScan 85
2.7.1.1 BrdUrd-pulse labelling 85
2.7.1.2 Cell harvesting and fixing 85
2.7.1.3 Cellular staining for BrdUrd 86
2.7.1.4 Detection of labelled nuclei 86
2.7.2 Propidium iodide (PI) staining 86
2.7.3 Flow cytometry data collection 87

3. Cell survival after acute low-dose irradiation **89**

3.1 Aims 89

3.2 Modification of growth conditions 89
3.2.1 Introduction 89
3.2.2 Specific materials and methods 90
3.2.2.1 Reduction in incubation temperature 90
3.2.2.2 Reduction in foetal calf serum concentration 91
3.2.2.3 Confluence arrest 91
3.2.3 Results 91
3.2.3.1 Reduction in incubation temperature 91
3.2.3.2 Reduction in foetal calf serum concentration 92

3.2.3.3 Confluence arrest 93
3.2.4 Discussion 104

3.3 Assessment of prevalence of HRS/IRR to acute doses of radiation in cell lines in vitro 107
3.3.1 Introduction 107
3.3.2 Assessment of acute dose cell survival 108
3.3.2.1 Dynamic microscope image processing scanner 108
3.3.2.2 FACS Vantage cell sorter 108
3.3.2.3 Data analysis 109
3.3.3 Results 110
3.3.4 Discussion 121

4. The effect of low dose-rate ^{60}Cobalt irradiation on cell survival **125**

4.1 Aims 125

4.2 Introduction 125

4.3 Development of ^{60}Cobalt irradiation system 127
4.3.1 Specific materials and methods 127
4.3.1.1 Dosimetry 128
4.3.2 Results and discussion 130

4.4 Low dose-rate irradiations of cells using ^{60}Cobalt 136
4.4.1 Materials and methods 136
4.4.1.1 Data analysis 138
4.4.2 Results 139
4.4.3 Discussion 167

5. The survival of human tumour cells after low dose-rate irradiation with ^{125}Iodine **174**

5.1 Aims 174

5.2 Introduction 174

5.3 Materials and methods 176
5.3.1 ^{125}Iodine seeds 176
5.3.2 Suspension culture 176

5.3.3 ^{125}Iodine seed irradiator plaques 177
5.3.3.1 Data analysis 178

5.4 Results 181
5.4.1 Suspension culture 181
5.4.2 ^{125}Iodine seed irradiators 181

5.5 Discussion 206

6. The effect of subsequent acute dose irradiation after low dose-rate exposures on cell survival in vitro **212**

6.1 Aims 212

6.2 Introduction 212

6.3 Materials and methods 213

6.4 Data analysis 214

6.5 Results 214

6.6 Discussion 238

7. Cell-cycle characteristics and the effect of radiation on cell-cycle progression **253**

7.1 Aims 253

7.2 Introduction 253

7.3 Materials and methods 256
7.3.1 Data analysis 256
7.3.1.1 Cell-cycle time (T_C) 256
7.3.1.2 S-phase duration (T_S) 257
7.3.1.3 G2/M-phase duration (T_{G2+M}) 257
7.3.1.4 G0/G1-phase duration (T_{G1}) 258
7.3.1.5 G1 delay 258
7.3.1.6 G2 delay 258
7.4 Results 261

7.5 Discussion 266

8. Final discussion **268**

8.1 Low dose-rate irradiation and cell survival 269
8.1.1 Introduction 268
8.1.2 The survival of cells after low dose-rate irradiation 268
8.1.3 Comparison between irradiation methods 269
8.1.4 Comparison with published data 269

8.2 Homology between HRS/IRR and the inverse dose-rate effect 272
8.2.1 Prevalence of both responses 272
8.2.2 Cell-cycle effects 272
8.2.2.1 HRS/IRR 273
8.2.2.2 Inverse dose-rate effect 273

8.3 Possible mechanisms of HRS/IRR and the inverse dose-rate effect 274
8.3.1 Evidence for a threshold for the triggering of IRR 274
8.3.2 Possible mechanisms and future work 276

8.4 Potential clinical importance of the inverse dose-rate effect and HRS/IRR 279
8.4.1 HRS/IRR 279
8.4.2 Inverse dose-rate effect 281

8.5 Implications for radioprotection 283

8.6 Conclusions 285

Appendices **286**
Appendix 1 286
Appendix 2 291
Appendix 3 294

REFERENCES **295**

Index of figures

Chapter 1

Figure 1.1	A survival curve and 2-dose fractionation curve of "clone A" cells. From Elkind and Sutton (1959).	36
Figure 1.2	An initial survival curve and fractionation survival curve for "clone A" cells. From Elkind and Sutton (1959).	37
Figure 1.3	The low dose-rate sparing observed in Chinese hamster cells exposed to γ-rays. From Bedford (1973).	38
Figure 1.4	The inverse dose-rate effect observed in HeLa cells. From Mitchell (1979).	42
Figure 1.5	The high and low LET mutation and transformation yield and surviving fraction of 2 cell lines relative to cell-cycle position. From Burki (1980) and Miller (1995).	49
Figure 1.6	The calculated fractional change in cell survival for pulsed-dose rate compared with continuous low-dose rate as a function of assumed half time of repair. From Brenner (1996).	66

Chapter 2

Figure 2.1	A photograph of the Pantak X-ray unit.	76
Figure 2.2	A photograph of the ^{60}Co γ-source used to give high dose-rate irradiations.	77
Figure 2.3	A photograph of the ^{60}Co Mobaltron γ-source used to give low dose-rate irradiations.	78
Figure 2.4	A photograph of the Dynamic Microscope Imaging Processing Scanner (DMIPS).	81
Figure 2.5	A photograph of the cell sorter.	83
Figure 2.6	A diagrammatic representation of the cell sorter.	84
Figure 2.7	A photograph of the FACScan flow cytometer.	88

Chapter 3

Figure 3.1	The growth of RT112 cells at 29°C, 30°C, 32°C and 37°C showing cell count, plating efficiency and proportion of cells in each phase of the cell cycle.	94
Figure 3.2	The number of RT112 cells present in supernatant extracted from cells grown at different temperatures.	96
Figure 3.3	The results of 3 DMIPS experiments on RT112 cells grown at 37°C and 30°C.	97
Figure 3.4	The growth of T98G cells in monolayer culture	

	incubated with 0.5, 1, 2, 7.5 and 10% FCS showing cell count, plating efficiency and proportion of cells in each phase of the cell cycle.	98
Figure 3.5	The growth of T98G cells in suspension culture incubated with 0.5, 1, 2 and 7.5% FCS showing cell count and plating efficiency.	99
Figure 3.6	The proportion of T98G cells in each phase of the cell cycle after incubation with 0.5 and 7.5% FCS in suspension culture.	100
Figure 3.7	The results of 5 DMIPS experiments using T98G cells grown in 0.5% FCS in suspension culture for 5 days.	101
Figure 3.8	The growth of T98G cells kept confluent for 8 days showing cell count, plating efficiency, proportion of cells in each phase of the cell cycle and cells present in supernatant.	102
Figure 3.9	The results of 3 DMIPS and 3 cell sort experiments on confluent T98G cells.	111
Figure 3.10	The results of 5 DMIPS and 4 cell sort experiments on PC3 cells.	112
Figure 3.11	The results of 3 DMIPS and 4 cell sort experiments on DU145 cells.	113
Figure 3.12	The results of 3 DMIPS and 4 cell sort experiments on LNCaP cells.	114
Figure 3.13	The results of 4 DMIPS and 3 cell sort experiments on A7 cells.	115
Figure 3.14	The relationship between surviving fraction at 2 Gy and the α_s/α_r value for cell lines tested *in vitro*.	120

Chapter 4

Figure 4.1	Photographs of the ^{60}Cobalt water tank system.	131
Figure 4.2	The dosimetry of the ^{60}Cobalt water tank system using an ionisation chamber.	133
Figure 4.3	The dosimetry of the ^{60}Cobalt water tank system using Fricke solution.	134
Figure 4.4	The results of LDR irradiations on asynchronous T98G cells using the ^{60}Cobalt water tank system expressed as relative clonogens per flask.	140
Figure 4.5	The results of LDR irradiations on asynchronous T98G cells using the ^{60}Cobalt water tank system expressed as cell counts and surviving fraction.	141

Figure 4.6	The distribution of asynchronous T98G cells in each phase of the cell cycle after irradiation with ^{60}Co at 100 and 5 cGy h^{-1}.	143
Figure 4.7	The results of LDR irradiations on confluent T98G cells using the ^{60}Cobalt water tank system expressed as relative clonogens per flask.	144
Figure 4.8	The results of LDR irradiations on confluent T98G cells using the ^{60}Cobalt water tank system expressed as cell counts and surviving fraction.	145
Figure 4.9	The distribution of confluent T98G cells in each phase of the cell cycle after irradiation with ^{60}Co at 60 and 5 cGy h^{-1}.	147
Figure 4.10	The results of LDR irradiations on asynchronous A7 cells using the ^{60}Cobalt water tank system expressed as relative clonogens per flask.	148
Figure 4.11	The results of LDR irradiations on asynchronous A7 cells using the ^{60}Cobalt water tank system expressed as cell counts and surviving fraction.	149
Figure 4.12	The distribution of asynchronous A7 cells in each phase of the cell cycle after irradiation with ^{60}Co at 100 and 5 cGy h^{-1}.	151
Figure 4.13	The results of LDR irradiations on asynchronous PC3 cells using the ^{60}Cobalt water tank system expressed as relative clonogens per flask.	152
Figure 4.14	The results of LDR irradiations on asynchronous PC3 cells using the ^{60}Cobalt water tank system expressed as cell counts and surviving fraction.	153
Figure 4.15	The distribution of asynchronous PC3 cells in each phase of the cell cycle after irradiation with ^{60}Co at 100 and 5 cGy h^{-1}.	155
Figure 4.16	The results of LDR irradiations on asynchronous U373MG cells using the ^{60}Cobalt water tank system expressed as relative clonogens per flask.	156
Figure 4.17	The results of LDR irradiations on asynchronous U373MG cells using the ^{60}Cobalt water tank system expressed as cell counts and surviving fraction.	157
Figure 4.18	The distribution of asynchronous U373MG cells in each phase of the cell cycle after irradiation with ^{60}Co at 60 and 5 cGy h^{-1}.	159
Figure 4.19	The results in Figure 4.4 (asynchronous T98G)	

plotted as dose rate versus $\log_n$ gradient, *a*, obtained from fitting $SF=e^{-adose}$. 160
Figure 4.20 The results in Figure 4.7 (confluent T98G) plotted as dose rate versus $\log_n$ gradient, *a*, obtained from fitting $SF=e^{-adose}$. 160
Figure 4.21 The results in Figure 4.9 (asynchronous A7) plotted as dose rate versus $\log_n$ gradient, *a*, obtained from fitting $SF=e^{-adose}$. 161
Figure 4.22 The results in Figure 4.12 (asynchronous PC3) plotted as dose rate versus $\log_n$ gradient, *a*, obtained from fitting $SF=e^{-adose}$. 161
Figure 4.23 The results in Figure 4.15 (asynchronous U373MG) plotted as dose rate versus $\log_n$ gradient, *a*, obtained from fitting $SF=e^{-adose}$. 162
Figure 4.24 The distribution of asynchronous T98G cells in each phase of the cell cycle, 0, 3 and 24 h after irradiation with ^{60}Co at 100 and 5 cGy h^{-1} to 5 Gy. 165
Figure 4.25 The results of LDR irradiations on asynchronous T98G cells using the ^{60}Cobalt water tank system at 100 cGy h^{-1} at 5.7 and 31.0 cm into the water tank. 166

Chapter 5

Figure 5.1 A diagram of the cross-section through an ^{125}Iodine seed. 183
Figure 5.2 An isodose plot using ^{125}Iodine seeds for prostate cancer. 184
Figure 5.3 A diagram of the ^{125}Iodine seed irradiator. 185
Figure 5.4 (A & B). Photographs of the ^{125}Iodine seed irradiator. 186
Figure 5.5 The results of Fricke dosimetry in a suspension culture bottle containing one 370 MBq (10 mCi) ^{125}Iodine seed. 188
Figure 5.6 The results of Fricke dosimetry on two X-ray irradiated flasks measured at wavelengths of 224 and 304 nm. 189
Figure 5.7 The standardised results from Figure 5.6. 190
Figure 5.8 The optical density spectrum curve for unirradiated Fricke solution. 191
Figure 5.9 The results of LDR irradiations of confluent T98G cells using the "old" seed irradiator. 192
Figure 5.10 (A–D). The results of LDR irradiations of confluent T98G cells using seed irradiators 1 to 4. 194
Figure 5.11 The results in Figure 5.9 ("old" seed irradiator) plotted as dose rate plotted versus gradient, *a*,

obtained from fitting $SF=e^{-adose}$. 202
Figure 5.12 The results in Figure 5.10A (seed irradiator 1) plotted as dose rate plotted versus gradient, *a*, obtained from fitting $SF=e^{-adose}$. 203
Figure 5.13 The results in Figure 5.10B (seed irradiator 2) plotted as dose rate plotted versus gradient, *a*, obtained from fitting $SF=e^{-adose}$. 203
Figure 5.14 The results in Figure 5.10C (seed irradiator 3) plotted as dose rate plotted versus gradient, *a*, obtained from fitting $SF=e^{-adose}$. 204
Figure 5.15 The results in Figure 5.10D (seed irradiator 4) plotted as dose rate plotted versus gradient, *a*, obtained from fitting $SF=e^{-adose}$. 204
Figure 5.16 The results of all seed irradiators plotted as dose rate versus gradient, *a*, obtained from fitting $SF=e^{-adose}$. 205

Chapter 6

Figure 6.1 The results of irradiating asynchronous T98G at LDR at 60, 30, 10 and 5 cGy h^{-1} to total doses of 2 and 5 Gy then at HDR with 0 h between irradiations. 220
Figure 6.2 The results of irradiating confluent T98G at LDR at 60, 30, 10 and 5 cGy h^{-1} to total doses of 2 and 5 Gy then at HDR with 0 h between irradiations. 227
Figure 6.3 The results of irradiating confluent T98G at LDR at 60, 30, 10 and 5 cGy h^{-1} to total doses of 2 and 5 Gy then at HDR with 4 h between irradiations. 234
Figure 6.4 A threshold model for the induction of IRR at LDRs. 242
Figure 6.5 A diagram of the "distance" method of analysis. 245
Figure 6.6 A diagram of the "area" method of analysis. 246
Figure 6.7 (A–C) Comparisons of the degree of HRS obtained by irradiating T98G cells at various LDR then subsequently with HDR as calculated by 3 different methods. 248
Figure 6.8 The relationship between surviving fraction at 2 Gy and the "distance" method of analysis for cell lines tested *in vitro*. 251
Figure 6.9 The relationship between surviving fraction at 2 Gy and the "area" method of analysis for cell lines tested *in vitro*. 252

Chapter 7

Figure 7.1 Diagram of cell-cycle regulation in mammalian cells. 255
Figure 7.2 A typical dot plot of cell-cycle analysis using BrdUrd

	and flow cytometry.	259
Figure 7.3	Histograms used in cell-cycle phase length and cell-cycle analysis.	260
Figure 7.4	The results of BrdUrd pulse-labelling experiments using asynchronous T98G cells to measure cell-cycle time.	262
Figure 7.5	The results of BrdUrd pulse-labelling experiments using asynchronous T98G cells to measure G1 delay after irradiation with 2 Gy at HDR.	263
Figure 7.6	The results of BrdUrd pulse-labelling experiments using asynchronous T98G cells to measure G2 delay after irradiation with 2 Gy at HDR.	264

Index of Tables

Chapter 1

Table 1.1	The cell lines screened for the presence of HRS.	28
Table 1.2	Selected international variations in age-adjusted prostate cancer mortality rates.	56
Table 1.3	The degree of side effects using various treatments for prostate cancer.	56
Table 1.4	A comparison of acute and late toxicities for HDR, LDR and PDR brachytherapy.	65

Chapter 2

Table 2.1	The characteristics of 7 cell lines used in this study.	69

Chapter 3

Table 3.1	The results of BrdUrd pulse-labelling of RT112 cells grown at 37, 32 and 30°C to obtain cell-cycle times.	96
Table 3.2	Summary of data obtained from DMIPS experiments on 6 human tumour cell lines.	116
Table 3.3	Summary of data obtained from cell sort experiments on 5 human tumour cell lines.	117
Table 3.4	The results of fitting cell survival data to the equation $SF = C\exp\left(-\alpha d - \beta d^2\right)$.	118
Table 3.5	Summary data from cell sort and DMIPS experiments on T98G under cell-cycle modified conditions.	119

Chapter 4

Table 4.1	The distance along ^{60}Cobalt water tank where flasks were positioned to give desired dose rate.	135
Table 4.2	The comparison between survival curves obtained irradiating asynchronous T98G cells with ^{60}Co γ-rays.	142
Table 4.3	The comparison between survival curves obtained irradiating confluent T98G cells with ^{60}Co γ-rays.	146
Table 4.4	The comparison between survival curves obtained irradiating asynchronous A7 cells with ^{60}Co γ-rays.	150
Table 4.5	The comparison between survival curves obtained irradiating asynchronous PC3 cells with ^{60}Co γ-rays.	154
Table 4.6	The comparison between survival curves obtained irradiating asynchronous U373MG cells with ^{60}Co γ-rays.	158
Table 4.7	The comparison between the percentage of cells in each	

phase of the cell cycle after LDR ^{60}Co γ-ray irradiation at 100 or 60 and 5 cGy h^{-1}. 163

Chapter 5

Table 5.1 The activity of ^{125}Iodine seeds as measured in an ionisation chamber then used for Fricke dosimetry in suspension culture. 180

Table 5.2 The activity of ^{125}Iodine seeds as measured in an ionisation chamber then placed in seed irradiators. 180

Table 5.3 The comparison between survival curves obtained irradiating confluent T98G cells with the "old" ^{125}Iodine seed irradiator. 193

Table 5.4 The comparison between survival curves obtained irradiating confluent T98G cells with no.1 ^{125}Iodine seed irradiator. 195

Table 5.5 The comparison between survival curves obtained irradiating confluent T98G cells with no.2 ^{125}Iodine seed irradiator. 197

Table 5.6 The comparison between survival curves obtained irradiating confluent T98G cells with no.3 ^{125}Iodine seed irradiator. 199

Table 5.7 The comparison between survival curves obtained irradiating confluent T98G cells with no.4 ^{125}Iodine seed irradiator. 201

Chapter 6

Table 6.1 Summary of the results of irradiating asynchronous T98G at LDR at 60, 30, 10 and 5 cGy h^{-1} to total doses of 2 and 5 Gy then at HDR with 0 h between irradiations. 217

Table 6.2 The results from Figure 6.1 fitted to the equation $SF = C\exp\left(-\alpha d - \beta d^{2}\right)$. 218

Table 6.3 The presence or absence of significant HRS in data from Figure 6.1 using 4 methods of analysis. 219

Table 6.4 Summary of the results of irradiating confluent T98G at LDR at 60, 30, 10 and 5 cGy h^{-1} to total doses of 2 and 5 Gy then at HDR with 0 h between irradiations. 224

Table 6.5 The results from Figure 6.2 fitted to the equation $SF = C\exp\left(-\alpha d - \beta d^{2}\right)$. 225

Table 6.6 The presence or absence of significant HRS in data from Figure 6.2 using 4 methods of analysis. 226

Table 6.7 Summary of the results of irradiating confluent T98G at LDR at 60, 30, 10 and 5 cGy h^{-1} to total doses of 2 and 5 Gy then at HDR with 4 h between irradiations. 231

Table 6.8 The results from Figure 6.3 fitted to the equation $SF = C\exp(-\alpha d - \beta d^2)$. 232

Table 6.9 The presence or absence of significant HRS in data from Figure 6.3 using 4 methods of analysis. 233

Table 6.10 The degree of HRS as measured using 3 methods in all LDR then HDR experiments. 247

Chapter 7

Table 7.1 The cell-cycle phase times and delays after 2 Gy HDR X-rays for asynchronous T98G, A7, PC3 and U373MG cell lines. 265

Abbreviations

ANOVA	analysis of variance
AT	ataxia telangiectasia
α	alpha
β	beta
BED	biologically effective dose
BrdUrd	5'-bromo-deoxyuridine
CAK	cdk activity kinase
Cdk	cyclin dependent kinase
CS	cell sorter
C-Scan	cell recognition program
CT	computed tomography
DMF	dose modifying factor
DMIPS	dynamic microscope image processing scanner
DNA	deoxyribonucleic acid
DNA-PK	DNA-protein kinase
DSB	Double strand break
DVH	Dose-volume histogram
EDTA	ethylenediaminetetraacetic acid
EMEM	eagle's minimum essential medium
FACS	fluorescence activated cell sorter
FCS	foetal calf serum
FITC	fluorescein isothiocyanate
G0	quiescent or resting phase of the cell cycle
G1	first gap phase of the cell cycle
G2	second gap phase of the cell cycle
Gy	Gray
h	hours
HDR	high dose rate
HRS	hyper-radiosensitivity
IRR	increased-radioresistance
IR	induced repair
keV	kiloelectron volts
kV	kilovolt
kVp	kilovoltage peak
L	litre
LET	linear energy transfer
LDR	low dose rate
LI	labelling index

LPL	lethal and potentially lethal model
LQ	Linear-Quadratic model
LQR	Linear-Quadratic-resensitisation model
M	mitosis
mA	milliamps
MBq	megabequerels
mCi	milliCurie
MeV	megaelectron volts
mg	milligram
MI	mitotic index
min	minute
ml	millilitre
mM	millimolar
MRI	magnetic resonance imaging
MW	molecular weight
n	extrapolation number
NER	nucleotide excision repair
NHEJ	non-homologous end joining
PARP	poly (ADP-robose) polymerase
PBS	phosphate buffered saline
PDR	pulsed dose rate
PE	plating efficiency
PI	propidium iodide
PK	protein kinase
PLD	potentially lethal damage
RMSE	residual mean square error
RNase	ribonuclease
RPR	repair-misrepair model
S	S phase of the cell cycle
S-Scan	cell revisiting program
SD	standard deviation
SEM	standard error of the mean
SF	surviving fraction
SF2	surviving fraction at 2 Gy
SLD	sublethal damage
SSB	single strand break
T_C	length of cell cycle
T_{G1}	duration of G1
$T_{G2/M}$	duration of G2/M phase
T_S	duration of S phase

Chapter 1. Introduction

1.1. Introduction

Over 70% of new cases of cancer are in people over the age of sixty (Parkin *et al.* 1999). Carcinogenesis is a multistep accumulation of genetic lesions that may result in uncontrolled cellular proliferation, a decrease in cell death or apoptosis, invasion, metastatic spread and a blockade of differentiation. The accumulation of these genetic lesions throughout life may culminate in cancer. The acquisition of a number of genetic mutations in one cell may eventually lead to loss of proliferative control of this host cell. This cell will start dividing uncontrollably, invading adjacent normal tissue and spreading around the body via the blood or lymphatic system.

Radiotherapy is one of the most effective treatments for cancer, second only to surgery. It generally achieves good tumour control whilst giving a good cosmetic result and has replaced surgery in the control of tumours of the head and neck, prostate, cervix, bladder and skin. A range of studies have been carried out to develop a regime that maximises tumour cell kill whilst sparing surrounding normal tissues in a short overall treatment time (Saunders *et al.* 1997, Saunders and Dische 1992, Roed *et al.* 1996, Zamorano *et al.* 1992, Blasko *et al.* 2000). Many of these have been tailored to a specific tumour type.

1.2 Cellular effects of ionising radiation

Charged particles enter biological material and have two immediate effects. They interact with orbital electrons, ejecting some of them from the atoms (ionisation) and raise the energy levels of other electrons (excitation). Depending on the energy, these secondary electrons may give rise to a cascade of ionisation events. At therapeutic doses, the number of ionisation events initiated by X-rays is very large, with a dose of 1 Gy producing approximately 10^5 ionisation events per cell. Different radiation types deposit energy at different rates producing different biological effects (Pogozelski *et al.* 1999). Linear Energy Transfer (LET) describes the rate of energy deposition for disparate radiations. It is defined as the mean energy given up by a particle travelling 1 μm. High-LET radiation, such as neutrons is densely ionising and has a greater biological effect per unit dose compared with γ-rays which are less densely ionising.

X- and γ-rays mediate their effects primarily through indirect action on the surrounding tissue (reviewed by Ward 1986). A photon of energy dislodges an electron from an atom, which reacts with water molecules producing hydroxyl radicals. These are thought to diffuse to and react with the DNA, producing lesions such as single and double-strand breaks (SSB and DSB). More than 100 free radical-induced DNA radiolysis products have been identified and they include a broad spectrum of damage to the purine and

pyrimidine rings, SSB and sites of base loss (Wallace 1998). It is estimated that 60–70% of X-ray damage to cellular DNA in mammalian cells is due to the hydroxyl radical (Ward 1988).

High-LET radiations, act primarily directly on the DNA. High-LET radiation-induced lesions will possess a high-structural complexity, that is, breaks associated with aberrant chemical structures such as modified base/sugars and crosslinks. Higher proportions of DSB are produced with high-LET radiation compared with SSB.

1.2.1 DNA damage

There is strong circumstantial evidence to indicate that DNA is the principal target for the biological effects of radiation, including cell killing, mutation and carcinogenesis. Exposure to ionising radiation produces a number of chemical changes in the DNA of the cell including SSB and DSB, base damage and DNA protein-protein crosslinks (Ward 1988). The DNA strand break is the most important lesion produced in the cell in response to radiation. When cells are irradiated with X-rays, the number of SSB increases linearly with dose (Ward 1990, Iliakis 1991). SSB are of little consequence biologically as they may be repaired using the other strand as a template. DSB are, however of greater biological importance. Breakage of both strands at areas well separated on the DNA strand may still be repaired using the opposite strand as a template. However, SSB in the same area or opposite on the DNA strand results in no template available for repair and the chromosome will snap into two pieces. DNA DSB production is proportional to dose (Ward 1990) and although the nature of the lesion(s) responsible for cell death, lethal lesions, is unknown, there is much evidence implicating DNA DSB in cell killing. Indeed a linear relationship between lethal lesions and the induction of DSB has been observed (Radford 1985).

DSB differ in their character depending on the inducing agent and the location of the DSB in time (phase of cell cycle) and space (chromatin site).

1.2.2 Cell killing

There are three primary pathways through which radiation damage leads to cell death (Dahm Daphi *et al.* 1998, Cohen-Jonathan *et al.* 1999). Cells either die from failure to undergo mitosis (mitotic death), undergo programmed cell death (apoptotic death) or pass through several differentiation steps allowing survival at the expense of reproductive capability. Mitotic death results from structural chromosome aberrations which either preclude symmetrical segregation of chromatids to daughter nuclei (dicentrics, rings, triradials) or which result in the loss of essential genetic information due to fragment deletion (terminal, interstitial deletion, chromatid breaks) or translocations. All the lethal

types of aberrations have a DNA DSB as a common precursor. After irradiation, most normal cells, wild type for p53 and p21, are blocked at the G1/S border. Some of these cells will be able to re-enter the cell cycle, but will be blocked at the G2/M border. At this point cells with damaged chromosomes will fail to reproduce (mitotic death). Cells which undergo mitosis, may divide several times and then die (eventual reproductive death). In contrast, apoptosis is a genetically programmed form of cell death. It is characterised by cell shrinkage, chromosomal condensation and in some cases endonuclease activation leading to DNA cleavage (Rowan and Fisher 1997). It has been seen to occur after irradiation *in vitro* (Yount *et al.* 1996).

1.2.3 DNA repair

Pro- and eukaryotic cells induce the expression of genes of various functions in response to agents which cause damage to DNA. This response is essential for cells and organisms to adapt to life-threatening environmental conditions and maintain their genetic material with the highest fidelity for duplication and transcription. DNA repair may be defined as those mechanistically diverse cellular responses associated with the restoration of the normal nucleotide sequence following events which damage or alter the genome (Eckardt Schupp and Klaus 1999). There is much biological evidence in favour of the existence of radiation-inducible DNA-repair mechanisms in eukaryotes. Two main experimental schemes have been used to deduce the existence of these. Split dose experiments have been carried out where radioadaptive responses have been found (Section 1.4). A low-dose conditioning treatment was found to protect against the effects of a subsequent exposure to a larger challenge dose. In this situation a reduction in the number of chromatid aberrations, sister chromatid exchanges, deletion-type mutations and micronuclei have been seen compared with a single high dose (Olivieri *et al.* 1984, Ikushima 1987, Wojewodzka 1994, Rigaud and Moustacchi 1996, Wojcik *et al.* 1999). The second experimental scheme was to study any deviations from a typical survival curve (Section 1.3). Low-dose HRS reflects an increased sensitivity of cells to very low-radiation doses where survival is lower than predicted by high-dose data. This effect is thought to be due to an inability to induce repair mechanisms by very low doses. Cell-cycle related mechanisms have been ruled out and various experimental modifications of the effect support the relevance of inducible DNA repair as the effect is blocked by inhibiting poly (ADP ribose) polymerase (PARP), topoisomerase I (topo I) and general protein synthesis (Joiner *et al.* 1996).

Experiments using yeast have found clear evidence that UV and ionising radiation-inducible responses depend on newly synthesised mRNA and proteins and after the induction of these, survival is improved and the frequency of genetic events such as gene conversions and recombinations are increased (reviewed by Haynes *et al.* 1984, Lewis and

Resnick 2000, Siede and Eckardt 1984, Kunz *et al.* 1985, Eckardt Schupp and Klaus 1999, Roush *et al.* 1998, Boreham and Mitchel 1991). Genes which are known to facilitate either recombinational repair or nucleotide excision repair were shown to be upregulated in response to ionising radiation (*e.*g. RAD54, RAD5 and RAD16) (Budd and Mortimer 1984, Siede *et al.* 1985, Siede and Eckardt Schupp 1986, Waters *et al.* 1993, Scott and Waters 1997, Teng *et al.* 1998).

The cellular response pathways that are involved in radiation-induced DNA repair are complex. These damage-sensing proteins are organised into pathways for checkpoint control, to block DNA replication and the cell cycle if DNA damage is encountered (Kiser and Weinert 1996, Hendrickson 1997), and in several mechanistically diverse repair pathways, which either eliminate or tolerate DNA damage to maintain the structural and functional integrity of the genome.

1.2.3.1 Excision repair

Two major pathways for removing different types of DNA alterations are base excision repair (BER) and nucleotide excision repair (NER). BER is the process for removing many types of base damage produced in DNA (*e.g.* by uracil, 8-oxoguanine, and 3-methyladenine). The initial step is the removal of the damaged base by one of a series of lesion-specific DNA glycosylases to generate a gap which is subsequently filled by DNA polymerase β and is sealed using a DNA ligase (Seeberg *et al.* 1995). NER removes a large variety of lesions in DNA, which result in major distortions of the double helical structure. The DNA damage is recognised and helicase activities open out the structure. The DNA is cut on either side of the damage and DNA polymerase and accessory proteins fill in the gap and the new DNA is joined to the old by DNA ligase (Lehmann 1995).

1.2.3.2 DSB repair

DSB are particularly lethal, and there are at least two ways of repairing DSB in eukaryotes. The first, which predominates in yeast, involves homologous recombination with a sister duplex *i.e.* exchange of DNA with another homologous region which then acts as a template for new strand formation (Shinohara and Ogawa 1995). The second pathway, which is thought to be the dominant mode of DSB repair in cells of multicellular eukaryotes is non-homologous end-joining (NHEJ) (Labhart 1999). This process is biphasic with a fast component with a $t_{1/2}$ in the region of 20–40 min and a slow phase with a $t_{1/2}$ of several hours (Lieber *et al.* 1997). NHEJ employs the DNA-dependent protein kinase (DNA-PK). This is recruited and activated when a hetero-dimeric protein, made up of subunits Ku70, Ku80 and DNA-PKcs, binds to the double strand ends (Feldmann and Winnacker 1993, Troelstra and Jaspers 1994, Siede *et al.* 1996, Jeggo

1997, Kumaravel *et al.* 1998, Kasten *et al.* 1999, Wachsberger *et al.* 1999). DNA-PK acts to promote rejoining of the strands by DNA ligase IV through an, as yet, unknown pathway (Jackson and Jeggo 1995, Jeggo 1998). The activity of DNA-PK is known to vary with the phase of the cell cycle, with a maximum activity in G1 and a minimum in S phase (Lee *et al.* 1997) and after irradiation, Ku70 may form complexes with cABL and p21 suggesting a role in cell-cycle arrest (Kumaravel *et al.* 1998). Brown *et al.* (2000) recently showed that Ku70 was up-regulated in response to ionising radiation and that the activation of DNA-PK does not require Ku70 up-regulation. These findings suggest that Ku70 up-regulation provides the cell with a means of assuring either proper DNA repair or an appropriate response to DNA damage independent of DNA-PKcs activation.

A significant correlation between radiosensitivity and DSB repair has been found in many studies (reviewed by (Foray *et al.* 1997a)). Paterson *et al.* (1976) identified AT fibroblasts as being deficient in DNA excision repair of radiation-induced DNA damage and postulated that this might be the cause of the extreme radiosensitivity in AT patients. Mutants derived from hamster cell lines (CHO), have shown large reductions in the rate and extent of DSB rejoining and a substantial increase in radiosensitivity (Kemp *et al.* 1984, Kysela *et al.* 1993). Other examples include murine lymphoblast cell lines (Wlodek and Hittelman 1988), AT cell lines (Coquerelle *et al.* 1987, Foray *et al.* 1997b) and tumour cell lines (Kelland *et al.* 1988c, Giaccia *et al.* 1992, Lambin *et al.* 1992, Zaffaroni *et al.* 1994). However, a correlation has not been found in all studies (Olive *et al.* 1994, Whitaker *et al.* 1995, Powell *et al.* 1992, Woudstra *et al.* 1996a, Woudstra *et al.* 1996b, Smeets *et al.* 1994, Lehmann *et al.* 1977, vanAnkeren *et al.* 1988). Although it is difficult to compare studies due to differences in cell lines, assays, endpoints and time-courses used, the variable results obtained highlight that the relationship between DNA-repair pathways and radiosensitivity is a complex one.

1.3 Survival at acute low doses of radiation

1.3.1 Low-dose hyper-radiosesitivity (HRS)

There is evidence for a deviation from the Linear-Quadratic curve, where enhanced sensitivity occurs at very low doses of radiation (below 1 Gy). Experiments carried out by Eriksson (1963) studied the effects of acute low-dose γ-ray exposures in maize. His data analysed by Chadwick and Leenhouts (1975), demonstrated that at doses below 0.5 Gy there appeared to be an enhanced sensitivity to radiation both in pollen production and mutation induction. A similar sensitivity was observed in the budding yeast *Sarcomyces Cerevisiae* (Beam *et al.* 1954) and in the green algae *Oedegonium cardiacum* (Horsley and Pujara 1969). Observations made by Calkins (1967) on the dose-survival relationship

of the protozoan *Tetrahymena pyriformis*, found that a dip in the survival curve occurred in the low-dose region together with an *increase* in cell survival at higher doses (above 0.5 Gy). This was explained as two separate repair systems, a constitutive and a triggered mechanism which occurs at larger doses leading to increased cell survival. Similarly, the response of a lepidopteran cell line to low doses was also multiphasic (Koval 1984).

Up until recently, the study of low-dose HRS in mammalian cells was not possible as an exact assessment of clonogenicity could not be gained. Accurate measurement of cell survival at very low doses of radiation (below 1 Gy) requires specialised techniques. For many years, the low-dose region of the cell-survival curve was predicted to follow the extrapolation of the Linear-Quadratic model, as accurate measurement of this region could not be gained by conventional methods. These conventional "Puck and Marcus" (Puck and Marcus 1956) survival assays relied on a certain number of cells being plated as a result of multiple dilutions. There are considerable errors inherent when using this method (Boag 1975) including sampling errors and the precise number of cells plated is not known.

During the last decade two new methods to measure cell survival accurately at low doses have been developed using either the Dynamic Microscopic Image Processing Scanner (the DMIPS) or a cell sorter. The DMIPS is an automated microscope which scans a flask containing single cells, identifies the attached cells and stores their locations so that the exact cell positions can be revisited to manually score for colony formation. This allows a very accurate measurement of clonogenic survival on a cell-by-cell basis. The cell sorter uses the reflectance properties of the cells when illuminated by laser light to sort individual cells on the basis of cell size and granularity without the use of a cell stain (Durand 1986). A precise number can be plated before or after irradiation, thereby omitting sampling error (Boag 1975). These two methods have been used to measure the survival of tumour cells after very low doses of radiation (Marples and Joiner 1993, Skarsgard *et al.* 1991). Both the DMIPS, developed at the Gray Laboratory and the cell sorter have shown surviving fractions at high doses comparable to data obtained using a conventional dilution assay (Marples and Joiner 1993).

With this increase in the sensitivity of techniques used, the low-dose region of the mammalian cell-survival curve could be studied in more detail. Similar findings to non-mammalian cell lines were obtained. In 1993, Marples and Joiner published the results of the first low-dose survival curve using mammalian cells. They used the DMIPS to study the survival of asynchronously growing V79 cells (rodent fibroblasts) after irradiation. They found an enhanced sensitivity to radiation in the low-dose region (below 1 Gy), deviating from the prediction modelled from the high-dose data. This increase in

sensitivity has been termed low-dose hyper-radiosensitivity (HRS). As the dose is increased above 0.4 Gy, radioresistance increases until it is maximal beyond 1 Gy and the survival curve then follows the usual downward-bending curve with increasing dose. This increase in resistance has been termed increased radioresistance (IRR). The authors suggest that this IRR response is due to the triggering of repair or radioprotective mechanisms which are switched on at a sufficiently high dose, *i.e.* above 0.4 Gy.

1.3.2 LET

This low-dose HRS was not observed in cells irradiated with high-LET neutrons which would suggest that neutrons do not induce repair mechanisms. Studies comparing the effects of LET over the whole dose range in V79 (Marples and Joiner 1993) and HT29 (Lambin *et al.* 1993) concluded that in the low-dose region, both high and low LET produced a similar response, but at higher doses, an increased sensitivity was seen with high-LET radiation. This would suggest that IRR does not occur at high doses in cells irradiated with high-LET radiation. Alternatively IRR may be switched on in both cases, but the resulting repair processes may not be effective in repairing damage caused by high-LET irradiation.

1.3.3 Hypoxia

Oxygen has a radiosensitising effect on cells, an effect which decreases with decreasing dose (Revesz and Palcic 1985) (Skarsgard *et al.* 1991). V79 cells show HRS when irradiated in both oxic and hypoxic conditions (Marples *et al.* 1994). This would suggest that oxygen is not required for HRS. However the IRR response occurred at higher doses (the d_C value for oxic cells was 0.5 Gy compared with 0.69 Gy in hypoxic cells). This oxygen dependency was also observed in lepidopteran cells (Koval 1984). Modelling by Dasu and Denekamp (1998) has predicted that at very low doses where HRS occurs, hypoxia may produce an increase in *sensitivity*, not resistance. This could be a potential benefit when clinically treating hypoxic tumours with low doses per fraction (Dasu and Denekamp 1999).

1.3.4 Prevalence of HRS in vitro

Over the past 7 years, in the Gray Laboratory and Vancouver, 28 cell lines have been assessed for the presence of HRS, including the ones described in this thesis (see Table 1.1). These include both normal and tumour cell lines of both rodent and human origin. Only five of these cell lines do not show HRS.

Cell line	Type	Reference	HRS?
V79	Hamster fibroblast	(Marples and Joiner 1993)	✔
HT29	Human colon adenocarcinoma	(Lambin *et al.* 1993)	✔
Be11	Human melanoma	(Lambin *et al.* 1996)	✔
MeWo	Human melanoma	(Lambin *et al.* 1996)	✔
U1	Human melanoma	(Wouters *et al.* 1996)	✔
RT112	Human bladder carcinoma	(Lambin *et al.* 1994b)	✔
DU145	Human prostate carcinoma	(Wouters *et al.* 1996)	✔
A549	Human lung carcinoma	(Wouters *et al.* 1996)	✔
T98G	Human glioblastoma	(Short *et al.* 1999a)	✔
L132	Human embryonic lung	(Singh *et al.* 1994)	✔
A7	Human glioblastoma	(Short *et al.* 1999b)	✔
U373MG	Human glioblastoma	(Short *et al.* 1999b)	✘
U87MG	Human glioblastoma	(Short *et al.* 1999b)	✔
SiHa	Human cervical carcinoma	(Wouters *et al.* 1996)	✘
SW48	Human colonic carcinoma	(Lambin *et al.* 1996)	✘
HX142	Human neuroblastoma	(Lambin *et al.* 1996)	✘
RKO	Human colorectal carcinoma	Joiner *et al.* pers. comm.	✔
LNCaP	Human prostate carcinoma	Mayes *et al.* 1999 unpublished data	✔
SNB19	Human glioblastoma	Joiner *et al.* pers. comm.	✔
U118	Human glioblastoma	Joiner *et al.* pers. comm.	✔
U138	Human glioblastoma	(Short *et al.* 1999b)	✔
HGL21	Human glioblastoma	(Short *et al.* 1999b)	✔
MSU1.1	Human fibroblast	Joiner *et al.* pers. comm.	✔
UMUC3	Human bladder carcinoma	Joiner *et al.* pers. comm.	✔
MCF7	Human breast carcinoma	Joiner *et al.* pers. comm.	✘
DBTRG	Human glioblastoma	Joiner *et al.* pers. comm.	✔
PC3	Human prostate carcinoma	Mayes *et al.* 1999 unpublished data	✔

Table 1.1
Shows the cell lines screened for the presence of low-dose HRS.

1.4 The adaptive response

This increase in radiosensitivity in the low-dose region may be related to an "adaptive response" to radiation in which a small conditioning dose of radiation induces a resistance to a subsequent higher dose. This response has been described in many prokaryote and lower eukaryote cell lines. Early work by Hillova and Drasil (1967) showed an adaptive response in the green unicellular algae, *ChlamydomonasReinhardti.* Experiments by Hendry on fern spores from *Osmunda* showed that radioresistence would increase by a factor of 3–4 if an initial priming dose was given 5 h earlier. This radioresistant effect was no longer present after 24 h (Hendry 1986). The adaptive response has also been found in *Escherichia Coli* (Pollard and Achey 1975, Huang and Claycamp 1993), *Closterium* (Howard and Cowie 1976), yeast (Boreham and Mitchel 1991) and insect cell lines (Koval 1988).

Variations in radiosensitivity throughout the cell cycle have been proposed to explain HRS. The rationale for HRS/IRR is that cells in a sensitive phase of the cell cycle would be killed with a low dose of radiation and higher doses would then be needed to kill cells in more resistant phases of the cell cycle. This was termed the "two population model". A cell-cycle effect could also be argued for the adaptive response. The first dose of radiation would kill off the most sensitive cells and induce cell synchrony within the cell cycle. A higher subsequent dose would then be needed to kill cells in the more resistant phases of the cell cycle. These cells would then appear more radioresistant than cells which had not received a priming dose. This could not be the explanation for some of the adaptive responses seen in non-mammalian systems such as the photosynthesising desmid *Closterium* which shows an adaptive response to radiation when kept in the dark, where cells are effectively in cell-cycle arrest (Howard and Cowie 1978). This adaptive response was blocked by the presence of cycloheximide, a potent protein inhibitor, and they therefore suggested that their adaptive response was due to the induction of a repair enzyme after the initial priming dose which protected the cells from the subsequent dose of radiation. Cell-cycle effects could also be ruled out in the green algae, *Oedogonium* as the increased survival after the second dose was much greater than could be explained by any cell-cycle progression (Horsley and Laszlo 1971). Similar effects have been seen in other types of algae including *Chlamydomonas* and *Chlorella* (Bryant 1972).

The adaptive response has been shown to occur in mammalian cell lines. Olivieri *et al.* (1984) carried out experiments demonstrating this effect on human lymphocytes. They found that those cells receiving both an initial small priming dose and a higher subsequent dose of X-rays had fewer chromatid aberrations than cells receiving only the higher dose. Other studies have been carried out on lymphocytes using chemicals for the initial or challenge dose. Conditioning doses of bleomycin (Vijayalaxmi and Burkart 1989a,

Vijayalaxmi and Burkart 1989b) and hydrogen peroxide (Wolff *et al.* 1989, Cortes *et al.* 1990) and challenging doses of bleomycin, mytomycin C (Wolff *et al.* 1989), BCNU, *cis*-platin and etoposide (Shadley and Dai 1993) have been studied and all result in significant reductions in chromosome aberrations when compared with a single low dose. (Shadley 1994) reviewed this work and concluded that the adaptive response is caused by induced-repair activity involving proteins that repair lesions in the DNA. Other studies have found the adaptive-type response in human tumours (Seong and Kim 1994, Wouters and Skarsgard 1997) and normal cell lines (Cai and Liu 1990, Azzam *et al.* 1994) and in rodent cells (Marples and Joiner 1995, Sasaki 1995) measuring endpoints such as chromosome aberrations, mutations, genetic instability and clonogenic survival.

Although there appears to be a certain degree of homology between the adaptive response and HRS/IRR, a study using HT29 cells by Wouters and Skarsgard (1997) suggests that they may be distinct phenomena. Their results show that priming doses prevent HRS but have no effect on the high-dose region of the survival curve. Experiments by Short (1999) have shown that the time course for the effect to become apparent and the persistence of the effect is much greater in the adaptive response, mitigating against a mechanistic relationship.

1.5 Possible mechanisms of HRS/IRR

1.5.1 Apoptosis

Apoptosis, or programmed cell death, is a form of cell death which is distinct from necrosis. The process is defined by morphological changes resulting in non-pathogenic cell loss. Evidence suggests that apoptosis is NOT involved in the HRS/IRR response. An original hypothesis was that at small doses of radiation, cells undergo apoptosis as a means of removing genomically-unstable cells from the population. This does not seem to be the case for the HRS-positive cell line T98G which does not show an increase in apoptosis after 0.4 Gy, a dose at which HRS is observed in this cell line (Short 1999). Nine of the 27 cell line studied were glioma cell lines of which 8 (89%) showed low-dose HRS. Stapper *et al.* (1995) showed that apoptosis is not the primary mode of cell death in glioma cell lines. In both U373MG (HRS –ve) and T98G (HRS +ve) cell lines, apoptosis does not occur due to an abnormally high activity of protein kinase C (PKC). This promotes the production of BCL-xL, a protein which inhibits apoptosis. However, the inhibition of PKC induces apoptosis in these cell lines (Leirdal and Sioud 1999). Unpublished data from Power (1998) show that two cell lines, HT29 and Be11, both characterised by a high level of HRS/IRR, show different levels of apoptosis in both unirradiated and irradiated populations over a range of doses. Thus, the level of apoptosis

is not correlated with the presence of HRS/IRR.

1.5.2 Cell cycle

As with the non-mammalian systems, it was argued that low-dose HRS was a consequence of a cell-cycle effect. The "two population" model was used to explain substructure in the survival curve of mammalian cell lines at higher doses (between 1–4 Gy) which disappears when the population is synchronised. This was shown to occur in V79 cells (Marples and Joiner1993, Skarsgard *et al.* 1996). Calculations made on the sensitivity of cells throughout the cell cycle could only account for a 2–3 fold increase in radiosensitivity in the low-dose region, whereas the sensitivity observed for cell lines such as HT29 was as much as a factor of 81 (Lambin *et al.* 1996). This would suggest that cell-cycle perturbations are not the major component of HRS. Modification of the cell cycle to promote cell-cycle synchronicity or arrest did not prevent HRS in V79 cells (Marples and Joiner 1993) and not in the human glioblastoma, T98G which shows HRS when serum deprived and under confluence arrest (Short *et al.* 1999a).

Work carried out by Joiner *et al.* (pers. comm.) showed a variation in the magnitude of the HRS effect throughout the cell cycle. Experiments were carried out using a cell sorter to select a population of T98G cells in a certain phase of the cell cycle. Survival curves show the greatest HRS/IRR effect in the G2/M phase. This effect was less marked during G1 phase and even less in S phase. This increase in HRS response parallels changes in high-dose radiosensitivity in different phases of the cell cycle. Variations in DNA-repair capacity during different cell-cycle phases therefore seem to influence clonogenic survival after both low and high-dose irradiation. These experiments also show that low-dose HRS could not be due to a sensitive subpopulation of cells, as all cells selected on the basis of a single cell-cycle phase for an experiment showed a similar radiosensitivity.

1.5.3 DNA repair

Evidence has been accumulating that DNA repair is one of the main mechanisms underlying the phenomenon of low-dose HRS and IRR (Joiner and Marples 1992). The nature of this repair, whether it be a constitutive or induced process is still yet to be determined. Low-dose HRS tends to occur in relatively radioresistant cell lines. The magnitude of the response can be as great as 20 times as much as the radiosensitivity seen in doses above 1 Gy where IRR occurs. Some radiosensitive cell lines such as HX142 and SW48 do not show an apparent HRS/IRR response, but show a high level of radiosensitivity along the whole survival curve. Cells may be radiosensitive as it is the lack of IRR at high doses rather than HRS that results in a sensitive response. These cells may have a reduced repair capacity and the lack of IRR in these cell lines suggests that IRR may be linked to the DNA-repair ability.

Further evidence suggests that DNA repair is involved in the HRS/IRR response. Chemical inhibitors of DNA repair have been shown to block the effect. Cycloheximide, a protein synthesis inhibitor, blocks the adaptive response and the HRS/IRR effect (Marples and Joiner 1995). This would suggest that synthesis of new proteins occurs as a radioprotective mechanism. 3-Aminobenzamide also abolishes the HRS/IRR effect in V79 cells (Marples *et al.* 1997) suggesting that repair pathways encompassing Poly (ADP ribose) polymerase (PARP) may be involved. Skov *et al.* (1994) examined 3 rodent cell lines, each with a different DNA-repair deficiency, and determined the presence or absence of HRS/IRR for each. HRS was found in the BER-deficient cell line, EM9, which would imply that BER is not an important factor in IRR. HRS/IRR was not present in either the DSB-repair deficient cell line, XR-V15B, or the NER-deficient cell line, UV-20, suggesting that these pathways are induced after radiation. The XR-V15B cell line is defective in the Ku80 subunit of the DNA-PK complex that repairs DNA DSB (Jeggo 1997). Further evidence for the involvement of DNA-PK in IRR was obtained by (Vaganay-Juéry *et al.* 2000) who found a decrease in DNA-PK activity at 0.2 Gy in cell lines displaying HRS and an increase in activity in cell lines which did not show a HRS response. DNA-PK, however is not thought to be involved in the adaptive response. A study comparing DNA-PK-deficient murine fibroblasts with normal fibroblasts found no difference in the adaptive response, implying that DNA-PK is not involved in this effect (Odegaard *et al.* 1998). This result suggests that the mechanisms behind the adaptive response and HRS/IRR may be different.

1.6 Low dose-rate irradiation

The dose of radiation (energy absorbed per gram of biological material) to a cell is an important factor affecting the biological response, However the rate of energy absorption (the dose rate) is also of fundamental importance. Reports in the literature dating back to the 1920s suggest that the dose rate can affect division delay in chick tissue cultures (Canti and Spear 1927), chromosome aberrations in *Tradescantia* (Sax 1939), cleavage delay in *Arbacia* eggs (Henshaw *et al.* 1933) and growth inhibition of roots of *Vicia faba* (Gray and Scholes 1951). Since the discovery of X-rays by Röntgen over a hundred years ago and the subsequent development of radiation as an cancer treatment, the time over which a dose of radiation has been delivered has been cause for debate. High dose-rate radiotherapy appeared to produce a high tumour cell kill, but low dose-rate irradiation spared surrounding normal tissue from damage. In general low-dose rates tend to have a "sparing" effect on cell survival where less cell kill is observed per unit dose. However an "inverse" dose-rate effect has been observed in some studies where a reduction in dose rate leads to an *increased* cell kill. This is described in detail in Section 1.6.4.

1.6.1 Low dose-rate sparing

Elkind and Sutton (1959) conducted experiments where the single-dose radiation survival of a Chinese hamster ovarian cell line (Clone A) was compared with doses which were split and given in two fractions. They produced a "2-dose fractionation curve" where surviving fraction was plotted against the time interval between the two fractions (Figure 1.1). Cells appeared more resistant to cell kill than with single dose exposure. This increase in resistance could be measured when the time interval between doses was as little as 30 minutes. In a second series of experiments (Figure 1.2) they irradiated cells with an initial dose of 5 Gy, followed by an 18 h incubation was given and survival was then assessed following further irradiation with doses ranging from 2 to 8 Gy. The resulting survival curve lay above the curve obtained from a single exposure. These data suggest that cells were repairing sublethal damage in the time interval before the second fraction of radiation. In 1961 Lajtha and Oliver (1961) used the results from Elkind and Suttons' acute and split-dose experiments to predict survival curves for continuous low dose-rate exposures. They made two predictions, the first being a reduced efficiency of radiation cell kill at lower dose rates. They hypothesised that as the dose rate was lowered, the survival curve would become progressively less steep. Continuous low dose–rate irradiation could be considered as an infinite number of fractions and so sublethal damage would be repaired during the irradiation time. They therefore hypothesised that as the dose rate was reduced (equivalent to reducing the dose per fraction) and the irradiation time to reach a target total dose was increased (equivalent to increasing the number of fractions), that the radiation would be less efficient at cell killing than at higher or acute dose rates. This effect has been termed the "dose-rate effect" or "dose-rate sparing".

The second prediction put forward by Lajtha and Oliver from Elkind and Suttons' data was a change in the form of the dose-response curve from a sigmoid (Equation 1.2) for acute irradiation, to a simple exponential (Equation 1.3) for protracted irradiation.
The shoulder region of the survival curve which can be seen at acute doses, was predicted to be absent in the fractionated dose-response curve. They suggested that the accumulation of hits at sensitive DNA sites, which explains the shoulder region on the acute dose curve, would occur continuously during low dose–rate irradiation. Sublethal-damage repair would take place at these hit sites at the same time. The result would be that the continuous low dose–rate survival curve would approximate to a straight line on a linear-log plot. Similar predictions were made by Elkind and Whitmore (1967) regarding cell survival after multiple fractions.

The first experimental data on the effects of low dose-rate irradiation on mammalian cell survival were published in 1962. Berry and Cohen (1962) carried out experiments *in vivo* where tumour bearing mice were placed in cages at right angles to a ^{60}Co γ-source. A dose

rate of 20 or 40 rad h^{-1} (20 or 40 cGy h^{-1}) was obtained at the centre of the cage. The experiment was designed so that the random movements of the mice around the source averaged out the dose rate to each mouse. The total accumulated dose was reported to be as accurate within ± 5%. The survival of the tumour cells were assessed using a dilution assay technique and were compared with tumour cells taken from mice irradiated at an acute dose rate of 115 rad min^{-1} (115 cGy min^{-1}). There were many inherent problems with the dosimetry in this type of experiment and there was an absence of oxygen during irradiation which may have increased the radioresistance and made the survival curves appear shallower. Under these conditions the oxygen enhancement ratio was not known with any certainty, so survival curves in the presence of oxygen could not be accurately estimated. However, survival curves were obtained which supported the predictions made by Lajtha and Oliver a year earlier (Lajtha 1961). The cells irradiated at the lowest dose rates showed less cell kill than cells irradiated at acute doses.

Bedford and Hall carried out experiments *in vitro* with HeLa (human cervical carcinoma) cells under aerobic conditions using radium (Bedford 1963) and cobalt (Hall 1964) as a source of γ-rays. A wide range of dose rates were studied. A dose-rate effect was observed and the findings reported were in general agreement with experiments by previous investigators. The predictions made by Lajtha and Oliver concerning differences in the shape of the survival curve for acute (sigmoid) and low dose-rate (exponential) irradiation (Lajtha 1961) were substantiated by Hall and Bedford (Bedford 1963, Hall 1964). The dose–rate effect appeared most dramatic between 100 and 1 rad min^{-1} (100 and 1 cGy min^{-1}), although the effect was apparent at dose rates as low as 30 rads per day (1.25 cGy h^{-1}) (Nias and Lajtha 1964). Figure 1.3 shows the dose-rate effect in Chinese hamster cells.

1.6.2 Mechanisms

Various mechanisms have been suggested for the increased protection of LDR irradiation (reviewed by Gentner 1992). Firstly, a cell-repair system that may be saturated with lesions requiring repair when irradiated at HDR is thought to be more effective in repairing radiation injury if sufficient time is allowed. Secondly, there are physical differences in the radiation intensity or distribution of ionisations between HDR and LDR exposure (Russell *et al.* 1958) and dispersed or unclustered ionisation as a result of LDR exposure have less chance of producing DSB compared with HDR exposure. Therefore, following LDR, a cell may have a greater number of repairable lesions than after HDR and consequently a repair-proficient cell may be able to better repair these critical lesions. Finally an adaptive or induced response has been suggested where at LDR the cell receives a priming dose, switching on repair mechanisms which leaves it better able to repair the subsequent damage (Sasaki 1995, Stecca and Gerber 1998).

Experiments using genetically modified cell lines have further implicated the involvement of DNA-repair mechanisms in dose-rate sparing. The mouse lymphoma cell line showed increased survival at low-dose rate, while its X-ray-sensitive derivative LY-S, showed only a slight dose-rate effect (Evans *et al.* 1985). Similarly, CHO K-1 cells had a 2.5 fold increase in survival at low-dose rate compared with acute exposure, while their X-ray-sensitive mutants, *xrs-5*, *xrs-6* (Nagasawa *et al.* 1989) and *irs-20* (Stackhouse and Bedford 1993) exhibited no dose-rate effect. These sensitive cell lines are believed to be deficient in DSB repair.

Chemicals which block dose-rate sparing can lead to greater understanding of the mechanisms behind the effect and may possibly be useful as clinical radiosensitisers. The dose-rate sparing effect can be blocked by chemical inhibitors of protein synthesis, such as 3-aminobenzamide (a PARP inhibitor) (Kelland *et al.* 1988b, Kelland *et al.* 1988a, Kelland and Tonkin 1989) novobiocin and hydroxyurea (Kelland and Steel 1988c) suggesting that the sublethal-damage repair pathway involves the production of new proteins. These inhibitors reduced survival by a similar extent at high (150 cGy min^{-1}) or low-dose rates (3.2 cGy min^{-1}). The effects of DNA polymerase inhibitors β-arabionofuranosyladenine (β-ara A) (blocks α and β-polymerase) and aphidicolin (blocks α-polymerase) on low dose-rate sparing were studied. The former reduced survival during low dose-rate irradiation whilst the latter had no effect suggesting β-polymerase, but not α-polymerase is involved in the effect (Kelland and Steel 1988b). However, the radiosensitising effect of β-ara A, varied between cell lines, producing greater sensitivity on the most radiosensitive lines. This did not favour the use of β-ara A in the treatment of intrinsically radioresistant human tumours (Chavaudra *et al.* 1989). Caffeine, which prevents a G2 block in cell-cycle progression, reduced survival during low dose-rate irradiation possibly by allowing less time for the operation of DNA-repair processes induced after irradiation (Kelland and Steel 1988b, Dillehay *et al.* 1988, Sakurai *et al.* 1999). Camptothecin, a topoisimerase I inhibitor, abolished dose-rate sparing in a human bladder carcinoma cell line, whereas the topoisomerase II inhibitor, VP16 had no effect. This suggests topoisomerase I, but not II, is involved in DNA repair during LDR irradiation (Musk and Steel 1990). The halogenated pyrimidine bromodeoxyuridine (BrdUrd) has also been shown to block dose-rate sparing, although the mechanism has yet to be fully elucidated (Morstyn *et al.* 1984, Mitchell *et al.* 1989). The chemotherapeutic agents, adriamycin (Sherman *et al.* 1982, Peacock *et al.* 1985), mytomycin (Fu *et al.* 1984) and cisplatinum (Fu *et al.* 1985, Wilkins *et al.* 1996, Raaphorst *et al.* 1996a, Raaphorst *et al.* 1996b, Raaphorst *et al.* 1997, Raaphorst *et al.* 1998) all appeared to sensitise cells to low dose-rate irradiation. In fact, cisplatinum combined with LDR irradiation is now in common usage clinically (Gaspar *et al.* 2000, Micheletti *et al.* 1996, Kaye *et al.* 1992).

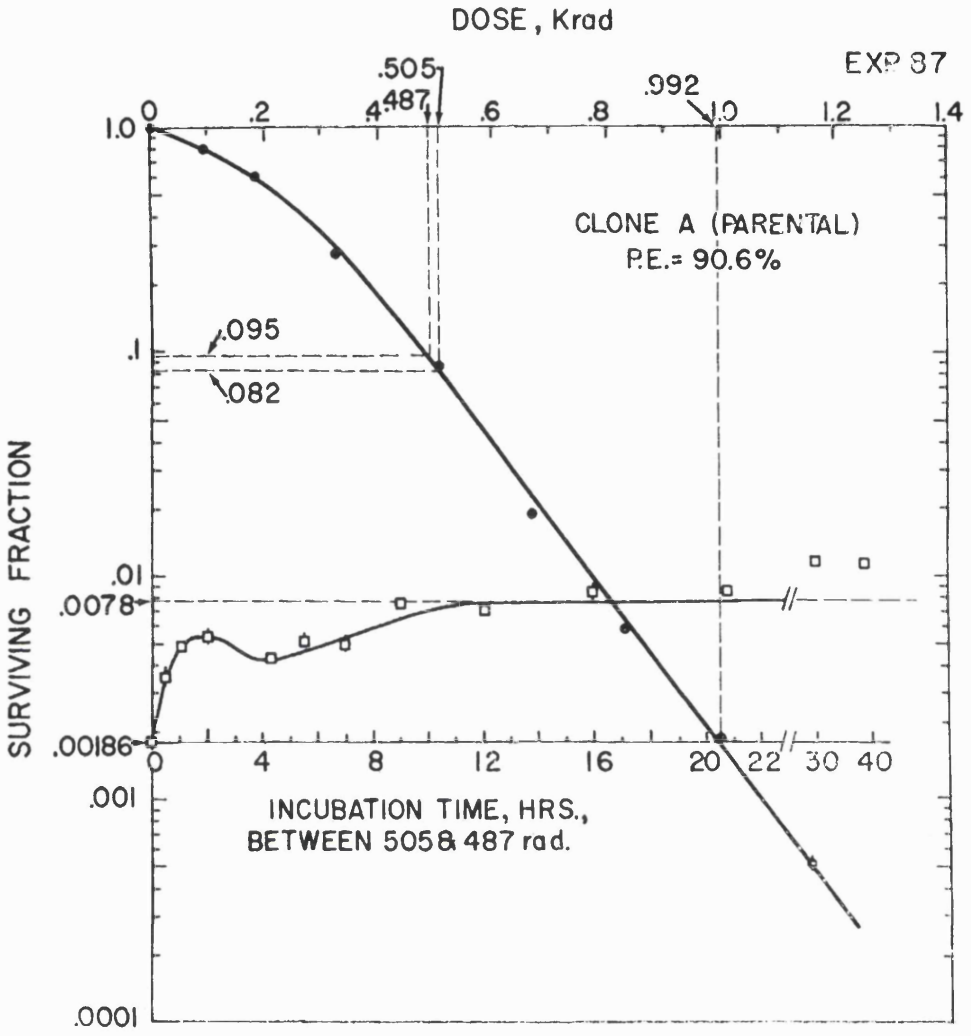

Figure 1.1
Shows an acute-dose survival curve (closed circles) and "2-dose fractionation curve" (open squares) of "clone A" cultured Chinese hamster cells. From Elkind (1959).

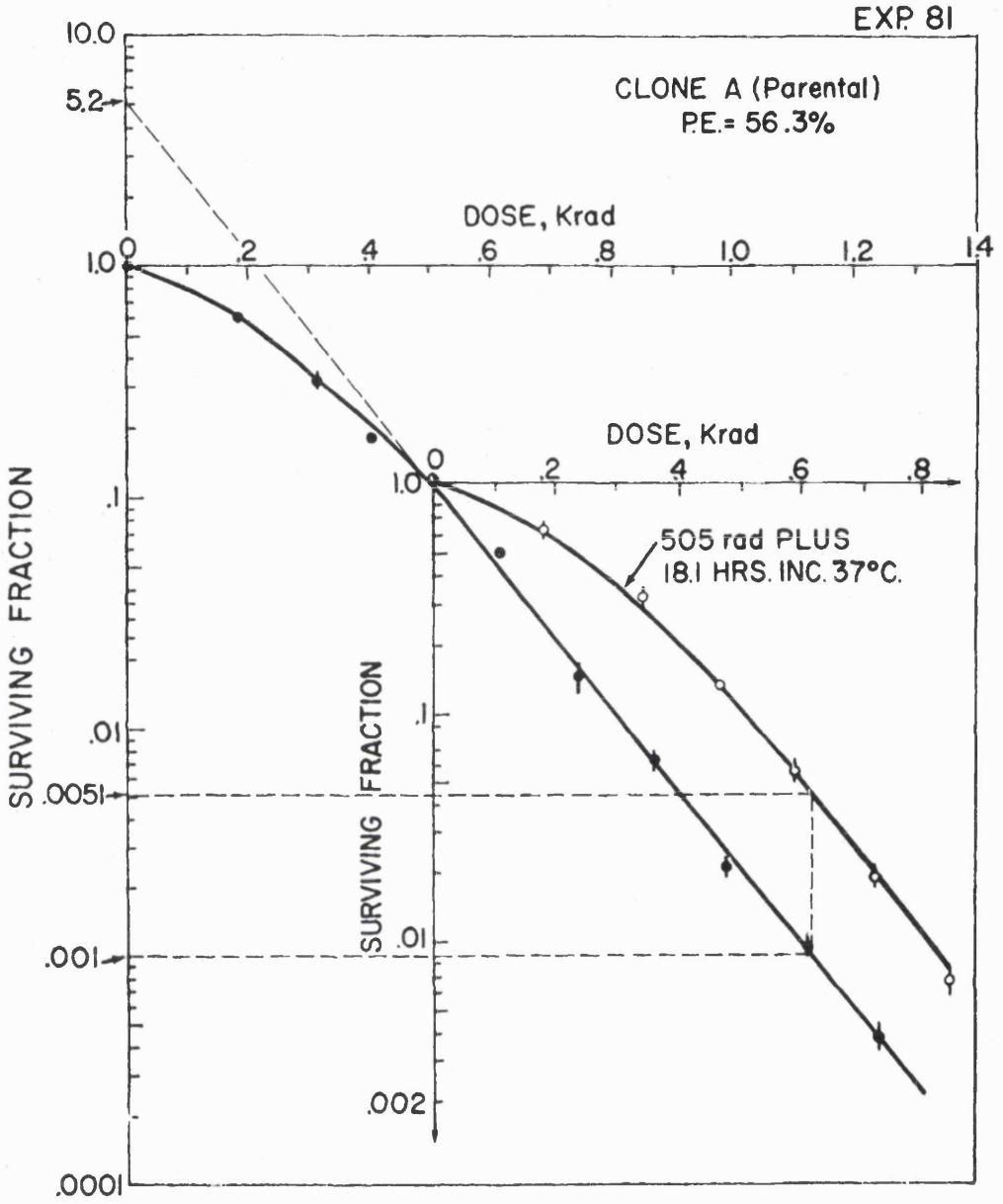

Figure 1.2
Shows acute-dose survival curve (closed circles) and fractionation survival curve (open circles) for "clone A" cultured Chinese hamster cells. From Elkind (1959).

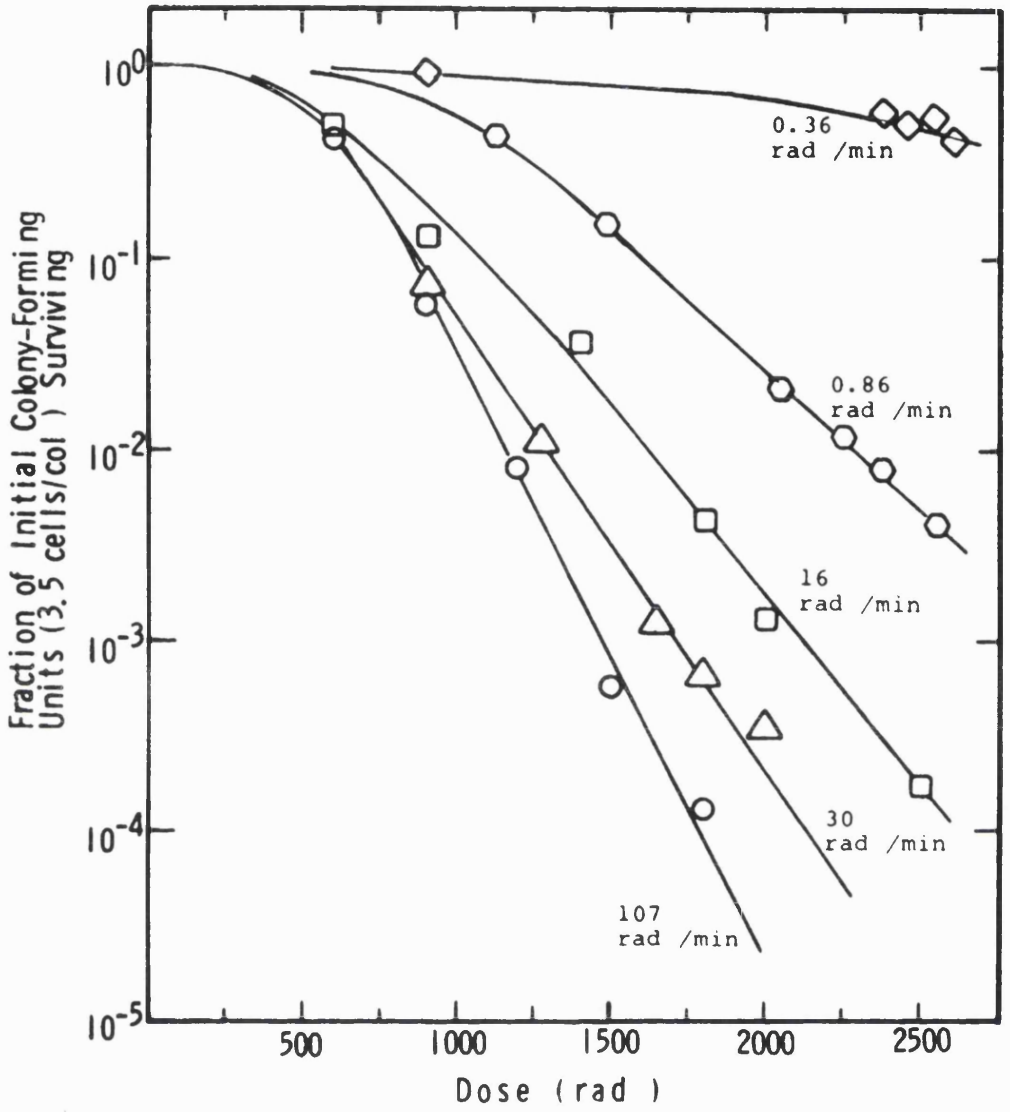

Figure 1.3
Shows dose response curves for Chinese hamster cells (CHL-F line) grown *in vitro* and exposed to ^{60}Co γ-rays. Low dose-rate sparing is observed with cell survival increasing as the dose rate is reduced. From Bedford and Mitchell (1973).

1.6.3 Discrimination of cell radioresponsiveness

The dose-rate effect varies considerably between cell lines. In some studies the radiosensitivity of the cell line has been correlated with the amount of dose-rate sparing and the potential clinical implications for use in predictive testing are described below. The size of the initial shoulder of the acute-dose survival curve has been shown to correspond with the magnitude of the sparing effect at low-dose rates. For example HeLa cells show a small shoulder and the dose-rate effect is small (Bedford 1963). The reverse is true for Chinese hamster cells (Bedford and Mitchell 1973).

Different cell types have different shaped survival curves. Sensitive cell lines tend to be characterised by a survival curve with a very small initial shoulder region. Therefore, as the maximum amount of dose-rate sparing in a cell line generally approximates to the initial slope (α slope) (Section 1.6.1) of an acute dose survival curve, a greater separation between sensitive and resistant cells may be seen at low-dose rates. Since inherent sensitivity to ionising radiation is an important factor involved in determining how well a cancer patient will respond to a radical course of radiotherapy, this could prove a useful tool in predicting the response of a patient to radiotherapy. Evidence for the ability of LDR exposure to amplify inter-individual differences comes from work carried out with normal tissues (Little and Nove 1990, Burnet *et al.* 1994, Jones *et al.* 1995, Burnet *et al.* 1996, Sproston *et al.* 1996), human tumour cell lines (Fertil and Malaise 1981, Deacon *et al.* 1984, Malaise *et al.* 1987, Kelland and Steel 1988a, Tonkin *et al.* 1989, Bjork-Eriksson *et al.* 1998) experimental tumours (Bristow and Hill 1990) and mathematical models (Tucker and Thames 1989), although it has not been found in all studies (Geara *et al.* 1992). Clinical studies have subsequently supported these findings, and some have shown that the measurement of tumour radiosensitivity is prognostic for the outcome of patients treated with radical radiotherapy in certain tumour sites (West *et al.* 1993, Girinsky *et al.* 1994, West *et al.* 1997).

Since the initial slope of the survival curve may be the most important parameter when evaluating radiosensitivity of tissues, the most useful predictive measures of tumour control probability are those which describe this region. These parameters are the surviving fraction at 2 Gy (SF_2) (this is the usual dose given per fraction in radiotherapy), the mean inactivation dose (D_{bar}) and α. The most widely used of these parameters is SF_2 and differences in SF_2 values between tumour cells *in vitro* have been shown to correlate with clinical outcome (Deacon *et al.* 1984, Fertil and Malaise 1985, reviewed by West 1995). However the SF_2 value is generally limited to a fairly narrow range (*e.g.* 0.15–0.9) which may make it more difficult to discriminate between different tumour radiosensitivities. Dividing the total dose of 2 Gy into a series of 5 or 6 fractions has increased the reproducibility of these measurements compared with a single

2 Gy dose (Raaphorst 1993, Gerweck and Zaidi 1996), and irradiating the cells at LDR (0.01–0.05 Gy min^{-1}) has been shown to discriminate better than HDR irradiation between tumour cell lines of differing radiosensitivities (Steel *et al.* 1987). However this effect has not been found in all studies. Marchese *et al.* (1987) found no dose-rate effect in a series of 6 tumour and 3 normal fibroblast lines in the dose-rate range of 1.16–0.27 cGy min^{-1}. If irradiating cells at low-dose rate to discriminate between radiosensitivities was to be used as a prognostic indicator, the reproducibility and discrimination would have to be further improved.

Incorporating a measurement of cellular repair of sublethal damage following exposure to LDR irradiation may improve the discrimination between radioresponse groups (Raaphorst 1993). To assess DNA damage, a number of studies have used a range of assays to measure initial and residual DNA damage after HDR and LDR irradiation and examine correlations with intrinsic radiosensitivity. In a review of the correlation between DSB induction and cell killing by Foray *et al.* (1997a) they found that only in a minority (20%) of tumour cells studied was the intrinsic radiosensitivity related to DSB induction level and this relationship was not seen in fibroblasts (Foray *et al.* 1997a). A weak correlation between the level of initial DNA strand breakage and survival after HDR and LDR irradiation was found (Ruiz de Almodovar *et al.* 1994, Hu and Hill 1996), although not in every study (Wurm *et al.* 1994, Marples *et al.* 1998) (HDR). A stronger correlation has been observed between the level of residual damage (the damage measured after cells were allowed time to repair) and radiosensitivity, with a positive correlation being found in 89/100 tumour cell lines in a review by Foray *et al.* (1997a). Foray *et al.* (1997b) examined residual DNA damage in AT and control cells using two protocols: LDR irradiation (0.01 Gy min^{-1}) at 37°C (which allows repair during irradiation) and irradiation at HDR (1 Gy min^{-1}) at 4°C (followed by repair at 37°C). They found that the former protocol allowed a cleaner distinction between the AT and the control cells as it selects for those DSB which are most slowly repaired and/or unrepairable DSB. Marples *et al.* (1998) found a significant correlation between HDR and LDR SF_2 values and the ratio of the slopes of the initial and residual DNA DSB dose-response curves, representing the fraction of DNA damage remaining. They suggested that the assay used (neutral comet) could be used to predict radiosensitivity.

There are many inherent problems when trying to develop a predictive test for the measurement of intrinsic radiosensitivity in a clinical setting. The ideal assay would have to be easy to carry out, reliable, be able to give a clear discrimination between radiosensitive and normal patients and need to be rapid. At the present time no single test fulfills all these criteria and it remains to be seen whether a sufficiently sensitive test can be developed.

1.6.4 Inverse dose-rate effect and cell survival

In some cell systems an *inverse* dose-rate effect has been demonstrated. Experiments by (Mitchell 1979) showed that reducing the dose rate from 1.54 to 0.37 Gy h^{-1} in HeLa cells results in greater killing for a given absorbed dose (Figure 1.4).

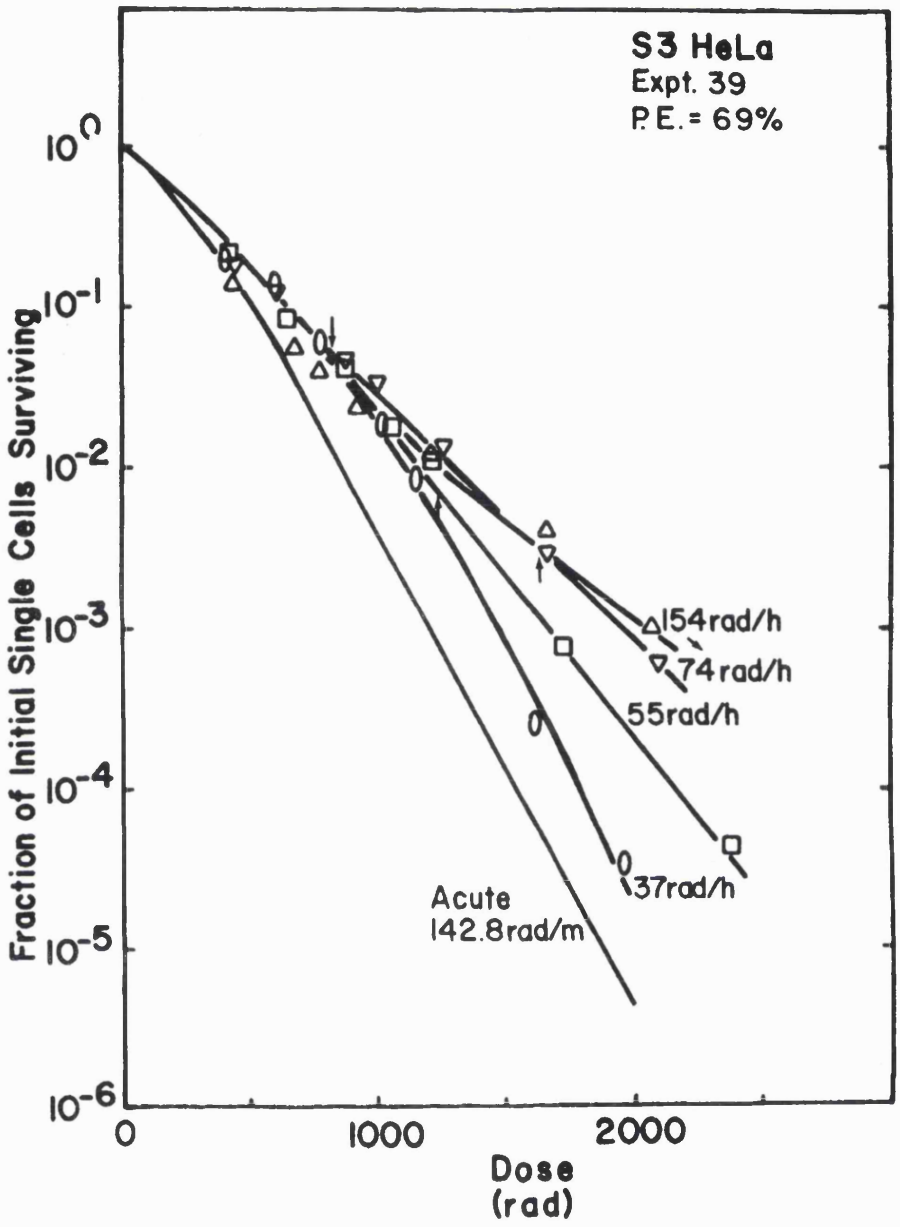

Figure 1.4
Shows dose response curves for HeLa cells. An inverse dose-rate effect is present whereby survival decreases as the dose-rate is reduced. From Mitchell (1979).

1.6.4.1 Cell cycle

Studies examining the cell–cycle phase lengths in HeLa and V79 cells during low dose-rate (Bedford and Mitchell 1973) and fractionated exposures (Mitchell and Bedford 1977) showed an accumulation of cells in the G2/M phase of the cell cycle. This was also seen in rat rhabdomysarcoma cells (Kal *et al.* 1975) and bone marrow cells (Frindel *et al.* 1972). A possible explanation is that most cells undergo a G2 delay in response to acute doses of irradiation and then move out of G2 when they have successfully repaired most of the radiation-induced damage. At low-dose rates cells are constantly being exposed to radiation and so are unable to repair all damage during irradiation. This results in a permanent delay in progression into mitosis and therefore an accumulation of cells in G2. The G2/M phase is proposed to be the most radiosensitive of the cell-cycle phases (Sinclair 1968). Mitchell *et al.* (1979) concluded that their apparent inverse dose-rate effect was due to a build up of cells in the G2 phase of the cell cycle during low dose-rate irradiation causing an increase in radiosensitivity. Mitchell *et al.* (1979) also showed that this inverse dose-rate effect was present in HeLa cells, but not V79 cells and proposed that this this was a consequence of V79 cells having a shorter cell-cycle time. Several recent studies have found a similar inverse dose-rate effect in different cell lines. Furre *et al.* (1999) examined the *in vitro* sensitivity of a human cervical cancer cell line, NHIK3025, to low (0.37 Gy h^{-1}) and high (1.54 Gy h^{-1}) dose-rate irradiation at various times after mitotic selection. An inverse dose-rate effect after doses of 7 Gy was found which appeared greater in cells irradiated 15 h after mitotic selection (*i.e.* cells in G2) compared with cells irradiated 2h after mitotic selection (G1 cells). They concluded that cells accumulated in G2 after low dose-rate exposures and this resulted in increased cellular toxicity. G2/M accumulation has also been suggested as one of the underlying mechanisms responsible for the larger than expected efficacy of low dose-rate radioimmunotherapy in the treatment of lymphoma (Knox *et al.* 1993). DeWeese (1998) examined LDR (0.25 Gy h^{-1} irradiation) vs. HDR (60 Gy min^{-1}) *in vitro* in a range of human prostate cell lines (LNCaP, PC3, PPC1, TSUPr1 and DU145). They found an inverse dose-rate effect in the majority of the cell lines irradiated at LDR compared with a HDR. The authors showed that although a premitotic accumulation was observed in some of the cell lines, the sensitivity of the different prostate cell lines to protracted LDR irradiation did not correlate with cell-cycle redistribution phenotype. They also showed no correlation between the LDR-sensitive cell lines and the presence or absence of p53 mutations, a gene known to be important in cell-cycle regulation. An earlier publication by the same authors compared an RKO colonic carcinoma cell line, which showed an accumulation of cells at the G1 and G2 checkpoint after LDR irradiation, with a genetically modified RKO subline which expressed oncogenic human papillomavirus E6 and E7 transforming proteins and also lacked a G1 cell-cycle checkpoint. The RKO parental and the control transfected cell lines have been shown in another study to exhibit HRS/IRR (M.C. Joiner, pers. comm).

DeWeese *et al.* (1997) showed that the E6 and E7 RKO subline exhibited a similar LDR radiosensitivity as the parental line despite demonstrating different cell-cycle redistribution patterns, *i.e.* an accumulation in just G2 as opposed to both G1 and G2, during protracted LDR exposure. These results suggest that cells arresting in G1 during LDR exposure may be as radiosensitive as cells arresting in G2 (Sinclair and Morton 1966, Sinclair 1968) or that cell-cycle distribution may not be the dominant determinant of radiosensitivity of all cancer cells treated with LDR γ-irradiation. DeWeese *et al.* (1997) suggested that LDR radiation treatment of RKO cells resulted in a prolonged delay in the progression from early G2 (radioresistant) to late G2 (radiosensitive). Therefore, cells which accumulated in G1 and G2 and G2 only, would show a similar radiosensitivity. Cao *et al.* (1983) also found that redistribution of cells in G2 was not the explanation for an inverse dose-rate effect on growth of Bp8 mouse ascites sarcoma *in vivo*. The authors suggested that an induction of repair, dependent both on dose rate and on total dose, may explain the higher efficiency of protracted irradiation.

An alternative hypothesis to explain the enhanced sensitivity seen at low-dose rates is that cellular resensitisation occurs during protracted irradiation of a heterogeneous cell population. The sequence of events was first discussed by Elkind *et al.* (1965). A single dose of radiation given to an asynchronous population of cells will kill cells in the most sensitive parts of the cell cycle, *i.e.* G2 phase. The cell population will therefore be more radioresistant to a second dose of radiation. If the time between irradiations is increased, the preferentially spared resistant cells will, by cell-cycle progression and loss of cell-cycle synchrony, eventually be redistributed among the more sensitive cell-cycle phases no longer occupied by the cells killed by the first dose, thereby resensitising the population back to the original level, to a second dose of radiation. This theory has been used to explain the inverse dose-rate effect during protracted exposures and was modelled by Hahnfeldt (1996). However, a cell population such as that seen within a solid tumour, is made up of many different cell subpopulations. A cell from such a population may undergo changes in radiosensitivity not only through a change in cell-cycle phase but also through a movement from one subpopulation to another, *e.g.* by a shift in microenvironment due to an altered oxygen tension (Thames and Hendry 1987, Hlatky *et al.* 1994, Hlatky *et al.* 1995). A more general mathematical model which reflects these other factors affecting cellular resensitisation was developed by the same authors in 1998 (Hahnfeldt and Hlatky 1998). Although this model did not take into account changes in growth parameters due to tumour BED effects and stochastic effects, the authors concluded that it was sufficiently robust to explain that the inverse dose-rate effect was due to cellular resensitisation.

1.6.4.2 Hypoxia

A further hypothesis proposed to explain the mechanisms of the inverse dose-rate effect was hypoxia. Tumour hypoxia is an important prognostic factor influencing radiocurability in cancer. After or during irradiation, reoxygenation can occur transiently or take several days to be completed. Therefore, tumours treated over a longer time (*i.e.* irradiated at a lower dose rate) are less likely to display hypoxia than tumours irradiated with acute exposures. However, as hypoxia is more specific to solid tumours, this phenomenon is not expected to occur in normal tissues or *in vitro*. An *in vivo* study of LDR irradiation on mouse ascites sarcoma cells found an inverse dose-rate effect and as these cells were not in a solid tumour, the authors rejected hypoxia as a possible explanation (Cao *et al.* 1983). In addition, as hypoxia does not normally occur *in vitro*, the inverse dose-rate effect first observed in HeLa cells by (Mitchell 1979) cannot be explained by this phenomenon.

1.6.4.3 IRR

The dose-rate sparing effect has been blocked by several chemical modifiers of protein synthesis (Kelland and Steel 1988c) (Kelland *et al.* 1988b). The inverse dose-rate effect may reflect the inability to induce sublethal-damage repair mechanisms dependent on protein synthesis. If the dose rate is sufficiently low, the damage produced per unit time, would not cross a putative threshold level for the triggering of repair pathways. The net effect of this would be a reduction in survival at very LDR irradiation. This was the explanation given by Cao *et al.*(1983) for the inverse dose-rate effect observed for the survival of mouse ascites sarcoma cells *in vitro*. A clinical study comparing the early effects of two dose rates in brachytherapy of cervical carcinoma (Lambin *et al.* 1994a) found an inverse dose-rate effect, with significantly more sterilisations observed in the LDR group ($p<0.01$). They also suggested that this effect may be due to a lack of induced resistance.

The inverse dose-rate effect may be similar to the HRS/IRR effect seen at low-acute doses (Section 1.3.1). Cell lines such as DU145, a prostate carcinoma have been shown to display HRS (Wouters *et al.* 1996) and an inverse dose-rate effect (DeWeese *et al.* 1998), further suggesting a link between the two. One of the aims of this thesis is to evaluate whether HRS/IRR and the inverse dose-rate effect are related.

Although it is currently proposed that HRS/IRR and the adaptive response are distinct phenomena, adaption can be observed in some cells following continuous LDR irradiation. Experiments carried out on *Chlamydomonas*, showed an increase in resistance to a second dose of LDR γ-rays after an initial priming dose (Bryant 1972). A similar result was reported by Santier *et al.* (1985) using *Chorella* cells and several authors have reported a

cytogenetic adaptive response in mammalian cells *in vitro* (Ikushima 1987, Shadley and Wiencke 1989). These results suggest the active induction of repair mechanisms at low-dose rates.

Further reducing the dose rate below the region where an inverse dose-rate effect occurs, ablates the inverse dose-rate effect as cells escape the G2 block and divide. Cell proliferation may then occur during protracted exposure and survival increases which offsets cell killing due to irradiation.

1.6.5 Inverse dose-rate effect in mutation induction

Previous studies on cellular HRS have shown an inverse dose-rate effect on mutation induction at very low-dose rates, with lower dose rates causing an enhanced mutational or transformational endpoints relative to acute exposures (Little 1990). This effect has been observed after both high and low-LET irradiations (Hall *et al.* 1991) (Colussi and Lohman 1997). Evidence, both *in vitro* and *in vivo*, has accumulated for an increase in oncogene transformation when cells are exposed to low dose-rate neutrons compared with acute exposures. Hill *et al.* (1982) first observed this inverse dose-rate effect *in vitro* in C3H1OT1/2 cells. They found that after a given low dose of neutrons (5–30 cGy), the transformation incidence was much higher if the radiation was delivered at LDR, or as a series of fractions over 5 days, than if delivered in a single HDR exposure. Further studies on the same cell line found a similar effect (Hill *et al.* 1984, Hill *et al.* 1985, Miller *et al.* 1988, Miller *et al.* 1989, Miller *et al.* 1990, Miller and Hall 1991). This inverse dose-rate effect on oncogene transformation has also been found in many other cell systems *in vitro* (reviewed by Hall *et al.* 1991) in Syrian hamster embryo cells (Jones *et al.* 1989), human hybrid cells (Redpath *et al.* 1990) and a human HGPRT mutation in V79 cells (Kubota and Hill 1989) and *in vivo* in humans (Hornung and Meinhardt 1987, Chmelevsky *et al.* 1988, Darby and Doll 1990, Lubin *et al.* 1990) and in animals (Ullrich 1984, Little *et al.* 1985). This effect has not been found in all studies (Balcer Kubiczek *et al.* 1994, Saran *et al.* 1994)(fractionated) (Elkind 1994). An example of an enhanced mutation induction at low-dose rates of *low*-LET radiation includes the human HPRT locus of human lymphoblastoid WI-L2-NS cells, where low dose-rate X-rays induced larger deletions than high-dose rates (Colussi and Lohman 1997). This effect has also been observed using γ-rays (Crompton *et al.* 1985, Crompton *et al.* 1990, Lorenz *et al.* 1993, Amundson and Chen 1996, Furuno Fukushi *et al.* 1996, Vilenchik and Knudson 2000) and α particles (Bettega *et al.* 1997). However, this is not a universal finding (Colussi *et al.* 1998, Spivak and Kolman 1998, Kolman and Harms Ringdahl 1996, Han *et al.* 1980, Komatsu *et al.* 1993). Edwards *et al.* (1997) studied the spectrum of deletion sizes in HPRT mutants of two human bladder carcinoma cell lines of widely differing radiosensitivity. No difference in mutation frequency and deletion size was observed between high and low-dose rates

although a lower incidence was found in the sensitive cell line. The results are consistent with the hypothesis that large deletions tend to lead to the loss of adjacent essential genes and thereby to the death of potential mutants.

Following studies by Rossi and Kellerer (1986) on variations in oncogenic transformation throughout the cell cycle, inverse dose-rate effects have often been explained on the basis of 'a window of sensitivity' in the cell cycle (Brenner and Hall 1990). This window was established for low-LET radiations to be in late G2/M phase (Redpath and Sun 1990, Cao *et al.* 1992, Miller *et al.* 1992, Cao *et al.* 1993, Wells *et al.* 1993). On the basis of this biophysical model Elkind (1991, 1994) detailed the different effects of high and low LET during low dose-rate exposures. With high-LET radiation, because of the nature of the radiation, even repair-competent cells are unable to repair damage during exposures. It is proposed that, similarly, transformation-susceptible cells are not able to repair damage. Consequently, cell kinetics in the absence of repair is the principal biological process that modulates the effectiveness of low-dose rates. During a protracted exposure, extra cells can enter this sensitive window by cell-cycle progression, resulting in the effects of irradiation being enhanced as irradiation time is increased. This enhancement requires some kind of "saturation" of hits to the cell resulting in a less than proportional increase in the probability of damage. Such saturation can produce an inverse dose-rate effect through a larger number of wasted hits during acute dose exposure during an acute exposure to cells in a sensitive window, compared with a protracted exposure. Rossi and Kellerer (1986) speculated on the existence of a short "window of sensitivity" in the cell cycle lasting around 10 minutes, in which cells were more than an order of magnitude more sensitive than in the rest of the cell cycle. However, many of the ideas behind this explanation were based on a widely criticised theory previously published by these authors (Section 1.7.2). Their theory of dual radiation action whereby lesions interact to produce cell kill proportional to dose squared (Kellerer and Rossi 1972), is not widely accepted. The dose-effect relationship using this hypothesis did not take into account LET and any biological repair processes which may occur. Goodhead (1982) criticised the model on the basis of a lack of experimental evidence and his experiments showed the probability of lesion interaction is very small. Although there may be apparent evidence for a window of sensitivity in radiation-induced oncogenic transformation (Kennedy 1985, Kamiya *et al.* 1995, Selvanayagam *et al.* 1995), there is no evidence for this in the induction of mutagenesis, so this appears a controversial explanation for any inverse dose-rate effects occurring at high-LET radiations.

At low LET there is evidence for a correlation between cell killing and mutation and their variations throughout the cell cycle (Burki 1980, Jostes *et al.* 1980, Watanabe and Horikawa 1980, Chuang and Liber 1995) which is not apparent at high LETs (Miller *et al.*

1995, Redpath *et al.* 1995, Pazzaglia *et al.* 1996). Figure 1.5 shows survival, yield of mutants and oncogenically transformed cells throughout the cell cycle from 2 cell lines irradiated at high and low LET. Brenner *et al.* (1996a) used this assumption and suggested a model based on the Linear-Quadratic equation called Linear-Quadratic and resensitisation (LQR). Their theory was that a positive correlation through the cell cycle between killing and mutagenesis implies that, for acute irradiation, cells, which have undergone mutation, are preferentially killed, and cells resistant to killing have a below average chance of mutagenesis. So for acute exposure, the correlation between killing and mutagenesis decreases the observed mutation rate per surviving cell. By contrast, at low-dose rates, cell cycling can cause mutated cells to progress to resistant phases before they are killed, resulting in previously resistant surviving cells progressing to a sensitive part of the cell cycle, where they can undergo mutagenesis. This results in an overall inverse dose-rate effect on mutation induction.

Despite much evidence of the existence of an inverse dose-rate effect on mutation induction/oncogenic transformation, there is still much controversy over whether enhanced mutation/transformation exists after low-acute doses. At present there is no method sensitive enough to detect mutations, if indeed there are any, after such small doses. If, as the evidence suggests, there is an inverse dose-rate effect on mutation induction/transformation, it is still open to debate whether this is mechanistically related to the inverse dose-rate effect observed with cell survival.

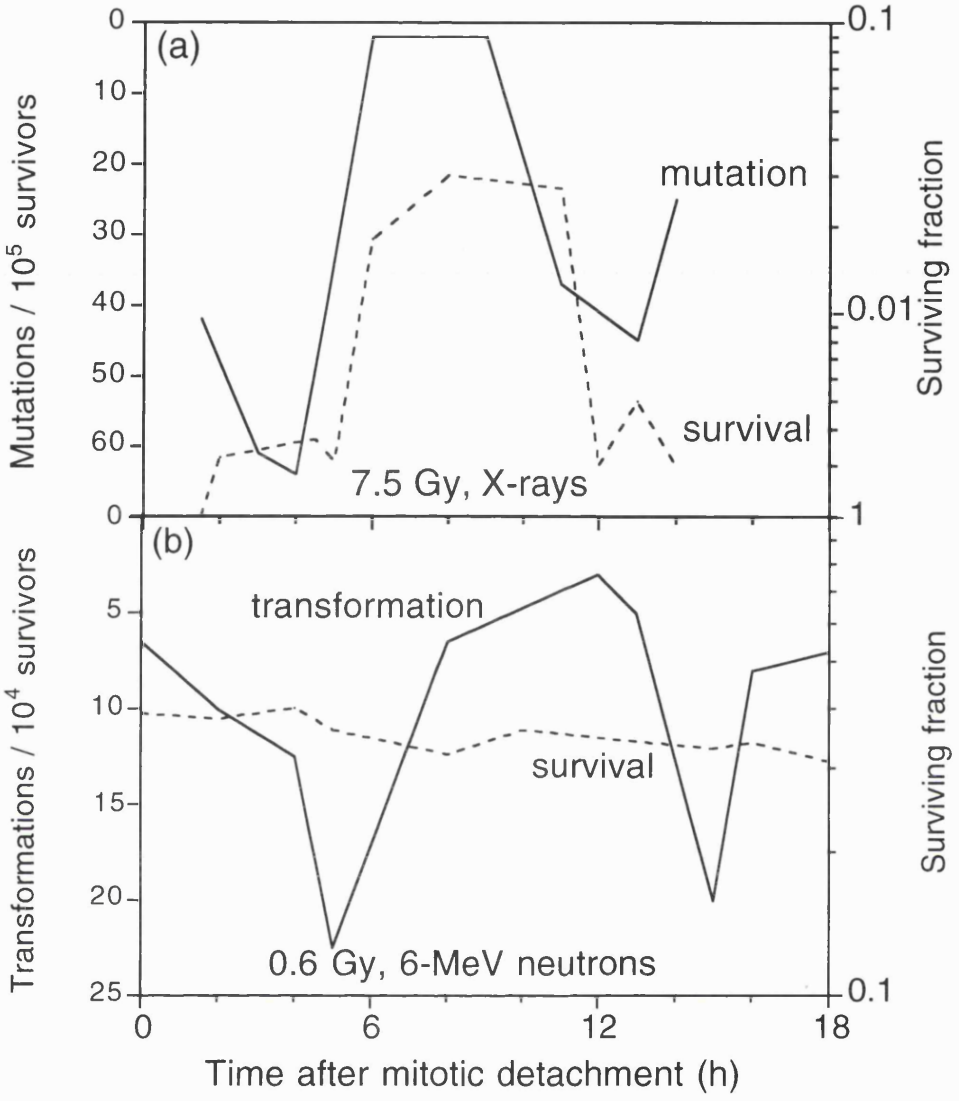

Figure 1.5
Shows (a) X-ray induced surviving fraction and yield of 6-thioguanine-resistant mutant clones per survivor, as a function of cell-cycle position (time after mitotic detachment) in CHO cells (from Burki (1980)).
(b) Neutron-induced surviving fraction and yield of oncogenically transformed cells per survivor as a function of cell-cycle position in CH310T1/2 cells (from Miller *et al.* (1995)).
Diagram redrawn from Brenner *et al.* (1996a).

1.7 Cell-survival curves

1.7.1 Early models

Puck and Marcus published the first *in vitro* irradiation cell-survival curve for mammalian cells in 1956. They irradiated HeLa cells with doses up to 700 rads (7 Gy) and assessed colony-forming ability. The cell-survival curve they obtained had a characteristic shape which differed from the previously published survival curves for non-mammalian cells. The low-dose region of the curve is characterised by an initial shoulder which suggests that small doses of radiation are relatively inefficient at cell killing. Higher doses of radiation, however, are more efficient at producing cell kill and so the high-dose region approximates to a straight line on a log-linear plot. This shape disagrees with the single–target, single–hit, theory of radiation cell kill, which proposes that one hit of a sensitive DNA target will inactivate the cell. This shape of survival curve is found in non–mammalian cells.

$$\mathrm{SF} = e^{-d/D_0} \qquad \text{Equation 1.1}$$

Where SF is surviving fraction, d is dose and D_0 is the dose where survival is reduced to 37%. d/D_0 is the average number of hits per cell.

This model did not fit the HeLa data obtained by Puck and Marcus, and so the authors suggested a second model. This was the multiple–hit, single–site model which proposes that single-hit inactivation of multiple targets are necessary for cell killing. This allows for the "shoulder" region on the HeLa survival curve as at lower doses fewer targets are inactivated giving a reduction in cell kill.

$$\mathrm{SF} = 1 - \left(1 - e^{-d/D_0}\right)^n \qquad \text{Equation 1.2}$$

where n is number of sensitive sites. At higher doses the form of the curve returns to the simple exponential.

$$\mathrm{SF} = ne^{-d/D_0} \qquad \text{Equation 1.3}$$

This curve will intercept the y axis at the theoretical number of target sites, n. n is also known as the extrapolation number. Puck and Marcus obtained an extrapolation number of 2 for their HeLa data. This would suggest that two DNA targets would need to be hit in order to cause cell death. At the low-dose region there may not be enough radiation hits to knock out both targets so a shoulder region on the survival curve would be observed.

1.7.2 Linear-Quadratic (LQ) model

A mathematical description of a survival curve which describes cell kill as a linear or quadratic (LQ) function was first described on theoretical grounds by Kellerer and Rossi (1972) and Chadwick and Leenhouts (1973). This Linear-Quadratic (LQ) model, is perhaps the best description of radiation response (Fowler 1989)

$$SF = e^{(-\alpha d - \beta d^2)} \qquad \text{Equation 1.4}$$

which describes the cell kill due to both the linear contribution (α) and the quadratic contribution (β). Survival curves described by this model are continuously bending and the shape is determined by the α and β factors. The α/β ratio represents the dose at which the linear contribution to cell death (αd) is equal to the quadratic contribution (βd^2).

Kellerer and Rossi (1972) derived a form of the LQ equation based on their idea that low-LET radiation acted in a dual fashion, causing two lesions to interact and produce killing proportional to the dose squared. The linear aspect of this equation was based on the theory that at high LETs could produce single hit killing. This equation could be used to calculate a yield of sublesions:

$$Yield = k(\xi D + D^2) \qquad \text{Equation 1.5}$$

Where ξ is the average specific energy in individual events, D is the dose and k is a constant. Chadwick and Leenhouts (1973) considered cell death being due to one particle causing two SSB on the adjacent strands of the DNA spiral. These interact and produce a dose squared relationship with cell kill. The LQ was fitted was fitted to experimental data using X-rays on mouse skin by Douglas and Fowler (1975). They postulated that damage to two chromosomes was involved and not simply two SSB of the double DNA helix. Two SSB caused by the passage of two particles would give a linear relationship. Experiments were carried out by using soft X-rays which produce ionisations over a few nanometers (Raju *et al.* 1987, Thacker *et al.* 1986). This distance is too small to allow for lesion interaction as described by Kellerer, but mutation induction and inactivation still occurs suggesting that complex lesions can be formed as a result of a single irradiation track (Goodhead 1982, Powell 1996).

1.7.3 Induced-Repair (IR) model

A modification of the Linear-Quadratic model was developed to take into account low-dose HRS/ IRR (Joiner and Johns 1988). This is termed the Induced-Repair (IR) curve.

$$SF = \left(\exp - \alpha_r \left(1 + \left(\frac{\alpha_s}{\alpha_r} - 1 \right) e^{-d/d_C} \right) d - \beta d^2 \right) \qquad \text{Equation 1.6}$$

Where d is dose, α_r is α at high doses and α_s is α at low doses. d_c is the dose where repair is 63% complete. β is unmodified from the Linear-Quadratic formula. It is unchanged with low-dose HRS as the β parameter only influences the survival curve at high doses.

1.7.4 Two-population model

An alternative hypothesis for the presence of HRS is that a sensitive subpopulation are killed off at very low doses leaving a more resistant subpopulation to be killed at higher doses (Skarsgard *et al.* 1993, Skarsgard *et al.* 1996). This would equate to a sensitive response in the low-dose region and has been termed the two population model.

$$SF = f(e^{-\alpha_s d - \beta_s d^2}) + (1 - f)(e^{-\alpha_r d - \beta_r d^2}) \qquad \text{Equation 1.7}$$

where f is the fraction of the population which is sensitive and α_s and β_s are the LQ parameters in the sensitive population and α_r and β_r the LQ parameters in the resistant population.

1.7.5 Low dose-rate modelling

The LQ model has been modified for continuous low dose-rate and fractionated radiotherapy by Thames (1985) (1987).

To predict survival at continuous low-dose rates:

$$BED = D\left[1 + g\frac{d}{\alpha/\beta}\right] \qquad \text{Equation 1.8}$$

Where $g = 2\dfrac{\left[\mu t - 1 + e^{-\mu t}\right]}{(\mu t)^2}$ where t is exposure duration and

$\mu = \dfrac{\ln 2}{T_{1/2}}$ where $T_{1/2}$ is the half time of repair for that cell line.

Ever since Elkind and Sutton (1959) produced the first fractionation data, many authors have come up with possible models for cell survival. The aim was to produce the best fractionation or low dose-rate schedule that causes the highest tumour cell kill whilst sparing normal tissues. Lajtha and Oliver (1961) used the Elkind and Sutton data to predict survival responses at continuous low-dose rate. They observed that the increase in dose required from a low dose-rate exposure to achieve the same effect as a high dose-rate exposure could satisfactorily explained by the concept of an 'effective dose' that decays exponentially in time, or equivalently, of a 'dose-equivalent of incomplete repair' (Oliver 1964) in a split dose experiment. They assumed that the repair of radiation damage was an exponential function of time and that the cell-survival curve could be described adequately by the Linear-Quadratic (LQ) formalism. This incomplete repair model was developed further by Liversage (1969) to show an equivalence of doses between protracted and fractionated acute exposures. Further incorporation of ideas from a variety of other prominent models were carried out by Kellerer & Rossi (1972) (1978), Chadwick and Leenhouts (1978) and (Pohlit and Heyder 1981). However, the incomplete repair model did not take into account split dose recovery, dose equivalence of incomplete repair or define an acute exposure. The incomplete repair model was revised once again by Thames (1985) who addressed many of these problems and then again in 1990 by Nilsson (1990) who showed that incomplete repair model was critically dependent on alpha/beta, repair half-time, treatment time and interfraction interval. Their generalised incomplete-repair equation was equivalent to an expression derived by (Dale *et al.* 1988) for analysis of tissue effects of fractionated irradiations at varying dose rates. The generally accepted definitive model was published in 1993 by Millar *et al.* (1993b, 1993a). They produced two papers which covered a wide range of fractionation and LDR possibilities. The first (Millar and Canney 1993b), evaluated equations for fractionated protracted irradiation where the dose-rate was constant during each fraction or changed from fraction to fraction. The resultant equations show that the apparent alpha/beta ratio derived from the analysis of equivalent protocols may be protocol dependent and should therefore be only used as a tool in carefully designed radiobiological experiments. In the second paper they applied the equations to fit a wide range of mouse lung data accrued from a spectrum of different protocols including different radiation qualities, interfraction times and dose-rates (Millar and Canney 1993a).

In 1982 Curtis suggested a model to describe survival at low-dose rates termed the lethal and potentially lethal (LPL) model (Curtis 1982). It evolved in part from a previous model, the repair-misrepair (RPR) model, suggested by Tobias *et al.* (1980) and combined the ideas of lesion interaction, irreparable lesions caused by single tracts, linear lesion fixation, lesion repair via first order kinetics and binary misrepair. Two different kinds of lesions

were hypothesised: irreparable (lethal) and repairable (potentially lethal) lesions. This model gives reasonably good predictions of the effect of interfraction interval, dose per fraction, and dose rate on cell survival *in vivo* and on tissue responses. However this model also had it disadvantages. The incomplete repair and LPL models were compared by Thames (1985) who found that the two models were equivalent, given certain constraints on the size of dose per fraction and dose rate. This was substantiated by Steel *et al.* (1987). *In vitro* data on 12 cell lines derived from a variety of human tumours irradiated over the dose-rate range from 150 to 1.6 cGy min^{-1} were equally well fitted by the two models.

1.8 Prostate cancer

Prostate cancer is the most common solid tumour in American men and the second most common cause of cancer deaths in the US. The incidence and mortality rates are changing throughout the world at an accelerating pace. In the United States, age-adjusted prostate cancer mortality rates have increased by 28% from 20.5 to 26.3 per 100,000 in the last 35 years (Society 1996). In 1996 there were approximately 41400 prostate cancer deaths compared with 14941 in 1961. Between 1965 and 1985 mortality increased by 13% in the UK, 13% in Denmark, 10% in Japan, 5% in Australia and 8% in Canada (Coleman *et al.* 1993). The incidence of prostate cancer varies considerably around the world (Table 1.2). Post mortem data show clearly that approximately one in three men over 50 and nearly two in three over 70 have cancerous prostates (Stemmerman 1992, Sakr 1994). However the clinical relevance of these malignancies is uncertain, because the majority of men die *with* prostate cancer and not *of* prostate cancer. Why the increase? The international variation has been attributed to exogenous factors rather than genetically determined predisposition, by the fact that risk appears to be modified by migration (Shimizu *et al.* 1991). Nutritional differences between countries seems to play a major role as age adjusted mortality rates in different countries correlate with a variation in fat. Whittemore *et al.* (1995) studied patients with prostate cancer and normal healthy controls from a variety of ethnic backgrounds who were all resident in America. They found a statistically significant association of prostate cancer risk with total fat intake for all ethnic groups. High consumption of dietary fats (Fradet *et al.* 1999), alcohol (Breslow *et al.* 1999), calcium (Grant 1999). They also found that African-Americans had the highest incidence of prostate cancer (Natarajan *et al.* 1989, Sakr *et al.* 1994, Pienta *et al.* 1995). This would suggest that variation in nutrition is not the only factor involved in increasing the risk of prostate cancer, but genetic factors also play a role.

Histological changes are present in the prostates of men in their twenties and the diagnosis is typically made 3 or 4 decades later. This implies that the development of the disease involves a multistep process that requires androgens (Carter *et al.* 1990). Men who are castrated or who become hypopituitary before the age of 40 years rarely develop prostate cancer (Zuckerman 1936). Malignancies develop with varying frequencies in each of the five zones of the prostate. These are not directly proportional to the amount of glandular tissue present in each zone. 20% of cancers develop in the transition zone that surrounds the prostatic urethra, although benign prostatic hypertrophy occurs more frequently in this location than cancer. The central zone, which occupies 15–20% of the gland, has an incidence of 5–10% of prostate cancers occurring here. The peripheral zone surrounds the central zone and is the palpable portion of the gland on digital rectal examination. 70% of prostate cancers occur in this location.

Country	Deaths from prostate cancer per 10 000 population
Switzerland	22.5
Norway	21.7
Sweden	20.4
United States	16.8
United Kingdom	16.6
Germany	15.9
Hungary	15.7
Argentina	13.1
Italy	11.5
Mexico	10.6
Poland	9.8
Greece	8.1
Bulgaria	7.8
Singapore	4.2
Japan	3.8
Hong Kong	2.6

Table 1.2
Shows selected international variations in age-adjusted prostate cancer mortality rates per 10000 population, 1988–1991 (Boring *et al.* 1994).

Side effect	Radical prostectomy	External-beam Radiotherapy	Brachytherapy
Haematuria	+	+	+
Cystitis	o	++++	++++
Proctitis	o	+++	++++
Rectal injury	+	+	+
Colostomy	+	+	+
Stress incontinence	++	+	+
Impotence	++++	++	+++

Table 1.3
Shows degree of side effects using various treatments for prostate cancer.

Several histological grading systems have been proposed to determine the biological potential of a tumour. The Gleason system is the most widely utilised. This is a five-part scheme assigning a score of 1 to 5 for the primary and secondary growth patterns of a tumour. Pattern 1 tumours are the most differentiated with discrete glandular formation. Pattern 5 tumours are the most undifferentiated with virtually complete loss of glandular architecture (Gleason 1966). The two scores are combined to give a total score of 2 through to 10. The higher the score, the greater the probability of extracapsular spread, nodal involvement and subsequent metastases (Gleason 1992).

The major treatment strategies for prostate cancer are surgery, external-beam radiotherapy, hormone treatment, and brachytherapy. All treatments have varying degrees of side effects (Table 1.3).

1.9 Brachytherapy

Brachytherapy is a type of radiotherapy whereby radioactive implants are used to kill tumours cells. These implants, known as needles or seeds, contain a radioisotope encapsulated in a metal (*e.g.* titanium) sheath. Interstitial brachytherapy is based upon continuous low dose–rate irradiation with a dose rate of about 0.6–1 Gy h^{-1}. The advantage of brachytherapy is that a substantial total dose can be given in a short overall time, usually less than a week. Furthermore, the very localised placement of the sources, may result in an increased sparing of normal tissues compared with external-beam therapy.

The discovery of radium by Marie Curie in 1898 (Strebel 1903), provided a new treatment for prostate cancer in the form of brachytherapy ^{226}Ra became more widely available for treatment in the early 1900s where it was encapsulated in the form of needles. The first interstitial implantation of radium into the prostate was demonstrated by Barringer (1917), who inserted radium needles transperineally into the rectum, guided with a finger. This was a disadvantage in general use as the constant presence of radium sources in the patient led to unwanted exposures to clinical staff. After initial popularity, this problem combined with poor clinical outcome resulted in brachytherapy treatments falling into decline.

Brachytherapy as a treatment for prostate carcinoma enjoyed a recent, brief period of popularity after Whitmore *et al.* (1972) introduced their method of retropubic implantation of ^{125}Iodine radionuclides. The procedure required surgical exposure of the gland, and the seeding needles were inserted into the prostate freehand. Initial reports of minimal incontinence and impotence compared with competing treatment modalities were favourably received, and the iodine implant delivered high-dose radiation to the prostate, higher doses than could safely be administered by external-beam radiation. The technique

promised improved local control, while the short tissue penetration of the isotope (half-value layer 1.3 cm) spared adjacent tissue from high-dose radiation injury. Follow-up, however, disclosed a high rate of local failure with these ^{125}Iodine implants. Advances in external-beam radiation and radical prostectomy techniques of that time period eventually led to a waning of interest in brachytherapy as a treatment for prostate carcinoma. However, it is likely that these early brachytherapy failures were due to a number of reasons: flawed dosimetry, non–homogeneous distribution of dose, selection of patients with locally advanced (Stage C) disease and the suggestion that the dose rate of ^{125}Iodine implants (8 cGy h^{-1}) was too low to cause cell death and counteract proliferation in aggressively growing tumours.

The positioning of the implant and the resulting dose distributions within the tumour are important for clinical efficacy. In the early 20th century when Barringer first introduced brachytherapy for the prostate, the implant positioning was very inaccurate due to the inability to visualise the tumour, calculate adequate dose distributions and inadequacies in freehand source placement techniques. Widespread clinical use of the implants prompted the development of methods to guide the planning of the placement of radioactive sources in the tumour and subsequent dose prescription for the patient. Rules to distribute radium needles in planar or volume implants were devised by Parker and Paterson (1934), aimed at producing uniform irradiation in a plane parallel to the implanted sources or at a distance outside the implanted volume (Meredith 1967). These rules demanded a variety of radium needles of different activities. The rules were simplified by Quimby (1953) (1963), who took into account that such a variety of needles were not always available.
X-ray films were used to visualise the prostate, tumour masses and the positions of the needles once implanted. These systems helped to determine the number of sources, source strength and spacing between sources to calculate the greatest clinical efficacy within the approximate dimensions of the tumour. The rules used were general and only limited individualisation of treatment between patients was available and X-ray film only gave a 2 dimensional representation of the tumour and prostate so that the prostate tumour volume could not be seen.

Developments in computer technology have meant a further increase in accuracy and individualisation of prostate brachytherapy treatment regimes. Imaging and the calculation of dose distributions in 3 dimensions are now possible. This was first developed for external-beam radiotherapy, but the technology is now also applied to brachytherapy to enable pre- and post-implant evaluations for individual patients. Based on the description by Watanabe *et al.* (1975) of prostate ultrasound anatomy, in 1983, Holm *et al.* (1983) first reported the use of transrectal ultrasound to plan and verify needle position within the prostate. Today this is performed as a two stage procedure. The first stage is to use

transrectal ultrasound to define the prostate volume and use the information from the template co-ordinates to plan the number and position of radioactive sources required to deliver a homogeneous dose to the prostate. At the second stage, sources are inserted into their pre-planned position in the prostate using a template. Needles are inserted through the perineal skin as a closed procedure. Advantages of transrectal ultrasound guided implantation over the previously used retropubic method include this ability to preplan implants based on transrectal ultrasound images, verify proper needle placement before source insertion and the convenience of outpatient treatment. The development of computer aided tomography (CT) and magnetic resonance imaging (MRI) have lead to a better understanding of the implant process. Source placement in the tumour can potentially be optimised, doses to tumour and normal tissue volumes can be calculated accurately and summarised in the form of dose–volume histograms (DVHs). DVHs are useful to compare treatment plans and in the development of dose prescriptions for individual patients. These improvements in techniques have led to more dose with a homogeneous distribution being delivered to the tumour whilst sparing surrounding tissues.

Today two forms of prostate brachytherapy are in clinical use, permanent and temporary implants. Permanent implants are the commonest form of prostate brachytherapy. These implants are left within the prostate and deliver their radiation over several weeks or months. ^{125}Iodine (Storey *et al.* 1999, Beyer and Priestley 1997) and ^{103}Palladium (Blasko *et al.* 2000) are common isotopes used in permanent implants. ^{125}Iodine is an Auger emitter, but the short range, highly effective electrons cannot pass out of the titanium capsule, so the radiation damage caused is effectively due to γ-rays. It has a short half-life of 60 days and it is usual to prescribe a minimum peripheral dose of 145 Gy, which includes the prostate capsule plus a 2 or 3 mm margin. Placement of ^{125}Iodine seeds in the prostate is calculated to give a initial mean peripheral dose rate of approximately 8 cGy h^{-1}. This means that 73 Gy is delivered in the first 60 days and the remainder at decreasing dose rates over the next 4–6 months. ^{103}Palladium emits its γ-rays through K-capture, has a higher dose rate (20–24 cGy h^{-1}) and its half-life is 17 days. As a higher dose rate is thought to be more biologically effective, the minimum peripheral dose is reduced to 120 Gy. ^{125}Iodine and ^{103}Palladium are low-energy isotopes (emitting γ-rays of 27–35 and 20–23 keV respectively). Their penetration distance is very small which is advantageous in protecting critical organ structures such as the rectum and neurovascular bundles, but has the disadvantage of not reaching tumour cells which have spread more than 3 or 4 mm outside the prostate capsule.

Temporary implants are removed at the completion of treatment. Needles or tubes, which carry the source, are placed in the prostate. These can be afterloaded with a radioactive

source. There are two types of implants used in temporary-implant brachytherapy: continuous LDR implants using iridium wire and HDR implants which consist of cylindrical iridium sources of diameter <1 mm. They have a high activity (100–400 GBq) and are used to give a fractionated-treatment schedule. High-activity sources deliver a pulse of radiation to the prostate. Four to six fractions are given over 2 or 3 days or in two separate applications (Ash *et al.* 1998).

1.9.1 Comparison between treatments

Pulsed dose-rate (PDR) brachytherapy is a new type of afterloading brachytherapy in which a continuous low dose-rate (LDR) treatment is simulated by a series of "pulses," *i.e.*, fractions of short duration (*e.g.* 10–20 minutes) with intervals between fractions of 1 to several hours. The term "PDR brachytherapy" is generally used for treatment schedules with a large number of fractions (at least four per day), while the term "fractionated high dose-rate (HDR) brachytherapy" is used for treatment schedules with just one or two brachytherapy fractions per day. Both treatments can be applied as alternatives for LDR. PDR is different from HDR afterloading machines in two ways. The first is that the afterloader in PDR is computerised and gives multiple dose fractions at a fixed chosen time interval. The second way is that the single ^{192}Ir source in the machine is approximately a factor of 10 weaker than the sources commonly used in HDR afterloaders, *i.e.* 37 GBq instead of 370 GBq (Visser *et al.* 1996).

1.9.1.1 High dose-rate (HDR) vs. low dose-rate (LDR) brachytherapy

Low dose-rate brachytherapy used in the treatment of endometrial cancer is 22% more expensive than high dose-rate treatments, according to a national survey carried out in the USA in 1998 (Pinilla 1998). It would therefore seem more cost efficient to use HDR treatments, but are they more effective radiobiologically? An *in vitro* study using a ^{137}Cs source found that fractionated HDR treatment gave greater cell kill than LDR on human tumour spheroids *in vitro* (Omura *et al.* 1998). In radiotherapy, the dose-limiting factor is often damage to normal tissue in the treatment field. Continuous low-dose rate is a useful treatment as it theoretically kills tumour cells whilst better sparing surrounding tissues compared with HDR treatments. The sparing effect of a low-dose rate is particularly effective on late responding tissues such as nervous tissue and sub-mucosa, but is it as effective as high-dose treatments at killing tumour cells? Several clinical studies have been published on this subject, most of them non-randomised retrospective studies on a small number of patients. Moreover, their conclusions are contradictory. Mazeron *et al.* (1991a) examined ^{192}Iridium implants on patients with T1-T3 breast cancer. They compared 3 dose-rate ranges 0.32–0.49 Gy h^{-1}, 0.50–0.59 Gy h^{-1} and 0.60–0.90 Gy h^{-1} and concluded that to maximise local control an implant dose rate of greater than or equal to 0.6 Gy h^{-1} should be used. Conversely, a clinical study compared the early effects of two dose rates

in brachytherapy of cervical carcinoma (Lambin *et al.* 1994a). They irradiated patients with stage I and stage IIp cervical cancer at dose rates of 0.38 and 0.73 Gy h^{-1} each to a total dose of 60 Gy. They found an inverse dose-rate effect in medium sized tumours, with significantly more sterilisations observed in stage IIp in the lower dose-rate group ($p<0.01$). They suggested that this effect may be due to hypoxia or induced resistance (Section 1.3.1 and 1.5). Other clinical studies have given contradictory results. One study showed that HDR brachytherapy in cervical carcinoma was as effective as LDR but with a lower risk of late complications (Orton 1998). Conversely a phase I/II study comparing fractionated HDR with LDR for interstitial brachytherapy for early stage squamous cell carcinoma of the tongue found that local-control rates for the tumours were lower than controls treated using low-dose rate. They also found a higher incidence of severe complications for the HDR patients (Lau *et al.* 1996). A similar result was obtained in a phase III study comparing HDR and LDR treatments for carcinoma of the tongue (Inoue *et al.* 1996, Inoue *et al.* 1998, Inoue *et al.* 2000). One of the main advantages of HDR compared with LDR treatments is that it is easier to obtain precise dose distributions, so biological advantages, if any, may be outweighed by these physical considerations when choosing a brachytherapy treatment.

1.9.1.2 Pulsed dose-rate (PDR) vs. low dose-rate (LDR) brachytherapy

In 1991 Brenner and Hall suggested that pulsed brachytherapy may be biologically equivalent to continuous LDR brachytherapy (Brenner and Hall 1991). Pulsed dose-rate machines use an ^{192}Iridium source 1mm in length with an activity of 37 GBq and a dose rate of 0.428 cGy h^{-1} at one metre. The iridium source moves stepwise through the implant. The dose and dose rate can be prescribed for each point along the implant. An iridium source can deliver the pulse dose (dose per pulse) in an implant in 10 min or less. The advantage of a pulsed-dose rate is that there is no radiation exposure to the staff between the pulses, only one source is needed and no treatment interruptions are necessary so the dose rate over the whole treatment time remains constant (Hall and Brenner 1992). The dosimetry may also be optimised for all sorts of configurations of the implant by varying the dwell time of the source for each position in the implant, compensating for cold and hot spots. Using PDR, the problems for trying to compensate for a variable dose rate to maintain local tumour control and minimise the late damage to normal tissues would then be eliminated (Hall and Brenner 1992).

There may be physical advantages of using PDR compared with LDR, but are there biological disadvantages? Indeed, if so, these may be outweighed by the increase in precision and convenience of using PDR. Hall and Bedford first addressed the question of equivalent pulse regimes (Hall 1964). They showed, that for HeLa cells, an effective dose rate of 0.17 Gy min^{-1} could be mimicked by exposing at 0.45 Gy min^{-1} for

23 seconds of every minute, whereas an effective dose rate of 0.024 $Gymin^{-1}$ could be mimicked by exposing at 0.45 $Gy\ min^{-1}$ for 30 seconds every 10 minutes. In 1991 Brenner and Hall examined data from 36 cell lines of human origin. They suggested that a pulsed regime consisting of 0.6 Gy given in a 10 min pulse and repeated every hour would, in practice, be indistinguishable from continuous low dose-rate irradiation at 0.6 $Gy\ h^{-1}$, as far as early responding endpoints are concerned (Brenner and Hall 1991). This conclusion was based on calculations for each cell line using the values of the radiobiological parameters α, β and $t_{1/2}$, obtained from analysing low dose-rate data. Subsequent mathematical modelling was carried out by Fowler and Mount (1992) and Visser *et al.* (1996) who arrived at a similar conclusion. This proposal has been followed by a number of centres using pulsed brachytherapy in a clinical situation (Mazeron *et al.* 1991b, McLean 1994, Fritz *et al.* 1997, Levendag *et al.* 1997, Pizzi and Marchetti 1997, Swift *et al.* 1997, de Pree *et al.* 1999) who, as yet, have found no significant difference in early response between PDR treatment and those of a previous series using LDR brachytherapy (Gaddis *et al.* 1983, Aristizabal *et al.* 1987, Esche *et al.* 1988, Pernot *et al.* 1994).

Experiments comparing the effects of LDR and PDR on the regeneration of mouse jejunal crypts *in vivo* have found similar results (Mason *et al.* 1994). Many studies have also considered the effectiveness of PDR treatments compared with LDR. A range of dose rates, size of pulse and duration between pulses were tested and no difference was found for acute endpoints between the two treatments when an equivalent pulse to dose rate is given in human tumour cells *in vitro* (Chen *et al.* 1997, Pomp *et al.* 1999), rat tumour cells *in vitro* (Armour *et al.* 1992), guinea pig skin *in vivo* (Brock *et al.* 1995) or rat eyes *in vivo* (Brenner *et al.* 1996b). Conversely a study on mouse lip mucosa concluded that LDR is the most efficient way to deliver radiation if recovery is to be maximised and the overall time kept as short as possible (Stuben *et al.* 1997). Experiments have shown that if the pulse interval is increased, PDR becomes more effective than LDR for a given dose. A study by Chen *et al.* (1997) showed that by increasing the time between pulses, PDR produces greater biological effectiveness compared with LDR, when the total dose and time were kept constant. This was also shown in other studies (Armour *et al.* 1992, Brenner *et al.* 1996b). Pomp *et al.* (1999) observed that when the dose rate during pulses was increased, cell survival decreased. In their study they examined two human tumour cell lines of widely differing SF_2 values. They found that this effect was most pronounced in the radiosensitive cell line and to a greater extent than values predicted by the Linear-Quadratic model.

A pulsed low dose-rate regime may seem beneficial from a practical standpoint and may produce equal or greater biological effectiveness as far as early responding endpoints are

concerned. However, several authors have commented on the need for caution with regard to late effects of PDR (Brenner and Hall 1991, Fowler 1993, Pop *et al.* 1996) because late-responding tissues are more sensitive than early responding tissues to changes in fractionation patterns (Hall 1994). The higher dose rate element of PDR may cause greater toxicity to late responding tissues than LDR and so it is therefore important to consider longer-term follow-up endpoints when comparing the two. In two studies examining normal tissues, late effects, such as telangiectasia and soft tissue necrosis, were found to be greater with PDR than LDR (Brock *et al.* 1995, Fritz *et al.* 1995). Another study examining cataract formation in rats found no difference in late effects between PDR and LDR (Brenner *et al.* 1996b). An equivalence in late endpoints was also seen between PDR and LDR treatments on guinea pig skin (Brock *et al.* 1995). Using a rat model to examine late rectal injury, Armour *et al.* (1997) showed that responses to PDR pulse sizes up to 1.5 Gy every 2 h were indistinguishable from LDR at a dose rate of 0.25 Gy h^{-1}. Recent clinical data also indicates no significant difference in late effects between PDR and LDR (de Pree *et al.* 1999). However, it is worthy of mention that reporting in most brachytherapy series, no distinction is made between acute and delayed complications. Table 1.4 shows a comparison the acute and late toxicity found in a number of studies.

Fowler (1993) suggests that the efficacy of PDR depends on the rates of sublethal-damage repair in early and late-responding tissues. This is because if tissues have a $T_{1/2}$ (half time of repair) which is short (0.1 to 1 h), the pulse interval can be kept small and so an equivalent total dose can be given in the same overall time as LDR. If the $T_{1/2}$ is large, the pulse interval must be large to allow for sparing of the tissue. This increases the overall irradiation time and in this case, LDR produces the greatest biological effect over a shorter time whilst sparing surrounding tissues. Increasing the dose per fraction could be carried out to compensate for the increase in pulse interval, but this would equate to a HDR fractionation schedule thus increasing late effect toxicity. Brenner *et al.* (1996b) calculated the fractional change in cell survival for PDR compared with LDR as a function of assumed half time of repair (Figure 1.6).

If PDR brachytherapy is to prove a viable option for clinical use, the $T_{1/2}$ for tumour tissues must be larger than surrounding tissues. In general, rapidly proliferating tissues seem to have a smaller $T_{1/2}$ than slower growing tissues, but this trend has as yet not been substantiated. It is true that the shortest half times of repair in normal tissues *in situ* occur in the rapidly proliferating cells of the small intestine and the longest half times in the late-responding tissues of the spinal cord, in several species. However this trend is not uniform. The $T_{1/2}$ for rapidly proliferating mouse skin is 1.3 h or longer (Henkelman *et al.* 1980, Kelland and Steel 1989, Rojas and Joiner 1989). The $T_{1/2}$ for repair in lung (a slowly proliferating late-responding organ) has been determined in various experiments in

mice as 0.7–0.9 h (Travis *et al.* 1987, Thames 1989). Rojas and Joiner (1989) discussed the large range in repair half times and concluded that there was a considerable overlap in repair times for tumours and normal tissues. It is therefore incorrect to assume that normal tissues and tumours have distinct $t_{1/2}$ times and so assuming the same effectiveness on tumour cell kill for both LDR and PDR treatments, increased normal tissue toxicity using PDR cannot be ruled out.

Reference	No. of patients	Site of tumour	Type of brachytherapy	Acute toxicity (% of patients)	Late toxicity (% of patients)
Inoue 1998	16	Floor of mouth	HDR LDR	NM NM	38 32
Swift 1997	41	Pelvic tumour	PDR	6.5	15
Beauvois 1994	237	Lip	LDR	16*	0.4
Mazeron 1991	279	Mobile tongue Floor of mouth	LDR	NM	21
De Pree 1999	24 17	Pelvic Head and neck	PDR PDR	4.2 23.5	13.6 6

NM= not mentioned.
*Grade not specified.

Table 1.4
Shows the comparison of acute and late toxicities for HDR, LDR and PDR brachytherapy used in clinical studies (de Pree *et al.* 1999).

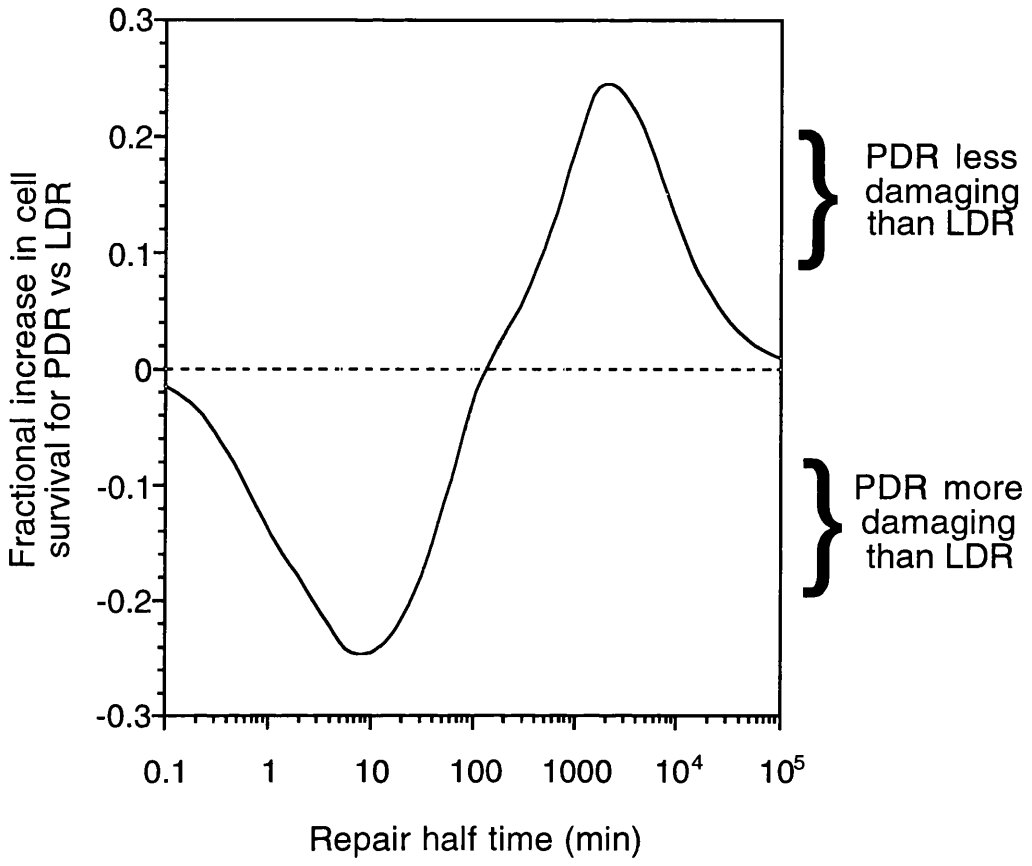

Figure 1.6
Shows calculated fractional change in cell survival for pulsed-dose rate (PDR) compared with continuous low-dose rate (LDR) as a function of the assumed half time of repair. Redrawn from Brenner *et al.* (1996b).

1.10 Aims of thesis

The aims of the research described in this thesis were:

1. To establish whether cell proliferation can be halted or slowed by modification of growth conditions and determine the presence or absence of HRS/IRR at acute doses in cells after exposure to these growth conditions.
2. To determine the prevalence of HRS/IRR to acute doses of radiation in cell lines *in vitro*.
3. To establish whether an increase in sensitivity of cell survival is observed at very low-dose rates of ^{60}Co γ- rays and ^{125}Iodine and to detect whether any effect observed could be due to cell-cycle perturbations.
4. To determine the effect of pretreatment with LDR irradiation on the HRS/IRR response.
5. To investigate the effects of a high dose given at HDR on cell-cycle progression of cell lines used in this study.

Chapter 2. Materials and methods

2.1 Introduction

This Chapter describes the materials and methods used routinely throughout the course of this project, that is descriptions of cell culture techniques, irradiations, dosimetry, survival curve protocols, clonogenic survival measurements and cell-cycle analysis. Any additional procedures or adaptations of existing protocols are described separately in the relevant chapters together with details of statistical analysis and data presentation.

2.2 Cell lines

A total of 7 human tumour cell lines were used in this study. They consist of 3 gliomas (T98G, A7 and U373MG), 3 prostate carcinomas (PC3, DU145 and LNCaP) and one bladder carcinoma (RT112). Their key features are described in Table 2.1.

2.3 Cell culture

2.3.1 Media

RT112, T98G, LNCAP, A7, U373MG and DU145 cells were maintained in exponential growth in monolayer culture *in vitro*, in Eagles minimum essential medium (MEM) with Earle's salts supplemented with 10% foetal calf serum (FCS, Sigma), $1.5\,g\,L^{-1}$ sodium bicarbonate, $10\,ml\,L^{-1}$ sodium pyruvate (Sigma), 20 μM L-glutamine (Sigma), $10\,ml\,L^{-1}$ non-essential amino acids (10 × stock, Sigma), 50 μg streptomycin (Sigma) and $50\,\mu m l^{-1}$ penicillin (Sigma).

PC3 cells were maintained in Hams F12 and Glutamax media (Life Technologies) with 10% FCS, 50 μg streptomycin and $50\,\mu m l^{-1}$ penicillin.

2.3.1.1 Monolayer culture

Cells were maintained routinely in exponential culture with media changes every 2–5 days, depending on growth rate, at 37°C in an atmosphere of 5% CO_2 + 5% O_2 (balance N_2). Every 3 months, cells were replaced with fresh cells from frozen stocks to prevent exhaustion of cell cultures. Cells were tested monthly for mycoplasma infection (Section 2.3.4) and any cell line that tested positive was discarded.

Cell line	Primary histology	Supplied by	Doubling time (h)	p53 status	SF_2
RT112	Human bladder carcinoma	ATCC*, 1993	38.7 (Power 1998)	Mutant (Chresta *et al.* 1996)	0.62 (Power 1998)
A7	Human astrocytoma	Massachusetts General Hospital, 1996	NK	NK	0.85 (Short *et al.* 1999)
T98G	Human glioblastoma	ECACC**, 1996	26 (Stein 1979)	Mutant (Van Meir *et al.* 1994)	0.75 (Short *et al.* 1999)
PC3	Human prostate carcinoma	Nycomed Amersham, 1997	31 (Algan *et al.* 1996)	Mutant (Isaacs *et al.* 1991)	0.32 (Leith *et al.* 1993)
LNCaP	Human prostate carcinoma	Paterson Institute, 1998	24.6 (Leith 1994)	Wild type (Israel *et al.* 1995)	0.51 (Leith 1994)
U373MG	Human glioblastoma	ATCC*, 1996	NK	Mutant (Van Meir *et al.* 1994)	0.55 (Short *et al.* 1999)
DU145	Human prostate carcinoma	Paterson Institute, 1998	18 (Algan *et al.* 1996)	Mutant (Isaacs *et al.* 1991)	0.60 (Leith *et al.* 1993)

Table 2.1
Shows the key features of the seven cell lines used in this study.
NK= not known. *American Tissue Culture Collection. **European Collection of Animal Cell Cultures

2.3.1.2 Suspension culture

T98G cells were grown *in vitro* in suspension culture using Minimum Essential Medium for Suspension culture (MEMS). The medium was modified for suspension culture by the removal of calcium and magnesium salts and the addition of 7.5% foetal calf serum (FCS) instead of 10% which is usual for attached cell culture. 500 ml rotating rod suspension culture bottles containing 100 ml suspension medium were seeded with a known number of cells and the media was gassed with 5% CO_2 + 95% air prior to being put on a magnetic stirrer pad at 100 r.p.m. in a 37°C warm room.

2.3.2 Sub culture

2.3.2.1 Monolayer culture

Cells grown in monolayer culture were passaged on a twice-weekly basis. The medium in the flasks was removed and discarded and the cells were rinsed twice with phosphate buffered saline (PBS). An appropriate volume, (2 ml for a 25 cm^2 flask, 3 ml for a 75 cm^2 flask and 8 ml for a 150 cm^2 flask) of 0.05% trypsin + 0.02% ethylene-diamine tetra-acetic acid (EDTA) was added to the flask and was allowed contact with the cells for 2–5 minutes. During this time, the flask was gently rotated to encourage detachment of the cells. The flask was then inspected using an inverting microscope to observe the detachment of cells from the growth surface. When the majority of cells could be seen floating in the trypsin, the action of the trypsin + EDTA was stopped by the addition of an equal volume of culture medium. The cells were then decanted into a 20 ml plastic universal container and centrifuged for 5 minutes at 1000 r.p.m. The supernatant was then aspirated and the cell pellet was momentarily whirl-mixed before dilution in fresh medium. The cells were syringed twice through a 21 gauge needle to give a single-cell suspension and an aliquot was placed into a tissue culture flask containing pre-warmed medium. The cells were then incubated at 37°C in a 5% CO_2 + 5% O_2 (balance N_2) gassed incubator.

2.3.2.2 Suspension culture

Cells in suspension culture were passaged twice weekly. Medium was aspirated from the suspension culture vessel into two plastic 50 ml universals. These were then centrifuged for 5 minutes at 1000 r.p.m. The supernatant was discarded and the pellet was whirl mixed and resuspended in 5 ml fresh medium. The cells were passed twice through a 21-gauge needle attached to a syringe to give a single-cell suspension. An aliquot of this cell suspension was placed back in a fresh suspension culture bottle containing 100 ml pre-warmed, pre-gassed media. The suspension culture vessel was then placed on a stirrer pad in a 37°C environment.

2.3.3 Frozen Stocks

Frozen stocks of cells were obtained by resuspending cells, after harvesting, in culture media containing 10% dimethylsulfoxide (DMSO). The cells were resuspended giving a final concentration of 2–4 $\times$ 10^6 cells ml^{-1}. 1 ml of this cell suspension was pipetted into a plastic 2 ml freezing vial. Cells were frozen quickly to -70°C for 24 h before storage in liquid nitrogen.

2.3.4 Mycoplasma testing

A coverslip, previously sterilised with 70% IMS, was placed in a 5 cm^2 petri dish and overlaid with 4 ml of antibiotic–free medium containing a single cell suspension at a concentration of 1 $\times$ 10^5. The dish was then placed in a 37°C incubator for at least 72 h to allow proliferation. After this time, the dish was checked to ensure that the cells were at least 50% confluent. The coverslip was then washed twice with PBS, fixed with 70% IMS for 30 min and allowed to air dry. After washing again twice with PBS, 2 ml of a 0.5 µg ml^{-1} solution of Hoechst 33342 was added to the cells and left for 15–20 min at room temperature in the dark. The coverslip was then inversely mounted on a clean glass slide with PBS + glycerol (1:1) and viewed with a fluorescent microscope at 400 nm. The slide was inspected for bright cytoplasmic staining in discrete dots which indicates mycoplasma contamination.

2.4 Cell growth experiments

2.4.1. Assessment of cell growth (also see Section 3.2.2)

These experiments were carried out to assess cell growth under various culture conditions.

2.4.1.1 Cell number

A known number of cells in exponential growth were plated into 25 cm^2 tissue culture flasks containing 5 ml of medium. Flasks were incubated at 37°C with 5% CO_2 + 5% O_2 (balance N_2) for 24 h to allow cells to attach. Flasks were then exposed to a variety of culture conditions. Experiments were conducted where flasks were placed in incubators heated to 37, 32, 30, 28 and 25°C. Other experiments involved exposing the cells to media containing varying amounts of FCS. These are described in detail in Section 3.2.2. Cell growth under these conditions was measured by detaching the cells from the flasks, centrifuging and resuspending in 5 ml of medium every 24 h as described in Section 2.3.2.1. An aliquot was pipetted onto a Modified Fuchs Rosenthal haemocytometer. Cells were visualised by placing the haemocytometer under a Nikon

Diaphot inverting microscope and were then counted to assess the number of cells extracted from the flask. Three readings per flask were taken and an average count was recorded. Counts were normalised using the following equation:

$$\text{Normalised count} = \frac{\text{no. cells at time t}}{\text{no. cells at time zero}}$$

The normalised count was plotted against time and enabled an assessment of the effect of the culture conditions on cell growth. It also allowed the effects of different culture conditions to be compared (Section 3.2.3).

2.4.1.2 Plating efficiency

The effect of culture conditions on colony forming ability was also assessed. After counting using the haemocytometer, a known number of cells were plated into 25 cm^2 flasks containing 5 ml pre-warmed MEM at an appropriate concentration to produce 100–200 colonies. These were incubated at 37°C until colonies were greater than 50 cells in number (10–14 days). Flasks were then removed from the incubator and the medium was discarded. Colonies were stained using 2 ml 2% crystal violet which was left in the flasks for at least 20 min. The stain was then removed and the flasks were rinsed 3 times with water. Flasks were then allowed to dry at room temperature for 24 h. The number of colonies were counted manually using a colony counter.

The remaining cells from these culture condition experiments, after cell number and plating efficiency were assessed, were fixed in 100% ethanol and cell-cycle distribution was assessed (Section 2.7.2).

2.4.1.3 Confluent T98G cells

5 x 10^5 T98G cells were plated into 25 cm^2 tissue culture flasks containing 5 ml EMEM. Flasks were incubated at 37°C with 5% CO_2 + 5% O_2 (balance N_2) for 4 days when they were observed to be confluent under an inverting microscope.

2.4.1.4 Supernatant

The supernatant was poured off each flask prior to trypsinisation and counting. It was examined under a microscope using a haemocytometer. The number of whole cells present was recorded.

2.4.1.5 Suspension culture

The cell number, plating efficiency and cell-cycle characteristics were assessed for cells grown in suspension culture under different FCS concentrations (Section 3.2.2.2). 2ml aliquots were taken from the suspension culture every 24 h, centrifuged at 1000r.p.m. for 5 minutes and resuspended in 5ml medium. Cells were counted using a haemocytometer, (Section 2.4.1.1) plating efficiency (Section 2.4.1.2) and cell-cycle characteristics were assessed (Section 2.7.2).

2.5 Irradiations

2.5.1 X- ray irradiations

Cells were irradiated at acute doses using a Pantak unit operating at 240kVp at a dose rate of 0.23 Gy min^{-1} for doses less than 1 Gy and 0.44 Gy min^{-1} for doses greater than 1 Gy. Flasks were irradiated in a Stuart perspex incubator heated to 37°C (Figure 2.1).

2.5.2 ^{60}Cobalt irradiations

Acute high-dose ^{60}Co irradiations were carried out on a ^{60}Cobalt source at a dose rate of 0.552 Gy min^{-1} (Figure 2.2). Dosimetry measurements were carried out using the method described in Section 2.5.4. Prior to HDR irradiation, a 0.5cm thick perspex sheet was fitted to allow build up of ^{60}Co radiation across the perspex, ensuring the correct dose of radiation was delivered to the cells. The source-object distance was corrected each month to maintain a constant dose rate. Cells were irradiated with 3 flasks placed in a perspex holder facing the source. These irradiations were carried out at room temperature.

Low dose rate irradiations (1–100 cGy h^{-1}) were carried out using Mobaltron 100 ^{60}Cobalt source (T.E.M. Instruments Ltd, Crawley, Sussex, England) (Figure 2.3) with flasks placed in an attenuating water tank using the method described in Section 4.3.1.

2.5.3 ^{125}Iodine irradiations

Low dose rate irradiations (3–40 cGy h^{-1}) were carried out using ^{125}Iodine brachytherapy implants described in Section 5.4.2.

2.5.4 Fricke dosimetry

Fricke dosimetry was used in ^{60}Co irradiations, both for acute dose (Section 2.5.2) and LDR (Section 4.3.1.1) and for ^{125}I dosimetry (Section 5.3.2). Fricke proposed this system as a radiation dosimeter in 1929 (Matthews, 1973, Matthews, 1978). Fricke

solution contains H_2SO_4, ferrous sulphate and a salt. Acidic conditions are required as the iron salts are not stable in neutral solutions. The reaction involved is the oxidation of the acid solution of ferrous sulphate to the ferric salt, in the presence of oxygen atoms (supplied by the water) and under the influence of radiation. A salt such as KCl or NaCl is added to desensitise the solution to organic impurities. The production of the ferric salt can be measured on a spectrophotometer as a change in absorbance of light at a wavelength of 304 nm or 224 nm. The dose of radiation given is linearly related to the change in absorbance of the Fricke solution. The dose of radiation received can be calculated as follows:

G (number of Fe^{2+} molecules changed per 100 eV deposited) = 14.3

1 Gy deposits 10^4 ergs gram^{-1}

1 erg = 6.242 x 10^{11} eV

1 Mole = 6.023 x 10^{23} molecules

Specific density of Fricke solution for 0.4 M H_2SO_4 @ 20°C = 1.0268 (calculated by plotting known specific densities for different molarities and then finding the equation of the curve)

Molar extinction coefficient (MEC) of ferric ion @ wavelength of 224 nm = 4565

(224 nm was used, as absorbance at that wavelength is almost temperature independent)

ΔA represents change in measured absorbance at 224 nm

B is the molar change in Fe^{3+} concentration per Gy

$$\Delta A = \text{Radiation dose} \times (B \times MEC)$$

$$\therefore \text{Radiation dose} = \Delta A \times \frac{1}{B \times MEC}$$

$$B = \frac{(10^4 \times 6.242 \times 10^{11}) \times (14.3/100)}{6.023 \times 10^{23}} \times 1000 \times 1.027$$

$$= 1.522 \times 10^{-6}$$

$$\therefore \frac{1}{B \times MEC} = \frac{1}{1.522 \times 10^{-6} \times 4565}$$

$$= 143.93$$

$$\therefore \text{Dose} = \Delta A \times 143.93$$

Fricke dosimetry solution was made up by adding 0.278 g of $FeSO_4 \cdot 7H_20$ and 0.058 g NaCl to 1 litre of 0.4 M H_2SO_4. A dose response curve of the Fricke solution to X-rays was obtained. 600 ml of the solution was added to two 75 cm^2 tissue culture flasks and irradiated with 60 Gy of ^{60}Co γ-rays for 1 h to radiochemically clean the flasks. The solution was then poured off and the flasks were rinsed three times with fresh Fricke solution. 600 ml of Fricke solution was then added to the flasks and the flasks were then irradiated with X-rays at a dose rate of 0.44 Gy min^{-1}. When the flasks had received 10 Gy, a 15 ml aliquot of the Fricke solution was removed and the flasks were irradiated for a further 10 Gy up to 60 Gy. 1 ml of the aliquot was used to rinse out a microcuvette before the addition of the irradiated sample. The absorbencies of the solutions from both flasks were measured at a wavelength of 224 nm on a spectrophotometer. The spectrophotometer was blanked using unirradiated Fricke solution before the absorbance of the irradiated solution was measured. After a dose response curve was obtained, the Fricke solution was irradiated using the experimental set-up and the absorbance was measured at 224 nm on the spectrophotometer. The dose received by the Fricke solution could then be read off the standard curve at the absorbance measured.

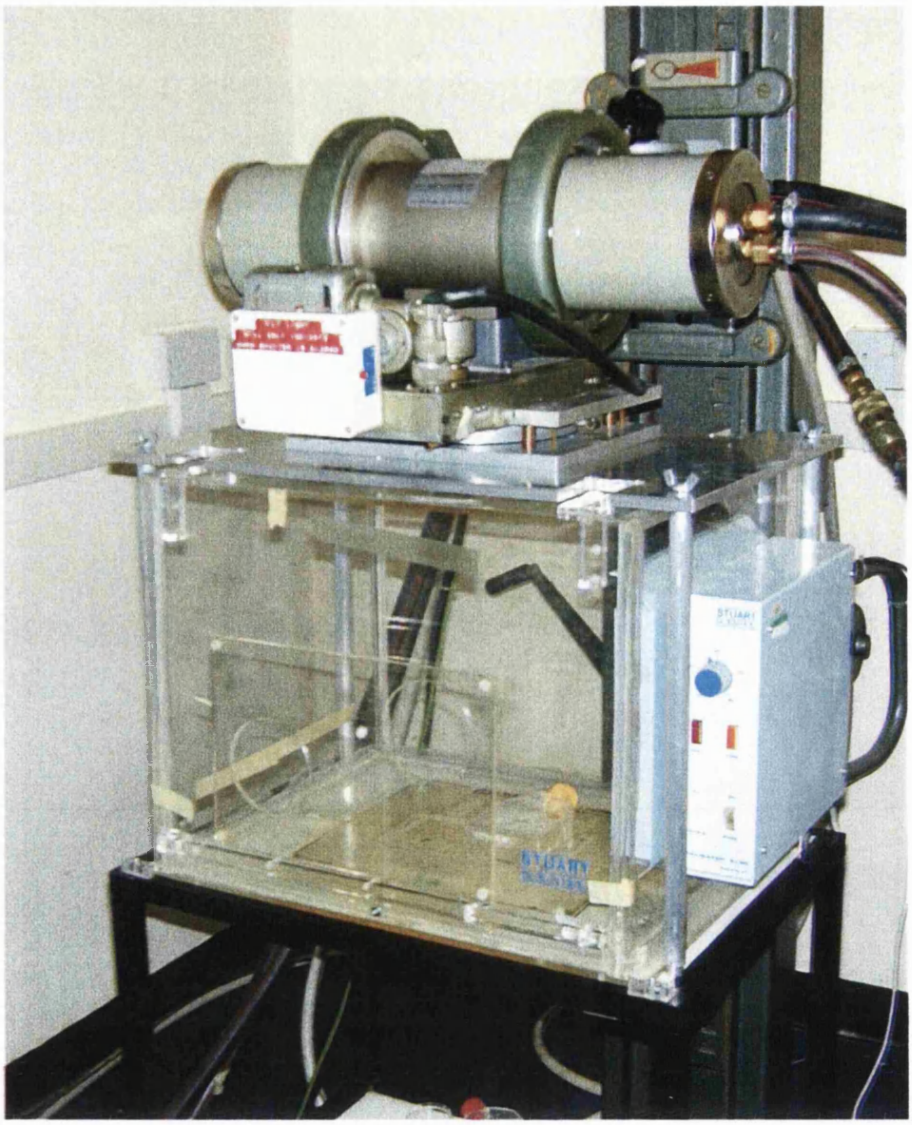

Figure 2.1
Shows the Pantak X-ray unit with a Stuart incubator used to keep the cells at 37°C during irradiations.

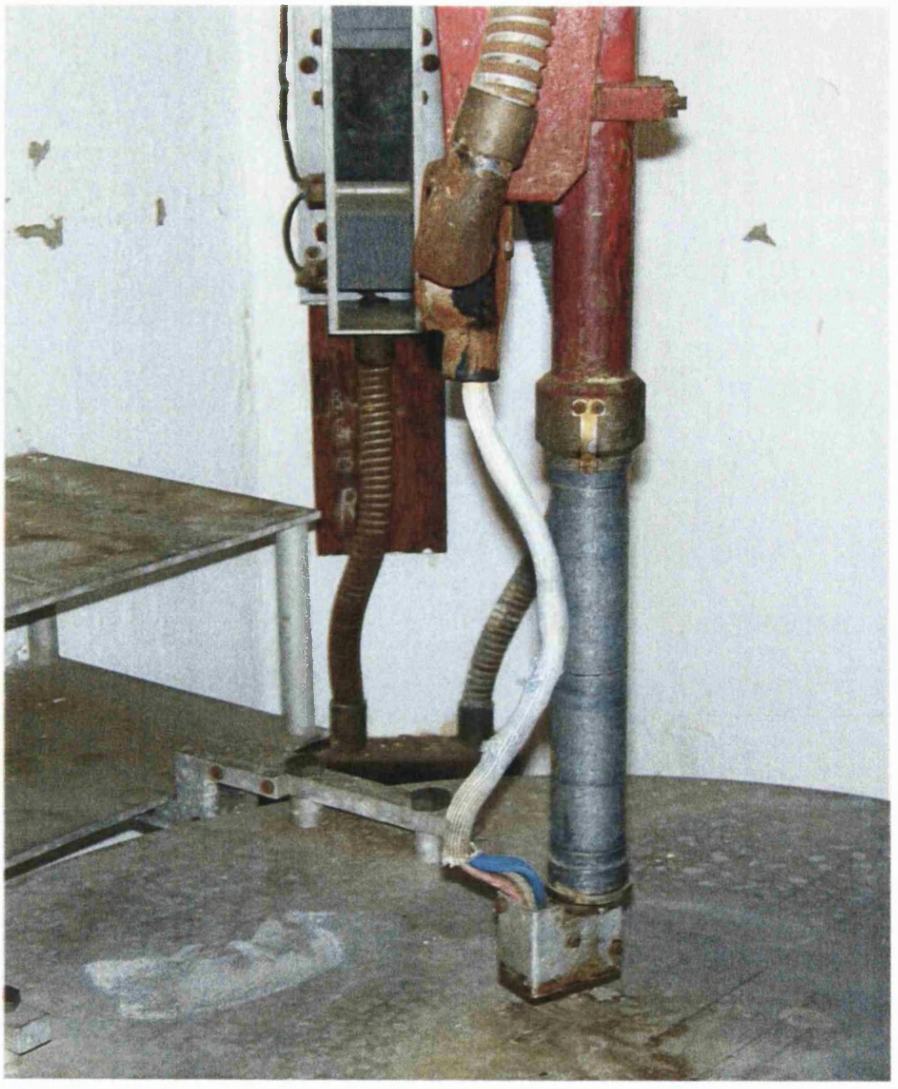

Figure 2.2
Shows the ^{60}Co γ-ray source used to give acute dose irradiations.

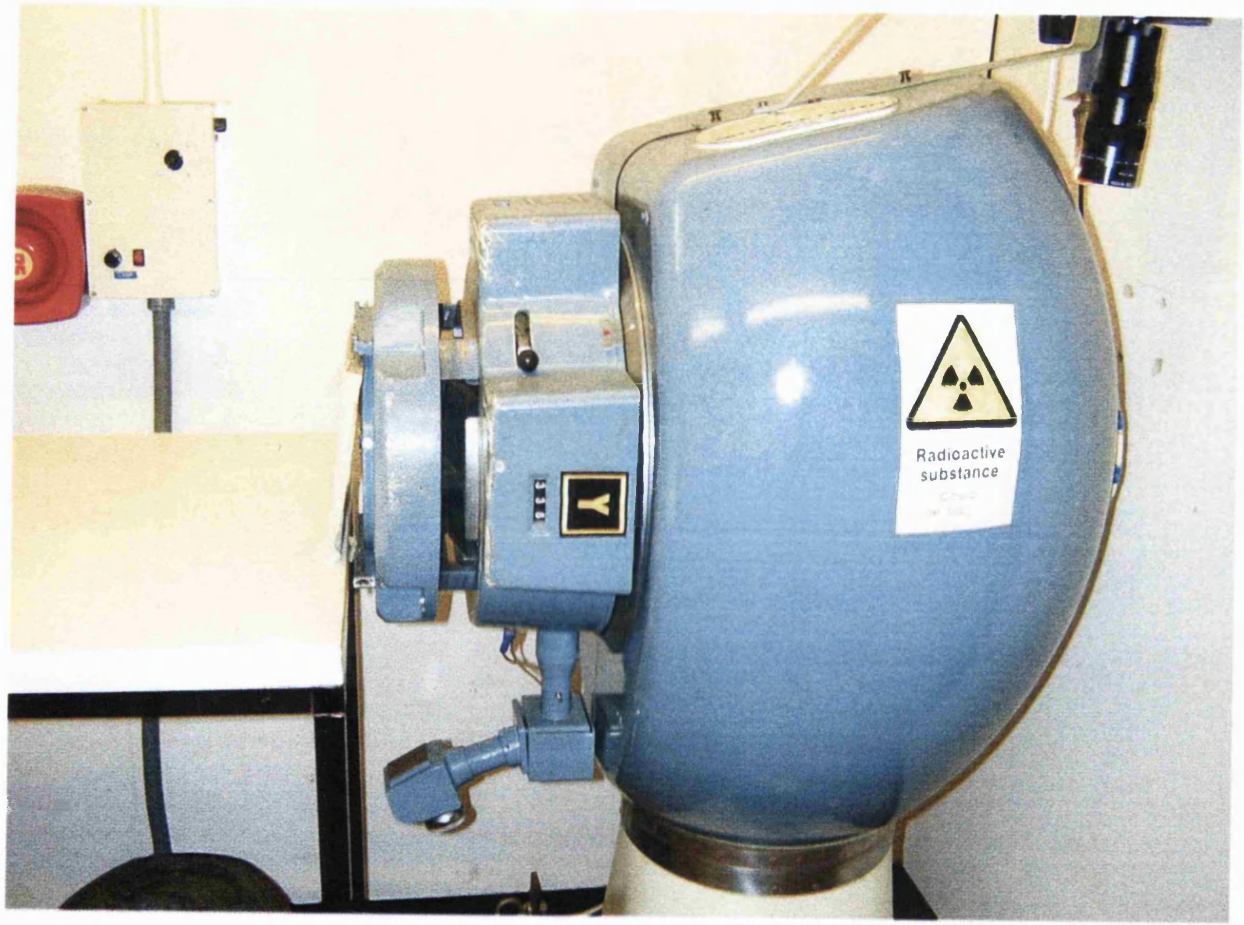

Figure 2.3
Shows the Mobaltron ^{60}Co γ-ray source used to give low dose-rate irradiations.

2.6 Cell-survival assays

2.6.1 Dynamic Microscope Image Processing Scanner (DMIPS)

2.6.1.1 Introduction

The Dynamic Microscope Image Processing Scanner (DMIPS) is an automated microscope which scans a flask of cells, identifies single live cells attached to the bottom of the flask and stores their locations so that the cell positions can be revisited to score for colony formation. This gives a very accurate measure of clonogenic survival following irradiation, on a cell-by-cell basis. It has applications in the study of cell growth and motility as well as accurate determination of clonogenic cell survival (Palcic and Jaggi 1986, Spadinger *et al.* 1989, Spadinger and Palcic 1993).

The DMIPS consists of an IBM-PC AT host computer, a Nikon TMD inverted microscope, a microscope stage plate, a solid state image sensor and a stage incubator. A photograph of the DMIPS is shown in Figure 2.4. To assess cell survival, the host computer uses a cell recognition program; C scan (cell recognition algorithm), in which the flask is scanned by the microscope and single cells are identified. The entire area of the flask is scanned by the movement of the microscope stage plate which is mobile along the X and Y planes and is controlled by the computer. The solid state image sensor consists of a linear array of photo diodes, which detect the bright field microscopic image, and identifies cells as changes in the light intensity. Each flask is scanned in 11 separate bands, each 40 mm long and 2.25 mm wide by moving the flasks perpendicular to the sensor array. The sensor is sensitive enough to distinguish the cells from debris and irregularities in the surface of the tissue culture flask. The locations of these cells are stored on computer as two-dimensional co-ordinates. The host computer then allows manual confirmation of the presence of a single cell in each of these logged areas. A second computer program, S Scan (cell-survival monitoring) is used approximately 10 to 14 days later. This program revisits the logged co-ordinates and allows manual scoring for the presence or absence of colonies in the logged area of the flask.

The C-scan program will exclude cells which are too close together as colonies grown from these would overlap making it difficult to accurately assess colony formation. The distance at which this exclusion occurs is set so that cells are spaced by at least the maximum diameter (δ) of a typical colony, this then determines the optimum number of cells to be plated in each flask. The exclusion distance is then related to the number of cells plated by:

$$Nc = \frac{1}{0.0016\delta^2}$$

Where δ is the exclusion distance and *Nc* is the number of cells plated.
The number of usable cells in a 2.5 cm region of the flask is then given by:

$$N = Nc\, e^{-0.0016 Nc \delta^2}$$

It was found previously that an exclusion distance of 350–400 μm and a cell count of 3500 per 25 cm^2 flask produced optimal cell recognition and colony counting for V79 cells. The distances used in these experiments were based on these values.

2.6.1.2 Cell culture, irradiation and assessment of cell survival

Cells in exponential growth were trypsinised and then counted using a haemocytometer. 3000 were plated into 25 cm^2 high optical clarity Nunclon tissue culture flasks with 5 ml pre-warmed medium. Flasks were incubated at 37°C with lids loose for 30 min to 2 h to allow the cells to attach. The attachment time was found to vary between cell line. A time was chosen where a large number of cells would attach, but a minimum had flattened down so that the optimal number could be scanned on the DMIPS. The medium was then discarded and flasks were then completely filled with fresh medium to increase optical definition when C scanned. Cells were irradiated with doses from 0.05 Gy to 5 Gy with 240 kVp X-rays as described in Section 2.5.1. Flasks were C scanned on the DMIPS in a random order at 37°C. Locations were checked manually for the presence of a single cell. Empty locations and doublets were discarded. They were then incubated at 37°C for 7–10 days to allow colony growth and were then rescanned using the S-scan program by the DMIPS to score colony formation. A location was deemed to be positive for a colony if >50 cells were visible. The surviving fraction of the cells could be calculated and plotted against dose.

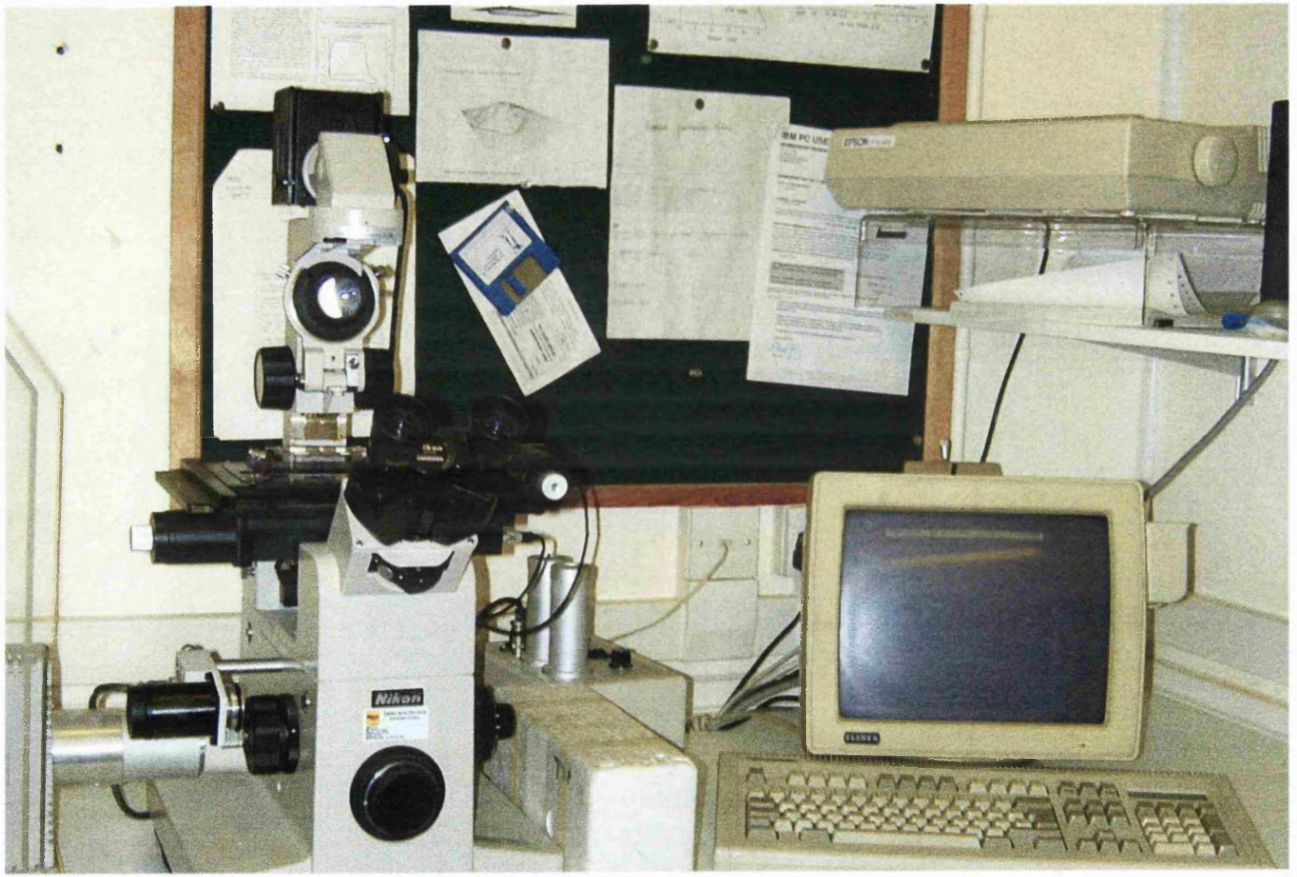

Figure 2.4
Shows the DMIPS.

2.6.2 FACS Vantage cell sorter

2.6.2.1 Introduction

The Fluorescence Activated Cell Sorter, FACSVantage (Becton Dickinson) is an automated flow cytometer which is attached to a computer. It is similarly equipped as the FACScan (Section 2.7.1) with an additional sort facility. It uses the reflectance properties of the cells when illuminated by laser light to sort individual cells on the basis of cell size (forward scatter) and granularity (side (perpendicular) light scatter) without the use of a cell stain (Durand 1986). The cells are visualised on the computer screen which enables regions to be drawn around the subpopulations of cells to be selected. A droplet sorting method is used in which the cells of choice exit the flow chamber in a jet which breaks up into regular droplets containing a known number of cells. The cells are charged and passed through a high voltage electrostatic field where they are deflected into a 25 cm^2 flask. A precise number of cells can be dispensed into a flask; thus, a clonogenic assay plated in this way can give a very accurate assessment of cell survival at low doses. A photograph of the cell sorter is shown in Figure 2.5 and a diagrammatic representation of the sorting method is shown in Figure 2.6.

2.6.2.2 Cell culture, irradiation and assessment of cell survival

Cells were trypsinised, centrifuged and resuspended as described in Section 2.3.2.1, The cell suspension whirl mixed and decanted into 5 ml, round-bottomed polystyrene sample tubes (Becton Dickinson Labware 'Falcon 205L' tubes) which was positioned below the Vantage sampling port. The cells were then passed through to the cell sorter. The cells were sorted on the basis of side and forward scatter, and a region was gated round the healthy cell population to exclude doublets and debris. These cells were then dispensed directly into a 25 cm^2 flask containing 5 ml pre-gassed, pre-warmed medium. A precise number were sorted into each flask, depending on predicted survival for that cell line per dose. The dishes were incubated at 37°C with 5% CO_2 + 5% O_2 (balance N_2) for 2 h to allow the cells to attach. Flasks were then irradiated in the same order as were plated with doses from 0.05 Gy to 5 Gy with 240 kVp X-rays (Section 2.5.1). These were then placed in an incubated at 37°C for 10–14 days to allow for colony formation, before being stained with crystal violet and counted manually to obtain the surviving fraction.

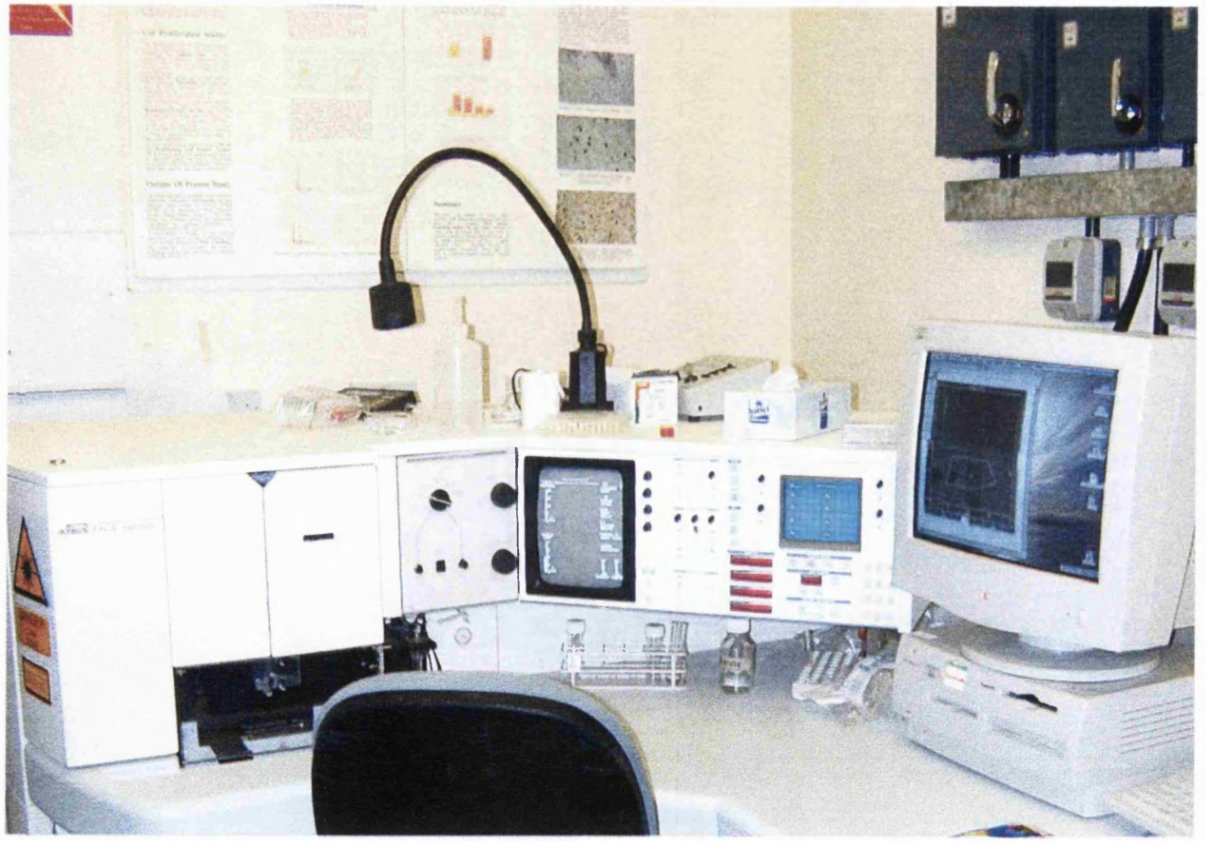

Figure 2.5
Shows the cell sorter.

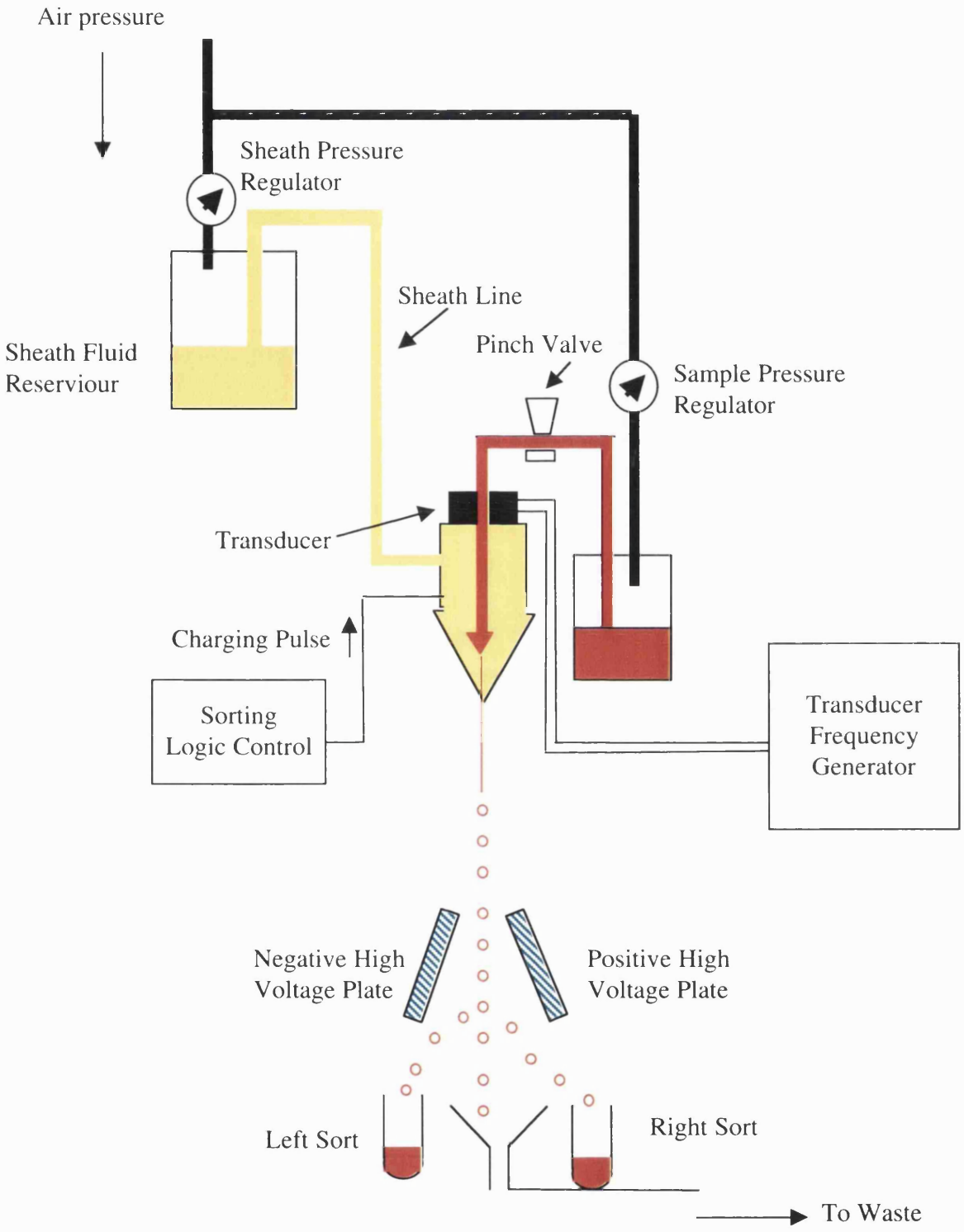

Figure 2.6
Shows a generalised droplet system used for cell sorting. The droplets containing selected cells are electrically charged as they pass through a high voltage electrostatic field and are deflected into a dish or flask.

2.7 Cell-cycle analysis

2.7.1 Flow cytometry: The FACScan

The cell cycle was assessed by flow cytometry using a Becton-Dickinson FACScan. The FACScan is equipped with a 15 mWatt Argon-ion laser with an excitable wavelength of 488 nm and is capable of measuring five optical parameters simultaneously:- forward scatter, side scatter and three spectral regions of fluorescence. It has three high performance photomultipliers with band pass filters of 530 nm, 585 nm and >650 nm. The single cells to be analysed are enclosed in a pressurised saline solution and passed through a flowcell where they generate up to 5 signal pulses simultaneously. These pulses are processed by an analogue-digital converter and stored by the computer system for analysis. A photograph is shown in Figure 2.7.

2.7.2.1 BrdUrd-pulse labelling

To look more closely at the phase lengths of the cell cycle in each cell line, cells were pulse labelled with 5-bromo-2'-deoxyuridine (BrdUrd), labelled with a monoclonal antibody against BrdUrd and stained with a second antibody before analysis on the flow cytometer. BrdUrd is a thymidine analogue which is incorporated into DNA only during S phase. Cellular nuclei can then be extracted and labelled with monoclonal antibodies against BrdUrd.

Cells were grown exponentially *in vitro* in monolayer culture in 75 cm^2 tissue culture flasks at 37°C. When the cells were approximately 70% confluent, BrdUrd (Sigma) was added to each to give a final concentration of 20 µM. After 20 minutes the medium was removed and the flasks were washed 3 times with phosphate buffered saline pre-warmed to 37°C to remove all unbound BrdUrd. Fresh medium was added and cells were returned to the incubator to allow progression through the cell cycle. Irradiations with 2 Gy were carried out using 240 kVp at a dose rate of 0.44 Gy min^{-1}. Flasks were irradiated in a Stuart warm box maintained at 37°C to minimise heat loss and possible cell-cycle perturbations. Control flasks were sham-irradiated to determine the effect, if any, on cell-cycle progression of any heat loss during transit to and from the incubator. Following irradiation flasks were returned to the incubator.

2.7.2.2 Cell harvesting and fixing

At 4 h intervals, for up to 36 h after removal of BrdUrd, cells were harvested. Cells were scraped from the flask and centrifuged for 5 minutes at 0°C at 2000 r.p.m. The pellet was then re-suspended in 200 µl of PBS and fixed in 5 ml of ice cold 70% ethanol and stored at 4°C.

2.7.2.3 Cellular staining for BrdUrd

To prepare the cells for staining, cells were centrifuged at 2000 r.p.m. for 5 minutes and the ethanol was removed. The cells were re suspended in 2.5 ml of 2 M HCl containing 0.1 mg ml^{-1} pepsin solution for 20 minutes. The resulting nuclei were then washed twice in 10 ml PBS and re-suspended in 0.5 ml of PBS containing 0.5% normal goat serum, 0.5% Tween 20 and 36 µl rat anti-BrdUrd monoclonal antibody. After 90 minutes of incubation with occasional mixing, 5 ml of PBS was added and nuclei were centrifuged at 2000 r.p.m. for 5 minutes. They were then re suspended in 0.5 ml PBS containing NGS + Tween 20 and 25 µl anti-rat IgG fluoresein isothiocyanate conjugate (FITC) and incubated in the dark at room temperature for 60 minutes. Finally the nuclei were centrifuged as before, washed in 10 ml PBS and re-suspended in 1 ml PBS containing 10 µg ml^{-1} propidium iodide. Samples were then vortexed prior to analysis on the flow cytometer.

2.7.2.4 Detection of labelled nuclei

The sample was analysed using a Becton–Dickinson FACScan incorporating Lysis II software. The BrdUrd incorporated cells labelled with FITC (green emission) were collected on the FL1 channel, while the propidium iodide emission (DNA content) was collected on the FL3 channel. Samples were gated on the FL3 area and width signals to eliminate debris, doublets and clumps. The FL1 signal was collected on a log scale and the FL3 signal on a linear scale to achieve optimum separation of the BrdUrd incorporated and unincorporated cells. For each sample, 10000 events were recorded. Analysis of the sample was performed using the Lysis II software package.

2.7.3 Propidium Iodide (PI) labelling

The DNA distributions of the cell populations used during asynchronous and confluent irradiation experiments were measured. Cells were stained with Propidium iodide to assess the proportion of cells in each phase of the cell-cycle. PI is incorporated into the DNA and enables the DNA content of the cells to be measured by flow cytometry. Cells were centrifuged at
1000 r.p.m. for 5 minutes. The supernatant was removed, the pellet was resuspended in 200 µl PBS and fixed in 10 ml of 70% ethanol. To determine the proportion of cells in each cell-cycle phase, cells were stained using a solution of propidium iodide (PI) (1 µg ml^{-1}) and ribonuclease (5 µg ml^{-1}). Stained samples were then analysed on a FACScan flow cytometer.

2.7.4 Flow cytometry data collection

A FACScan flow cytometer was used to visualise BrdUrd and PI staining. BrdUrd incorporation gives off a green FITC emission signal (515 < 1 < 545 nm) and was collected on a log scale to discriminate total labelled and unlabelled populations. The red PI emission signal (620nm) was collected on a linear scale for best discrimination of DNA content in each cell-cycle phase. Application of the doublet discrimination module on the PI signal (Becton-Dickinson) was used to exclude collection of debris and clusters of cells. 10000 cells from each sample were collected for analysis.

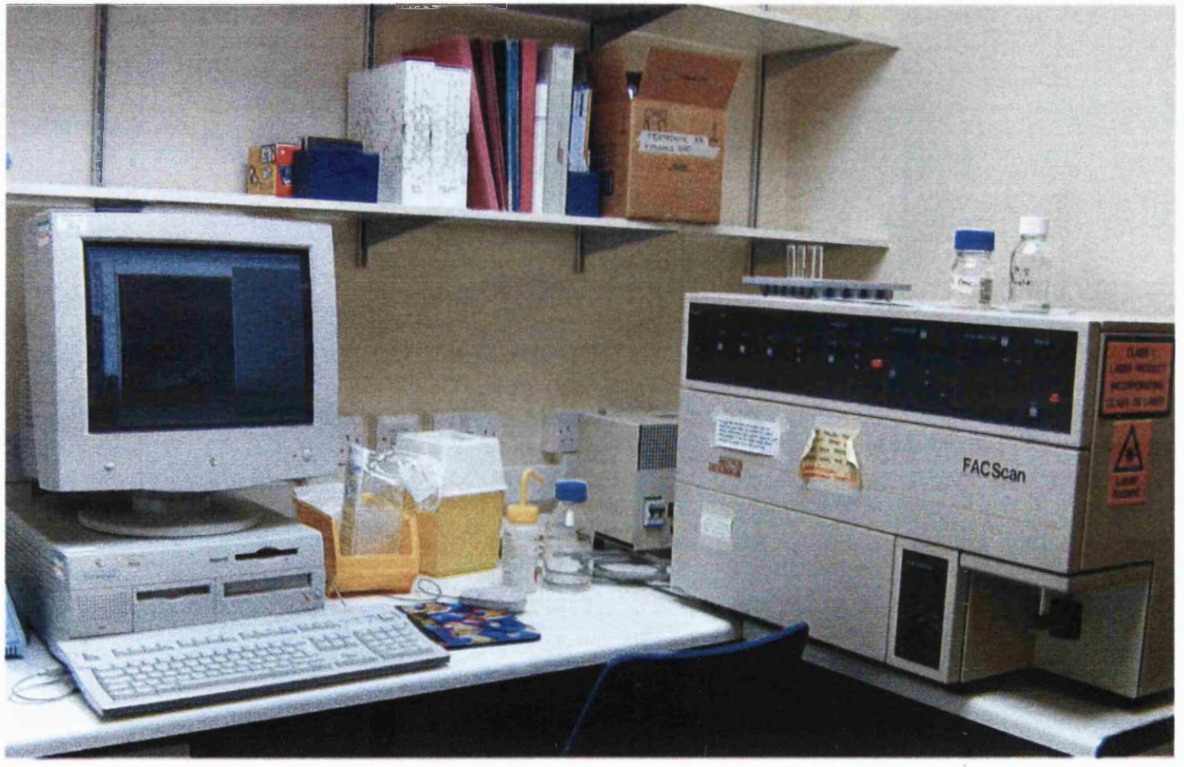

Figure 2.7
Shows the FACScan flow cytometer.

Chapter 3. Cell survival after acute low-dose irradiation

3.1 Aims

The aims of these experiments were:

1) To determine the prevalence and extent of HRS/IRR to acute doses of radiation in cell lines *in vitro*.

2) To establish whether proliferation in specific cell lines could be halted or slowed by modification of growth conditions and to determine if this affected the extent of HRS/IRR at acute doses of radiation after exposure to these growth conditions.

3.2. Modification of growth conditions

3.2.1 Introduction

Optimal growth conditions for an asynchronous cell population lead to continuing mitotic activity and an increase in cell number. With acute irradiation doses, exposures are so short that a known number of cells can be irradiated to the same dose and survival assessed by the number of them dividing to form colonies. However, low dose-rate exposures may occur over a long time period in order to achieve the same total dose as acute exposures. In this case, the exposure time may be greater than the cell-cycle time, so the number of cells will increase during irradiation. This produces an additional complication when assessing the cell survival. Cells surviving at the end of irradiation may have only been "born" during the exposure and therefore not received the full dose compared with other cells present throughout the irradiation. These experiments, to study the effects of low dose-rate irradiation of the range 1–100 cGy h^{-1} on human cells, necessitates irradiating cells over long periods of time (*e.g.* up to 10 days for a dose of 12 Gy given at a dose rate of 5 cGy h^{-1}). In contrast, in a non-proliferating population, cells present at the end of irradiation have received the same total dose and so assessment of cell survival is made much simpler.

Both HRS/IRR and inverse dose-rate effect have been explained by changes in sensitivity throughout the cell cycle. As discussed in Section 1.5.2., a substructure in the survival curve was hypothesised to be due to a sensitive subpopulation of cells (Skarsgard *et al.* 1996). Although this theory for HRS/IRR has been discounted by many authors (Lambin *et al.* 1993, Wouters *et al.* 1996, Wouters and Skarsgard 1997), the presence of HRS/IRR in a non-cycling population would prove definitively that HRS/IRR was not related to cell-cycle progression, as shown by Short (1999a). The inverse dose-rate effect also has a cell-cycle based explanation (Section 1.5.3.1). Work carried out by Mitchell (1979) suggested that a G2 accumulation during irradiation could account for an increase in sensitivity seen

at the lower dose rates below 154 cGy h^{-1} in HeLa cells (Figure 1.4). This was supported by several other authors (Furre *et al.* 1999, DeWeese *et al.* 1998).

In order to assess survival after low dose-rate irradiations without the variations in sensitivity throughout cell cycle affecting the results, methods to stop or slow cell-cycle progression have to be used. The first aim was to develop and optimise these irradiation conditions. Three possible methods of slowing cell proliferation were investigated:

1. reducing the incubation temperature to below 37°C (generally the optimum for cell growth)
2. reducing the concentration of foetal calf serum in the growth medium to below 10%
3. growing T98G cells to confluence.

The methods used were chosen as they caused minimal stress to the cells. Such stress might itself alter radiosensitivity and abolish HRS. After these growth conditions were investigated, cells were then tested for the presence of HRS/IRR.

3.2.2 Specific materials and methods

3.2.2.1 Reduction in incubation temperature (see also Section 2.4)

10^3 RT112 cells in monolayer culture were seeded into 25 cm^2 tissue culture flasks containing 5 ml of MEM. Flasks were incubated at 37°C with lids loose in 5% CO_2 + 5% O_2 (balance N_2) for 24 hours to allow cells to attach. The flask lids were then tightened and the flasks were transferred to an incubator at a lower temperature of 25, 29, 30, 32 or 35°C. The medium in each flask was changed and flasks were gassed using 5% CO_2 + 5% O_2 (balance N_2) every 3 days.

After three days of incubation at the required temperature, cells were harvested from 3 of the flasks every 24 hours until 7 days after initial plating. Cell growth, plating efficiency and cell-cycle characteristics were assessed at each temperature point (Section 2.4.1). At least 2 experiments were carried out at each temperature.

BrdUrd Labelling and staining (Section 2.7.2.1 to 4) was also carried out for RT112 incubated at 30, 32 and 37°C to ascertain the cell-cycle time at the various temperatures. Cells were plated and incubated at 37°C until they were 60% confluent. They were then transferred to an incubator heated to the appropriate temperature, 24 hours before starting the experiment and held at that temperature throughout the experiment.

The presence of low-dose HRS in cells incubated at 37 and 30°C temperatures was investigated using the DMIPS protocol (Section 2.6.1.2 and 3.3.2.1). Stock flasks were incubated at the appropriate temperature for 24 hours before plating. After plating, flasks were left to attach at that temperature for 12 hours. Media was then discarded and flasks were filled with media heated to the either 30 or 37°C. Throughout irradiations and C

scanning (Section 2.6.1.1) the cells were maintained at the appropriate temperature. They were placed back in a 37°C incubator 6–8 hours after irradiation.

3.2.2.2 Reduction in foetal calf serum concentration

The effects of serum depletion on T98G cells in monolayer culture were investigated using a method similar to that employed in the study of temperature on RT112 cells (Section 2.4 and 3.2.2.1). T98G cells were chosen as they have been shown to exhibit a reversible G1 arrest when grown in serum-deprived cultures (Stein 1979) (Short *et .al.* 1999a). Five different concentrations of foetal calf serum in the medium (0.5, 1, 2, 7.5 and 10%) were compared. The medium in each flask was changed every 72 hours. Plating efficiency, supernatant cell content and cell-cycle analysis with PI staining were also examined (Section 2.4.1 and 2.7.3). At least 3 experiments were carried out at each FCS concentration.

T98G cells were grown *in vitro* in suspension culture as described in Section 2.3.1.2. The effect of serum depletion on the cells was assessed by replacing the medium containing the original concentration of FCS with medium supplemented with 0.5, 1 or 2% FCS. Cell growth was ascertained using methods described in Section 2.4.1.2.

3.2.2.3 Confluence arrest

T98G cells are known to exhibit reversible confluence arrest in the G1 phase of the cell cycle (Stein 1979). 5 x 10^3 T98G cells were plated into 25 cm^2 flasks with 5 ml medium. Flasks were left for 4 days to grow to confluence, *i.e.* day 1 on the graph (Figure 3.8) indicates the first day the cultures were observed as being confluent. The media was changed every 48 hours and cell growth, plating efficiency, supernatant cell concentration (Section 2.4) and cell-cycle proportions (2.7.3) were monitored every day for up to 14 days after plating. 3 flasks per day were harvested and 3 experiments were carried out in total.

To assess whether holding T98G in confluence affected the T98G low-dose HRS response, confluent cell survival was assessed using the DMIPS (Section 2.6.1.2 and 3.3.2.1) and cell-sort (Section 2.6.2 and 3.3.2.2) protocols. Cells were plated from a stock flask which was observed as being confluent for 4 days.

3.2.3 Results

3.2.3.1 Reduction in incubation temperature

RT112 cells grown at 37°C had a faster growth rate than cells grown at lower temperatures. Figure 3.1A shows that as the temperature was lowered the rate of proliferation was lowered correspondingly. After day 5, in flasks incubated at 37°C, there was a reduction in the cell number which did not occur with cells incubated at lower

temperatures. Cells from flasks incubated at 37°C had a fairly constant plating efficiency with a mean of 45.6% over the whole time period (see Figure 3.1B). The plating efficiency was lower for cells incubated at lower temperatures, *i.e.*, the mean PE was approximately 6% lower per °C below 37°C. The proportion of cells in each phase of the cell cycle was measured by flow cytometry. There appeared to be a difference between cells grown at 37°C and those at lower temperatures (see Figure 3.1C). With increasing time, cells incubated at 37°C showed a higher proportion of cells in the G1 phase of the cell cycle (with 68.9% in G1 at day 3 rising to 79.0% by day 6). The proportion of cells in each phase of the cell cycle was unchanged over time at lower temperatures (approximately 61% of cells in G1, 17% in S and 22% in G2). Table 3.1 shows the calculated cell-cycle times of RT112 cells at temperatures of 30°C, 32°C and 37°C. The cell-cycle time lengthened as the temperature was reduced (from 24.7 h and 37°C down to 56.5 h at 30°C). The results of supernatant analysis (Figure 3.2) showed a higher cell number in flasks incubated at 37°C. As the temperature was reduced there were fewer cells in the supernatant.

RT112 cells grown at 37°C and 30°C exhibited a HRS response to very low doses of radiation (see Figure 3.3). Cells incubated at 30°C showed a more resistant response to radiation over the whole survival curve and slightly less HRS than those grown at 37°C.

3.2.3.2 Reduction in foetal calf serum concentration

In monolayer culture, T98G cells continued to grow using serum concentrations below 10%, albeit at a slower rate (Figure 3.4). The mean plating efficiency over the 5 days decreased exponentially for cells grown with the lower concentrations of serum from 36.3% at 10%, down to 23.0% at 0.5% FCS. Examination of the cell-cycle phase proportions with PI staining showed a normal distribution under these conditions (*i.e.* a mean of 65.5% cells in G1, 15.8% in S and 18.4% in G2).

Figures 3.5 and 3.6 show the results of growing T98G cells in suspension culture, in various FCS concentrations. Serum depletion at both 0.5% and 1% FCS appeared to halt T98G cell proliferation as demonstrated by the constant cell number between day 0 and day 3 followed by a sharp decline after this time. This was in contrast to cells grown in 2 and 7.5% FCS which continued to proliferate. At all serum concentrations, the cell number decreased transiently after the medium change at day 2 and 4. This probably reflected the cell loss following centrifugation. The plating efficiency in suspension cultures with 1, 2 and 7.5% FCS was similar to that of cells grown in 10% FCS in monolayer culture. However, cells grown in 0.5% FCS had a significantly lower plating efficiency.

By staining the cells with propidium iodide (Figure 3.6) and analysis on the flow cytometer, it was found that the cessation of cell proliferation in 0.5% and 1% FCS was due to cells arresting in G1 (see Figure 3.6).

Figure 3.7 shows the results of 5 DMIPS experiments carried out with Dr. S. Short on cells grown in 0.5% FCS. Analysis of the radiation response showed that HRS was present and an Induced-Repair curve was fitted to the data.

3.2.3.3 Confluence arrest

The cell number remained constant at a mean count of 4.4 x 10^5 cells per flask while held for 8 days in confluence. The plating efficiency was also constant at a mean of 28.3% over the 8 days. The supernatant contained relatively few dead cells and staining with PI showed cells to be in G1 arrest with 86.6% cells in G1 by day 8 compared with a mean of 64% in asynchronous cultures (see Figure 3.8). Figure 3.9 shows the results of confluent cells assessed for the presence of HRS/IRR using the DMIPS and cell-sort protocols showing that it was indeed present. The results are summarised in Tables 3.2 to 3.5.

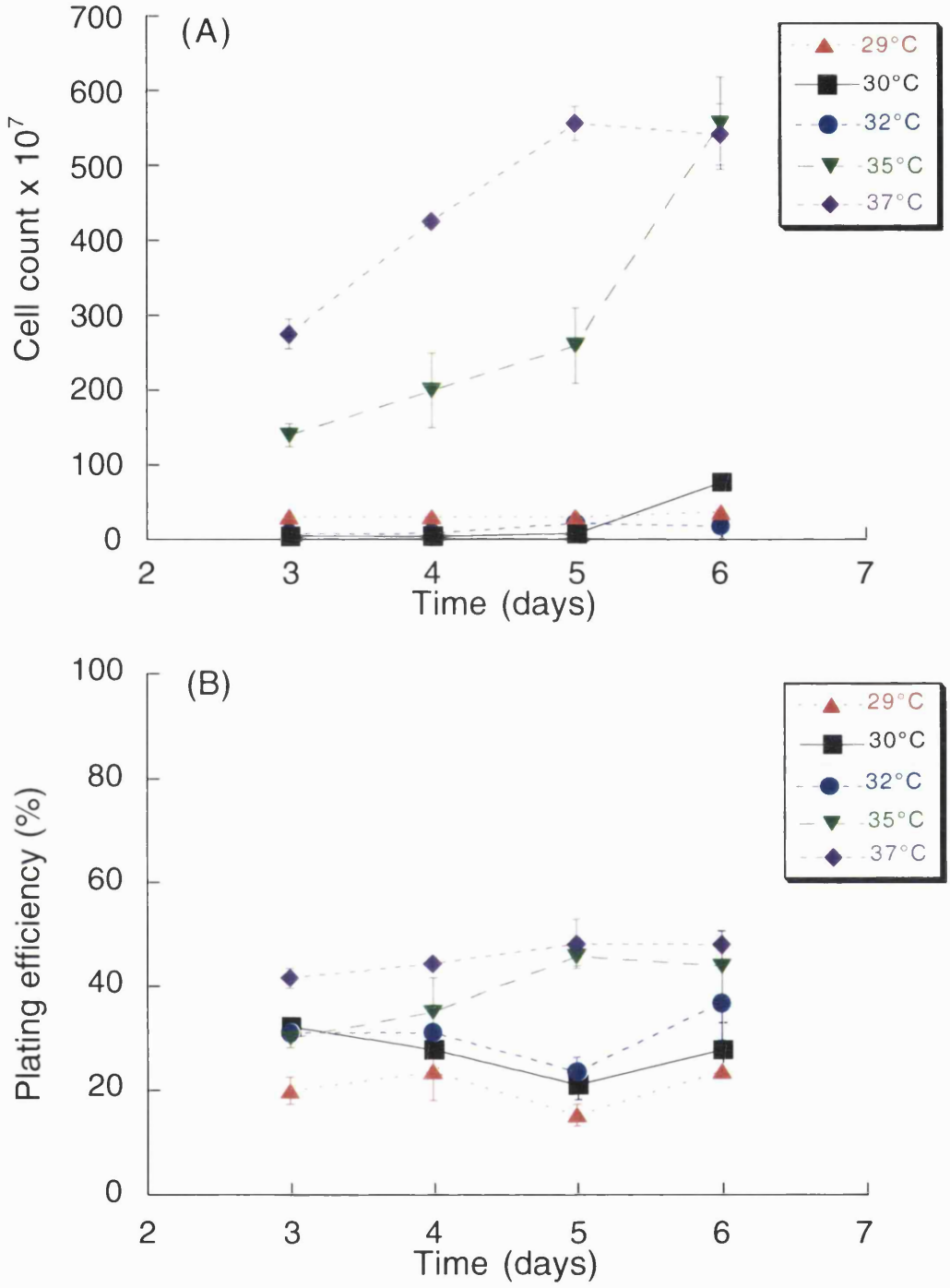

Figure 3.1
Shows the growth of RT112 cells incubated at 29°C, 30°C, 32°C, 35°C and 37°C seeded with an initial concentration of 10^5 cells (plotted as the mean ± SEM).
(A) Shows cell counts from flasks
(B) Shows plating efficiency

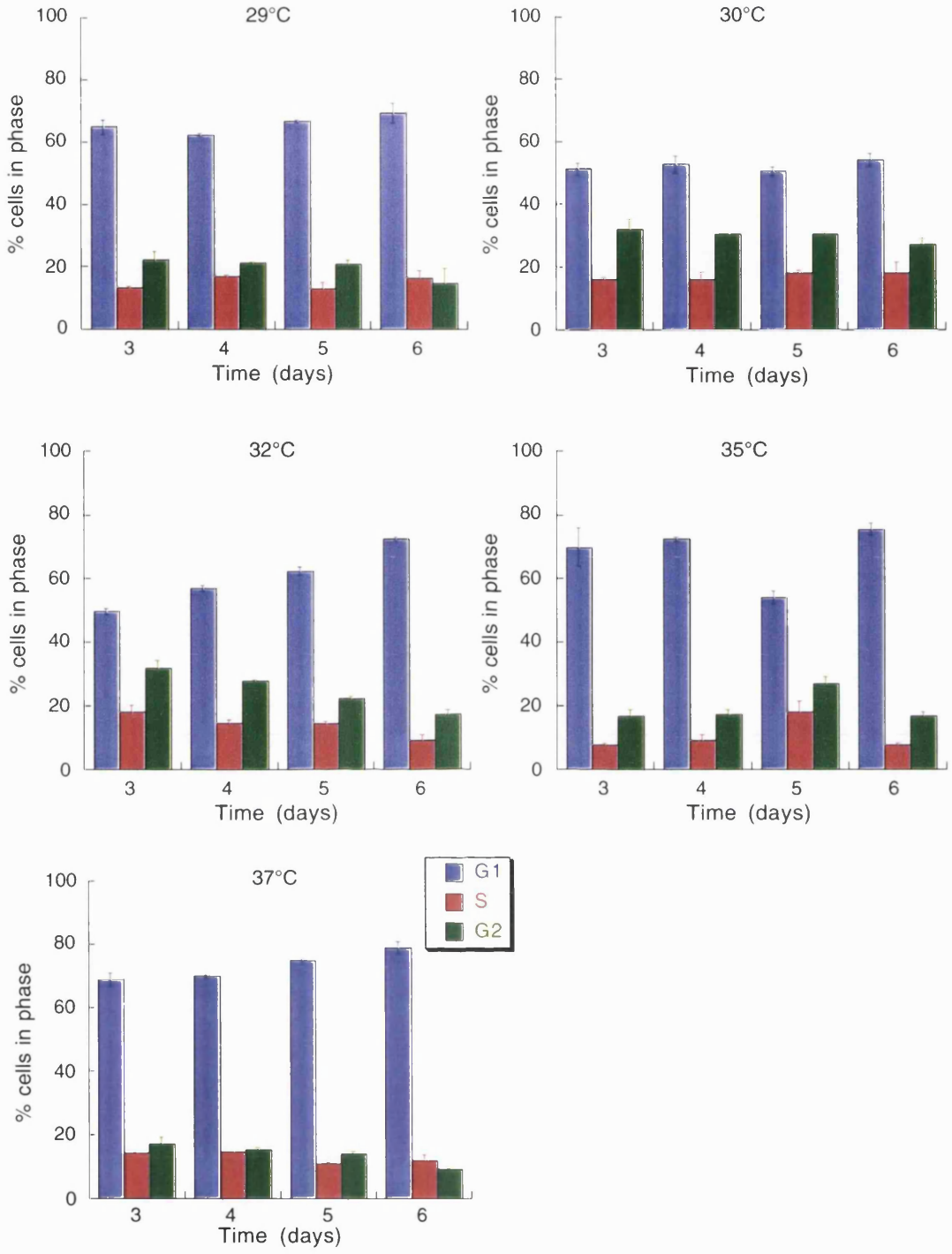

Figure 3.1 (continued)
(C) Shows percentage of RT112 cells in each stage of the cell cycle as determined by propidium iodide staining and analysis on a flow cytometer (plotted as the mean ± SEM).

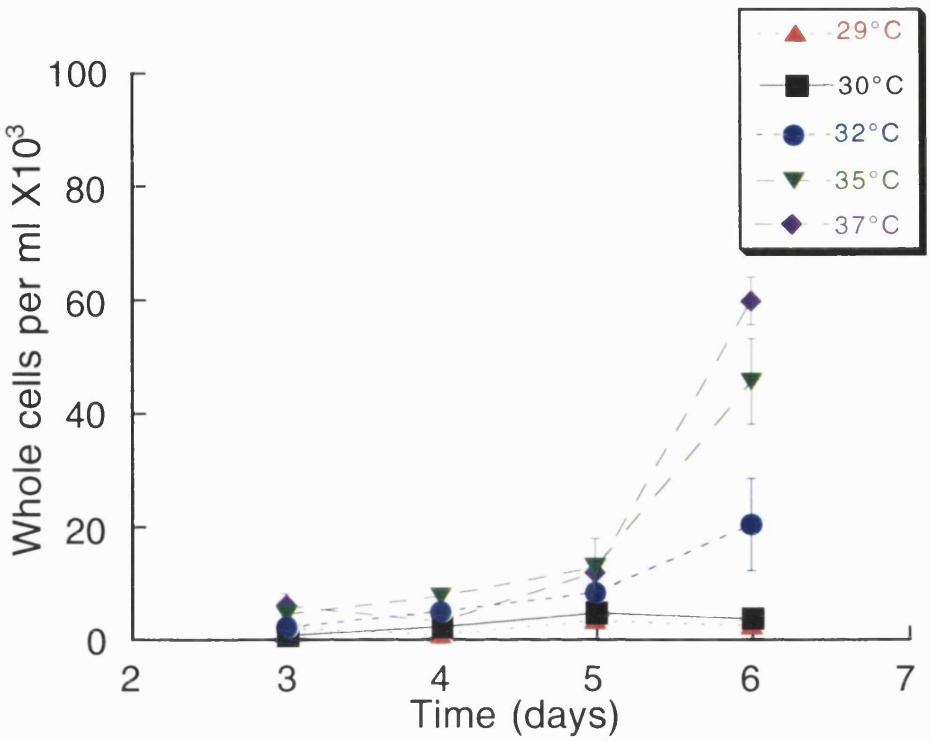

Figure 3.2
Shows the number of whole cells present per ml of supernatant removed from each flask as assessed by counting using a haemocytometer (plotted as the mean ± SEM).

	Duration (hours)		
Phase	37°C	32°C	30°C
Cell-cycle time (T_C)	24.7 ± 5.2	30.2 ± 7.1	56.5 ± 10.1
Time in G2 and M phases (T_{G2+M})	2.3 ± 0.4 (0.09)	3.2 ± 0.2 (0.1)	5.2 ± 1.3 (0.09)
Time in S phase (T_S)	11.9 ± 2.4 (0.48)	12.7 ± 3.5 (0.42)	26.4 ± 11.4 (0.47)
Time in G1/G0 ($T_{G1/G0}$)	10.5 (0.42)	14.3 (0.47)	24.9 (0.44)

Table 3.1
Shows the cell-cycle times and duration of each individual phase of RT112 cells (mean ± SEM) as assessed by labelling of BrdUrd and analysis on the flow cytometer. The fraction of total cell-cycle time occupied by each phase is indicated in brackets.

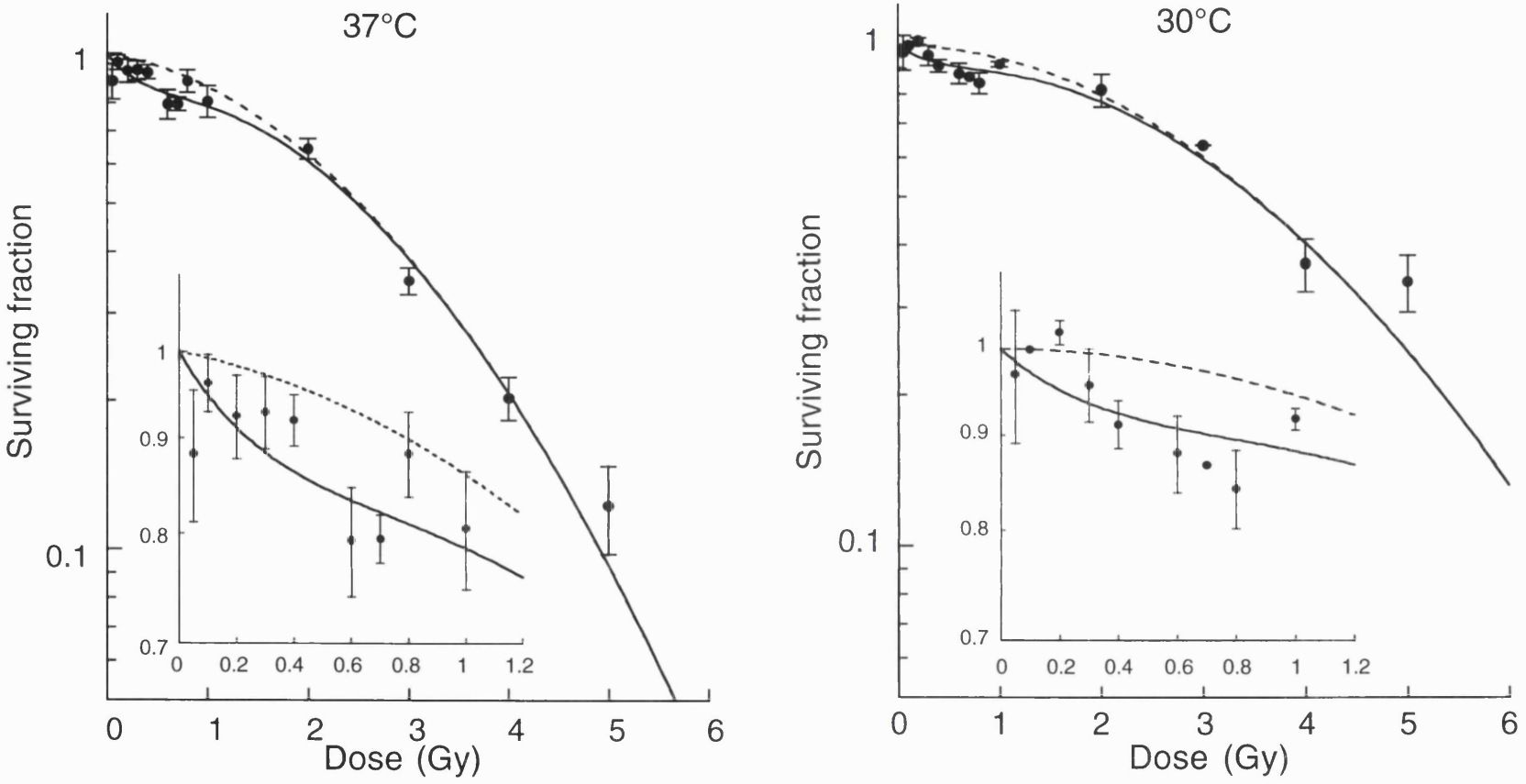

Figure 3.3
Shows the results of DMIPS experiments using RT112 human bladder carcinoma cells incubated at 37°C and 30°C. Plotted as mean ± SEM.
3 experiments were carried out for each. The data have been fitted to the Induced-Repair equation (solid line) and the broken line represents the Linear-Quadratic fit derived from high-dose IR parameters. The insert shows the low-dose region in greater detail.

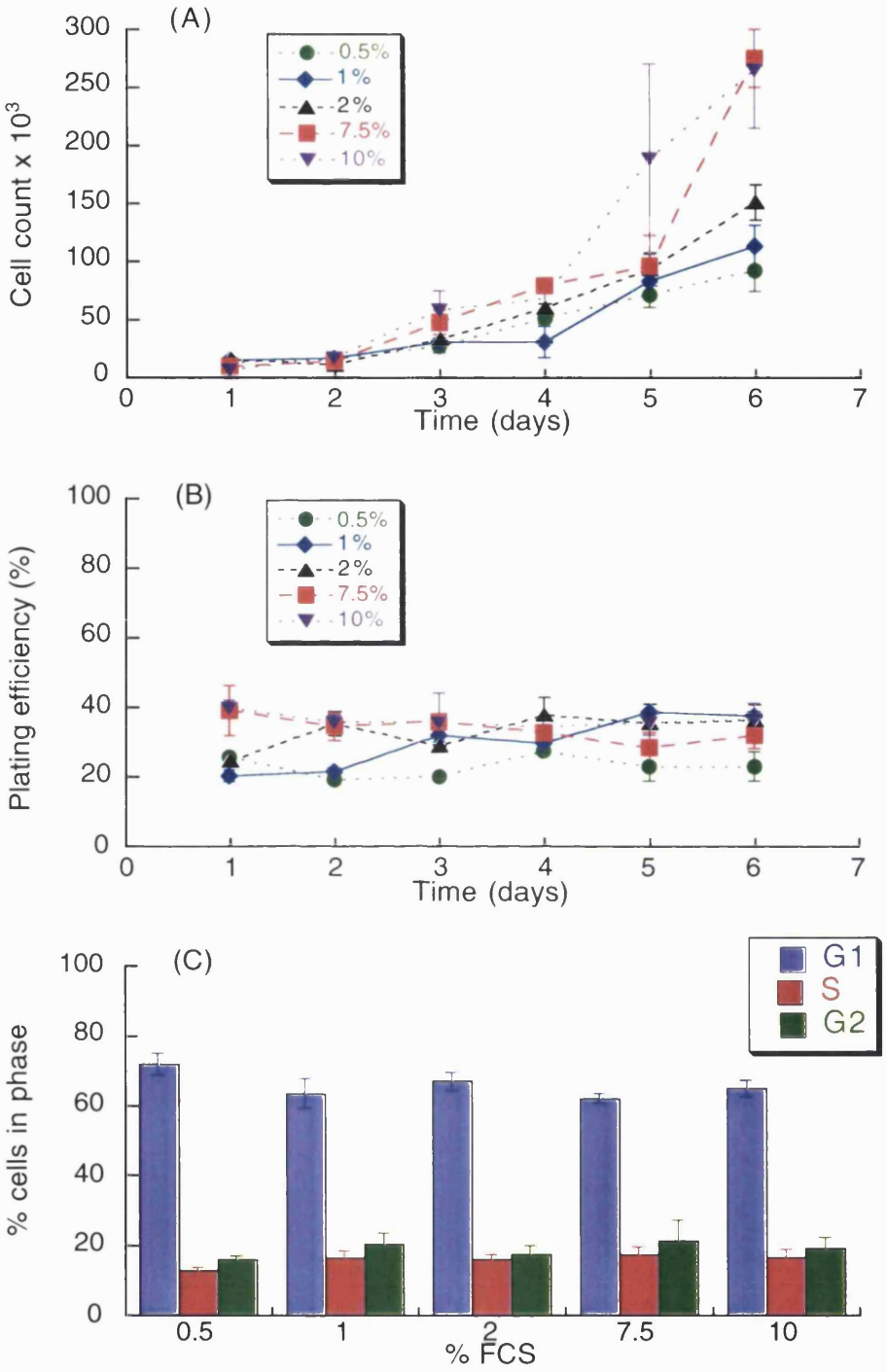

Figure 3.4
Shows T98G cells grown in monolayer culture in various concentrations of foetal calf serum (0.5, 1, 2, 7.5 and 10%) over a period of 6 days.
(A) Shows cell number
(B) Shows plating efficiency
(C) Shows proportion of cells in each phase of the cell cycle on day 6 for each FCS concentration as assessed by PI staining and detection on a flow cytometer

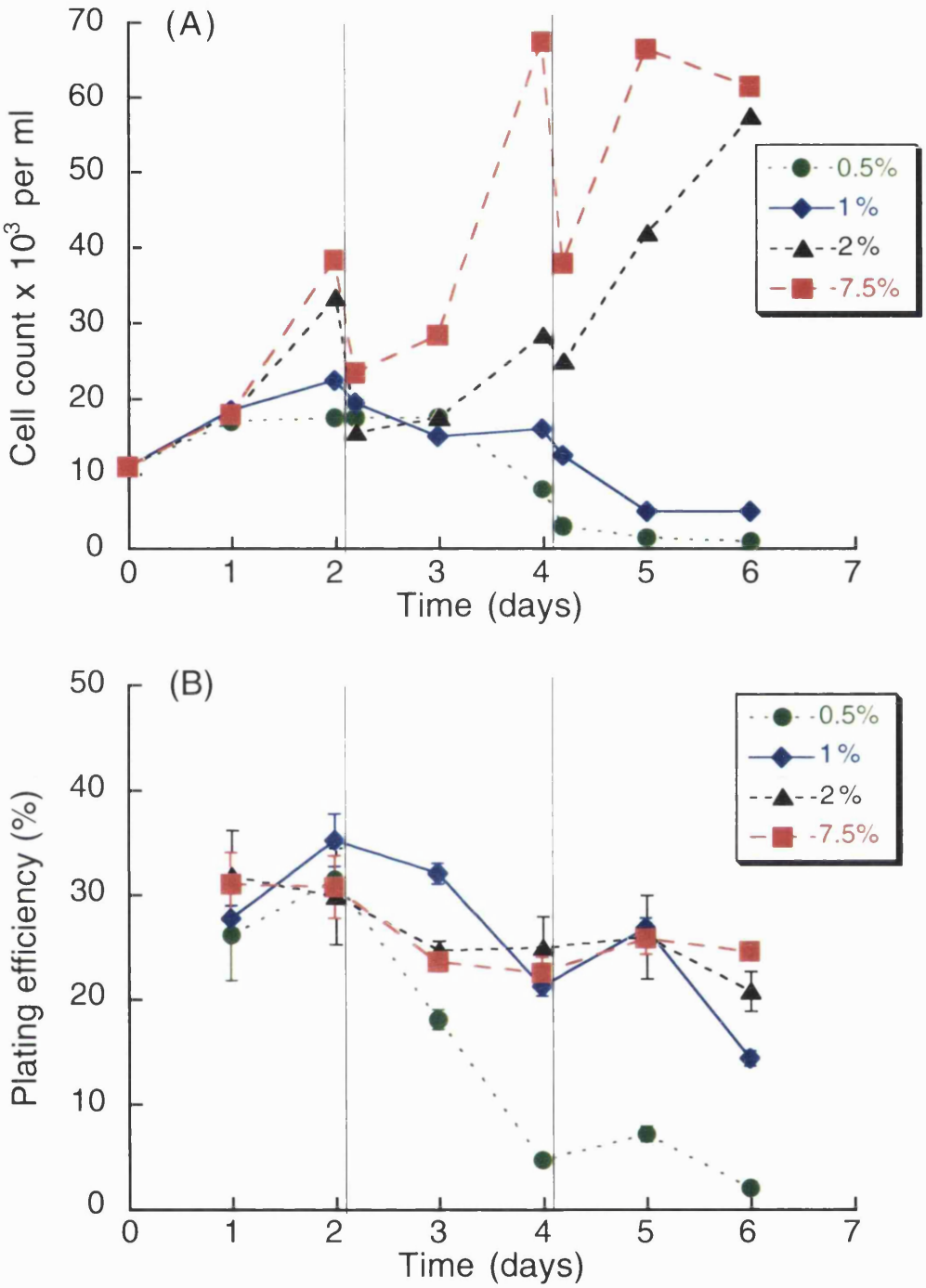

Figure 3.5
Shows T98G cells grown in suspension with various concentrations of foetal calf serum. A solid vertical line denotes a change in medium.
(A) Shows cell counts per flask (No error bars are shown as only one reading per sample was taken)
(B) Shows plating efficiency

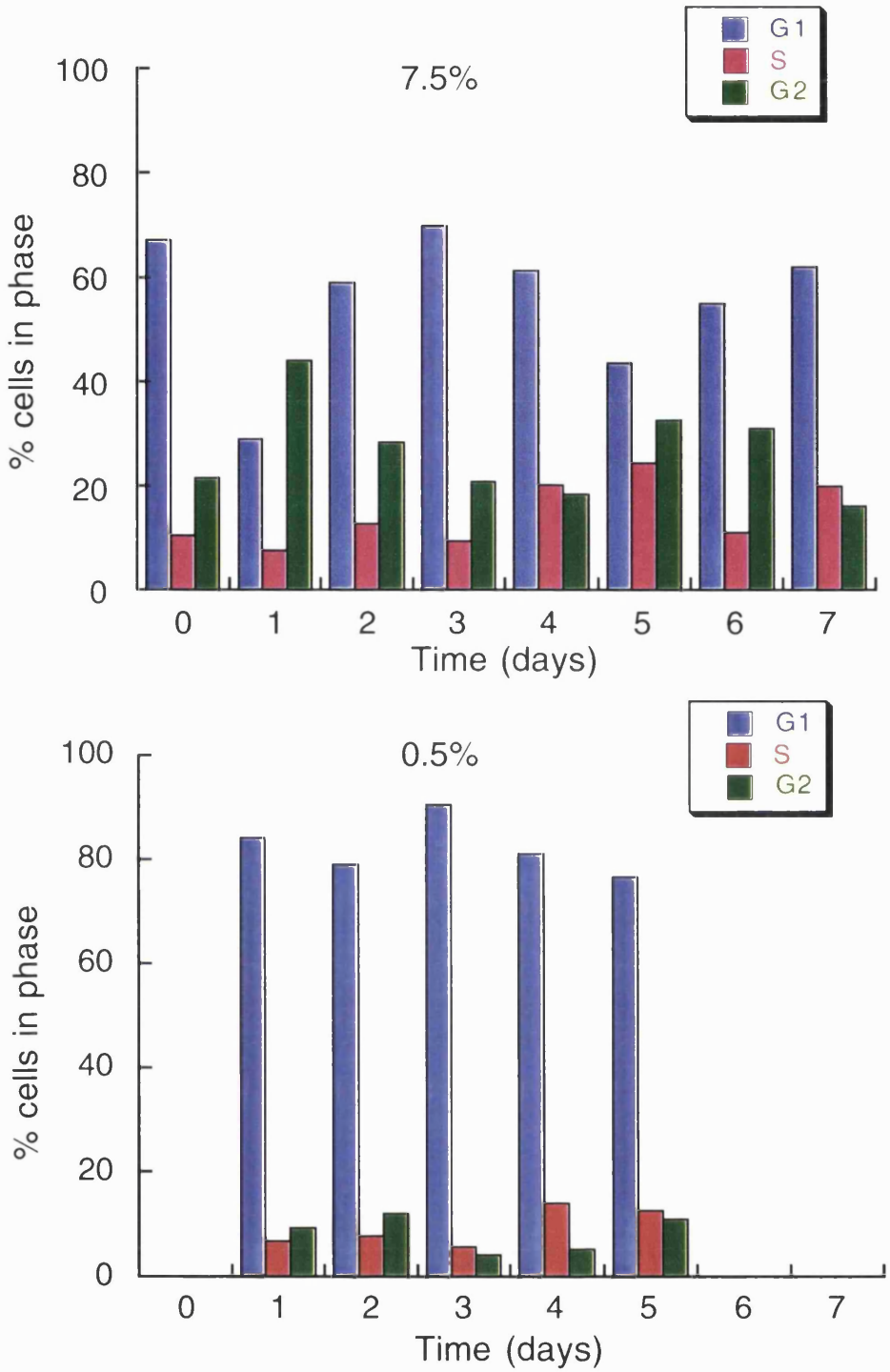

Figure 3.6

Shows the cell-cycle characteristics of T98G cells grown in 7.5% (upper panel) and 0.5% (lower panel) FCS in suspension culture. A medium change was carried out after 2 days and 4 days where the original medium was replaced by new medium containing the same serum levels. (No error bars are shown as only one reading per sample was taken).

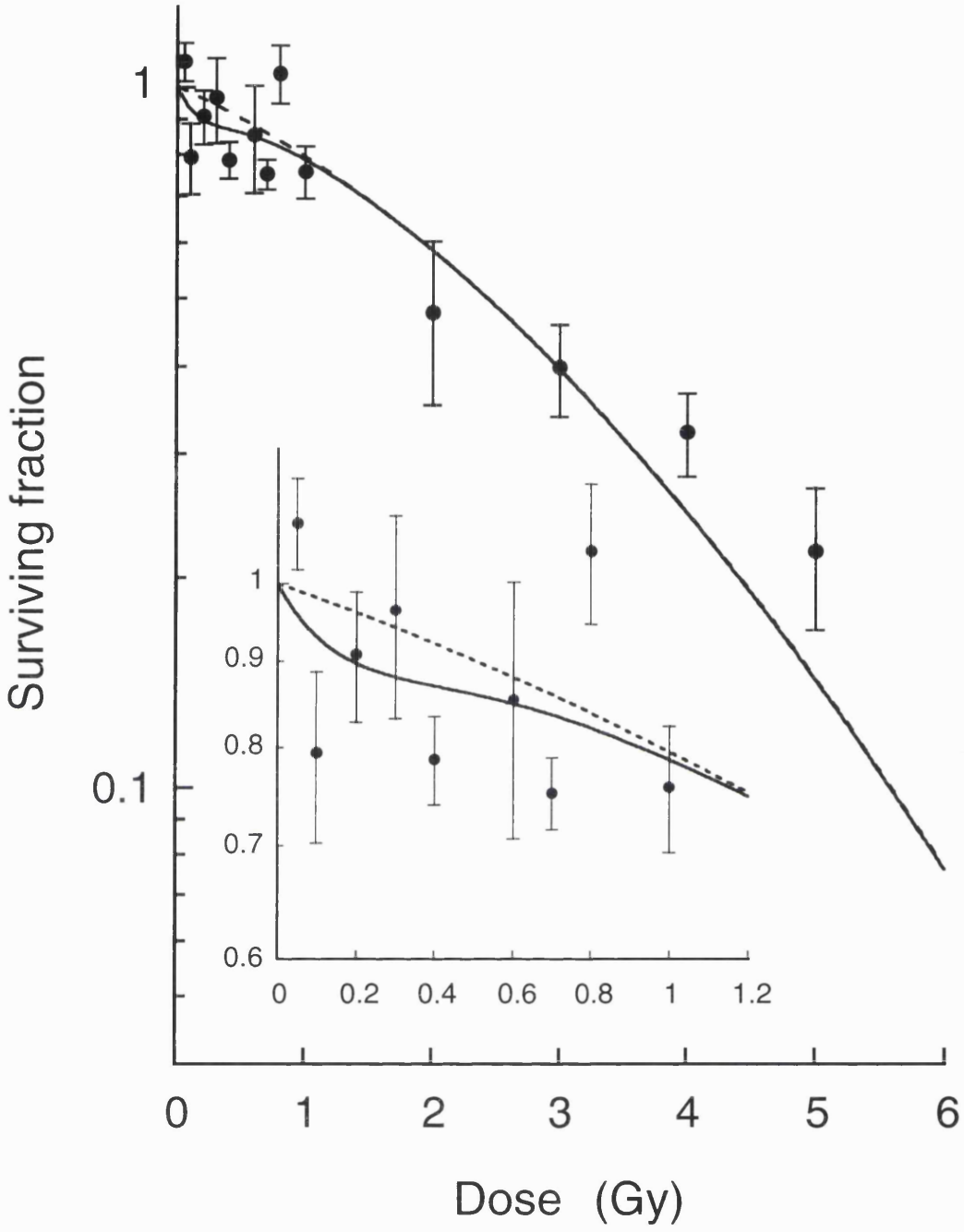

Figure 3.7
Shows the survival curve of T98G cells grown in 0.5% serum for 5 days. Data from 5 DMIPS experiments. Plotted as mean ± SEM. The data have been fitted to the Induced-Repair equation (solid line) and the broken line represents the Linear-Quadratic fit derived from high-dose IR parameters. The insert shows the low-dose region in greater detail. Data from S.C. Short.

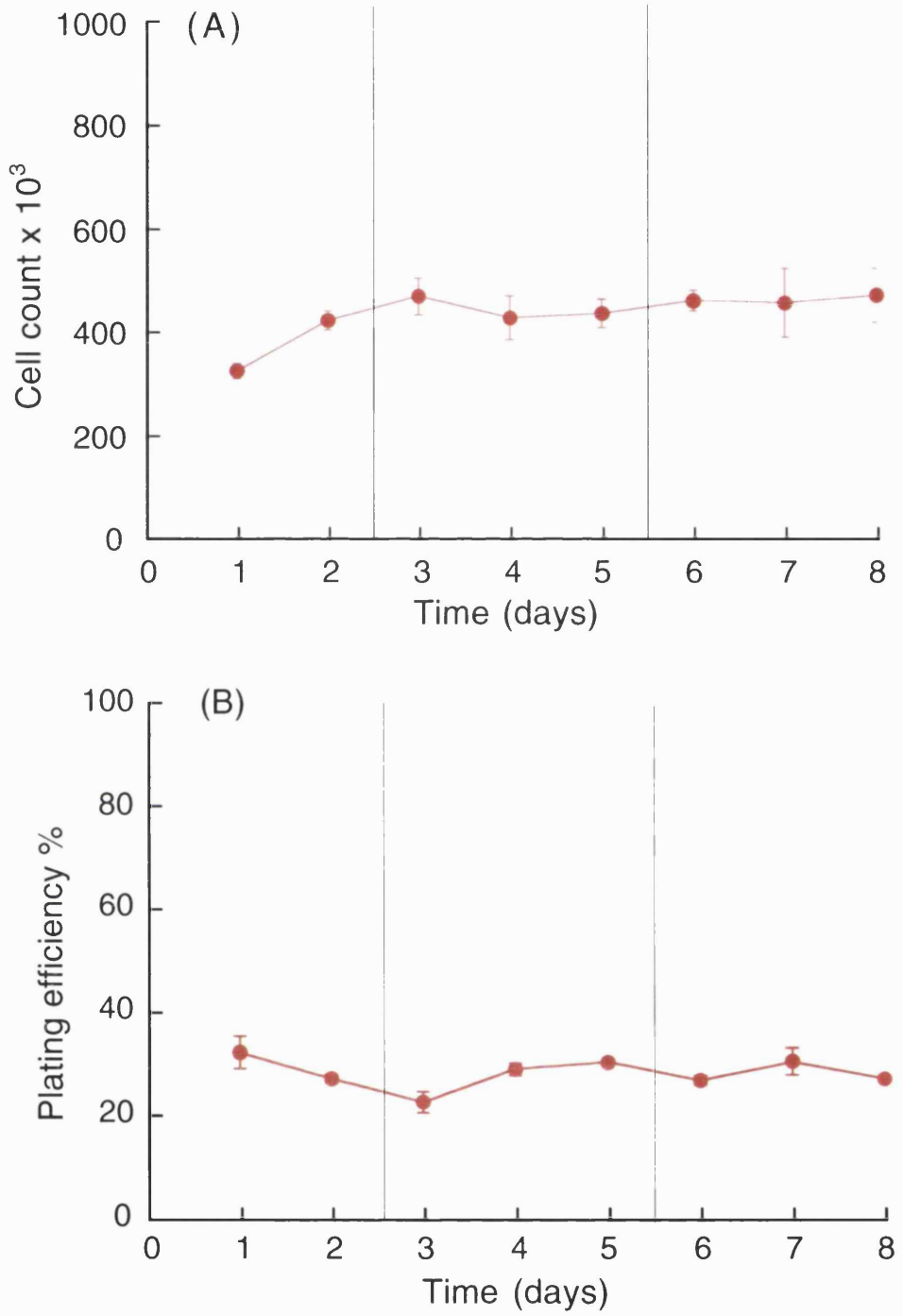

Figure 3.8
Shows T98G cells kept confluent in flasks for 8 days. Data plotted as mean ± SEM. Solid vertical lines denote the time when a medium change took place.
(A) Shows cell counts from flasks
(B) Shows plating efficiency

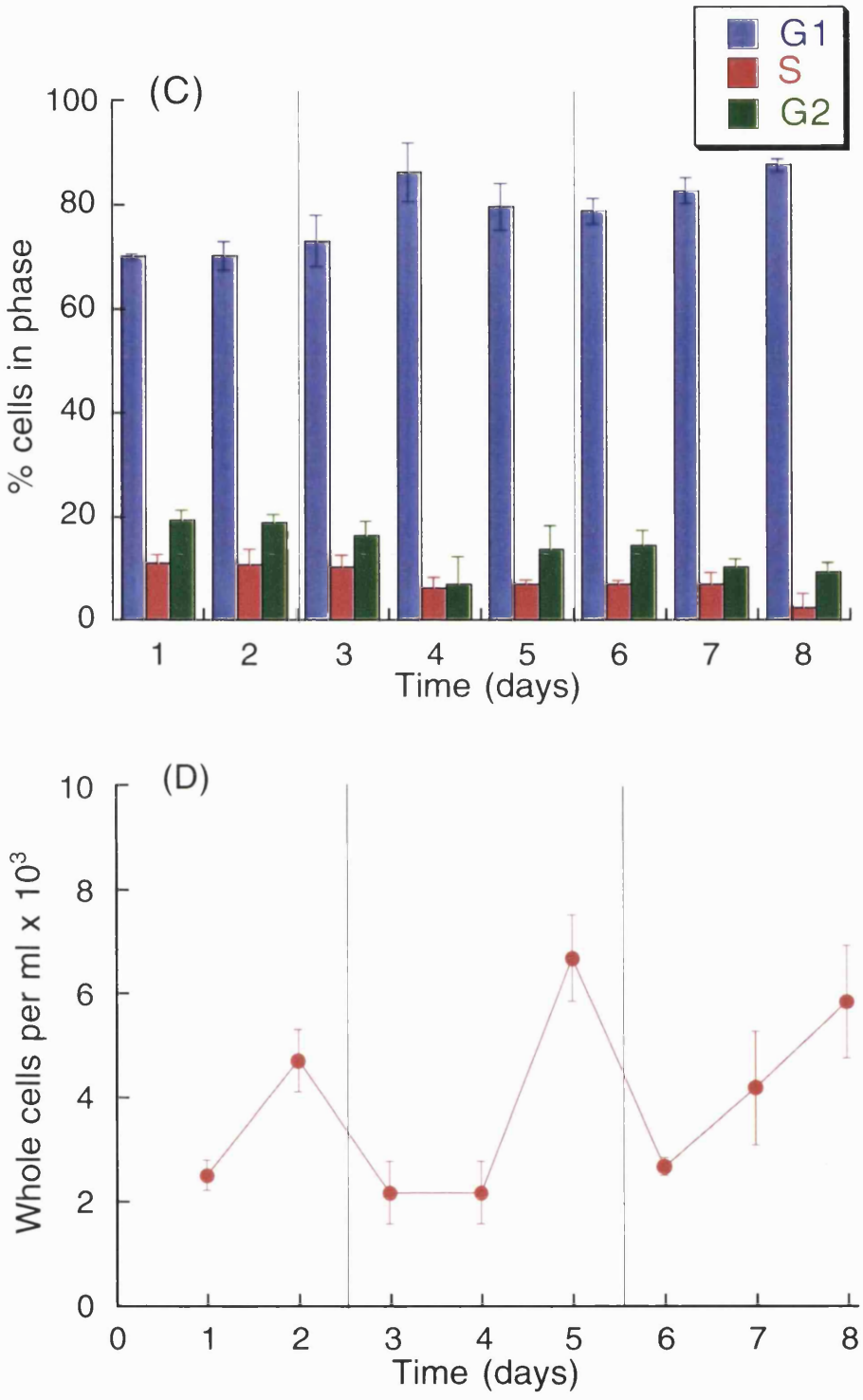

Figure 3.8 (continued)
(C) Shows fraction of cells in each stage of the cell cycle as determined by PI staining and detection using a flow cytometer
(D) Shows cells present in the supernatant

3.2.4 Discussion

Altering culture conditions to below optimum for cell growth was carried out in an attempt to slow or halt proliferation. This would allow LDR irradiations to be carried out over a long period without cell-cycle progression affecting cell survival. Changing the culture conditions were chosen as a method to do this, as opposed to chemical inhibitors of cell-cycle progression in order to minimise stress to the cells. Such stress itself may result in an induction of radioprotective mechanisms thereby affecting cell survival. The following methods were therefore tested to try to slow the cell cycle without causing a radioprotective effect: reducing the incubation temperature below 37°C, reducing the FCS concentration and growing T98G cells to confluence.

Figure 3.1A shows that as expected, RT112 cells grown at 37°C have a faster growth rate than cells grown at lower temperatures. Over time, cells incubated at 37°C will become overcrowded. This can be seen on day 4, as cells stop proliferating and begin to die and detach. This does not occur with cells incubated at lower temperatures. Presumably this would occur in these cultures at later times, but this was not tested. The plating efficiency is lower for cells incubated at lower temperatures indicating that they may be stressed, therefore resulting in lower survival. Results from analysis of the supernatant show that the constant cell number counted at the lower temperatures is not due to a balance of birth and death of cells, but is indeed due to slowing in proliferation. This evidence was supported up by the cell-cycle time increasing to 56.5 h at 30°C compared with 24.7 h at 37°C (Table 3.1). When the proportion of cells in each individual phase of the cell cycle was measured by flow cytometry, with increasing time, cells incubated at 37°C show a higher proportion of cells in the G1 phase of the cell cycle (Figure 3.1C). As the medium is changed frequently (every 3 days), this is likely to be due to overcrowding rather than nutrient depletion, which is inhibiting DNA synthesis and therefore preventing proliferation. In contrast with cells incubated at 37°C, the proportion of cells in each phase of the cell cycle seems unchanged over time at lower temperatures (see Figure 3.1C), suggesting that cells grown at lower incubation temperatures are not overcrowded.

RT112 cells grown at 30°C exhibit a HRS response to very low doses of radiation. This effect appears more marked compared with control cells grown at 37°C, with the α_s/α_r value for 30°C being 8.15×10^{16} compared with 7.91 for 37°C. The α_s/α_r value is used to determine the degree of HRS present based on the α predicted for the low-dose data from the high-dose data points (α_r) and the actual shape of the survival curve obtained by fitting the IR model (Section 1.7.3) to the data (α_s). The α_s/α_r value obtained for the 30°C data is very large, this may reflect an increase in radioresistance at higher doses compared with cells irradiated at 37°C rather than an increase in HRS/IRR. The SF_2 is 0.82 for 30°C, whereas the SF_2 value obtained for cells grown at 37°C was much lower at 0.66 and similar to the published data of 0.7 (Woudstra *et al.* 1996). A possible explanation may be

that at higher radiation doses, the increase in cell-cycle time allows more time for repair mechanisms to act prior to mitosis allowing more efficient repair of DNA damage compared with growth at 37°C. At lower doses however, these repair mechanisms may not be induced so repair is limited. It may be the contrast between an increased radioresistance at higher radiation doses and no repair at low doses that makes the HRS appear more marked at 30°C.

Reducing the serum concentration in T98G glioma cells slows proliferation both in monolayer and suspension culture. The concentration at which the cell number remains constant was not found for monolayer culture as cell growth was still occurring at 0.5% FCS, the lowest concentration examined. In suspension culture with 0.5% FCS, the cell number can be kept constant for 3 days, but at the cost of substantially reducing the plating efficiency. Analysis of the cell-cycle phase characteristics shows that by day 5, 76.6 ± 2.4% of cells are in G1. Experiments carried out with S. Short, have shown that T98G cells grown in suspension culture at 0.5% FCS exhibit HRS/IRR (Figure 3.7).

In 1979, Stein described a cell line that could enter a reversible G1 arrest when grown to confluence. Observations made in the experiments reported here confirmed this. The cell number could be kept constant for at least 8 days. The high-plating efficiency indicates that cells are not stressed due to overcrowding. Analysis of the supernatant also showed that this constancy in cell number was unlikely to be due to cells dropping off and regrowing. The cell-cycle profile shows that by day 8, 86.6 ± 1.2% of cells are in the G1 phase of the cell cycle. This is different to serum deprivation where the number in G1 was only 76.6 ± 2.4%. Using the DMIPS and cell-sort protocols, confluent T98G cells were shown to exhibit HRS/IRR (Figure 3.9).

Low-dose HRS is present in T98G cells growing both asynchronously and predominantly in the G1 phase. Table 3.5 summarises the data obtained using both the DMIPS and the cell sorter with cells which have been serum deprived (grown in 0.5% FCS), grown to confluence or using the cell sorter to directly select cells from a G1 population. The plating efficiency of G1 cells is slightly reduced compared with asynchronous cells in most cases, possibly due to added stress or because of an increase of cells in G0. The SF_2 is also lower in G1 cells compared with asynchronous cells in
3 out of 4 assays probably because the radioresistant S-phase population is not present to contribute to the SF_2. The degree of HRS/IRR varies considerably between assays. The confluence-arrested cells show a higher α_s/α_r value than asynchronous cells for both protocols. This may indicate that by putting cells into confluence arrest, different genes and proteins may be induced/ suppressed than in an asynchronous population. As with the serum-deprived cultures, confluent cells are not all in G1; only an average of 76.6% (serum deprived) and 88.7% (confluent), therefore they will have had some contamination

with cells from other cell-cycle phases contributing to the effects seen. Data is shown in Table 3.4 from the cell-sort protocol in which cells are labelled with the DNA stain, hoechst 33342, and are gated for cells in G1. These cells are then sorted into dishes, irradiated and assessed for cell survival. This method is "cleaner" than experiments carried out on confluent cultures, as the cells are taken from an asynchronous population and so are not undergoing stresses such as overcrowding or serum deprivation. However, the α_s/α_r value for this assay is lower than for an asynchronous population. This would suggest that other phases of the cell cycle may show HRS to a greater degree, contributing to the asynchronous value. Experiments carried out with J. Kelly in this laboratory have shown that HRS occurs in T98G cells to a greater degree in the G2/M phase of the cell cycle, with the S phase exhibiting the least HRS and the G1 phase being intermediate between S and G2/M. One hypothesis for this is that IRR, which indirectly reflects HRS is very strong in G2/M due to the conformation of the DNA before mitosis. In the G2/M phase, a double complement of chromosomes are lined up ready for mitosis. If a threshold level of damage is reached, repair can more easily take place through homologous recombination between sister chromatids. This repair pathway has been found to contribute critically in the S and G2/M phases of the cell cycle (Thompson and Schild 1999). Thus, the potential for high-fidelity repair is much greater than chromosomes in the G1 phase where there is no "lining up" of chromosomes and there is a single complement. IRR therefore is greater in G2/M. The small degree of HRS in the S phase may be due to the more open conformation of the DNA during DNA replication allowing easier accessibility of repair complexes. Alternatively, the signalling pathway which determines IRR may be strongly cell-cycle dependent. These hypotheses have yet to be tested.

If HRS/IRR is present in all phases of the cell cycle, it is extremely unlikely that HRS/IRR itself is due to a sensitive subpopulation of cells in one particular phase. This is in agreement with the conclusions of Marples and Joiner (1993) who partially synchronised V79 cells and still observed HRS.

The methods investigated to slow or halt proliferation, reducing incubation temperature, serum deprivation or confluence arrest would all be useful for studying cell survival at low-dose rates of radiation. Conditions have been determined under which plating efficiency and HRS/IRR effects are not compromised and any effects of cell cycle on the survival of cells after LDR exposures, can be ruled out.

3.3 Assessment of the prevalence of HRS/IRR to acute doses of radiation in cell lines *in vitro*

3.3.1 Introduction

One of the aims of this thesis is to test whether a similar phenomenon to HRS occurs after low dose-rate exposures. This chapter describes how cell lines were tested for the presence of HRS at low-acute doses. Chapter 4 describes the results of some of these cell lines after low dose-rate irradiation.

So far 25 cell lines have been tested for the presence of HRS/IRR; of these 5 have not shown the effect (Table 1.4). Two of these, the SW48 human colonic carcinoma and HX142 human neuroblastoma, have SF_2s of below 0.2 (SW48 0.179 and HX142 0.033) and this is extremely radiosensitive compared with the majority of other cell lines tested. The two other cell lines, that do not show HRS/IRR are relatively radioresistant (SF_2s of 0.62 U373MG and 0.63 SiHa). These are useful cell lines to study in comparison with HRS+ve lines as differences may elucidate possible mechanisms of HRS/IRR. For example SW48 is mismatch-repair deficient, suggesting that this may be involved in HRS/IRR. When the α_s/α_r values are plotted against SF_2 for all 25 cell lines (Figure 3.14), there is a general trend that the more radioresistant a cell line, the greater the degree of HRS observed, producing a positive trend with r= 0.199, although this was not significant, p= 0.333. This phenomenon therefore appears to be more characteristic of radioresistant cell lines. It is possible that the repair mechanisms involved in IRR in these cell lines also contribute to resistance seen at higher doses. This may explain why the cell lines with very low SF_2, SW48 and HX142, do not show HRS as they may have an absence of these repair mechanisms and are therefore radiosensitive along the whole survival curve.

Of the 25 cell lines studied, 8 have been assessed using the DMIPS protocol and 14 using the cell sorter. 3 cell lines have been tested using both methods. Short (1999b) studied HRS in a panel of human glioma cell lines with wide ranging radiosensitivity. They tested two of the cell lines used in this thesis, T98G and U373MG, using both protocols. As HRS/IRR was not present in U373MG no IR fit was obtained for comparison between protocols. The SF_2 was very similar using both protocols (0.62 DMIPS and 0.65 cell sort). Comparing the results from the two protocols tested on asynchronously growing T98G, the cell sorter gives a slightly higher SF_2 value (0.73 compared with 0.62). The degree of HRS/IRR is very similar for both protocols with the α_s/α_r value being 13.2 for the sorter and 14.3 for the DMIPS. These results suggest that the two methods are sensitive enough to detect the presence, or in the case of U373MG, the absence of HRS/IRR. The human colon adenocarcinoma cell line, HT29, has also been studied in two laboratories using the two protocols (Lambin *et al.* 1993, Wouters *et al.* 1996). The

results were consistent as they both indicated the presence of HRS/IRR, although a larger α_s/α_r value was obtained for the DMIPS data, 20.54 (Lambin *et al.* 1993) compared with the cell-sort protocol, 6.89 (Wouters *et al.* 1996).

3.3.2 Assessment of acute dose cell survival

Two methods were employed to accurately assess cell survival at very low-acute doses. They are described in detail in Section 2.6.

3.3.2.1 Dynamic Microscopic Image Processing Scanner

The DMIPS was used to obtain accurate survival curves (Section 2.6.1) for the following cell lines: RT112, T98G (confluent), A7, LNCaP, PC3 and DU145. A photograph of the DMIPS is shown in Figure 2.4.

Confluent T98G cells were grown as described in Section 2.4.1.3 and were used in these experiments only after they had been observed as confluent for 4 days.

During a single experiment 3000–3500 cells were plated into 16 flasks. This cell number gives a maximum number of logged locations in the C-scan program without allowing overlap of colonies when they reach >50 cells (see Section 2.6.1). 16 flasks are the maximum number that can be handled by this protocol in one day. Flasks were incubated with their lids loose with 5% CO_2 + 5% O_2 (balance N_2) for 40–60 min to allow the cells to attach. Attachment time varied between cell line. Flasks were then filled with fresh medium. Of the 16 flasks plated, 3 were 0 Gy controls which were sham irradiated on the X-ray set for 2 min. The other 13 flasks were irradiated as described in Section 2.5.1 at doses between 0.05 Gy and 5 Gy, with 1 flask per dose. After 10–14 days incubation, flasks were S-scanned. The number of days incubated depended on the doubling time of the cells. At least 3 experiments were carried out per cell line.

3.3.2.2 FACSVantage cell sorter

The following cell lines were assessed for cell survival using the cell-sort protocol (Section 2.6.2): T98G (confluent), A7, LNCaP, PC3 and DU145.

As with the DMIPS protocol, confluent T98G cells were observed as confluent for 4 days (Section 2.4.1.3).

The cell sorter was used to dispense a known number of cells into a 25 cm^2 flask containing 5 ml medium. The number of cells dispensed depended on the plating efficiency of the cell line and the dose of radiation the cells would receive. Sufficient cells were plated to give 100–200 surviving colonies per flask. 3–6 flasks were plated per dose point. 6–12 of these flasks were designated controls. Flasks were incubated for 2 hours

prior to irradiation. 2 hours allowed enough time to for cells to attach, but not enough for them to divide. Irradiations were carried out as described in Section 2.5.1 at doses between 0.05 Gy and 5 Gy. Flasks were then incubated for 10–14 days and then stained with crystal violet and colonies counted using a manual colony counter.

3.3.2.3 Data analysis

In DMIPS and cell-sort experiments the plating efficiency (PE) was calculated using the following equation:

$$\mathrm{PE} = \frac{\text{number of colonies}}{\text{number of cells plated}}$$

A mean PE value was calculated from the controls for each experiment. The surviving fraction (SF) for each flask was calculated using the following equation:

$$\mathrm{SF} = \frac{\text{PE of each flask}}{\text{mean control PE}}$$

Data from the experiments were plotted as SF versus dose, then fitted with the Linear-Quadratic (LQ) equation or the Induced-Repair (IR) equations.

The LQ equation models cell survival (SF) as:

$$\mathrm{SF} = \exp\left(-\alpha d - \beta d^2\right) \qquad \text{Equation 3.1}$$

where d is dose and α and β are constants.

The IR equation models cell survival (SF) as:

$$\mathrm{SF} = \left(\exp - \alpha_r \left(1 + \left(\frac{\alpha_s}{\alpha_r} - 1 \right) e^{-d/d_C} \right) d - \beta d^2 \right) \qquad \text{Equation 3.2}$$

where d is dose and α_s is the low-dose value of α (derived from the response at very low doses), α_r is the value of α extrapolated from the conventional high-dose response. d_c is a measure of the dose range over which low-dose HRS occurs (where the change from α_s to α_r is 63% complete) and β is a constant as in the LQ equation.

The two equations were fitted to all data points of the cell survival data using JMP® software to produce parameters which best fitted each model. Confidence limits were given as the estimate of uncertainty for each fit.

Data was also fitted to a modification of the LQ curve. This equation allows data points below the LQ model in the low-dose region force the curve fit down. This produces a fit which intercepts the survival-axis below 1 if significant HRS is present.

$$\mathrm{SF} = C\exp\left(-\alpha d - \beta d^2\right) \qquad \text{Equation 3.3}$$

Where C is the survival-axis intercept.

3.3.3 Results

Figures 3.9 to 3.13 show the results of low-dose cell-survival measurements made on 5 human tumour cell lines using the DMIPS and cell-sort protocols. These figures show the mean surviving fraction plotted against dose on a log-linear plot with the Linear-Quadratic and Induced-Repair curve fits superimposed on the data. Data were fitted to the LQ and IR equations, using all the raw data from each cell line to fit all parameters simultaneously. For the LQ curve, values of α and β obtained from the IR fitting were used to generate the dashed lines.

Tables 3.2 and 3.3 summarise the values of the surviving fraction at 2 Gy, mean plating efficiency obtained and the LQ and IR parameters acquired after fitting the data to the models. 95% confidence limits are shown where possible.

All cell lines showed substructure in the low-dose region, where an enhanced sensitivity was detected below that predicted by the LQ model. In all cases an LQ and IR fit was obtained, although confidence limits within 95% were not obtained for all parameters in each survival curve. Table 3.4 summarises the parameters obtained when data were fitted to a modification of the linear-quadratic model (Equation 3.3).

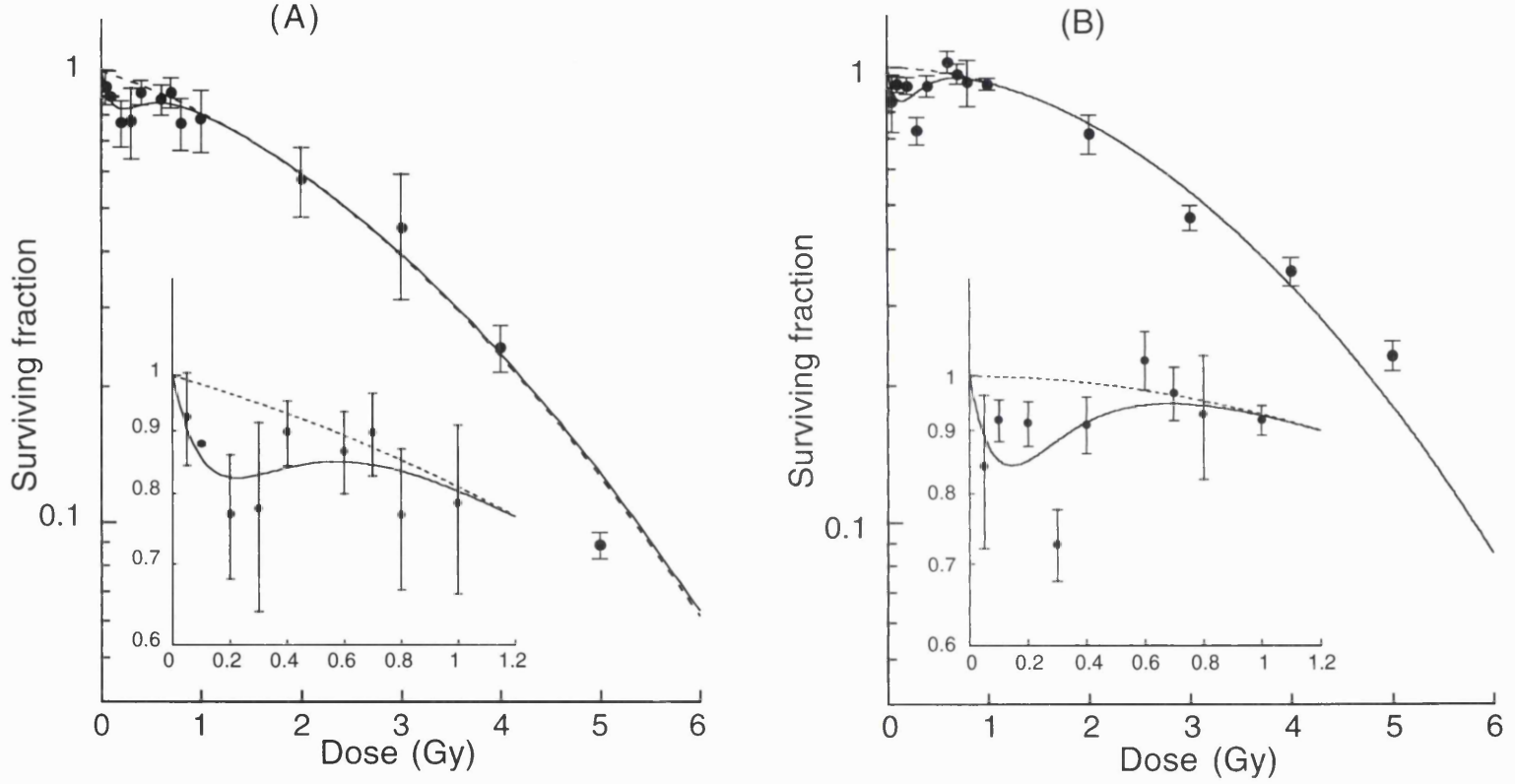

Figure 3.9
Shows the survival curve obtained after irradiating T98G, human glioblastoma cells observed as being in confluence for 4 days. Plotted as mean ± SEM. The data have been fitted to the Induced-Repair equation (solid line) and the broken line represents the Linear-Quadratic fit derived from high-dose IR parameters. The insert shows the low-dose region in greater detail.
(A) Results of 3 experiments using the DMIPS protocol.
(B) Results of 3 experiments using the cell-sort protocol

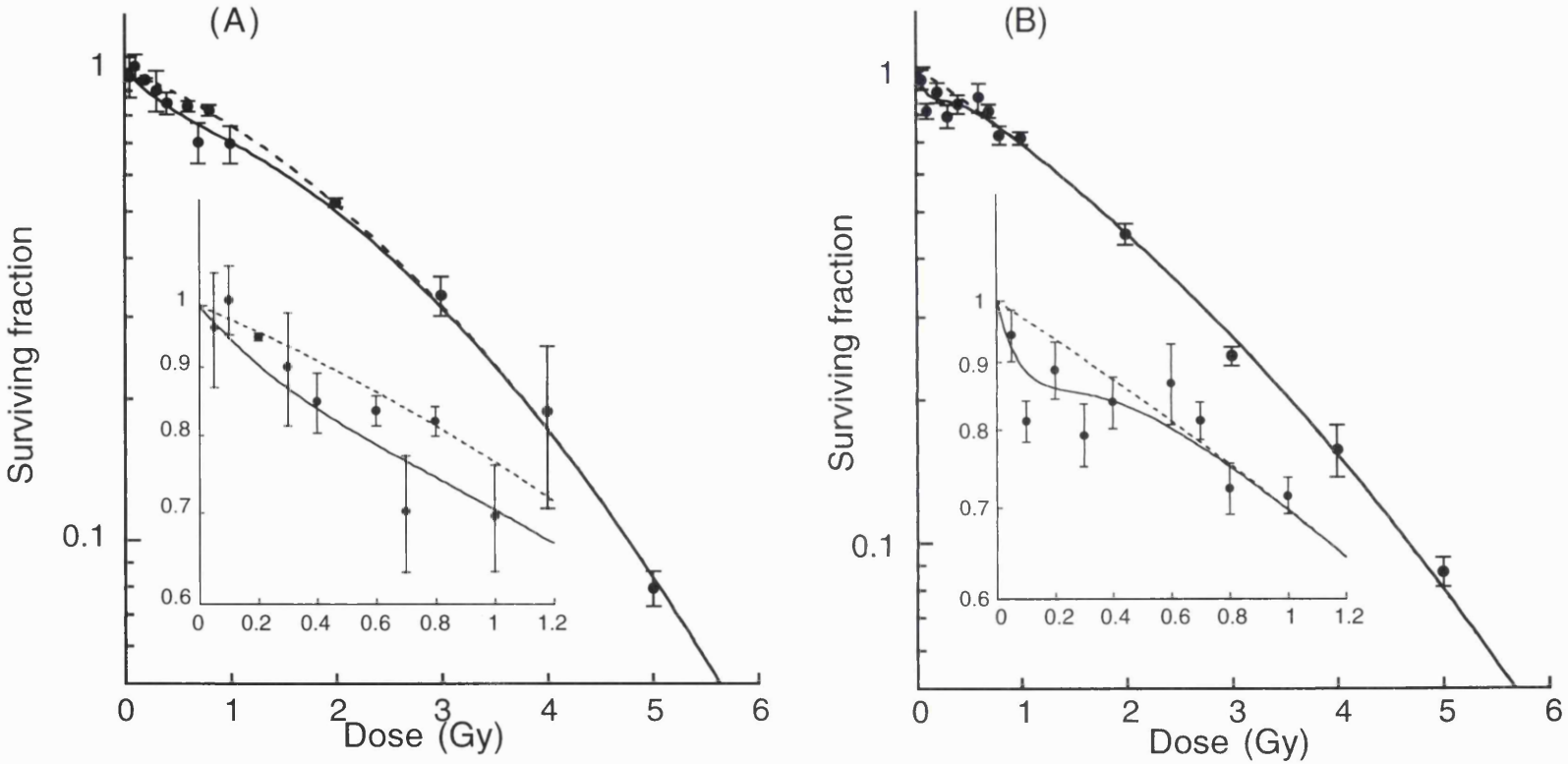

Figure 3.10
Shows the survival curve obtained from irradiating PC3 human prostate carcinoma cells. Plotted as mean ± SEM. The data have been fitted to the Induced-Repair equation (solid line) and the broken line represents the Linear-Quadratic fit derived from high-dose IR parameters. The insert shows the low-dose region in greater detail.
(A) Results of 5 experiments using the DMIPS protocol
(B) Results of 4 experiments using the cell-sort protocol

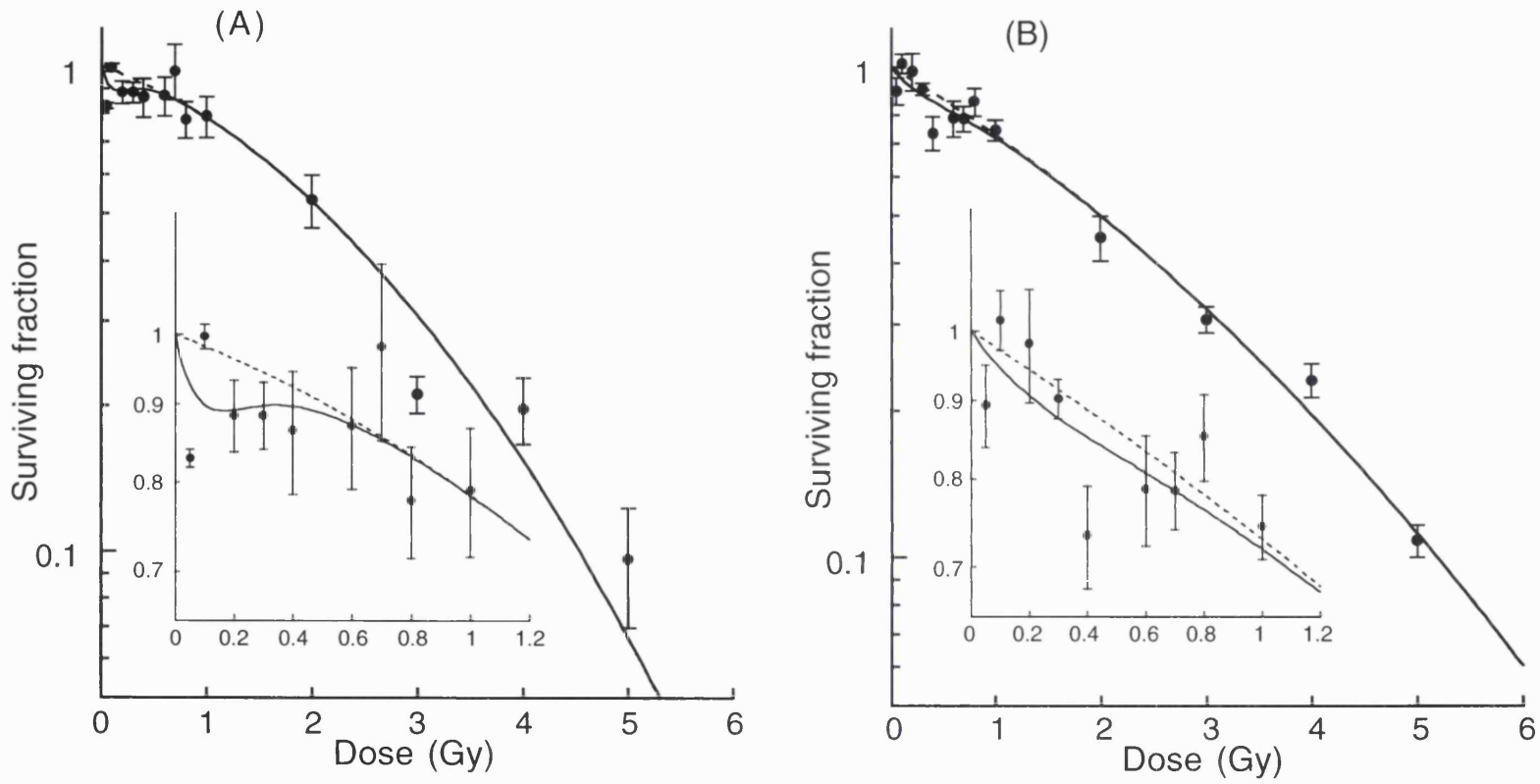

Figure 3.11
Shows the survival curve obtained from irradiating DU145 human prostate carcinoma cells. Plotted as mean ± SEM. The data have been fitted to the Induced-Repair equation (solid line) and the broken line represents the Linear-Quadratic fit derived from high-dose IR parameters. The insert shows the low-dose region in greater detail.
(A) Results of 3 experiments using the DMIPS protocol
(B) Results of 4 experiments using the cell-sort protocol

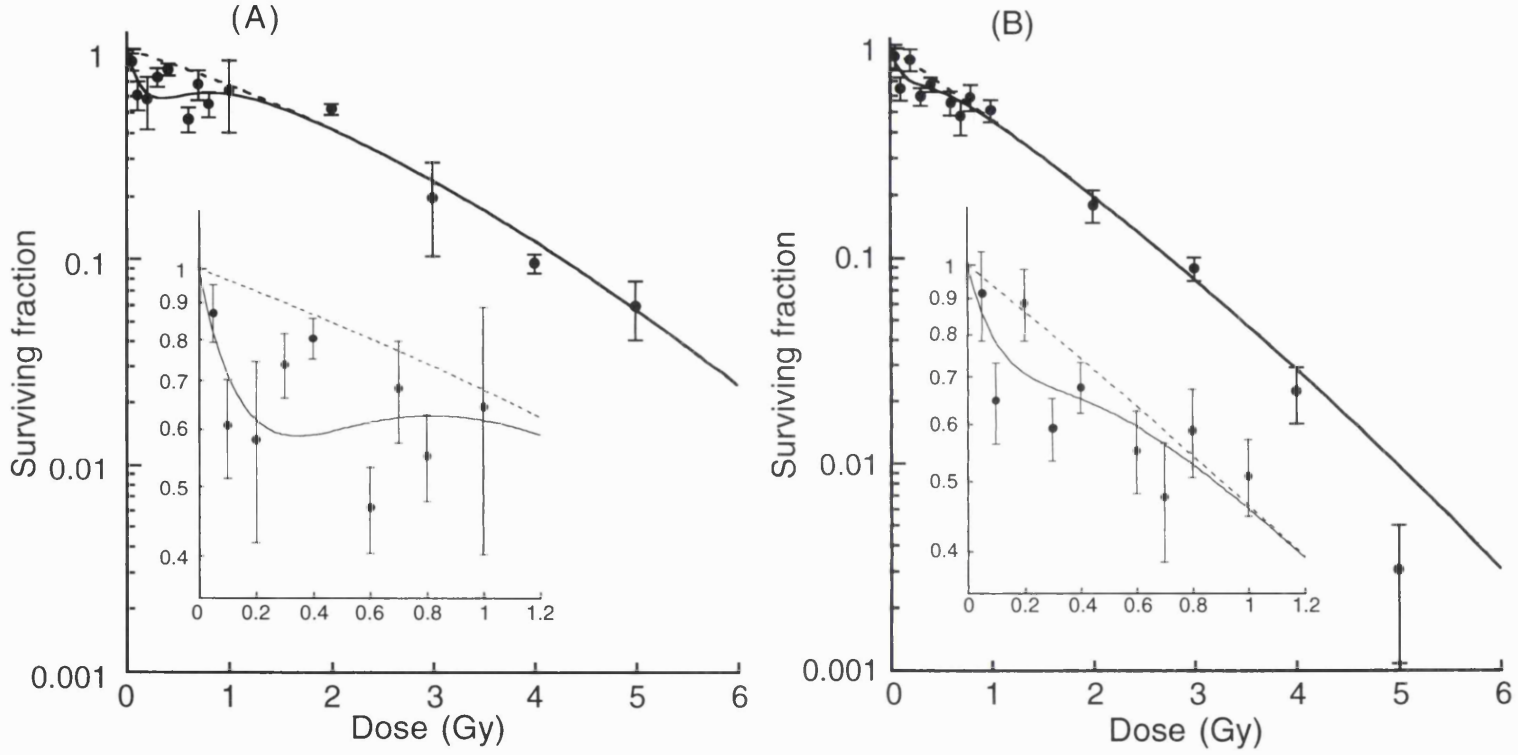

Figure 3.12
Shows the survival curve obtained from irradiating LNCaP human prostate carcinoma cells. Plotted as mean ± SEM. The data have been fitted to the Induced-Repair equation (solid line) and the broken line represents the Linear-Quadratic fit derived from high-dose IR parameters. The insert shows the low-dose region in greater detail.
(A) Results of 3 experiments using the DMIPS protocol
(B) Results of 4 experiments using the cell-sort protocol

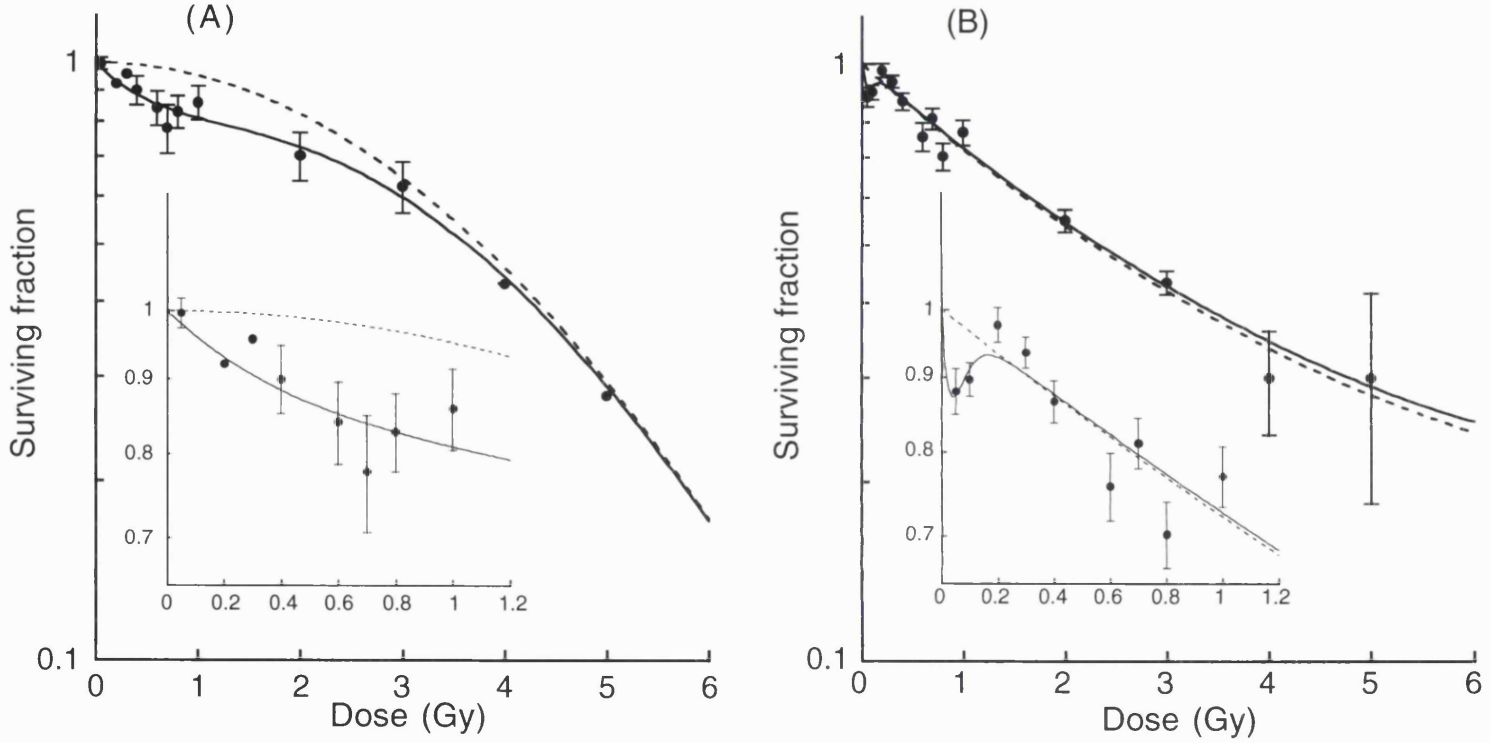

Figure 3.13
Shows the survival curve obtained from irradiating A7 human glioblastoma cells. Plotted as mean ± SEM. The data have been fitted to the Induced-Repair equation (solid line) and the broken line represents the Linear-Quadratic fit derived from high-dose IR parameters. The insert shows the low-dose region in greater detail.
(A) Results of 4 experiments using the DMIPS protocol
(B) Results of 3 experiments using the cell-sort protocol

Cell line	PE	Pub. SF_2	Exp. SF_2	LQ fit			IR fit					RMSE	
				α	β	α/β	α_s	α_r	dc	β	α_s/α_r	LQ	IR
RT112 (37°C) n=3	0.53 (0.031)	0.70 (Woudstra)	0.66	0.213 (0.139-0.287)	0.0391 (0.136-0. 676)	5.4	0.546 (0.237-)	0.069 (-0.5-0.185)	0.557	0.081 (0.048-0.24)	7.91	0.077	0.073
RT112 (30°C) n=3	0.61 (0.032)		0.82	0.0908 (0.32-0.151)	0.0334 (0.159-0.518)	2.7	0.326 (0.133-0.588)	4×10^{-18} (0.0735-0.074)	0.645	0.0562 (-0.0562)	8.15×10^{16}	0.07	0.064
T98G (confl) n=3	0.47 (0.027)		0.58	0.253 (0.115-0.399)	0.0244 (-0.019-0.076)	10.4	2.632 (0.81-6.48)	0.16 (-0.017-0.31)	0.177	0.0504 (0.035-0.107)	16.45	0.141	0.127
PC3 n=5	0.52 (0.030)	0.32 (Leith)	0.52	0.358 (0.259-0.46)	0.0158 (-0.019-0.0574)	22.7	0.599 (0.326-)	0.212 (-0.451)	0.643	0.0568 (-0.012)	2.82	0.099	0.099
DU145 n=3	0.48 (0.023)	0.60 (Leith)	0.53	0.208 (0.08-0.333)	0.0601 (0.012-0.127)	3.45	2.205 (0.228-)	0.167	0.12 (-0.988)	0.0751 (0.007-0.164)	13.2	0.119	0.116
LNCaP n=3	0.06 (0.012)	0.51 (Leith)	0.52	0.965 (0.535-1.53)	-0.1183 (-0.251-0.158)	8.16	4.736 (1.81-27.0)	0.337 (-1.05)	0.263 (0.0565-)	0.04721 (-0.15)	14.1	0.237	0.187
A7 n=4	0.59 (0.058)	0.59 (Taghian)	0.7	0.194 (0.117-0.272)	0.0012 (0.022-0.026)	164.7	0.423 (0.205-)	0.000056	1.05 (-0.988)	0.0488 (0.007-0.164)	7561.5	0.087	0.0807

Table 3.2

Shows summary data from DMIPS experiments on 6 human cell lines. Plating efficiency (PE) shown is the mean from all experiments (n) for each cell line. The SEM and upper and lower confidence limits where available are shown in brackets. Published and experimental (exp.) SF_2 are shown for comparison. LQ and IR fit parameters are those obtained by fitting the Linear-Quadratic and Induced-Repair equations to all of the data for each cell line. The RMSE is shown as a measure of 'goodness of fit' for each model to the data.

Cell line	PE	Pub. SF_2	Exp. SF_2	LQ fit			IR fit					RMSE	
				α	β	α/β	α_s	α_r	dc	β	α_s/α_r	LQ	IR
T98G (confl) n=3	0.29 (0.022)		0.72	0.0626 (-0.016-0.142)	0.0503 (0.025-0. 078)	1.24	3.239 (1.42-6.43)	0.0058 (-0.080-0.087)	0.142 (0.086-0.223)	0.067 (0.041-0.099)	562.7	0.165	0.151
PC3 n=4	0.63 (0.037)	0.32 (Leith)	0.45	0.358 (0.301-0.429)	0.0236 (-0.001-0. 052)	15.5	2.662 (1.36-4.95)	0.307 (0.227-0.375)	0.133 (0.079-0.233)	0.0435 (0.016-0.078)	8.67	0.098	0.088
DU145 n=4	0.30 (0.020)	0.60 (Leith)	0.45	0.334 (0.251-0.418)	0.016 (-0.012-0.05)	20.9	0.662 (0.417-0.911)	0.283 (0.194-0.393)	0.311 (0.109-43.62)	0.0308 (-0.013-0.058)	2.34	0.161	0.161
LNCaP n=4	0.029 (0.0015)	0.51 (Leith)	0.18	0.976 (0.744-1.206)	-0.067 (-0.158-0.127)	14.4	3.763 (1.43-16.71)	0.73 (0.73-1.086)	0.18 (0.0408-0.18)	0.0389 (-0.123-0.039)	5.16	0.291	0.285
A7 n=3	0.16 (0.025)	0.59 (Taghian)	0.55	0.347 (0.292-0.402)	-0.0211 (-0.041-0.002)	16.4	9.79 (3.13-9.79)	0.337 (0.283-0.39)	0.036 (0.016-0.067)	-0.0179 (-0.038-0.005	29.05	0.123	0.118

Table 3.3

Shows summary data from cell-sort experiments on 5 human cell lines. Plating efficiency (PE) shown is the mean from all experiments (n) for each cell line. The SEM and upper and lower confidence limits where available are shown in brackets. Published and experimental (exp.) SF_2 are shown for comparison. LQ and IR fit parameters are those obtained by fitting the Linear-Quadratic and Induced Repair equations to all of the data for each cell line. The RMSE is shown as a measure of 'goodness of fit' for each model to the data.

Cell Line	Protocol	Survival-axis intercept (C)	95% confidence limits
RT112 (37°C)	DMIPS	0.930	0.882-0.979
RT112 (30°C)	DMIPS	0.964	0.917-1.012
T98G (confl)	DMIPS	0.872	0.786-0.961
T98G (confl)	Cell sort	0.888	0.827-0.949
PC3	DMIPS	0.950	0.879-1.023
PC3	Cell sort	0.904	0.864-0.945
DU145	DMIPS	0.917	0.835-0.999
DU145	Cell sort	0.967	0.908-1.028
LNCaP	DMIPS	0.660	0.510-0.822
LNCaP	Cell sort	0.823	0.711-0.936
A7	DMIPS	0.950	0.876-1.026
A7	Cell sort	0.950	0.913-0.987

Table 3.4

Shows the results of fitting cell-survival data to the equation $SF = C\exp\left(-\alpha d - \beta d^2\right)$. This produces a Linear-Quadratic curve which intercepts the survival axis below 1 if significant HRS is present. This is the case in all the cell lines tested.

Assay		*DMIPS Asynchronous	*DMIPS G1 arrested Serum deprivation	DMIPS G1 arrested confluence	†Cell sort Asynchronous	**Cell sort G1 sort	Cell sort G1 arrested confluence
SF_2		0.62	0.55	0.58	0.74	0.58	0.72
PE		0.31 (0.1174)	0.25 (0.067)	0.47 (0.027)	0.39 (0.078)	0.23 (0.055)	0.29 (0.022)
IR parameters	α_s	1.16 (0.19-5.8)	0.39	2.63 (0.81-6.48)	1.56 (0.77-2.9)	0.73 (0.39-10.2)	3.24 (1.42-6.43)
	α_r	0.081 (-0.22-0.38)	0.27	0.16 (-0.017-0.31)	0.12 (0.071-0.16)	0.17 (-0.42)	0.0058 (-0.080-0.087)
	β	0.075 (-0.02-0.13)	0.015	0.05 (0.035-0.107)	0.019 (0.0066-0.032)	0.036 (-0.031-)	0.067 (0.041-0.099)
	dc	0.39	0.29	0.18	0.21 (0.13-0.36)	0.67 (0.034-)	0.142 (0.086-0.223)
	α_s/α_r	14.3	1.44	16.45	13.2	4.3	562.7
LQ parameters	α	0.26 (0.08-0.46)	0.19 (0.048-0.33)	0.25 (0.115-0.399)	0.15 (0.11-0.2)	0.37 (0.28-0.45)	0.063 (-0.016-0.142)
	β	0.019 (-0.04-0.102)	0.041 (-0.0046-0.099)	0.024 (-0.019-0.076)	0.0107 (-0.0007-0.023)	-0.014 (-0.038-0.014)	0.0503 (0.025-0.078)
	α/β	13.7	4.6	10.4	14.0	26.43	1.25

Table 3.5
Shows the summary data from cell-sort and DMIPS experiments on T98G human glioma cell line under cell-cycle modified conditions. Plating efficiency (PE) and SF_2 is shown for each protocol. The SEM and upper and lower confidence limits where available are shown in brackets. LQ and IR fit parameters are those obtained by fitting the Linear-Quadratic and Induced-Repair equations to all of the data for each protocol. Data from *S. Short, †M. Woodcock and **J. Kelly.

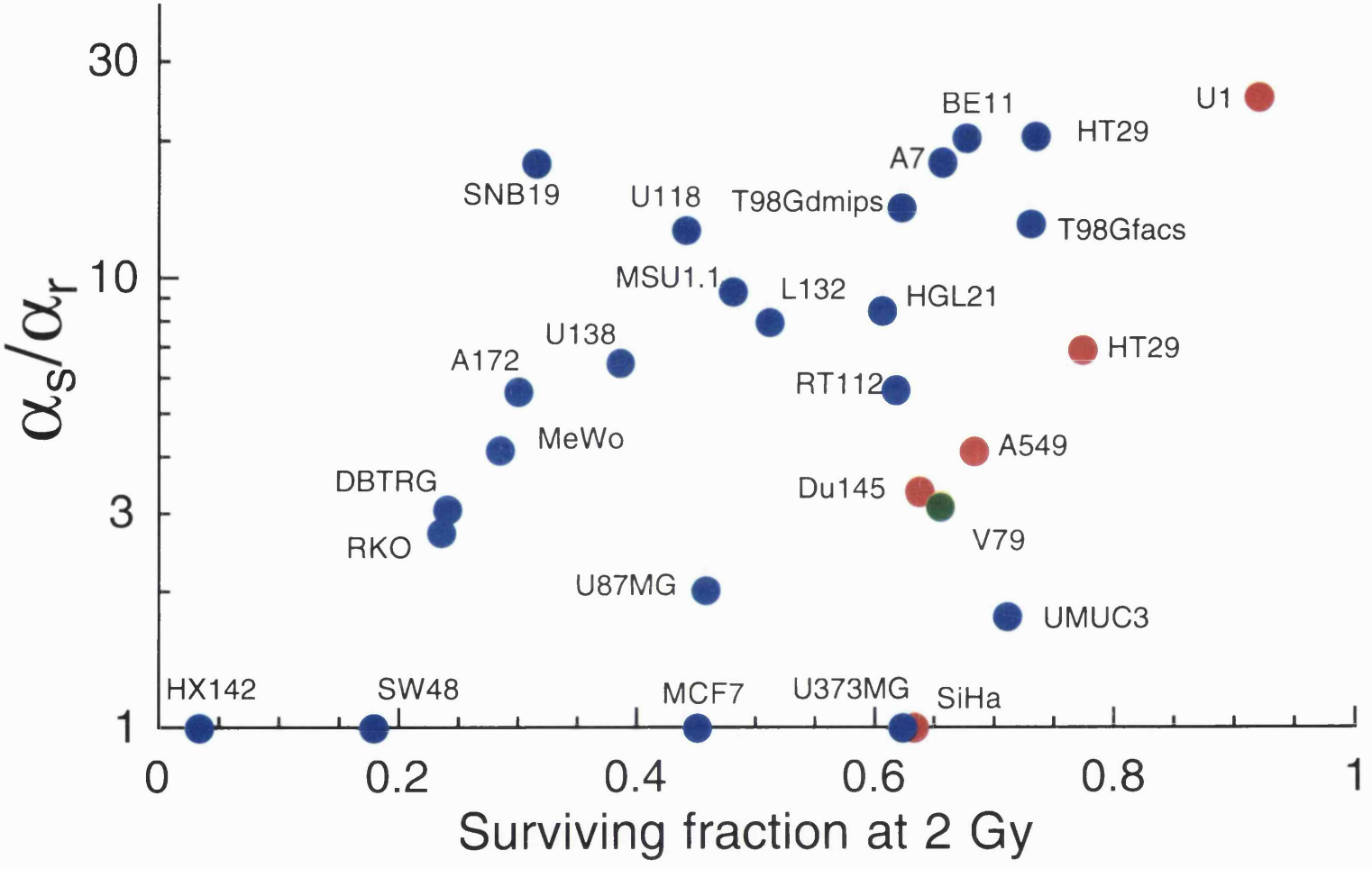

Figure 3.14
Shows the relationship between surviving fraction at 2 Gy (SF_2) and the degree of HRS/IRR measured, that is the α_s/α_r value for cell lines tested *in vitro*. Blue circles represent human cell lines tested in the Gray laboratory, UK, red circles represent human cell lines tested in the British Columbia Research Centre, Vancouver, Canada, and the green circle represents a rodent cell line tested at the Gray Laboratory.

3.3.4 Discussion

HRS was present in all cell lines using both techniques. This was in agreement with previously published data for the DU145 cell line which was shown by Wouters (1996) to exhibit HRS using the cell-sort protocol. The other cell lines PC3, LNCaP, A7 and confluent T98G, have not previously been tested for low-dose survival using the cell-sort technique, although the human glioblastoma T98G has been shown to exhibit HRS/IRR in asynchronous growth and under serum deprived conditions (Short *et al.* 1999a). Using the DMIPS protocol, only the human glioblastoma A7 out of the cell lines studied in these experiments had previously been tested for HRS/IRR (Short *et al.* 1999b). The results obtained in the present experiments were in agreement with that study that HRS/IRR was present. Although a negative value of β was acquired for A7 cell-sort data fitted to the IR model, when the data were fitted to Equation 3.3 (see Table 3.4) which incorporated the intercept, C, in the survival axis, C was significantly below 1, in all cases, showing that in these experiments HRS was present.

DU145 was more radiosensitive along the whole survival curve using both protocols (SF_2s of 0.45 cell sort and 0.53 DMIPS) compared with the published values of 0.64 (Wouters *et al.* 1996) who used the cell-sort protocol and 0.60 (Leith *et al.* 1993). However, different medium was used to culture the cells and possibly different plastic culture vessels. Wouters also had a slightly different protocol when using the cell sorter. In the present experiments the cells were sorted directly into flasks. Wouters sorted the cells directly into test tubes with 5 ml medium and poured their contents into flasks. In this protocol, cells may have been left behind resulting fewer actual cells being placed in the flask than were counted into the tube. If this was done inconsistently between samples more errors would have been introduced. The method described in this thesis was more accurate as a known number of cells was plated into he actual dish used to grow the colonies. This increased handling error using the Wouters protocol, may have also accounted for the differences in PE and radiosensitivity. The size of the HRS/IRR response was slightly greater in the Wouters data as the α_s/α_r value was 3.35 which was larger than the cell-sort value of 2.34 for these experiments. This follows in the general trend of the cell lines tested so far where the higher the SF_2 the greater the degree of HRS/IRR as measured by the α_s/α_r value.

Although both published data (Short *et al.* 1999b) and the present experiments, agree that HRS/IRR occurs in the A7 cell line using the DMIPS protocol, the shape of the survival curve in the low-dose region was very different. In the DMIPS experiments carried out by Short *et al.* (1999b), a significant value of 18.3 for α_s/α_r was obtained for A7. In the present experiments the α_s/α_r value for A7 was very high (7560) due to the α_r being very low, but this was not significant. The values for α_s and α_r obtained in these experiments did not fall within the 95% confidence limits of the Short data. This would suggest a

difference between the two data sets. The SF_2 value was also slightly higher in these experiments. As the work in this publication was carried out in the same laboratory, differences cannot be explained by difference in culture conditions or experimental protocol. Variability may be introduced when carrying out these experiments on this particular cell line as the cells do not form tight discrete colonies, but are spread out, diffuse which may lead to greater errors when counting. However, the cell-sort data for A7 obtained in the present experiments show a significant value of α_s/α_r to be 29.1 and this is within the 95% confidence limits of the Short data.

Prostate carcinoma cell lines, PC3 and LNCaP have not previously been tested for survival at low doses before. LNCaP had a very low SF_2 compared with published values for both protocols. Although great care was taken, this cell line was very difficult to use as the cells were not firmly attached to the growth surface of the culture flask. Those attached could be disturbed easily. It is possible that this may have occurred inconsistently between flasks in these experiments reducing the observed surviving fraction. In contrast to this, PC3 had a higher SF_2 using both protocols than published values. There could be several reasons for this. First, it is possible that handling the cells in a slightly different way may have altered their low-dose response, for example by exposing them to non-specific cellular stress such as pH changes during the experiment. Second, it is possible that because a different passage number and origin of PC3 cells was used, their radiation response was different.

The two protocols yielded different shaped survival curves, often with one protocol producing an increase or decrease in plating efficiency, radioresistance and amount of HRS compared with the other. This varied between cell lines. The α_s/α_r value obtained for each survival curve gives a measure of the increase in sensitivity at low doses. Published data on the human colon carcinoma, HT29, from two different laboratories allows a comparison between the two techniques (Lambin *et al.* 1993, Wouters *et al.* 1996). The survival curve obtained using the DMIPS protocol showed a higher α_s/α_r value than measured with the cell sorter. Three of the 5 cell lines in this study, DU145, LNCaP and A7 also showed a higher α_s/α_r value when survival was assessed using the DMIPS protocol rather than the cell sorter. The reverse was true for PC3 and confluent T98G, and published values for asynchronous T98G (Short *et al.* 1999a) showed that the cell-sort protocol produced a very similar α_s/α_r value (13.2) to the DMIPS (14.3). The sensitivity of the overall survival curve also varied between protocols, with the DMIPS producing a trend towards a slightly more resistant response in 4 out of the 5 cell lines tested although this was not significant in any of these. Published data for the T98G cell line agrees with these data that the SF_2 was higher with the cell-sort protocol (Short *et al.* 1999a). There were also large differences in the plating efficiencies between the different protocols with all, but the PC3, having a higher PE using the DMIPS technique. This effect was quite dramatic depending on the cell line, with the A7 PE being 0.16 using the cell-sort protocol

which was more than 70% lower than the PE for the DMIPS at 0.59. Lowered PE may suggest that the cells were stressed in some way that may already increase activity of repair mechanisms and so may reduce the size of a HRS response. This may be the case as in this study as 3 of the cell lines which showed reduced PE in the cell-sort protocol (DU145, LNCaP and A7), also showed reduced α_s/α_r values.

There were substantial differences between the protocols, which may account for the differences in survival curves observed. After trypsinisation, the cells were plated into flasks. In the DMIPS protocol, these flasks were filled with medium and sealed. The initial pH of the medium was between pH 7.4–8.0. This changed over time as CO_2 is released from the cells decreasing the pH to below 7. This contrasted with the cell-sort protocol, where the medium is exposed to a CO_2 balanced atmosphere prior to plating and a smaller volume had to be conditioned. Each cell line may have preferred more alkaline or acid conditions in order to grow so one protocol may have been more favourable than the other depending on the cell line in question.

The number of cells plated per flask was constrained in the DMIPS protocol as the set. exclusion distance allowed a certain maximum density for optimal recognition (Section 2.6.1.1), so 3000 cells were plated for all doses. The cell-sort protocol, however, had no such constraints on cell number and cell number plated could be adjusted for each dose, so that the average number of colonies counted was between 100–200. More cells meant that more CO_2 was being produced and the medium was conditioned quicker. This may have been an advantage to cells that favoured acidic conditions and a disadvantage to those that did not. It may have meant that at lower doses DMIPS flasks had more cells than sort flasks and *vice versa* at higher doses, therefore as well as the difference in the conditioning of the medium, there may have been a "feeder layer effect" from surrounding cells. There is evidence that increased survivors might compete for nutrients and produce an artificially low surviving fraction. Pomp (1996) showed that some cell lines *in vitro* do not produce a linear relationship between cell number plated and plating efficiency at high density. This may have meant that in DMIPS experiments at low doses the SF may be lower than expected. This is unlikely to have happened in these experiments as in 3 out of 5 cell lines, the response was more resistant in the low-dose region using the DMIPS protocol, *i.e.*, the α_s/α_r was lower using the DMIPS rather than the cell sorter.

In general, however, the two techniques show up low-dose HRS in all cell lines. They even are consistent in not showing HRS in cell line where it is not present *e.g.* the glioblastoma U373MG which has been tested using both techniques by Short (1999b). In most cases the SF_2 values for both techniques and the published data were not widely differing. This would suggest that both techniques were sensitive enough to accurately assess cell survival and in these experiments have shown significant HRS in all cell lines tested.

These experiments were carried out to assess the prevalence of HRS/IRR in cell lines in asynchronous cultures and under growth modified conditions. In all cell lines tested, HRS/IRR was present. This suggested that these cell lines were good candidates for assessment of cell survival at low-dose rates. Since HRS was present, a similar hypersensitive response in these cell lines at low-dose rates, if also detected, would suggest a mechanistic relationship between effects at acute low doses and low-dose rates. Survival of some of these cell lines after low dose-rate irradiation is described in Chapters 4 and 5.

Chapter 4. The effect of low dose-rate ^{60}Cobalt irradiation on cell survival

4.1 Aims

The aim of the experiments described in this chapter was to test sensitivity of cells to killing by exposure to ^{60}Co γ-rays at very low-dose rates and to measure any effects due to radiation-induced cell-cycle perturbations.

4.2 Introduction

The amount of radiation dose received by a cell is the primary factor in determining the response of that cell. However, the time over which that radiation dose is delivered is also important in most biological systems. A dose of radiation, irrespective of the time it takes to be delivered, will produce an identical number of ionisations, and for a given quantity of ionisations we may expect a given amount biological damage. However, it is often observed that at lower dose rates a smaller biological response is observed than at higher dose rates. This effect, known as sparing, was first described by Lajtha and Oliver (1961) who made predictions based on fractionation experiments carried out by Elkind and Sutton (1959). They suggested that the difference in biological response between low and high-exposures was due to repair of damage occurring during the irradiation time. Bedford and Hall carried out experiments where they irradiated the human cervical carcinoma cell line, HeLa *in vitro* using radium (Bedford 1963) and cobalt (Hall 1964) as a source of γ-rays. They found a sparing effect. Bedford *et al.* (1973) examined the cell cycle during low dose-rate exposures and fractionated exposures with his co-worker Mitchell (1977). They found that in HeLa cells during low dose-rate irradiation, there was an accumulation of cells in the G2 phase of the cell cycle. Their theory was that most cells undergo a G2 delay in response to acute doses of irradiation and they move out of G2 when they have successfully repaired most of the radiation-induced damage. At low-dose rates cells are constantly being irradiated and so do not get the chance to repair all damage during irradiation. This results in a permanent delay in progression into mitosis and therefore an accumulation of cells in G2. In 1979, Mitchell found that by irradiating HeLa cells at a dose rate of 37 cGy h^{-1}, that there was less survival than cells irradiated at 154 cGy h^{-1} (Mitchell 1979). This contrasted with the sparing effect found in previous studies (Berry 1962, Nias and Lajtha 1964, Bedford 1963, Hall 1964). Mitchell (1979) concluded that this inverse dose-rate effect was due to increased pre-mitotic accumulation in G2, the most radiosensitive phase of the cell cycle, during LDR exposures.

This hypothesis has been tested in several further studies with contradictory results. Knox *et al.* (1993) carried out low dose-rate irradiations on human tumour cells *in vivo* and found a

correlation of tumour radiosensitivity to low dose-rate irradiation with G2/M-phase block. Similar results were found in a previous study (van Oostrum *et al.* 1990). *In vitro* experiments by Furre *et al.* (1999) found an inverse dose-rate effect in a human cervical carcinoma cell line at dose rates below 86 cGy h^{-1} which correlated with an increased number of cells in G2. Similar findings were obtained *in vitro* for glioblastoma cell lines at dose rates below 49 cGy h^{-1} (Marin *et al.* 1991). In the clinic several studies have observed changes in tumour cell-cycle distribution which correlate with curability of squamous cell cancers of the cervix (Rutgers 1988, Rutgers *et al.* 1989). Other *in vitro* studies have suggested that the increased cellular sensitivity seen is due an increase in apoptosis occurring when cells accumulate in G2 (Macklis *et al.* 1994, Palayoor *et al.* 1995, Ning and Knox 1999). Conversely, other studies have questioned whether any increased cell kill at low-dose rates is due to the accumulation of cells in G2 phase of the cell cycle. DeWeese *et al.* (1998) found an inverse dose-rate effect in 6 prostate cell lines irradiated *in vitro*, but pre-mitotic accumulation did not occur in all 6 cell lines. They also found no correlation between p53 status (a gene known to control cell cycle) and the inverse dose-rate effect. Earlier work by the same authors found a similar inverse dose-rate effect in two related sublines which showed different cell-cycle distributions after LDR irradiation (DeWeese *et al.* 1997). These data suggest that cell-cycle perturbations may *not* be the dominant determinant of protracted low dose-rate radiation cell killing. Cao *et al.*(1983) carried out irradiations on mouse ascites sarcoma *in vivo* and also rejected premitotic accumulation as a reason for the inverse dose-rate effect observed. In fact, these authors suggest that the effect may be due to the lack of induction of repair process occurring at the lowest dose rates.

At very low-acute doses an increase in radiosensitivity has been detected in a number of cell lines *in vitro*. This low-dose HRS effect is where cells exhibit decreased cell survival, compared with the prediction by the linear quadratic model based on extrapolation from higher dose (1–5 Gy) data. This phenomenon has not been studied until fairly recently as the technology to detect survival accurately at very low doses has not been available. However, the two methods most widely used, the Dynamic Microscope Image Processing Scanner (Section 2.6.1) and the cell sorter (Section 2.6.2) are now used on a routine basis to search for the presence of HRS/IRR in cell lines. So far 25 cell lines have been tested and only 5 do not show this effect. The major hypothesis to explain the effect is that at very low-acute doses, cells do not detect damage and so radioprotective repair mechanisms are not triggered to restrict damage and therefore an increase in cell kill results. This effect has also been seen after fractionated exposures, where 0.4 Gy fractions were given 3 times a day for 5 days resulting in greater cell kill than a 1.2 Gy fraction given once a day for 5 days (Short 1999). It is still to be determined whether a similar sensitivity can be seen with even smaller,

more numerous fractions with smaller inter-fraction intervals, or indeed after continuous low dose-rate exposures which is the subject of this thesis.

This chapter describes the development of a low dose-rate ^{60}Cobalt irradiation system and describes experiments in which 3 cell lines known to show HRS at low-acute doses (T98G, A7 and PC3) were irradiated at low-dose rate to test for the presence of an inverse dose-rate effect. The cell-cycle characteristics were also examined to observe whether G2 accumulation was present. One cell line, T98G, was also grown to confluence to see whether any inverse dose-rate effect could be detected when cell-cycle progression occurred at a reduced rate. A HRS/IRR negative cell line, U373MG was also irradiated at low-dose rate to observe whether any low dose-rate sensitivity could be detected and therefore to elucidate further whether any relationship exists between HRS/IRR and a putative inverse dose-rate effect.

4.3 Development of a ^{60}Cobalt irradiation system

Experiments were carried out with cells irradiated on a cobalt unit at various dose rates (1–100 cGy h^{-1}). As the room in which the ^{60}Cobalt source was situated was relatively short in length, to irradiate as many cells simultaneously at as many dose rates as possible, a large spread of dose rates over a small area was needed. This was made possible by carrying out the irradiations in water as this concentrated the dose fall-off of the radiation field producing a wide range of accessible dose rates over a relatively small area. A water-tank system was designed and built to carry out these experiments at the required temperatures.

4.3.1 Specific materials and methods

Low dose-rate irradiations using the ^{60}Co source were carried out in a modified water tank. A 30 cm × 90 cm water tank was positioned with the 30 cm face at 154 cm from a Mobaltron 100 ^{60}Cobalt source (T.E.M. Instruments Ltd, Crawley, Sussex, England) (activity was recorded in 1991 as being > 2 kCi). This large distance between the source and the tank, ensured that the gamma-ray beam (width approximately 40 cm) was uniform and free of Compton Scattered photons. De ionised water was added to a depth of 20 cm and the temperature was maintained at 37°C with a circulating pump-heater. Four specially-designed plastic flask holders, each able to hold eight 25 cm^2 tissue culture flasks (T25), were attached to the floor of the tank. In order that all flasks in the same holder received the same dose rate, flasks were positioned back to back so that the growth surfaces of the flasks were adjacent to each other.

4.3.1.1 Dosimetry

Reference dosimetry was carried out using an ionisation chamber (chamber :35cc model 2530/1 and meter: Farmer dosimeter, type 2502/3, both from Nuclear Enterprises Ltd, Reading, England) on 17th Dec 1997 (Figure 4.1). This was the only time the dosimetry was checked by using an ionisation chamber with the tank in this position. Changes in dosimetry due to ^{60}Co decay were calculated based on this original dosimetry. The water tank was filled to a depth of 20 cm and the water heated to 37°C. The ionisation probe was covered with a latex glove to protect it from water damage. The flask holders were positioned at distances of 5 cm, 32 cm, 59 cm and 86 cm into the tank away from the ^{60}Co source. Each holder contained eight 25 cm^2 orange capped (Corning, UK) T25 flasks which were filled with water. Measurements were taken with the probe positioned at the bottom of the water tank, in the middle of each flask holder along the central axis. During a measurement, flasks were removed from that particular flask holder. Measurements were also made at points 10 cm either side of the central axis so that an overall dose distribution could be gauged.

Dosimetry was confirmed by the use of Fricke dosimetry on 5th Jan 1998 (Figure 4.3). The method is described in section 2.5.4. Flask holders were positioned at distances of 61.49, 48.57, 28.09 and 15.17 cm from the front of the tank so as to give dose rates of approximately 5, 10, 30 and 60 cGy h^{-1} respectively as calculated from the ionisation chamber dosimetry. 12 flasks (3 per flask holder) were filled with Fricke solution, placed in the water tank in the flask holders. The remaining 5 spaces in each flask holder was filled with flasks containing water. Flasks were irradiated in the dark for 65 hours. After irradiation, the Fricke solution was removed and the absorbance was measured at a wavelengths of 224 nm using a spectrophotometer. From the absorbance measurements, the dose was calculated using the equations in Section 2.5.4.

The radioactive decay of ^{60}Co ($t_{1/2}$= 63.24 months) over time would mean a decrease in dose rate at the positions of the flask holders between experiments. In order to keep the experimental dose rate the same, the flasks were moved slightly towards the ^{60}Co source. The new distances for the dose rates required were calculated as follows:

The equation of the line from the graph dose rate vs. distance into tank can be defined as:

$$y_{x,t} = y_{0,t}e^{-sx}$$

Where y is the dose rate at distance x into the tank, y_0 the dose rate at distance 0 and s is the slope of the curve.

The decay for ^{60}Co with time can be calculated by:

$$y_{x,t} = y_{x,0}e^{-\lambda t} \quad \text{where} \quad \lambda = \frac{\ln 2}{t_{1/2}}$$

Where $y_{x,o}$ is the activity at time 0 and $y_{x,t}$ is the activity at time t and $t_{1/2}$ (^{60}Co) is 63.24 months.

To calculate the new dose rate, at distance x, after decay time t:

$$y_{x,t} = y_{0,0}e^{-\lambda t}e^{-sx}$$

This can be rearranged to give the new distances from the source:

$$x_t = \frac{\ln\left(\frac{y_{0,0}}{y_{x,t}} - \lambda t\right)}{s}$$

The source-flask holder distance was corrected each month to allow for ^{60}Co decay.

4.3.2 Results and discussion

Figure 4.1 shows photographs of the water tank irradiation set up. Figure 4.2 shows the dose rate measured by the ionisation chamber along the central axis and 10 cm either side. The results show a decrease in dose rate as the probe is moved away from the source, further into the tank. Figure 4.3 shows the results of Fricke dosimetry. Similarly, using this method of dosimetry, the dose rate is decreased as the distance from the source increases.

The two dosimetry methods were inter-compared. The lines of best fit to the Fricke and ionisation chamber data were plotted, confidence limits were obtained and those for the slope of the curve (distance) were found to overlap. Multiple regression analysis was also used to test for a significant difference between the lines and a p-value of 0.1107 was obtained which therefore suggests that there was no difference. However, the 95% confidence limits for the intercept, did not overlap. The greatest divergence of the lines occurs at the intercept, which is 0 distance into the tank. It is not entirely understood why the Fricke should show a larger dose rate here than the ionisation chamber. There are more variations that can occur using Fricke dosimetry, such as contamination from other chemicals which are present in apparently clean glassware or flasks or during manipulations. Efforts were made to reduce such contamination, by filling flasks with Fricke solution and irradiating to a high dose (effectively radiochemically cleaning them) and then emptying before use in the experiment. However, the divergence between measurements is not widely different and as the ionisation chamber measurements gave the least standard error it was deemed more accurate and used as standard for these experiments (Table 4.1).

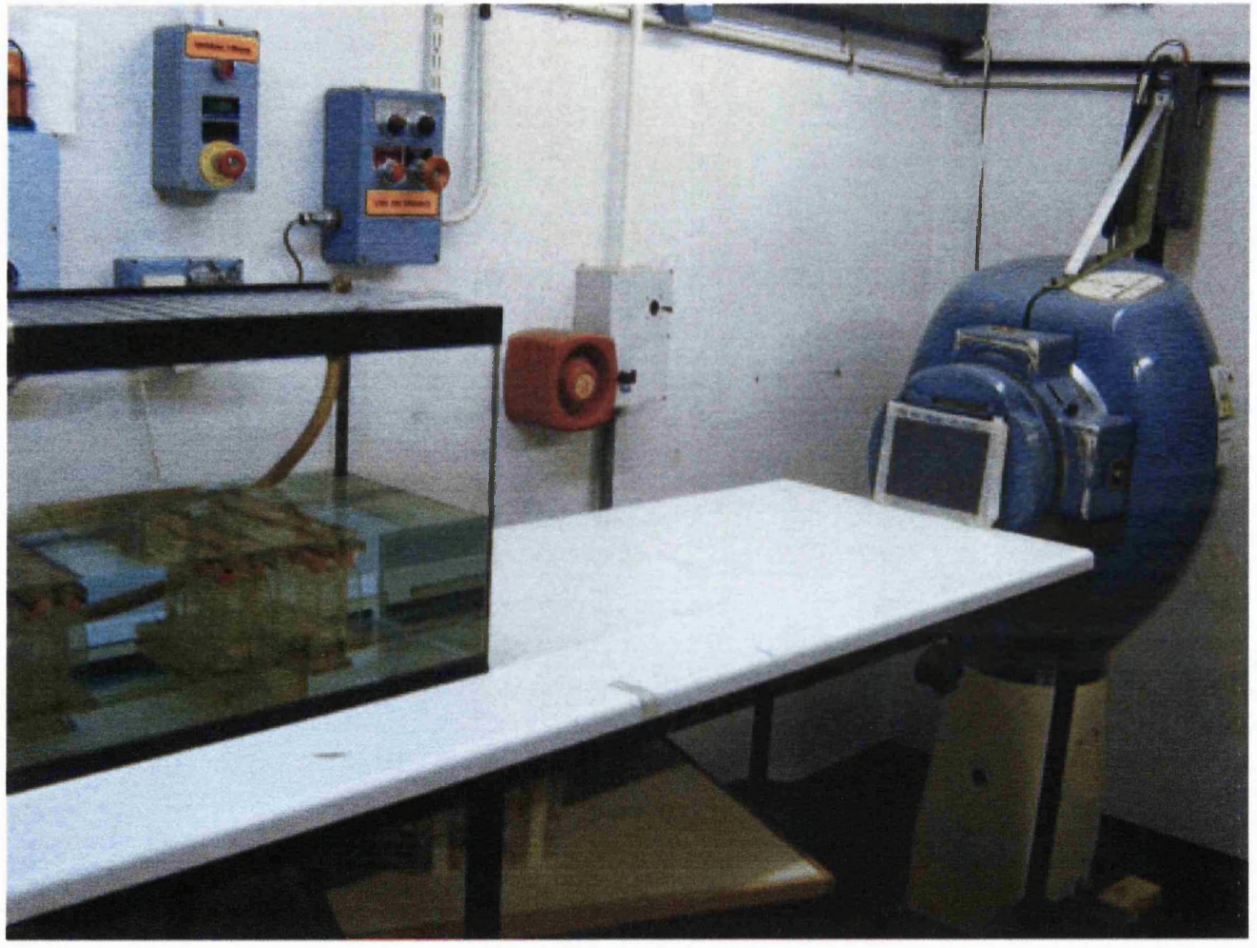

Figure 4.1(a)
Shows the ^{60}Cobalt water tank irradiation system, with the ^{60}Co source (right) and the water tank containing flasks of cells (left).

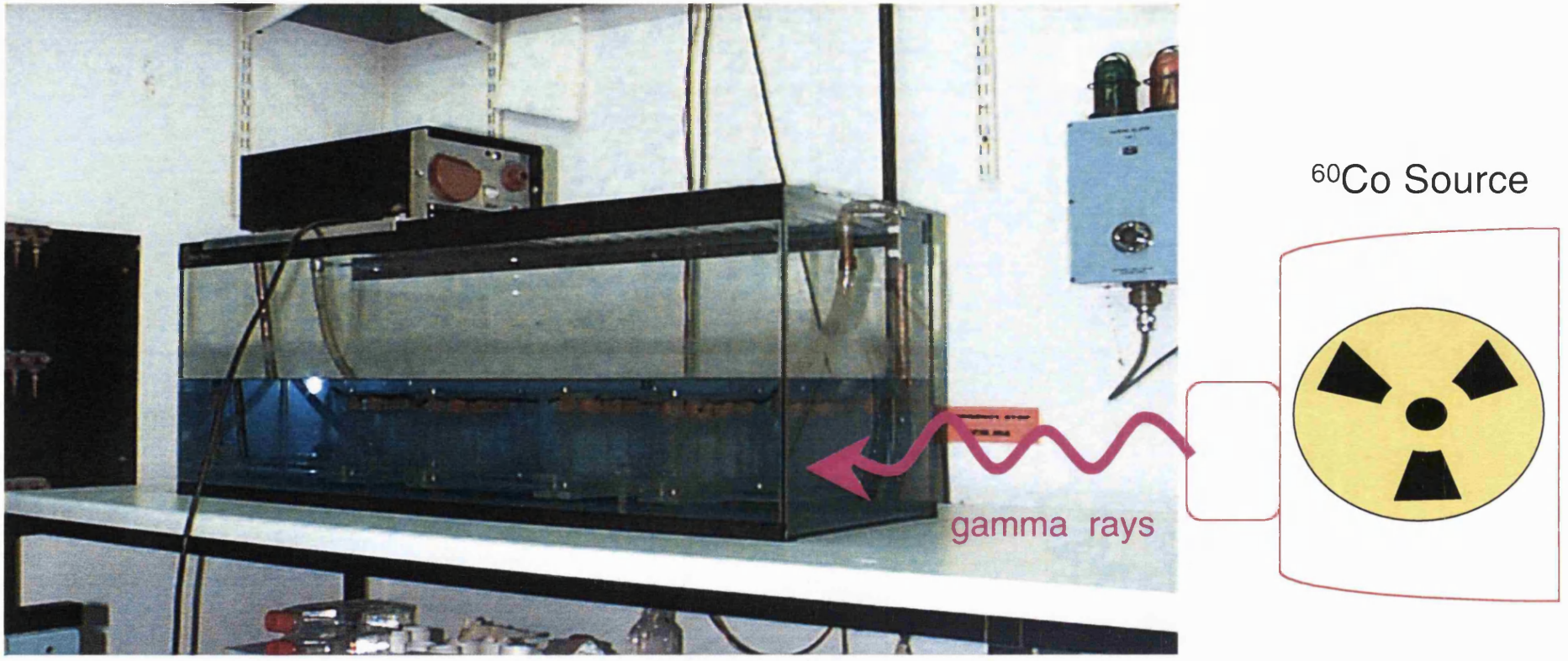

Figure 4.1 (b)
Shows a representation of the ^{60}Co water tank irradiation system. The γ-rays enter the tank and are concentrated, allowing a large range of dose rates over a relatively small area. Cells can be irradiated simultaneously at 4 different dose rates ranging from 1–100 cGy h^{-1}.

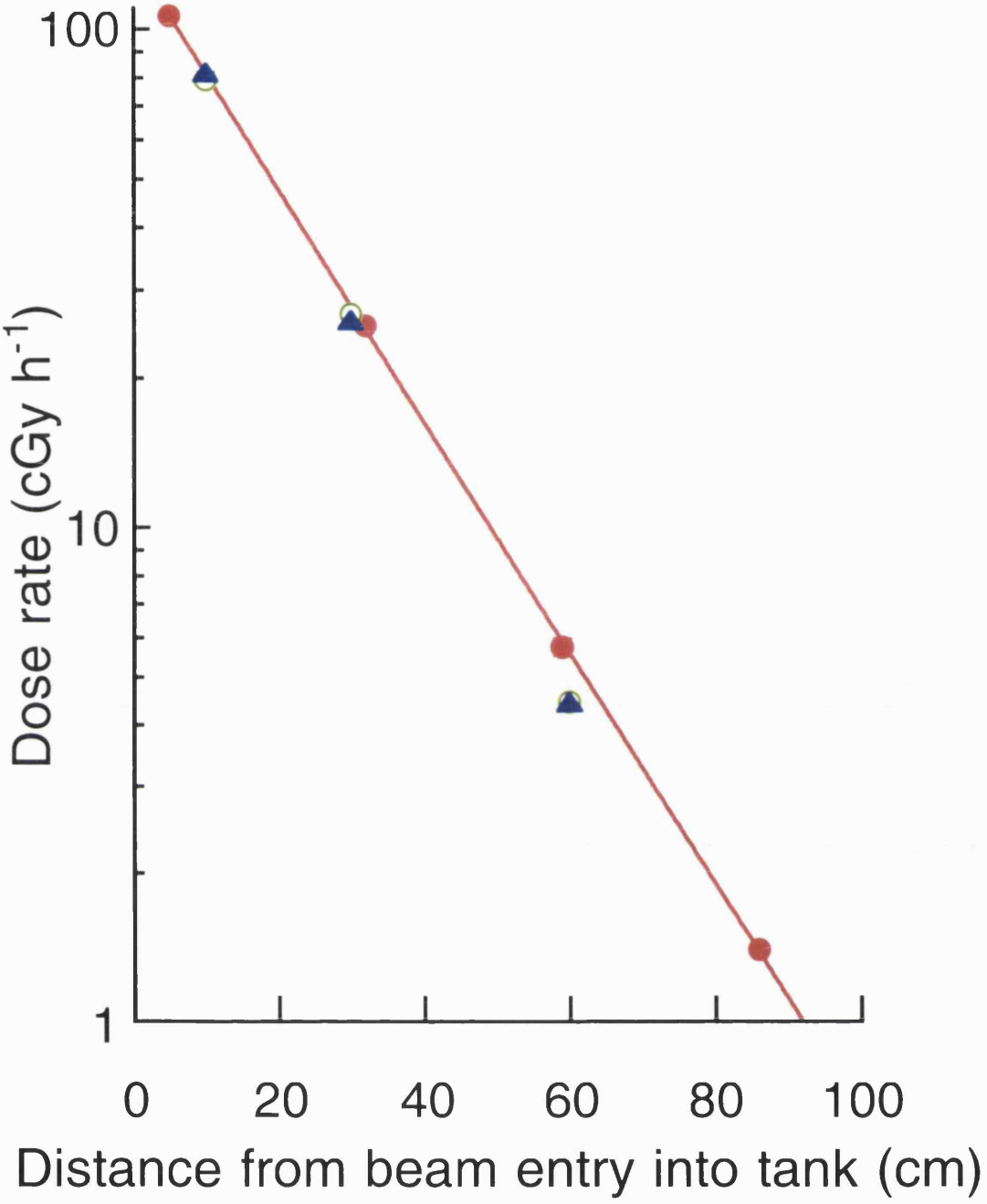

Figure 4.2
Shows the dose rate against distance along water tank measured using an ionisation chamber. Measurements were taken along the central axis (red circles), 10 cm left (green circles) and 10 cm right (blue triangles) of central axis with flasks in place. The line of best fit is shown for the central axis measurements;

$$y = 139.38e^{-0.054x}.$$

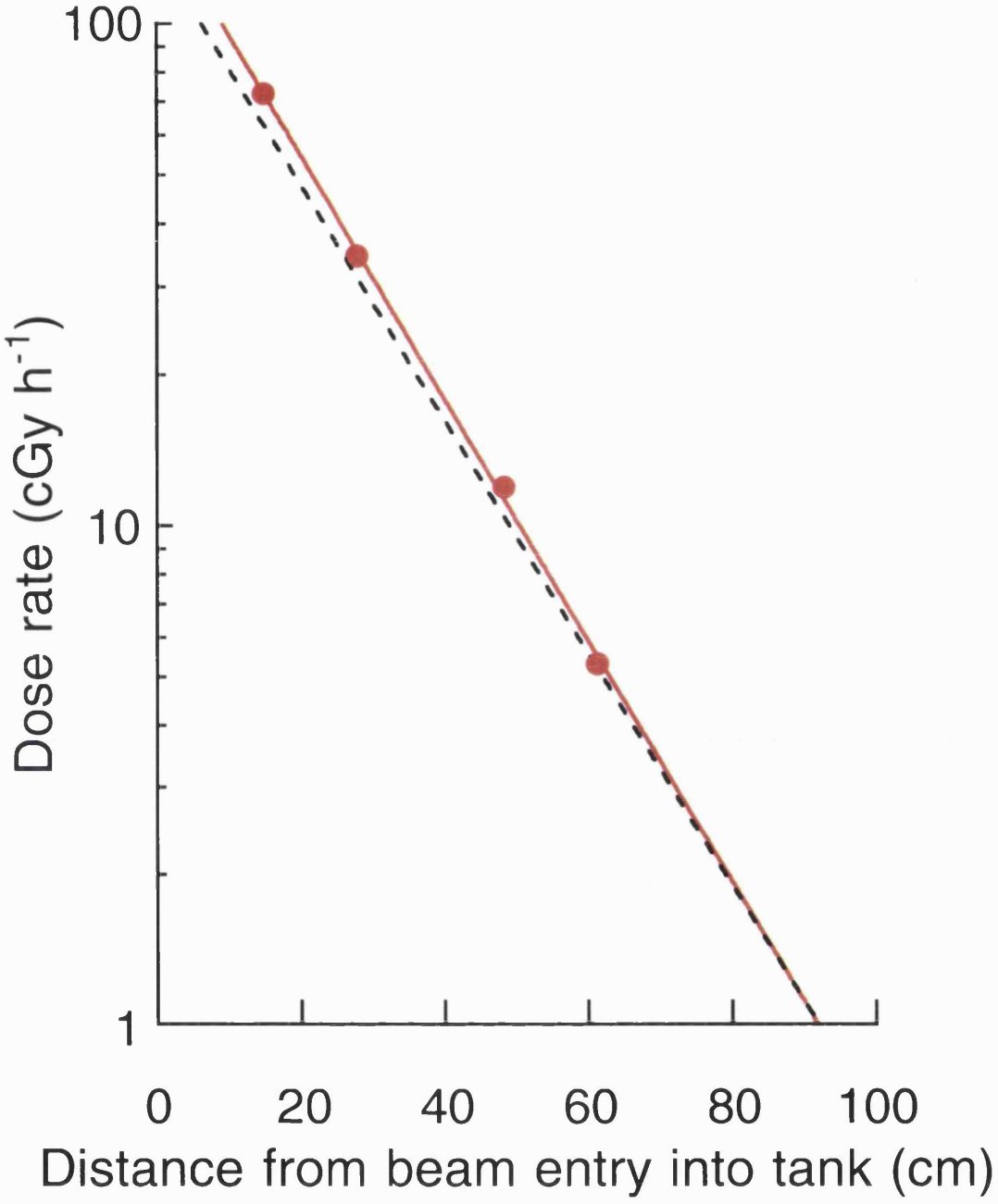

Figure 4.3

Shows the dose rate against distance along water tank measured using Fricke dosimetry (solid line). Flasks containing Fricke solution were placed in the flask holders at distances 61.49, 48.57, 28.09 and 15.17 cm respectively from the front of the tank. The flasks were irradiated for 65 hours and the absorbance measured. The line of best fit is shown;

$$y = 169.24e^{-0.56x}.$$

The line of best fit from dosimetry using the ionisation chamber (Figure 4.2) is also shown (dashed line).

Measurement date : 17.12.97	
Dose rate (cGy h^{-1})	Distance into tank (cm) (x_0)
2	78.6
5	61.5
10	48.6
30	28.1
60	15.2
100	5.7

Table 4.1.
Shows the distance along tank where flask holders were positioned to give desired dose rate.

4.4 Low dose-rate irradiations of cells using ^{60}Cobalt

After the irradiation system was set up with accurate determination of dose rates made possible, human tumour cells were irradiated at various low-dose rates with cell survival and cell-cycle distribution assessed.

4.4.1 Materials and methods

The cell survival at low-dose rates using the water tank system was assessed for the following cell lines: T98G (confluent and asynchronously growing), A7, PC3 and U373MG. 5×10^3 asynchronously growing cells were plated into orange capped (Corning, UK) T25 25 cm^2 tissue culture flasks containing 5 ml of medium. In confluent T98G experiments, 5×10^5 cells were plated. In all experiments, flasks were incubated at 37°C with 5% CO_2 + 5% O_2 (balance N_2) overnight to allow cells to attach. The medium was then removed and each flask was then fully filled with fresh medium. Strips of parafilm were wound round the lid to form a watertight seal. Half the flasks were removed from the incubator and were attached to the holders in the water tank with 8 flasks at each dose-rate position (Table 4.1). Cells were then irradiated in the dark. After the required dose (2, 5, 12 and 18 Gy for dose rates above 5 cGy h^{-1}, 2, 5, 8 and 12 Gy at 5 cGy h^{-1} and 1, 2, 4 and 5 Gy for 2 cGy h^{-1}), flasks were removed from the water tank and replaced with flasks containing water so the dose distribution was not disturbed for the remaining flasks. The remaining flasks in the incubator were kept in there for the duration of the irradiations to act as unirradiated controls. Cells in the irradiated and control flasks were then assessed for clonogenic survival. The media was removed and the flasks washed twice with PBS. Cells were harvested using EDTA/trypsin and centrifuged at 1000 r.p.m. for 5 minutes. The pellet was resuspended in 5 ml of medium before being passed through a 21 gauge needle. Cell number was calculated by haemocytometer counting and a known number of cells were plated in petri dishes containing 5 ml of medium. These dishes were incubated at 37°C for 14 days before being stained with crystal violet and the colonies were manually counted to assess cell survival.

The sample remaining after plating was centrifuged at 1000 r.p.m. for 5 minutes, resuspended in 70% ethanol and stored at 4°C. At a later date, cells were centrifuged at 2000 r.p.m. for 5 minutes and were resuspended in 500 µl PBS containing 1 µg ml^{-1} propidium iodide and 5 µg ml^{-1} ribonuclease, as described in Section 2.7.3. Samples were then analysed for cell-cycle distribution on a FACScan flow cytometer (Section 2.7.1 and 2.7.4).

The survival of T98G cells grown to confluence was also tested at low-dose rates. In these experiments 5×10^5 cells were plated into 25 cm^2 tissue culture flasks containing 5 ml EMEM. Flasks were incubated at 37°C with 5% CO_2/5% O_2 (balance N_2) until they were

observed to be confluent for 4 days. Flasks were then irradiated as described above for asynchronous cultures.

To examine recovery of the cell cycle post irradiation, 12 flasks of asynchronously-growing T98G cells were irradiated as described above to at total dose of 5 Gy, six flasks at a dose rate of 100 cGy h^{-1} and the other 6 flasks at 5 cGy h^{-1}. Two flasks at each dose rate were trypsinised immediately after irradiation and the cells were fixed in 70% ethanol. The remaining flasks were incubated at 37°C for either 3 hours or 12 hours post irradiation before being trypsinised and fixed. The samples were then processed, stained with PI and analysed on a FACScan flow cytometer as described in Section 2.7.3 to 2.7.4.

To check for radiation quality changes as the γ-rays pass through the water, the tank was moved forward so that a dose rate of 100 cGy h^{-1} was achieved 31.0 cm from beam entry into the tank. Dosimetry was redone as described in Section 4.3.1.1. Asynchronously growing T98G cells were irradiated in this position to total doses of 2, 5, 12 and 18 Gy and flasks were processed as described before, cells were counted and surviving fraction was calculated. The resulting survival curve was compared with the curve obtained for cells irradiated at 100 cGy h^{-1} in the previous position which was 5.7 cm into the tank.

An acute dose survival curve using ^{60}Co was obtained for the following cell lines T98G (confluent and asynchronously growing), A7, PC3 and U373MG. In the case of asynchronous cultures, 1×10^4 cells were plated out into 25 cm^2 flasks containing 5 ml pre-warmed medium and incubated at 37°C with 5% CO_2 + 5% O_2 (balance N_2) two days prior to irradiation. Confluent cells were plated out as described in Section 2.4.1.3 and were observed to be in confluence for 4 days prior to irradiation. Flasks were irradiated at a dose rate of 0.52 Gy min^{-1} to doses ranging from 1 to 5 Gy as described in Section 2.5.2. Cells were then trypsinised, counted and plated out for a colony forming assay (Section 2.4.1.2). They were incubated for 10–14 days at 37°C and then stained using crystal violet. Colonies were then counted manually. Acute dose survival curves were plotted onto the same graph as the LDR data to allow for comparison.

4.4.1.1 Data analysis

Cell survival was defined in asynchronous cultures as surviving clonogens per flask:

$$\text{Surviving clonogens per flask} = \text{Surviving fraction} \times \text{Relative yield}$$

Where,

$$\text{Relative yield} = \frac{\text{no. cells counted in irradiated flask}}{\text{no. cells counted in control flask}}$$

at the conclusion of irradiation and

$$\text{Surviving fraction} = \frac{\text{no. colonies counted}}{\text{no. cells plated}}$$

Surviving clonogens per flask was plotted against total dose for each dose rate.

To test for significance of any differences seen between survival at different dose rates, multiple regression analysis was carried out between survival curves and a p-value for differences was obtained.

A second method of analysis was employed to give a general assessment of survival at different dose rates. In this method, each survival curve was represented by a single value. This value was derived on the assumption that each survival curve is linear on a log scale. Each data set was fitted to the equation, $SF = e^{-a\,dose}$, where a is the gradient of the line. The value of a was calculated, then plotted against dose rate and a line of best fit was obtained. Analysis of variance was used to obtain a p-value. A one-way analysis of variance was used to test whether the variability between groups was significantly higher than the variability within groups.

To test for significance of any differences between cell-cycle distributions at different dose rates, each phase of the cell cycle was compared with the corresponding phase at the same total dose for the highest and lowest dose rates. Analysis of variance was used to obtain p-values.

4.4.2 Results

Figures 4.4, 4.7, 4.10, 4.13 and 4.16 show the survival curves obtained for asynchronous T98G, confluent T98G, asynchronous A7, PC3 and U373MG cells respectively, when irradiated with low dose-rate ^{60}Cobalt γ-rays using the water tank irradiation system. An inverse dose-rate effect was apparent in asynchronous T98G, A7 and PC3 cells. Tables 4.2 to 4.6 show the p-values obtained by multiple regression analysis when survival curves within each cell line was compared and Figures 4.19 to 4.23 show the plots the gradient of each fitted survival curve against dose rate within each cell line. One-way ANOVA was used to compare inter and intra variability and these were significantly different from each other in all, but the U373MG cell lines suggesting that a real effect was present. Figures 4.5, 4.8, 4.11, 4.14 and 4.17 show a breakdown for each cell line of the surviving fraction and the relative yield of cell for each dose rate. Figures 4.6, 4.9, 4.12, 4.15 and 4.18 show the proportion of cells in each phase of the cell cycle as observed by PI staining and flow cytometry. Figure 4.24 shows the cell-cycle distribution of asynchronous T98G irradiated at 5 and 100 cGy h^{-1} to a total dose of 5 Gy, directly after irradiation and then 3 and 24 h later. Table 4.7 shows the p-values obtained when the percentage of cells in each phase of the cell cycle for a certain total dose is compared for the highest and lowest dose rates for each cell line. In Figure 4.6 the lowest dose rate for asynchronous T98G shown is 5 cGy h^{-1} rather than 2 cGy h^{-1} as the total doses allow a better comparison with the higher dose rates. The survival curve obtained when the water tank has been moved to a new position and the cells are irradiated at 100 cGy h^{-1} is compared with the same dose rate in the old position is shown in Figure 4.25 and there is no significant difference between these survival curves.

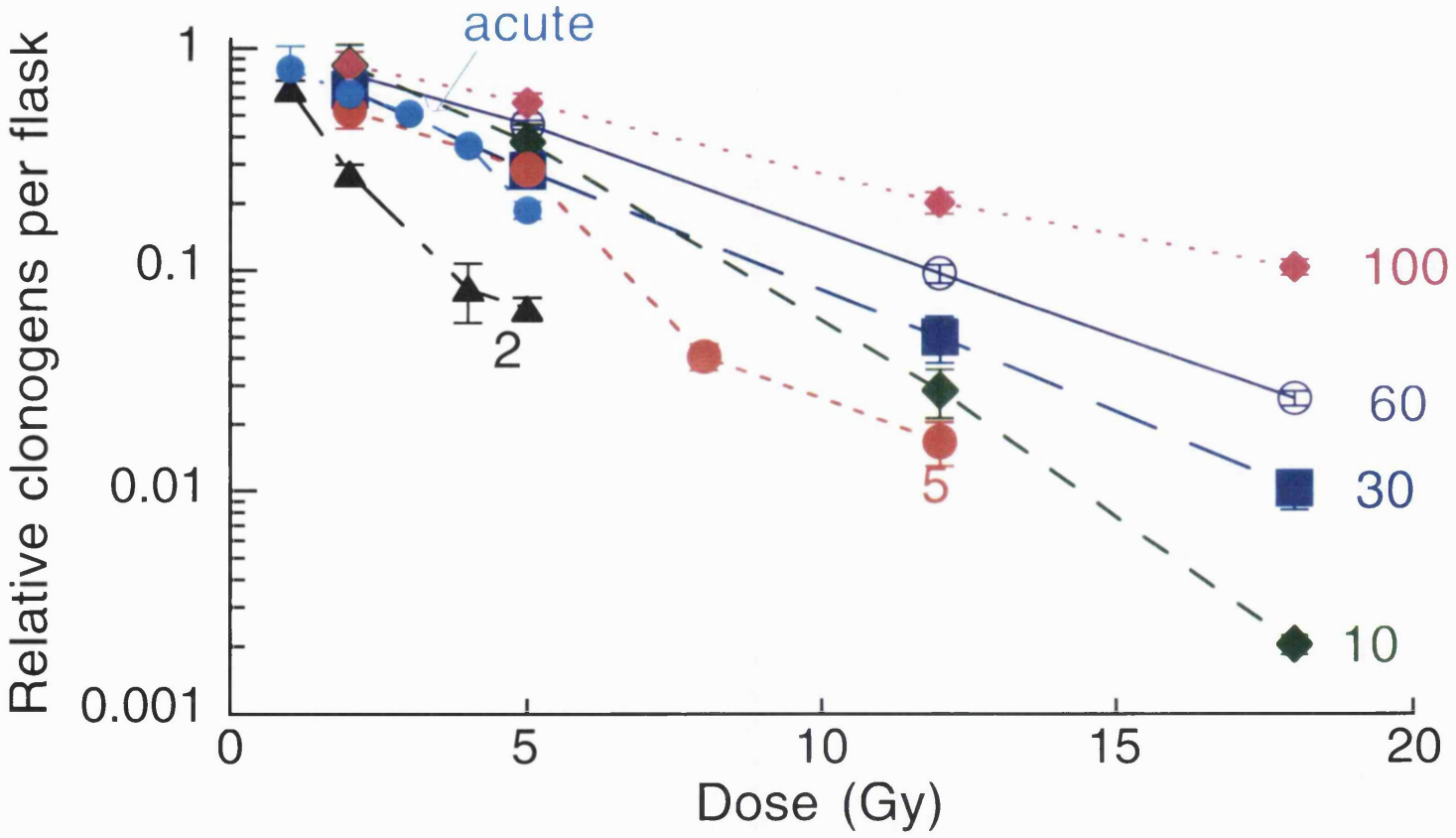

Figure 4.4
Shows survival curves obtained after irradiating asynchronous T98G cells (human glioblastoma) using the ^{60}Cobalt water tank irradiation system. Dose rates shown are in cGy h^{-1}. Relative clonogens per flask is calculated by multiplying the surviving fraction by the relative yield as described in Section 4.4.1.1. Each data point is plotted as mean ± SEM. The acute dose rate was 33 Gy h^{-1}.

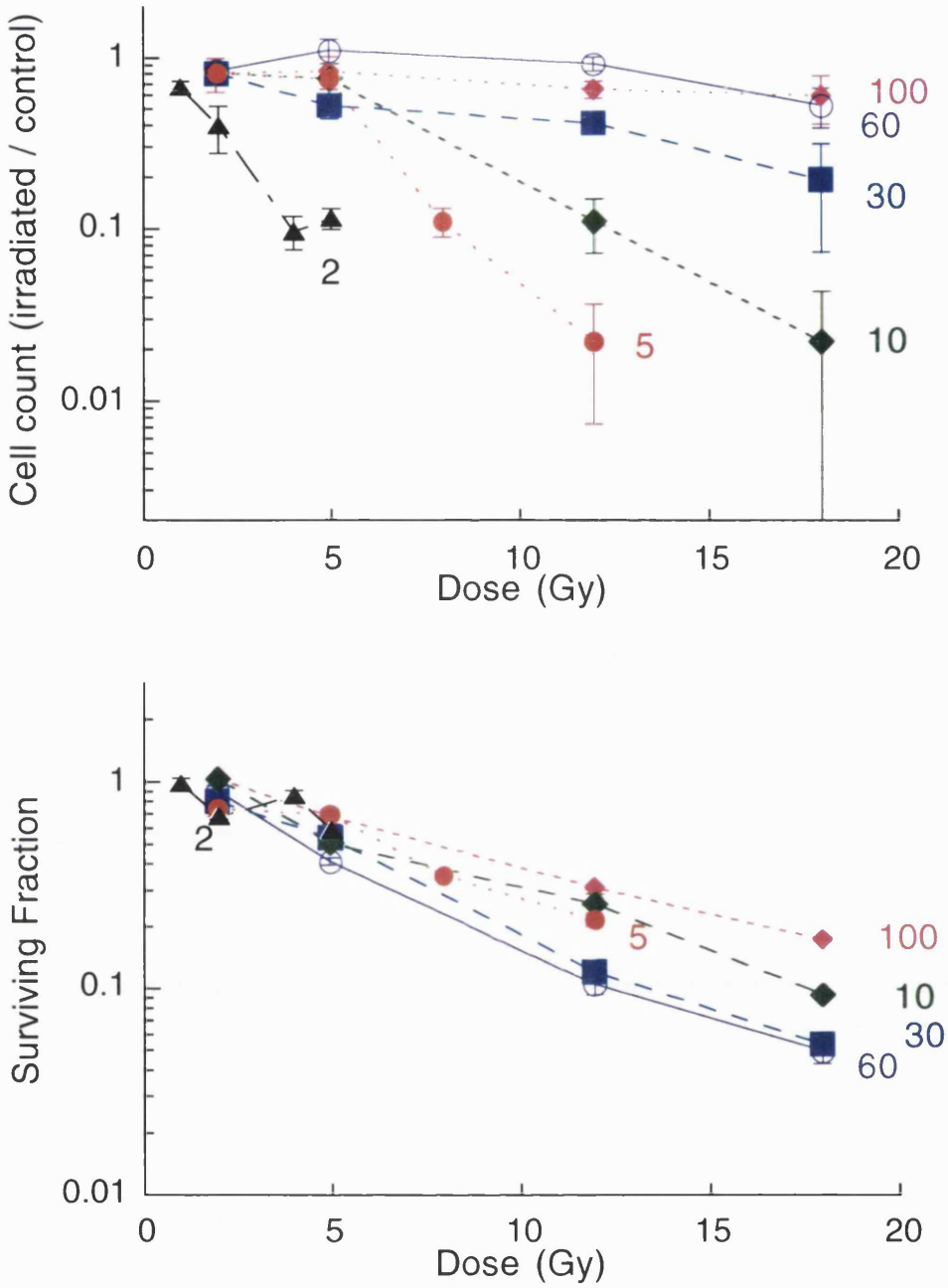

Figure 4.5
Shows survival curves obtained after irradiating asynchronous T98G cells (human glioblastoma) using the ^{60}Cobalt water tank irradiation system. Dose rates shown are in cGy h^{-1}. The upper panel shows the cells counted per flask after trypsinisation divided by the number of cells in the control flask. The lower panel shows the surviving fraction obtained when cells are plated out and colonies counted. Each data point is plotted as mean ± SEM.

Comparison between survival curves at dose rates (cGy h^{-1})		p-value
100	60	**0.0024***
100	30	**0.0144***
100	10	0.0587
100	5	**0.0061***
100	2	**0.0207***
60	30	0.0357
60	10	0.5962
60	5	**0.0325***
60	2	**0.0095***
30	10	0.6264
30	5	0.1728
30	2	**0.0429***
10	5	0.1185
10	2	**0.0082***
5	2	0.0691
acute	100	**0.0042***
acute	60	**0.0144***
acute	30	0.3181
acute	10	**0.0062***
acute	5	0.5290
acute	2	**0.0056***

Table 4.2
Shows the comparison between survival curves obtained after irradiating asynchronous T98G cells with ^{60}Cobalt γ-rays at dose rates shown. Multiple regression analysis was carried out to obtain a p-value for the difference between survival curves. *denotes survival curves which are significantly different from one another. The acute dose rate is 33 Gy h^{-1}.

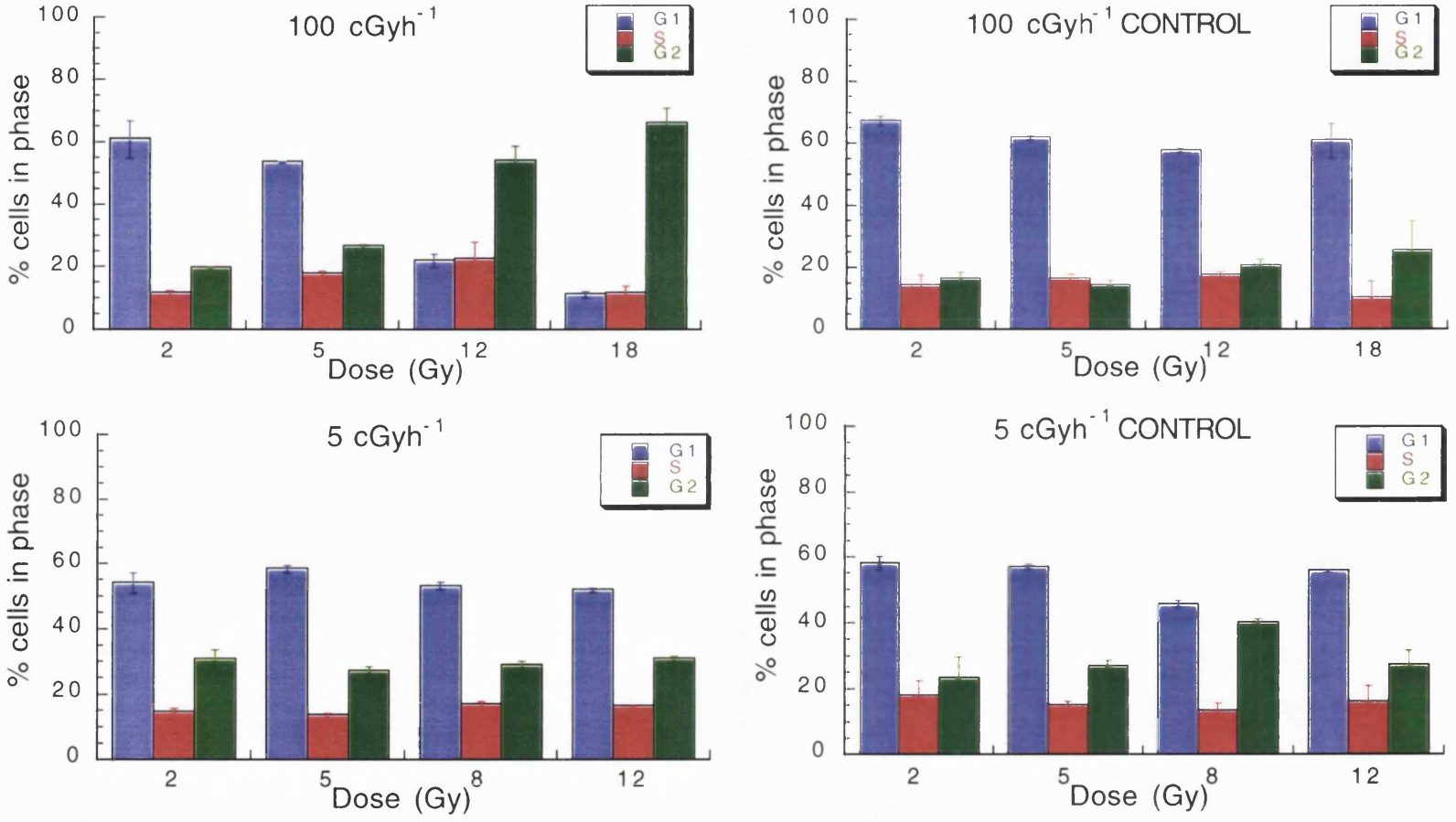

Figure 4.6

Shows the distribution of asynchronous T98G cells in each phase of the cell cycle after irradiation with ^{60}Cobalt γ-rays at dose rates of 100 cGy h^{-1} (top panel) and 5 cGy h^{-1} (bottom panel). The distributions of unirradiated controls sampled at the same time are shown.

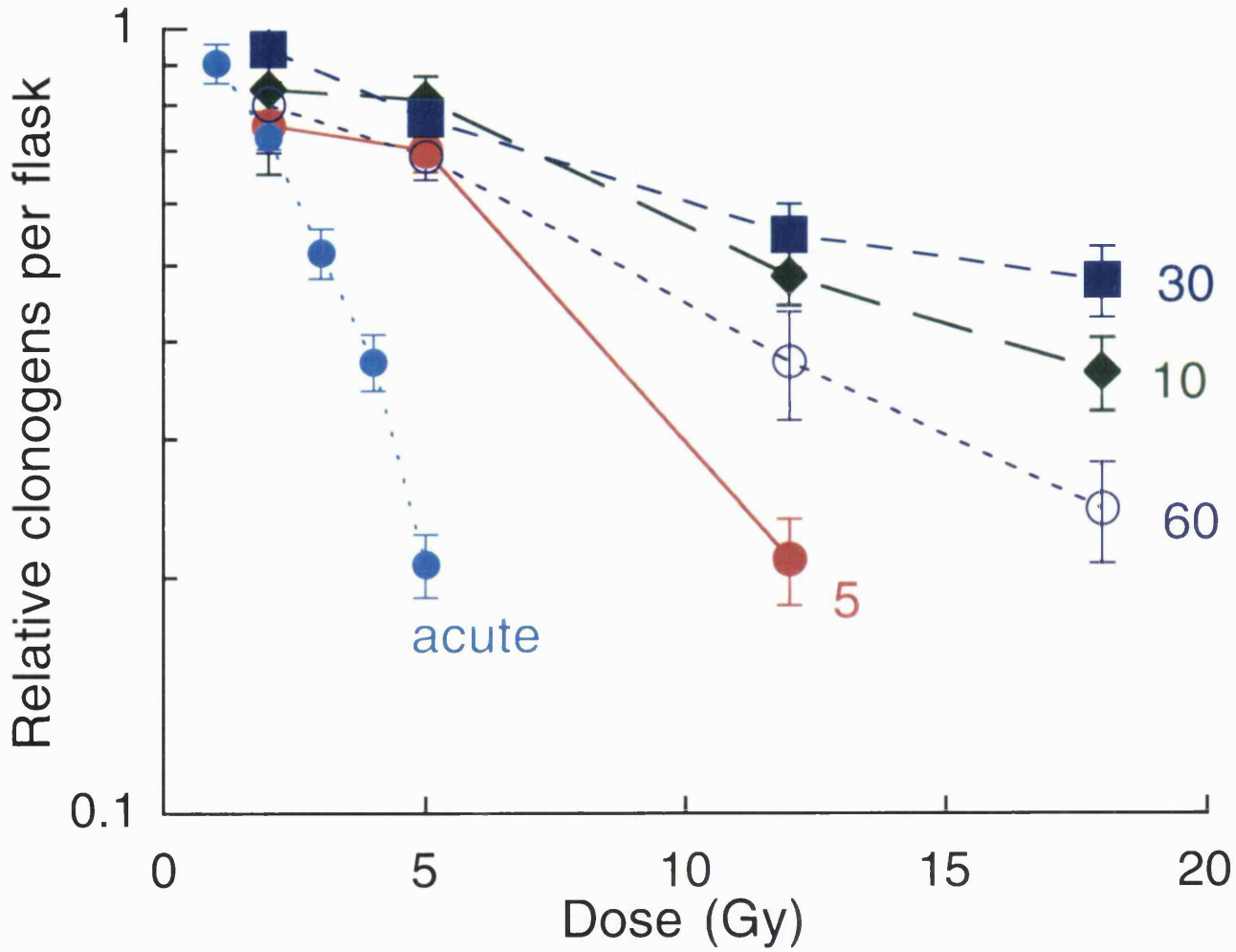

Figure 4.7
Shows survival curves obtained after irradiating confluent T98G (human glioblastoma) cells using the ^{60}Cobalt water tank irradiation system. Dose rates shown are in cGy h^{-1}. Each data point is plotted as mean ± SEM. The acute dose rate was 33 Gy h^{-1}

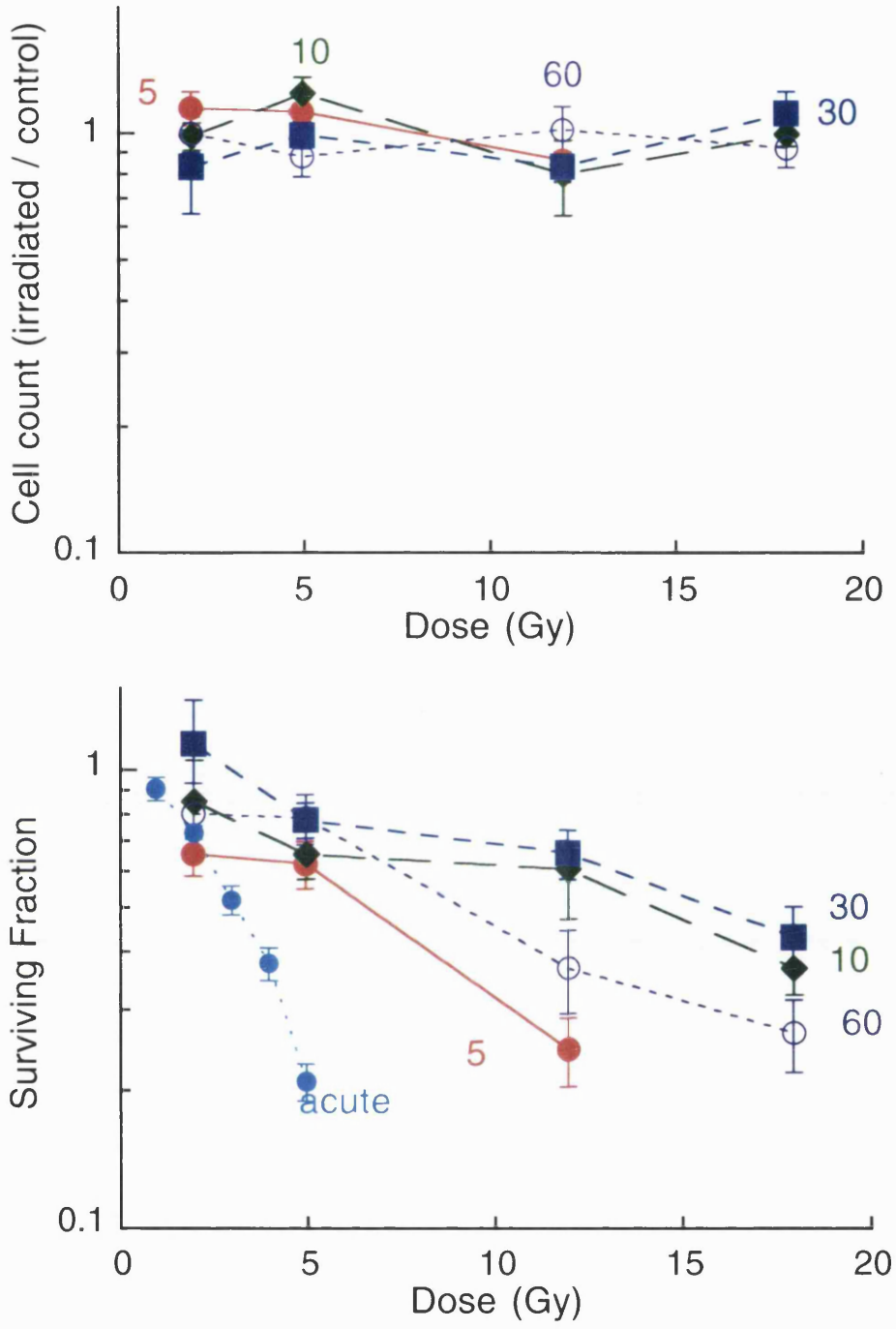

Figure 4.8
Shows survival curves obtained after irradiating confluent T98G cells (human glioblastoma) using the ^{60}Cobalt water-tank irradiation system. Dose rates shown are in cGy h^{-1}. The upper panel shows the cells counted per flask after trypsinisation divided by the number of cells in the control flask. The lower panel shows the surviving fraction obtained when cells are plated out and colonies counted. Each data point is plotted as mean ± SEM

Comparison between survival curves at dose rates (cGy h^{-1})		p-value
60	30	**0.0135***
60	10	**0.0346***
60	5	0.2372
30	10	0.1572
30	5	0.0554
10	5	0.0775
acute	60	**0.0478***
acute	30	**0.0124***
acute	10	**0.0331***
acute	5	0.1005

Table 4.3
Shows the comparison between survival curves obtained irradiating confluent T98G cells, with ^{60}Cobalt γ-rays at dose rates shown. Multiple regression analysis was carried out to obtain a p-value for the difference between survival curves. *denotes survival curves which are significantly different from one another. The acute dose rate is 33 Gy h^{-1}.

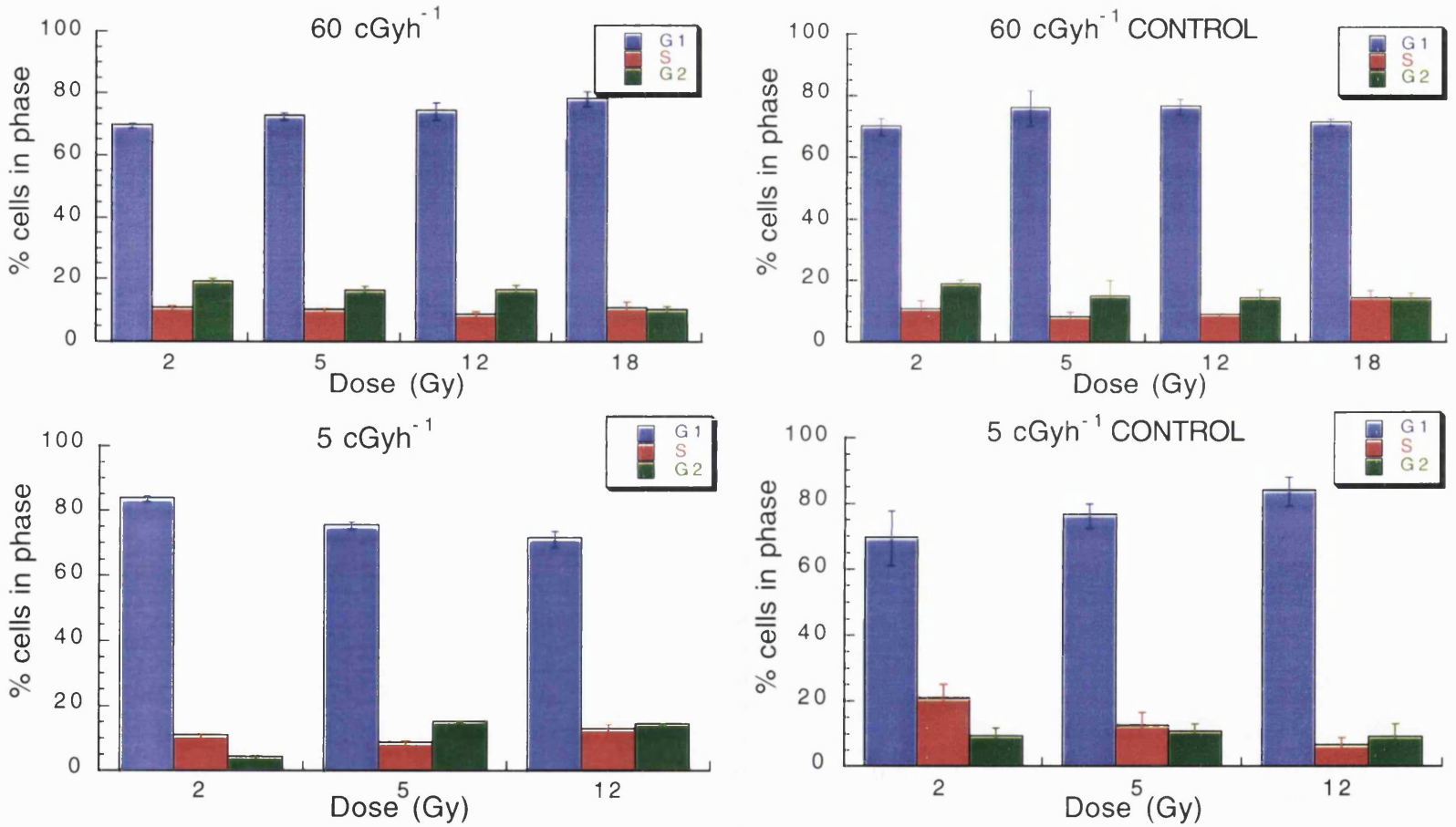

Figure 4.9

Shows the distribution of confluent T98G cells in each phase of the cell cycle after irradiation with ^{60}Cobalt γ-rays at dose rates of 60 cGy h^{-1} (top panel) and 5 cGy h^{-1} (bottom panel). The distributions of unirradiated controls sampled at the same time are shown.

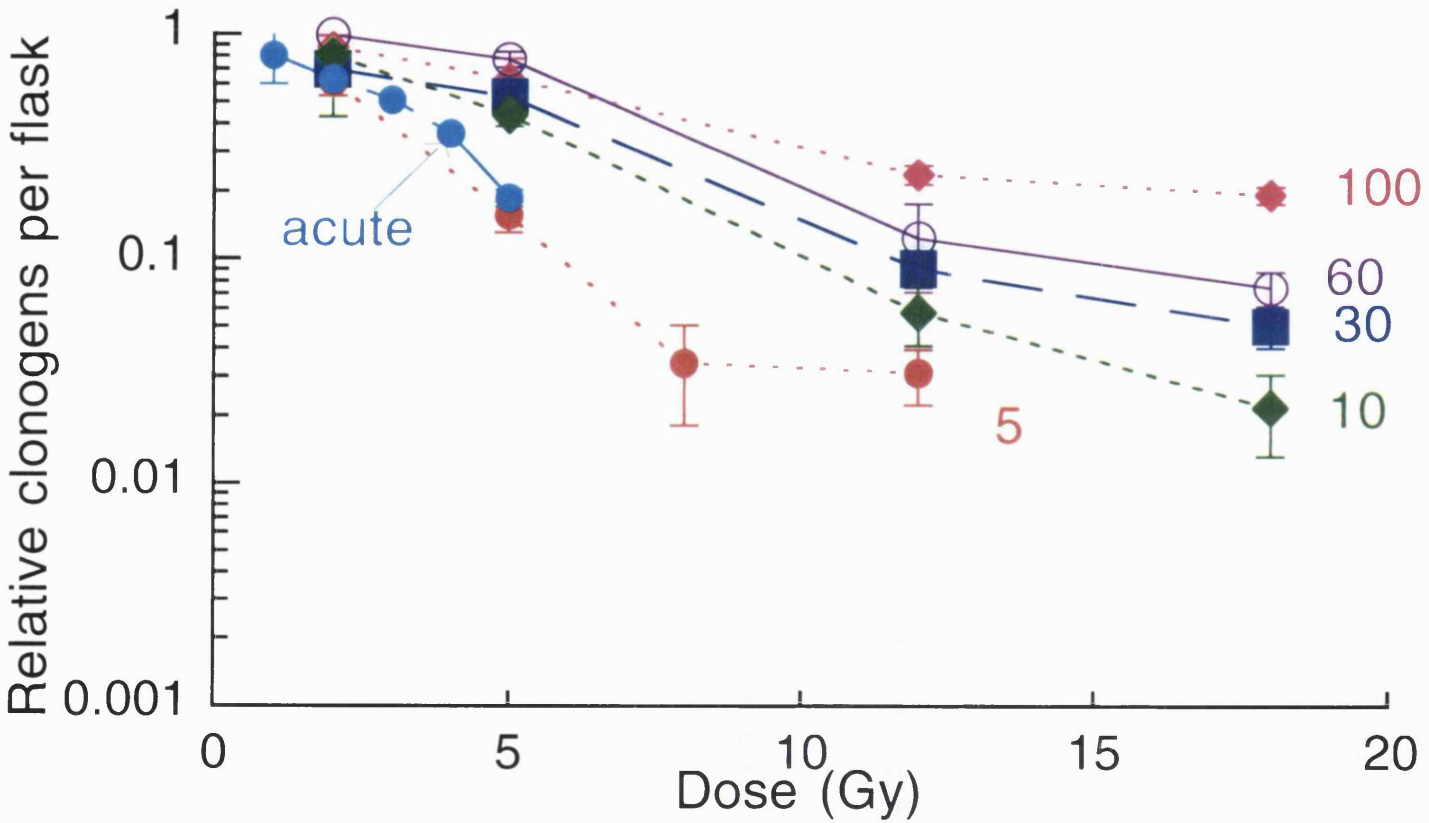

Figure 4.10
Shows survival curves obtained after irradiating asynchronous A7 (human glioma) cells using the ^{60}Cobalt water tank irradiation system. Dose rates shown are in cGy h^{-1}. Relative clonogens per flask is calculated by multiplying the surviving fraction by the relative yield as described in Section 4.4.1.1. Each data point is plotted as mean ± SEM. The acute dose rate was 33 Gy h^{-1}.

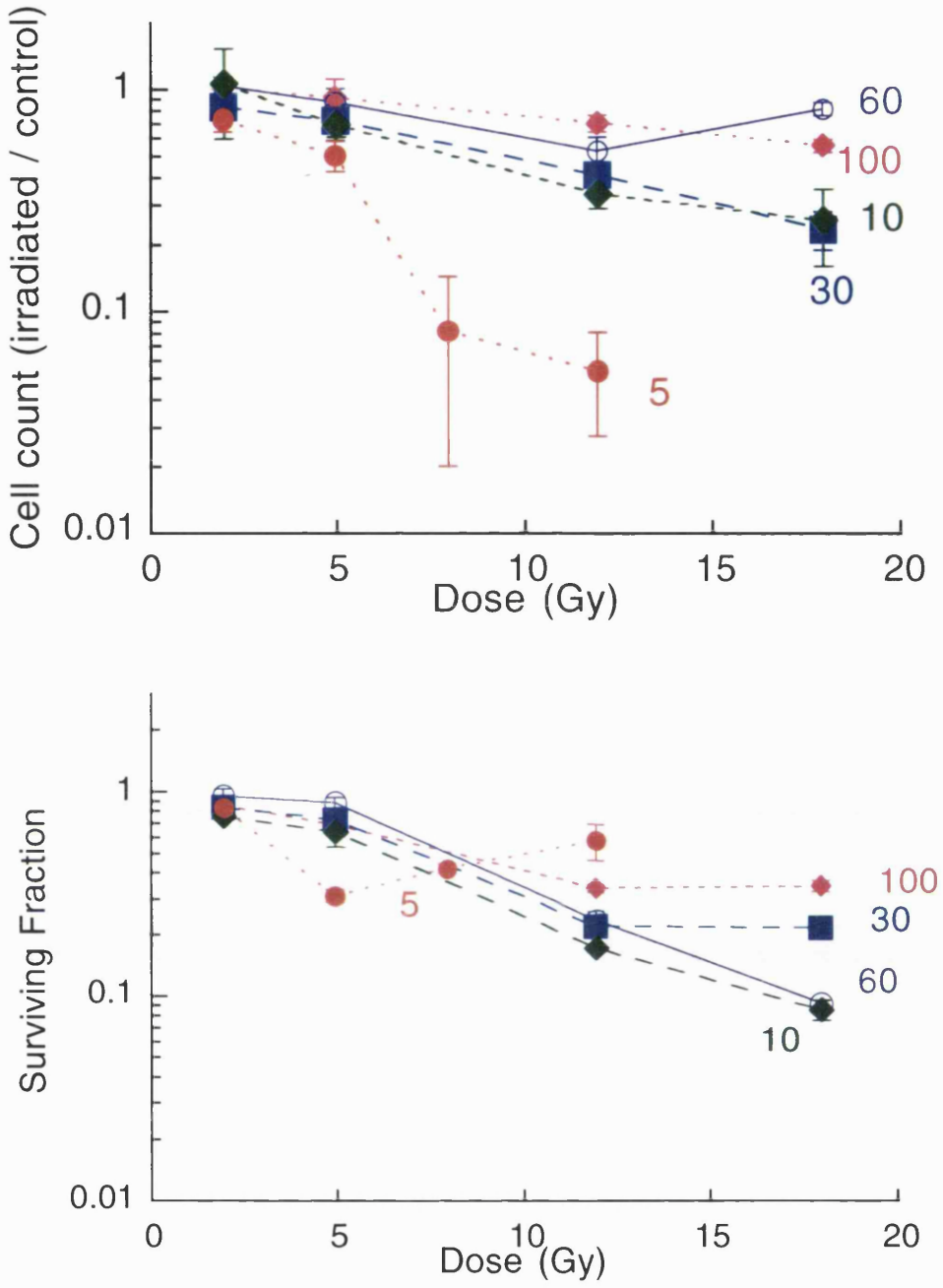

Figure 4.11
Shows survival curves obtained after irradiating asynchronous A7 cells (human glioblastoma) using the ^{60}Cobalt water tank irradiation system. Dose rates shown are in cGy h^{-1}. The upper panel shows the cells counted per flask after trypsinisation divided by the number of cells in the control flask. The lower panel shows the surviving fraction obtained when cells are plated out and colonies counted. Each data point is plotted as mean ± SEM.

Comparison between survival curves at dose rates ($cGy\ h^{-1}$)		p-value
100	60	0.9483
100	30	**0.0035***
100	10	**0.0035***
100	5	**0.0132***
60	30	0.2143
60	10	0.0548
60	5	**0.0387***
30	10	0.7546
30	5	0.0599
10	5	0.0868
acute	100	**0.0022***
acute	60	**0.0167***
acute	30	**0.0388***
acute	10	**0.0047***
acute	5	0.3397

Table 4.4
Shows the comparison between survival curves obtained after irradiating asynchronous A7 cells with ^{60}Cobalt γ-rays at dose rates shown. Multiple regression analysis was carried out to obtain a p-value for the difference between survival curves. *denotes survival curves which are significantly different from one another. The acute dose rate is 33 Gy h^{-1}.

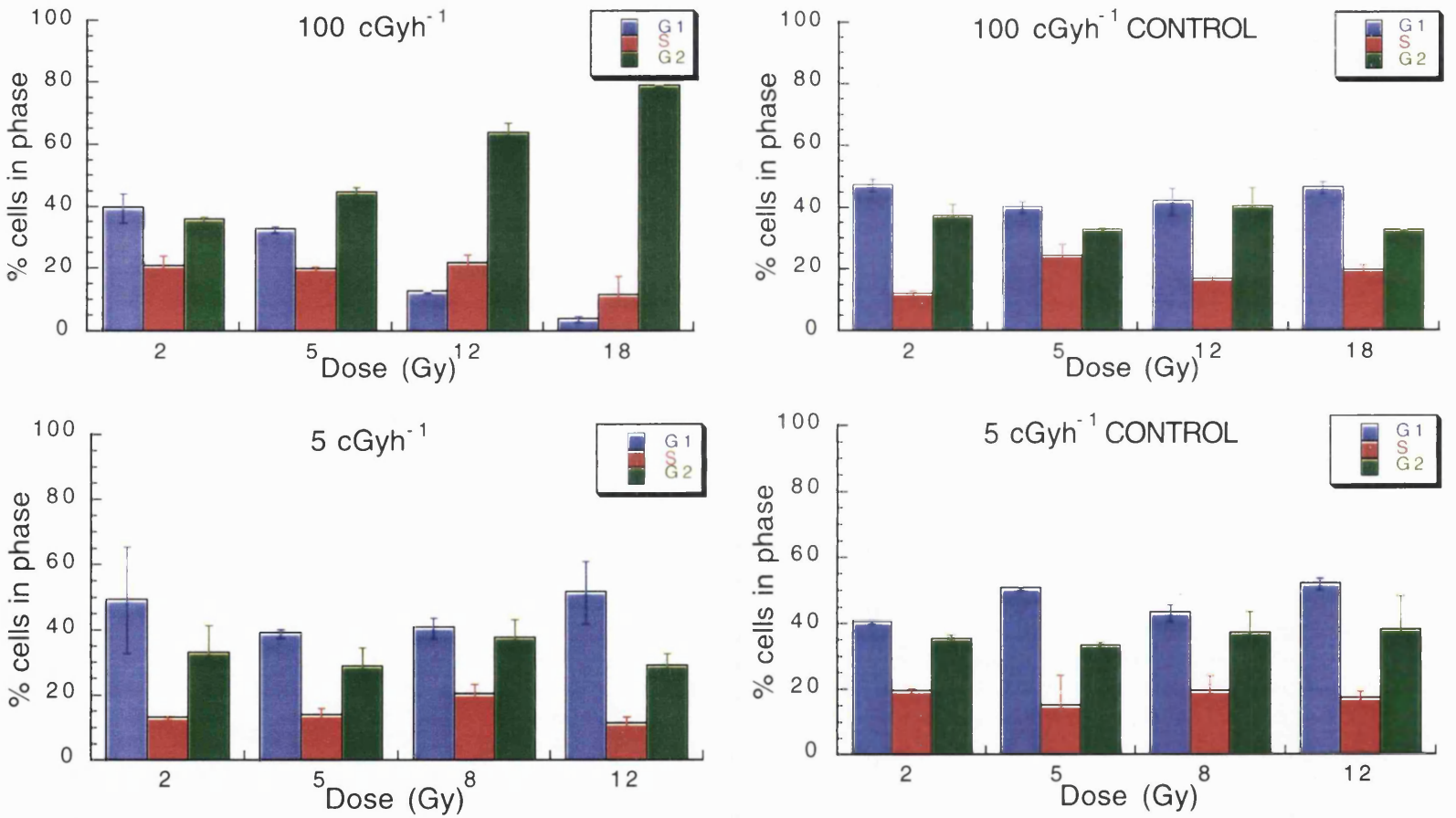

Figure 4.12

Shows the distribution of asynchronous A7 cells in each phase of the cell cycle after irradiation with ^{60}Cobalt γ-rays at dose rates of 100 cGy h^{-1} (top panel) and 5 cGy h^{-1} (bottom panel). The distributions of unirradiated controls sampled at the same time are shown.

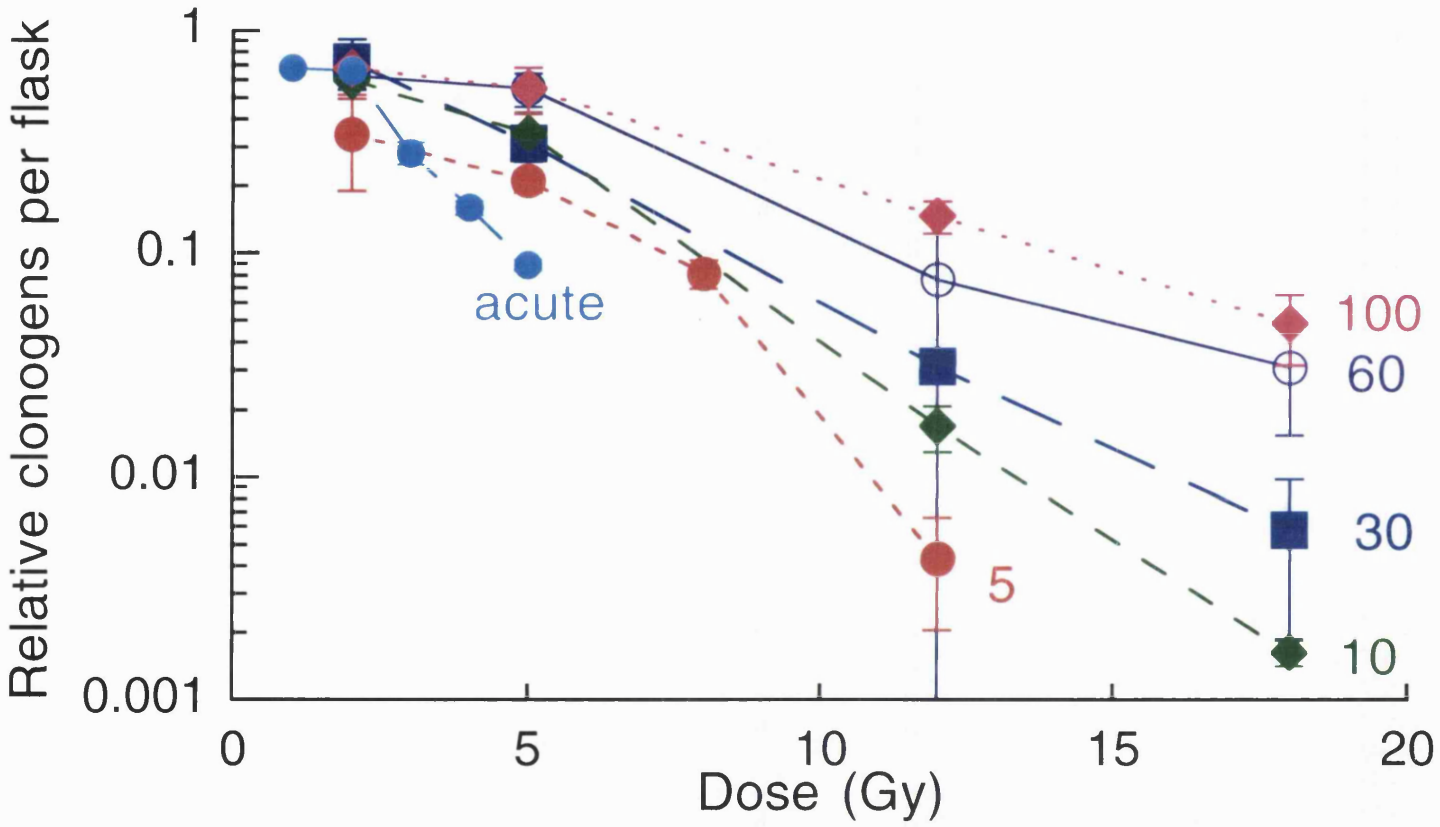

Figure 4.13
Shows survival curves obtained after irradiating asynchronous PC3 (human prostate carcinoma) cells using the ^{60}Cobalt water tank irradiation system. Dose rates shown are in cGy h^{-1}. Relative clonogens per flask is calculated by multiplying the surviving fraction by the relative yield as described in Section 4.4.1.1. Each data point is plotted as mean ± SEM. The acute dose rate was 33 Gy h^{-1}.

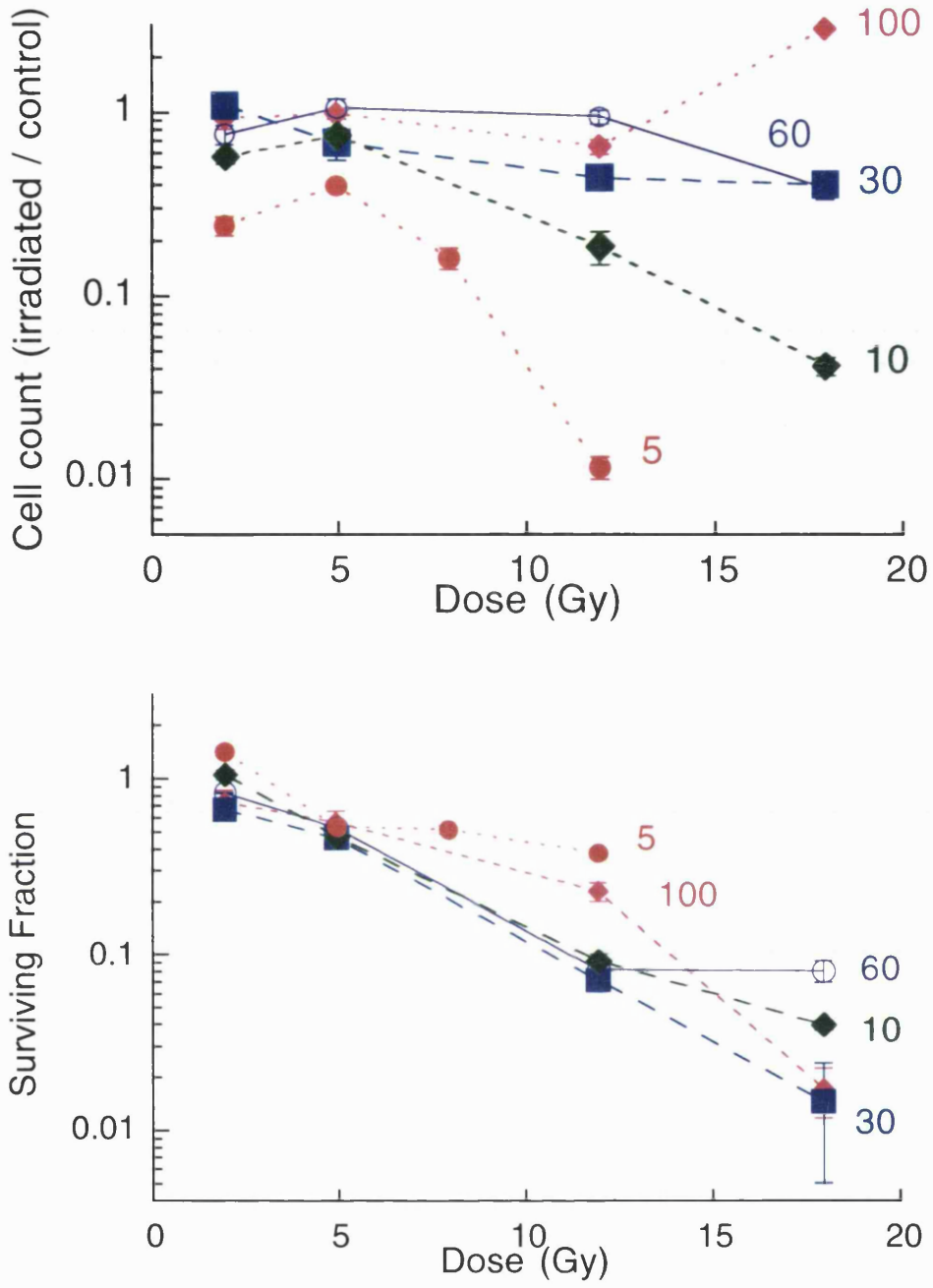

Figure 4.14
Shows survival curves obtained after irradiating asynchronous PC3 cells (human prostate carcinoma) using the ^{60}Cobalt water tank irradiation system. Dose rates shown are in cGy h^{-1}. The upper panel shows the cells counted per flask after trypsinisation divided by the number of cells in the control flask. The lower panel shows the surviving fraction obtained when cells are plated out and colonies counted. Each data point is plotted as mean ± SEM.

Comparison between survival curves at dose rates ($cGy\ h^{-1}$)		p-value
100	60	0.1052
100	30	0.1724
100	10	**0.0246***
100	5	**0.001***
60	30	0.4342
60	10	0.1474
60	5	**0.0055***
30	10	0.4802
30	5	0.0627
10	5	**0.0374***
acute	100	**0.0332***
acute	60	0.0527
acute	30	**0.0386***
acute	10	0.1077
acute	5	0.7184

Table 4.5
Shows the comparison between survival curves obtained after irradiating asynchronous PC3 cells with ^{60}Cobalt γ-rays at dose rates shown. Multiple regression analysis was carried out to obtain a p-value for the difference between survival curves. *denotes survival curves which are significantly different from one another. The acute dose rate is 33 $Gy\ h^{-1}$.

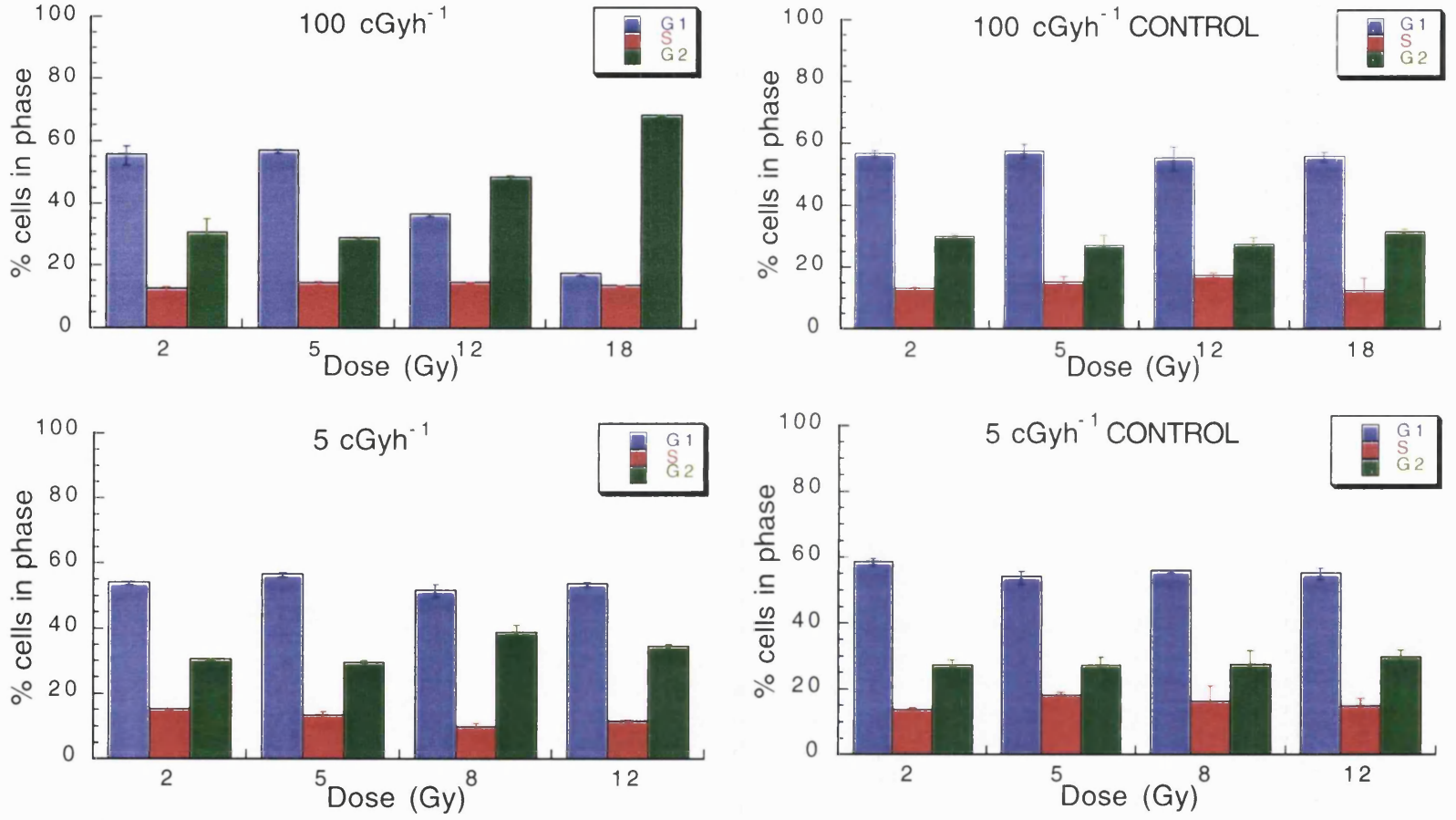

Figure 4.15

Shows the distribution of asynchronous PC3 cells in each phase of the cell cycle after irradiation with ^{60}Cobalt γ-rays at dose rates of 100 cGy h^{-1} (top panel) and 5 cGy h^{-1} (bottom panel). The distributions of unirradiated controls sampled at the same time are shown.

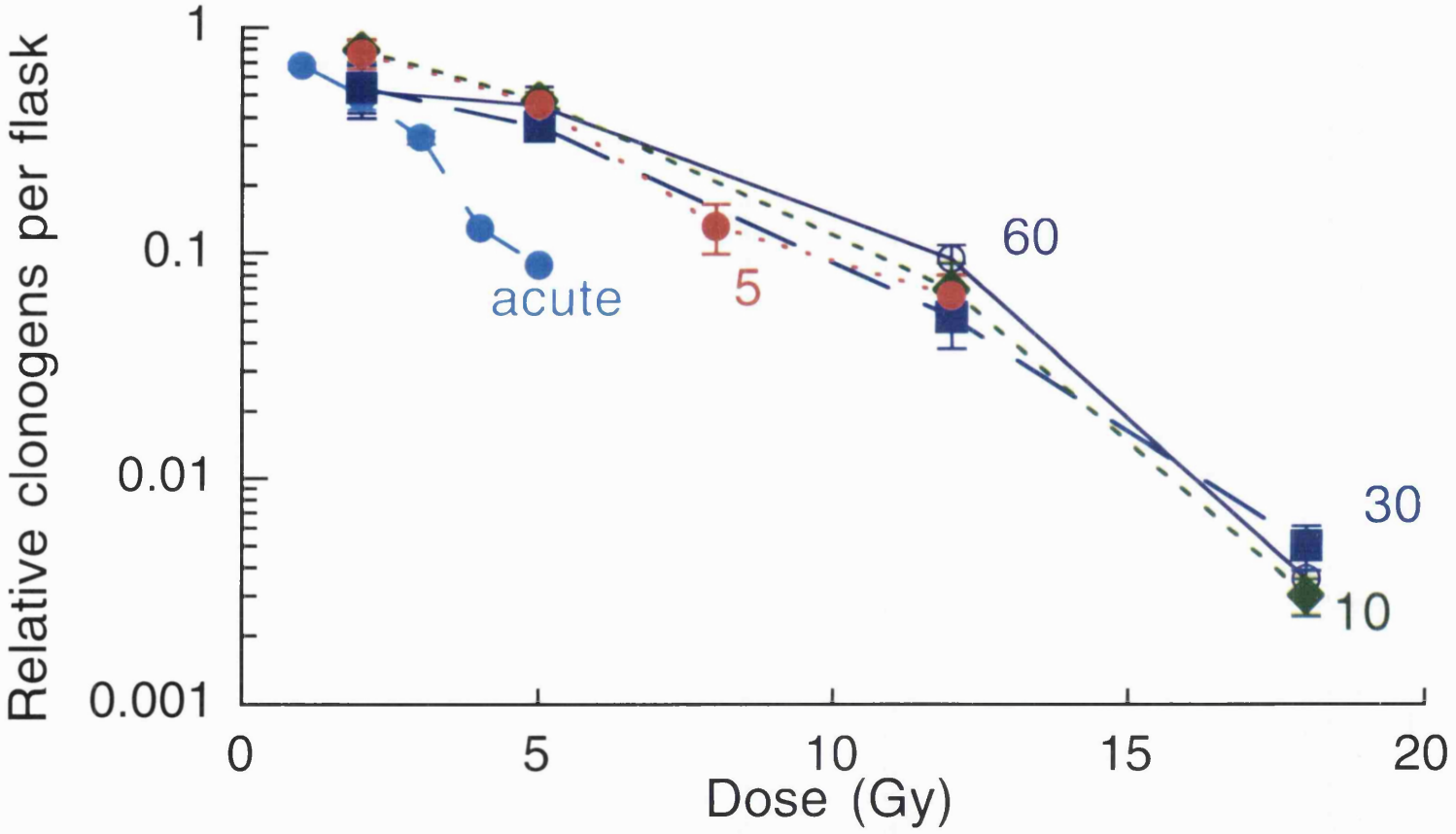

Figure 4.16
Shows survival curves obtained after irradiating asynchronous U373MG cells (human glioblastoma) using the ^{60}Cobalt water tank irradiation system. Dose rates shown are in cGy h^{-1}. Relative clonogens per flask is calculated by multiplying the surviving fraction by the relative yield as described in Section 4.4.1.1. Each data point is plotted as mean ± SEM. The acute dose rate was 33 Gy h^{-1}.

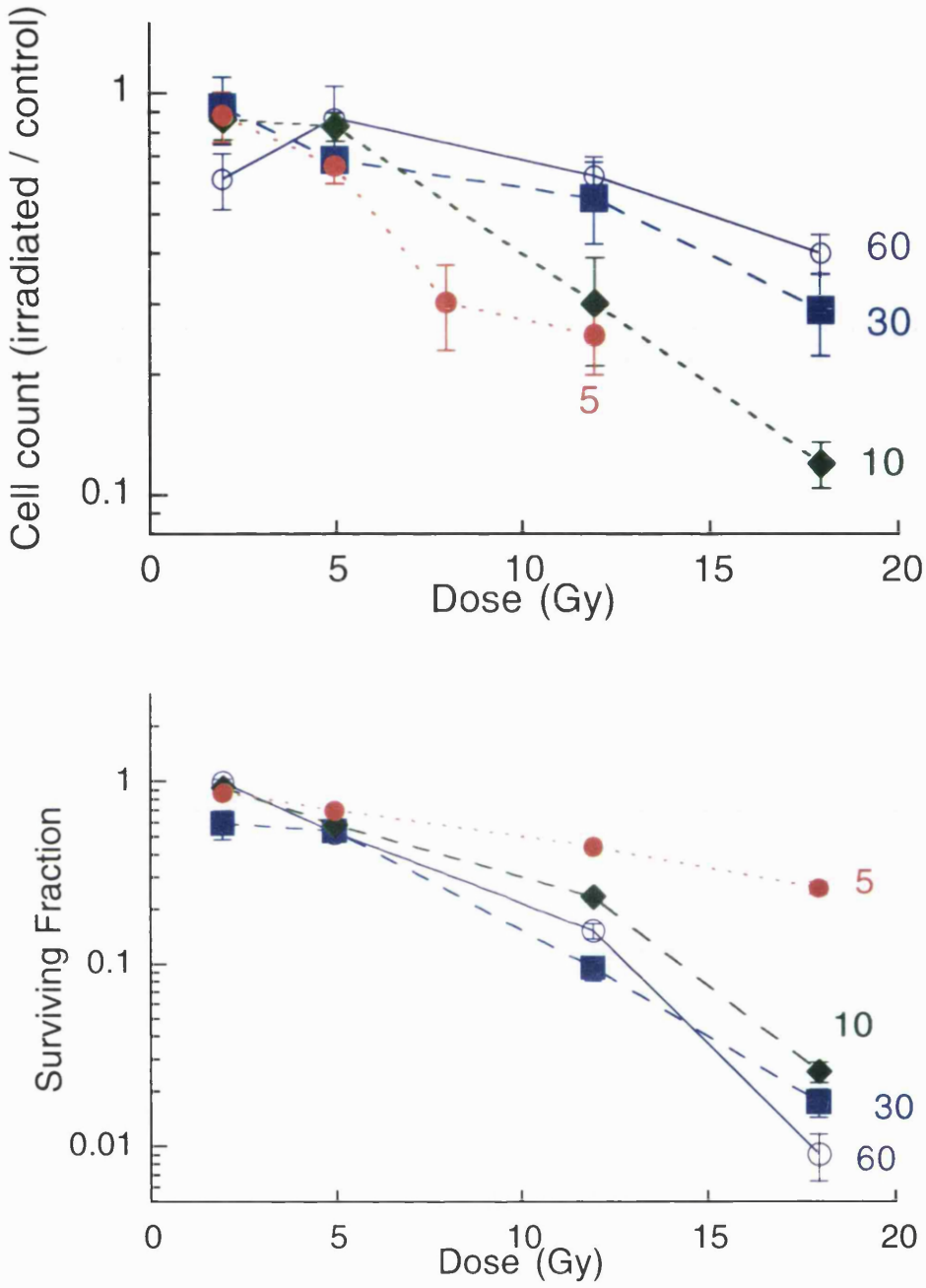

Figure 4.17
Shows survival curves obtained after irradiating asynchronous U373MG cells (human glioblastoma) using the ^{60}Cobalt water tank irradiation system. Dose rates shown are in cGy h^{-1}. The upper panel shows the cells counted per flask after trypsinisation divided by the number of cells in the control flask. The lower panel shows the surviving fraction obtained when cells are plated out and colonies counted. Each data point is plotted as mean ± SEM.

Comparison between survival curves at dose rates ($cGy\ h^{-1}$)		p-value
60	30	0.4064
60	10	0.3357
60	5	0.6405
30	10	0.1339
30	5	0.2424
10	5	0.2941
acute	60	0.0786
acute	30	0.0679
acute	10	**0.0452***
acute	5	**0.0195***

Table 4.6
Shows the comparison between survival curves obtained after irradiating asynchronous U373MG cells with ^{60}Cobalt γ-rays at dose rates shown. Multiple regression analysis was carried out to obtain a p-value for the difference between survival curves. *denotes survival curves which are significantly different from one another. The acute dose rate is 33 $Gy\ h^{-1}$.

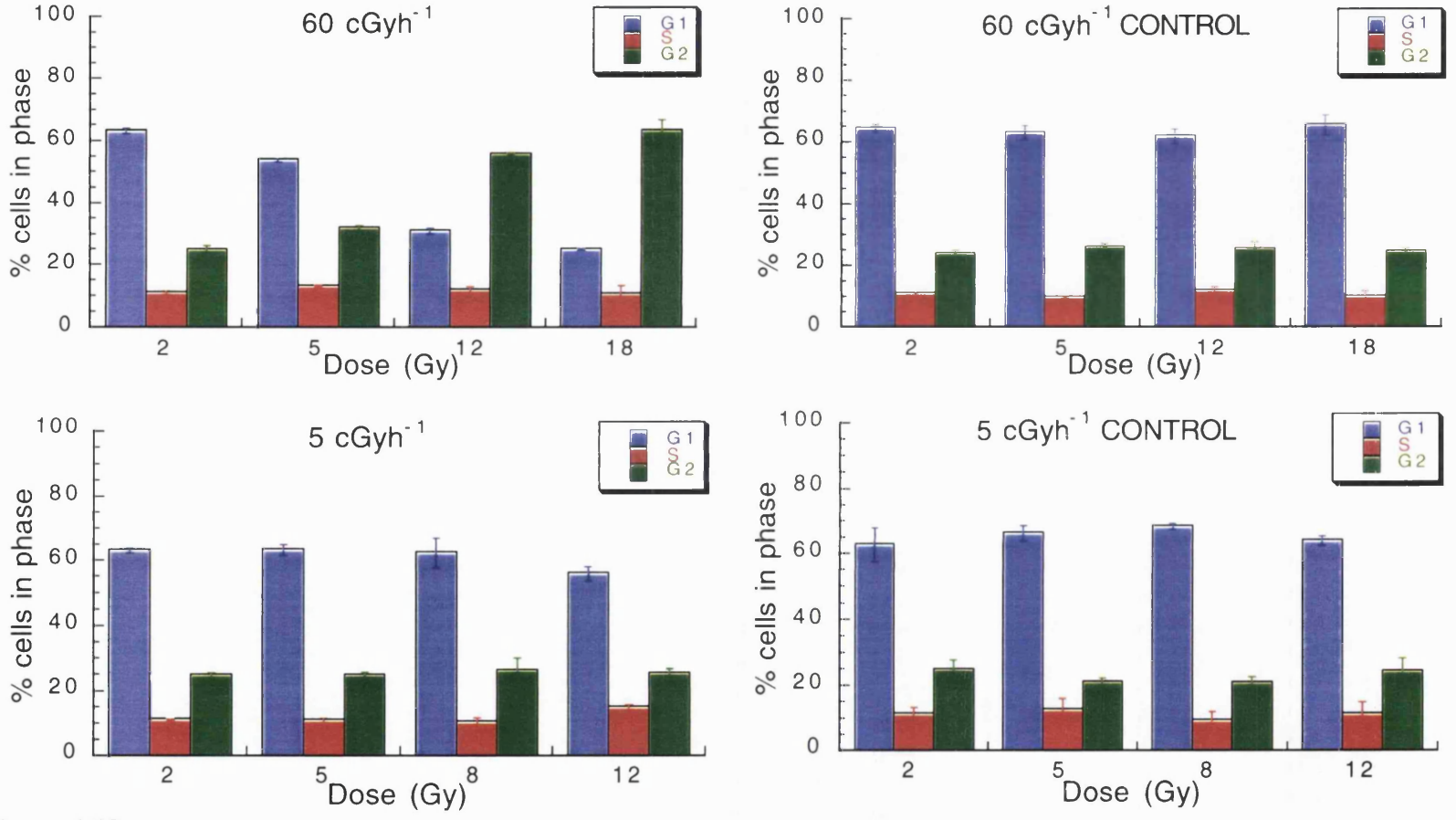

Figure 4.18

Shows the distribution of asynchronous U373MG cells in each phase of the cell cycle after irradiation with ^{60}Cobalt γ-rays at dose rates of 60 cGy h^{-1} (top panel) and 5 cGy h^{-1} (bottom panel). The distributions of unirradiated controls sampled at the same time are shown.

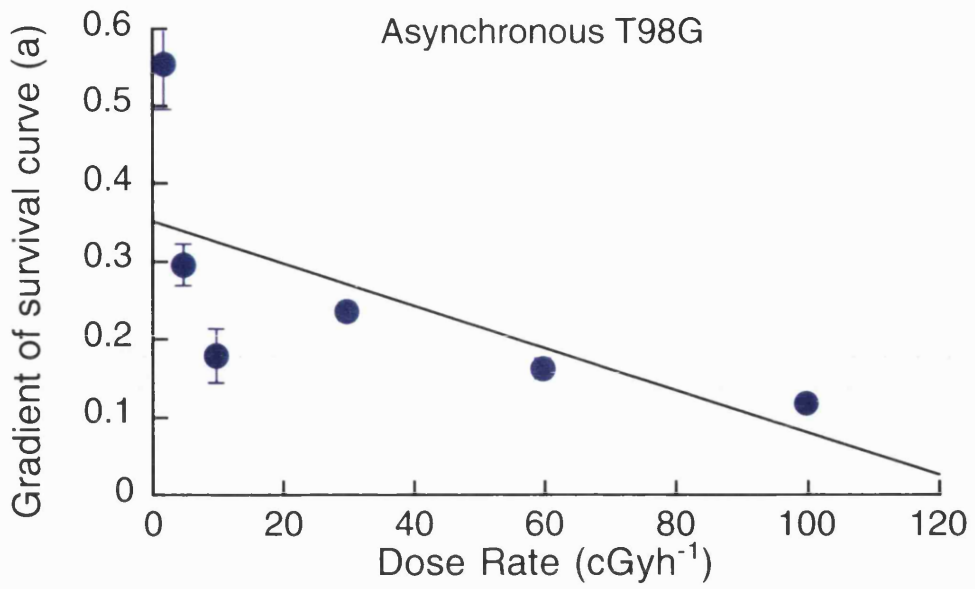

Figure 4.19
Shows dose rate plotted against the gradient obtained, *a*, when asynchronous T98G survival curves are fitted to the following equation, $SF = e^{-adose}$. One-way ANOVA shows that the variability between dose rates is significantly greater than the variability within dose rates ($p=4\times10^{-8}$). Data points shown are mean ± SEM

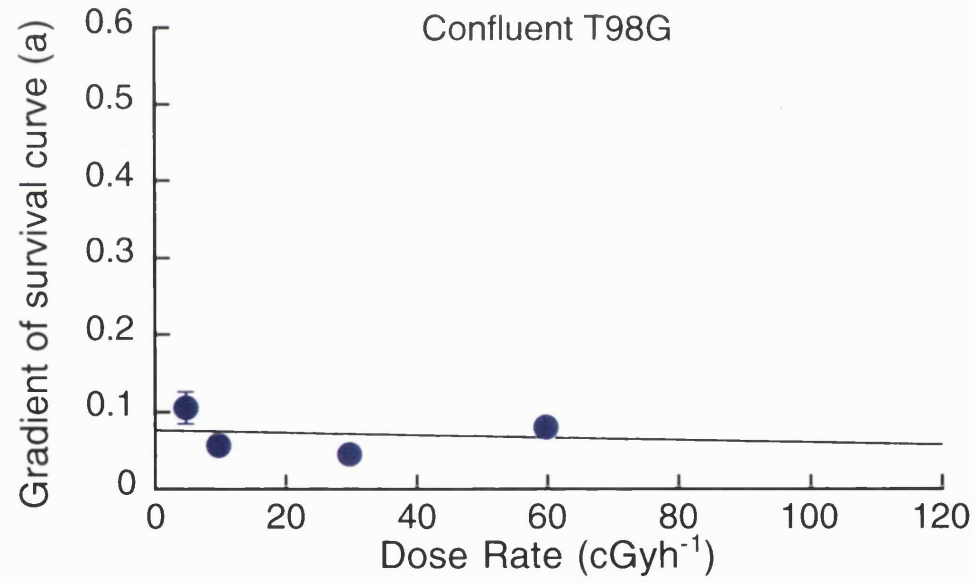

Figure 4.20
Shows dose rate plotted against the gradient obtained, *a*, when confluent T98G survival curves are fitted to the following equation, $SF = e^{-adose}$. One-way ANOVA shows that the variability between dose rates is significantly greater than the variability within dose rates ($p= 0.040$). Data points shown are mean ± SEM.

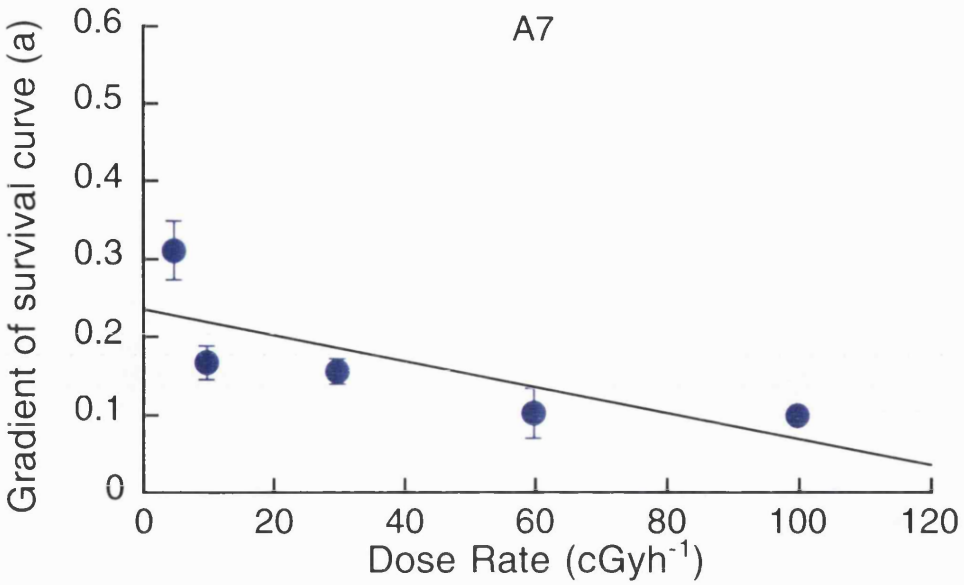

Figure 4.21
Shows dose rate plotted against the gradient obtained, a, when asynchronous A7 survival curves are fitted to the following equation, $SF = e^{-adose}$. One-way ANOVA shows that the variability between dose rates is significantly greater than the variability within dose rates (p= 0.050). Data points shown are mean ± SEM.

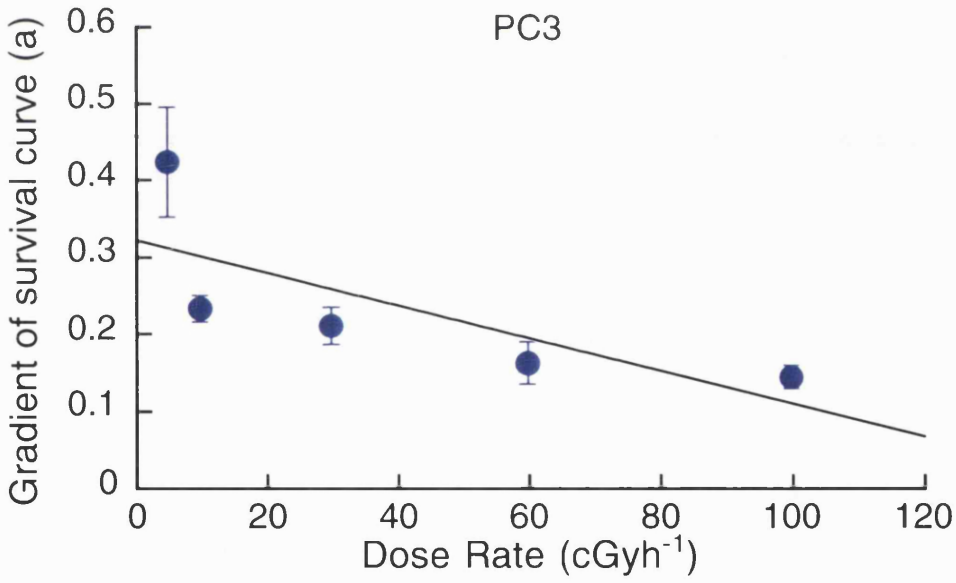

Figure 4.22
Shows dose rate plotted against the gradient obtained, a, when asynchronous PC3 survival curves are fitted to the following equation, $SF = e^{-adose}$. One-way ANOVA shows that the variability between dose rates is significantly greater than the variability within dose rates (p= 0.00023). Data points shown are mean ± SEM.

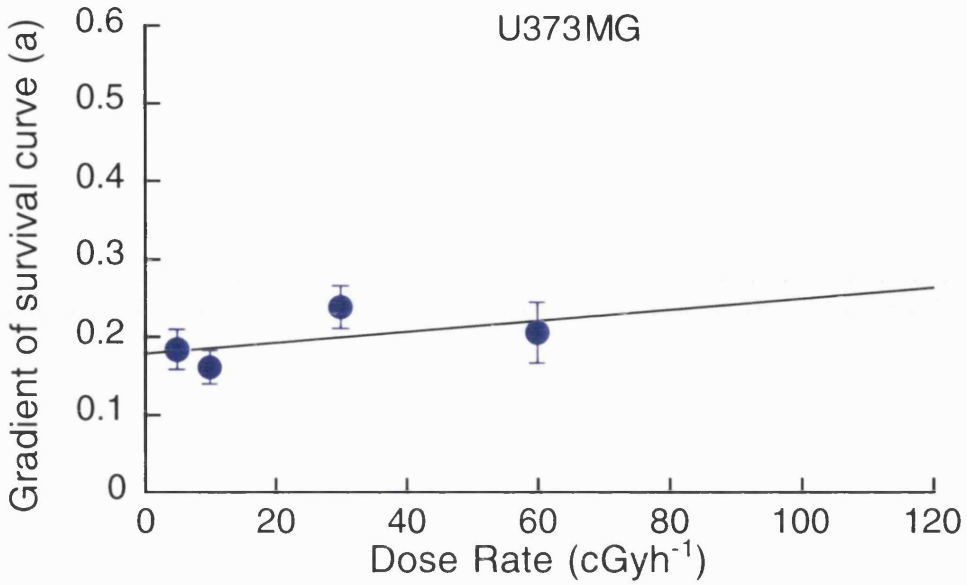

Figure 4.23
Shows dose rate plotted against the gradient obtained, a, when asynchronous U373MG survival curves are fitted to the following equation, $SF = e^{-adose}$. One-way ANOVA shows that the variability between dose rates is not significantly greater than the variability within dose rates (p= 0.43). Data points shown are mean ± SEM.

Cell line	Dose (Gy)	Dose rates to compare (cGy h^{-1})		Cell-cycle phase	p-value
Async T98G	2	100	5	G1	0.3634
Async T98G	2	100	5	S	0.753
Async T98G	2	100	5	G2	**0.0184***
Async T98G	5	100	5	G1	**0.0190***
Async T98G	5	100	5	S	**0.0131***
Async T98G	5	100	5	G2	0.0611
Async T98G	12	100	5	G1	**0.0002***
Async T98G	12	100	5	S	0.3128
Async T98G	12	100	5	G2	**0.0107***
A7	2	100	5	G1	0.5945
A7	2	100	5	S	**0.0848***
A7	2	100	5	G2	0.7642
A7	5	100	5	G1	**0.0202***
A7	5	100	5	S	0.0842
A7	5	100	5	G2	0.0592
A7	12	100	5	G1	**0.0158***
A7	12	100	5	S	**0.0441***
A7	12	100	5	G2	**0.0023***
PC3	2	100	5	G1	0.6758
PC3	2	100	5	S	**0.0328***
PC3	2	100	5	G2	0.9675
PC3	5	100	5	G1	0.8339
PC3	5	100	5	S	0.4884
PC3	5	100	5	G2	0.5687
PC3	12	100	5	G1	**<0.0001***
PC3	12	100	5	S	**0.0064***
PC3	12	100	5	G2	**0.0004***

Table 4.7
Shows p-values obtained when the percentage of cells in each phase of the cell cycle are compared for two different dose rates at the same total dose for each cell line. p-values were obtained using ANOVA t-test. * denotes values which show a significant difference between the two dose rates.

Cell line	Dose (Gy)	Dose rates to compare (cGy h^{-1})		Cell-cycle phase	p-value
U373MG	2	60	5	G1	0.9798
U373MG	2	60	5	S	0.9889
U373MG	2	60	5	G2	0.9226
U373MG	5	60	5	G1	**0.0043***
U373MG	5	60	5	S	0.0562
U373MG	5	60	5	G2	**0.0035***
U373MG	12	60	5	G1	**0.0005***
U373MG	12	60	5	S	0.0857
U373MG	12	60	5	G2	**<0.0001***
Conf T98G	2	60	5	G1	**0.0002***
Conf T98G	2	60	5	S	0.8793
Conf T98G	2	60	5	G2	0.1152
Conf T98G	5	60	5	G1	0.1444
Conf T98G	5	60	5	S	0.2170
Conf T98G	5	60	5	G2	0.5228
Conf T98G	12	60	5	G1	0.4832
Conf T98G	12	60	5	S	0.1209
Conf T98G	12	60	5	G2	0.2765

Table 4.7 (continued)
Shows p-values obtained when the percentage of cells in each phase of the cell cycle are compared for two different dose rates at the same total dose for each cell line. p-values were obtained using ANOVA t-test. * denotes values which show a significant difference between the two dose rates.

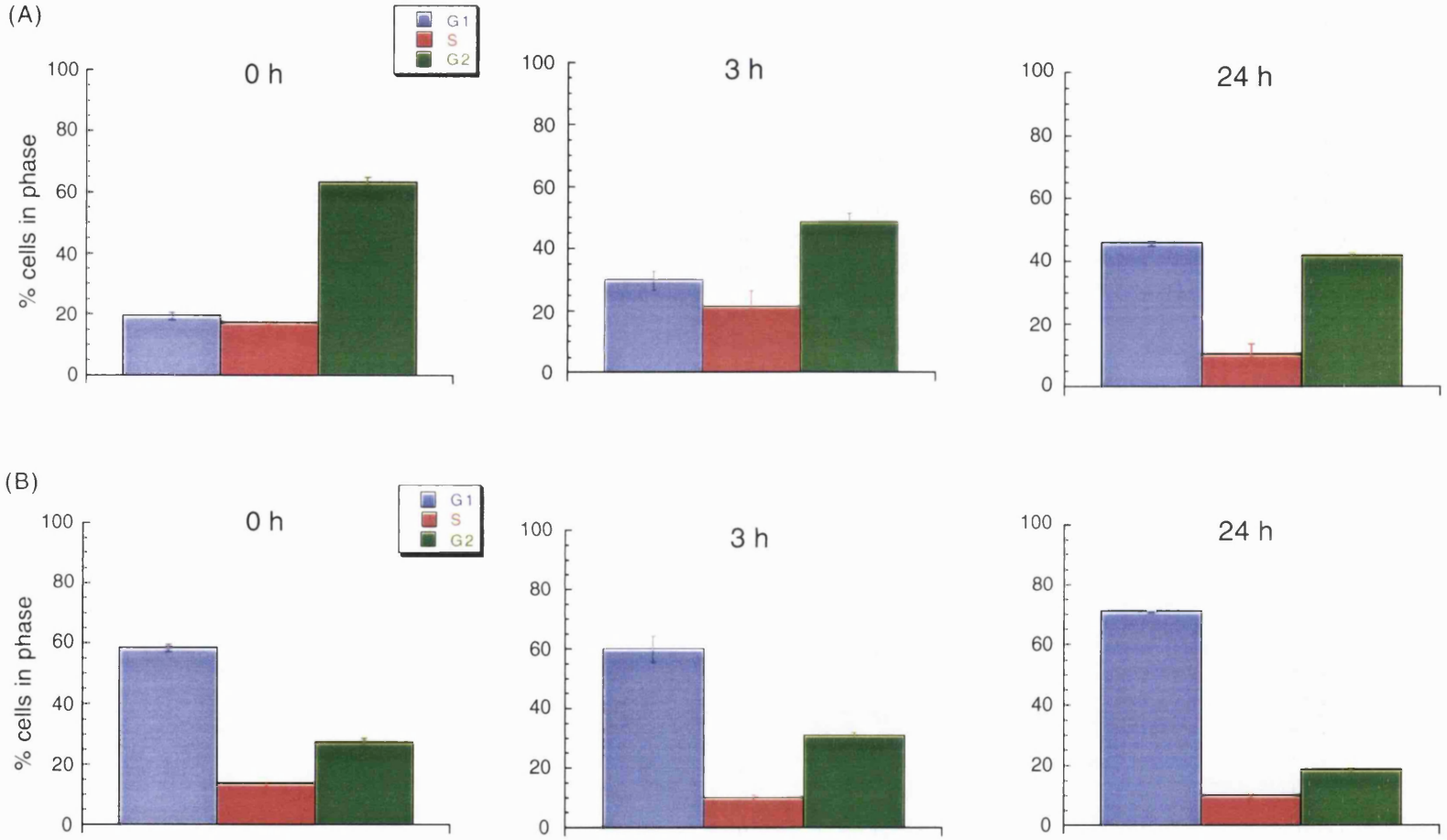

Figure 4.24
Shows the distribution of asynchronous T98G cells in each phase of the cell cycle after irradiation to a total dose of 5 Gy with ^{60}Cobalt γ-rays at dose rates of (A) 100 cGy h^{-1} (top panels) and (B) 5 cGy h^{-1} (bottom panels). The distributions are shown 0, 3 and 24 hours after irradiation.

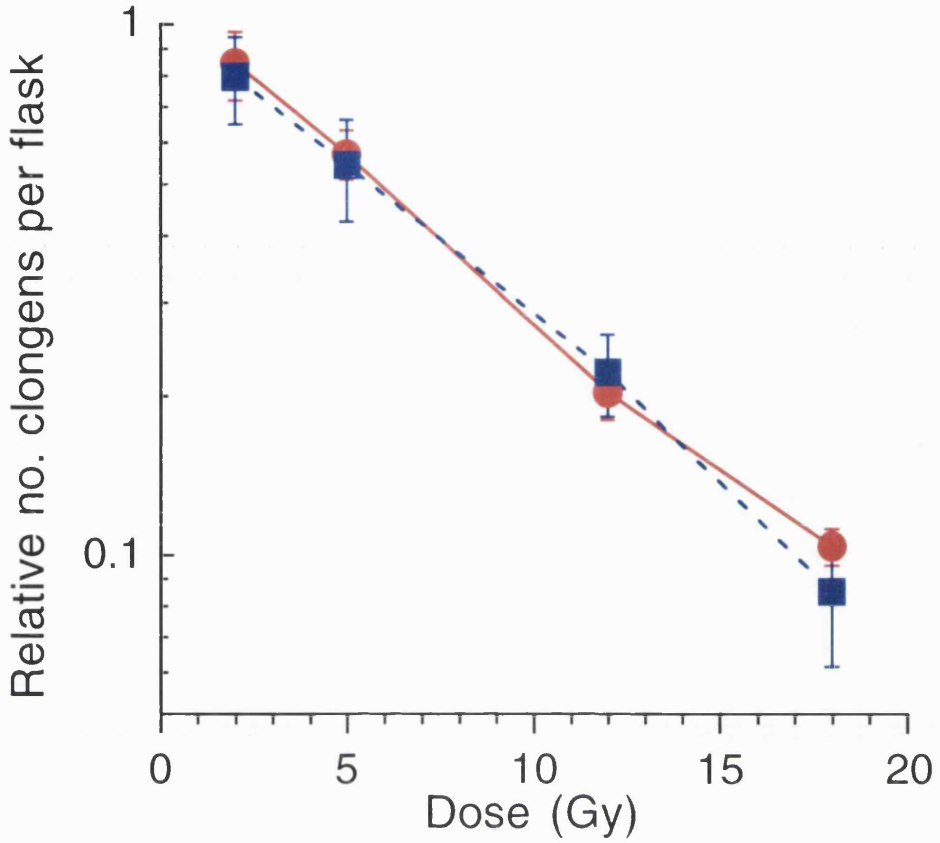

Figure 4.25
Shows the survival curves obtained when asynchronous T98G cells are irradiated with ^{60}Cobalt γ-rays at a dose rate of 100 cGy h^{-1}. The red symbols indicate survival obtained when cells were placed in the water tank at a distance of 5.7 cm from beam entry into the tank. The blue symbols show survival when the tank is moved towards the ^{60}Cobalt source and flasks are positioned 31.0 cm from beam entry into the tank.

4.4.3 Discussion

An inverse dose-rate effect was detected in asynchronous and confluent T98G cells, asynchronous A7 and PC3 cells when irradiated with low dose-rates of ^{60}Cobalt γ-rays. The effect was not seen in asynchronously growing U373MG cells. Tables 4.2 to 4.6 show the results when pairs of survival curves were compared using multiple regression analysis. For asynchronous T98G, A7 and PC3 the survival curves obtained at the highest dose rate were significantly more radioresistant than that obtained for the lowest. This is an unexpected result as the considered opinion is that as the dose rate is reduced, an increase in cell survival is observed and therefore more total dose is required to see the same amount of cell kill compared with higher dose rates (Lajtha 1961, Elkind 1967). This does not occur in these experiments, however, the U373MG cell line did not show the inverse dose-rate effect. With no significant differences between the survival curves observed and maximal dose-rate sparing appears to occur at 60 cGy h^{-1}. The cell lines in which the inverse dose-rate effect was observed all showed low-dose HRS at acute doses and the HRS-negative U373MG cell line did not show an effect. This may reflect a relationship between HRS/IRR and the inverse dose-rate effect seen in these experiments.

Figures 4.19 to 4.23 show plots obtained when all survival curves for each cell line were fitted to $SF = e^{-adose}$ and the gradient, *a*, is then plotted against dose rate and analysed as described in Section 4.4.1.1. For the cell lines where a significant inverse dose rate is present in the above analysis (asynchronous and confluent T98G, A7 and PC3), the gradient of a slope drawn approximately through the points, was negative (*i.e.* as the dose rate increases the cell-survival curve becomes shallower). A one-way analysis of variance showed that the variability between values of *a* obtained for a particular dose rate was significantly greater than the variability within *a* obtained for a particular dose rate. This suggested than an effect was real and the pattern of the data was not merely due to variability in the results. It was possible that the survival curves obtained at LDR approximated more to a curve than a straight line on a log linear plot. Therefore a second method of analysis was employed where the points from all survival curves from each cell line were fitted to the LQ model and if a significant β was obtained then, for that survival curve, the α value for the LQ fit was plotted. However, after fitting a straight line, the highest p and r values were obtained using the original *a* value from the exponential fit. Figures 4.19 to 4.22 show the best fits obtained. The lack of a linear relationship between dose rate and *a* may reflect a biphasic inverse dose-rate response where at the lowest dose rates (below 20 cGy h^{-1}), the cells have an initial extremely sensitive response and then above this dose rate a second, less sensitive effect occurs which decreases as the dose rate is increased. This may reflect damage levels approaching an IRR trigger threshold and so not showing an inverse dose-rate response to such a great degree (see

Chapter 6). The U373MG cell line (Figure 4.22) did not show a negative gradient, possibly suggesting a slight dose-rate sparing effect. The data do suggest that the dose rate vs. *a*, may not have a linear relationship. One-way analysis of variance was carried out to assess whether the variability between dose rates is greater than the variability within each dose rate. This difference was found not to be significant for the U373MG cell line, thus suggesting that there is no inverse dose-rate effect on survival of U373MG when the dose rate is lowered.

In these cell lines the highest dose rate was also significantly different from the acute dose survival curve. Dose-rate sparing was occurring between these dose rates. At what point the sparing response turns into an inverse dose-rate effect is not known in these experiments as survival at dose rates between 100 cGy h^{-1} and 33 Gy h^{-1} was not investigated. Conventional radiobiological modelling such as that carried out by Lajtha and Oliver (1961) suggests that at maximum dose-rate sparing, the slope of the LDR survival curve approximates to the initial slope of the acute dose survival curve (α). For asynchronously growing T98G, when the initial slope of the acute dose survival curve was measured an α value of 0.218 was obtained. The slope of a line fitted to the 100 cGy h^{-1} survival curve, was 0.118 which gave greater dose-rate sparing than predicted from the α value. These numbers, however were not significantly different as determined by their 95% confidence intervals, which would suggest that maximum dose-rate sparing was indeed occurring at 100 cGy h^{-1} and so increasing the dose rate further would give a similar or more radiosensitive response. A similar effect was also observed in PC3 and U373MG (at 60 cGy h^{-1}) where the LDR slope and the HDR α value were not significantly different. The A7 cell line, however, showed a significant difference between the two values, where irradiation at low-dose rate gave more sparing than predicted from the acute dose survival curve. This is not in agreement with the established opinion that maximum repair of sublethal damage occurs when the slope of the LDR curve is equal to α. However, in these experiments an inverse dose-rate effect at lower dose rates was seen. This cannot be explained by conventional "sublethal" damage repair theories such as the incomplete repair model (Thames 1985) as it is expected to see more repair occurring at low-dose rates and therefore a more resistant response. Responses to irradiation at low-dose rate are more complex than Thames' theory, so the maximum sparing effect seen may not be simply due to maximal sublethal damage repair, but a complex combination of effects. This may explain the results obtained for A7.

It was also a consideration whether the value of α obtained from the acute dose survival curve, which is plotted as SF against dose, could be justly compared with a line fitted to the LDR survival curve which is a plot of relative clonogens per flask vs. dose. As the relative clonogens per flask value was made up of SF multiplied by cell yield which takes into account

proliferation during irradiation, it was judged that this was a valid comparison. The proliferation at acute doses was equivalent to 1 and so the SF at acute doses was equivalent to the relative number of clonogens per flask. The reason that cell survival is not defined by the surviving fraction or the cell number alone in the present experiments, is that cells are irradiated for different periods of time depending on the dose rate. At the lower dose rates, the irradiation time is long and cells may go through several cell divisions. Daughter cells will not receive enough radiation damage to affect their surviving fraction, so the survival of the population as a whole is taken into account by the slowing in proliferation, *i.e.* cell number. For cells irradiated with higher dose rates *e.g.* 100 cGy h^{-1}, the irradiation time is much shorter (5 Gy takes 5 hours) and the cells do not have time to go through a whole cell cycle. In this situation, the surviving fraction is a more accurate representation of the cell survival. This was apparent when the two parameters are plotted separately as shown in Figures 4.5, 4.11, 4.14 and 4.17. This is not the case in confluent cultures where the cell number remains constant throughout irradiation time (Figure 4.8). Differences in growth kinetics between cell lines cannot be used to explain the inverse dose-rate effect as U373MG cells have a similar cell-cycle time to T98G (27.9±6.6 h for U373MG compared with 23.3±0.8 h for asynchronous T98G (Table 7.1)).

To investigate whether the degree of the inverse dose-rate effect at a particular dose rate for a specific cell line bore a relationship with parameters obtained from the acute dose survival curve, the gradient, *a*, of the survival curve for a single dose rate of each cell line was plotted against the d_C, α_s/α_r and SF_2 values obtained at acute doses for that cell line (graphs not shown). Analysis of variance showed there was no correlation between the gradient, *a*, and any of these parameters for any dose rate whether they were obtained using the cell sort or DMIPS protocols.

Confluent T98G cells showed a different pattern to asynchronously growing cells. They also showed an inverse dose-rate effect but it occurred at lower dose rates. At 30 cGy h^{-1}, there was a decrease in cell kill per unit dose compared with 60 cGy h^{-1}, so at these dose rates the cells effectively showed conventional dose-rate sparing. At dose rates below 30 cGy h^{-1}, there was an increase in cell kill per unit dose and so an inverse dose-rate effect occurred. In this case the α value for the survival curve obtained when confluent T98G cells were irradiated with ^{60}Cobalt at a dose rate of 33 Gy h^{-1}, was 0.056. When a curve was fitted to the survival curve obtained at 30 cGy h^{-1} and forced through 1, the slope was 0.045. The two numbers were not significantly different and this suggests that a maximal amount of sparing occurred at 30 cGy h^{-1} in confluent T98G cells. If the dose rate was further reduced, a similar or more radiosensitive response should be seen, and in this case the latter was observed.

The reason for the difference in effect between the confluent and asynchronous T98G, is likely to have reflected the different cell-cycle distributions. Confluent cells had few cells in the G2 phase of the cell cycle. This phase tends to be the most radiosensitive phase of the cell cycle (Sinclair and Morton 1965). In confluent cultures there were fewer than 20% of cells in G2 and so cells may have shown a more resistant response to radiation. This may explain why a sensitive response was only seen at the lowest dose rates in confluent cultures compared with an inverse dose-rate effect at higher dose rates in asynchronous cells. A second explanation may be that HRS/IRR is more pronounced in the G2 phase of the cell cycle than the other phases, so that confluent cells may appear more resistant. Recent evidence for this cell-cycle effect on HRS/IRR at acute doses has been gathered in this laboratory showing the most extensive HRS/IRR response in G2 and the least in S phase with G1 being intermediate (J. Kelly pers. comm.).

Changes in the distribution of cells within the cell cycle have been hypothesised as the explanation for the inverse dose-rate effects reported in the past. Studies irradiating HeLa and V79 cells at low-dose rate (Bedford and Mitchell 1973) and after fractionated exposures (Mitchell and Bedford 1977) showed an accumulation of cells in the G2/M phase of the cell cycle. Mitchell *et al.* (1979) later showed an inverse dose-rate effect on cell survival. This pre-mitotic accumulation is now generally accepted to be the explanation for this effect. In the experiments reported in this thesis, cells were irradiated at low-dose rate and cells remaining after counting and plating were fixed in 70% ethanol. At a later time they were stained with the DNA stain propidium iodide and analysed on a flow cytometer. Figures 4.6, 4.9, 4.12, 4.15 and 4.18 show the profiles obtained at the highest and lowest dose rates for each cell line. The profiles for the intermediate dose rates are shown in Appendix I. The percentage of cells in each phase of the cell cycle at a certain total dose was compared for the highest and lowest dose rates. The results are shown in Table 4.7. At the highest total dose compared, *i.e.* 12 Gy in all asynchronous cultures, there were significantly more cells in G2 at the higher dose rate. These data for the highest dose rates are similar to the findings of Mitchell *et al.* (1979) described previously. There did not appear to be any G2 accumulation at the higher dose rate in confluent T98G cultures. At the highest dose rate and in all cell lines (except the confluent T98G), as the total dose increases there was an increase in proportion of cells in G2/M phase of the cell cycle. However, at the lowest dose rates, where the greatest cell kill occurs in 3 of the cell lines, there was no significant pre-mitotic accumulation. This is comparable to the findings of Skladowski *et al.* (1993) who observed no G2 accumulation in the human bladder carcinoma cell line MGH-U1 irradiated with ^{60}Co γ-rays at a dose rate of 6 cGy h^{-1} but did see the pre-mitotic accumulation at a dose rates of 84 cGy h^{-1}. This occurred in the present study

in all asynchronous cell lines tested, including the U373MG which did not show an inverse dose-rate effect. This suggested that the inverse dose-rate effect seen was not due to G2/M accumulation. The fact that U373MG did not show a more sensitive response at 60 cGy h^{-1}, than at lower dose rates, despite having a greater proportion of cells in G2/M phase of the cell cycle, would suggest that the having more cells in this phase of the cell cycle, does not in itself alter radiosensitivity and the effect Mitchell *et al.* (1979) observed may not have necessarily been due to pre-mitotic accumulation as they hypothesised.

After HDR irradiations, in some cell lines, cells accumulate in the G1 phase of the cell cycle, *i.e.* a G1 delay occurs, and although a G2/M delay may be present it is masked by the cells not getting through the G1 block. At lower dose rates, it is possible that there is not enough damage to cause a G1 block and so the cells pile up in G2. At very low-dose rates (below 20 $cGyh^{-1}$) there may not be enough recognised damage even to block cells in G2. However, radiation induced delays in G1 are essentially related to the status of the p53 gene and cells lacking functional p53 protein generally lose the ability to arrest in G1 in response to radiation (Kastan *et al.* 1992, Kastan and Kuerbitz 1993, Kuerbitz *et al.* 1992). All the cell lines used in these experiments are p53 mutant. p53 is known to control cells progressing into the S phase of the cell cycle, if a mutation occurs, cells may not show a G1 delay after ionising radiation (Paulovich *et al.* 1997), indeed when the cell lines were irradiated to 2 Gy at HDR (Chapter 7) they did not show a G1 delay, but did show a G2 delay.

Cells irradiated at the upper end of the low-dose rate scale (60 and 100 cGy h^{-1}), showed an accumulation of cells in G2 with increasing dose. This was not a permanent state as the cells reverted back to a control profile within 24 h after irradiation (Figure 4.24). At the lowest dose rates, however, no delays are apparent from the cell-cycle distribution profiles, but cell-cycle delay time course experiments using BrdUrd-incorporation (Section 2.7.1 and 7.3) were not carried out. Several studies have shown a correlation between a long G2 delay and radioresistance (Ehmann *et al.* 1975, Bates and Lavin 1989), as may occur at the higher dose rates. However these studies were carried out at acute doses of radiation where any resulting accumulation of cells in G2 were not subsequently irradiated as would occur in continuous LDR exposures possibly increasing cell kill. Conversely there are other studies that show correlations between large G2/M delays and radiosensitivity (Nagasawa *et al.* 1994, Power 1998) and others which show no correlation (Smeets *et al.* 1994). Therefore a conclusion cannot be drawn that the increased radioresistance seen at higher dose rates is due to a G2 delay.

In these cell lines there may have been a threshold level of damage at which a delay occurs and at dose rates producing damage below this threshold, cells do not accumulate in G2. In this scenario cells would have less time to undergo DNA damage repair in G2 before progressing through mitosis and this could, to some extent, explain the increased cell kill observed at the lowest dose rates. However it seems unlikely that cells will receive such a small amount of damage as to escape a G2 block, but then subsequently die after they go through mitosis, as even a dose as small as 0.25 Gy in HL60 given at acute doses is enough to induce a G2/M delay (Gilbertz *et al.* 1998). It is possible at LDR that a HRS-like response is occurring in which the cells are not recognising damage both in terms of repair and delaying their cell-cycle progression and it is a combination of both that leads to increased cell kill. However, in T98G, at an acute dose of 0.4 Gy where HRS occurs, a G2/M delay was present and this is of similar magnitude to that found at 2 Gy where HRS was not present (Short 1999). Furthermore, in another study no correlation between HRS and cell-cycle perturbations was found in a series of HRS positive and negative cell lines studied in this laboratory (Power 1998). This would suggest that HRS is a separate response to cell-cycle perturbations, and it may be that in this study HRS occurred independently of the absence of the G2 block. The fact that the HRS negative cell line U373MG, shows a similar pattern of radiation-induced cell-cycle perturbation, but no increased cell kill at lower dose rates is support for this position. Further evidence for HRS being the explanation for the inverse dose-rate effect, rather than G2 accumulation, was that the effect was observed, albeit at a lower dose rate, in confluent cells. In this situation there was no G2 accumulation at higher or LDR (Figure 4.9), but an inverse dose-rate effect was still apparent (Figure 4.7). This would suggest that cell-cycle perturbations did not play the major role on the inverse dose-rate effect observed.

It was possible that the inverse dose-rate effect observed was due to a physical rather than biological effect. Different radiation types deposit energies at different densities, which is characterised by the Linear Electron Transfer (LET) defined as the mean energy given up to the medium by a particle travelling a distance of 1 μm. Differences in relative biological effectiveness (RBE) are dependent on the energy and spacing of ionisation events in biological structures and high-LET radiations which are more densely ionising have a higher RBE. ^{60}Cobalt γ-rays have a low-LET but may undergo a number of physical changes as they pass through the water in the tank. The major process is electron pair production. This happens when the photon interacts with the field around the nucleus of an atom and the whole of the photons energy is converted to the mass and kinetic energy of a positron and an electron. This will happen to a greater extent as the γ-rays move through the absorber, in this case water, so that the γ-rays reaching flasks at the back of the tank will have lost energy. These secondary electrons produce more dense ionisations (clusters) than the higher energy

photons at the front of the tank and therefore the radiation would effectively be of higher LET than at the front of the tank. Higher-LET radiation is more effective in killing cells, and although this is thought to be a small effect, it may be a reason for the increase in cell kill seen at the lowest dose rates rather than a biological inverse dose-rate effect. To test whether this was the case, the water tank was moved forward towards the source. This meant that a dose rate of 100 cGy h^{-1} received by cells, which was originally obtained by placing the flasks 6 cm from the beam entry into the tank, was now achievable by placing the flasks 31 cm into the tank. The γ-rays therefore had to pass through 25 cm more water to achieve the same dose rate. Asynchronous T98G cell survival was measured in this position using the same method as before. Figure 4.25 shows the survival curves obtained in both positions. By eye, there seemed to be no difference at all between the two survival curves. Multiple regression analysis also revealed that the survival curves were not significantly different ($p=0.306$). This therefore, showed that the inverse dose-rate effect observed in these experiments cannot be explained by physical changes in radiation quality as it passes through the water and must be due to a biological effect. The cell line U373MG did not show an inverse dose-rate effect despite being placed in a similar position at the rear of the tank as with the other cell lines. This also indicates that the inverse dose-rate effects must be related to biological rather than physical mechanisms.

Chapter 5. The survival of human tumour cells after low dose-rate irradiation with ^{125}Iodine

5.1 Aims

As an inverse dose-rate effect occurs when cells are irradiated with LDR ^{60}Cobalt γ-rays (Chapter 4), the aim of the experiments described in this chapter was to elucidate whether a similar effect could be detected when cells were irradiated with LDR ^{125}Iodine.

5.2 Introduction

In the clinic, low dose-rate exposures are often given in the form of brachytherapy. This is a treatment method where tumours such as prostate and pancreatic carcinomas are irradiated using interstitial implants containing radioisotopes. The most commonly used radioisotopes are ^{125}I (Storey *et al.* 1999, Beyer and Priestley 1997), ^{103}Pd (Blasko *et al.* 2000), ^{198}Au (Butler *et al.* 1997) and ^{89}Sr. These isotopes have relatively short half-lives and the low-energy photons they emit requires only a small amount of shielding. ^{125}Iodine has been used since the early 1970s, but techniques of implantation and the accuracy of dosimetry have greatly improved since that time. In North America, large numbers of implantations are now performed and the technique is beginning to be used extensively in the UK. ^{125}Iodine has a short half-life, compared with ^{103}Pd, ^{198}Au and ^{89}Sr, of 59.6 days and delivers very low-dose rate radiation to the surrounding tumours cells, typically 7 cGy h^{-1} at the start of a course of treatment. An example of an isodose plot using ^{125}I seeds for brachytherapy is shown in Figure 5.2.

The inverse dose-rate effect, whereby a decrease in dose rate causes a greater cell kill, was first documented by Mitchell (1979) in HeLa cells. As dose rates tend to be low in brachytherapy treatments (normally below 1 Gy h^{-1}), the inverse dose-rate effect may have a bearing on the treatment outcomes. Since those initial experiments, more studies have been carried out investigating this effect. It is now accepted that normal and neoplastic cells from different anatomical sites respond differently to ionising radiation exposure, whether the radiation is administered at high-dose rate or low-dose rate (Malaise *et al.* 1996, Steel 1991). Typically, when treated with ionising radiation, most proliferating cells delay progression throughout the replicative cell cycle via the activation of cell-cycle checkpoints (Hartwell and Kastan 1994, Tolmach *et al.* 1977, Leeper *et al.* 1973). Mitchell *et al.* (1979) found an accumulation of cells in the G2 phase of the cell cycle as the dose rate was reduced. This phase was considered the most sensitive phase of the cell cycle and so any increase in cell killing seen at low-dose rate was explained by this pre-mitotic accumulation. However, results reported in Chapter 4 of this thesis suggest that the inverse dose-rate effect is not due to G2 accumulation. This is consistent with the findings of other studies (DeWeese *et al.* 1997, DeWeese *et al.* 1998) who conclude that radiation-

associated perturbations in cell-cycle progression are not the dominant determinants of low dose-rate radiation killing efficacy.

Low-dose HRS occurs in several tumour cell lines *in vitro*, as observed in Chapter 3 and in other studies (Marples and Joiner 1993, Lambin *et al.* 1993, Wouters *et al.* 1996, Short *et al.* 1999a, Short *et al.* 1999b). HRS produces a decrease in cell survival at doses of less than 1 Gy, below the prediction of the Linear-Quadratic model which is based on extrapolation from higher doses. The effect may be more apparent in radioresistant cell lines (Section 3.3.1). It has been proposed that HRS reflects a differential triggering or induction of repair mechanisms, so that at very low doses, below a threshold, DNA repair mechanisms are not triggered and cells remain sensitive. It is possible that HRS could translate into a similar sensitivity when cells are continuously exposed to radiation at very low-dose rates and results obtained in Chapter 4 would strongly suggest this. As with low-acute doses, during low dose-rate exposures, cells would be receiving very small amounts of radiation per unit time and it is proposed that not enough sudden damage will be caused to induce the activation of repair mechanisms within the cell. In Chapter 4, an inverse dose-rate effect was found using ^{60}Co γ-rays to irradiate 3 cell lines which show HRS at low-acute doses of X-rays. Furthermore a cell line which did not show HRS, did not display an inverse dose-rate effect at very low-dose rates. This suggests that HRS and the inverse dose-rate effect observed may be mechanistically linked. It is also possible that cells irradiated with using ^{125}Iodine at very low-dose rates may also display an inverse dose-rate effect.

During low dose-rate brachytherapy treatments, as tumour cells are irradiated with dose rates usually below 1 Gy h^{-1}, it is possible that an inverse dose-rate response, possibly due to HRS, will occur in some of the cells. In this case more cells would be killed than would be predicted by dosimetry alone. The implications for this may be that brachytherapy implants containing a radioisotope that emits a very low-dose rate over a long period of time, may be better at tumour cell kill than higher dose-rate implants. This may also be true for pulsed dose-rate or fractionated treatments.

The experiments described in this chapter were designed to study the effect of low dose-rate ^{125}Iodine implants on the survival of human tumour cells *in vitro*, in protocols which could possibly mimic, to some extent, a clinical situation. The cell line used, T98G, a human glioblastoma, was held in confluence to rule out cell-cycle effects and has previously been shown to exhibit low-dose HRS (Chapter 3) and an inverse dose-rate effect using ^{60}Co γ-rays (Chapter 4), under these conditions.

5.3 Materials and methods

5.3.1 ^{125}Iodine seeds

The sources used in these experiments were ^{125}Iodine seeds, code IMC 6702, obtained from Nycomed Amersham. Figure 5.1 shows a cross-section of a seed. Each source consisted of a welded titanium capsule containing ^{125}Iodine adsorbed on anion exchange resin spheres. The air kerma rates at 1 m of the sources used were in the range 12.7 to 15.1 μ Gy h^{-1}, equivalent activities in the range 370 to 440.3 MBq (10.0 to 11.9 mCi). Each source emitted Tellurium X-rays of 27-32 keV and γ-rays at 35.5 keV and the dose distribution around each seed was not isotropic. The half-life of ^{125}Iodine is 59.4 days. Seeds of this model are commonly used for treatment of malignant brain tumours using temporary stereotactic interstitial implantations. Nycomed Amersham also produced lower activity seeds (code IMC6711) with air kerma rates of 0.24 to 7.92 μ Gy h^{-1}, with equivalent activities of 10.4 to 38.5 MBq (0.28 to 1.04 mCi) and these were used for permanent implantation of the prostate. The physical characteristics of both seeds are similar and the slight differences in anisotropy and spectrum of radiation were not considered significant for biological experiments. The former seeds were therefore used in these experiments as a higher initial dose rate meant that a larger range of dose rates could be studied.

The first goal was to develop a method of irradiating cells with the ^{125}Iodine seeds. The first method developed was to place cells in suspension culture with one 370 MBq (10 mCi) ^{125}Iodine seed and then to assess survival by haemocytometer counting and a clonogenic assay (Section 5.3.2). The second method developed was to fix nine of the seeds in a "plaque" structure and expose a petri dish of attached cells, by placing it on top of the plaque. Survival in this case would also be assessed by a clonogenic assay (Section 5.3.3). Dosimetry was carried out on both methods before exposure to cells.

5.3.2 Suspension culture

Proliferation during irradiation may mean difficulties in assessing cell kill for reasons outlined in Section 3.2.1. Therefore in an attempt to stop proliferation, the effect of serum deprivation was investigated. T98G cells were grown in various concentrations of FCS in suspension culture and cell number was counted as described in Section 2.3.1.2. Section 3.2.3.2 and Figures 3.5 and 3.6, show the results of these experiments. They indicated than a serum concentration of 0.5% to 1% was needed to halt proliferation in suspension cultures of T98G cells.

Dosimetry was carried out on the proposed irradiation system using suspension culture vessels containing 100 ml Fricke radiation dosimeter solution (Section 2.5.3) and one 370 MBq (10 mCi) ^{125}I seed. The hypothesis was that the dose measured by the Fricke solution would reflect the average dose to the cells in an experiment. The vessel was placed

on a magnetic stirrer pad. Titanium-encapsulated ^{125}Iodine seeds (model number IMC 6702) were obtained from Nycomed Amersham. In these experiments, each seed was designated an identification number on receipt (26/6/97) and the activity of each ^{125}I seed was measured using an ionisation chamber. The results are shown in Table 5.1.

The dosimetry for the ^{125}I seed in suspension culture was then measured. 100 ml Fricke solution was added to a 250 ml spinner bottle and one ^{125}I seed was placed into the bottle. The bottle was then placed on a magnetic stirrer and surrounded by foil to exclude light. A 5 ml sample was pipetted from the bottle into a plastic universal container every 48 h. The cuvette was first rinsed with 70% IMS before the addition of unirradiated Fricke solution which was used to calibrate the machine. The absorbance of a 1 ml sample of the irradiated Fricke was measured in a cuvette at a wavelength of 224 nm on a spectrophotometer. This procedure was then repeated twice per sample and was carried out for each ^{125}I seed. The dose measured was calculated from the spectrophotometer reading as described in Section 2.5.3.

5.3.3 ^{125}I seed irradiator plaques

Low dose-rate ^{125}Iodine irradiations were carried out using bespoke ^{125}Iodine seed irradiators. Nine titanium-encapsulated ^{125}Iodine seeds (model number IMC 6702, 388.5–462.5 MBq (10.5–12.5 mCi), Nycomed Amersham) were fixed into individual compartments in a plaque made from cross-linked polystyrene, chosen for its approximate tissue equivalence (for ^{125}Iodine radiation) and very high resistance to radiation damage. The seeds were fixed in a circular arrangement with one central seed and eight peripheral seeds located 15 mm from the centre and equally distributed around the periphery. The seeds were "sandwiched" between two other pieces of polystyrene such that the seeds were secure, constrained from moving. The polystyrene layer above the seeds was 6 mm thick and was designed to support the cell dish. The base of the irradiator was fixed to the inside of an 80 mm high steel cylindrical container, with a steel and lead lid to prevent radiation leakage. Figure 5.3 shows a diagram of this set up and Figure 5.4 (A & B) shows photographs of the irradiator. A 3.5 cm petri dish containing cells was placed 6 mm above the seeds. The dish was held in place using a plastic holder which could be rotated 360°. This was designed to give a homogenous dose of radiation to the cells. The irradiator was placed in an incubator and the lid was propped open slightly to permit gaseous exchange with the cell dish. Manipulations of the cell dishes were undertaken using tongs and wearing lead lined gloves.

Prior to loading the plaques, the activity of each individual seed was measured in an ionisation chamber (see Table 5.2). This enabled the dose rate of each seed irradiator to be calculated (dosimetry calculations are shown in Appendix 2). After loading the plaque, the distribution of the seeds was checked by autoradiography. It was also possible to do this

check on a gamma camera using a pinhole collimator. To verify the dose rate at 6 mm from the seeds, various dosimetric methods were considered. Disc-type ion chambers were considered, but rejected on the grounds of lack of sensitivity and high level of energy dependence in this energy range. Photographic film was useful to check the distributions of the sources, but was not an accurate dosimeter. A batch of high-sensitivity TLD was used. These were calibrated using a superficial X-ray tube with filtration and kVp to produce an average energy close to that of ^{125}Iodine photons. In order to deal with hot spots over seeds (except for the one central seed), the plaque was rotated by 22.5° (half-angle between peripheral seeds) half way through exposure of each culture dish. Five seed irradiators were built, 1 "old" irradiator (measurement date 29/01/98), 4 "new" irradiators designated 1 to 4 (measurement date 14/05/98).

Cell-survival curves were obtained for confluent T98G cells for each dose rate as the ^{125}Iodine decayed. 10^5 T98G cells were plated into a 3.5 cm petri dish containing 2 ml medium. Cells were then incubated to confluence for 4 days and the medium was then replaced with fresh medium. The dish was then placed on the irradiator situated in an incubator. Control dishes were placed on a "dummy" irradiator which was identical to the ^{125}I irradiator, but did not contain seeds. This was put into the same incubator. The media was replaced in all dishes every 3 days. It was impractical to divide the total irradiation time by 16 and rotate the cell dish by 22.5° after every time period, to avoid hot spots within the dose distribution (as was carried out during dosimetry measurements). This would have meant rotations occurring during the night in some cases, which was not practical. Therefore total irradiation time was divided into 4 periods which was considered a much easier way to arrange experiments that did not occur at unsociable times. After each period the plastic holder was rotated 90°. At the end of the radiation time, the dish was removed from the irradiator and cell survival was assessed using a clonogenic assay. Cells were harvested using a cell scraper. They were then centrifuged at 1500 r.p.m. for 5 minutes. The pellet was then resuspended in 5 ml medium and passed repeatedly through a 21-gauge needle. A haemocytometer was used to calculate cell number and a known number of cells were plated into 6 cm petri dishes containing 5 ml medium. These dishes were incubated for 2 weeks and were then stained with crystal violet. Colonies were counted manually to evaluate surviving fraction.

5.3.3.1 Data analysis

To test for significance of any differences seen between survival at different dose rates, multiple regression analysis was carried out between survival curves and a p-value for differences was obtained.

A second method of analysis was employed to give a general assessment of survival at different dose rates. Each survival curve was represented by a single value. This value was

determined on the assumption that each survival curve is linear on a plot of log survival versus dose. Each data set was fitted to the equation, $SF = e^{-adose}$, where a is the gradient of the line. The value of a was calculated, then plotted against dose rate and a line of best fit was obtained. One-way analysis of variance was used to compare inter- and intra-point variability.

Seed no.	Activity measured (MBq)
1	360.6 ± 0.03
2	359.4 ± 0.03
3	360.0 ± 0.03
4	360.2 ± 0.06

Table 5.1
Shows activity in MBq of ^{125}Iodine seeds as measured in an ionisation chamber on 26 June 1997 and then used for Fricke dosimetry for the suspension culture method (Section 5.3.1).

	^{125}Iodine irradiators				
	old	**1**	**2**	**3**	**4**
Measurement date	29/01/98	14/05/98	14/05/98	14/05/98	14/05/98
Activity of Peripheral seeds (MBq)	543.9 536.5 543.9 536.0 537.0 543.9 543.9 543.9	545.1 542.9 552.0 531.5 555.4 556.0 539.6 514.6	515.1 518.1 510.9 488.0 497.7 505.0 512.9 517.9	514.0 517.1 501.2 519.9 495.3 494.8 526.8 507.9	494.3 502.5 497.1 511.8 490.0 510.2 501.3 511.6
Activity of central seed (MBq)	444.0	601.0	520.2	525.6	516.2
Dose rate on measurement date (cGy h^{-1})	40.8	53.5	50.5	50.6	49.8

Table 5.2
Shows the activity of individual ^{125}Iodine seeds used in a specially designed irradiator system as measured in an ionisation chamber. Irradiators were designated a name, either a number or "old" (for the irradiator with an earlier measurement date).

5.4 Results

5.4.1 Suspension culture

The results of the dosimetry carried out with one ^{125}Iodine seed in a spinner bottle containing Fricke solution are shown in Figure 5.5. As expected, the absorbance of the Fricke solution increased with irradiation exposure time, although this is not a linear relationship and is highly variable both intra- and inter-experimentally.

As the results of the dosimetry using this method showed much variability, experiments were carried out to assess whether the variation seen was due to the methods of detection or variability in the chemistry, rather than the variation in the dose received by the Fricke solution. A stock solution of Fricke was irradiated with X-rays up to a total dose of 60 Gy to obtain a standard curve as described in Section 2.5.3. The absorbance of solutions taken from two separately irradiated stock flasks were measured at a wavelength of 224 nm and 304 nm using two different spectrophotometers. In these suspension culture experiments 224 nm was used to measure absorbance, however a wavelength of 304 nm has also been used in the past to measure absorbance when using Fricke dosimetry (Spinks and Woods 1990). On the optical density spectrum curve, 224 nm is on a shoulder region compared with 304 nm which is on a flatter area (Figure 5.8). Measuring absorbance at 224 nm, as was done, may therefore be a more sensitive method as small changes would be measured more accurately. The two wavelengths were compared. The results are shown in Figure 5.6. Figure 5.7 shows the same graphs normalised to allow a comparison of variability. Results were standardised by fitting a line through all points in Figure 5.6 and dividing each individual point by the gradient of the line. Results were then replotted and a line fitted to obtain the residual mean square error (RMSE). RMSE for 224 nm is 3.38 and 304 nm is 2.31 suggesting that using a lower wavelength of 224 nm did increase the variability. The intra and inter-seed variability from the suspension culture seed experiments (Figure 5.5) was calculated. A line was fitted through the data points for each seed and the RMSE was also calculated (seed 1: 6.108, seed 2: 3.23, seed 3: 6.45 and seed 4: 5.82). The RMSE for readings using X-ray irradiated Fricke at 224 nm from 2 separate flasks on both spectrophotometers was at 30 Gy and was 3.38. The curves obtained using each seed were significantly different by multiple regression analysis ($P < 0.0001$).

5.4.2 ^{125}Iodine seed irradiators

Figure 5.9 shows survival curves from confluent T98G cells irradiated on the "old" seed irradiator at a range of dose rates. The dose rates at the start of irradiation time are shown. Table 5.3 shows p-values obtained by multiple regression analysis when survival curves from the "old" irradiator are compared. Data from this irradiator shows a general trend towards an inverse dose-rate effect with the highest dose rate giving the least cell kill,

however this was not found to be significant. Figure 5.10 shows survival curves from confluent T98G cells irradiated on the "new" seed irradiators (1–4) at a range of dose rates and Tables 5.4 to 5.7 show significant differences between survival curves of different dose rates. Figures 5.11–15 show the plots of the gradient of each fitted survival curve against dose rate for each irradiator and Figure 5.16 shows this for all dose rates and all irradiators. Seed irradiator no. 1 showed a large spread in survival curves (Figure 5.10A), and although there are incidences where the lower dose rates gave increased cell kill, there was no overall trend towards an inverse dose-rate effect (Figure 5.12). There was also no trend towards an inverse dose-rate effect when cells were irradiated with seed irradiators 2 or 3 (Figures 5.10B and C and 5.13 and 5.14). Survival curves obtained using seed irradiator 4 (Figure 5.10D) did show an inverse dose-rate effect although this too was not significant (Figure 5.15). When data from all irradiators were considered (Figure 5.16), a slight inverse dose-rate effect was observed, although one-way analysis of variance showed that variability within a data point was not significantly different from variability between data points. This suggested that no effect was present or that variations in experimental technique *etc.* was masking any effects.

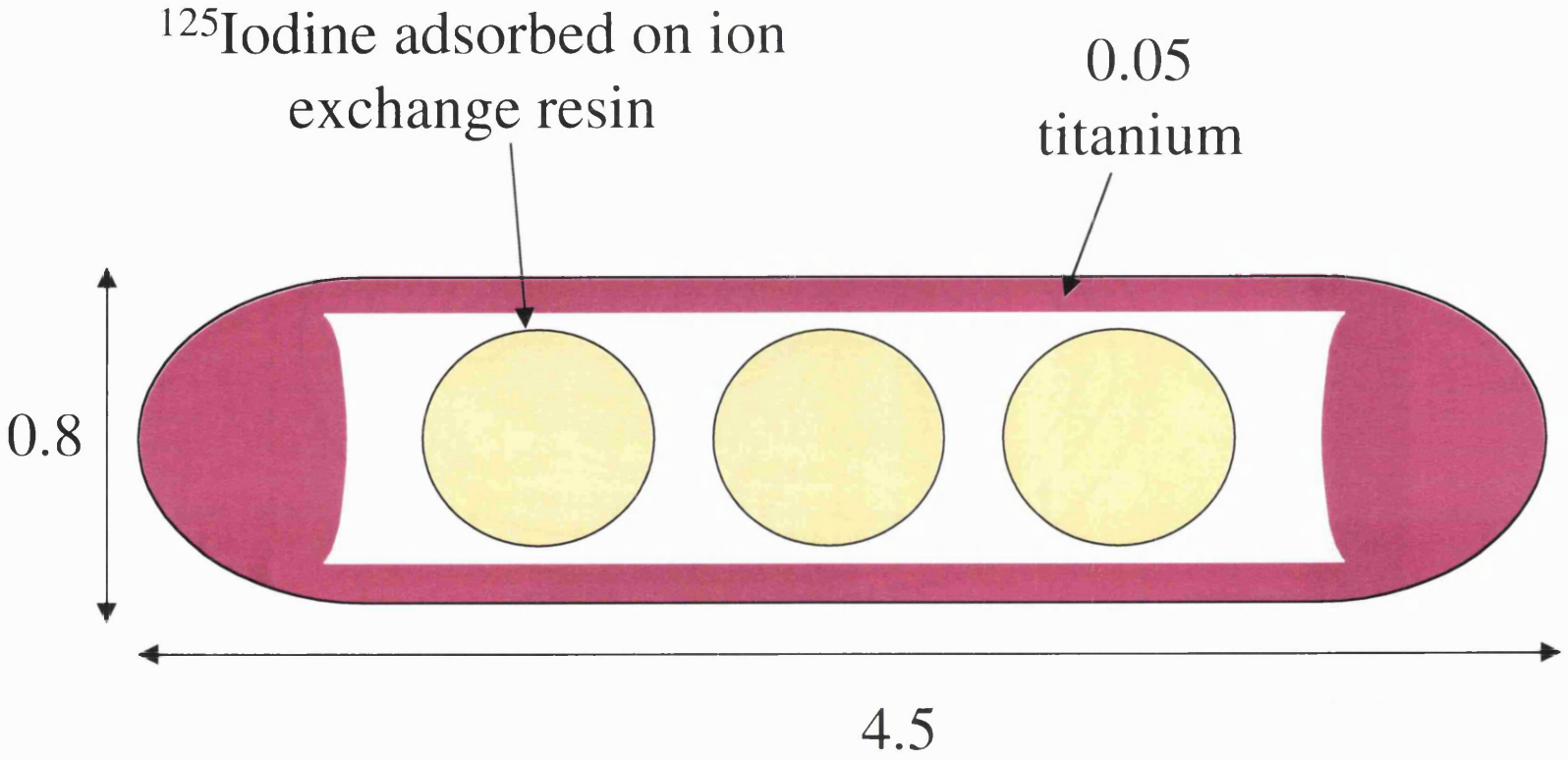

Figure 5.1
Shows a diagram of the cross-section through a ^{125}Iodine seed (Nycomed Amersham, code IMC 6702). Measurements are shown in mm. The seed consists of a welded titanium capsule containing ^{125}Iodine adsorbed on anion exchange resin spheres.

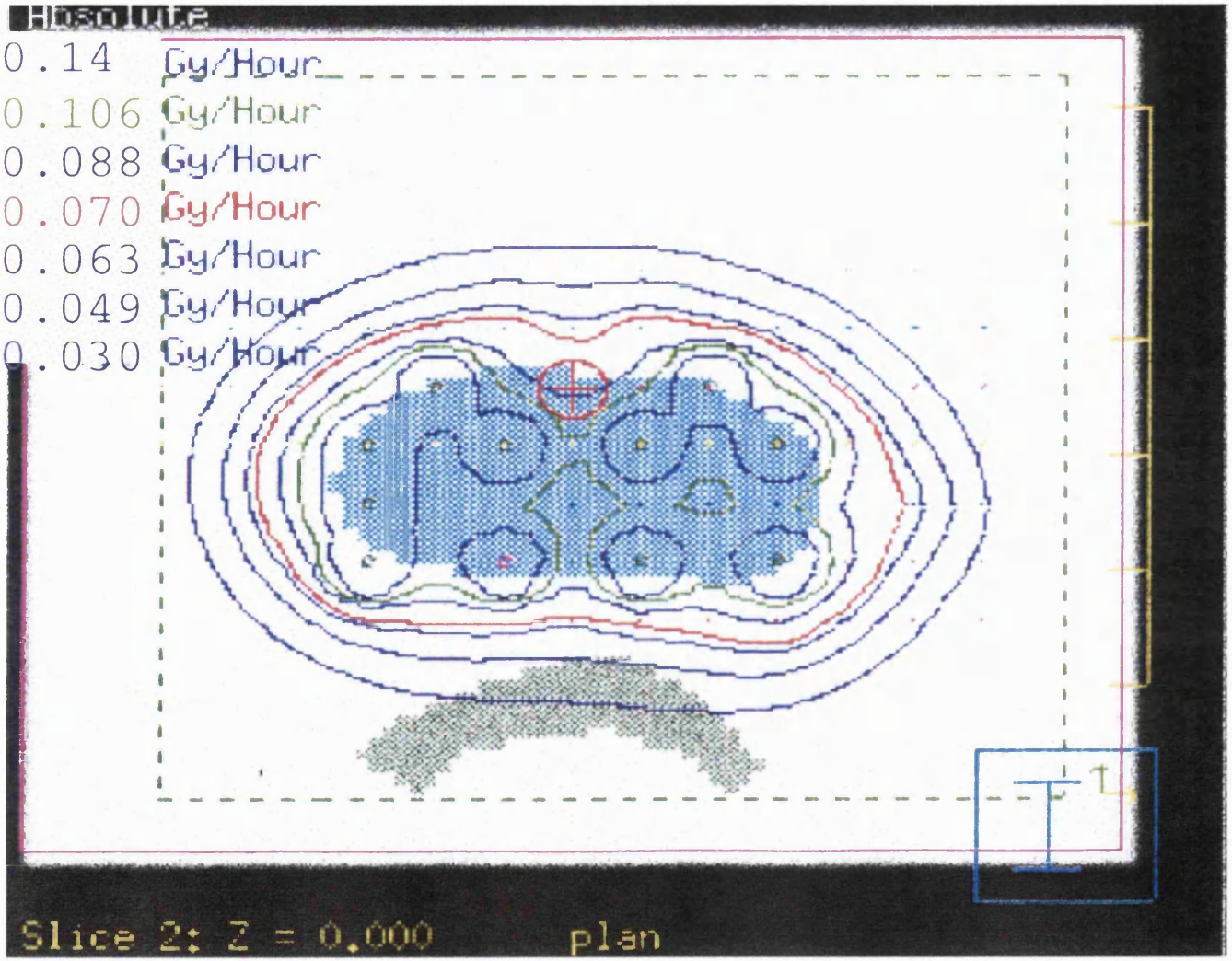

Figure 5.2
Shows an example of an isodose plot using ^{125}Iodine seeds for prostate cancer. The blue stippled area represents the prostate, and the green stippled area is the rectum. Brachytherapy implants are represented by small circles. The contours indicate the dose rates at a particular distance from each source at the start of treatment.

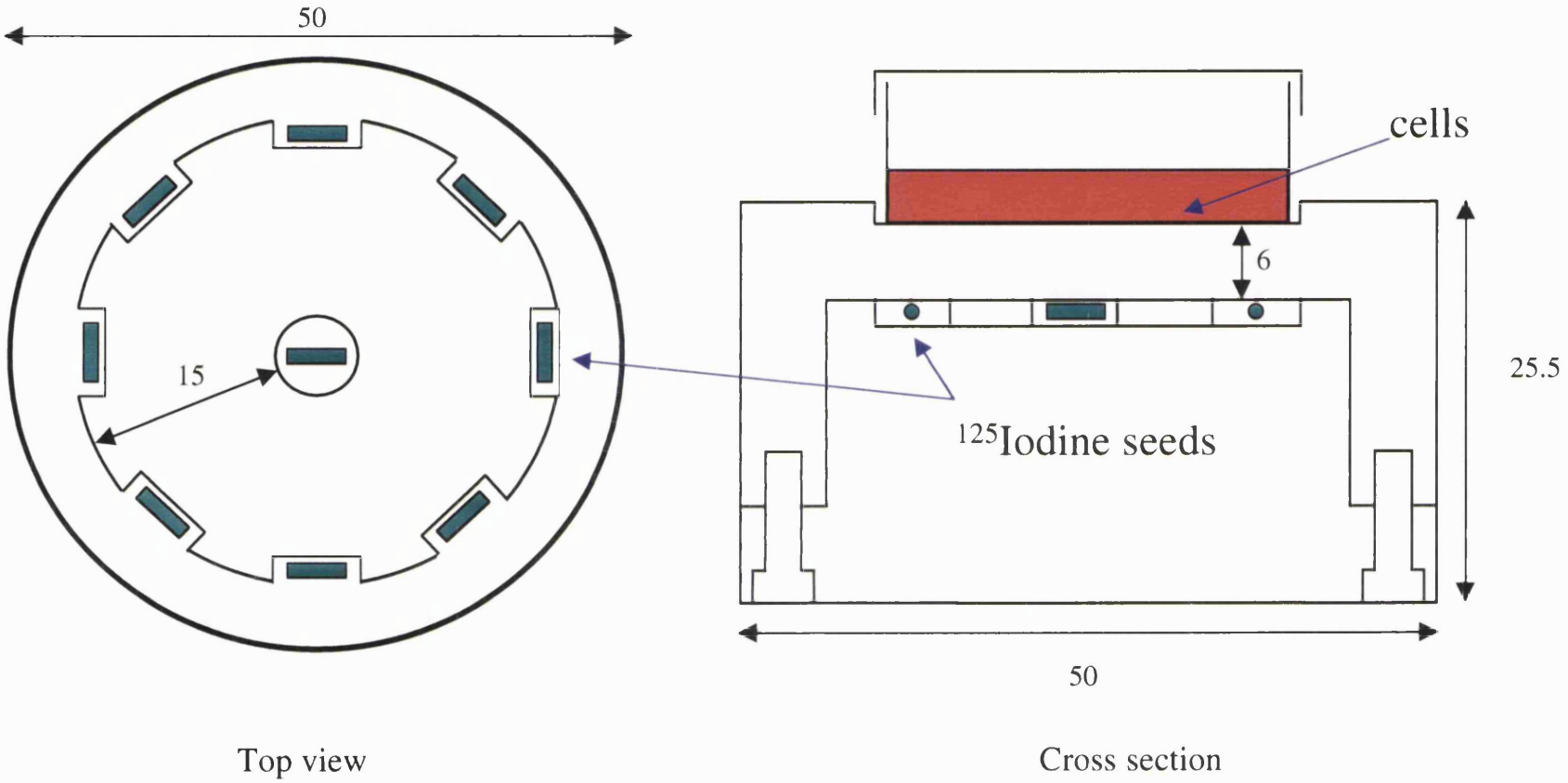

Figure 5.3
Shows a diagram of the ^{125}Iodine seed irradiator used to irradiated confluent T98G human glioblastoma cells. Measurements are shown in mm. The irradiator is made from cross-linked polythene and contains nine 370–440.3 MBq (10–11.5 mCi) ^{125}Iodine seeds (Nycomed Amersham, code IMC 6702).

Figure 5.4A
Shows the ^{125}Iodine seed irradiator inside an 80 mm high cylindrical steel container.

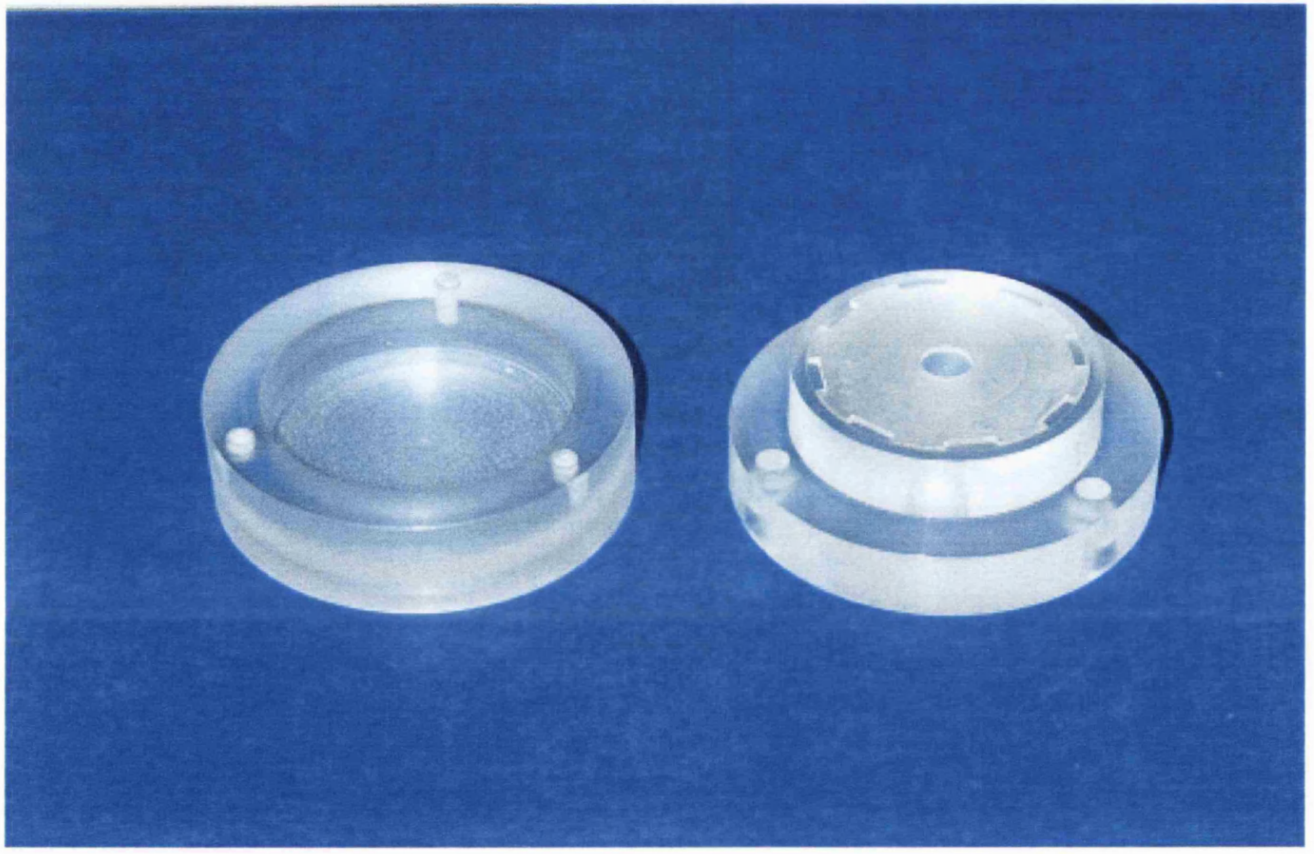

Figure 5.4B
Shows the ^{125}Iodine seed irradiator. The plaque is made from cross-linked polythene. The lid of the plaque is shown on the left. This is bolted to the seed-containing piece on the right.

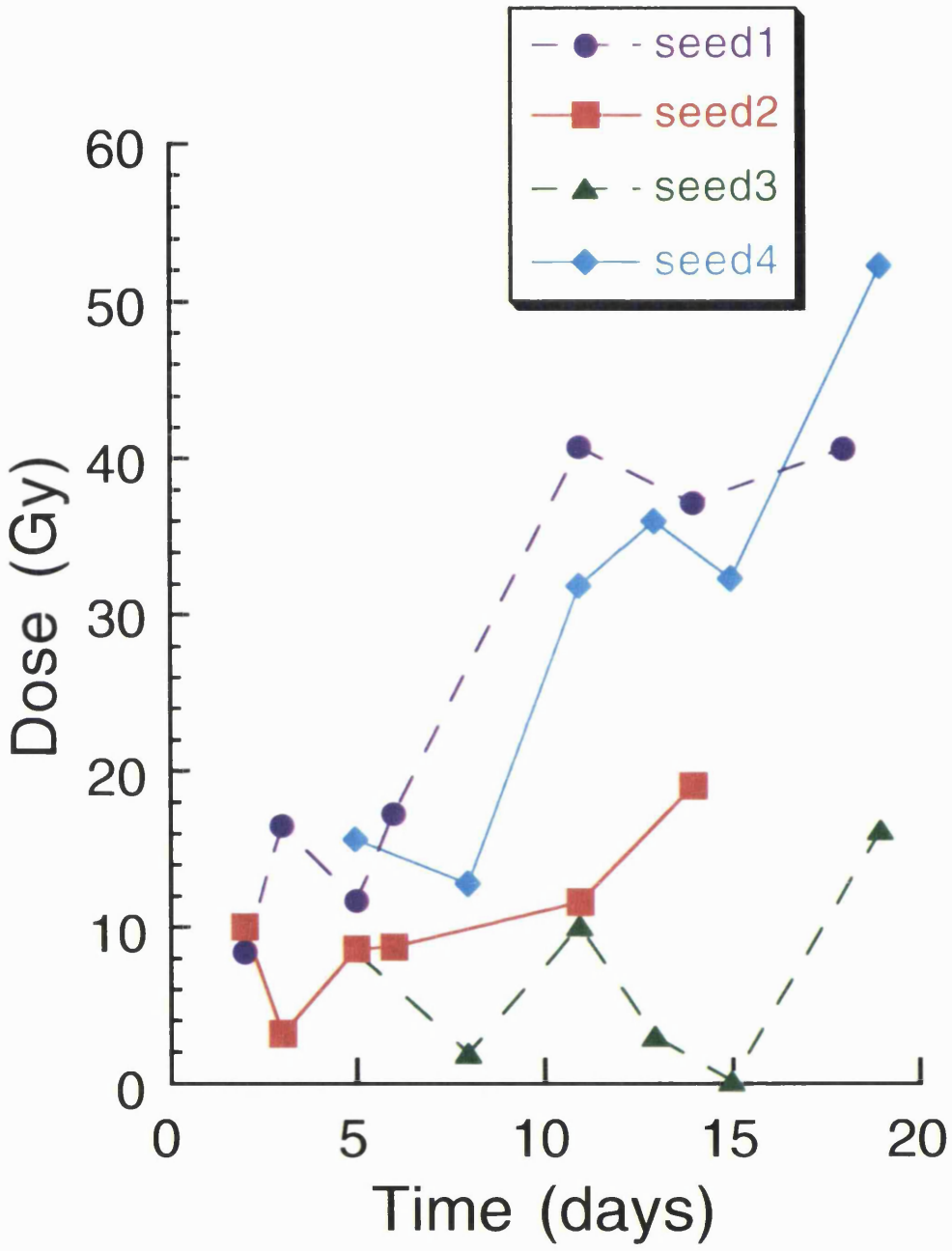

Figure 5.5
Shows the results of 4 independent experiments where calculated dose to Fricke solution in a suspension culture bottle containing one 370 MBq (10 mCi) ^{125}Iodine seed is plotted against time. The dose was calculated from the measured absorbance of Fricke solution at a wavelength of 224 nm (Section 2.5.3).

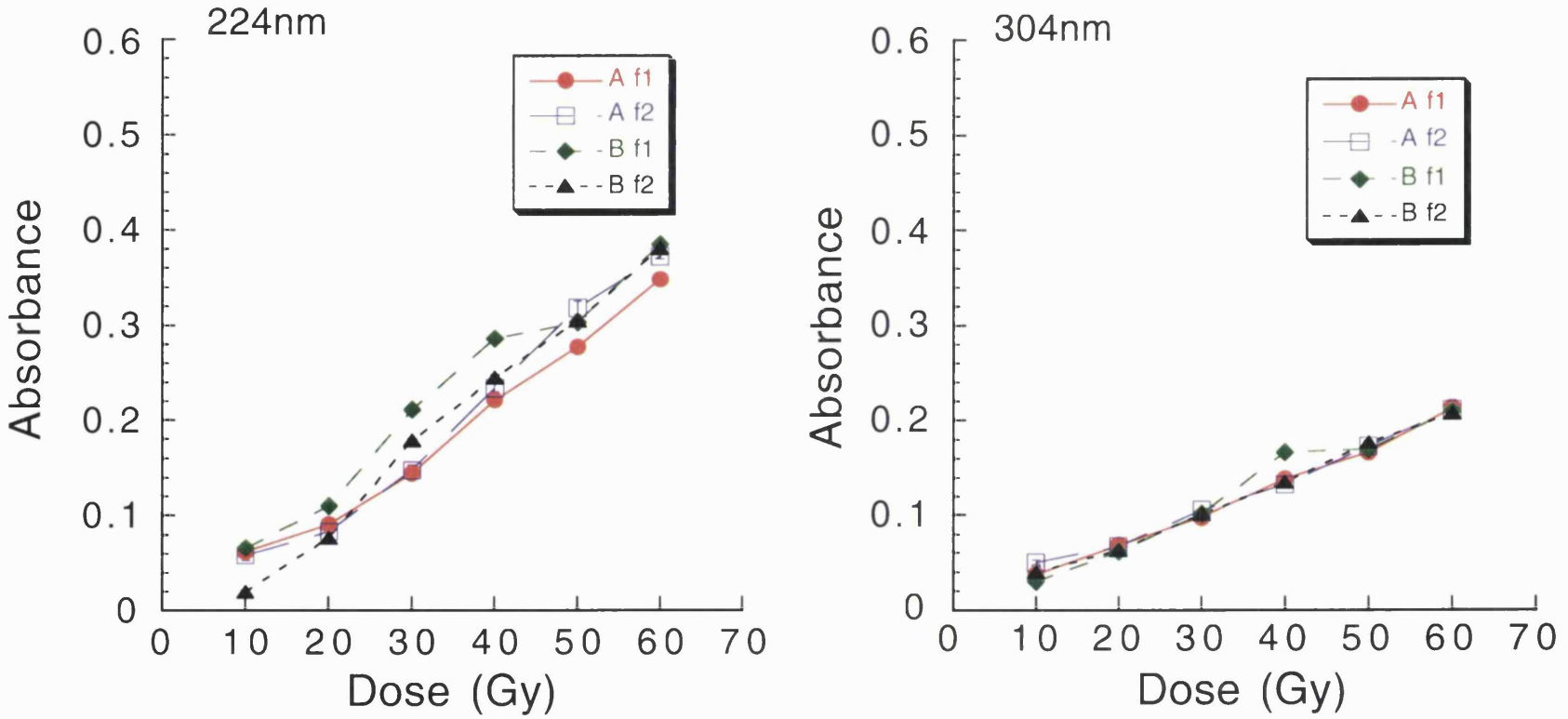

Figure 5.6
Shows the absorbance measured for Fricke solution containing 0.4M H_2SO_4 at wavelengths of 224 nm and 304 nm. Samples were taken from two separately X-ray irradiated stock flasks (f1 and f2) and were measured on two different spectrophotometers (A and B). When all the data at each wavelength were pooled, the following linear fits were obtained: for 224 nm (y= -0.0250+0.00660x, r= 0.983) and 304 nm (y= 0.0009+0.00346x, r= 0.992).

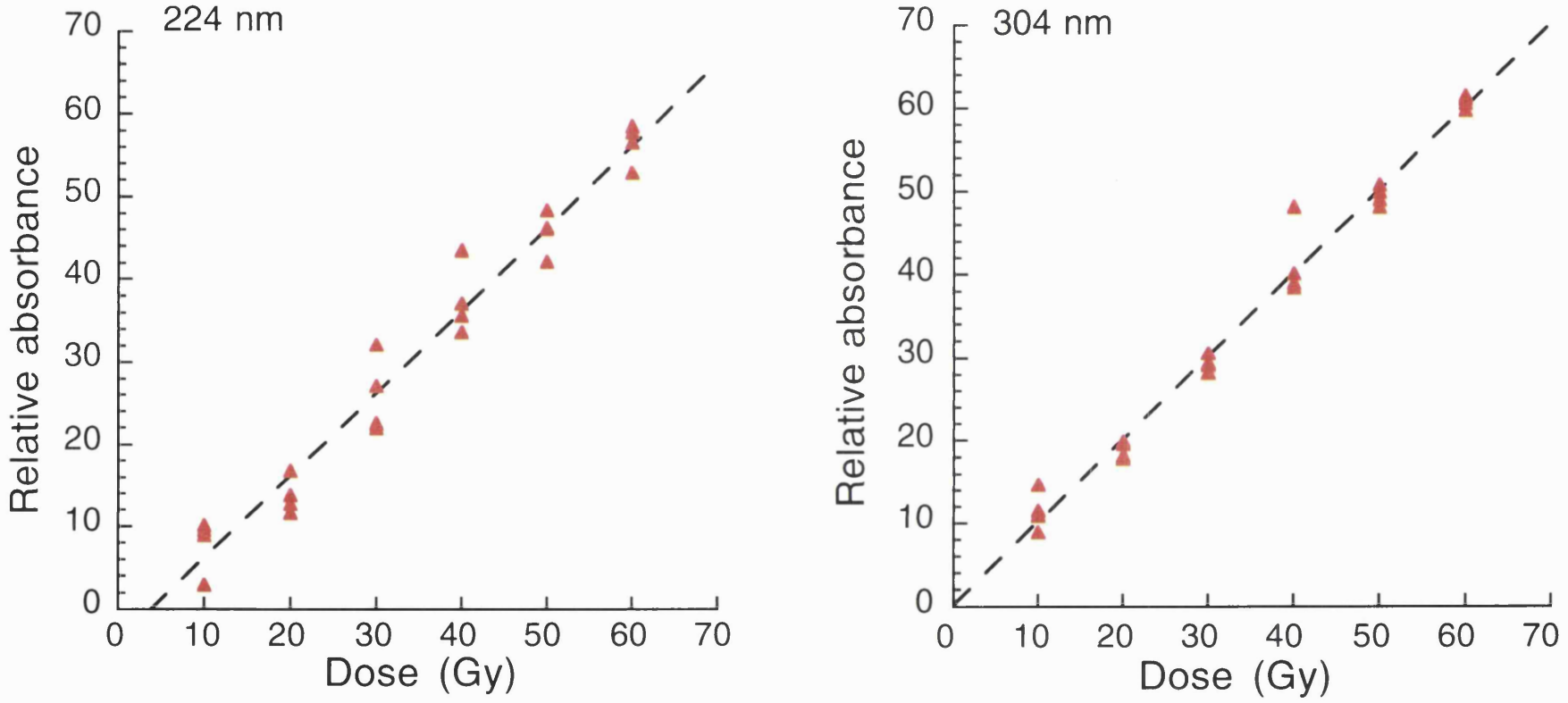

Figure 5.7
Shows standardised measurements of Figure 5.5. Results were standardised by fitting a line through all points in Figure 5.5 and dividing each individual point by the gradient of the line. Results were then replotted and a line fitted to the 224 nm (y= -3.78+x, r=0.983) and 304 nm (y= 0.2954+0.99x, r=0.992). The mean square error (MSE) for 224 nm is 11.42 and 304 nm is 5.33.

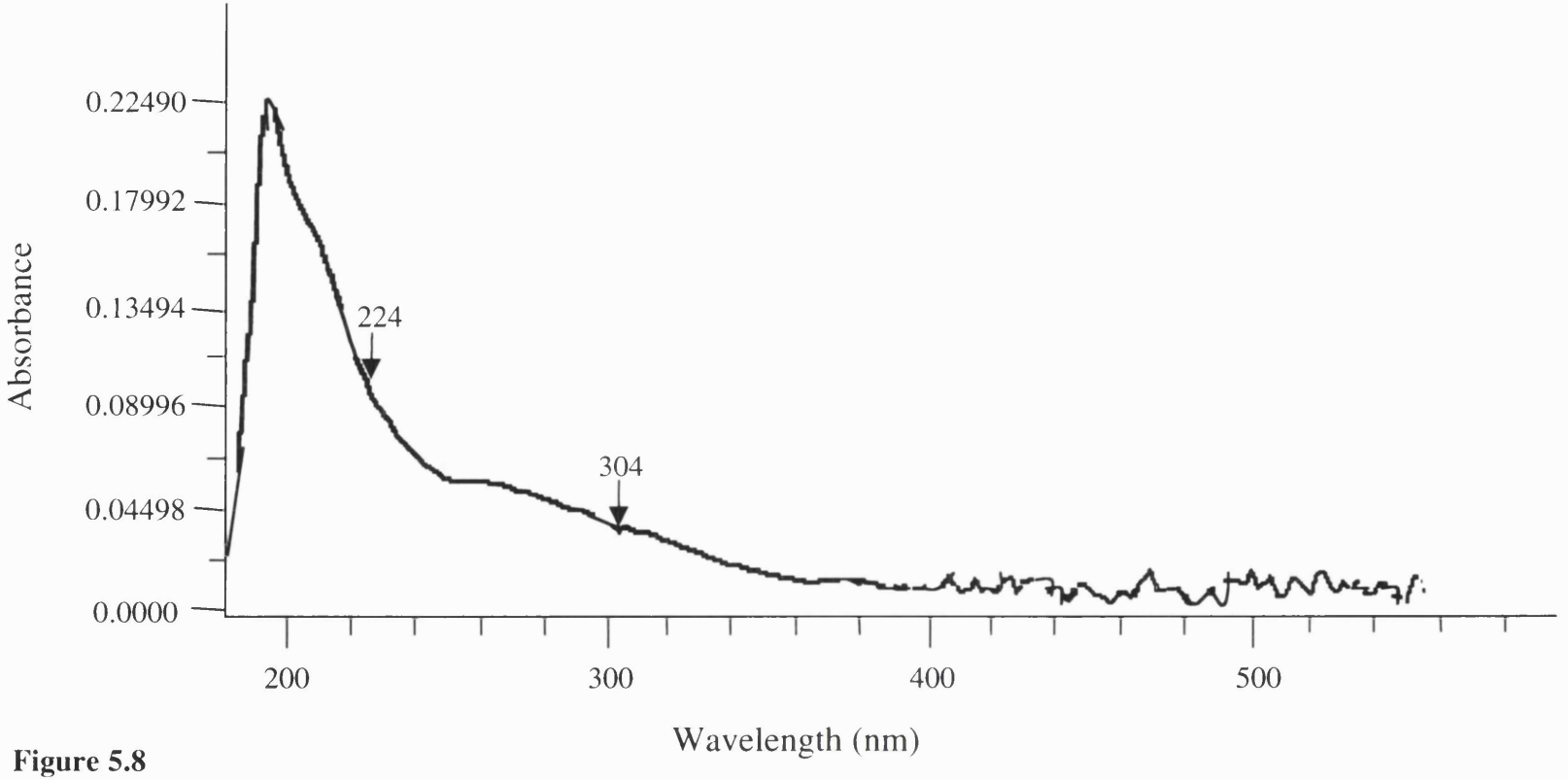

Figure 5.8
Shows the optical density spectrum curve for unirradiated Fricke solution. The two wavelengths, 224 and 304 nm, used in these experiments to determine the absorbance of the Fricke solution are shown.

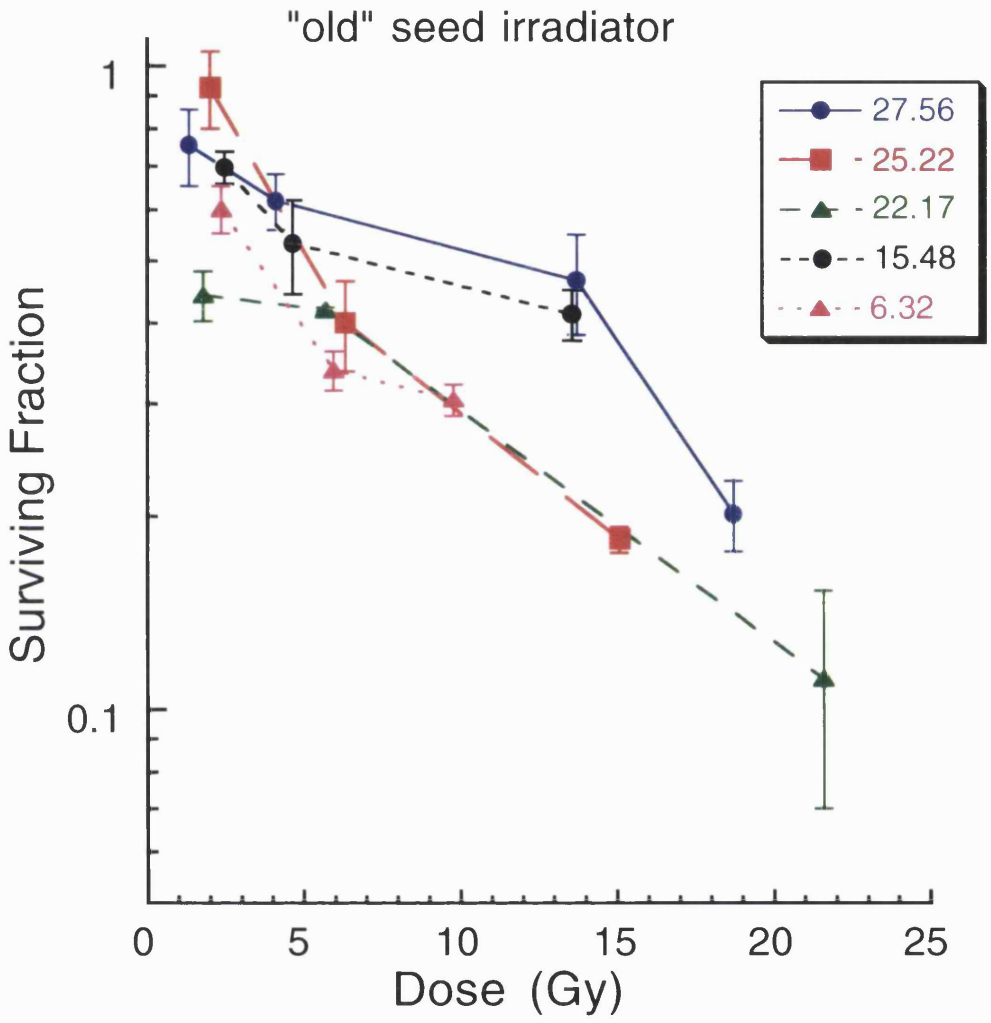

Figure 5.9
Shows survival curves obtained after irradiating confluent T98G cells using the "old" ^{125}Iodine seed irradiator. Dose rates shown are in cGy h^{-1} and are the calculated dose rate at the start of the irradiation period. Each data point is plotted as mean ± SEM.

Comparison with survival curves at dose rates (cGy h^{-1})		p-value
6.32	15.48	0.1185
6.32	22.17	0.8273
6.32	25.22	0.2418
6.32	27.56	**0.0489***
15.48	22.17	**0.0350***
15.48	25.22	0.9686
15.48	27.56	0.8421
22.17	25.22	0.5052
22.17	27.56	**0.0324***
25.22	27.56	0.6744

Table 5.3
Shows the comparison between survival curves obtained using the "old" seed irradiator at dose rates shown. Multiple regression analysis was carried out to obtain a p-value for the difference between survival curves. *denotes survival curves which are significantly different from one another.

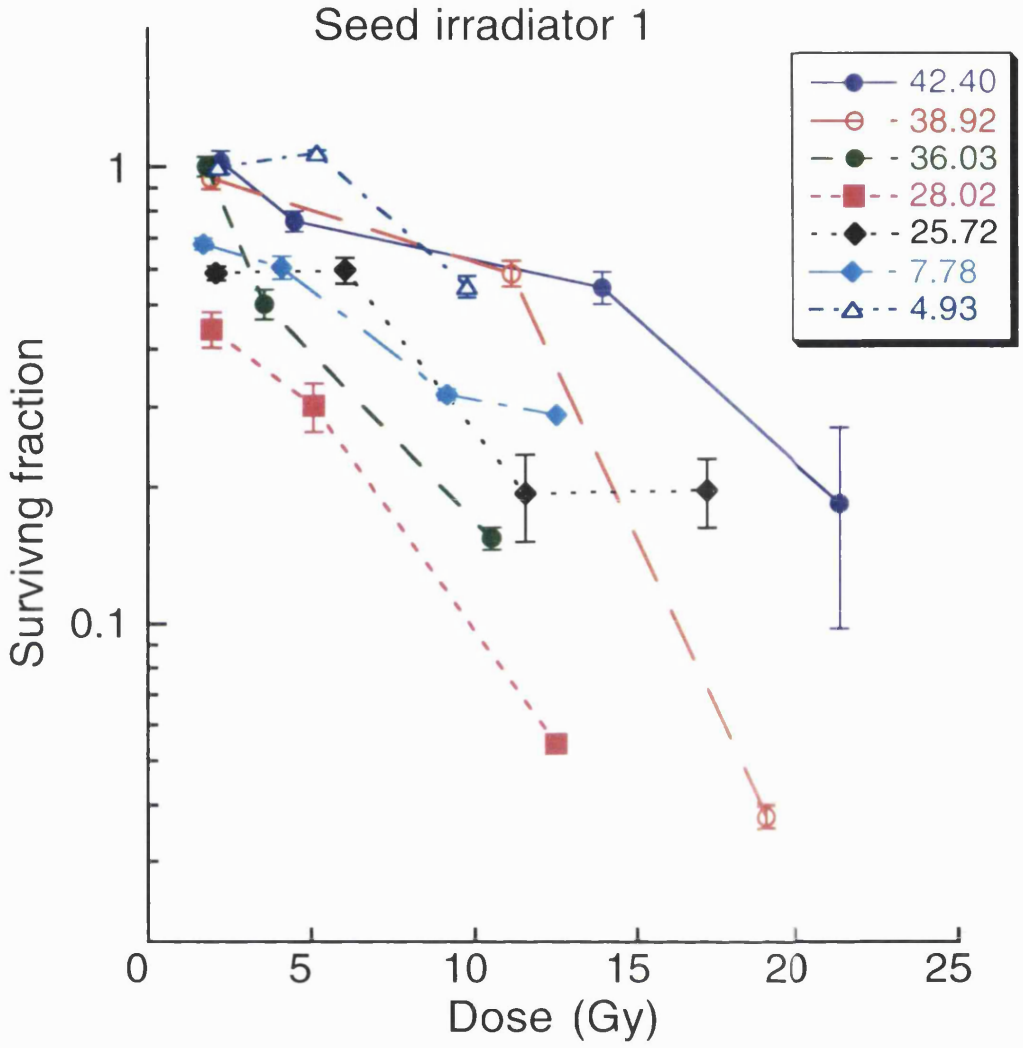

Figure 5.10(A)
Shows survival curves obtained after irradiating confluent T98G cells using the "new" ^{125}Iodine seed irradiator no. 1, which had an initial dose rate of 53.5 cGy h^{-1}. Dose rates shown are in cGy h^{-1} and are the calculated dose rate at the start of the irradiation period. Each data point is plotted as mean ± SEM.

Comparison with survival curves at dose rates (cGy h^{-1})		p-value
42.40	38.92	0.2963
42.40	36.03	0.1484
42.40	28.02	**0.0007***
42.40	25.72	0.0119*
42.40	7.78	**0.0021***
42.40	4.93	0.7270
38.92	36.03	0.1864
38.92	28.02	**0.0093***
38.92	25.72	0.1347
38.92	7.78	**0.0220***
38.92	4.93	0.5694
36.03	28.02	0.2806
36.03	25.72	0.9468
36.03	7.78	0.9524
36.03	4.93	0.1142
28.02	25.72	**0.0378***
28.02	7.78	**0.0022***
28.02	4.93	**0.0151***
25.72	7.78	0.9916
25.72	4.93	0.0501
7.78	4.93	**0.0216***

Table 5.4
Shows the comparison between survival curves obtained using the "new" seed irradiator no. 1, at dose rates shown. Multiple regression analysis was carried out to obtain a p-value for the difference between survival curves. *denotes survival curves which are significantly different from one another.

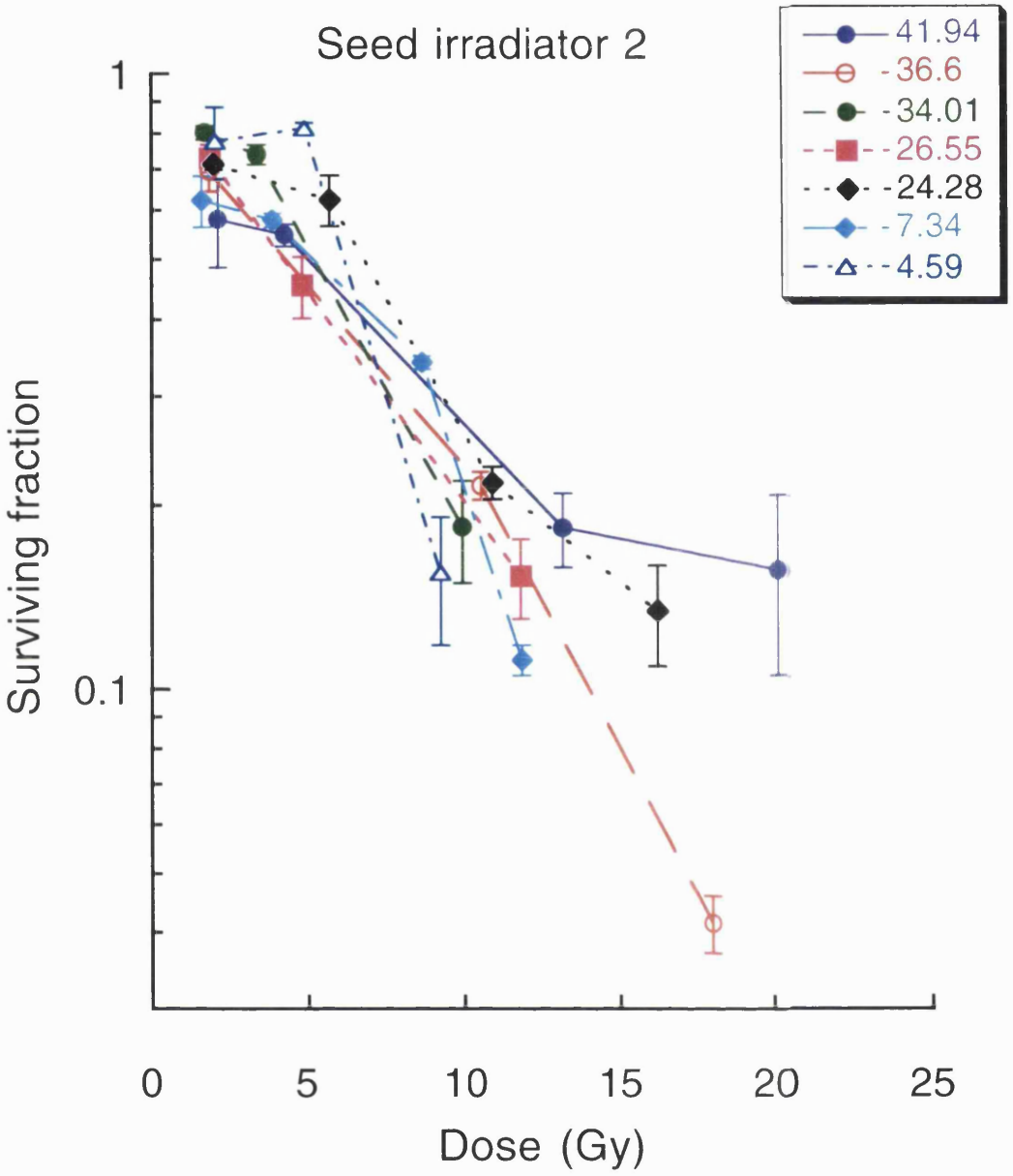

Figure 5.10(B)
Shows survival curves obtained after irradiating confluent T98G cells using the "new" ^{125}Iodine seed irradiator no. 2, which had an initial dose rate of 50.5 cGy h^{-1}. Dose rates shown are in cGy h^{-1} and are the calculated dose rate at the start of the irradiation period. Each data point is plotted as mean ± SEM.

Comparison with survival curves at dose rates (cGy h^{-1})		p-value
41.94	36.60	0.6054
41.94	34.01	0.7745
41.94	26.55	0.6822
41.94	24.28	0.8638
41.94	7.34	0.4261
41.94	4.59	0.7247
36.60	34.01	0.9612
36.60	26.55	0.5786
36.60	24.28	0.5502
36.60	7.34	0.3273
36.60	4.59	0.8724
34.01	26.55	0.4826
34.01	24.28	0.6809
34.01	7.34	0.3130
34.01	4.59	0.7538
26.55	24.28	0.2222
26.55	7.34	0.7538
26.55	4.59	0.5814
24.28	7.34	0.0819
24.28	4.59	0.9183
7.34	4.59	0.4397

Table 5.5
Shows the comparison between survival curves obtained using the "new" seed irradiator no. 2, at dose rates shown. Multiple regression analysis was carried out to obtain a p-value for the difference between survival curves. *denotes survival curves which are significantly different from one another.

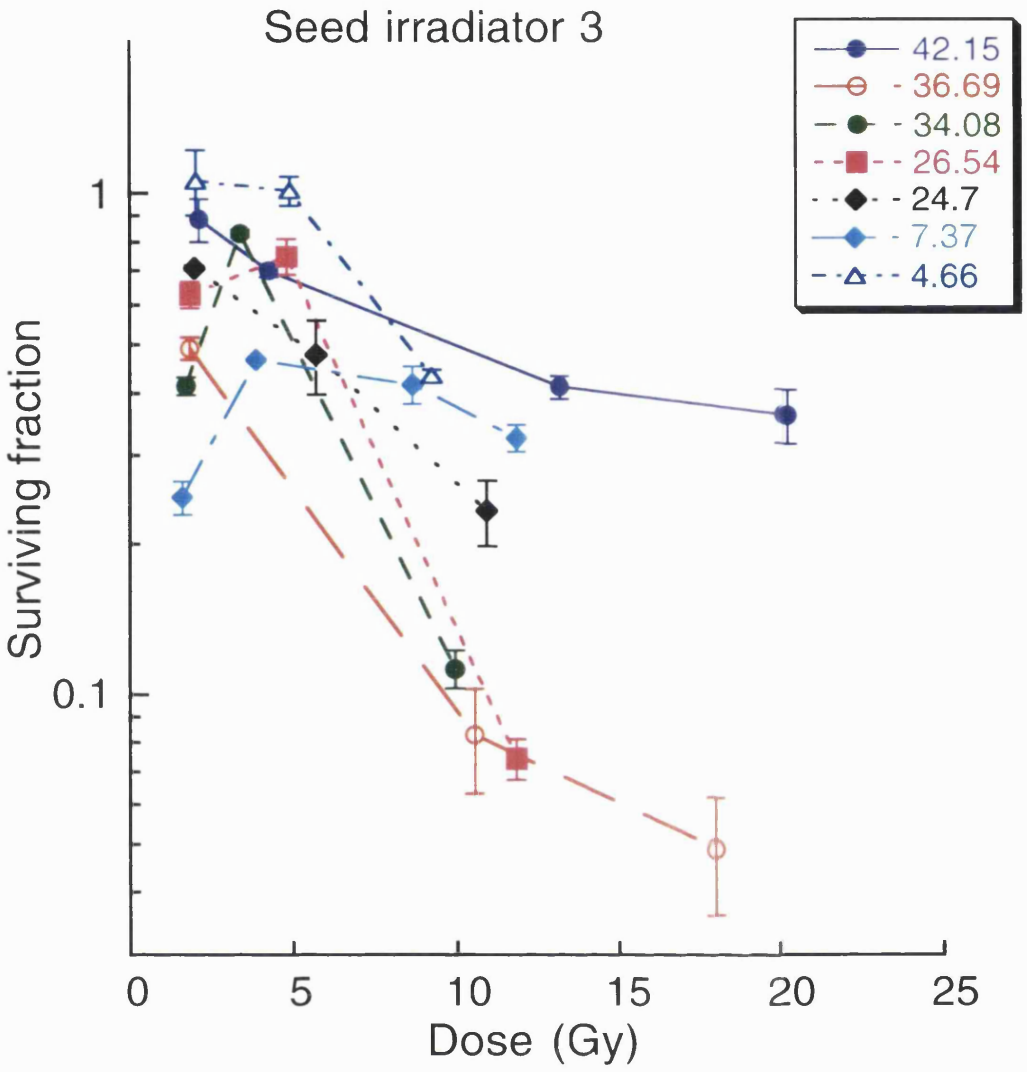

Figure 5.10(C)
Shows survival curves obtained after irradiating confluent T98G cells using the "new" ^{125}Iodine seed irradiator no. 3, which had an initial dose rate of 50.6 cGy h^{-1}. Dose rates shown are in cGy h^{-1} and are the calculated dose rate at the start of the irradiation period. Each data point is plotted as mean ± SEM.

Comparison with survival curves at dose rates (cGy h^{-1})		p-value
42.15	36.69	**0.0073***
42.15	34.08	0.1657
42.15	26.54	0.1617
42.15	24.70	**0.0415***
42.15	7.37	**0.0327***
42.15	4.66	0.6088
36.69	34.08	0.7819
36.69	26.54	0.5137
36.69	24.70	0.2754
36.69	7.37	0.4849
36.69	4.66	0.0992
34.08	26.54	0.6534
34.08	24.70	0.6642
34.08	7.37	0.7766
34.08	4.66	0.1339
26.54	24.70	0.9262
26.54	7.37	0.5554
26.54	4.66	0.1319
24.70	7.37	0.4550
24.70	4.66	0.0622
7.37	4.66	0.0698

Table 5.6
Shows the comparison between survival curves obtained using the "new" seed irradiator no. 3, at dose rates shown. Multiple regression analysis was carried out to obtain a p-value for the difference between survival curves. *denotes survival curves which are significantly different from one another.

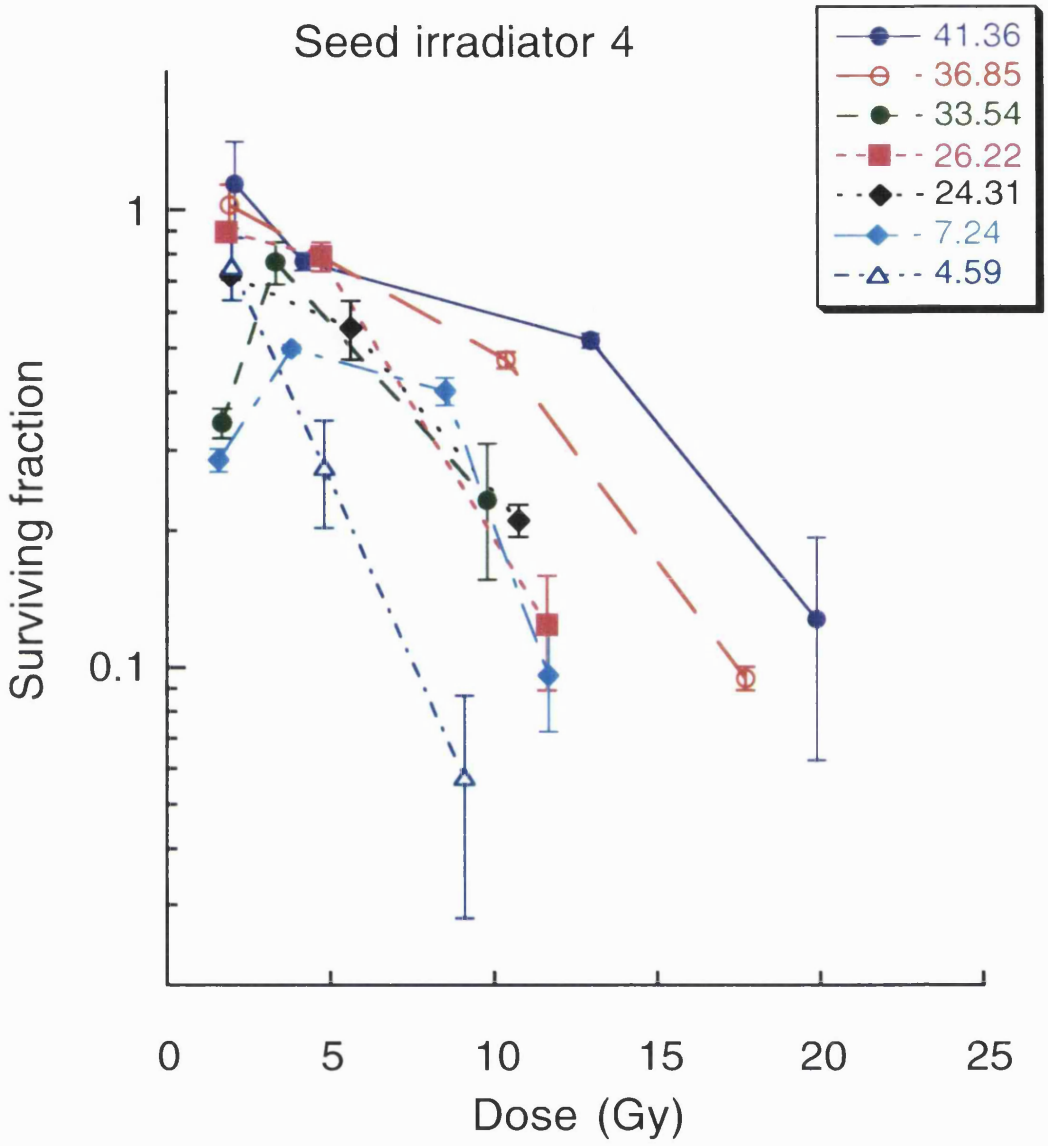

Figure 5.10(D)
Shows survival curves obtained after irradiating confluent T98G cells using the "new" ^{125}Iodine seed irradiator no. 4, which had an initial dose rate of 49.8 cGy h^{-1}. Dose rates shown are in cGy h^{-1} and are the calculated dose rate at the start of the irradiation period. Each data point is plotted as mean ± SEM.

Comparison with survival curves at dose rates (cGy h^{-1})		p-value
41.36	36.85	0.2911
41.36	33.54	0.0659
41.36	26.22	0.1076
41.36	24.31	**0.0135***
41.36	7.24	**0.0130***
41.36	4.59	**0.0176***
36.85	33.54	0.1724
36.85	26.22	0.1281
36.85	24.31	**0.0028***
36.85	7.24	0.0585
36.85	4.59	**0.0304***
33.54	26.22	0.3456
33.54	24.31	0.6133
33.54	7.24	0.6187
34.08	4.59	0.7824
26.22	24.31	0.2276
26.22	7.24	0.1718
26.22	4.59	**0.0466***
24.31	7.24	0.22489
24.31	4.59	0.2278
7.24	4.59	0.9796

Table 5.7
Shows the comparison between survival curves obtained using the "new" seed irradiator no. 4, at dose rates shown. Multiple regression analysis was carried out to obtain a p-value for the difference between survival curves. *denotes survival curves which are significantly different from one another.

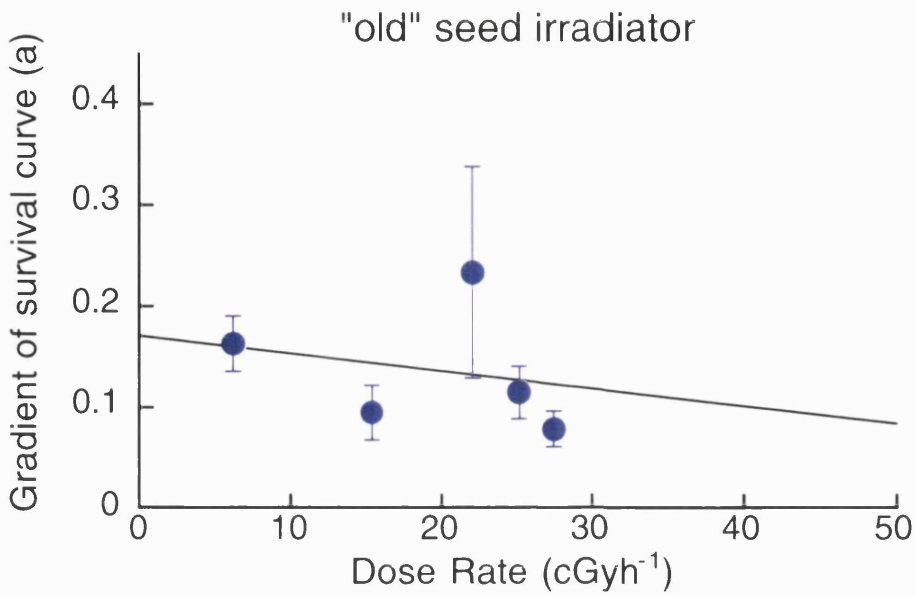

Figure 5.11.
Shows dose rate plotted against the gradient obtained, a, when survival curves obtained using the "old" seed irradiator are fitted to the following equation: $SF = e^{-adose}$. One-way ANOVA shows that the variability between dose rates is not significantly greater than the variability within dose rates.

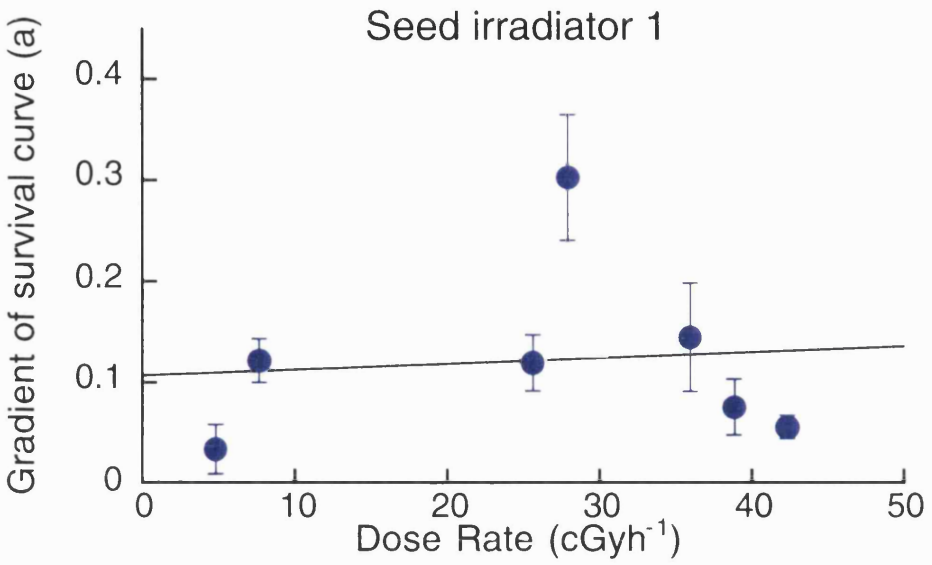

Figure 5.12
Shows dose rate plotted against the gradient obtained, *a*, when survival curves obtained using seed irradiator 1 are fitted to the following equation: $SF = e^{-adose}$. One-way ANOVA shows that the variability between dose rates is not significantly greater than the variability within dose rates.

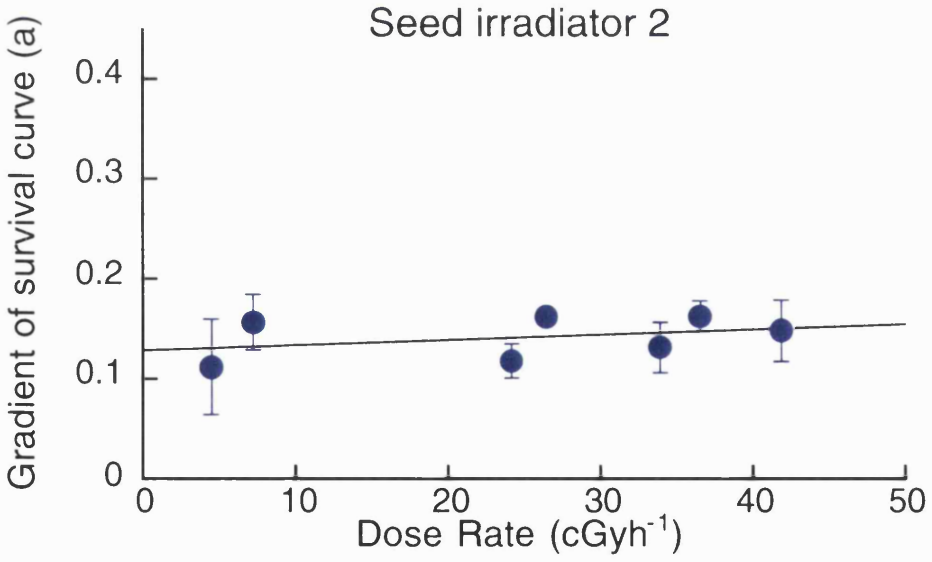

Figure 5.13
Shows dose rate plotted against the gradient obtained, *a*, when survival curves obtained using seed irradiator 2 are fitted to the following equation: $SF = e^{-adose}$. One-way ANOVA shows that the variability between dose rates is not significantly greater than the variability within dose rates.

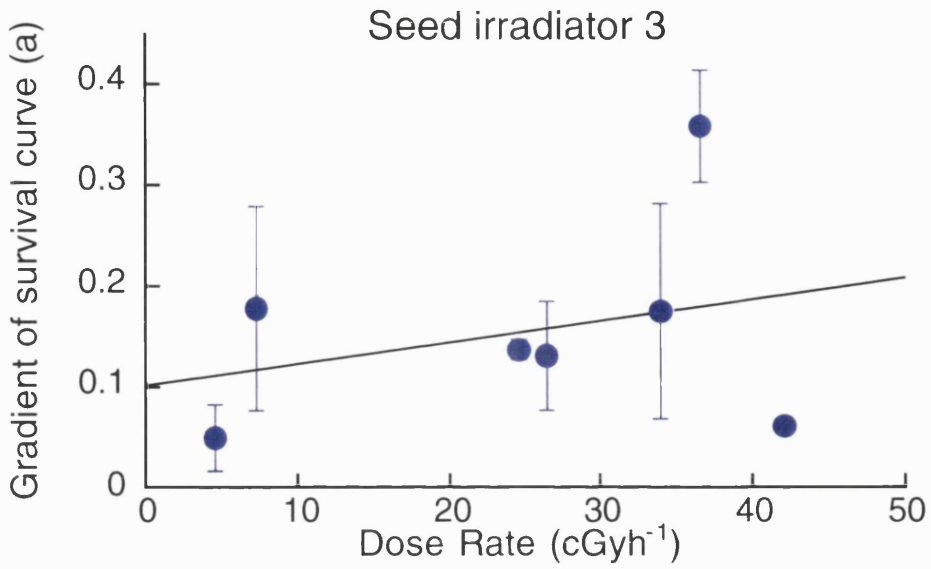

Figure 5.14
Shows dose rate plotted against the gradient obtained, *a*, when survival curves obtained using seed irradiator 3 are fitted to the following equation: $SF = e^{-adose}$. One-way ANOVA shows that the variability between dose rates is not significantly greater than the variability within dose rates.

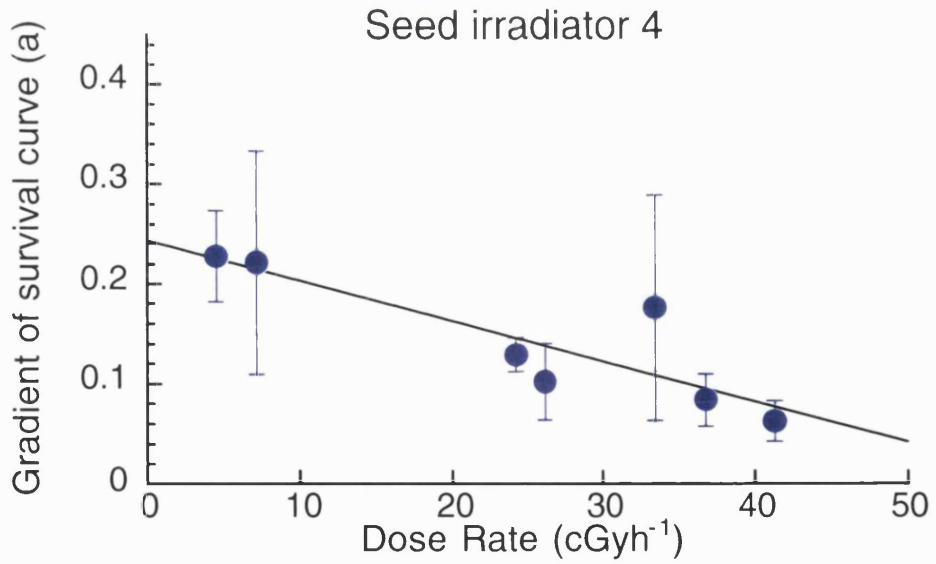

Figure 5.15
Shows dose rate plotted against the gradient obtained, *a*, when survival curves obtained using seed irradiator 4 are fitted to the following equation: $SF = e^{-adose}$. One-way ANOVA shows that the variability between dose rates is not significantly greater than the variability within dose rates.

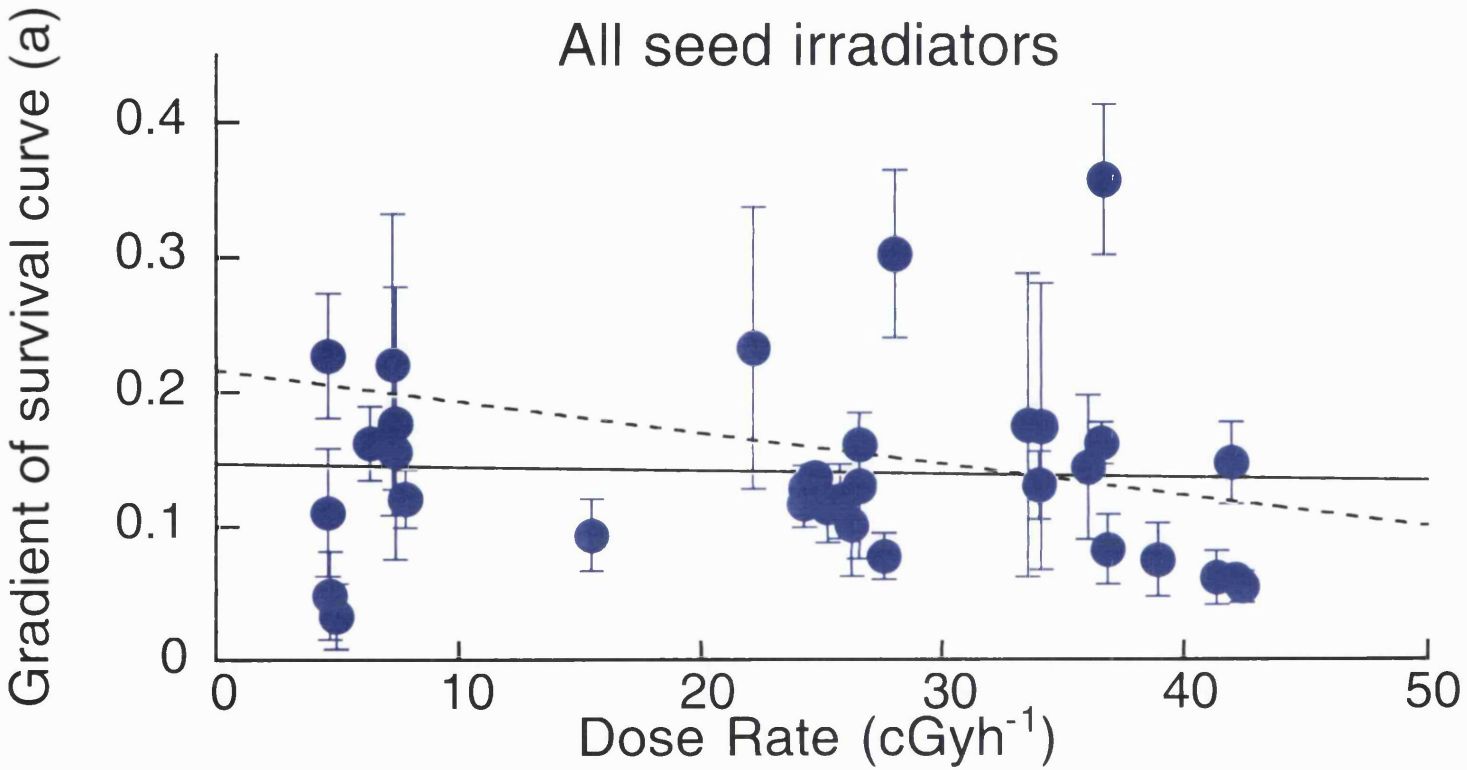

Figure 5.16
Shows dose rate plotted against the gradient obtained, *a*, when survival curves obtained using all seed irradiators are fitted to the following equation: $SF = e^{-adose}$. One-way ANOVA shows that the variability between dose rates is not significantly greater than the variability within dose rates.

5.5 Discussion

The first method developed to irradiate cells with low dose-rate ^{125}Iodine was to place one seed with tumour cells in a suspension culture bottle. Dosimetry was carried out using Fricke solution to determine the dose to the cells. The calculated dose using Fricke solution did not appear to increase linearly with time as expected. There was both inter-experimental variation between spinner flask set ups and intra-experimental variation between readings taken from one flask. This could have been due to variability in the method of measuring the absorbance of the Fricke. A wavelength of 304 nm has been used previously to measure absorbance (Spinks and Woods 1990). On the optical density spectrum curve 224 nm is on a shoulder region and 304 nm is on the flatter area (Figure 5.8). Therefore it may be more sensitive to measure absorbance at 224 nm, as we have done, as small changes would be measured more accurately which is advantageous when irradiating with very low doses. It is also possible however, that increasing the sensitivity may also increase the background "noise" and this may explain the high variability between measurements for the seeds in spinner. An experiment was therefore performed to compare the two wavelengths and determine the variability at 224 nm by measuring the absorbance of Fricke solution irradiated on an X-ray set with a known dose. From Figure 5.8 it is seen that absorbance measured at 304 nm appeared less variable, but the range of absorbance covered is smaller compared with the absorbance at 224 nm. This would mean that small changes in absorbance could not be measured accurately. Figure 5.7 shows the same graphs which have been normalised to allow a comparison of variability. The residual mean square error from a fitted line was 3.38 at 224 nm and 2.31 at 304 nm suggesting that reducing the wavelength to 224 nm did in fact increase the variability.

However, the increased variability due to the wavelength at which the Fricke was measured (224 nm), could not account for the high inter or intra-experimental variability. The RMSE between readings using X-ray irradiated Fricke at 224 nm was only 3.38, compared with the RMSE measured when lines were fitted through the Fricke data for each seed (seed 1: 6.108, seed 2: 3.23, seed 3: 6.45 and seed 4: 5.82). 3 out of the 4 seed experiments gave a higher RMSE than the X-irradiated Fricke solution. This showed that for seeds 1, 3 and 4, the variability seen for the seed data could not be explained by errors when measuring the absorbance of the Fricke solution. Seed 2, however, showed a similar RMSE to the X-ray irradiated Fricke solution suggesting that the variation observed was due to measurement error. The variation in Fricke readings from the seed experiment may have been due to a number of factors. Firstly, the position of the seed in the bottle will determine how much exposure the seed will have to the dosimetry solution. If the seed lies in a corner and only one side is exposed to the Fricke solution, then less dose will be recorded than a seed spinning in the centre of the bottle. The time over which the seed spends in one particular place will also have introduced variation. When the readings for each individual seed were

corrected for differences in initial activity, the resulting curves could be compared. A multiple regression analysis was carried out and the dosimetry curves where found to be significantly different from one another ($P< 0.0001$). In an ideal situation these curves should have been the same. Differences between each experimental set-up therefore existed. As well as the differences in seed position within the bottle outlined above, there may have been other factors increasing variability within each flask. The speed of the propeller within the suspension bottle may have been slightly different for each causing the seed to be pushed out to the side or pulled into the centre of the bottle and therefore introducing variations in dosimetry.

Although this suspension culture system for low-dose irradiation was developed, it proved to be inappropriate for irradiating cells at low-dose rates. Apart from the high variation in delivered dose after prolonged exposure to the Fricke solution (3 weeks), the ^{125}Iodine seeds appeared to suffer from corrosion and one seed actually disintegrated. This occurred despite the Nycomed Amersham specifications stating that these seeds should withstand acid with concentrations up to 1M. In these experiments the seeds were exposed to 0.4M and so should not have undergone corrosion. The option of having the seeds sealed into the propeller of the spinner vessel was explored, but this too proved unsuccessful as the seeds would possibly undergo excessive mechanical stress in a laminator necessary to seal them. A further potential problem in irradiating cells in spinner culture, is that each cell would receive a variable dose of radiation. Cells momentarily closer to the seed would receive a high-instantaneous dose that could induce radio resistance even if the 'average' dose was low. Therefore even if some cells exhibit HRS the overall result might not be marked. This method was therefore deemed inappropriate for ^{125}Iodine LDR irradiations and no further experiments were carried out using cells.

However, the second method which was developed, the ^{125}Iodine seed irradiator, proved to give a consistent dose and was used to study LDR ^{125}Iodine irradiation on human glioma cells. The survival curves obtained are shown in Figures 5.9 and 5.10. The data were compared using two methods. The first method used multiple regression analysis to compare the survival curves of different dose rates and gave a p-value for any differences. The second method condensed each individual survival curve into a single value, the gradient of a line fitted through the points, *a*. If a data set showed a large amount of cell kill the value of *a* would be large. These *a* values were then plotted against dose rate and a line was fitted through this data. If an inverse dose rate effect was present, then *a* would be expected to be greatest at the lowest dose rates and a negative value for the gradient of the fit would be obtained. A one-way ANOVA would also show a significant effect.

Using the "old" ^{125}Iodine seed irradiator, it was possible to compare survival at each dose rate using multiple regression. Table 5.3 shows the p-value when each survival curve was

compared with all the others. The survival curves obtained using this irradiator showed a general trend of an inverse dose-rate effect with the highest dose rate giving the least cell kill and the lowest showing the greatest (Figure 5.9). When compared, the p-values for the difference between the following survival curves were significant, 6.32 cGy h^{-1} versus 27.56 cGy h^{-1} and 22.17 cGy h^{-1} versus 27. 56 cGy h^{-1}, with the lower dose rate showing the greater cell kill. 15.48 cGy h^{-1} versus 22.17 cGy h^{-1} also showed a significant difference, but in this case the higher dose rate showed the greatest cell kill, *i.e.*, an inverse dose rate was not present in this comparison. When all curves were fitted to $SF = e^{-adose}$ and the gradient, *a*, was then plotted against dose rate (Figure 5.11) and analysed as described in Section 5.3.3.1. A one-way analysis of variance showed that the variability between values of *a* obtained for a particular dose rate was not significantly greater than the variability within *a* obtained for a particular dose rate. This suggested that altering the dose rate had no effect on *a*, or that there was sufficient variability within the measurement system that masked any effect. However, there was a general trend towards a negative slope if a line was drawn approximately through the data, (although a p-value on this line could not be obtained as the errors could not be incorporated into the curve fit) showing that using this irradiator there is a trend towards an inverse dose-rate effect, but this was not significant.

Seed irradiator number 1, showed a large spread in survival curves (Figure 5.10A). There were several significant differences between survival curves (Table 5.4). Most of which were centred around data obtained at a dose rate of 28.02 cGy h^{-1} (the calculated dose rate at the start of the irradiation) which appeared very low, 5 out of the 6 survival curves obtained at remaining dose rates were significantly higher than this survival curve. The survival curve obtained at 42.4 cGy h^{-1}, the highest dose rate was significantly higher than 25.72 cGy h^{-1} and the lowest 7.78 cGy h^{-1}. The data obtained for 7.78 cGy h^{-1} was also significantly lower than 38.92 cGy h^{-1}. Although there were incidences in which lower dose rates gave greater cell kill than high, overall there was no trend towards an inverse dose-rate effect. A one-way analysis of variance shows that variation within *a* at a particular dose rate was not significantly different from the variability between *a* at different dose rates. Suggesting an effect was not present. This is supported by Figure 5.12 where the gradient of a line drawn approximately though the data points was slightly positive, therefore showing no inverse dose-rate effect.

The survival curves obtained for seed irradiator number 2, showed much less variability (Figure 5.10B). Although the highest dose rate gave the least cell kill and the lowest gave the most, there were no significant differences between any of the survival curves (Table 5.5). In general there was no trend towards an inverse dose-rate effect as is seen from Figure 5.13 where the gradient was also slightly positive and one-way ANOVA also showed no significant effect other than variation within each data point.

Seed irradiator number 3 did show significant differences where some lower dose rates showed more cell kill than higher (Figure 5.10C and Table 5.6). At 42.15 cGy h^{-1} cell kill was significantly higher than at 7.37 cGy h^{-1}, 24.7 cGy h^{-1} and 36.69 cGy h^{-1}. Although survival at other dose rates on this irradiator followed no apparent pattern. This was reflected when the values of *a* were plotted against dose rate (Figure 5.14), the gradient obtained was positive and ANOVA also showed much variation within and between data points giving no significant effects.

Survival curves obtained using seed irradiator 4 (Figure 5.10D and Table 5.7) followed a strong inverse dose-rate pattern with the highest dose rate of 41.36 cGy h^{-1} giving significantly less cell kill than 24.31, 7.24, 4.59 cGy h^{-1}. The survival curves for 36.85 cGy h^{-1} and 26.22 cGy h^{-1} were also significantly higher than the lowest dose rate of 4.59 cGy h^{-1}. A significant negative gradient was obtained when *a* was plotted against dose rate (Figure 5.15) (-0.0296, p= 0.168), although this cannot be considered truly significant as the error bars were not incorporated into this analysis. One-way analysis of variance also did not give a significant effect as the variation in results were large, although the p-value was low at 0.09. This suggested a trend towards an inverse dose-rate effect using this seed irradiator, although this is not significant.

When all data from all irradiators is considered, a slight negative gradient was obtained when a line is drawn approximately through the points (Figure 5.16). This showed that there was a very slight trend towards the presence of an inverse dose-rate effect. However, when data from dose rates above 20 cGy h^{-1} were studied, omitting data from below this dose rate, the gradient of the linear fit was slightly steeper. This may suggest that an inverse dose-rate effect occurred to a greater degree at dose rates above 20 cGy h^{-1}, which plateau as the dose rate is reduced further. In these experiments a p-value for these lines drawn through the data could not be obtained as errors could not be incorporated into the curve fits. One-way analysis of variance showed that the variability within a data point is not significantly different from variability between data points suggesting that no effect is present or that the variations in experimental technique *etc.* may be masking an effect. However, it would have been useful in these experiments to have obtained survival curves at even higher dose rates, to see whether the value of *a* obtained is further reduced, thus producing a steeper, and possibly significant, linear fit when combined with the low-dose data. This however was not practical in these experiments as higher activity ^{125}Iodine seeds would have to be used in the irradiator to give a higher overall dose rate, and this was not feasible under the radiation protection licensing for this institution.

The cell survival at the lowest dose rates may have not shown an inverse dose-rate effect to such a great extent as higher dose rates (> 20 cGy h^{-1}), possibly because the dose rate was

so low that not enough damage is done to the cells to even overcome constitutive repair processes occurring during irradiation, so that the net effect was very little cell kill. At higher dose rates, enough damage may have occurred to overcome this constitutive repair, but not enough to trigger inducible repair mechanisms and so cell kill appeared greater. At even higher dose rates these are triggered and so therefore cells "appear" more resistant. This hypothesis, however, is not supported by the data obtained in Chapter 4 of this thesis, where the inverse dose-rate effect occurs greatest at dose rates below 20 cGy h^{-1}. Furthermore the analysis of variance between intra and inter-point variability in the current experiments suggested that there was no overall effect, either mono- or biphasic. There was also more variability within the data in the low dose-rate region, there were fewer data points obtained and in this case the irradiation time is longer, therefore the potential for variation in irradiation conditions was greatest suggesting against a biphasic effect, if any.

Although a significant inverse dose-rate effect was not apparent in these experiments, there was a slight overall trend towards an effect (Figure 5.13). The lack of such a response may have been due more to the design of the experiment rather than the absence of an effect. The experiments were carried out using seed irradiators which, when tested, did not give an overall homogenous dose of radiation. It was impractical to rotate the dishes by 22.5° sixteen times as was carried out in the dosimetry to give a homogeneous dose, and by rotating the dish by a more practical 90° four times during the irradiation, would have introduced errors, with some cells receiving up to a10% higher or lower dose rate than the mean dose rate increasing the variability in results. If the dish was rotated by 22.5° then cells would have spent half the irradiation time over the high dose-rate areas of where they received 110% of the mean dose rate and half the time over areas where they received 90% of the mean dose rate. All cells would have therefore received the same total dose. Flasks that were rotated 90° were in a similar position to the start, with the same cells over the "hot" areas and the same cells over the "cold" areas. At the end of irradiation, some cells in these flasks would have received 10% more dose and some 10% less dose than the overall mean. In this situation, the results of the cell-survival assay would have given a more resistant response than in flasks where cells all received the same dose, as the relationship between survival and dose is not linear, but logarithmic. However, during LDR exposures this may not make such a large difference, as LDR survival curves are more linear and are less steep. The problem of "hot spots" is further complicated if HRS/IRR occurs, as, whether the flasks are rotated by 22.5° or not, some cells will be exposed to higher dose rates than others. These higher dose rates may lead to an induction of repair mechanisms in some cells in the population and not in others which are in "colder" areas. Therefore even if the cells receive the same total dose, IRR may mean the population shows a more resistant response overall compared with a population where the cells are receiving a constant homogeneous dose rate.

As well as the possible experimental design flaws, there were other factors which may have caused variability in results and so masked any inverse dose-rate effects. The experiments were carried out on a small number of cells. There was also the problem of the actual dose rate received by the cells. The dose rates shown in Figures 5.9 and 5.10 are the initial dose rates at the start of the irradiation time. At the higher dose rates the dose rate was dropping rapidly, which although may closely mimic the clinical situation, made it difficult to assess the survival of cells at a particular dose rate. This, however, was not such a problem at lower dose rates where the dose rate was dropping less rapidly, therefore it was easier to more accurately estimate the dose rate received by the cells. In some ways it may have been better to use an irradiator with a longer half life *e.g.* as used by DeWeese (1998) who used ^{137}Caesium. They compared survival of prostate cells using a HDR (60 cGy h^{-1}) and a LDR (25 cGy h^{-1}) irradiator. These irradiators would give a constant dose rate to the cells, but unlike the set up used in the experiments described here, they did not mimic the clinical situation, *i.e.* they did not use a common brachytherapy radioisotope and the uniformity of their dose rate is not comparable to implants in patients.

Although the inverse dose-rate effect was not largely apparent in these experiments, this may have been due to the problems of increased difficulties in measuring an actual dose rate, the variations in homogeneity of irradiation field, the small numbers of cells available and the fact that there was only one data point obtained for a particular dose rate. It may have been these variable irradiation conditions; indeed the ANOVA used suggested large variations within single measurements, which were masking any inverse dose-rate effects occurring. Although much effort was made to overcome these problems, it was not possible to overcome the limitations of this ^{125}I seed approach to measuring the effects of LDR irradiations on cell survival. The water tank method of measuring survival to low dose-rate irradiation described in Chapter 4 did not have these problems. Therefore a more accurate determination of cell survival could be made and in this case an inverse dose-rate effect on cell survival was apparent.

Chapter 6. The effect of subsequent acute dose irradiation after low dose-rate exposures on cell survival in vitro

6.1 Aims

Under the hypothesis that HRS and the inverse dose-rate effect (Chapter 4) are mechanistically related, the aim of experiments described in this chapter was to determine which combinations of dose and dose-rate trigger IRR.

6.2 Introduction

There is much evidence to suggest the involvement of DNA-repair complexes in IRR. Many studies have shown the correlation between experimental radiosensitivity (measured as SF_2) and the ability of DNA-repair complexes to mend DSBs in both normal and tumour cells (Kiltie *et al.* 1997, Mitchell *et al.* 2000, Herring *et al.* 1998, Ward and Marples 2000). Cell lines with different repair abilities have been tested for the presence of HRS at low doses and the results imply that DSB repair and nucleotide excision repair, but not base excision repair, are involved in IRR (Skov *et al.* 1994). Inhibitors of PARP have also been shown to block IRR suggesting that pathways encompassing Poly (ADP ribose) polymerase (PARP) may be involved (Marples *et al.* 1997) and further studies have shown evidence of protein synthesis (Marples and Joiner 1995) and DNA-PK (Skov *et al.* 1994, Jeggo 1997) involvement in IRR.

The evidence suggests that DNA repair is involved in IRR, however the trigger and the mechanisms by which it acts are as yet unknown. There are two major hypotheses to explain the involvement of DNA repair in HRS/IRR. The simplest idea is that IRR corresponds to *constitutive* DNA-repair processes, *i.e.* no proteins or genes are actually induced by radiation as they are already present. Under this hypothesis DNA repair is proposed to occur due to either one of two mechanisms. Firstly DNA repair operates when the cell recognises a level of damage that exists over a certain putative threshold, thus producing a more resistant response at doses above 0.5 Gy. Secondly, when DNA damage levels increase, the access to the DNA for the repair complexes increases, thus allowing more repair.

The second hypothesis is that IRR in high-dose resistant human cell lines reflects the level of *induced* DNA repair, possibly controlled by a mechanism that responds to increasing levels of DNA damage (Marples *et al.* 1997). This mechanism was thought to be similar to that of the adaptive response, however recent evidence has accumulated against this. Wouters and Skarsgard (1997) suggested that IRR and the adaptive response are different phenomena. Their results show that priming doses prevent HRS, but have no effect on the high-dose region. Other experiments have shown that the time course for the effect to become apparent and the persistence of the effect is much

greater for the adaptive response suggesting against a mechanistic relationship between the two.

Whether DNA repair is constitutive or induced, a dose exists at which increased radioresistance mechanisms become active. This threshold level may be fixed, below which DNA-repair mechanisms are not triggered, or there may be an interaction between damage levels and repair ability, making repair less efficient at low doses. If there is a threshold level where constitutive processes start operating or DNA is actively induced, the object of experiments described in this chapter was to determine the combination of dose and dose rate this is achieved, during low dose-rate exposures.

6.3 Materials and methods

T98G cells were taken from monolayer culture and plated into orange capped (Corning, UK) 25 cm^2 tissue culture flasks containing 5 ml of medium. 5×10^3 cells were plated to determine survival in asynchronous growth and 5×10^5 cells were plated to determine the survival of cells grown to confluence. In all experiments flasks were incubated at 37°C with 5% CO_2 + 5% O_2 (balance N_2) overnight to allow cells to attach. The medium was then removed and the flask was then fully filled with fresh medium. Strips of parafilm were wound round the lid to form a tight seal. Flasks to be used in confluence survival experiments were then placed in a 37°C incubator until observed to be in confluence for 4 days. Cells were then irradiated with LDR ^{60}Co γ-rays in the water tank set up described in Section 4.4.1. Control flasks remained in the incubator while flasks to be irradiated were attached to the holders in the water tank with 8 flasks at each dose-rate position. Flasks were then irradiated in the dark. After the required dose, the flasks were removed from the water tank. They were then placed in an incubator for 0 or 4 h at 37°C. Flasks were then irradiated with acute doses of 240 kVp X-rays at dose rates of 0.23 Gy min^{-1} for doses less than 1 Gy and 0.44 Gy min^{-1} for doses greater than 1 Gy. Irradiations were carried out as described in Section 2.5.1 at doses of between 0.05 Gy and 5 Gy. Flasks were then incubated for a further 3 h to allow cells to recover. The medium was removed and the flasks washed out twice with PBS. Cells were then harvested using EDTA/trypsin and centrifuged at 1000 r.p.m. for 5 minutes. The pellet was resuspended in 5 ml of medium before being passed through a 21-gauge needle. The cell sorter was then used to dispense a known concentration of cells into a 25 cm^2 flask containing 5 ml medium (Section 2.6.2). The number of cells dispensed depended on the expected plating efficiency of the cell line and estimated survival after the dose and dose-rate of radiation the cells received. Cells were plated to give 100–200 colonies per flask. 3–6 flasks were plated per dose point. 6–12 of these flasks were designated controls. Flasks were then incubated for 10–14 days and then stained with crystal violet and colonies were counted using a manual colony counter.

In these experiments asynchronously growing T98G cells were irradiated at low-dose rates of 5, 10, 30 and 60 cGy h^{-1} to total doses of either 2 or 5 Gy. No time was left between LDR and HDR irradiations. Confluent T98G cells were irradiated at the same dose rates to total doses of 2 or 5 Gy. Two sets of experiments were carried out where 0 h or 4 h was left between LDR and HDR irradiations. As only eight flasks could be irradiated in one dose-rate position at any one time, using the water tank set up, two experiments were carried out per dose and dose rate combination to obtain more than 8 doses in the final survival curve. In the first experiment, flasks were irradiated with HDR X-rays to doses of 0.05, 0.2, 0.4, 0.7, 1, 3 and 5 Gy with one control flask irradiated at LDR only. The remaining intermediary data points, 0.1, 0.3, 0.6, 0.5, 0.8, 2 and 4 Gy and one control flask were obtained in a second experiment.

6.4 Data analysis

The plating efficiency and surviving fraction were calculated and data analysed by fitting to the IR equation as described in Section 3.3.2.3. If non-overlapping 95% confidence limits on the α_s and α_r parameters were obtained and 95% confidence limits on the d_C parameter which did not include zero, by fitting data to the IR model, significant HRS was considered to be present using this analysis. Data was also fitted to a modification of the Linear-Quadratic equation:

$$SF = C\exp(-\alpha d - \beta d^2) \qquad \text{Equation 6.1}$$

This takes into account how the low-dose data "pull" down the survival-axis intercept, C, to below one. In this analysis, significant HRS is deemed to be present if the upper 95% confidence limit on C is less than 1. In a third method of analysis, data were fitted to two separate LQ equations. The first fit was carried out using all data in the survival curve to obtain an LQ fit and the second fit omitted the low-dose data (<1 Gy), using only the high-dose data to obtain a curve fit. Data points in the low-dose region were then assessed to be above or below each LQ curve. A t-test was used to determine whether this number of data points below the curve, in each case, was significant.

6.5 Results

Figures 6.1 (A to H) show the survival curves obtained from irradiating asynchronous T98G cells at various LDRs of ^{60}Co γ-rays to total doses of 2 or 5 Gy, then exposing them immediately to HDR X-rays. Significant HRS/IRR was observed in at least one test when analysing the data using the 4 statistical tests described above, in all experiments (Table 6.3). Parameters obtained from IR curve fits are summarised in Table 6.1. IR curve fits were obtained for all but one experiment (60 cGy h^{-1}, 2 Gy). Significant 95% confidence limits on the IR fit (as described in Section 6.4) were

obtained for 4 of the 8 experiments (60, 30) and 10 cGy h^{-1} to a total dose of 5 Gy and 5 cGy h^{-1} to a total dose of 2 Gy). The outcome of assessing the C-intercept of the y-axis after fitting the LQ modification (Section 6.4) is shown in Table 6.2. Using this method of analysis all experiments show significant HRS, with the upper 95% confidence limit on the y-axis intercept, C, being below 1. When an LQ fit was obtained for the high-dose data only (doses ≥ 1) in each of the experiments (as described Section 6.4), five of the data sets (60, 30 and 10 cGy h^{-1} to a total dose of 5 Gy and 30 and 5 cGy h^{-1} to a total dose of 2 Gy) had a significant number of points in the low-dose region below the LQ fit. Of these five, four (60, 30 and 10 cGy h^{-1} to a total dose of 5 Gy and 30 cGy h^{-1} to a total dose of 2 Gy) also had a significant number of points below the LQ fit obtained using all data were the low-dose data points were included. All of the data sets showed significant HRS using at least one of the 4 statistical methods.

Figures 6.2 (A to H) show the results of experiments where the cells were held in confluence arrest. In these experiments a 0 h interval was used between LDR and HDR irradiations. HRS was present in the majority of experiments (in 6 out of 8) using the 4 analytical methods described in Section 6.4. However, HRS was not observed in cells irradiated with 5 Gy at dose rates of 30 and 60 cGy h^{-1}. Table 6.4 shows a summary of these data and the results of the data analysis are shown in Tables 6.5 and 6.6. In two of the 8 experiments (30 and 60 cGy h^{-1} to a total dose of 5 Gy), an IR curve fit was not obtained. Of the six IR fits, 5 showed significant HRS at 95% confidence limits (10 and 5 cGy h^{-1} to a total dose of 5 Gy and 60, 30 and 10 cGy h^{-1} to a total dose of 2 Gy). Only one data set showed significant HRS when the C-intercept method of analysis was studied (10 cGy h^{-1} to a total dose of 5 Gy), although 6 of the 8 crossed the y-axis below 1 (60, 30 10 and 5 cGy h^{-1} to a total dose of 2 Gy and 10 and 5 cGy h^{-1} to a total dose of 5 Gy). Only 3 experiments showed a significant number of low-dose data points below the "high-dose only" LQ fit (10 and 5 cGy h^{-1} to a total dose of 5 Gy and 5 cGy h^{-1} to a total dose of 2 Gy) and only 2 of these showed HRS using the "all data" LQ fit (5 cGy h^{-1} to a total dose of both 2 and 5 Gy). Two of the 8 survival curves, (60 cGy h^{-1} to 5 Gy and 30 cGy h^{-1} to5 Gy) did not show significant HRS using any of the statistical methods.

The results of experiments where the cells were held in confluence arrest and a 0 h interval was left between LDR and HDR irradiations are shown in Figures 6.3 (A to H). A summary of IR curve fit parameters obtained are shown in Table 6.7. In all experiments an IR fit was obtained with 5 of the 8 being significant (60, 30 and 10 cGy h^{-1} to a total dose of 2 Gy and 30 and 5 cGy h^{-1} to a total dose of 5 Gy). The results of the data analysis are shown in Tables 6.8 and 6.9. In all 8 experiments the modified LQ curves intercepted the survival axis (C) below 1, although only 5 were significant (60, 30 and 5 cGy h^{-1} to a total dose of 5 Gy and 10 and 5 cGy h^{-1} to a total dose of 2 Gy).

Four data sets showed significant HRS when fitted to the "high-dose LQ" fit (60 and 10 cGy h^{-1} to a total dose of 5 Gy and 30 and 5 cGy h^{-1} to a total dose of 2 Gy) and only 2 of these (60 cGy h^{-1} to a total dose of 5 Gy and 30 cGy h^{-1} to a total dose of 2 Gy) were significant when fitted to the "all-data" LQ fit. All of the data sets showed significant HRS using at least one of the 4 statistical methods.

Dose rate ($cGy\,h^{-1}$)	Total Dose (Gy)	Interval between LDR & HDR (h)	Fig. 6.1	Sig. HRS?	LQ fit			IR fit					RMSE	
					α	β	α/β	α_s	α_r	d_C	β	α_s/α_r	LQ	IR
60	2	0	(G)	×	0.725 (0.451-1.03)	-0.0811 (-0.178–0.0750)	8.95						0.235	
60	5	0	(H)	✓	0.655 (0.498-0.828)	-0.0681 (-0.111–0.0210)	9.62	3.14 (1.77-6.13)	0.345 (-0.258-0.164)	0.389 (0.162-0.581)	0.00761 (-0.0541-0.102)	19.1	0.133	0.150
30	2	0	(E)	×	0.807 (0.675-0.948)	-0.102 (-0.139–0.0571)	7.93	1.77 (1.42-2.54)	0.158 (-0.473)	0.682 (0.387-3.15)	0.0743 (-0.0233-)	11.2	0.149	0.126
30	5	0	(F)	✓	0.333 (0.247-0.421)	-0.00512 (-0.0341-0.0271)	60.2	3.87 (1.81-7.97)	0.257 (0.162-0.344)	0.134 (0.0831-0.224)	0.017 (-0.012-0.053)	15.0	0.126	0.107
10	2	0	(C)	×	0.574 (0.455-0.698)	-0.0346 (-0.0712-0.00761)	16.6	17.1 (2.57-)	0.558 (0.444-0.671)	0.0281 (-0.0784)	-0.0301 (-0.0662-0.00631)	18.5	0.106	0.0991
10	5	0	(D)	✓	1.073 (0.900-1.26)	-0.145 (-0.191–0.0870)	7.39	7.22 (3.56-15.6)	0.820 (0.563-1.00)	0.149 (0.0862-0.287)	-0.0841 (-0.142–0.287)	8.82	0.156	0.117
5	2	0	(A)	✓	0.203 (0.119-0.290)	0.0228 (-0.00511-0.0532)	89.0	0.823 (0.351-2.16)	0.0641 (-0.243-0.164)	0.389 (0.162-1.87)	0.0620 (0.00611-0.130)	12.9	0.133	0.128
5	5	0	(B)	×	0.366 (0.263-0.474)	-0.0105 (-0.0412-0.0241)	36.6	0.603 (0.312-)	0.248	0.607	0.0194	2.43	0.111	0.112

Table 6.1

Shows summary data from experiments on asynchronously growing T98G cells (Figure 6.1). Cells were irradiated with LDR ^{60}Co γ-rays and then with HDR X-rays and a survival curve was obtained. LQ and IR fit parameters are those obtained by fitting the Linear-Quadratic and Induced-Repair equations to all of the data for each set of experiments. The SEM and upper and lower confidence limits where available are shown in brackets. The RMSE is shown as a measure of 'goodness of fit' for each model to the data. Significant HRS shown is based on non overlapping 95% confidence limits for α_s and α_r and a lower 95% confidence limit for d_C above 0.

Dose rate ($cGy\,h^{-1}$)	Dose (Gy)	Interval between Irradiations (h)	Survival-axis intercept (C)	95% confidence limits
60	2	0	0.792	0.658-0.917
60	5	0	0.780	0.697-0.867
30	2	0	0.847	0.774-0.924
30	5	0	0.859	0.797-0.923
10	2	0	0.937	0.877-0.999
10	5	0	0.702	0.632-0.775
5	2	0	0.909	0.847-0.972
5	5	0	0.915	0.842-0.990

Table 6.2
Shows the results of experiments where asynchronously growing T98G cells are irradiated with LDR ^{60}Co γ-rays then HDR X-rays with no interval between these irradiations (summarised in Table 6.1 and shown in Figure 6.1). Results were fitted to the equation:

$$SF = C\exp\left(-\alpha d - \beta d^2\right)$$

This produces a Linear-Quadratic curve which intercepts the survival axis and has an upper 95% confidence limit below 1 if significant HRS is present.

Dose rate ($cGy\,h^{-1}$)	Dose (Gy)	IR model with sig. CL	Upper CL of C-intercept < 1	Sig. no. points below all data LQ fit	Sig. no. points below high-dose LQ fit
60	2	×	✓	×	×
60	5	✓	✓	✓	✓
30	2	×	✓	✓	✓
30	5	✓	✓	✓	✓
10	2	×	✓	×	×
10	5	✓	✓	✓	✓
5	2	✓	✓	×	✓
5	5	×	✓	×	×

Table 6.3
Shows the presence or absence of significant HRS using four different methods of analysis of results (described in Section 6.4) acquired by irradiating asynchronous T98G cells (Table 6.1 and Figure 6.1). Cells were irradiated with LDR ^{60}Co γ-rays and then with HDR X-rays with no interval between these irradiations and a survival curve was obtained.

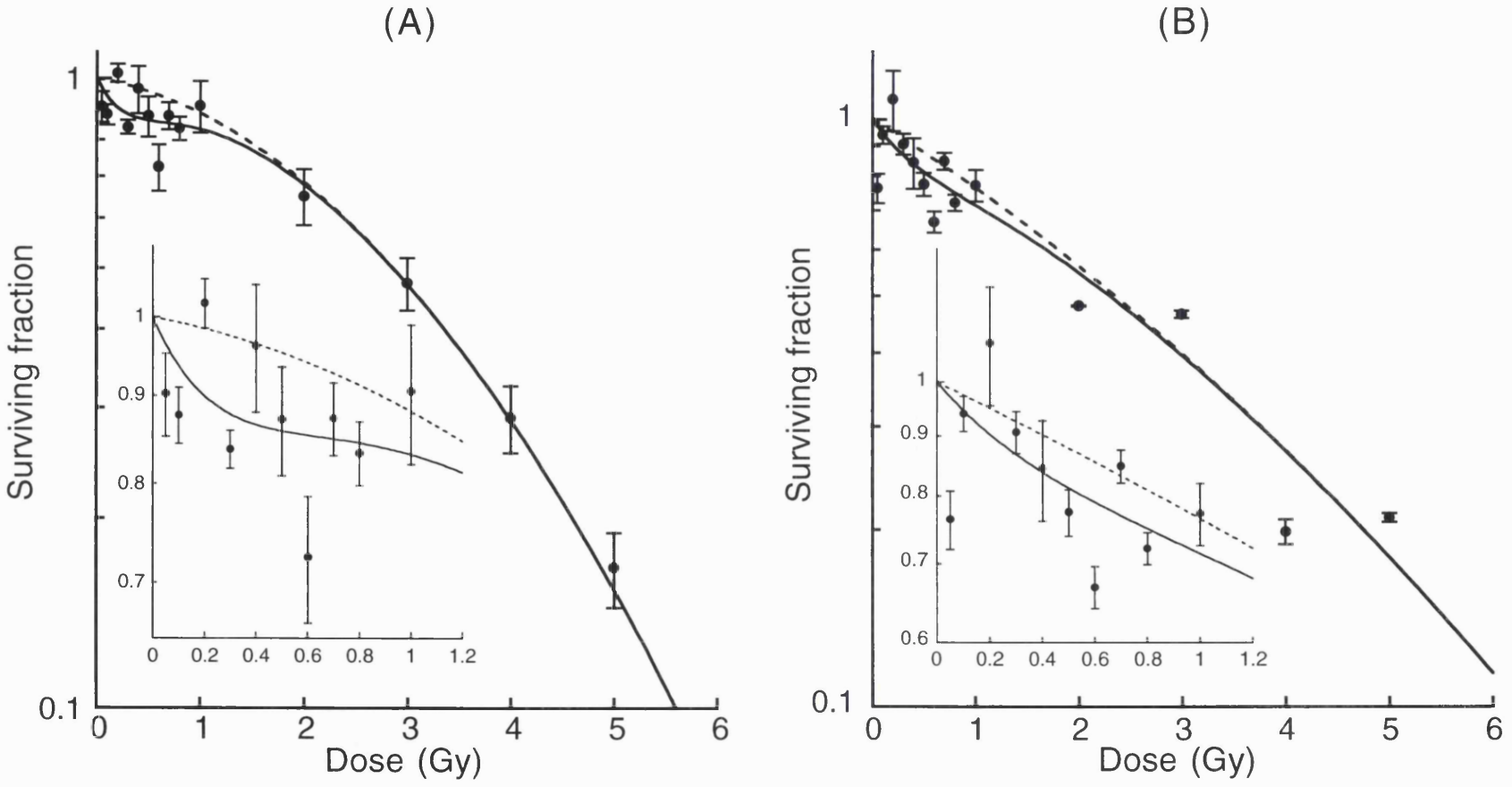

Figure 6.1
Shows the survival curve obtained from irradiating asynchronous T98G human glioma cells at low-dose rate and then at high-dose rate with 0h between irradiations. Survival was assessed using the cell sort protocol. Plotted as mean ± SEM. The data have been fitted to the Linear-Quadratic equation (broken line) and the Induced-Repair equation (solid line). The inserts show the low-dose regions in greater detail.
(A) LDR of 5 cGy h^{-1} irradiated to a total dose of 2 Gy
(B) LDR of 5 cGy h^{-1} irradiated to a total dose of 5 Gy

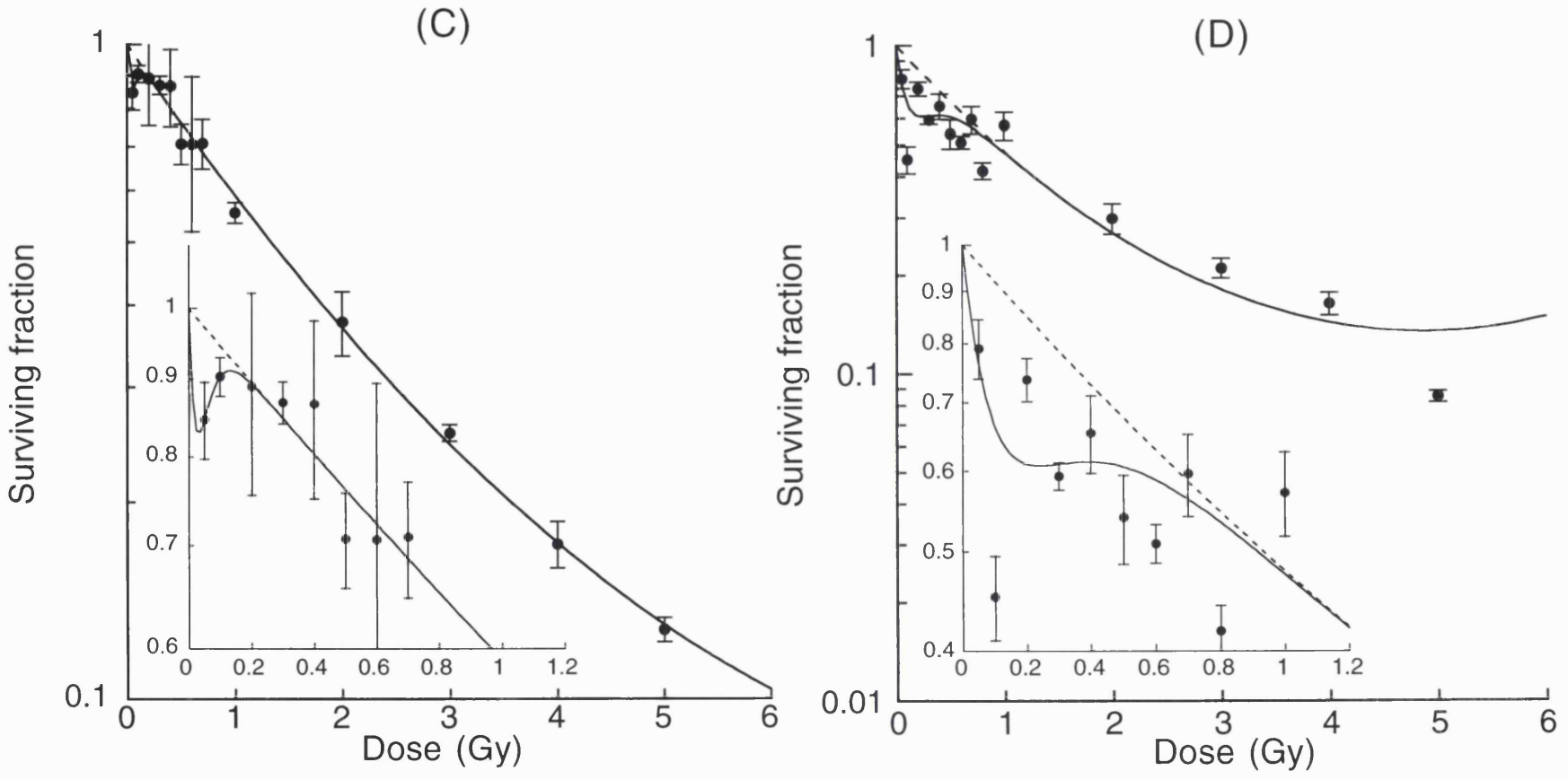

Figure 6.1 (continued)
Shows the survival curve obtained from irradiating asynchronous T98G human glioma cells at low-dose rate and then at high-dose rate with 0h between irradiations. Survival was assessed using the cell sort protocol. Plotted as mean ± SEM. The data have been fitted to the Linear-Quadratic equation (broken line) and the Induced-Repair equation (solid line). The inserts show the low-dose regions in greater detail.
(C) LDR of 10cGy h^{-1} irradiated to a total dose of 2Gy
(D) LDR of 10cGy h^{-1} irradiated to a total dose of 5Gy

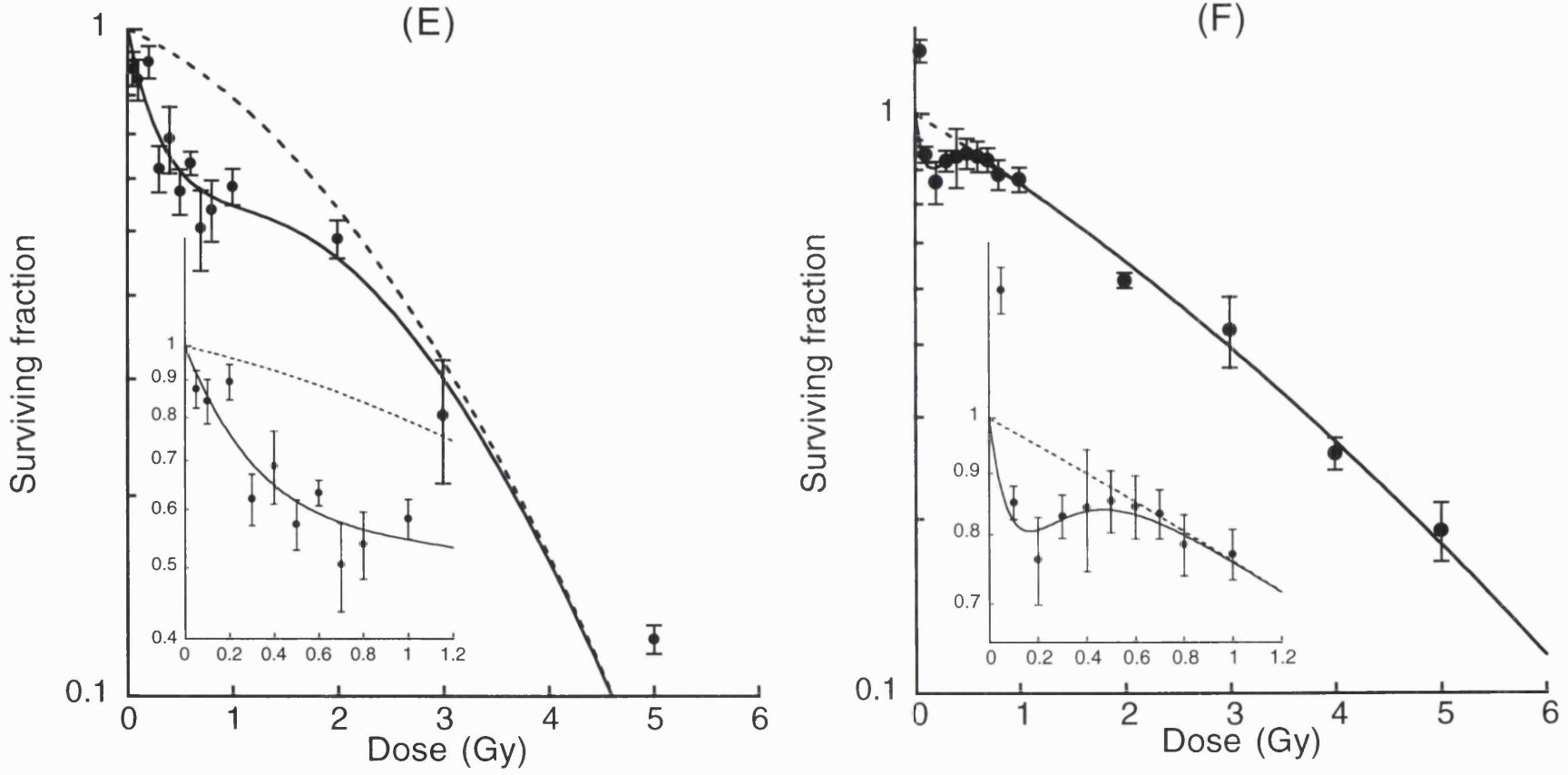

Figure 6.1 (continued)
Shows the survival curve obtained from irradiating asynchronous T98G human glioma cells at low-dose rate and then at high-dose rate with 0h between irradiations. Survival was assessed using the cell sort protocol. Plotted as mean ± SEM. The data have been fitted to the Linear-Quadratic equation (broken line) and the Induced-Repair equation (solid line). The inserts show the low-dose regions in greater detail.
(E) LDR of 30cGy h^{-1} irradiated to a total dose of 2Gy
(F) LDR of 30cGy h^{-1} irradiated to a total dose of 5Gy

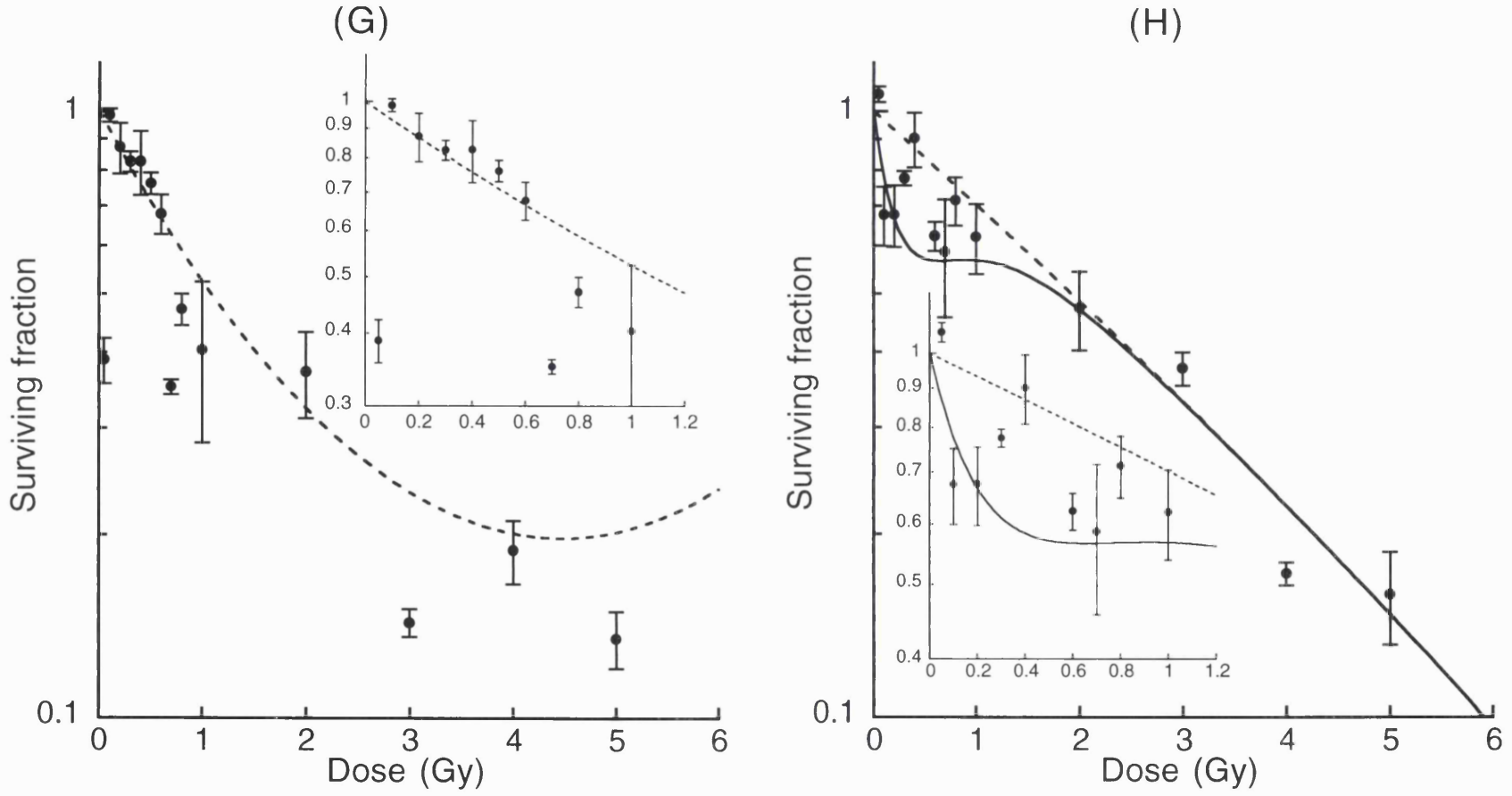

Figure 6.1 (continued)
Shows the survival curve obtained from irradiating asynchronous T98G human glioma cells at low-dose rate and then at high-dose rate with 0h between irradiations. Survival was assessed using the cell sort protocol. Plotted as mean ± SEM. The data have been fitted to the Linear-Quadratic equation (broken line) and the Induced-Repair equation (solid line). The inserts show the low-dose regions in greater detail.
(G) LDR of 60cGy h^{-1} irradiated to a total dose of 2Gy
(H) LDR of 60cGy h^{-1} irradiated to a total dose of 5Gy

Dose rate ($cGy\ h^{-1}$)	Total Dose (Gy)	Interval between LDR & HDR (h)	Fig. 6.2	Sig. HRS?	LQ fit			IR fit					RMSE	
					α	β	α/β	α_s	α_r	d_C	β	α_s/α_r	LQ	IR
60	2	0	(G)	✓	0.640 (0.504-0.786)	-0.0581 (-0.0991–0.00811)	11.0	0.860 (0.541-1.95)	0.293 (-0.491)	1.17 (0.530-)	0.0129 (-0.0171-0.461)	2.93	0.173	0.173
60	5	0	(H)	×	-0.113 (-0.304-0.713)	0.0872 (0.0282–0.171)	1.30						0.325	
30	2	0	(E)	✓	0.420 (0.302-0.542)	-0.0210 (-0.0571–0.0520)	20.0	6.43 (1.21-20.91	0.399 (0.283-0.519)	0.0651 (0.0271-0.163)	-0.158 (-0.0512-0.0271)	16.1	0.178	0.173
30	5	0	(F)	×	0.155 (0.086-0.224)	0.0441 (0.0190-0.0743)	3.52						0.112	
10	2	0	(C)	✓	0.299 (0.0421-0.559)	0.0320 (-0.0511-0.170)	9.3	4.45 (0.617-1.25)	0.187 (-0.205-0.466)	0.124 (0.0521-0.411)	0.0721 (-0.0271-0.280)	23.8	0.293	0.286
10	5	0	(D)	✓	0.367 (0.291-0.447)	-0.0202 (-0.0430–0.00431)	18.4	1.19 (0.482-9.90)	0.282 (0.157-0.404)	0.276 (0.0322-1.549)	0.00241 (-0.0321–0.0584)	4.22	0.114	0.109
5	2	0	(A)	×	0.397 (0.252-0.540)	-0.00412 (-0.0501-0.0553)	9.93	2.85 (0.32-6.89)	0.337 (0.0781-0.504)	0.139 (0.0150-1.08)	0.0141 (-0.116)	8.47	0.183	0.182
5	5	0	(B)	✓	0.245 (0.0622-0.444)	0.0111 (-0.0411-0.0801)	21.9	2.06 (0.612-4.54)	1×10^{-11} (-0.513-0.262)	0.316 (0.161-1.04)	0.0812 (0.000733-0.270)	2×10^{11}	0.279	0.265

Table 6.4

Shows summary data from experiments on confluent T98G cells (Figure 6.2). Cells were irradiated with LDR ^{60}Co γ-rays and then with HDR X-rays and a survival curve was obtained. LQ and IR fit parameters are those obtained by fitting the Linear-Quadratic and Induced-Repair equations to all of the data for each set of experiments. The SEM and upper and lower confidence limits where available are shown in brackets. The RMSE is shown as a measure of 'goodness of fit' for each model to the data. Significant HRS shown is based on non overlapping 95% confidence limits for α_s and α_r and a lower 95% confidence limit for d_C above 0.

Dose rate ($cGy\,h^{-1}$)	Dose (Gy)	Interval between Irradiations (h)	Survival-axis intercept (C)	95% confidence limits
60	2	0	0.939	0.849-1.032
60	5	0	1.210	0.968-1.281
30	2	0	0.931	0.847-1.018
30	5	0	1.107	1.057-1.158
10	2	0	0.894	0.740-1.050
10	5	0	0.917	0.865-0.970
5	2	0	0.915	0.774-1.058
5	5	0	0.879	0.747-1.016

Table 6.5
Shows the results of experiments where confluent T98G cells are irradiated with LDR ^{60}Co γ-rays then HDR X-rays with no interval between these irradiations (summarised in Table 6.4 and shown in Figure 6.2). Results were fitted to the equation:

$$SF = C\exp\left(-\alpha d - \beta d^2\right)$$

This produces a Linear-Quadratic curve which intercepts the survival axis and has an upper 95% confidence limit below 1 if significant HRS is present.

Dose rate ($cGy\ h^{-1}$)	Dose (Gy)	IR model with sig. CL	Upper CL of C-intercept < 1	Sig. no. points below all data LQ fit	Sig. no. points below high-dose LQ fit
60	2	✓	×	×	×
60	5	×	×	×	×
30	2	✓	×	×	×
30	5	×	×	×	×
10	2	✓	×	×	×
10	5	✓	✓	×	✓
5	2	×	×	✓	✓
5	5	✓	×	✓	✓

Table 6.6
Shows the presence or absence of significant HRS using four different methods of analysis (described in Section 6.4) of results acquired by irradiating confluent T98G cells (Table 6.4 and Figure 6.2). Cells were irradiated with LDR ^{60}Co γ-rays and then with HDR X-rays with no interval between these irradiations and a survival curve was obtained.

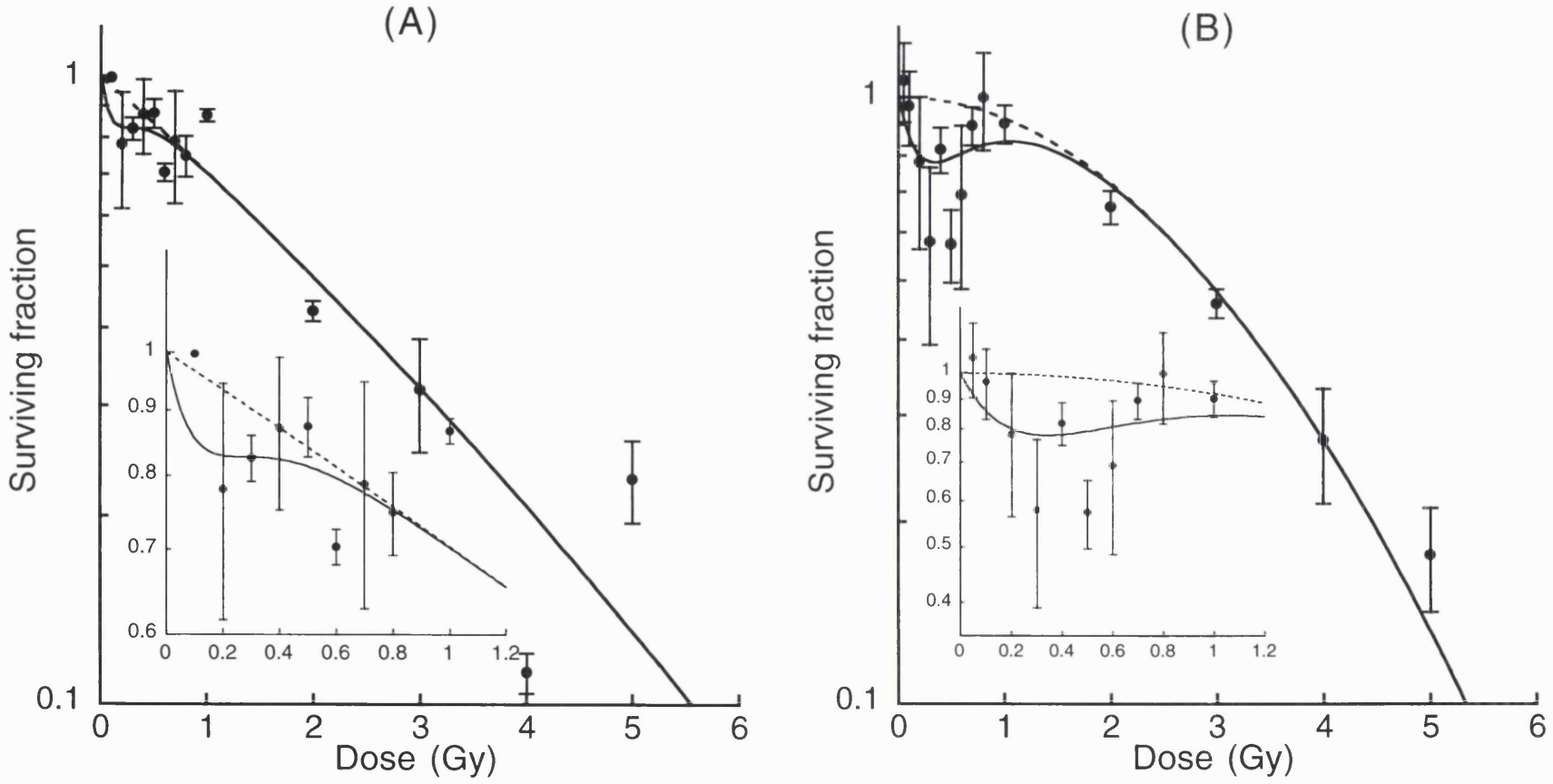

Figure 6.2
Shows the survival curve obtained from irradiating confluent T98G human glioma cells at low-dose rate and then at high-dose rate with 0 h between irradiations. Survival was assessed using the cell sort protocol. Plotted as mean ± SEM. The data have been fitted to the Linear-Quadratic equation (broken line) and the Induced-Repair equation (solid line). The inserts show the low-dose regions in greater detail.
(A) LDR of 5 cGy h^{-1} irradiated to a total dose of 2 Gy
(B) LDR of 5 cGy h^{-1} irradiated to a total dose of 5 Gy

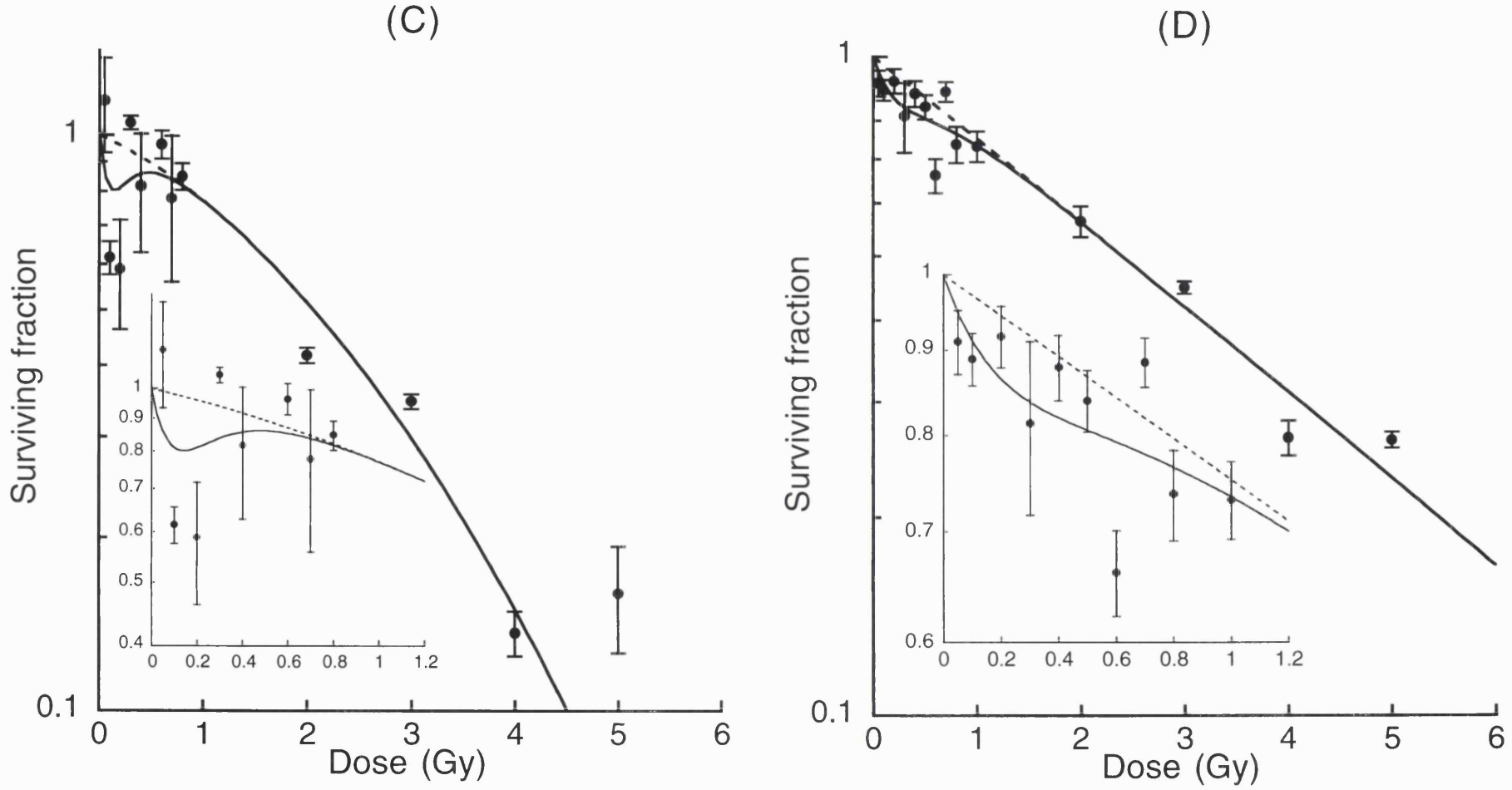

Figure 6.2 (continued)
Shows the survival curve obtained from irradiating confluent T98G human glioma cells at low-dose rate and then at high-dose rate with 0h between irradiations. Survival was assessed using the cell sort protocol. Plotted as mean ± SEM. The data have been fitted to the Linear-Quadratic equation (broken line) and the Induced-Repair equation (solid line). The inserts show the low-dose regions in greater detail.
(C) LDR of 10cGy h^{-1} irradiated to a total dose of 2Gy
(D) LDR of 10cGy h^{-1} irradiated to a total dose of 5Gy

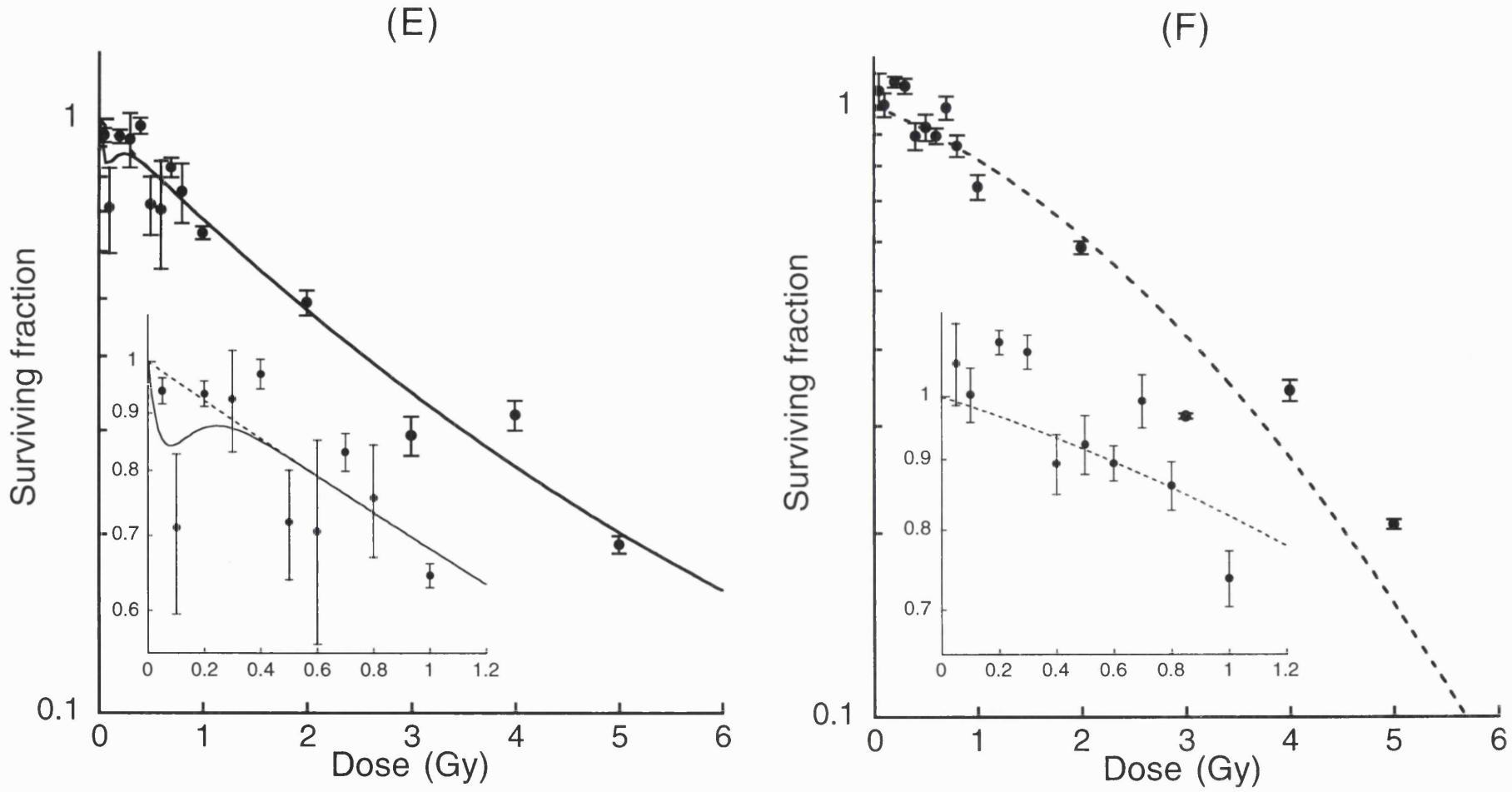

Figure 6.2 (continued)
Shows the survival curve obtained from irradiating confluent T98G human glioma cells at low-dose rate and then at high-dose rate with 0h between irradiations. Survival was assessed using the cell sort protocol. Plotted as mean ± SEM. The data have been fitted to the Linear-Quadratic equation (broken line) and the Induced-Repair equation (solid line). The inserts show the low-dose regions in greater detail.
(E) LDR of 30 cGy h^{-1} irradiated to a total dose of 2 Gy
(F) LDR of 30 cGy h^{-1} irradiated to a total dose of 5 Gy

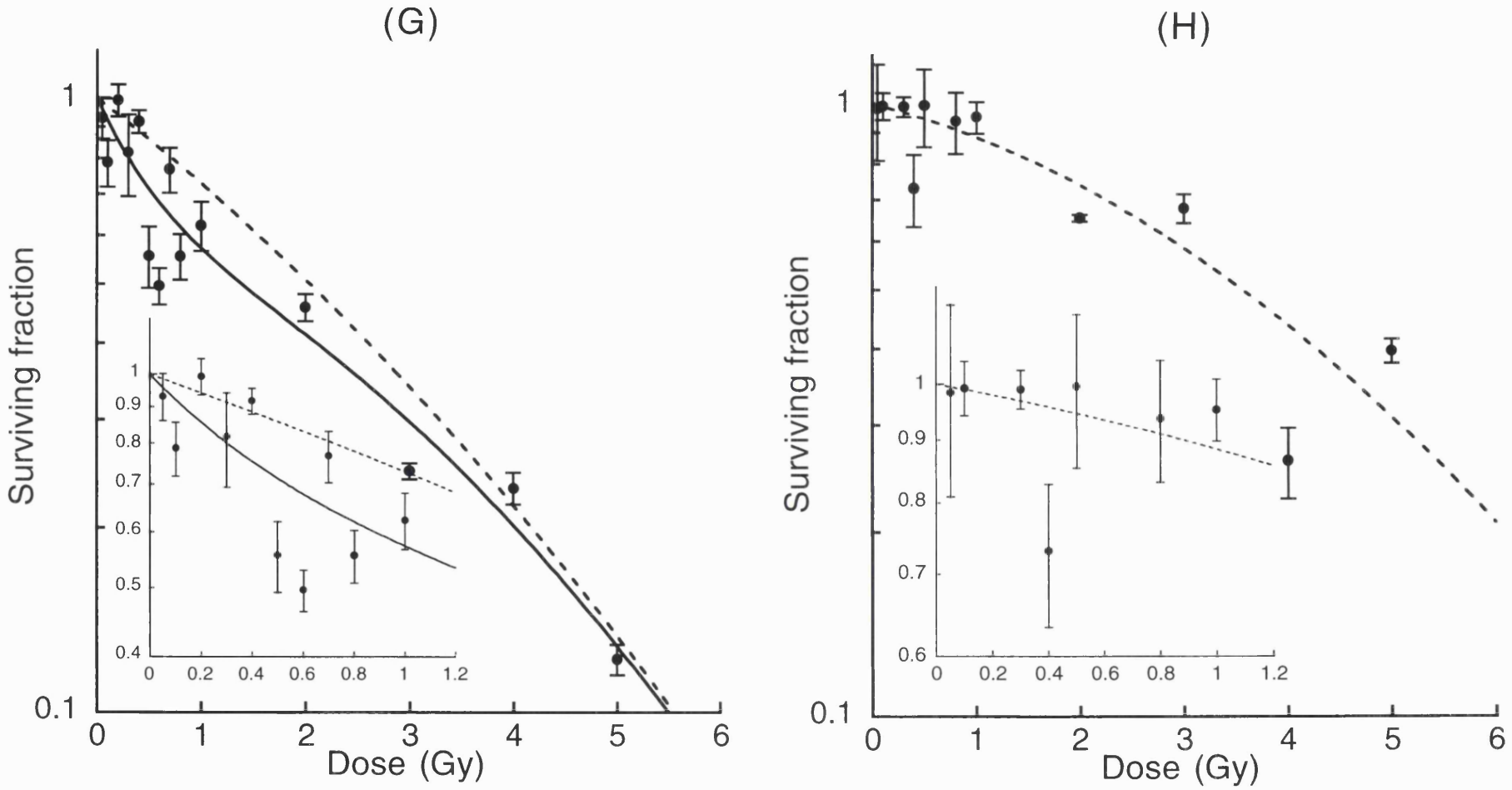

Figure 6.2 (continued)
Shows the survival curve obtained from irradiating confluent T98G human glioma cells at low-dose rate and then at high-dose rate with 0h between irradiations. Survival was assessed using the cell sort protocol. Plotted as mean ± SEM. The data have been fitted to the Linear-Quadratic equation (broken line) and the Induced-Repair equation (solid line). The inserts show the low-dose regions in greater detail.
(G) LDR of 60cGy h^{-1} irradiated to a total dose of 2Gy
(H) LDR of 60cGy h^{-1} irradiated to a total dose of 5Gy

Dose rate (cGy h^{-1})	Total Dose (Gy)	Interval between LDR & HDR (h)	Fig. 6.3	Sig. HRS?	LQ fit			IR fit					RMSE	
					α	β	α/β	α_s	α_r	d_C	β	α_s/α_r	LQ	IR
60	2	4	(G)	✓	0.544 (0.361-0.740)	-0.0320 (-0.0881–0.0460)	17.0	28.4 (5.74-170.)	0.520 (0.345-0.706)	0.0321 (0.00712-0.0630)	-0.0249 (-0.0801-0.0513)	54.6	0.237	0.227
60	5	4	(H)	×	0.281 (0.168-0.395)	0.0116 (-0.0191–0.0453)	24.2	0.817 (0.467-)	-0.161	2.02 (0.392-)	0.0853 (-0.135-0.308)	5.07	0.267	0.268
30	2	4	(E)	✓	0.291 (0.203-0.381)	-0.000511 (-0.0271–0.0302)	582	7.03 (2.57-14.5)	0.267 (0.183-0.353)	0.0812 (0.0431-0.127)	0.00592 (-0.0201-0.0353)	26.3	0.141	0.131
30	5	4	(F)	✓	0.425 (0.321-0.535)	-0.0243 (-0.0551-0.00900)	17.7	7.37 (2.00-27.4)	0.404 (0.302-0.508)	0.0652 (0.0263-0.148)	-0.0188 (-0.0481-0.0140)	18.2	0.159	0.151
10	2	4	(C)	✓	0.501 (0.374-0.635)	-0.0482 (-0.0833–0.0104)	10.4	18.2 (5.17-63.2)	0.481 (0.362-0.606)	0.0390 (0.0201-0.0710)	-0.043 (-0.0761-0.00741	37.8	0.179	0.168
10	5	4	(D)	×	0.181 (0.120-0.244)	0.0102 (-0.00811–0.0282)	18.1	1.58 (0.0651-5.65)	0.170 (0.105-0.235)	0.101 (0.0251-0.595)	0.0128 (-0.00502–0.0322)	9.29	0.105	0.104
5	2	4	(A)	×	0.600 (0.462-0.747)	-0.0651 (-0.103–0.0252)	9.23	4.60 (1.19-)	0.552 (0.407–0.699)	0.100 (0.0153-1.08)	-0.0531 (-0.0921–0.0112)	2.90	0.167	0.160
5	5	4	(B)	✓	0.665 (0.396-0.444)	-0.0871 (-0.162–0.00411)	7.64	4.08 (1.79-9.06)	0.287 (-0.101-0.647)	0.284 (0.120-0.666)	0.0100 (-0.0871-0.240)	14.2	0.290	0.257

Table 6.7

Shows summary data from experiments on confluent T98G cells (Figure 6.3). Cells were irradiated with LDR ^{60}Co γ-rays and then, after 4 h, with HDR X-rays and a survival curve was obtained. LQ and IR fit parameters are those obtained by fitting the Linear-Quadratic and Induced-Repair equations to all of the data for each set of experiments. The SEM and upper and lower confidence limits where available are shown in brackets. The RMSE is shown as a measure of 'goodness of fit' for each model to the data. Significant HRS shown is based on non overlapping 95% confidence limits for α_s and α_r and a lower 95% confidence limit for d_C above 0.

Dose rate ($cGy\,h^{-1}$)	Dose (Gy)	Interval between Irradiations (h)	Survival-axis intercept (C)	95% confidence limits
60	2	4	0.907	0.789-1.030
60	5	4	0.847	0.720-0.981
30	2	4	0.943	0.868-1.020
30	5	4	0.894	0.821-0.969
10	2	4	0.895	0.813-0.980
10	5	4	0.982	0.934-1.031
5	2	4	0.889	0.806-0.975
5	5	4	0.725	0.591-0.865

Table 6.8
Shows the results of experiments where confluent T98G cells are irradiated with LDR ^{60}Co γ-rays then HDR X-rays with a 4 h interval between these irradiations (summarised in Table 6.7 and shown in Figure 6.3). Results were fitted to the equation:

$$SF = C\exp\left(-\alpha d - \beta d^2\right)$$

This produces a Linear-Quadratic curve which intercepts the survival axis and has an upper 95% confidence limit below 1 if significant HRS is present.

Dose rate ($cGy\,h^{-1}$)	Dose (Gy)	IR model with sig. CL	Upper CL of C-intercept < 1	Sig. no. points below all data LQ fit	Sig. no. points below high-dose LQ fit
60	2	✓	×	×	×
60	5	×	✓	✓	✓
30	2	✓	×	✓	✓
30	5	✓	✓	×	×
10	2	✓	✓	×	×
10	5	×	×	×	✓
5	2	×	✓	×	✓
5	5	✓	✓	×	×

Table 6.9
Shows the presence or absence of significant HRS using four different methods of analysis (described in Section 6.4) of results acquired by irradiating confluent T98G cells(Table 6.7 and Figure 6.3). Cells were irradiated with LDR ^{60}Co γ-rays and then with HDR X-rays with a 4 h interval between these irradiations and a survival curve was obtained.

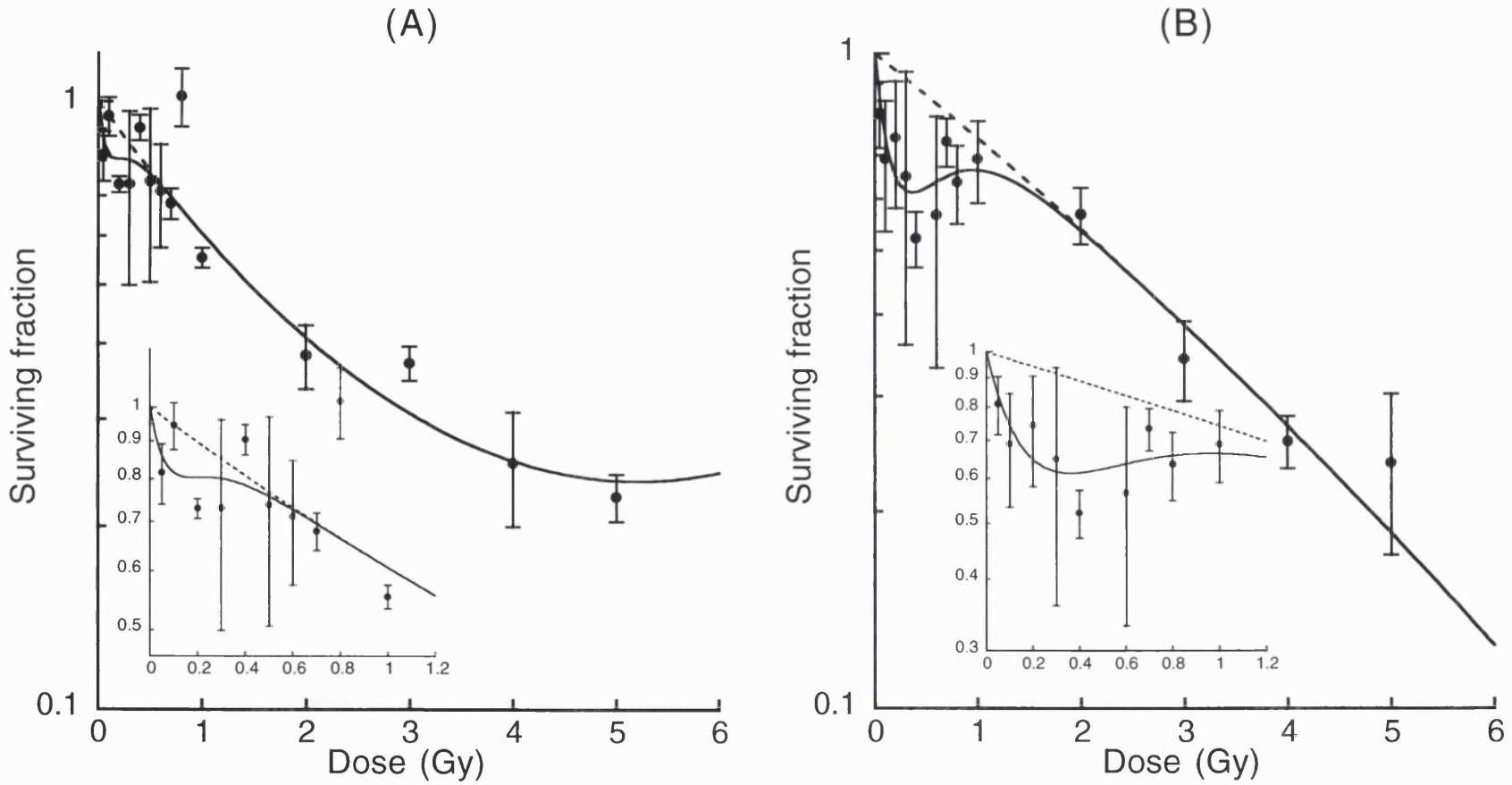

Figure 6.3
Shows the survival curve obtained from irradiating confluent T98G human glioma cells at low-dose rate and then at high-dose rate with 4 h between irradiations. Survival was assessed using the cell sort protocol. Plotted as mean ± SEM. The data have been fitted to the Linear-Quadratic equation (broken line) and the Induced-Repair equation (solid line). The inserts show the low-dose regions in greater detail.
(A) LDR of 5 cGy h^{-1} irradiated to a total dose of 2 Gy
(B) LDR of 5 cGy h^{-1} irradiated to a total dose of 5 Gy

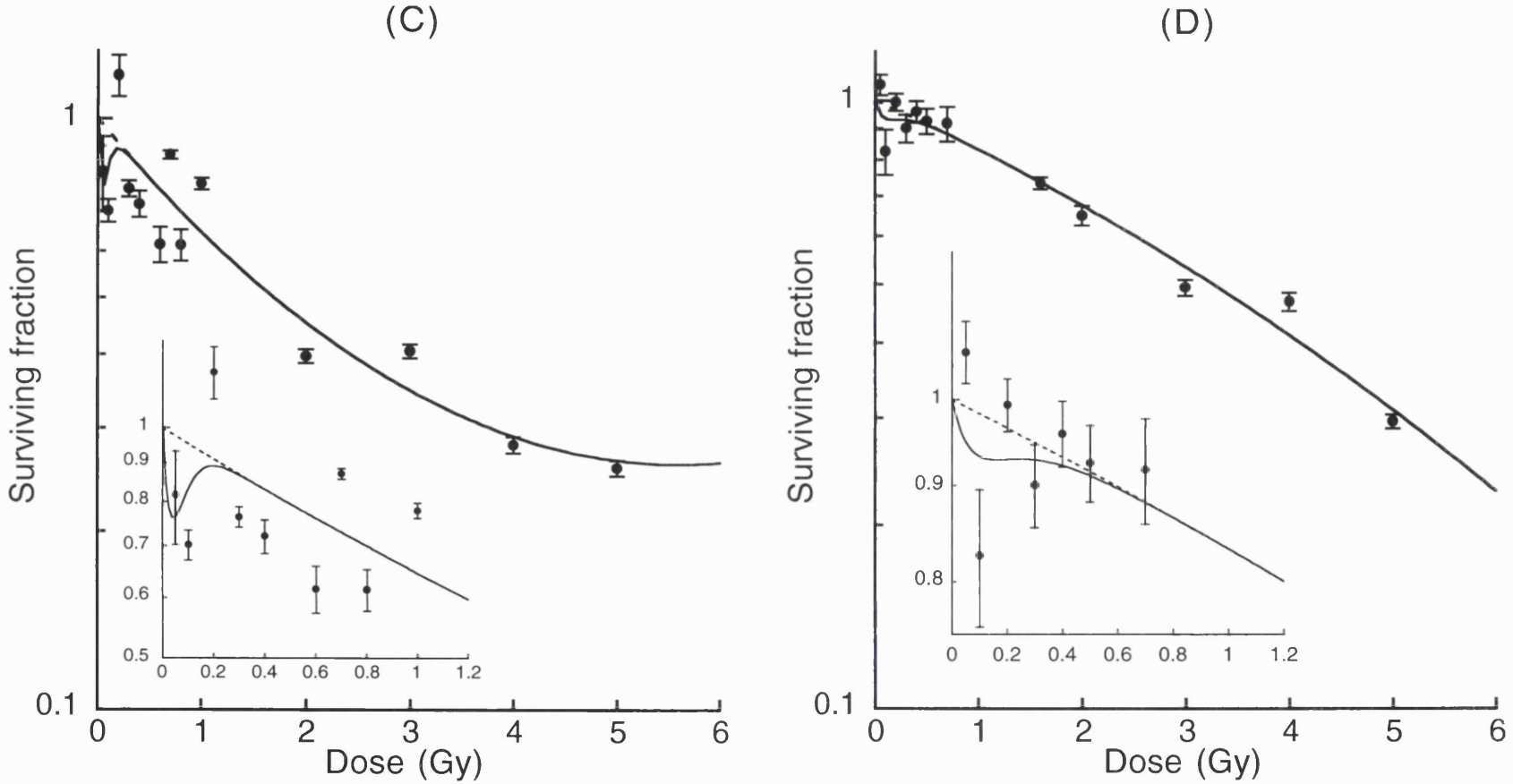

Figure 6.3 (continued)
Shows the survival curve obtained from irradiating confluent T98G human glioma cells at low-dose rate and then at high-dose rate with 4h between irradiations. Survival was assessed using the cell sort protocol. Plotted as mean ± SEM. The data have been fitted to the Linear-Quadratic equation (broken line) and the Induced-Repair equation (solid line). The inserts show the low-dose regions in greater detail.
(C) LDR of 10cGy h^{-1} irradiated to a total dose of 2Gy
(D) LDR of 10cGy h^{-1} irradiated to a total dose of 5Gy

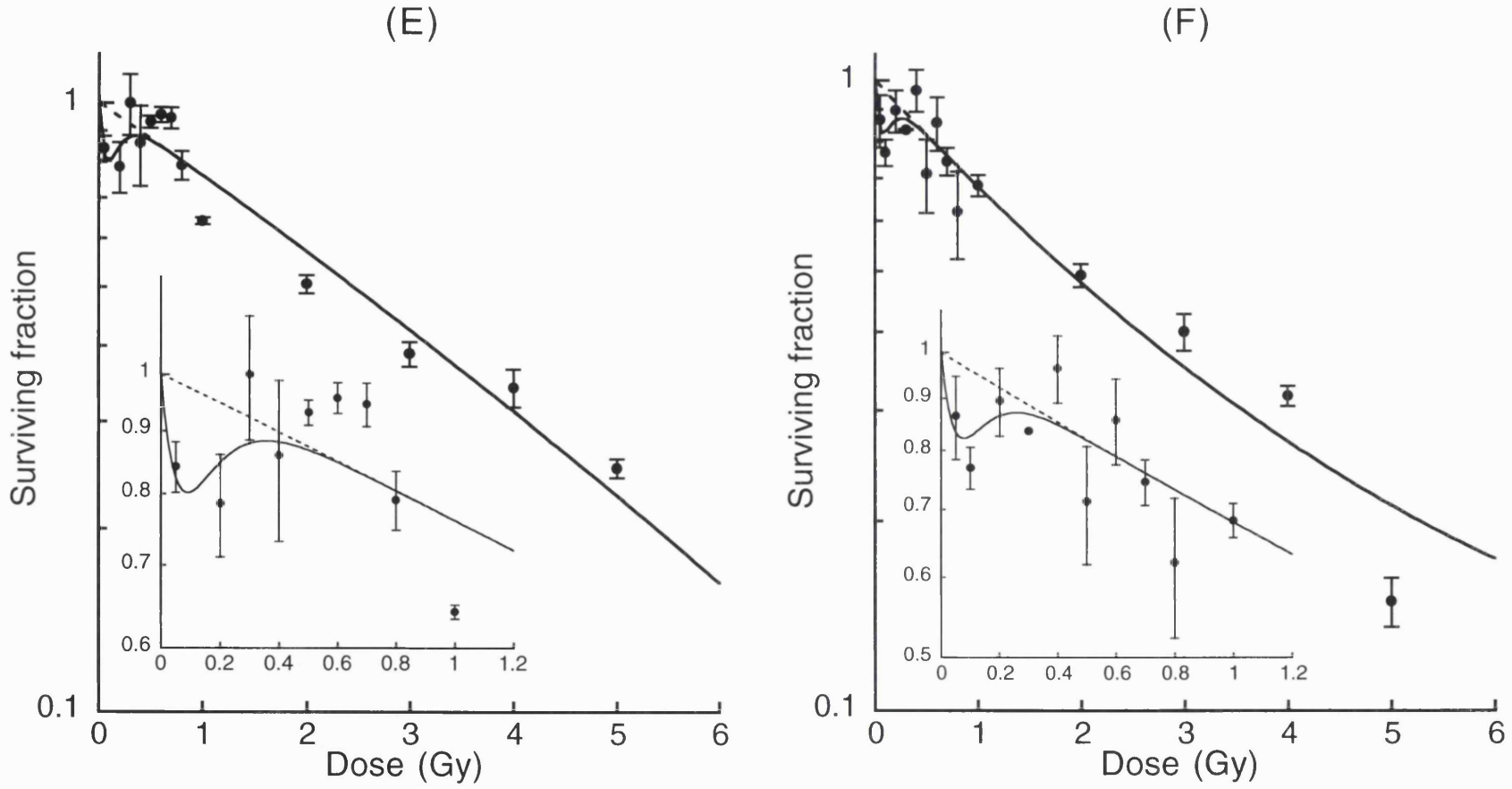

Figure 6.3 (continued)
Shows the survival curve obtained from irradiating confluent T98G human glioma cells at low-dose rate and then at high-dose rate with 4h between irradiations. Survival was assessed using the cell sort protocol. Plotted as mean ± SEM. The data have been fitted to the Linear-Quadratic equation (broken line) and the Induced-Repair equation (solid line). The inserts show the low-dose regions in greater detail.
(E) LDR of 30cGy h^{-1} irradiated to a total dose of 2Gy
(F) LDR of 30cGy h^{-1} irradiated to a total dose of 5Gy

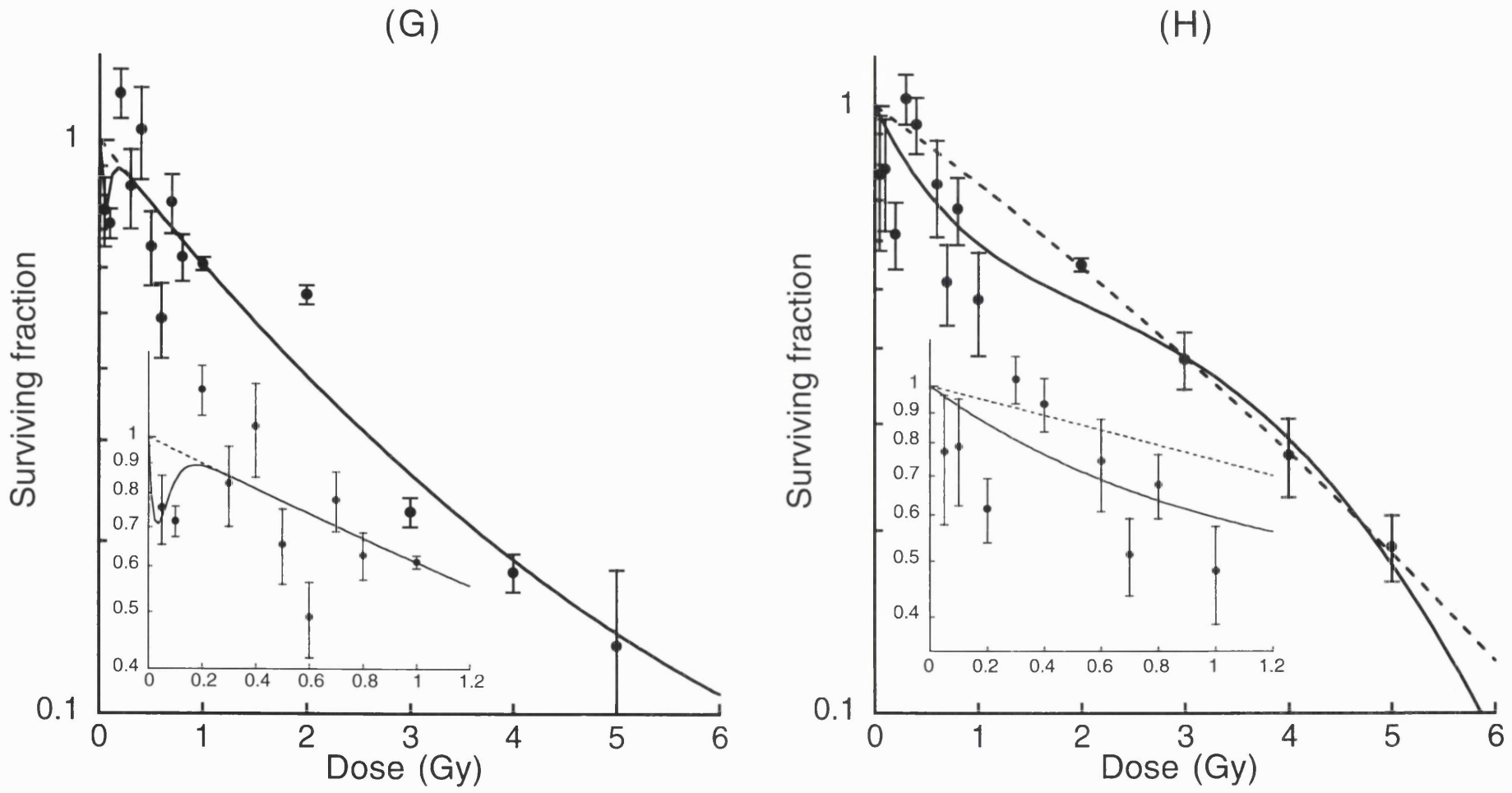

Figure 6.2 (continued)
Shows the survival curve obtained from irradiating confluent T98G human glioma cells at low-dose rate and then at high-dose rate with 4h between irradiations. Survival was assessed using the cell sort protocol. Plotted as mean ± SEM. The data have been fitted to the Linear-Quadratic equation (broken line) and the Induced-Repair equation (solid line). The inserts show the low-dose regions in greater detail.
(G) LDR of 60cGy h^{-1} irradiated to a total dose of 2Gy
(H) LDR of 60cGy h^{-1} irradiated to a total dose of 5Gy

6.6 Discussion

The experiments described in this chapter were designed to investigate the combination of "priming" dose and dose rate, given at LDR, that would decrease the size of, or block the HRS response, to subsequent HDR exposures. The presence or absence of HRS was investigated along with the "degree" of HRS as measured by the α_s/α_r value.

There is much evidence to suggest the involvement of DNA-repair processes in HRS/IRR. Whether this repair is constitutive or actively induced, there are two major hypotheses on how these repair mechanisms are triggered into action:
(1) that there is a fixed threshold level of damage where if damage levels exceed this, repair is switched on.
(2) that there is a continuous transition of increasing repair activity as damage levels increase.

In these experiments the presence or absence of HRS after various LDRs and various total doses, was examined. Hypothesis 1, that there is a fixed threshold for the triggering of repair, could be used to explain the results. HRS was present in asynchronously growing T98G cells irradiated with LDR ^{60}Co γ-rays to total doses of 2 and 5 Gy and then immediately irradiated with HDR X-rays. This would suggest that radioprotective mechanisms were not triggered in these experiments and that irradiating asynchronous T98G cells at dose rates below 60 cGy h^{-1} to 2 and 5 Gy did not cross a threshold level for the induction of radioresistance. However, confluent T98G irradiated under similar conditions did not always show HRS. Cells irradiated at a dose rate of 60 and 30 cGy h^{-1} to a total dose of 5 Gy (Figures 6.2 F and H) did not show significant HRS using any of the 4 methods of analysis. When the graphs were assessed visually, there was also no indication of HRS. It may have been possible that, in these two cases, a threshold level of damage for IRR was crossed, repair mechanisms were switched on and so no HRS was observed.

However, when confluent cells were irradiated in virtually identical experiments, but with a 4 h interval left between LDR and HDR irradiations, HRS was observed in all cases, including 60 and 30 cGy h^{-1} to 5 Gy. This may have reflected the triggered DNA-repair processes acting to reduce the amount of damage within those 4 h, to below a threshold level, and therefore when cells were irradiated at HDR, HRS was observed. The fact that HRS was observed following a total dose of 2 Gy at dose rates of 30 and 60 cGy h^{-1} and not following 5 Gy suggests that there may have been a fixed threshold level between 2 and 5 Gy for 30 to 60 cGy h^{-1} exposures. Further experiments could determine precisely this threshold level for a given dose rate.

Four statistical methods were used to determine the presence or absence of HRS. The first method involved fitting an Induced-Repair curve. If a curve fit could be obtained with the 95% confidence limits of the upper α_r and the lower α_s not overlapping and the lower d_C 95% confidence limit was above zero, then the experiment was judged to demonstrate significant HRS. In many cases a curve fit was obtained, but the confidence limits were not acquired or they were not significant. This suggested that HRS/IRR was present, but more experiments would be needed until it was proven. It is possible that in some cases that HRS was present, *i.e.* there were a number of sensitive data points in the low-dose region, but their distribution was not well described by the IR model so the JMP© program was unable to ascribe an accurate fit using the IR equation. As it was very important in these experiments to determine whether HRS was present or not, for these reasons, three other methods were used to try to determine the presence of HRS. The second method involved fitting the data to a modification of the Linear-Quadratic curve (Equation 6.1) which took into account the "pull" of the low-dose data. If significant HRS was present then the intercept (C) would intercept the survival below one and the upper 95% confidence limit of this value would also fall below 1. This method may have been useful in the above situation where the data points were not distributed in an IR curve shape and a fit could not be obtained. There were problems, however with this method if HRS was present and there were very few low-dose data points. In this case there may have not been enough "pull" stronger high-dose data for which there may have been a lot of points, resulting in the survival axis intercept being high, although HRS was present. However, this was a conservative method of analysis, so if the upper 95% was below 0 then it was very likely that significant HRS was present.

The last two methods to look for the presence of HRS involved using the JMP© software to fit a LQ curve. All data was fitted to a LQ curve and the data points that fell below the curve in the low-dose region (<1 Gy) were counted and assessed whether they were significantly different from the total number of data points in the low-dose region (using a t-test). This was also done with an LQ curve fitted omitting the low-dose data (*i.e.* using doses 1–5 Gy). The former method was more robust as if low-dose data had contributed to the shape of the curve, pulling it downwards, and the data set also showed a significant number of low-dose points below the curve, there was very strong evidence for the presence of HRS. The second method was weaker as the LQ curve was entirely defined by the high-dose data and the low-dose points made no contribution, however, the rational for HRS was an increased sensitivity, greater than predicted by the extrapolation of high-dose data and if a significant number of low-dose data points were found below this "high-dose" LQ curve it may have been acceptable to consider HRS present. There were some problems associated with these methods. For example, if the 1 Gy data point was very low it may have pulled down the curve resulting in fewer

points falling below it. In this case it may have been acceptable to use the data points for 2 to 5 Gy in the curve fit, omitting 1 Gy. It therefore seemed to be a matter of individual judgement which data points were used and this was not sound practice. In all the experiments described in his chapter, the same dose points were consistently included for analysis in each data set. There were problems with each method of analysis and the methods of detection for the presence of HRS could be ranked in the following order of robustness:

(1) IR fit with significant 95% confidence limits,

(2) Upper 95% confidence limit of C-intercept is <1 when fitted to:

$$SF = C\exp\left(-\alpha d - \beta d^2\right)$$

(3) Significant number of low-dose data points below "all data" LQ curve fit,

(4) Significant number of low-dose data points below "high-dose" LQ curve fit.

However, as each method detected a significant deviation from the LQ survival curve at low doses, for the experiments described in this chapter, if significant HRS in a data set was found by at least one method, then it was accepted that significant HRS was present in that experiment.

Hypothesis 2, that this threshold was not fixed with a specific on/off "trigger" level but the amount of repair may just have increased with increasing damage, was examined in these experiments by measuring the "degree" of HRS present. One way of doing this was by calculating the α_s/α_r value for each survival curve. In the asynchronously growing cells, for 3 out of the 4 dose rates (30, 10 and 5 cGy h^{-1}), the degree of HRS, as measured by the α_s/α_r value was greater at a total dose of 2 Gy than 5 Gy. This also seemed to be true in the confluent experiments where for 3 out of 4 dose rates (60, 30 and 10 cGy h^{-1}) for both 0 h and 4 h interval, the degree of HRS was greater at 2 Gy than 5 Gy. This may have been explained in terms of a transitional increase in repair (hypothesis 2) as the smaller degree of HRS, or none at all as occurred at 60 and 30 cGy h^{-1} in confluent cells, may have just reflected more repair mechanisms being switched on with increased damage at 5 Gy. It was surprising, however, that a greater degree of HRS was seen at 5 Gy rather than 2 Gy when cells were irradiated at 5 cGy h^{-1}. This was also seen in asynchronous cultures where the degree of HRS was smaller at 2 Gy compared with 5 Gy when irradiated at 60 cGy h^{-1}. It was difficult to explain this using a transitional threshold model as it would suggest that damage levels were higher at 2 Gy than 5 Gy, so that somehow less repair was occurring at 5 Gy than 2 Gy. This may have suggested the presence of some unknown constitutive repair mechanisms working during irradiations at very low-dose rates that reduced damage levels. This, however was unlikely to be the explanation as in the graph shown in Figure 4.4 of LDR ^{60}Co γ-irradiations of confluent cells, 5 cGy h^{-1} gave the greatest cell kill at 2 Gy of all the dose rates. It may have been more likely that the α_s/α_r value was not the most

accurate or appropriate measurement in assessing the "degree" of HRS. This, along with suggested alternative methods are discussed later in this chapter.

A pictorial representation of hypotheses 1 and 2 for confluent T98G cells irradiated at low-dose rates are shown in Figure 6.4. In acute dose situations >0.5 Gy, a high level of damage occurred very quickly, crossing the threshold level of IRR, or triggering the maximum amount of repair mechanisms. In the case of LDR of 10 and 5 cGy h^{-1} damage levels took longer to reach the IRR threshold, or trigger a large amount of repair and so a greater total dose could have been given before this maximum level or threshold was reached. Irradiating cells at 60 and 30 cGy h^{-1} to a total dose of 2 Gy, the threshold level or maximum repair activity was yet to be reached, but at a total dose of 5 Gy, HRS was not present, so the damage level had risen above the IRR threshold or had triggered maximum repair. If the cells were left to recover for 4 h before the second irradiation, repair mechanisms decreased damage levels to below the IRR threshold or to a level where the rate of repair was smaller. The degree of HRS as measured by α_s/α_r value was greater at 2 Gy than 5 Gy for 10, 30 and 60 cGy h^{-1} as more repair mechanisms were switched on at 5 Gy increasing resistance in the low-dose region of the survival curve. This seemed to be happening for all dose rates in asynchronous cultures.

The α_s/α_r values for confluent T98G irradiated at dose rates of 60, 30,and 10 cGy h^{-1} were higher in experiments given a 4 h interval between irradiations. The cells recovering in those 4 h, *i.e.* the damage levels falling to below the threshold level for the induction of repair, or falling to a level where there are fewer repair processes taking place, could have explained this and so HRS occurred to a greater extent. The timescale of 4 h was chosen as previous fractionation experiments on T98G by (Short 1999), showed that by giving two doses of 0.4 Gy separated in time, an increase in cell kill was observed, greater than observed after giving a single 0.8 Gy fraction. The optimum time for the increase in cell kill, *i.e.* for the "recovery" of HRS, was 4–6 h. In these experiments, the 4 h timescale between irradiations, after which HRS is observed may be equivalent to this single dose response. This may be further evidence for a relationship between HRS at low-acute doses and the inverse dose-rate effect observed in Chapter 4.

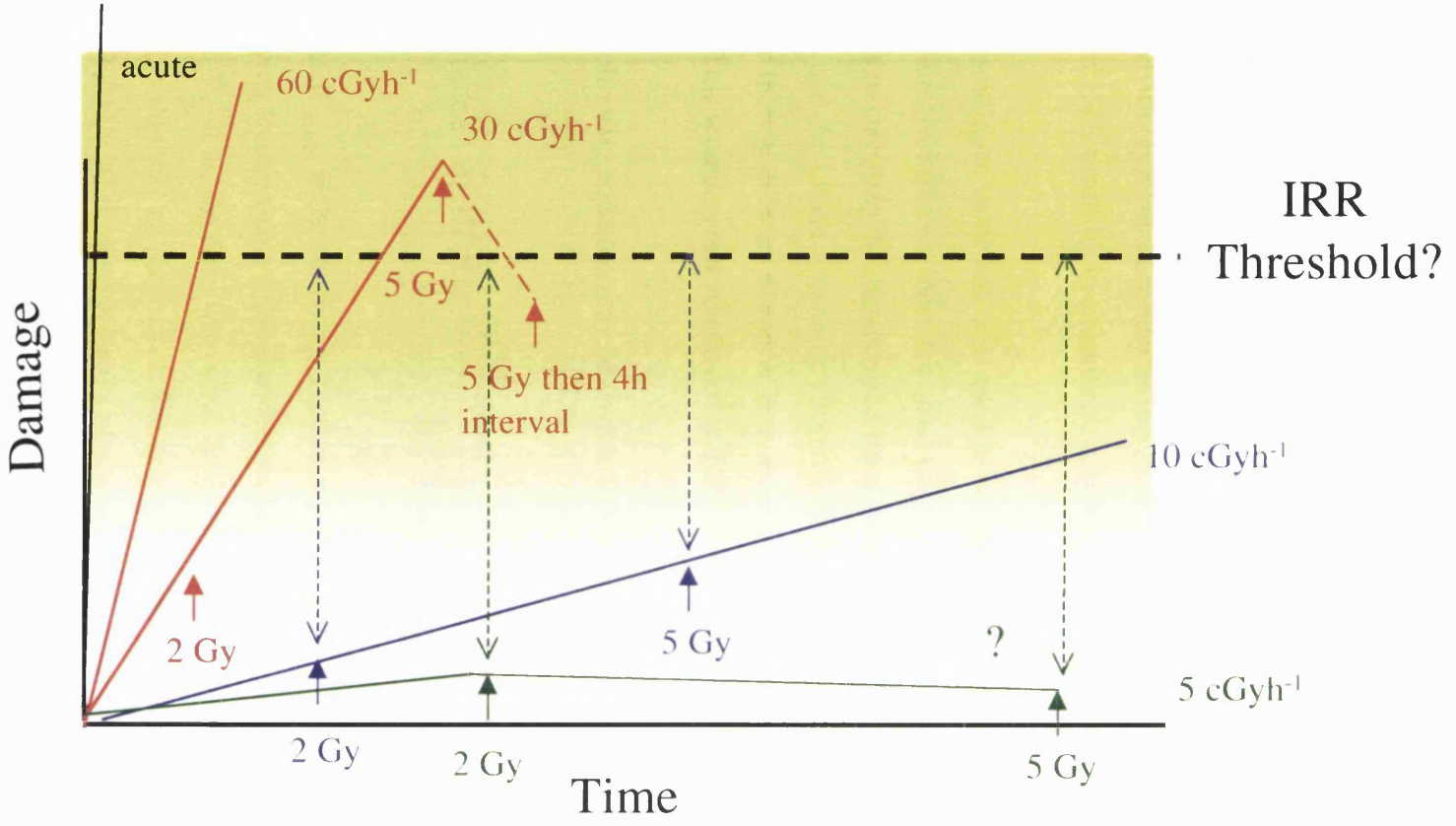

Figure 6.4
A model proposed for the induction of repair mechanisms in confluent T98G cells irradiated at low dose rates. Coloured lines represent damage at a particular dose rate, the dashed red line represents repair levels and the dashed blue and green lines represent the potential for HRS before the threshold or maximum repair is triggered. The longer the line, the greater the amount* of HRS observed. The dashed black line shows a fixed threshold level as described in hypothesis 1 (Section 6.6). The strength of the yellow colouring represents the rate of repair taking place as described by hypothesis 2 (Section 6.6). *as measued by α_s/α_r.

The results in Chapter 4 indicate that an inverse dose-rate effect is present in both asynchronously growing T98G and confluent cultures (Figures 4.4 & 4.7). However, there are differences between these two sets of data, as the "flip-over" from dose-rate sparing to the inverse dose-rate effect occurs at a much lower dose rate in confluent cells than the asynchronous. The possible reasons for this have been discussed in Chapter 4. However, the sparing effect in the confluent cultures at 60 and 30 cGy h^{-1}, which can only be seen at higher total doses (> 2 Gy), may be related to the results obtained in the experiments described in this chapter, *i.e.* the absence of HRS in the 60 and 30 cGy h^{-1} at 5 Gy may reflect the switching on of repair mechanisms and the lack of HRS resulting in a more resistant response in the two survival curves.

So far the α_s/α_r value has been used to calculate the degree of HRS in these experiments, however there are other ways in which to measure the extent of HRS. One way is to calculate the distance at a fixed point between the Induced-Repair survival curve and the Linear-Quadratic survival curve (shown as a blue line in Figure 6.5) and divide that by the total distance from the IR curve to 1 (shown as a red line in Figure 6.5). This would give a "distance" of HRS relative to the steepness of the curve.

The following equation may be used to calculate this distance:

$$\text{"Distance" of HRS} = \frac{\ln(SF_{doseIR}) - \ln(SF_{doseLQ})}{\ln(SF_{doseIR})} \qquad \text{Equation 6.2}$$

Where SF_{doseIR} is the surviving fraction at a fixed dose on the IR curve and SF_{doseLQ} is the surviving fraction on a fixed dose on the LQ curve. The decision over which dose to use was difficult as, the dose where the "kink" was situated varied between experiments. The d_C value was an obvious choice as it pinpointed the transition between HRS and IRR. Table 6.10 shows the results of analysis of the data using this method. The degree of HRS measured by the "distance" method for these experiments was compared with the α_s/α_r value obtained. If both methods produced a similar measurement of the degree of HRS, then when all the data was plotted against one another, a correlation of 1 should have been obtained. Figure 6.7 (A) shows a plot of α_s/α_r versus the "distance" measurement of HRS and there was clearly no linear correlation. There did however, appear to be a polynomial distribution, and a curve fit was obtained. This correlation

was not surprising since both methods used the same parameters to essentially estimate the same distance. However, the polynomial distribution did show that when a large degree of HRS was detected using α_s/α_r, the measure of HRS for the same experiment using the "distance" method was much more conservative.

The major problem with this "distance" analysis, was that if the d_C value was very small, the HRS effect may have looked small when assessed visually, but using the analysis, a large value for the amount of HRS may have been obtained. The degree of HRS was a proportion of the distance from the IR curve to the surviving fraction of 1 and if the distance was very small, the value may have appeared large in proportion although only a small amount of HRS could be seen by eye. In this situation it was difficult to assess whether this "distance" method gave a better measure of HRS than a "by eye" method as the "correct" or "most accurate" method of measuring HRS has yet to be defined.

A third method of assessing the degree of HRS may be to measure the area between the IR and LQ curves in the low-dose region (shown as a red shaded area in Figure 6.6) and take that as a proportion of the area above the IR curve to a surviving fraction of 1 and an upper dose of 2 (shown as the yellow shaded area in Figure 6.6).
The following equation was used:

$$\text{"Area" of HRS} = \frac{\int_0^2 \exp(-\alpha d - \beta d^2) - \int_0^2 \exp -\alpha_r \left(1 + \left(\alpha_s/\alpha_r - 1\right) e^{-d/d_c}\right) d - \beta^2}{2 - \int_0^2 \exp -\alpha_r \left(1 + \left(\alpha_s/\alpha_r - 1\right) e^{-d/d_c}\right) d - \beta d^2}$$

Equation 6.3

The results of this analysis of data are shown in Table 6.10. These results did not seem to correlate with α_s/α_r value (Figure 6.7(B)) or the "distance" method (Figure 6.7(C)) of assessing the degree of HRS. The major problem when using this method was, although an overall measurement of the size of the deviation between the IR and LQ was obtained, some survival curves where there were a few very sensitive points may have had a very narrow but "deep" dip in the curve. This would have resulted in there being a small overall area, but a large amount of HRS being observed by eye or measured by α_s/α_r or the "distance" method. Again it was difficult to reach a conclusion on which was the "correct" way to measure the degree of HRS.

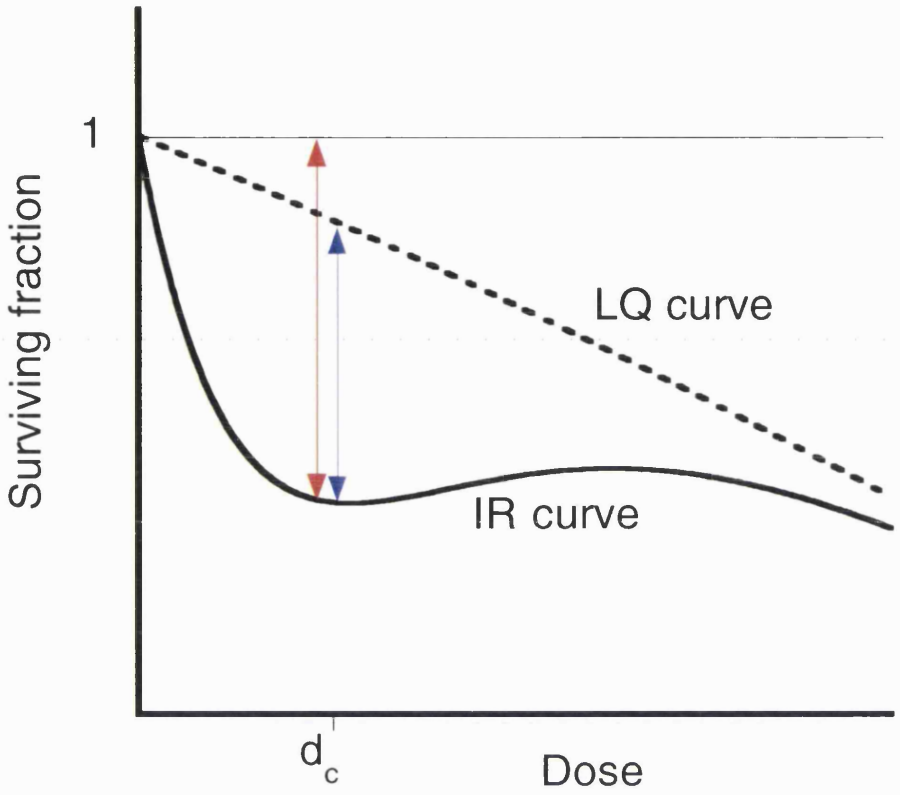

Figure 6.5
Shows the "distance" method of measuring the degree of HRS.
The difference between the natural logs of LQ and the IR curves (blue line) at d_C was divided by the distance between the natural logs of the SF of 1 and the IR curve at d_C (red line) (Equation 6.2).

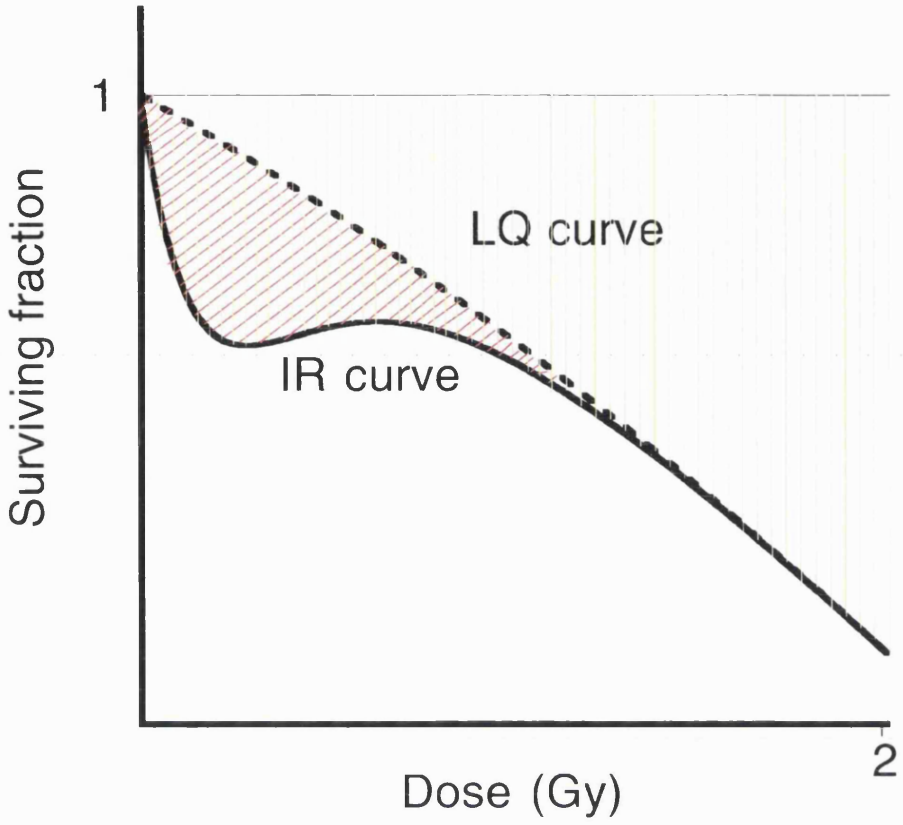

Figure 6.6
Shows the "area" method of measuring the degree of HRS.
The area between the LQ and the IR curves (red shaded area) between 0 and 2 Gy was divided by the area between the IR curve and a SF of 1 to an upper dose of 2 Gy (yellow shaded area) (Equation 6.3).

Cell growth status	Interval between LDR & HDR (h)	Dose rate ($cGy\,h^{-1}$)	LDR Dose (Gy)	Degree of HRS		
				"Distance" method	"Area" method	α_s/α_r value
async	0	60	2			
async	0	60	5	0.747	0.329	19.09
async	0	30	2	0.740	0.484	11.20
async	0	30	5	0.836	0.109	15.02
async	0	10	2	0.916	0.0154	18.54
async	0	10	5	0.745	0.0967	8.82
async	0	5	2	0.760	0.271	12.86
async	0	5	5	0.335	0.155	2.43
confl	0	60	2	0.376	0.334	2.93
confl	0	60	5			
confl	0	30	2	0.851	0.0371	16.12
confl	0	30	5			
confl	0	10	2	0.889	0.111	23.80
confl	0	10	5	0.542	0.107	4.22
confl	0	5	2	0.732	0.0695	8.47
confl	0	5	5	0.967	0.477	2×10^{11}
confl	4	60	2	0.942	0.033	54.60
confl	4	60	5	0.970	1.134	5.07
confl	4	30	2	0.903	0.078	26.33
confl	4	30	5	0.864	0.042	18.24
confl	4	10	2	0.931	0.035	37.82
confl	4	10	5	0.752	0.040	9.29
confl	4	5	2	0.731	0.0458	2.90
confl	4	5	5	0.828	0.314	14.22

Table 6.10
Shows values obtained using 3 different methods to measure the degree of HRS in all experiments described in this chapter. The α_s/α_r value obtained from the IR curve fit parameters is shown. The "distance" method used the LQ and IR curve fit parameters to measure the distance between curves at dose d_C. Equation 6.2 was used to calculate this. The "area" method measured the area between the LQ and IR graphs. In this method the parameters acquired from the two curve fits were used in Equation 6.3 to calculate the area within the dose range 0–2 Gy.

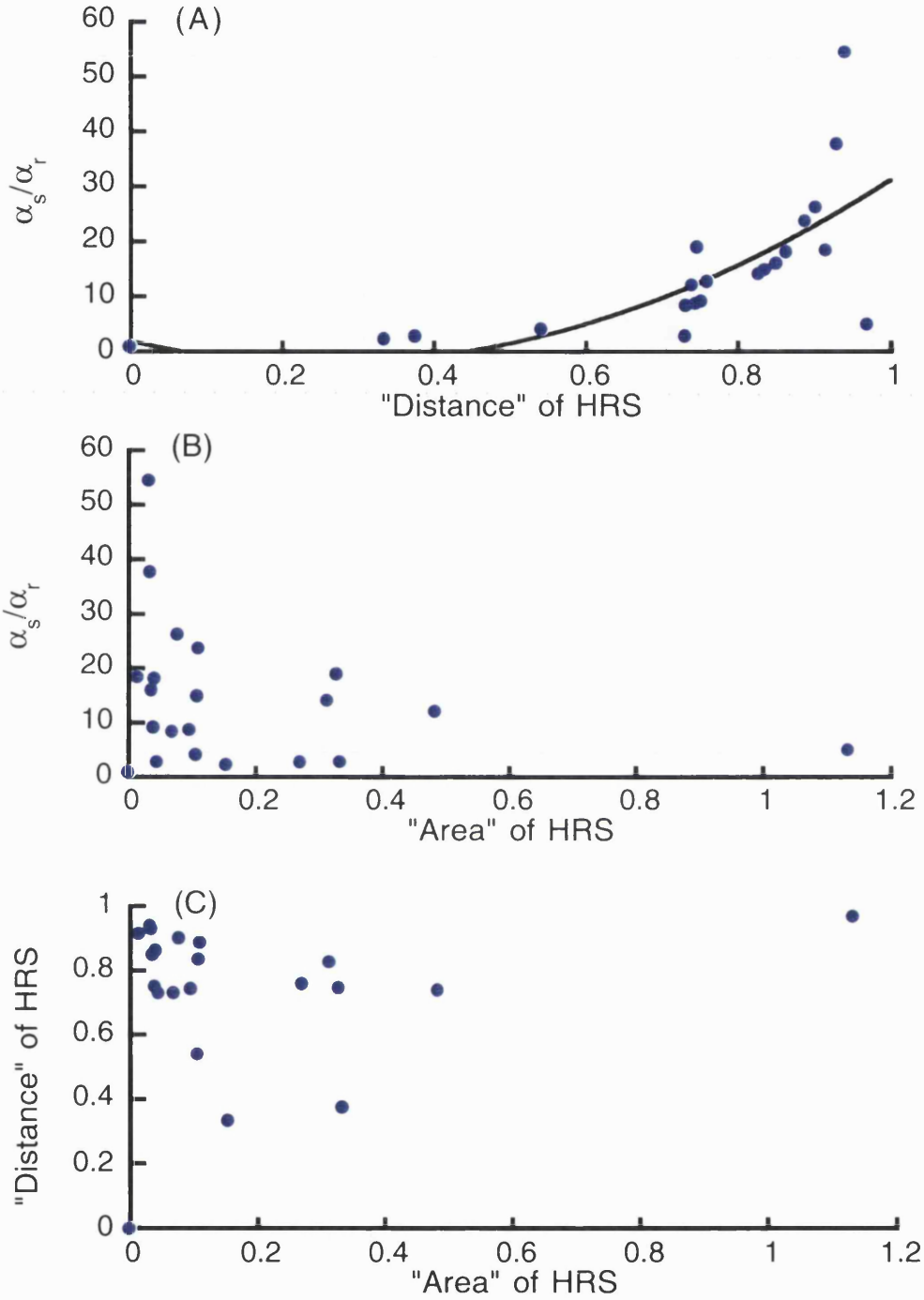

Figure 6.7
Shows plots of the degree of HRS as measured in all T98G cells irradiated at LDR then HDR as described in Section 6.3. Three methods were used to measure the degree of HRS, the α_s/α_r value, the "distance" method (Equation 6.2) and the "area" method (Equation 6.3). These are described in Section 6.6. (A) shows α_s/α_r plotted against "distance" where a curve fit was obtained: $y = 1.89 - 30.7x + 60.0x^2$ ($r=0.710$, $p<0.01$), (B) shows α_s/α_r plotted against "area" and (C) shows "distance" plotted against "area".

As mentioned in Chapter 3, there is a trend that the degree of HRS is related to radiosensitivity in the 25 cell lines tested. Figure 3.14 shows a graph plotted with SF at 2 Gy against degree of HRS as measured by α_s/α_r for all 25 cell lines. A positive trend was obtained (r= 0.198, p= 0.333). The 25 cell lines were also analysed using the other 2 methods described here to determine whether they would give a stronger correlation and therefore possibly a better method of measuring the degree of HRS. The graphs of each method plotted against SF at 2 Gy are shown in Figures 6.8 and 6.9. The "distance" method gave a correlation of r= 0.266 (p= 0.199) and the "area" method, r= 0.231 (p= 0.266). Although the "distance" method of measuring the amount of HRS gave a slightly better correlation with SF_2 than the other two methods, it was not significantly different. As these alternative methods of measuring the degree of HRS did not obtain a significantly stronger correlation with SF_2 ,they do not appear any "better" at measuring the degree of HRS than α_s/α_r. Therefore it was considered justifiable to use the established method, α_s/α_r, to determine the degree of HRS in the experiments described in this chapter.

A better correlation with SF_2 may have been obtained if the degree of HRS was plotted on a logarithmic scale, however, the "distance" and "area" methods could not be plotted on such a scale as zero was part of the co-ordinates for some of the points. The equations could be modified further to give results which are not equal to zero and therefore could be plotted on a log scale. It may also be possible to gain a stronger correlation using the "area" method when the upper limit is reduced from 2 Gy. There are infinite possibilities when it comes to methods used to measure the degree of HRS and possibly ones which would produce a better correlation with SF_2 for all the cell lines studied. Further investigation is needed to find the "optimum" method of measuring the degree of HRS.

Skarsgard and Wouters (1991, 1996) and Wouters *et al.* (1996) used the cell sort protocol to obtain survival curves extending down to low doses. In these papers two variations of the cell sort protocol were described. In the "post sort" protocol, cells were irradiated in suspension culture to a range of doses before sorting into petri dishes which were then stained and assessed after 10–14 days incubation. In the "pre sort" protocol, cells were sorted into aliquots in suspension before irradiation then plated into petri dishes. For DU145 cells, tested using both versions of this protocol, although the survival curves obtained were very similar, the pre sort protocol showed significantly less variability with consistently smaller standard errors (Wouters *et al.* 1996). This may be due to the pre sort protocol allowing a shorter handling time for each aliquot and variations between sorting and irradiation times could be more carefully controlled. The method used in Chapter 3 was a further modification of the pre sort protocol. The HRS response of cells may be affected if cells have to undergo the added stress of

trypsinisation after LDR irradiation, before X-irradiation as in these experiments. Therefore, a modification of the post-sort protocol was used in the experiments described in this chapter. Wouters' results indicate that the post sort protocol gives more variable data. This may explain, to some extent, the variability in these data.

The experiments described in this chapter were carried out to assess the prevalence and degree of HRS/IRR in T98G cells after various LDR "priming" treatments. The results suggest that the inverse dose-rate effect found in Chapter 4, where cell kill is enhanced at very low-dose rates, is due to a lack of induction, or decreased activity of DNA-repair mechanisms. The dose-rate sparing effect, whereby cell kill increases as dose rates decrease, may be caused by an induction or maximum activity of DNA repair. So far these hypotheses are speculative to some degree and further investigations are needed to further examine the role that DNA-repair mechanisms play, or don't play, in the inverse dose-rate effect.

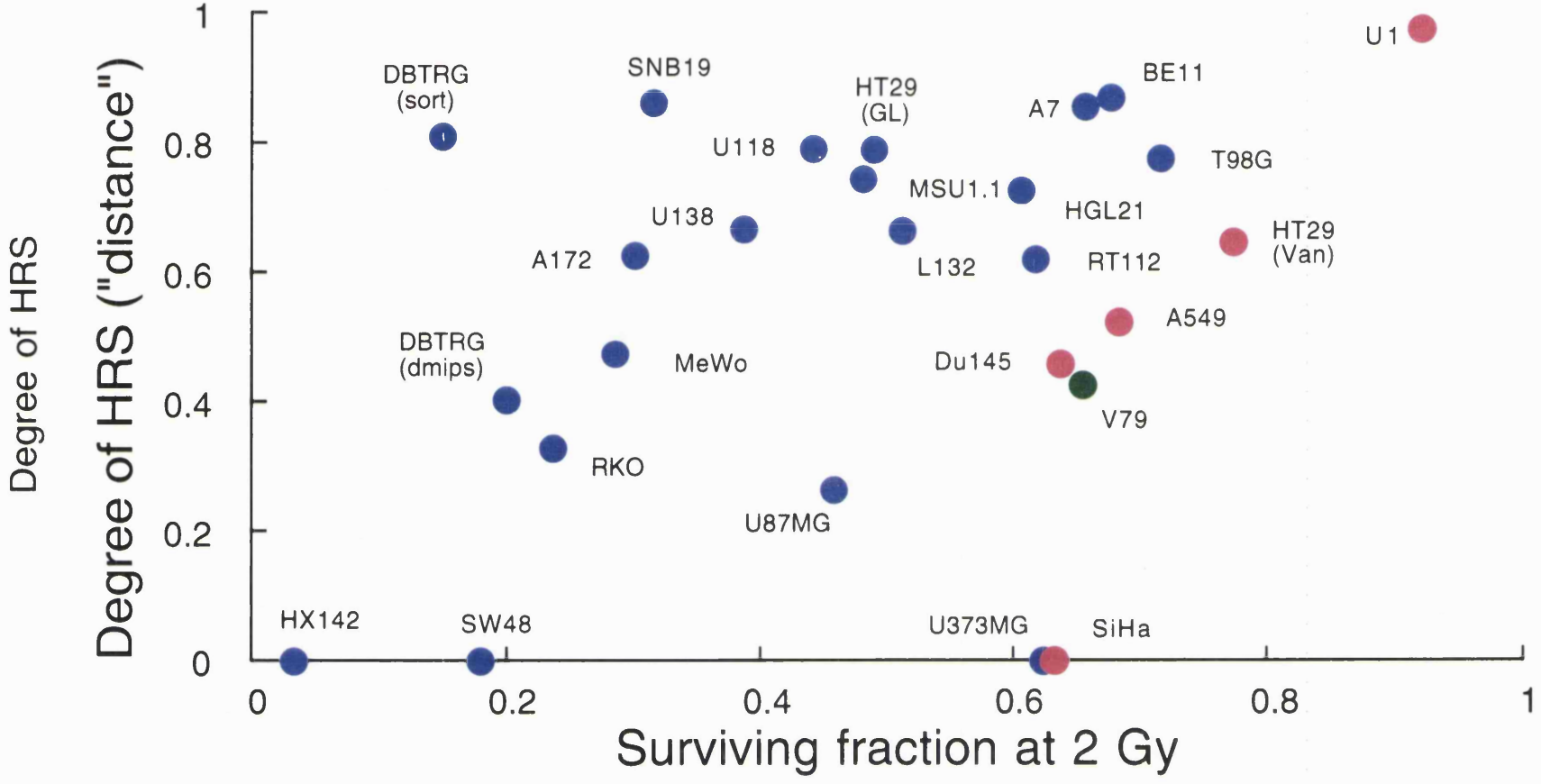

Figure 6.8
Shows the relationship between surviving fraction at 2 Gy (SF_2) and the degree of HRS/IRR measured using the "distance " method (Equation 6.2). Parameters obtained from the IR fit were used in Equation 6.2, where dose = d_C, for a number of cell lines tested for the presence of HRS/IRR in British Columbia Research Centre, Vancouver, Canada and at the Gray Laboratory, UK.

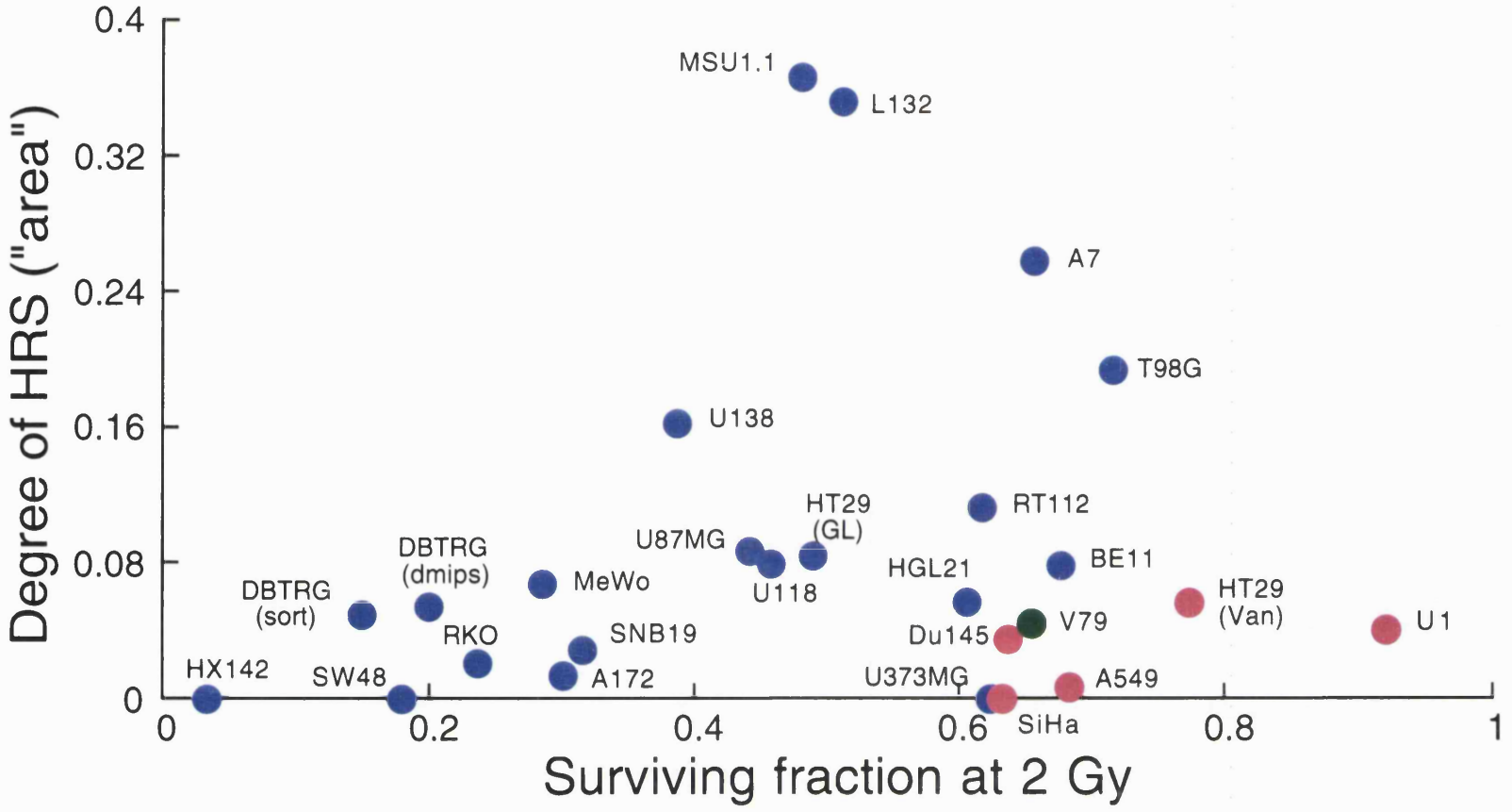

Figure 6.9
Shows the relationship between surviving fraction at 2 Gy (SF_2) and the degree of HRS/IRR measured using the "area" method (Equation 6.3). Parameters obtained from the IR fit were used in Equation 6.3 for a number of cell lines tested for the presence of HRS/IRR in British Columbia Research Centre, Vancouver, Canada and at the Gray Laboratory, UK.

Chapter 7. Cell-cycle characteristics and the effect of radiation on cell-cycle progression

7.1 Aims

The aims of these experiments were to:
(1) investigate the cell-cycle time of the cell lines studied in previous chapters,
(2) investigate the effect of a 2 Gy dose of HDR X-rays on cell-cycle progression for the cell lines studied in the previous chapters.

In this study, 4 cell lines, 3 of which known to be p53 mutant, (the p53 status of A7 is unknown) were analysed to establish background information such as the cell-cycle times and phase durations. They were also tested for the presence of any delays in cell-cycle progression after 2 Gy HDR X-rays. A dose of 2 Gy was chosen to mimic a clinical situation where radiotherapy treatments are generally given in a series of 2 Gy fractions.

7.2 Introduction

Experiments on *Vicia faba* roots by Howard and Pelc (1953), were the first to define two distinct events and four compartments in the reproductive cycle of eukaryotic cells. These were identified as DNA synthesis (S phase), mitosis (M phase) and the periods between these two events, labelled gap phases (G1 and G2). On a bio-molecular level, we now know that the cell cycle consists of a series of highly ordered processes which are primarily controlled by a set of protein complexes formed from protein kinases (Cdks) and cyclins, their activating proteins. Figure 7.1 summarises the key pathways involved in the regulation of the cell cycle in mammalian cells (Harris *et al.* 1998, Mitchell 1999).

Cell-cycle progression is characterised by checkpoints at which the cell ensures that the previous necessary steps have been completed before embarking on subsequent steps (Kaufmann and Paules 1996). In the cell cycle DNA synthesis begins when the cells have reached a certain size (G1/S checkpoint) and chromosome segregation only occurs when DNA synthesis is completed (G2/M checkpoint) (Wuarin and Nurse 1996). Checkpoint failure can lead to cancer, although this is dependent on many factors such as the type of damage the cell sustains and the phase of the cell cycle in which it occurs (Paulovich *et al.* 1997). Elongation of the checkpoints is also important in the response of cells to DNA damage which can be acquired during routine replication or additionally by treatment with DNA damaging agents such as radiation. The cell-cycle arrest resulting from such damage is caused by specific surveillance mechanisms that detect damage and induce inhibitors of key cell-cycle transitions (Szumiel 1998). Such elongation allows DNA integrity to be checked and the initiation of repair or apoptosis

before entry into replication and division phases (Sherr 1996). This inherent protection mechanism is vital in maintaining the integrity of the cell population as it prevents the transmission of DNA lesions which can be fixed in the genome and give rise to mutations in daughter cells.

p53 is a gene product that plays a major role in the control of cell division in response to DNA damaging agents. It is a key component of the DNA damage monitoring and signalling systems which respond to cellular insult (Szumiel 1998) (Somasundaram 2000) (Sionov and Haupt 1999). The p53 protein functions to halt cell-cycle progression in response to DNA damaging agents, such as radiation primarily by the transcription of the $p21^{WAF1/Cip1}$ gene. This protein inhibits the activation of cyclin/cdk complexes by binding directly to them which, in turn, delays the progression of cells through the cycle. Presumably this gives time for the cell to repair DNA damage or to commit itself to death before DNA replication is initiated.

The radiosensitivity of cells varies as they pass through different cell-cycle phases (Sinclair and Morton 1966). Cells generally tend to be more resistant in late S phase and are more sensitive in G2 and M phases. Radiation also affects cell-cycle progression, by inducing delays at the G1/S and G2/M checkpoints. The delays involve the inactivation of the cdk required for progression within or progression to the next cell-cycle stage (Iliakis 1997, Bernhard *et al.* 1995). The regulation of the G1 checkpoint generally requires p53 functionality (Kastan *et al.* 1991, Lee and Bernstein 1993). The p21 protein it activates causes G1 arrest. However, some tumour cell lines containing wild-type p53 do not undergo a G1 arrest in response to radiation, suggesting that factors other than p53 are also involved (Nagasawa *et al.* 1995, Li *et al.* 1995).

The genes and mechanisms underlying radiation-induced cell-cycle delays in S and G2 phase are not so well understood (Iliakis 1997, Schwartz and Rotter 1998). p53 has also been linked to the regulation of the G2/M checkpoint (Stewart *et al.* 1995, Guillouf *et al.* 1995, McKenna *et al.* 1996, Dasika *et al.* 1999). p53 is thought to prolong delay to enable more time for damage repair and it increases the efficiency of DNA repair in G2 (Schwartz and Rotter 1998). However, the major regulator of this checkpoint is $p34^{cdc2}$ kinase which is regulated by Cyclins A and B. Cyclin B complexes are retained in the cytoplasm in response to irradiation, reducing levels in the nucleus and resulting in a delay in progression into mitosis (Bernhard *et al.* 1995, Toyoshima *et al.* 1998).

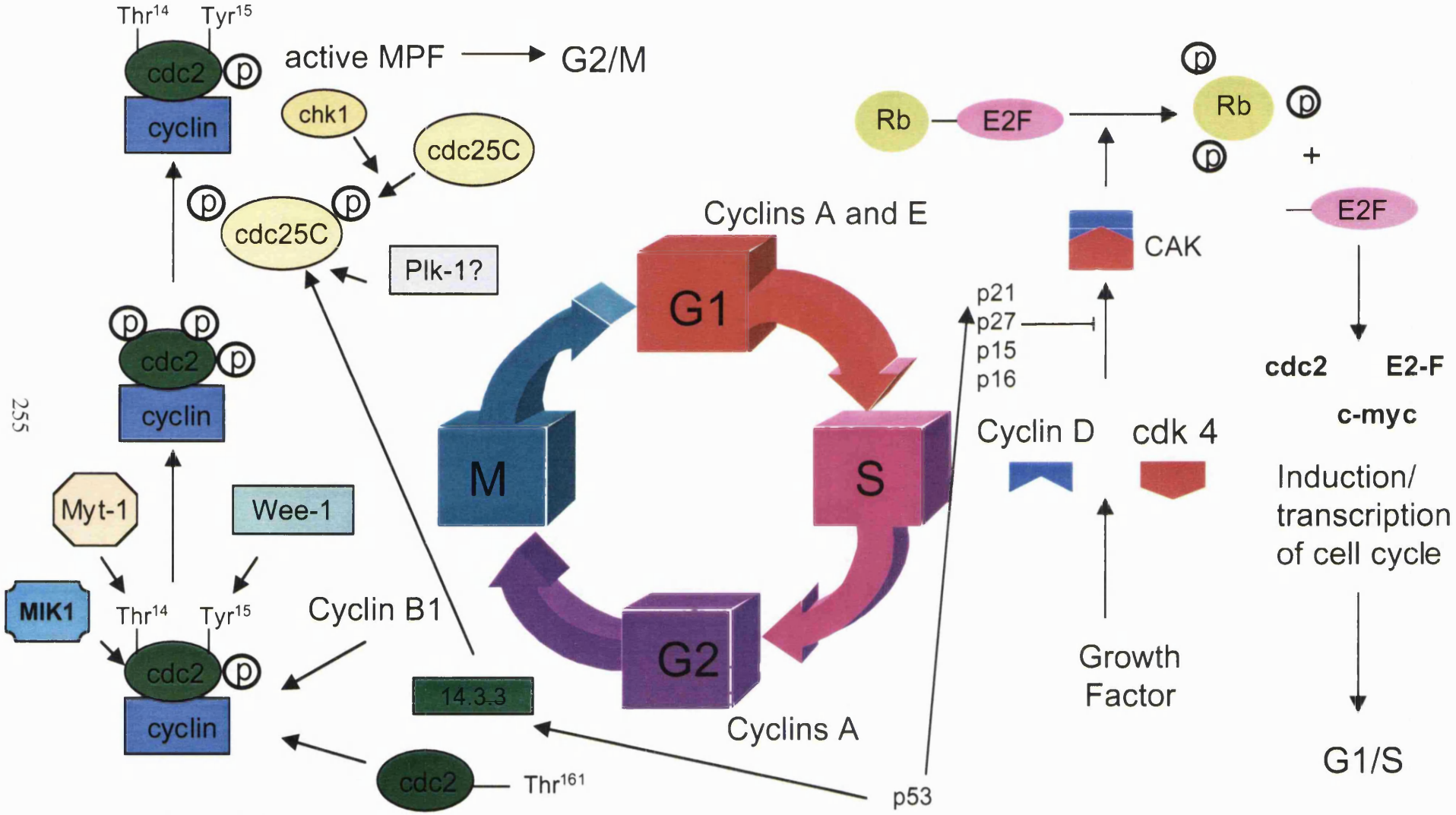

Figure 7.1.
Shows cell-cycle regulation in mammalian cells. The important transitions into both S phase and M phase are controlled primarily through the regulation of cyclin/cdk complex activation (Harris *et al.* 1999) and (Mitchell 1999).

7.3 Materials and methods

The progression of cells through the cell cycle was measured using incorporation of the thymidine analogue BrdUrd during S phase, and PI intercalation into double-stranded nucleic acids. In these experiments asynchronously growing T98G, A7, PC3 and U373MG were pulse labelled with BrdUrd as described in detail in Section 2.7. A separate set of flasks were irradiated with 2 Gy X-rays directly after BrdUrd removal (Section 2.7.2.1) to establish the effects of radiation on cell-cycle progression. Harvested samples were fixed in 70% ethanol and stored in labelled plastic test tubes at 4°C. For analysis, they were stained with FITC-labelled anti-BrdUrd antibody and propidium iodide. The stained specimens were then analysed on the Becton Dickinson FACScan as described in Section 2.7.4.

7.3.1 Data analysis

The following cell-cycle parameters were analysed:
(1) percentage of cells in G1, S and G2/M phases,
(2) duration of G1, S and G2/M phases,
(3) total cell-cycle time,
(4) delays in G1 and G2 phase following treatment with 2 Gy.
Data analysis was generally performed on bivariate dot plots (DNA versus BrdUrd content) with regions set around the various subsets of cells required to calculate the various parameters.

Using a series of plots showing BrdUrd incorporation with DNA content as demonstrated in Figure 7.2, BrdUrd labelled (R1) and unlabelled populations (R2) were distinguished by regions using the Lysys II© software package. At each time interval examined, cells in each of these regions were analysed separately for DNA content, (Figure 7.3A–C). The populations of interest, labelled M1-M5, were defined by eye on a plot of total DNA content (A) and superimposed onto the histograms of the BrdUrd-labelled (B) and unlabelled cells (C) only. These regions acted as analysis windows through which cell-cycle progression of each population was observed. This method was adapted from the cell-cycle analysis procedures reported by Karn (1989) and Higashikubo (1996).

7.3.1.1 Cell-cycle time (T_C)

The duration of the cell cycle, T_C, was calculated from the data generated by following the movement of cells through a narrow window, M4, located in mid-S phase (Figure 7.3). The ratio of BrdUrd-labelled cells to the total number of cells in this window was plotted against time and T_C was estimated as the time interval between the first and second peaks (Figure 7.4). A more accurate method of determining T_C was by the application of a curve fit model. An equation (shown in Appendix 3) was fitted to the

data using the JMP© statistics package and the midpoint of the second peak was calculated. The curve fit model used to fit the data, based on that reported by Watson and Taylor (Watson and Taylor 1977) and adapted by M.C. Joiner (pers. comm.), employed normally distributed mean times for the intermitotic times. This model (see Appendix 3 for formula) required the manual input of reasonable estimations of T_S and T_C in order to optimise the accuracy of fit for each cell line.

7.3.1.2 S-phase duration (T_S)

The length of S phase, T_S was calculated using the relative movement technique described by Begg (1985). The movement of S-phase cells relative to the positions of G1 and G2/M cells (relative movement, RM) was calculated as follows:

$$RM = \frac{F_L - F_{G1}}{F_{G2/M} - F_{G1}}$$

where F_L is the mean red fluorescence for the total G1 (M1) and G2/M (M3) populations respectively (see figure 7.3). At time zero RM=~0.5 as labelled cells were uniformly distributed throughout S phase, midway between the G1 and G2/M populations. RM increased towards 1 up to a time approximately equal to the time in S phase (T_S) as labelled cells progressed into G2. Values for RM were calculated at 4h intervals and were plotted against time. The following equation was then fitted to the linear part of the plot :

$$RM = a(time - S) + 1$$

Where S is T_S and *a* is a constant. T_S could then be calculated.

7.3.1.3 G2/M-phase duration (T_{G2+M})

The duration of G2/M phase, T_{G2+M}, was measured directly from the rate of entry of BrdUrd labelled cells into G1 phase (appearance in M1). At time zero, cells in late S-phase are ready to enter G2/M. The appearance of these cells in G1 relates to the time taken to complete G2/M. All cells appearing in this window have completed mitosis, and divided to form two daughter cells with G1-phase DNA content. This cell division was corrected for by application of the following formula which calculates the labelling index at time zero:

$$\text{Corrected cells in G1} = \frac{0.5 \times G1_{BrdUrd}}{Total_{BrdUrd} - 0.5 \times G1_{BrdUrd}}$$

where $G1_{BrdUrd}$ is the number of BrdUrd labelled cells in G1. These corrected values for the % BrdUrd labelled cells in G1 were plotted against time and followed a sigmoidal trend. The linear portion of the curve (between 2 and 8 hours) was fitted to the following equation:

$$\% \text{ BrdUrd labelled cells in G1} = a(\text{time} - G)$$

Where G is T_{G2+M} and *a* is a constant. Therefore a value of T_{G2+M} could be calculated.

7.3.1.4 G0/G1-phase duration (T_{G1})

The duration of G0/G1, (T_{G1}) cannot be calculated directly from the data collected using the BrdUrd method of cell-cycle analysis. However, an estimate can be obtained by subtraction of the sum of the calculated phase times from the cell-cycle time, *i.e.*,

$$T_{G0/G1} = T_C - (T_S + T_{G2/M})$$

7.3.1.5 G1 delay

G1 delay was assessed by analysing the movement of G1 cells into an early S-phase window (Figure 7.3, M5) expressed as a proportion of the total unlabelled population. This shows any delay of cells moving into or out of early S phase. The percentage of cells in early S was plotted against time for 0 Gy and 2 Gy so any G1 delays could be visualised (Figure 7.5). This can be quantified by estimating the area under the curves over the course of the cell-cycle duration (T_C), for irradiated and unirradiated cells and dividing the area at 0 Gy by the 2 Gy area.

7.3.1.6 G2 delay

The entry of BrdUrd-labelled cells into G1 was used to calculate a G2 delay of S-phase cells. This indicates a delay of S-phase cells entering G2/M phase or a delay of G2/M-phase cells entering G1 (Figure 7.6). The extent of G2/M delay of BrdUrd-labelled cells was determined from the shift in the inflection points of the best fit curves representing unirradiated controls and irradiated samples.

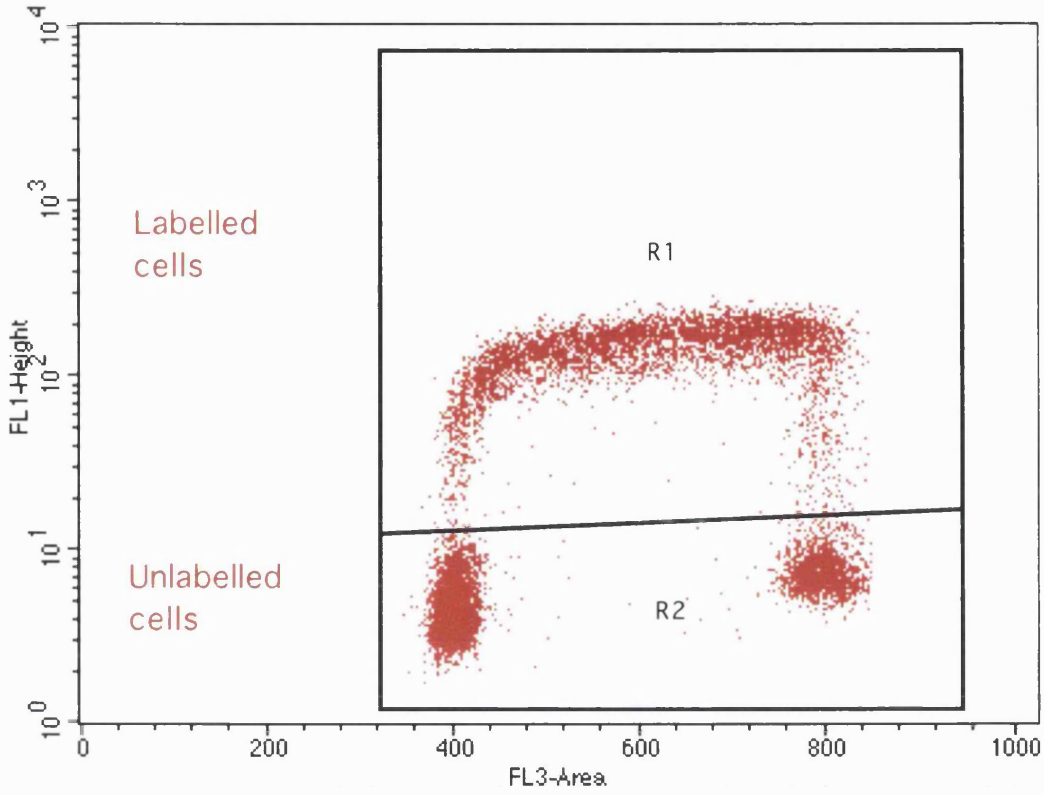

Figure 7.2
Cell-cycle analysis using BrdUrd and flow cytometry. The dot plot represents stained nuclei from human fibroblast cells harvested immediately after incubation with BrdUrd for 20 min. G1-phase cells have a 2N DNA content and no BrdUrd incorporation, whereas G2 and M-phase cells have a 4N DNA content and no BrdUrd incorporation. S-phase cells have a DNA content ranging between 2N and 4N, depending on the degree of completion of DNA synthesis and show a characteristic 'horseshoe profile'. BrdUrd incorporation is represented by the FL1 emission signal on the y-axis. DNA content is measured using the PI emission, plotted on the x-axis. Regions outlining the populations of interest are generated using the Lysys II© software (Becton Dickinson). BrdUrd-labelled cells are highlighted by R1 and unlabelled cells by R2.

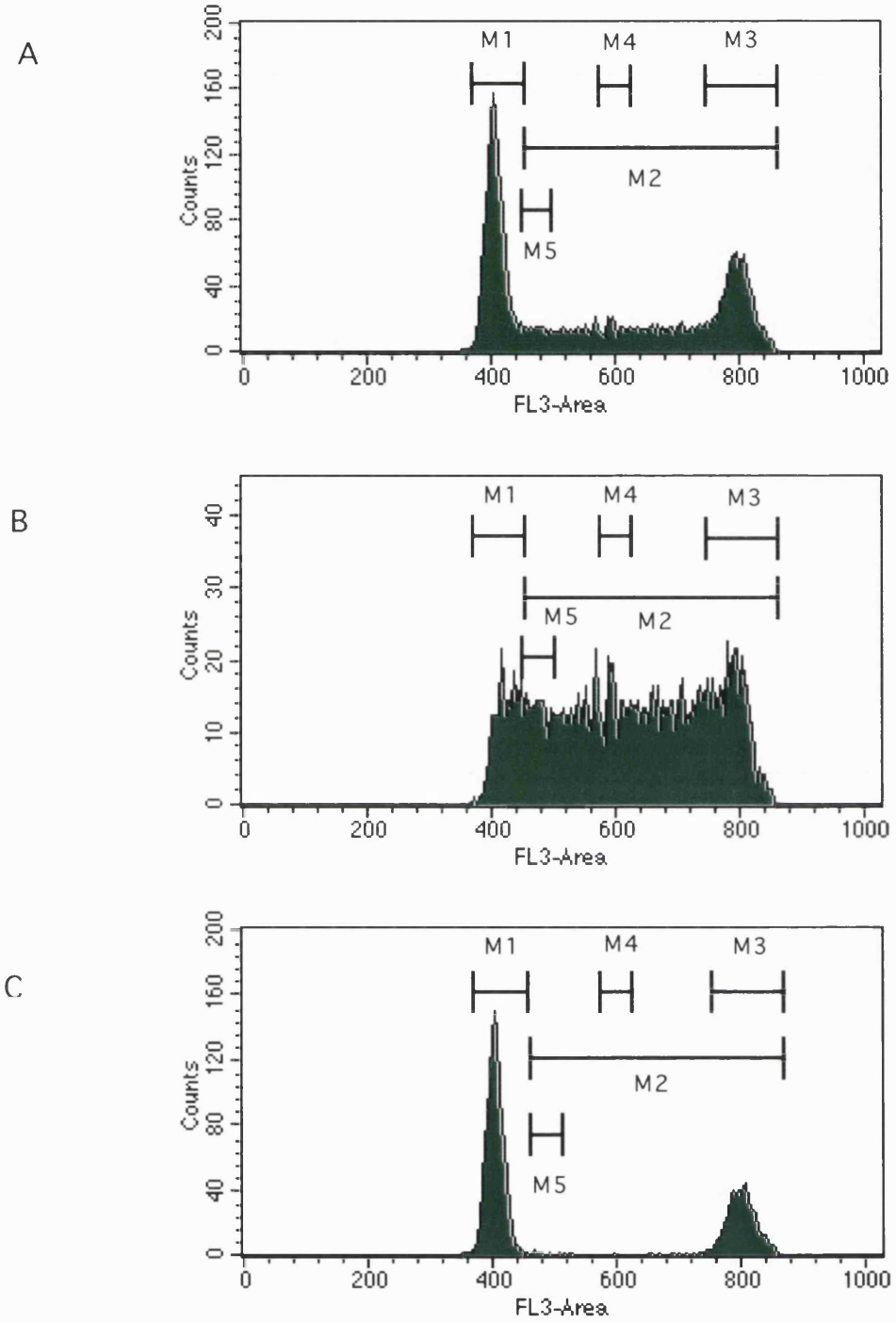

Figure 7.3
Shows cell-cycle phase length and cycle delay analysis of human fibroblast cells. Panel A shows the total cell population, and the markers (M1-M5) are initially defined on this plot. These are then overlaid onto individual plots of BrdUrd labelled (panel B) and unlabelled cells (panel C) only (from R1 and R2 respectively, Figure 7.2). Markers key is as follows: M1=G0/G1 cells, M2=G2/M and S-phase cells (for relative movement analysis), M3=G2/M cells, M4=mid S cells and M5=early S cells

7.4 Results.

Table 7.1 shows the results of BrdUrd staining and analysis for T98G, A7, PC3 and U373MG cell lines. The cell-cycle time is shown as well as the length of each individual phase, the length of any cell-cycle delays and the p53 status of the cell lines. Figures 7.4 to 7.6 show examples of the graphs used to calculate these values for asynchronously growing T98G cells. The results with and without irradiation are shown on the same plot for comparison. The cell-cycle time (T_C) for asynchronously growing T98G in these experiments was found to be 23.3±0.84 hours. This was slightly lower than the value of the population doubling time reported in the original paper describing the T98G clone (Stein 1979), of 26±2 hours, although the fact that the doubling time is longer than T_C may reflect some intrinsic cell death. The 3 other cell lines used in this study, A7, PC3 and U373MG showed slightly longer cell-cycle times of 25.8±0.5, 28.2±1.2 and 27.9±6.6 respectively. There is no published data concerning the cell-cycle times of these cell lines. All cell lines appeared to show the same amount of unlabelled cells in early S phase over the course of their cell-cycle time, whether irradiated with 0 or 2 Gy , suggesting that no G1 delays were present. G2 delays were observed after 2 Gy in all cell lines. This occurred to the greatest extent in U373MG which showed a G2 delay of 3.8±0.8 hours. The other cell lines, T98G, A7 and PC3 had shorter G2 delays of 2.9±0.7, 1.29±0.33 and 3.1±0.7 respectively.

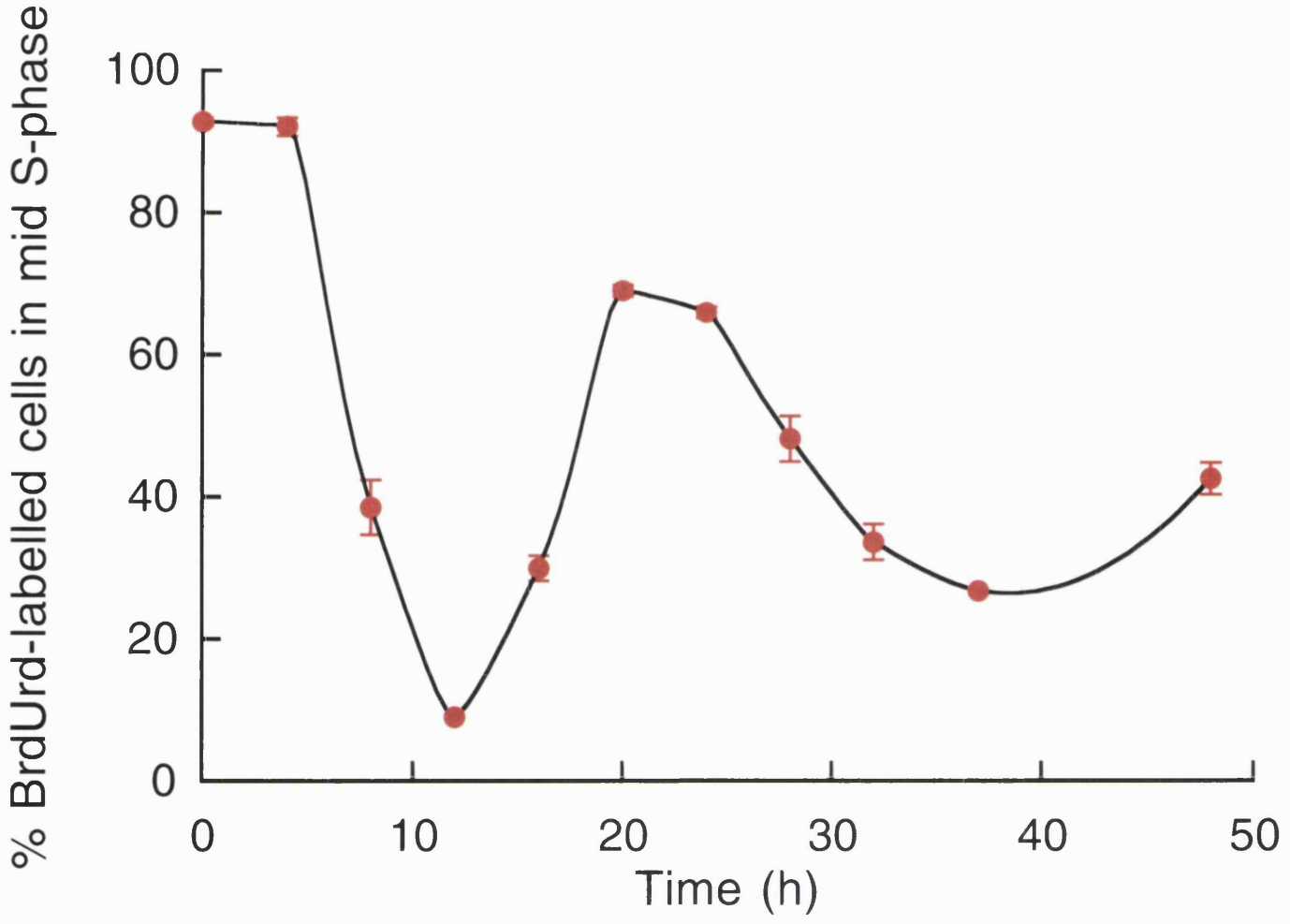

Figure 7.4
Shows the results of BrdUrd pulse-labelling experiments to measure cell-cycle time in asynchronously growing T98G cells
Points represent the mean ± SEM of three replicates from one experiment.

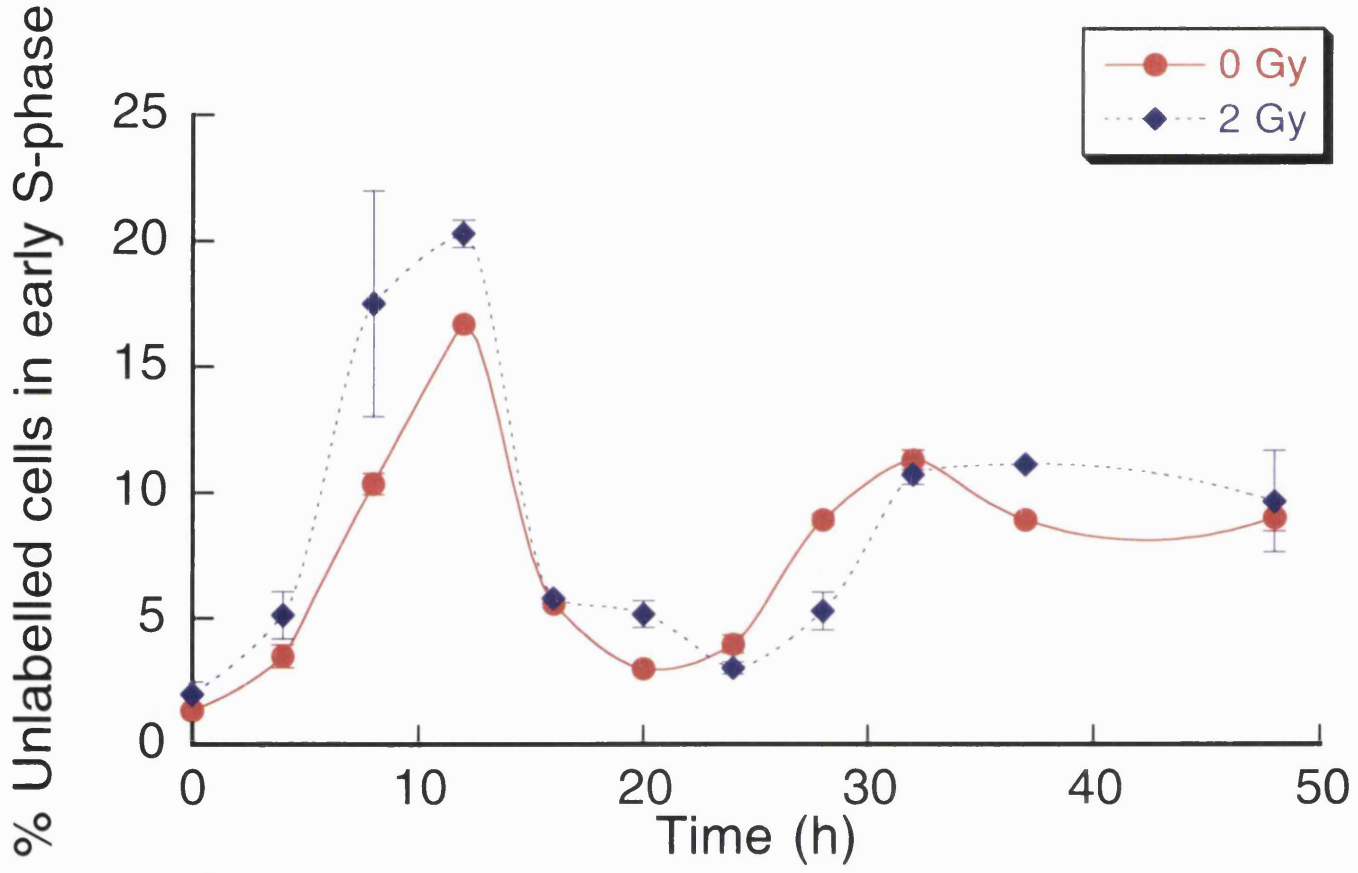

Figure 7.5
Shows the results of a BrdUrd pulse-labelling experiment using T98G cells. The percent unlabelled T98G cells in early S-phase is shown for unirradiated cells (red symbols) and 2 Gy irradiated cells (blue symbols) at times 0–48 hours after irradiation. The increase in unlabelled cells with time is a measure of progression through G1 phase. These data indicate that irradiation with 2 Gy does not result in a delay in progression through G1 phase in T98G cells. Points plotted represent the mean ± SEM of three replicates from one experiment.

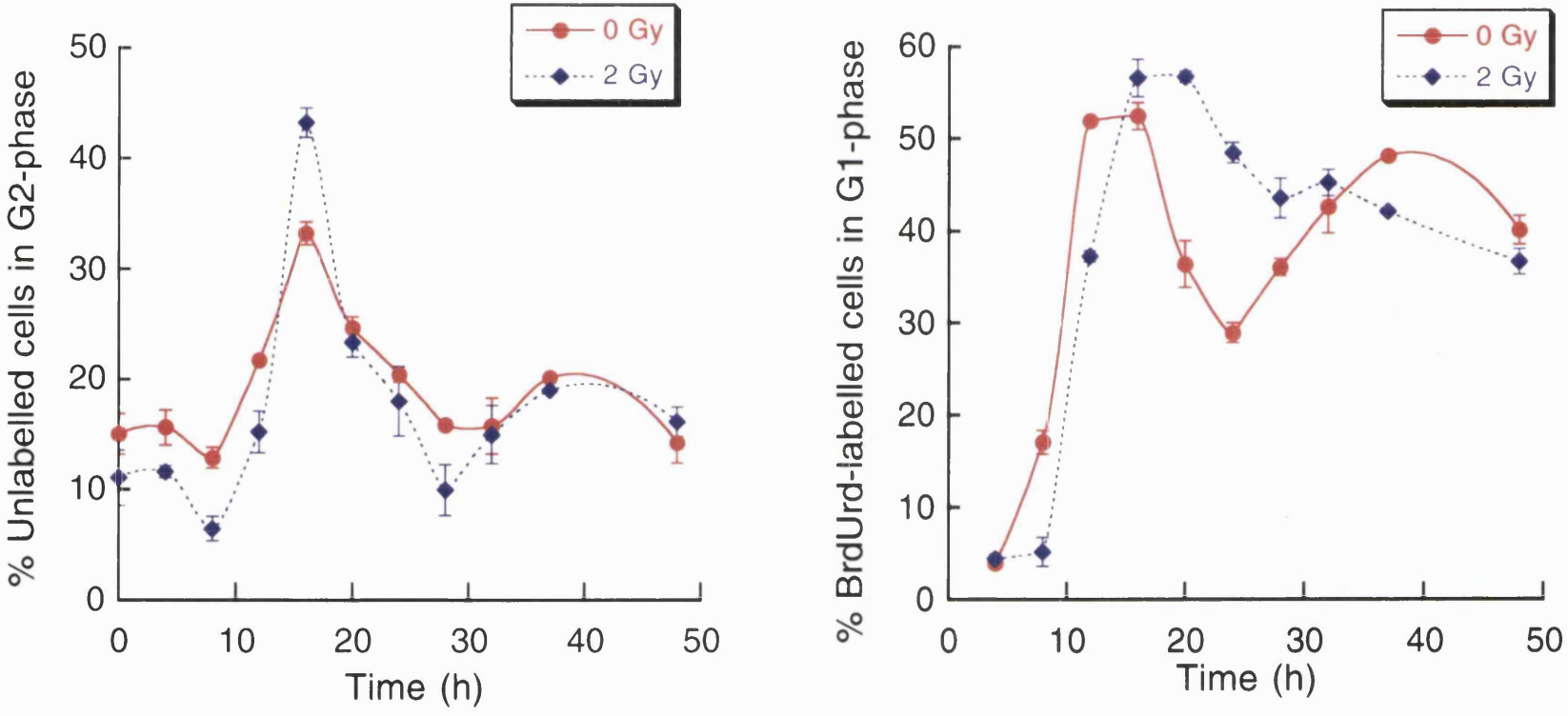

Figure 7.6
Shows the results of BrdUrd pulse-labelling experiments to assess the effect of 2 Gy irradiation on progression of T98G cells through G2 phase. This was assessed by measuring the percent unlabelled cells in G2-phase and the percent BrdUrd labelled cells in G1 phase with time (hours) after BrdUrd labelling. These data indicate that irradiation with 2 Gy produces a G2 delay in T98G cells of approximately 3 hours. Points plotted represent the mean ± SEM of three replicates from one experiment.

Cell line	Cell-cycle time (T_C)	Duration of Phases (h)			Delays after 2 Gy HDR X-rays		p53 status
		G1/G0 ($T_{G1/G0}$)	S (T_S)	G2/M ($T_{G2/M}$)	G1*	G2 (h)	
Asyn T98G	23.3±0.8	7.3	12.8±0.75	3.2±0.7	0	2.9±0.7	Mutant
A7	25.8±0.5	5.1	13.0±0.75	7.7±0.1	0	1.3±0.3	unknown
PC3	28.2±1.2	9.3	14.2±1.3	4.7±0.2	0	3.1±0.7	Mutant
U373MG	27.9±6.6	8.8	15.9±2.1	3.2±0.4	0	3.8±0.8	Mutant

*G1 delay occurring over the duration of T_C as measured by unlabelled cells in early S

Table 7.1
Shows the individual cell-cycle phase times in hours for T98G, A7, PC3 and U373MG cells as assessed by BrdUrd experiments. Plots of T98G distributions are shown in Figures 7.4 to 7.6. Data for each cell line is shown as the mean ± SEM of three replicates from one experiment. The G1-delay data is derived as described in Section 7.3.1.5.

7.5 Discussion

In order to further elucidate the characteristics of the cell lines used for LDR studies, the pre-irradiation cell-cycle phase lengths and cell-cycle delays in G0/G1 and G2/M phase after treatment with 2 Gy X-rays were examined in the 4 cell lines studied in this thesis. A dose of 2 Gy was chosen as it is both clinically relevant and is of sufficient magnitude to induce checkpoint delays. Cell-cycle progression was analysed using simultaneous analysis of BrdUrd incorporation and PI staining.

The value obtained for the cell-cycle time of asynchronously growing T98G, 23.3±0.84 h (Table 7.1), is significantly lower than the published value for the "generation" time, of approximately 26±2 h (SEM) (Stein 1979). However, the T_C is generally shorter than the cell doubling time in most cultures as all cells may not be in cycle or a small proportion die each division. This discrepancy may also be due to a measurement factors. In 1979, when this paper was published, the techniques for measuring cell-cycle time were not so advanced as they are now. Stein used tritiated thymidine and autoradiography to measured DNA synthesis over time. The techniques used today, *i.e.* BrdUrd incorporation and the use of flow cytometry, have increased the accuracy and specificity of the measurements. When these factors are taken into account, the 2–3 h difference in cell-cycle time measured is understandable. There is no published data on the cell-cycle times of the other 3 cell lines A7, PC3 and U373MG. PC3 had the longest cell-cycle time of the 4 cells lines studied, at 28.2±1.22 h. This cell line was derived from a prostate carcinoma and seemed to reflect the *in vivo* property of prostate tumours to generally be slow growing. This is traditionally why LDR treatments are given to prostate tumours as cell kill will not be overcome by proliferation.

The regulation of the G1 checkpoint requires p53 functionality (Kastan *et al.* 1991, Lee and Bernstein 1993, Hartwell and Kastan 1994). These cell lines showed no G1 delay in these experiments which was consistent with their mutant p53 status in 3 of the cell lines. The results for A7 suggest that this cell line is p53 mutant, although p53 *independent* G1 arrest has been documented in some cell lines, for example via MAP kinase induction of WAF1 (Carter *et al.* 1998, Russo *et al.* 1995). p53 is thought to be less important in controlling the G2 checkpoint after irradiation, and all these cell lines did show a G2/M delay in response to 2 Gy of radiation. The G2 checkpoint has multiple factors influencing its regulation (see Figure 7.1). Cell-cycle progression in T98G cells has also been studied after 0.4 Gy of ionising radiation and a G2/M delay of a similar magnitude was observed (Short 1999). This dose was the optimum for the presence of HRS in this cell line. HRS does not occur at 2 Gy, however the size of the delay was similar. This would further suggest that HRS is not mechanistically linked to changes in cell-cycle progression. In this study the HRS negative cell line, U373MG,

did not show marked differences in cell-cycle time or G2/M delays in comparison with the 3 HRS positive cell lines, also suggesting the lack of a relationship between HRS and cell-cycle progression.

Chapter 8. Final discussion

8.1 Low dose-rate irradiation and cell survival

8.1.1 Introduction

Since the first reported used of brachytherapy in the early 1900s, considerable research has been directed at optimising this treatment. This has resulted in better treatment planning and dosimetry and increased ease and accuracy in implantation of brachytherapy sources through advances in imaging techniques such as CT and MRI. These improvements have led to more dose with a homogenous distribution being delivered to the tumour with improved sparing of the surrounding tissues.

Advances in the type of radioisotope used in brachytherapy treatments have also been made. Isotopes such as radium are no longer in routine use, and have been replaced by ^{125}I and ^{103}Pd which are safer as they allow less harmful exposures to operators. However, there is still controversy about the optimal dose *rate* used in brachytherapy. High-dose rates give high-tumour cell kill, but also tend to damage normal cells. Lower dose rates spare normal tissues but may not provide sufficient tumour cell kill. The therapeutic gain of both treatments must be analysed so that a correct balance can be achieved between tumour and normal tissue damage and an optimal treatment regime can be given.

In 1979 Mitchell *et al.* (1979) discovered an inverse dose-rate effect on cell survival *in vitro* in a human tumour cell line, HeLa, whereby an increase in cell kill was observed as the dose rate was decreased. This effect, if present in tumour cells *in vivo*, could be potentially exploited in the clinic to increase overall therapeutic gain using LDR brachytherapy. This inverse dose-rate effect may be mechanistically linked to low-dose HRS seen at low-acute doses. The main aims of this thesis were to investigate this inverse dose-rate effect, the dose rate over which it occurs, the implication of cell-cycle position and whether it was linked to HRS observed at acute doses. This work could help elucidate whether LDR brachytherapy exposures could potentially have a higher therapeutic gain than HDR treatments due to an inverse dose-rate effect.

8.1.2 The survival of cells after low dose-rate irradiation

In this study two methods were used to examine survival in human tumour cells after low dose-rate exposures. The first method, irradiating cells with ^{60}Co γ-rays found an increase in cell kill when the dose rate was reduced from $100 cGy h^{-1}$ down to $2 cGy h^{-1}$ in 3 HRS positive (at acute doses) cell lines. In contrast no difference in cell kill was observed at lower dose rates in a HRS negative cell line (Chapter 4). The second method using ^{125}I brachytherapy seeds, produced a slight inverse dose-rate response in a HRS positive cell line although this was not significant in the dose-rate range studied (Chapter 5).

8.1.3 Comparison between irradiation methods

At face value, results from experiments carried out using the two methods would suggest that an inverse dose-rate effect is observed when cells are exposed to ^{60}Co but not to ^{125}I. Both radioisotopes produce γ-rays, which are responsible for the radiation damage and are both low LET radiation. This however is unlikely to account for the differences in cell survival between the two treatments. It is far more likely that this variation in response is caused by a physical difference in irradiation conditions rather than a biological response to a different radioisotope.

The most accurate assessment of dose rate and total dose received by the cells was made using the ^{60}Co-water tank method rather than the ^{125}I seed irradiator. The water tank dosimetry was carried out using two methods (ionisation chamber and Fricke dosimetry) and a γ-ray beam width of 40cm produced a uniform distribution of dose across the flasks. Using the water tank allowed large numbers of cells to be irradiated simultaneously and experiments at the same dose rate could be repeated by adjustment of the flask distance from the source to allow for decay of ^{60}Co. Due to the long half life of the ^{60}Co (63.24 months), the dose rates given to cells during exposure time was much more stable and the exact dose received by the cells was easier to determine than with the ^{125}I irradiator system. The ^{125}I irradiator method gave a less homogenous distribution of exposure and, although flasks were rotated in an attempt to avoid hot spots, this was not sufficient to give a uniform distribution and some cells would have received up to 20% more dose than others. The dose rates given to cells during irradiation time using the ^{125}I irradiator were subject to decay due to the shorter half-life of ^{125}I (59.6 days). Each dose rate could only be examined once and a limited number of cells could be irradiated due to the small size of the petri dishes used. The seed irradiator, however, is advantageous over the ^{60}Co system from a clinical perspective. The type of isotope used and the changes in dose rate during exposure time would more closely mimic a clinical situation where ^{125}I brachytherapy seeds are used. However, on the whole, the ^{60}Co water tank set-up gave more consistent results with a smaller standard error. This would suggest that the results obtained using this method give a better reflection of the real biological responses to low dose-rate irradiation. In the ^{125}I irradiator system where the results are more variable with larger standard errors, it is possible that any biological responses to ^{125}I, such as an inverse dose-rate effect, may have been masked due to poor irradiation conditions.

8.1.4 Comparison with published data

The inverse dose-rate effect was reported by DeWeese *et al.* (1998), where increased cell kill was observed with LDR compared with a fractionated HDR treatment in a number of prostate carcinoma cell lines. One of these, PC3, was included in the present study and the results of LDR ^{60}Co γ-ray exposure are shown in Chapter 4. DeWeese *et al.* (1998) studied the effects of ^{137}Cs γ-rays at a low-dose rate of 25cGy h^{-1} and a high-dose rate of

60 Gy h^{-1} on the survival of PC3 cells *in vitro*. The results described in Chapter 4 show that PC3 cells irradiated at HDR have a more radiosensitive response than the published data with the HDR SF_2 being 0.54 (Figure 4.13) compared with 0.71. However there are differences in irradiation conditions. ^{60}Co γ-rays have an energy of 2 MeV compared with 662 KeV for ^{137}Cs γ-rays which makes the ^{137}Cs γ-rays a slightly higher LET radiation. More damage would therefore be expected to occur after the high-LET exposure, but in this case the SF_2 is higher with the higher LET. The difference in radiosensitivity is therefore unlikely to be due to differences in LET. The HDRs used are also different with the PC3 cells irradiated at 60 Gy h^{-1} in the DeWeese *et al* (1998) study compared with the present experiments where cells were irradiated at 31 Gy h^{-1}. These dose rates are so high that it is unlikely that a dose-rate sparing response would occur, and even if such a response was present, the PC3 cells irradiated at 60 Gy h^{-1} (DeWeese *et al.* 1998) should show a more sensitive response, which is not the case.

At LDR there also seems to be differences in the radiosensitivity, but, conversely, in this case the PC3 cells used in the DeWeese study show a more sensitive response. When the surviving fractions at 18 Gy at dose rates of 25 cGy h^{-1} (DeWeese *et al.* 1998) and 30 cGy h^{-1} (the present study) are compared, the cell kill is greatest in the DeWeese study with an SF of 0.052 compared with 0.0142 (Figure 4.14). It would seem unlikely that a difference of 5 cGy h^{-1} in dose rate would result in such an extreme inverse dose-rate effect, especially as a lower dose rate of 10 cGy h^{-1} in the present study gives a higher SF of 0.0395 at the same dose (Figure 4.14). There is no mention in the DeWeese study that a correction for proliferation during irradiation was made. The cell-cycle time of PC3 cells is 28.2 h (Chapter 7). To give a dose of 18 Gy at 25 cGy h^{-1} an irradiation time of 72 h would be needed. Therefore PC3 cells would have potentially gone through two divisions during the irradiation time and so it is difficult to determine how much damage will have be done to each individual cell to have an effect on the overall surviving fraction. From Chapter 4 it is observed that considering the surviving fraction alone without taking into account the relative yield results in a more resistant radiation response than when proliferation is factored into the survival curve. This would suggest the PC3 cells used in the DeWeese study would have shown a more sensitive response had they considered cellular proliferation. However, it is interesting to note that when the DeWeese SF data is compared with the relative clonogens data in the present study (*i.e.* the SF data with proliferation factored in), the survival at 18 Gy for the two dose rates is very similar, that is 0.0052 (DeWeese study) compared with 0.0059 (present study (Figure 4.13)).

The effect of proliferation on survival seems also to have been omitted from other low dose-rate studies. Experiments carried out by Bedford and Hall (Bedford 1963) (Hall 1964) to examine the effects of using radium and ^{60}Co γ-rays at low dose rates on cell survival, found dose-rate sparing with dose rates ranging from 6000 to 60 cGy h^{-1} in HeLa

cells. At dose rates below this (the lowest studied by Bedford and Hall was 2.37cGyh^{-1}), there still seemed to be a sparing effect, although at these dose rates, cells will be proliferating during irradiation and they did not correct for this. This is comparable with the results obtained in the present study for the surviving fraction acquired at low-dose rates. Figure 4.5 (lower panel) shows the surviving fraction obtained for the cell line T98G. This graph shows that there is no significant inverse dose-rate effect for either 2 or 5cGyh^{-1} compared with the higher dose rates. It is only when proliferation is taken into account that the effect is apparent. This is also true for A7 and PC3 cell lines. More recent studies investigating the effect of LDR irradiation on cell survival have shown an inverse dose-rate effect on cell survival, but these have also not taken cellular proliferation into account. The effect detected may have been larger if this had been the case. Examples include the cervical carcinoma cell line NHIK3025 (Furre *et al.* 1999), human glioblastoma cell lines U251, U87MG (Marin *et al.* 1991) and U251 (Williams *et al.* 1998) and prostate carcinoma cell lines PC3 (described above), PPC-1 and TSU-Pr1 (DeWeese *et al.* 1998).

In an attempt to counteract the problems associated with proliferation during irradiation, Mitchell (1979b) carried out experiments using plateau-phase cultures of HeLa and V79 cells. Previous experiments by the same author have shown that an inverse dose-rate effect was not observed in asynchronous V79 cells (Mitchell 1979, Mitchell *et al.* 1979a) where a dose rate of 154cGyh^{-1} gave approximately 10 times more cell kill than 55cGyh^{-1} after 20Gy. Plateau phase cells were obtained by growing to confluence. However, cell cycling was still observed albeit at a slower rate with an increase in cell-cycle time from 9h to 52h. Under these conditions V79 cells showed an inverse dose-rate effect with a dose rate of 55cGyh^{-1} giving twice as much cell kill than 154cGyh^{-1}. This effect may have not been apparent in asynchronous cultures as the cell-cycle time was so short that, during low dose-rate treatments, not enough damage was done in one cell cycle to prevent proliferation. Therefore a high amount of proliferation may have masked any inverse dose-rate effect present. When the cell-cycle time was increased, there was a greater opportunity for damage accumulation and because there was much less proliferation, it was easier to assess damage to individual cells. Conversely, an inverse dose-rate effect was present in exponential cultures of HeLa cells (Mitchell *et al.* 1979b). A LDR of 55cGyh^{-1} gave approximately 10 times the cell kill at 25Gy than a HDR of 154cGyh^{-1}. When these cells were grown to confluence the cell-cycle time had increased from 25h to 66h. An inverse dose-rate effect was not apparent in HeLa cells when the cell-cycle time was increased as 154cGyh^{-1} gave the same magnitude of cell kill as 55cGyh^{-1}. This may be comparable with the results from confluence experiments on T98G cells in the present study (Chapter 4) where the proposed "flip-over" from dose-rate sparing to the inverse dose-rate effect occurs at much lower dose rates than in asynchronous cultures (below 30cGyh^{-1}). It would be interesting to examine the survival at dose rates below 55cGyh^{-1} for HeLa cells

to see whether an inverse dose-rate effect could be detected as occurred below 30cGyh^{-1} in the present study.

8.2 Homology between HRS/IRR and the inverse dose-rate effect

At the present time there is not sufficient evidence to categorically state that the inverse dose-rate effect and HRS/IRR are mechanistically related. Nevertheless, there is strong circumstantial evidence from the present study that this is the case.

8.2.1 Prevalence of both responses

Of the cell lines studied at acute and low-dose rates, three which did show HRS/IRR (T98G, A7 and PC3) also showed an inverse dose-rate effect and one which did not show a hypersensitive response at low-acute doses (U373MG) did not show an inverse dose-rate effect. There also seems to be a correlation between the presence of HRS and the inverse dose-rate effect in cell lines reported in the literature. V79 cells, for example, are known to exhibit HRS/IRR (Marples and Joiner 1993) and have been shown to exhibit an inverse dose-rate effect in plateau-phase cultures (Mitchell *et al.* 1979b). The glioblastoma cell line U87MG showed HRS/IRR (Short *et al.* 1999b) and a slight inverse dose-rate effect when uncorrected for proliferation (Marin *et al.* 1991). This was also seen in the prostate cell line, PC3, tested at acute doses and at low-dose rates in the present study. A further study also found an inverse dose-rate effect in this cell line (DeWeese *et al.* 1998). Conversely there are examples of cell lines which do show HRS/IRR, but not an inverse dose-rate effect. Examples include, the prostate cell lines LNCaP and DU145 which showed HRS/IRR in the present study and which, in the case of DU145, has been confirmed in other studies (Wouters *et al.* 1996). Experiments by DeWeese *et al.* (1998) did not reveal an inverse dose-rate effect, but, as mentioned before, proliferation was not corrected for in this study, so any effect may have been masked. Deacon *et al.* (1984) studied the effect of LDR irradiation on RT112 cells, a cell line which is known to display HRS/IRR (Lambin *et al.* 1994). They found a dose-rate sparing response, although their "low" dose rate was as high as 96cGyh^{-1}, which is at the top end of the range where an inverse dose-rate effect was observed in the present study. It is not possible to determine whether the slight inverse dose-rate effect observed in HeLa cells in the original experiments by Mitchell *et al.* (1979) was related to HRS/IRR as the presence of HRS/IRR in HeLa cells has not been determined as yet.

8.2.2 Cell-cycle effects

Both the inverse dose-rate effect and HRS/IRR appear to occur independently of variations in the cell-cycle phases, which further implies a homology between the two responses.

8.2.2.1 HRS/IRR

As described in Section 1.5.2, HRS/IRR can be observed in serum deprived (Short *et al.* 1999a), or synchronised cultures (Marples and Joiner 1993) and in individual phases of the cell cycle (M. C. Joiner pers. comm.). Calculations made on the sensitivity of cells throughout the cell cycle could only account for a 2–3 fold increase in radiosensitivity in the low-dose region, whereas the sensitivity observed for cell lines such as HT29 was as much as a factor of 81 (Lambin *et al.* 1996). All these findings suggest against a sensitive subpopulation of cells causing HRS/IRR. In this thesis HRS/IRR was observed in confluent cultures (Chapter 3).

8.2.2.2 Inverse dose-rate effect

In the present study an inverse dose-rate effect can be seen at dose rates below $60 cGy h^{-1}$. At dose rates below $10 cGy h^{-1}$ there does not appear to be a premitotic accumulation leading to increased sensitivity, which was the original hypothesis for this effect (Mitchell 1979). Furthermore, a cell line which did not show an inverse dose-rate effect (U373MG) showed a cell-cycle distribution before and after irradiation, similar to other cell lines where this effect could be detected. The effect is also apparent in confluent cultures where cell cycling is at a minimum. Other authors have rejected cell cycle as an explanation for the inverse dose-rate effect (DeWeese *et al.* 1998, DeWeese *et al.* 1997) as the sensitivity of cell lines which showed the effect was not correlated with cell-cycle redistribution phenotype or with the presence or absence of p53, a gene known to be involved in the regulation of the cell cycle.

In 1996, Brenner *et al.* introduced the linear quadratic and resensitisation (LQR) model to explain the inverse dose-rate effect on survival and mutagenesis at low-LET radiations (Brenner *et al.* 1996). This theory was based on a correlation between amounts of cell kill and mutagenesis and different phases of the cell cycle. They gave a simplified example that the cell cycle is split into two phases, one of which is resistant to radiation and another which is sensitive. If a single dose of radiation is given, cells will be killed off in both phases of the cell cycle, but a greater percentage will be killed in the sensitive phase. The surviving fraction will be an average of the cell kill in both phases. If the dose is split into two equal fractions, the first dose will kill more cells in the sensitive phase, but then cells in the resistant phase will move into the sensitive phase and the second dose will kill cells in this phase resulting in a lower surviving fraction than a single dose alone. Brenner *et al.* (1996) suggests that a dose of radiation given at low-dose rate can be considered as a large number of very small fractions and, during irradiation time, the cells are constantly cycling and are moving out of resistant into sensitive phases. This results in more cell kill than at acute doses, *i.e.* an inverse dose-rate effect occurs. Experiments described in this thesis show that asynchronously growing T98G cells irradiated at $100 cGy h^{-1}$ to a total dose of 5 Gy give a relative clonogen value of 0.572. Using the cellular resensitisation model in a

scenario where no cells are killed in the resistant phase, to result in a mean relative clonogen value of 0.572, the fraction of cells surviving in the sensitive phase is 0.144. However, by giving 5Gy in 2 fractions and allowing cells to resensitise through cell-cycle progression would produce a mean value for relative clonogens of 0.379. From experiments when asynchronous T98G cells are irradiated at $2cGyh^{-1}$ to 5Gy, the fraction of relative clonogens surviving is 0.0673, which is substantially lower than the 0.379 predicted from the LQR model (Brenner *et al.* 1996). This Brenner study did not examine the situation where a radiation dose was given in a greater number of fractions or at a low-dose rate. Using the LQR model, radiosensitivity is not increased further by increasing the fraction number above two or lowering the dose rate. Therefore the inverse dose-rate effect observed in asynchronous T98G in this thesis cannot be primarily due to the cellular resensitisation described by Brenner *et al.* (1996). It seems more likely to be due to an effect other than cell cycle, possibly related to HRS/IRR.

8.3 Possible mechanisms of HRS/IRR and the inverse dose-rate effect

8.3.1 Evidence for a threshold for the triggering of IRR

From experiments described in this thesis, there may be evidence for a threshold level for the "switching on" of a repair response at low-dose rates of irradiation leading to an increased survival of cells. This is analogous to the IRR seen with low-acute doses of X-rays. The data described in Chapter 6 for cells irradiated at low-dose rate followed by acute doses, suggests a lack of triggering of repair mechanisms when the inverse dose-rate effect occurs, as HRS/IRR can be observed after irradiation. An active induction of a radioprotective mechanisms may occur where dose-rate sparing is apparent in confluent cultures. This may be further evidence that HRS/IRR and the inverse dose-rate effect may be mechanistically related. So far this has only been observed in confluent cultures, where the "flip over" from sparing to the inverse dose-rate effect has been detected. It would be of interest to examine whether a similar effect occurs in asynchronous cultures. To do this, cell survival would need to be examined at dose rates between $100cGyh^{-1}$ (the "highest" low-dose rate studied in these experiments) and $33Gyh^{-1}$ (the acute dose rate). Between these dose rates the possible change from sparing to the inverse dose-rate effect may occur in these asynchronous cultures and the presence or absence of HRS/IRR after these exposures could be investigated.

The hypothesis for the presence of HRS at very low-acute doses and not at higher ones, is that at the lowest doses cells will not detect damage and therefore little or no repair will take place resulting in increased cell kill. As the dose is increased, a level of damage will be reached that the cell will detect and will then switch on repair mechanisms. The hypothesis for an inverse dose-rate effect is that cells will be irradiated so slowly that they will not

detect damage as it occurs and will not trigger repair. During protracted exposures, damage may accumulate and will therefore lead to greater cell kill than with a single acute dose. The experiments described in Chapter 6 were designed to assess whether there was a certain combination of dose and dose rate given prior to an acute dose that would affect the HRS response, possibly by triggering the "detection mechanisms" within the cell and switching on repair during the LDR irradiation. Therefore after a subsequent acute dose of radiation, the HRS/IRR effect would not be apparent. As described in Chapter 6 (Section 6.6), there are two hypotheses explaining how DNA-repair mechanisms are triggered:
(1) that there is a fixed threshold level of damage where repair is switched on if damage levels exceed this.
(2) that there is a continuous transition of increasing repair activity as damage levels increase.
A pictorial representation is given in Figure 6.4.

There appearss to be evidence for both hypotheses. In this study, the "switch" dose rate from dose-rate sparing to the inverse dose-rate effect was detected in confluent T98G cells. When cells were irradiated at the dose rate where dose-rate sparing was observed (60 to 30cGyh^{-1}) (Figure 4.6), no HRS/IRR could be detected after subsequent acute dose irradiation (Figure 6.2). Conversely cells irradiated at dose rates below 30cGyh^{-1}, where an inverse dose-rate effect was seen, continued to show HRS/IRR after an acute dose exposure. Furthermore the cells that showed dose-rate sparing, which did not show HRS/IRR when the acute dose was given immediately after the LDR irradiation, did show the response if there was a 4h time period between the low-dose rate and acute dose irradiations. This would suggest a threshold level of damage is accumulated at the dose rates where sparing occurs and this effect is explained by hypothesis 1. When a 4h interval is left between irradiations, DNA repair occurrs reducing damage levels to below the threshold level and HRS/IRR is recovered.

However, the second hypothesis may also explain this effect, and this involves examining the extent of the HRS response. In Chapter 6, the α_s/α_r value is used to measure the "degree" of HRS (other methods of measuring the extent of HRS are discussed in Section 6.6). After assessing the extent of HRS using the α_s/α_r value, the degree of HRS appears to be greater in cells irradiated at LDR to a total dose of 2Gy, compared with cells irradiated at the same dose rate to a total dose of 5Gy in both confluent and asynchronous cultures (with exceptions). This may reflect an increased rate of repair or a greater amount of repair mechanisms being switched on followed by increased damage at 5Gy.

Both hypotheses may also be applicable to low acute-dose studies. Time course experiments carried out by Short (1999), examined the amount of time required to "recover" from HRS, *i.e.* the shortest time between two 0.4Gy doses which would give a

sensitive response to the second dose. If the IRR was switched on over a fixed threshold level (hypothesis 1), then if a sensitive response was observed after the first dose, a second dose may increase the damage levels over this threshold resulting in a resistant response. Short (1999) found that an interval of 4h was needed to recover from the first dose. During that time DNA-repair processes may reduce damage levels and so a second subsequent dose would not cross the threshold and a sensitive response would be seen. The continuous transition of an increase in repair activity (hypothesis 2) may also be used to explain this. A single dose of 0.4Gy may give a sensitive response, but some repair mechanisms may be switched on to a small degree. A second dose may increase damage levels over the maximum repair levels so giving a resistant response. A 4h interval would allow a reduction in damage and a minimal amount of repair will be switched on and so a sensitive response will be observed.

8.3.2 Possible mechanisms and future work

The evidence from this thesis on the mechanisms behind HRS/IRR and the inverse dose-rate effect would suggest that they are related. More of the mechanisms underlying the HRS/IRR response have been elucidated than the inverse dose-rate effect. If, however, the inverse dose-rate effect has effectively the same underlying mechanism as HRS/IRR, but at low-dose rate, then elucidating the mechanisms of HRS/IRR will lead to further understanding of the inverse dose-rate response.

The evidence to date for mechanisms behind the HRS/IRR response strongly implicates the involvement of DNA repair. The response is not observed in very radiosensitive cell lines, *e.g.* SW48 and HX142. The involvement of DNA repair in HRS/IRR was studied by Skov *et al.* (1994) who measured the response of three repair deficient hamster cell lines to low doses of radiation. They concluded that HRS/IRR may be linked to double-strand break and nucleotide excision repair mechanisms, but not base excision repair as the base excision repair deficient cell line EM9 showed HRS/IRR. One of the cell lines they studied was XR-V15B, a V79-derived DSB repair deficient line. It is defective in the Ku80 subunit of the DNA-PK complex that repairs DNA DSBs (Jeggo 1997). Of the three pathways that are thought to repair DSB damage in eukaryotes, homologous recombination, direct repeat end joining and non-homologous end joining, the latter is the most common in mammals. This pathway requires the presence of DNA-PK to function. The proposed mechanism by which it acts, is by one of its subunits, Ku80, sensing DNA damage and binding to the DNA lwhich leads to the formation of DNA-PK. This then initiates a phosphorylation cascade leading to the binding of XRCC4 protein and ligase IV (Critchlow *et al.* 1997).

Cell lines deficient in DNA-PK show extreme radiosensitivity, *e.g.* the mutant cell line xrs5 (lacks Ku80) (Getts and Stamato 1994). This cell line has been shown to overcome

this extreme radiosensitivity when the Ku-80 gene is transfected into it (Gu *et al.* 1997). Another mutant cell line, MO59J fails to express DNA-PK. These cells are more radiosensitive than a DNA-PK competent cell line, MO59K, which was extracted from the same tumour biopsy (Allalunis Turner *et al.* 1993). Recent unpublished data has shown that both of these cell lines show HRS, however the M059J, which are deficient in DNA-PK, do not show an IRR response (Joiner, Marples, Johnston *et al.* pers. comm.). These experiments have implicated NHEJ as a pathway involved in IRR. A third cell line MO59J/fus-1 is derived from the original DNA-PK deficient MO59J cell line. This cell line has the Ku80 subunit transfected into it. Its radiosensitivity is similar to the MO59K cell line and a HRS/IRR response is apparent (Joiner, Marples, Johnston *et al.* pers. comm.). It therefore appears that DNA-PK is essential for IRR to occur in this cell line. Further studies involving DNA-PK inhibitors, such as OK1035 (Kruszewski *et al.* 1998, Take *et al.* 1995) and wortmannin (Chernikova *et al.* 1999, Okayasu *et al.* 1993, Sarkaria *et al.* 1998), would also prove useful in understanding the exact role of DNA-PK in HRS/IRR. A recent paper examining DNA-PK activity described a decrease in activity in the low-dose region (0.2Gy) of 6 cell lines which displayed HRS/IRR and an increase in DNA-PK activity in 4 cell lines which were HRS negative (Vaganay-Juéry *et al.* 2000). An examination of the movement of DNA-PK and its subunits within the cell after exposure to low-dose irradiation would be useful to determine the location of the sensing of damage and how this promotes DNA repair within the cell.

Poly (ADP-ribose) polymerase (PARP) has been implicated in DNA damage detection in IRR. Marples *et al.* (1997) showed that 3-aminobenzimide, a potent inhibitor of PARP, blocks IRR. These studies could be extended further to elucidate the timescale for the optimum inhibition of IRR in single and dual dosing experiments.

Recent data has implicated the presence of a gene which downregulates its protein production in response to low doses of ionising radiation. This gene, called DIR-1, was isolated from a cell line, L132, that shows HRS/IRR (Robson *et al.* 1999). Molecular and cellular characterisation of this gene reveals that it is unique but has similarities to a family of heat-shock-related proteins known as immunophilins. These have been implicated in various cellular functions including general stress responses. Antisense strategies have demonstrated that the DIR1 gene also appears to have some involvement in the control of the cell cycle. Furthermore, there appears be a potential role for this gene product in the phenomenon of IRR through a mechanism that increases the rate of DNA repair in cells exposed to X-rays and subsequently increases the cells' resistance to radiation (Robson *et al.* 2000). If this gene does potentiate a HRS/IRR response, it may prove a useful tool in radiotherapy treatments in the future. With further developments in gene therapy, incorporation of DIR-1 into cells may sensitise them to low doses of radiation. It could potentially be used in conjunction with ultrafractionation schedules (as described in

Section 8.4.1) to increase therapeutic gain in radioresistant tumours. However, much work remains to be carried out to further establish the role of DIR-1 in the HRS/IRR response.

It has been suggested that conformational changes in DNA structure may be an explanation for HRS/IRR seen at low doses of radiation. Chromatin structure and chromosomal organisation are widely accepted as key controlling mechanisms in DNA replication, transcription and associated processes such as differentiation, cell-cycle progression and onco-phenotypes. Chromatin structure may be an important determinant of radiosensitivity. Proteins such as histones which are associated with chromatin are major radioprotectors (Chiu *et al.* 1992, Elia and Bradley 1992, Nackerdien *et al.* 1989, Olive and Banath 1995). Cell cycle, and artificially-induced changes in chromatin structure have shown a strong correlation with radiosensitivity (Dahm-Daphi *et al.* 1993, Iliakis *et al.* 1993, Metzger and Iliakis 1991, Nackerdien *et al.* 1989, Okayasu *et al.* 1993, Raaphorst and Azzam 1981) and some radiation-sensitive cell lines and phenotypes often have associated alterations in chromatin structure (Malyapa *et al.* 1994, Schwartz *et al.* 1990, Schwartz and Vaughan 1989, Wlodek and Olive 1992, Yasui *et al.* 1991). It is possible that changes in DNA conformation are involved in HRS/IRR responses. After high doses of radiation, a large amount of DNA damage may occur causing the DNA conformation to "fall apart" leading to a more "open" state. In this state, repair complexes can reach damaged areas and repair them efficiently. It may be that at lower doses (below 0.5Gy), there is not enough DNA damage to alter the conformation and DNA-repair enzymes cannot reach the damaged sites, leading to more cell death. This is a passive response rather than an active induction of repair mechanisms and may be an explanation for changes in the degree of HRS/IRR seen in different phases of the cell cycle (M. C. Joiner pers. comm.). The greatest HRS/IRR response has been observed in G2. In this phase the DNA is in a tight conformation which may affect accessibility of repair complexes resulting in increased sensitivity at low doses. The S phase seems to show the least HRS and in this phase the DNA is stretched out for replication allowing repair enzymes to reach damaged sites. It would be interesting to investigate this hypothesis further and to monitor conformational changes in chromatin structure after low doses of irradiation in both HRS positive and negative cell lines. A combination of the DNA damage-measuring comet assay and fluorescence *in situ* hybridisation (FISH) could be used to do this. This technique would allow the examination of how compartmentalisation of DNA within the nucleus impacts on both the induction and repair of DNA damage (Heiskanen *et al.* 1994, McKelvey-Martin *et al.* 1998, Santos *et al.* 1997). This would establish whether a relationship exists between "constitutive" repair ability and HRS/IRR.

IRR after acute single doses and the adaptive response are similar because they both imply an active response to irradiation which leads to resistance. However, accumulating evidence

suggests that, the HRS/IRR response and the adaptive response are not as closely related as first thought. This was first proposed by Wouters and Skarsgard (1997). They found that although priming doses stop the HRS/IRR response, theyt do not have the effect of increasing resistance at the higher doses. The time course of adaption and HRS/IRR also appears to be different. In most systems adaption requires at least 4h to become apparent, whereas IRR is almost immediate and HRS returns to a sensitive response after 3h (Short 1999). However, an increase in activity of DNA-repair processes seems the most plausible explanation for the two phenomena. A further understanding of the mechanisms of HRS/IRR will provide evidence either for or against a homology between HRS/IRR and adaption.

There are other molecular techniques which could be employed to study and even evoke changes in DNA-repair pathways, and so further elucidate mechanisms of HRS/IRR and indeed the inverse dose-rate effect. This will be useful both from a scientific perspective to understand the processes involved and also from a clinical standpoint, where gene therapy or other methods could be used to induce HRS/IRR *in vivo*, or simple, fast, reliable predictive tests could be developed on the basis of these mechanisms to ultimately increase the therapeutic gain *in vivo*.

8.4 Potential clinical importance of the inverse dose-rate effect and HRS/IRR

8.4.1 HRS/IRR

The presence of HRS/IRR in the majority of cell lines tested *in vitro* may be of clinical importance. It would be extremely beneficial to be able to exploit the HRS/IRR response in radiotherapy. This may be of particular importance in the treatment of tumours that respond poorly to radiotherapy because of inherent radioresistance. Experiments *in vitro* have shown that, in some cell lines, a α_s/α_r value of greater than 20 can be obtained. If this HRS occurs after each dose in a fractionated regime, a very substantial increased cell kill would be predicted compared with the same total dose given as larger doses per fraction. Experiments carried out by Short (1999) have confirmed that this occurs in the T98G cell line *in vitro*. Short (1999) predicted that a multiple low-dose regime ('ultrafractionation") where 0.5Gy fractions were given instead of 2Gy fractions could increase the biological effect of a given dose by nearly two-fold. For a therapeutic gain to be obtained with ultrafractionation requires that a greater excess sensitivity occurs in the tumour than in critical normal tissues. The amount of increased sensitivity at lower doses depends on the parameter α_s/α_r and the rate at which the transition from α_r to α_s occurs with decreasing dose. Data on the mouse kidney have shown that HRS occurs to a lesser extent compared with T98G with an α_s/α_r of 6.6 (Joiner and Johns 1988) compared with 13.2 for T98G (Short 1999). The prediction of a 200% increase in biological effect due to

ultrafractionation by Short (1999) was calculated assuming an increase in cell kill due to HRS in T98G and a decrease in cell kill in rat kidney due to a lower value of α/β and a low value of d_c relative to the dose per fraction used.

This fractionated regime may be of use *in vivo* with tumours which appear more radioresistant. However, knowing which tumours would respond prior to radiotherapy, *i.e.* show a HRS response, would be beneficial. Low-dose HRS does not occur in all radioresistant lines *in vitro* and the development of a predictive assay to test for the presence of HRS in tumours *in vivo* would be a valuable tool. However, this is not a practical option at the present time. There are many difficulties in establishing tumour cell lines from primary cells and clonogenic assay survival curves on individual tumour cell lines are time consuming. For these reasons it is not practical to carry out experiments prior to commencing radiotherapy. In the future, however, the mechanisms underlying the response may be better understood and some which are being further investigated are described in Section 8.3.2. For example, a simple test may be developed to detect DNA-PK levels, specific gene defects, abnormalities in specific repair pathways or abnormal signalling post irradiation. If HRS can be detected then an ultrafractionated regime may be used instead of a conventional radiotherapy schedule to exploit this effect.

There is also concern about the effect of an ultrafractionation schedule on normal tissues surrounding the tumour. There is evidence for the presence of HRS/IRR in normal tissues in animal models and clearly if the magnitude of the HRS response is too high in human normal tissues then this would argue against a therapeutic gain from ultrafractionation. An enhanced sensitivity to low doses has been described in the mouse kidney (Joiner and Johns 1988), skin (Joiner *et al.* 1986) and lung (Parkins and Fowler 1986). The HRS/IRR occurring in mouse normal tissues appears to occur at lower doses and is less marked than in tumour cell lines studied *in vitro*. HRS/IRR has also been described in the rat spinal cord (Ang *et al.* 1985), although other studies have found no evidence of this (Wong *et al.* 1992, Wong *et al.* 1993, Lavey *et al.* 1994). These data would suggest that an ultrafractionation schedule would not be as damaging to normal tissues as to radioresistant tumours, at least in mice. A recent clinical study in Sweden on the effects of low doses per fraction on the basal cell density of human skin has shown evidence of an increased sensitivity to 0.45 Gy per fraction compared with 1.10 Gy per fraction. This effect was highly significant with a ratio between the slopes of these dose-response relationships (Dose Modifying Factor, DMF) of 1.8 (I. Turesson *et al.* pers. comm.). A similar study in the UK also examined the basal cell density and found evidence of HRS with doses of 0.3–0.5 Gy giving increased cell depletion compared with 1 Gy per fraction (Shah *et al.* pers.comm.). Further experiments are needed to establish whether other normal tissues show sensitivity to low doses in a clinical situation.

8.4.2 Inverse dose-rate effect

The data obtained in the present study imply that exposures to ionising radiation at low-dose rates are move effective than higher dose-rate exposures in killing tumour cells. The clinical implications of this work could be important where low dose-rate radiotherapy is used in cancer treatment. The major example is in prostate brachytherapy. Brachytherapy uses temporary or permanent radioactive implants to deliver a high dose at a continuous low-dose rate. The most common radioisotopes used in brachytherapy implants are ^{103}Pd, ^{198}Au and ^{125}I. These each have different properties and emit radiation at different dose rates. ^{103}Pd emits low-energy photons of 21 keV, has a half life of 17 days and it is usual to prescribe initial dose rates of 20–24 cGy h^{-1} to target tissues (Blasko *et al.* 2000). ^{198}Au emits higher energy photons of 420 keV, has a much shorter half life of 2.7 days and gives a higher initial dose rate of 60 cGy h^{-1} (Butler *et al.* 1997). ^{125}I, however, decays much more slowly, as it has a half life of 60 days emitting low-energy photons of 28 keV and giving an initial dose rate of 7–10 cGy h^{-1} to the prescription isodose contour (Storey *et al.* 1999, Beyer and Priestley 1997). ^{125}I and ^{103}Pd emit low-energy photons. This low energy means there is not much penetration into tissue and this combined with the inverse square law results in dose falling to less than 50% of the minimum peripheral dose within a few millimetres. This therefore provides a significant advantage in terms of reduction in dose to adjacent critical structures such as the rectum and neurovascular bundles but is equally a limitation in dealing with disease more than 3 or 4 mm outside the prostate capsule. Data from experiments described in this thesis, suggest that lowering the dose rate (below 60 cGy h^{-1}), will increase cell kill and therefore using ^{125}I brachytherapy may prove the most clinically beneficial compared with the other, slightly higher dose-rate isotopes. One of the cell lines used in this study was a prostate carcinoma line (PC3) and this cell line shows an inverse dose-rate effect below 60 cGy h^{-1} *in vitro*. Two other prostate carcinoma lines (LNCaP and DU145) have been shown to exhibit HRS/IRR at low-acute doses and with the current evidence so far on the homology between HRS/IRR and the inverse dose-rate effect, it is predicted that these cells would also show an inverse dose-rate effect. Treatment of prostate tumours using ^{125}I brachytherapy may be an ideal way of exploiting the HRS phenomenon clinically.

The greatest cell kill was observed in the present study at dose rates of 2–5 cGy h^{-1}. However, irradiating tumour cells at this dose rate may not give the greatest therapeutic gain, as the irradiation time would be so great that proliferation may offset any increase in cell kill. It is therefore important to address the balance between any increase in radiosensitivity by lowering of the dose rate, against the increased overall time needed to give a similar or reduced dose in order to counteract proliferation. This may prove crucial in establishing an optimal treatment regime.

Further investigations are required to try to maximise any increased cell kill *in vivo* due to the inverse dose-rate effect. It would be useful to test a wide range of primary prostate tumour cell lines to establish the prevalence of the inverse dose-rate effect. If indeed it was a universal effect then it may be wise to use ^{125}I rather than other isotopes in brachytherapy treatments in order to exploit this. The effect of decreasing dose rate with the ^{125}I decay *in vivo* could be studied *in vitro* using the ^{60}Co water tank apparatus. Stepping the dose rate downwards during exposure time could be investigated to mimic more closely the clinical situation. The development of a radiotherapy regime that will increase cell kill in a small overall treatment time whilst sparing the surrounding normal tissues is desirable. Combining LDR treatments with fractionation treatments may be a way forward in increasing therapeutic gain and a LDR treatment given prior to a high-dose fraction may be a way of achieving this. The rationale would be to reduce the overall treatment time required in clinical protocols for treatments involving very low-dose rates. The use of LDR would give enhanced cell kill whilst sparing the surrounding tissues and a single HDR fraction would increase the total dose delivered and therefore reduce the overall time of irradiation.

As with ultrafractionation, the effects of low dose-rate exposures on normal tissues is an important issue to address. Again, for a therapeutic gain to be obtained with low dose-rate exposures requires that more excess sensitivity occurs in the tumour than in critical normal tissues. If normal tissues also show an inverse dose-rate effect, then damage to these during brachytherapy treatments may prove deleterious. There is little evidence for the inverse dose-rate effect in normal tissues. The majority of studies have found a consistent dose-rate sparing response to dose rates ranging from 6000 down to $19 cGy h^{-1}$ (Badie *et al.* 1996). This effect appeared so consistent that many studies have been carried out to assess whether the α slope of the survival curve after LDR exposures can predict normal tissue radiosensitivity *in vivo* using dose rates as low as $12 cGy h^{-1}$ (Cox 1982, Burnet *et al.* 1996, Little and Nove 1990, Jones *et al.* 1995, Sproston *et al.* 1996). Furthermore, if the hypothesis that HRS/IRR and the inverse dose dose-rate effect are mechanistically related is true, then it is likely that normal tissues would show less inverse dose-rate effect, as HRS/IRR also appears less marked (Joiner and Johns 1988, Joiner *et al.* 1986, Parkins and Fowler 1986, Ang *et al.* 1985), or is absent (Wong *et al.* 1992, Wong *et al.* 1993, Lavey *et al.* 1994), in normal tissues compared with malignant cell lines. Even if normal tissues do show HRS (I. Turesson pers. comm., N. Shah pers. comm.), which *was* apparent at low-dose rates, with radioisotopes such as ^{125}I, the penetration distance is so short that even if a sensitive response occurs, the normal tissues will not receive sufficient total dose to cause extensive damage.

8.5 Implications for radioprotection

The effects of low dose-rate exposures on cell survival and mutagenesis has implications for radioprotection. Until recently, technology was not advanced enough to measure survival or mutagenesis at very small doses and low-dose rates. The dose-effect relationship in this region could only be considered indirectly and current risk estimates were based on Hiroshima atomic bomb survivors and occupationally and medically exposed patients. There are several possibilities for the relationship of very low doses/dose rates of radiation on cancer induction. The first is that there is a linear relationship between dose/dose rate and effect with or without a threshold, below which there is no effect. Alternatively, there may be a supra-linear relationship where there is an enhanced effect per dose at the lowest dose/dose rates or there may be a beneficial effect of low doses known as hormesis.

Some epidemiological studies suggest a hormetic effect of radiation (Lundell *et al.* 1999, Pollycove 1998, Cohen 1994). One hypothesis for this is that an adaptive response will occur after an initial exposure of very low doses/dose rates of radiation. The first radiation exposure will result in the switching on of repair processes. This may have a radioprotective effect by repairing subsequent spontaneous or radiation induced DNA damage occurring at a later date. *In vitro* evidence supports this whereby a low dose and low dose-rate exposure of γ-rays protected against neoplastic transformation below the level of spontaneous induction in C3H10T1/2 cells (Azzam *et al.* 1994, Azzam *et al.* 1996). The adaptive response is a similar effect to HRS/IRR, although as yet there is not sufficient evidence to link the two phenomena. However, both these phenomena, and perhaps also the inverse dose-rate effect, argue against a linear-no-threshold model for mutation induction at low doses/dose rates. If HRS did occur at very low doses/dose rates in normal tissues, then it could have a radioprotective effect by removing more potentially damaged cells from the population at risk. If the hypothesis from this thesis is true, that HRS/IRR and the inverse dose-rate effect are mechanistically related, a similar effect may be occurring at low-dose rates.

A recent paper by Little and Muirhead (2000) examined Japanese atomic bomb survivor data and found an *increased* risk of leukaemia and solid tumours at low doses of neutrons and gamma rays. It is also possible that HRS occurs when mutation is an endpoint, in which case an increase cell kill would be balanced by increased mutations. The presence of an inverse dose-rate effect on mutation induction has been documented in several studies (Section 1.6.5) with both high (Hill *et al.* 1984, Hill *et al.* 1985, Miller *et al.* 1988, Miller *et al.* 1989, Miller *et al.* 1990, Miller and Hall 1991, Hill *et al.* 1982, Hall *et al.* 1991, Hall *et al.* 1991, Redpath *et al.* 1990, Kubota and Hill 1989, Hornung and Meinhardt 1987, Chmelevsky *et al.* 1988, Darby and Doll 1990, Lubin *et al.* 1990) and low-LET irradiation

(Colussi and Lohman 1997, Crompton *et al.* 1985, Crompton *et al.* 1990, Lorenz *et al.* 1993, Amundson and Chen 1996, Furuno Fukushi *et al.* 1996, Bettega *et al.* 1997). However, this is a controversial issue as many other studies have found no effects at high LET (Balcer Kubiczek *et al.* 1994, Saran *et al.* 1994) (fractionated) (Elkind 1994) or low-LET irradiation (Colussi *et al.* 1998, Spivak and Kolman 1998, Kolman and Harms Ringdahl 1996, Han *et al.* 1980, Komatsu *et al.* 1993, Edwards *et al.* 1997). Most studies have examined either the hprt or tk loci and it remains to be seen whether any inverse dose-rate effect can be seen in more critical loci associated with oncogenes or tumour suppressor genes. It therefore seems that before any conclusions can be drawn as to the relevance of HRS/IRR and the inverse dose-rate effect with regards to radioprotection, a more detailed understanding of the mechanisms underlying these responses is required.

8.6 Overall conclusions of thesis

The present study allows several conclusions to be drawn:

(1) That low dose-rate exposure of ^{60}Co to HRS/IRR positive human tumour cell lines (T98G, PC3 and A7) *in vitro*, causes an inverse dose-rate effect at the lowest doses, whereby a reduction in dose rate results in a increase in cell kill.

(2) In a HRS/IRR negative cell line (U373MG) an inverse dose-rate effect is not evident.

(3) There is evidence that the inverse dose-rate effect is not due to cell-cycle perturbations:

- **(i)** There is no G2 accumulation in the lowest dose rates where the largest cell kill is observed.
- **(ii)** U373MG, which does not show an inverse dose-rate effect, has similar cell-cycle distributions as those cell lines which do.
- **(iii)** The effect has been observed in confluent cultures where cell-cycle progression is greatly reduced.

(4) A hypothesis may be formulated from the results of LDR "priming" experiments that dose-rate sparing, whereby an *increase* in cell survival is seen with a *decrease* in dose rate, may be linked to the increased activity of repair mechanisms and the inverse dose-rate effect, observed in these experiments, may occur due to a *lack* of activity of these mechanisms.

(5) There may be a mechanistic relationship between HRS/IRR observed at acute doses and the inverse dose-rate effect observed after continuous low dose-rate exposures. Further understanding of the mechanisms behind both phenomena may explain the exact nature of this relationship.

These observations may prove to be useful in the future planning of prostate brachytherapy treatments. Radioisotopes which deliver their dose at the lower dose rates, may be chosen over higher dose-rate treatments. Further experiments must be carried out to elucidate the mechanisms of the response and to develop a clinically therapeutic regime which exploits this inverse dose-rate effect to its full potential.

Appendix 1

Cell-cycle profiles of human tumour cells irradiated with LDR ^{60}Co (see Chapter 4).

(A) Asynchronous T98G (Figure 4.18)

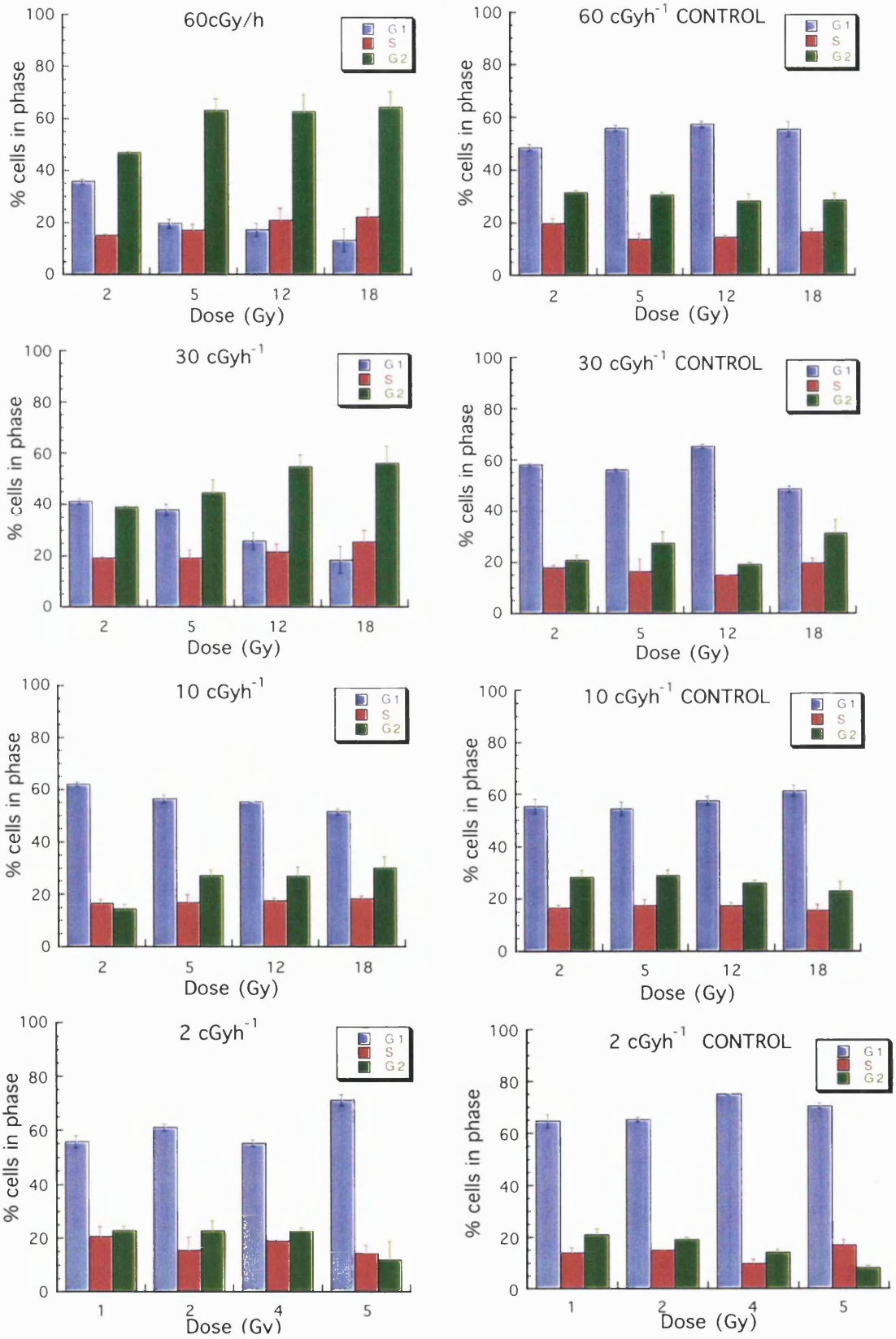

(B) Confluent T98G (Figure 4.19)

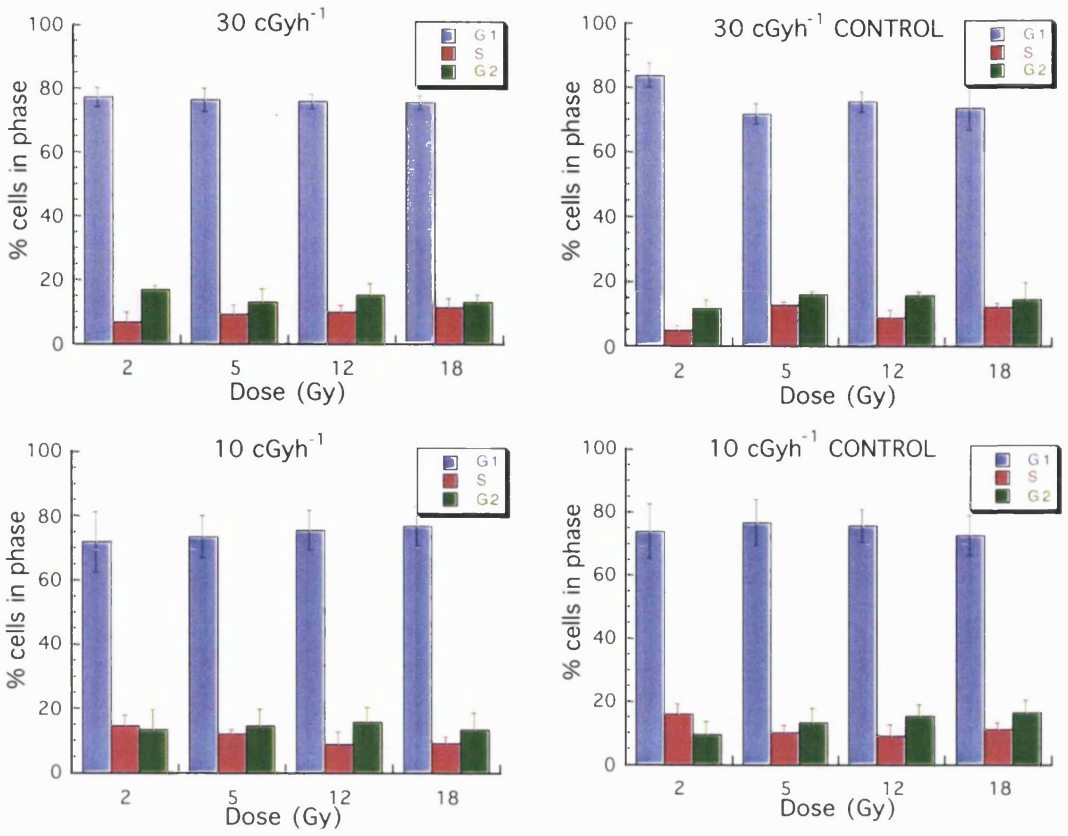

(C) Asynchronous A7 (Figure 4.20)

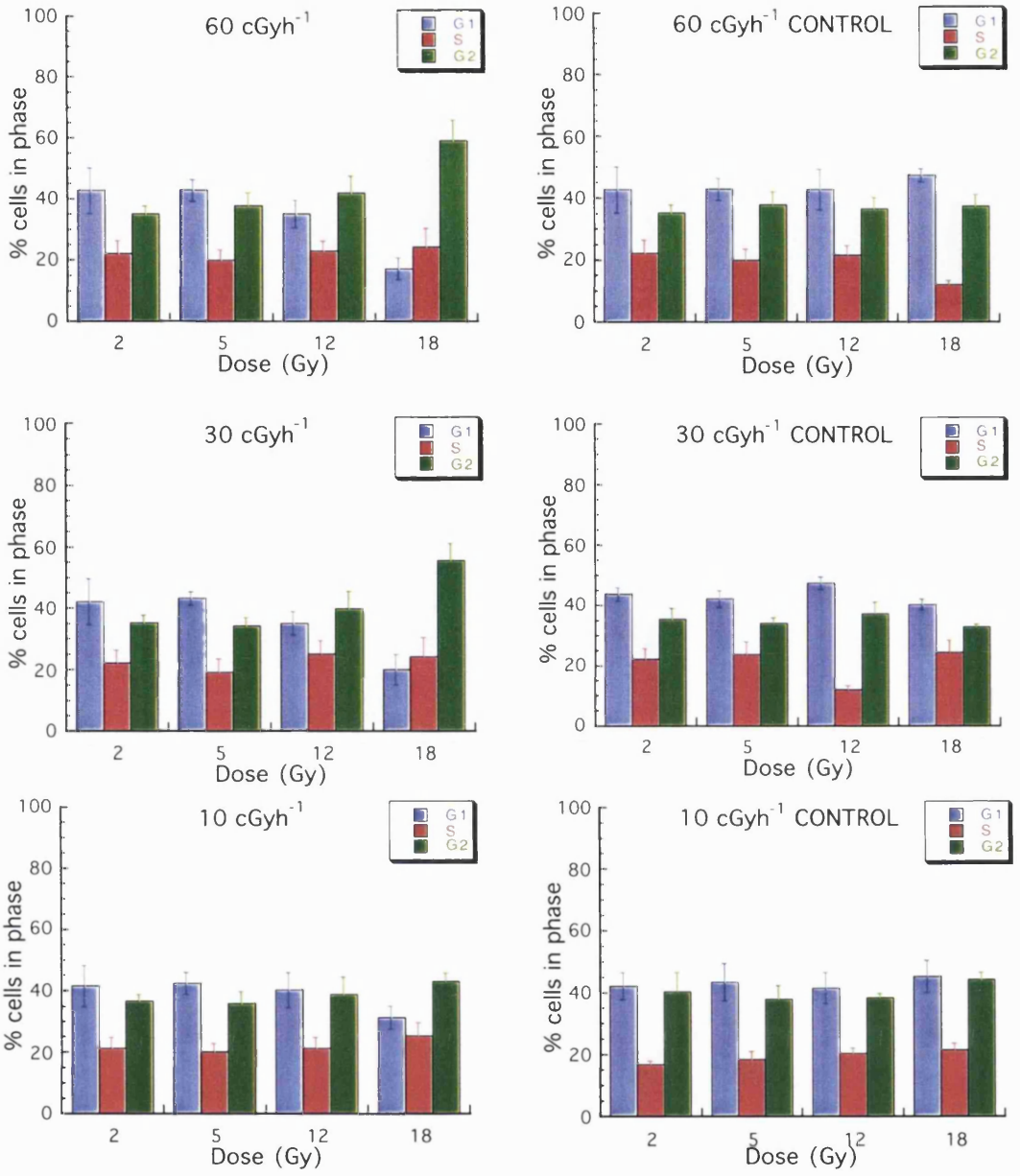

(D) Asynchronous PC3 (Figure 4.21)

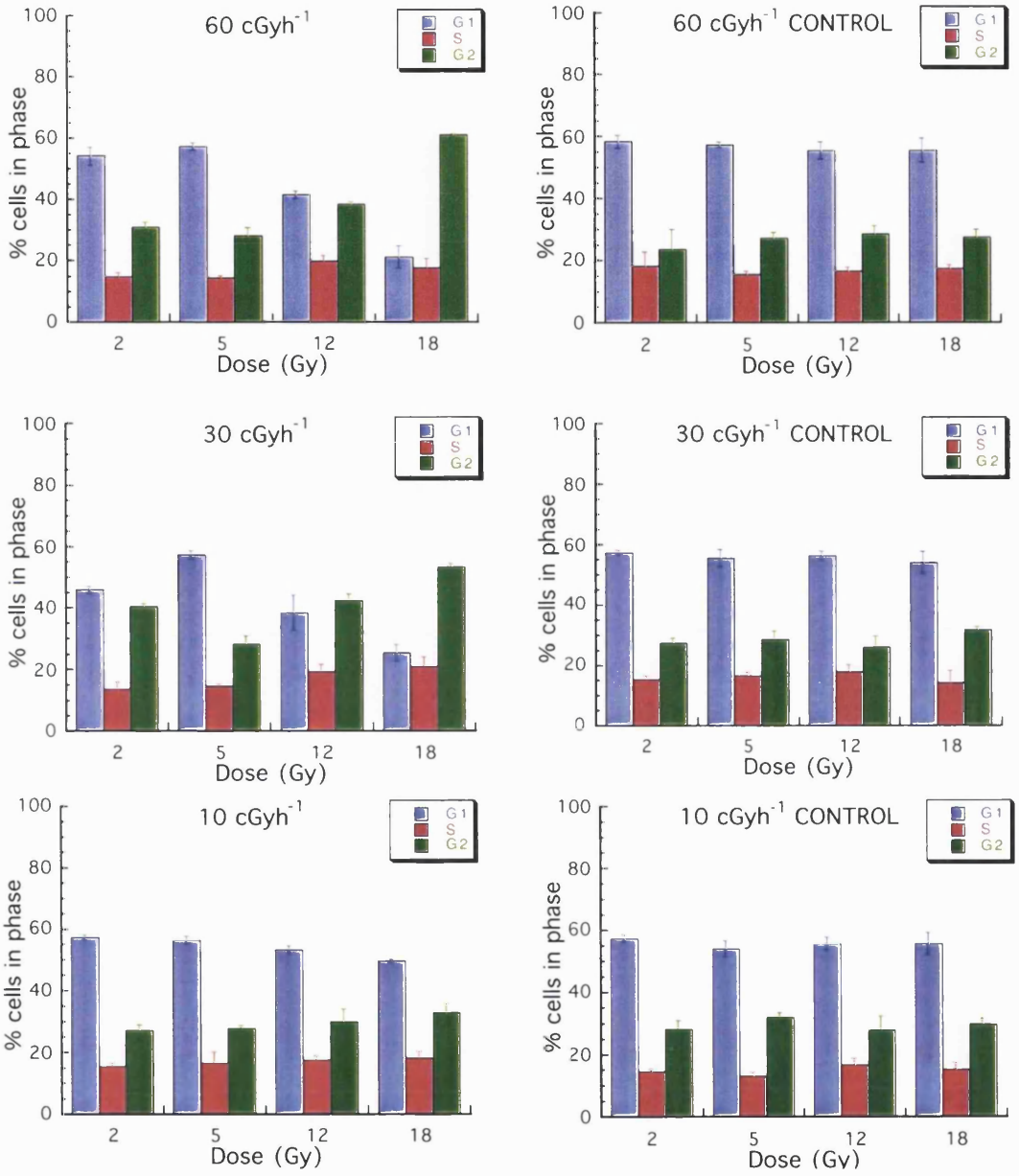

(E) Asynchronous U373MG (Figure 4.22)

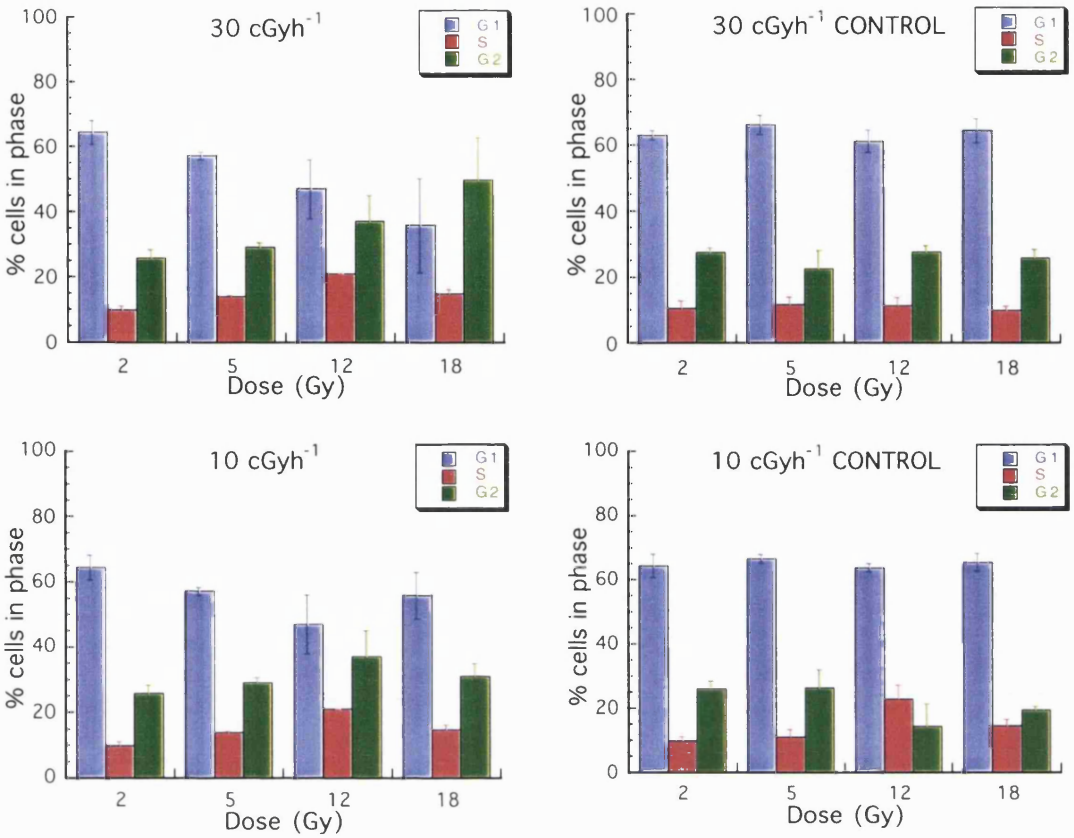

Appendix 2

Calculation of the initial dose rate for seed irradiator no.1

The dose rate DR (r,θ) at point (r,θ) is given by:

$$DR(r,\theta) = S_K A\left[\frac{G(r,\theta)}{G(r_o,\theta_o)}\right]g(r)F(r,\theta)$$

Where S_K= air kerma strength of the source ($\mu Gy\,m^2\,h^{-1}$)

A= dose-rate constant for ^{125}Iodine (a factor which transforms air kerma strength to dose rate in $cGy\,h^{-1}$ in water based measurements)

G(r,θ)= geometry factor, which accounts for the variation of relative dose due only to the spatial distribution of activity within the source.

$G(r_o,\theta_o)$= geometry factor for r_o= 1 cm and θ_o= Π/2

g(r)= radial dose function, which accounts for the effects of absorption and scatter in the medium along the transverse axis of the source

F(r,θ)= anisotrophy function, which accounts for the anisotrophy of dose distribution around the source, including the effects of absorption and scatter in the medium.

For the seeds loaded into the first plaque, the following calculations were made:

$$D(r) = \frac{S_K A}{r^2} = g(r)\overline{F}$$

Where S_KA and g(r) are as above and F is an average anisotrophy factor, taken to be 0.95 (for seed model 6702).

The set of seeds used on the first plaque had the following equivalent activities:

Central seed:	6.5 mCi
Peripheral seeds	8 × 7.9 mCi

Taking A= 0.93 cGy h^{-1}

and 1 mCi= 1.27 U

The dose rates at various points on the treatment plane (at 6 mm above seed plane) are given as follows:

Position	Dose rate in water (cGy h^{-1})
Above central seed	46.8
Above peripheral seed	43.3
Above a point half way between peripheral seeds	38.3
Above a point half way between peripheral and central seeds	38.0

If the hot spots are ignored, a mean dose rate can be taken as 39.3 cGy h^{-1}.

The total dose given in one week for this initial dose rate is:

$$\text{Total dose} = D_o \int_{t=o}^{t=T_e - \lambda t}$$

$$= 39.4\left[-\frac{1}{\lambda} e^{-\lambda t}\right]_{t=0}^{t=168}$$

$$= \frac{39.4 \times 1425.6}{0.693}[1 - 0.92]$$

$$= 6484 \text{ cGyh}^{-1} \text{ or } 64.84 \text{ Gy}$$

Alternatively, if it is wished to give 50 Gy at this initial dose rate then the length of irradiation, T hours, must be given from:

$$5000 = \frac{39.4 \times 1425.6}{0.693}\left[1 - e^{-\lambda t}\right]$$

T= 131 hours

Appendix 3

Formula used to calculate cell cycle time (T_C)

$$\left(\text{normDist}\left(\frac{\text{Time(h)} + \text{ts} \bullet 0.5}{\sqrt{\text{stc}^2 \bullet 0.00001}}\right) - \text{normDist}\left(\frac{\text{Time(h)} - \text{ts} \bullet 0.5}{\sqrt{\text{sts}^2}}\right)\right.$$

$$+\text{normDist}\left(\frac{\text{Time(h)} - \text{tc} + \text{ts} \bullet 0.5}{\sqrt{\text{stc}^2}}\right) - \text{normDist}\left(\frac{\text{Time(h)} - \text{tc} - \text{ts} \bullet 0.5}{\sqrt{\text{sts}^2 + \text{stc}^2}}\right)$$

$$+\text{normDist}\left(\frac{\text{Time(h)} - \text{tc} \bullet 2 - \text{ts} \bullet 0.5}{\sqrt{\text{stc}^2 \bullet 2}}\right) - \text{normDist}\left(\frac{\text{Time(h)} - \text{tc} \bullet 2 - \text{ts} \bullet 0.5}{\sqrt{\text{sts}^2 + \text{stc}^2 \bullet 2}}\right)$$

$$\left.+\text{normDist}\left(\frac{\text{Time(h)} - \text{tc} \bullet 3 + \text{ts} \bullet 0.5}{\sqrt{\text{stc}^2 \bullet 3}}\right) - \text{normDist}\left(\frac{\text{Time(h)} - \text{ts} \bullet 0.5 - \text{tc} \bullet 3}{\sqrt{\text{sts}^2 + \text{stc}^2 \bullet 3}}\right)\right) + \text{f}$$

REFERENCES

1 Algan, O., Stobbe, C.C., Helt, A.M., Hanks, G.E. and Chapman, J.D., 1996, Radiation inactivation of human prostate cancer cells: the role of apoptosis. *Radiation Research*, **146,** 267-75.

2 Allalunis Turner, M.J., Barron, G.M., Day, R.S.d., Dobler, K.D. and Mirzayans, R., 1993, Isolation of two cell lines from a human malignant glioma specimen differing in sensitivity to radiation and chemotherapeutic drugs. *Radiation Research*, **134,** 349-354.

3 Amundson, S.A. and Chen, D.J., 1996, Inverse dose-rate effect for mutation induction by gamma rays in human lymphoblasts. *International Journal of Radiation Biology*, **69,** 555-563.

4 Ang, K.K., van der Kogel, A.J. and van der Schueren, E., 1985, Lack of evidence for increased tolerance of rat spinal cord with decreasing fraction doses below 2 Gy. *Int-J-Radiat-Oncol-Biol-Phys*, **11,** 105-10 issn: 0360-3016.

5 Aristizabal, S.A., Woolfitt, B., Valencia, A., Ocampo, G., Surwit, E.A. and Sim, D., 1987, Interstitial parametrial implants in carcinoma of the cervix stage II-B. *Int J Radiat Oncol Biol Phys*, **13,** 445-50.

6 Armour, E., Wang, Z.H., Corry, P. and Martinez, A., 1992, Equivalence of continuous and pulse simulated low dose rate irradiation in 9L gliosarcoma cells at 37 degrees and 41 degrees C. *Int J Radiat Oncol Biol Phys*, **22,** 109-14.

7 Armour, E.P., White, J.R., Armin, A., Corry, P.M., Coffey, M., DeWitt, C. and Martinez, A., 1997, Pulsed low dose rate brachytherapy in a rat model: dependence of late rectal injury on radiation pulse size. *Int J Radiat Oncol Biol Phys*, **38,** 825-34.

8 Ash, D., Bottomly, D.M. and Carey, B.M., 1998, Prostate brachytherapy. *Prostate Cancer and Prostatic Diseases*, **1998,** 185-188.

9 Azzam, E.I., de Toledo, S.M., Raaphorst, G.P. and Mitchel, R.E., 1996, Low-dose ionizing radiation decreases the frequency of neoplastic transformation to a level below the spontaneous rate in C3H 10T1/2 cells. *Radiation Research*, **146,** 369-73.

10 Azzam, E.I., Raaphorst, G.P. and Mitchel, R.E., 1994, Radiation-induced adaptive response for protection against micronucleus formation and neoplastic transformation in C3H 10T1/2 mouse embryo cells. *Radiation Research*, **138,** S28-31.

11 Badie, C., Alsbeih, G., Reydellet, I., Arlett, C., Fertil, B. and Malaise, E.P., 1996, Dose-rate effects on the survival of irradiated hypersensitive and normal human fibroblasts. *International Journal of Radiation Biology*, **70,** 563-70.

12 Balcer Kubiczek, E.K., Harrison, G.H., Torres, B.A. and McCready, W.A., 1994, Application of the constant exposure time technique to transformation experiments with fission neutrons: failure to demonstrate dose-rate dependence. *International Journal of Radiation Biology*, **65,** 559-69.

13 Barringer, B.S., 1917, Radium in the treatment of carcinoma of the bladder and prostate. *J. Am. Med. Assoc.*, **68,** 1227–1230.

14 Bates, P.R. and Lavin, M.F., 1989, Comparison of gamma-radiation-induced accumulation of ataxia telangiectasia and control cells in G2 phase. *Mutation Research*, **218,** 165-70.

15 Beam, C.A., Mortimer, R.K., Wolfe, R.G. and Tobias, C.A., 1954, The relation of radioresistance to budding in saccharomyces cerevisiae. *Arch. Biochem. Biophys.*, **49,** 110–122.

16 Bedford, J.S., Hall, E.J.,, 1963, Survival of HeLa cells cultured *in vitro* and exposed to protracted gamma-irradiation. *Int. J. Rad. Biol.*, **7,** 377–383.

17 Bedford, J.S. and Mitchell, J.B., 1973, Dose-rate effects in synchronous mammalian cells in culture. *Radiation Research*, **54,** 316-27.

18 Begg, A.C., McNally, N.J., Shrieve, D.C. and Karcher, H., 1985, A method to measure the duration of DNA synthesis and the potential doubling time from a single sample. *Cytometry*, **6,** 620-6.

19 Bernhard, E.J., Maity, A., Muschel, R.J. and McKenna, W.G., 1995, Effects of ionizing radiation on cell cycle progression. A review. *Radiation and Environmental Biophysics*, **34,** 79-83.

20 Berry, R.J., Cohen, A.B., 1962, Some observations on the reproductive capacity of mammalian tumour cells exposed *in vivo* to gamma radiation at low dose-rates. *Br. J. Radiol.*, **35,** 489–491.

21 Bettega, D., Calzolari, P., Piazzolla, A., Tallone, L. and Redpath, J.L., 1997, Alpha-particle-induced neoplastic transformation in synchronized hybrid cells of HeLa and human skin fibroblasts. *International Journal of Radiation Biology*, **72,** 523-9.

22 Beyer, D.C. and Priestley, J.B., Jr., 1997, Biochemical disease-free survival following 125I prostate implantation. *International Journal of Radiation Oncology Biology Physics*, **37,** 559-63.

23 Bjork-Eriksson, T., West, C.M., Karlsson, E. and Mercke, C., 1998, Discrimination of human tumour radioresponsiveness using low-dose rate irradiation. *Int. J. Radiat. Oncol. Biol. Phys.*, **42,** 1147–1153.

24 Blasko, J.C., Grimm, P.D., Sylvester, J.E., Badiozamani, K.R., Hoak, D. and Cavanagh, W., 2000, Palladium-103 brachytherapy for prostate carcinoma. *Int J Radiat Oncol Biol Phys*, **46,** 839-50.

25 Boag, J.W., 1975, The statistical treatment of cell survival data. In: *Cell survival after Low Doses of Radiation: Theoretical and Clinical Implications*. Edited by: T. Alper. (Institute of Physics and John Wiley & Sons, London), pp. 40-53.

26 Boreham, D.R. and Mitchel, R.E., 1991, DNA lesions that signal the induction of radioresistance and DNA repair in yeast. *Radiation Research*, **128,** 19-28.

27 Boring, C.C., Squires, T.S., Tong, T. and Montgomery, S., 1994, Cancer statistics, 1994. *CA Cancer J Clin*, **44,** 7-26.

28 Brenner, D.J., Hahnfeldt, P., Amundson, S.A. and Sachs, R.K., 1996a, Interpretation of inverse dose-rate effects for mutagenesis by sparsely ionizing radiation. *International Journal of Radiation Biology*, **70,** 447-58.

29 Brenner, D.J. and Hall, E.J., 1990, The inverse dose-rate effect for oncogenic transformation by neutrons and charged particles: a plausible interpretation consistent with published data [see comments]. *International Journal of Radiation Biology*, **58,** 745-58.

30 Brenner, D.J. and Hall, E.J., 1991, Conditions for the equivalence of continuous to pulsed low dose rate brachytherapy. *Int J Radiat Oncol Biol Phys*, **20,** 181-90.

31 Brenner, D.J., Hall, E.J., Randers Pehrson, G., Huang, Y., Johnson, G.W., Miller, R.W., Wu, B., Vazquez, M.E., Medvedovsky, C. and Worgul, B.V., 1996b, Quantitative comparisons of continuous and pulsed low dose rate regimens in a model late-effect system. *Int J Radiat Oncol Biol Phys*, **34,** 905-10.

32 Breslow, R.A., Wideroff, L., Graubard, B.I., Erwin, D., Reichman, M.E., Ziegler, R.G. and Ballard Barbash, R., 1999, Alcohol and prostate cancer in the NHANES I epidemiologic follow-up study. First National Health and Nutrition Examination Survey of the United States. *Ann Epidemiol*, **9,** 254-61.

33 Bristow, R.G. and Hill, R.P., 1990, Comparison between in vitro radiosensitivity and in vivo radioresponse in murine tumor cell lines. II: In vivo radioresponse following fractionated treatment and in vitro/in vivo correlations. *International Journal of Radiation Oncology Biology Physics*, **18,** 331-45.

34 Brock, A., Prager, W., Pohlmann, S. and Friedrich, K., 1995, [The initial results on the radiobiological comparability of continuous LDR irradiation and PDR irradiation using a guinea pig skin animal model]. *Strahlenther Onkol*, **171,** 641-5.

35 Brown, K.D., Lataxes, T.A., Shangary, S., Mannino, J.L., Giardina, J.F., Chen, J. and Baskaran, R., 2000, Ionizing radiation exposure results in up-regulation of Ku70 via a p53/ataxia-telangiectasia-mutated protein-dependent mechanism. *Journal of Biological Chemistry*, **275,** 6651-6656.

36 Bryant, P.E., 1972, Changes in sensitivity of cells during exposure to radiation at low dose-rate. *International Journal of Radiation Biology*, **22,** 67-73.

37 Budd, M. and Mortimer, R.K., 1984, The effect of cycloheximide on repair in a temperature conditional radiation-sensitive mutant of Saccharomyces cerevisiae. *Radiation Research*, **99,** 582-90.

38 Burki, H.J., 1980, Ionizing radiation-induced 6-thioguanine-resistant clones in synchronous CHO cells. *Radiation Research*, **81,** 76-84.

39 Burnet, N.G., Nyman, J., Turesson, I., Wurm, R., Yarnold, J.R. and Peacock, J.H., 1994, The relationship between cellular radiation sensitivity and tissue response may provide the basis for individualising radiotherapy schedules [see comments]. *Radiotherapy and Oncology*, **33,** 228-38.

40 Burnet, N.G., Wurm, R. and Peacock, J.H., 1996, Low dose-rate fibroblast radiosensitivity and the prediction of patient response to radiotherapy. *International Journal of Radiation Biology*, **70,** 289-300.

41 Butler, E.B., Scardino, P.T., Teh, B.S., Uhl, B.M., Guerriero, W.G., Carlton, C.E., Berner, B.M., Dennis, W.S., Carpenter, L.S., Lu, H.H., Chiu, J.K., Kent, T.S. and Woo, S.Y., 1997, The Baylor College of Medicine experience with gold seed implantation. *Semin Surg Oncol*, **13,** 406-18.

42 Cai, L. and Liu, S.Z., 1990, Induction of cytogenetic adaptive response of somatic and germ cells in vivo and in vitro by low-dose X-irradiation. *International Journal of Radiation Biology*, **58,** 187-94.

43 Calkins, J., 1967, An unusual form of response in x-irradiated protozoa and a hypothesis as to its origin. *International Journal of Radiation Biology*, **12,** 297-301.

44 Canti, R.G. and Spear, F.G., 1927, Effect of gamma rays in mitosis *in vitro*. *Proc. Roy. Soc.*, **B102,** 92.

45 Cao, J., Wells, R.L. and Elkind, M.M., 1992, Enhanced sensitivity to neoplastic transformation by 137Cs gamma-rays of cells in the G2-/M-phase age interval. *International Journal of Radiation Biology*, **62,** 191-9.

46 Cao, J., Wells, R.L. and Elkind, M.M., 1993, Neoplastic transformation of C3H mouse embryo cells, 10T1/2: cell-cycle dependence for 50 kV X-rays and UV-B light. *International Journal of Radiation Biology*, **64,** 83-92.

47 Cao, S., Skog, S. and Tribukait, B., 1983, Comparison between protracted and conventional dose rates of irradiation on the growth of the Bp8 mouse ascites sarcoma. *Acta Radiol Oncol*, **22,** 35-47.

48 Carter, H.B., Piantadosi, S. and Isaacs, J.T., 1990, Clinical evidence for and implications of the multistep development of prostate cancer. *Journal of Urology*, **143,** 742-6.

49 Carter, S., Auer, K.L., Reardon, D.B., Birrer, M., Fisher, P.B., Valerie, K., Schmidt Ullrich, R., Mikkelsen, R. and Dent, P., 1998, Inhibition of the mitogen activated protein (MAP) kinase cascade potentiates cell killing by low dose ionizing radiation in A431 human squamous carcinoma cells. *Oncogene*, **16,** 2787-96 issn: 0950-9232.

50 Cassoni, A.M., McMillan, T.J., Peacock, J.H. and Steel, G.G., 1992, Differences in the level of DNA double-strand breaks in human tumour cell lines following low dose-rate irradiation. *European Journal of Cancer*, **28a,** 1610-4.

51 Chadwick, K.H. and Leenhouts, H.P., 1973, A molecular theory of cell survival. *Physics in Medicine and Biology*, **18,** 78-87.

52 Chadwick, K.H. and Leenhouts, H.P., 1975, The effect of an asynchronous population of cells on the initial slope of dose-effect curves. In: *Cell Survival After Low Doses of Radiation: Theoretical and Clinical Implications.* Edited by: T. Alper. (The Institute of Physics and John Wiley & Sons, London), pp. 57-63.

53 Chadwick, K.H. and Leenhouts, H.P., 1978, The rejoining of DNA double-strand breaks and a model for the formation of chromosomal rearrangements. *International Journal of Radiation Biology*, **33,** 517-529.

54 Chavaudra, N., Halimi, M., Parmentier, C., Gaillard, N., Grinfeld, S. and Malaise, E.P., 1989, The initial slope of human tumor cell survival curves: its modification by the oxic cell sensitizer beta-arabinofuranosyladenine. *International Journal of Radiation Oncology Biology Physics*, **16,** 1267-71.

55 Chen, C.Z., Huang, Y., Hall, E.J. and Brenner, D.J., 1997, Pulsed brachytherapy as a substitute for continuous low dose rate: an in vitro study with human carcinoma cells [see comments]. *Int J Radiat Oncol Biol Phys*, **37,** 137-43.

56 Chernikova, S.B., Wells, R.L. and Elkind, M.M., 1999, Wortmannin sensitizes mammalian cells to radiation by inhibiting the DNA-dependent protein kinase-mediated rejoining of double-strand breaks. *Radiation Research*, **151,** 159-166.

57 Chiu, S.M., Xue, L.Y., Friedman, L.R. and Oleinick, N.L., 1992, Chromatin compaction and the efficiency of formation of DNA-protein crosslinks in γ-irradiated mammalian cells. *Radiation Research*, **129,** 184-191.

58 Chmelevsky, D., Kellerer, A.M., Land, C.E., Mays, C.W. and Spiess, H., 1988, Time and dose dependency of bone-sarcomas in patients injected with radium-224. *Radiation and Environmental Biophysics*, **27,** 103-14.

59 Chresta, C.M., Arriola, E.L. and Hickman, J.A., 1996, Apoptosis and cancer chemotherapy. *Behring Inst Mitt*, **97,** 232-40.

60 Chuang, Y. and Liber, H.L. "Cell cycle effcts on x-ray mutagenesis at the thymine kinase locus in human lymphoblastoid cell line." In 43rd Annual meeting of the Radiation Research Society in San Jose, CA., Year.

61 Cohen, B.L., 1994, Dose-response relationship for radiation carcinogenesis in the low-dose region. *Int Arch Occup Environ Health*, **66,** 71-5.

62 Cohen-Jonathan, E., Bernhard, E.J. and McKenna, W.G., 1999, How does radiation kill cells? *Curr. Opin. Chem. Biol.*, **3,** 77–83.

63 Coleman, M.P., Esteve, J., Damiecki, P., Arslan, A. and Renard, H., 1993, Trends in cancer incidence and mortality. *IARC Sci Publ*, **121,** 1-806.

64 Colussi, N. and Lohman, P.H., 1997, Low dose-rate X-irradiation induces larger deletions at the human HPRT locus than high dose-rate X-irradiation. *International Journal of Radiation Biology*, **72,** 531-6.

65 Colussi, N., van Leeuwen, X. and Lohman, P.H., 1998, Similar mutational spectra in the HPRT gene of human and hamster cell lines after exposure to either low dose rate or high dose rate X-rays. *Mutation Research*, **401,** 89-97.

66 Coquerelle, T.M., Weibezahn, K.F. and Lucke Huhle, C., 1987, Rejoining of double strand breaks in normal human and ataxia-telangiectasia fibroblasts after exposure to 60Co gamma-rays, 241Am alpha-particles or bleomycin. *International Journal of Radiation Biology*, **51,** 209-18.

67 Cortes, F., Dominguez, I., Pinero, J. and Mateos, J.C., 1990, Adaptive response in human lymphocytes conditioned with hydrogen peroxide before irradiation with X-rays. *Mutagenesis*, **5,** 555-7.

68 Cox, R., 1982, A cellular description of the repair deficient ataxia-telangiectasia. In: *A cellular and molecular link between cancer, neuropathology and immune deficiency*. Edited by: B. A. B. a. D. G. Harden. (Wiley, Chichester), pp. 141-153.

69 Critchlow, S.E., Bowater, R.P. and Jackson, S.P., 1997, Mammalian DNA double-strand break repair protein XRCC4 interacts with DNA ligase IV. *Curr Biol*, **7,** 588-598.

70 Crompton, N.E.A., Barth, B. and Kiefer, J., 1990, Inverse Dose-Rate Effect for the Induction of 6-Thioguanine-Resistant Mutants in Chinese Hamster V79 Cells by 60Co gamma Rays. *Rad. Res.*, **124,** 300-308.

71 Crompton, N.E.A., Zoelzer, F., Schneider, E. and Kiefer, J., 1985, Increased mutant induction by very low dose-rate gamma irradiation. *Naturwissenschaften*, **72,** 439-440.

72 Curtis, S.B., 1982, *Lawrence Berkeley Laboratory report LBL-15913*,

73 Dahm Daphi, J., Dikomey, E. and Brammer, I., 1998, DNA-repair, cell killing and normal tissue damage. *Strahlenther Onkol*, **174 Suppl 3,** 8-11.

74 Dahm-Daphi, J., Dikomey, E., Pyttlik, C. and Jeggo, P.A., 1993, Reparable and non-reparable DNA strand breaks induced by X-irradiation in CHO K1 cells and the radiosensitive mutants *xrs1* and *xrs5*. *International Journal of Radiation Biology*, **64,** 19-26.

75 Dale, R.G., Huczkowski, J. and Trott, K.R., 1988, Possible dose rate dependence of recovery kinetics as deduced from a preliminary analysis of the effects of fractionated irradiations at varying dose rates. *British Journal of Radiology*, **61,** 153-7.

76 Darby, S.C. and Doll, R., 1990, Radiation and exposure rate [letter]. *Nature*, **344,** 824.

77 Dasika, G.K., Lin, S.C., Zhao, S., Sung, P., Tomkinson, A. and Lee, E.Y., 1999, DNA damage-induced cell cycle checkpoints and DNA strand break repair in development and tumorigenesis. *Oncogene*, **18,** 7883-99.

78 Dasu, A. and Denekamp, J., 1998, New insights into factors influencing the clinically relevant oxygen enhancement ratio. *Radiotherapy and Oncology*, **46,** 269-77.

79 Dasu, A. and Denekamp, J., 1999, Superfractionation as a potential hypoxic cell radiosensitizer: prediction of an optimum dose per fraction. *International Journal of Radiation Oncology Biology Physics*, **43,** 1083-94.

80 de Pree, C., Popowski, Y., Weber, D., Nouet, P., Rouzaud, M. and Kurtz, J.M., 1999, Feasibility and tolerance of pulsed dose rate interstitial brachytherapy. *Int J Radiat Oncol Biol Phys*, **43,** 971-6.

81 Deacon, J., Peckham, M.J. and Steel, G.G., 1984, The radioresponsiveness of human tumours and the initial slope of the cell survival curve. *Radiotherapy and Oncology*, **2,** 317-23.

82 DeWeese, T.L., Shipman, J.M., Dillehay, L.E. and Nelson, W.G., 1998, Sensitivity of human prostatic carcinoma cell lines to low dose rate radiation exposure. *Journal of Urology*, **159,** 591-8.

83 DeWeese, T.L., Walsh, J.C., Dillehay, L.E., Kessis, T.D., Hedrick, L., Cho, K.R. and Nelson, W.G., 1997, Human papillomavirus E6 and E7 oncoproteins alter cell cycle progression but not radiosensitivity of carcinoma cells treated with low-dose-rate radiation. *International Journal of Radiation Oncology Biology Physics*, **37,** 145-54.

84 Dillehay, L.E., Chang, G. and Williams, J.R., 1988, Effects of methylxanthines on cell-cycle redistribution and sensitization to killing by low-dose-rate radiation. *NCI Monographs*, **6,** 173-6.

85 Douglas, B.G. and Fowler, J.F., 1975, Fractionation schedules and a quadratic dose effect relationship. **48,** 502-504.

86 Durand, R.E., 1986, Use of a cell sorter for assays of cell clonogenicity. *Cancer Research*, **46,** 2775-8.

87 Eckardt Schupp, F. and Klaus, C., 1999, Radiation inducible DNA repair processes in eukaryotes. *Biochimie*, **81,** 161-71.

88 Edwards, S.M., Kent, C.R., McMillan, T.J. and Steel, G.G., 1997, Hprt- mutation spectrum in a closely related pair of human bladder tumour cell lines after gamma-irradiation at different dose-rates. *International Journal of Radiation Biology*, **71,** 177-84.

89 Ehmann, U.K., Williams, J.R., Nagle, W.A., Brown, J.A., Belli, J.A. and Lett, J.T., 1975, Perturbations in cell cycle progression from radioactive DNA precursors. *Nature*, **258,** 633-6.

90 Elia, M.C. and Bradley, M.O., 1992, Influence of chromatin structure on the induction of DNA double strand breaks by ionising radiation. *Cancer Research*, **52,** 1580-1586.

91 Elkind, M.M., Sutton, H., 1959, X-ray damage and recovery in mammalian cells in culture. *Nature*, **184,** 1293–1295.

92 Elkind, M.M., Whitmore, G.F., 1967, *The Radiobiology of cultured mammalian cells.* (Gordon and Breach, New York).

93 Elkind, M.M., 1991, Physical, biophysical, and cell-biological factors that can contribute to enhanced neoplastic transformation by fission-spectrum neutrons. *Radiation Research*, **128,** S47-52.

94 Elkind, M.M., 1994, Enhanced tumorigenesis by small, protracted doses of densely ionizing radiation. *Chin Med J Engl*, **107,** 414-9.

95 Elkind, M.M., Sutton-Gilbert, H., Moses, W.B., Alescio, T. and Swain, R.W., 1965, Radiation response of mammalian cells grown in culture. *Radiat. Res.*, **25,** 359-376.

96 Eriksson, G., 1963, Induction of waxy mutants in maize by acute and chronic gamma irradiation. *Hereditas.*, **50,** 161–178.

97 Esche, B.A., Haie, C.M., Gerbaulet, A.P., Eschwege, F., Richard, J.M. and Chassagne, D., 1988, Interstitial and external radiotherapy in carcinoma of the soft palate and uvula. *Int J Radiat Oncol Biol Phys*, **15,** 619-25.

98 Evans, H.H., Horng, M.F., Mencl, J., Glazier, K.G. and Beer, J.Z., 1985, The influence of dose rate on the lethal and mutagenic effects of X-rays in

proliferating L5178Y cells differing in radiation sensitivity. *International Journal of Radiation Biology*, **47,** 553-62.

99 Feldmann, H. and Winnacker, E.L., 1993, A putative homologue of the human autoantigen Ku from Saccharomyces cerevisiae. *Journal of Biological Chemistry*, **268,** 12895-900.

100 Fertil, B. and Malaise, E.P., 1981, Inherent cellular radiosensitivity as a basic concept for human tumor radiotherapy. *International Journal of Radiation Oncology Biology Physics*, **7,** 621-9.

101 Fertil, B. and Malaise, E.P., 1985, Intrinsic radiosensitivity of human cell lines is correlated with radioresponsiveness of human tumors: analysis of 101 published survival curves. *International Journal of Radiation Oncology Biology Physics*, **11,** 1699-707.

102 Foray, N., Arlett, C.F. and Malaise, E.P., 1997a, Radiation-induced DNA double-strand breaks and the radiosensitivity of human cells: a closer look. *Biochimie*, **79,** 567-75.

103 Foray, N., Priestley, A., Alsbeih, G., Badie, C., Capulas, E.P., Arlett, C.F. and Malaise, E.P., 1997b, Hypersensitivity of ataxia telangiectasia fibroblasts to ionizing radiation is associated with a repair deficiency of DNA double-strand breaks. *International Journal of Radiation Biology*, **72,** 271-83.

104 Fowler, J. and Mount, M., 1992, Pulsed brachytherapy: the conditions for no significant loss of therapeutic ratio compared with traditional low dose rate brachytherapy. *Int J Radiat Oncol Biol Phys*, **23,** 661-9.

105 Fowler, J.F., 1989, The linear-quadratic formula and progress in fractionated radiotherapy. *British Journal of Radiology*, **62,** 679-94.

106 Fowler, J.F., 1993, Why shorter half-times of repair lead to greater damage in pulsed brachytherapy [see comments]. *Int J Radiat Oncol Biol Phys*, **26,** 353-6.

107 Fradet, Y., Meyer, F., Bairati, I., Shadmani, R. and Moore, L., 1999, Dietary fat and prostate cancer progression and survival. *Eur Urol*, **35,** 388-91.

108 Frindel, E., Hahn, G.M., Robaglia, D. and Tubiana, M., 1972, Responses of bone marrow and tumor cells to acute and protracted irradiation. *Cancer Research*, **32,** 2096-103.

109 Fritz, P., Berns, C., Anton, H.W., Hensley, F., Assman, J., Flentje, M., von Fournier, D. and Wannenmacher, M., 1997, PDR brachytherapy with flexible implants for interstitial boost after breast-conserving surgery and external beam radiation therapy. *Radiother Oncol*, **45,** 23-32.

110 Fritz, P., Hensley, F.W., Berns, W. and Wannemacher, M., 1995, Effectiveness and sequelae of pulsed brachytherapy on human skin. *In: International*

brachytherapy, programme and abstracts of 8th international brachytherapy conference at Nice. Veenendaal, Netherlands: Nucletron–Odelft, 151–152.

111 Fu, K.K., Lam, K.N. and Rayner, P.A., 1985, The influence of time sequence of cisplatin administration and continuous low dose rate irradiation (CLDRI) on their combined effects on a murine squamous cell carcinoma. *International Journal of Radiation Oncology Biology Physics*, **11,** 2119-24.

112 Fu, K.K., Rayner, P.A. and Lam, K.N., 1984, Modification of the effects of continuous low dose rate irradiation by concurrent chemotherapy infusion. *International Journal of Radiation Oncology Biology Physics*, **10,** 1473-8.

113 Furre, T., Koritzinsky, M., Olsen, D.R. and Pettersen, E.O., 1999, Inverse dose-rate effect due to pre-mitotic accumulation during continuous low dose-rate irradiation of cervix carcinoma cells. *International Journal of Radiation Biology*, **75,** 699-707.

114 Furuno Fukushi, I., Tatsumi, K., Takahagi, M. and Tachibana, A., 1996, Quantitative and qualitative effect of gamma-ray dose-rate on mutagenesis in human lymphoblastoid cells. *International Journal of Radiation Biology*, **70,** 209-17.

115 Gaddis, O., Jr., Morrow, C.P., Klement, V., Schlaerth, J.B. and Nalick, R.H., 1983, Treatment of cervical carcinoma employing a template for transperineal interstitial Ir192 brachytherapy. *Int J Radiat Oncol Biol Phys*, **9,** 819-27.

116 Gaspar, L.E., Winter, K., Kocha, W.I., Coia, L.R., Herskovic, A. and Graham, M., 2000, A phase I/II study of external beam radiation, brachytherapy, and concurrent chemotherapy for patients with localized carcinoma of the esophagus (Radiation Therapy Oncology Group Study 9207): final report. *Cancer*, **88,** 988-95.

117 Geara, F.B., Peters, L.J., Ang, K.K., Wike, J.L., Sivon, S.S., Guttenberger, R., Callender, D.L., Malaise, E.P. and Brock, W.A., 1992, Intrinsic radiosensitivity of normal human fibroblasts and lymphocytes after high- and low-dose-rate irradiation. *Cancer Research*, **52,** 6348-52.

118 Gentner, N.E., 1992, Increased definition of abnormal radiosensitivity using low-dose rate testing. *Adv. Radiat. Biol.*, **16,** 293–302.

119 Gerweck, L.E. and Zaidi, S.T., 1996, The reproducibility and relationship between single and fractionated dose estimates of the surviving fraction at 2 Gy. *International Journal of Radiation Oncology Biology Physics*, **35,** 81-7.

120 Getts, R.C. and Stamato, T.D., 1994, Absence of a Ku-like DNA end binding activity in the xrs double-strand DNA repair-deficient mutant. *Journal of Biological Chemistry*, **269,** 15981-15984.

121 Giaccia, A.J., Schwartz, J., Shieh, J. and Brown, J.M., 1992, The use of asymmetric-field inversion gel electrophoresis to predict tumor cell radiosensitivity. *Radiotherapy and Oncology*, **24,** 231-8.

122 Gilbertz, K.P., Van Beuningen, D. and Rhein, A.P., 1998, Early changes in cell cycle kinetics after ionizing irradiation below 1 GY. *International Journal of Radiation Biology*, **73,** 187-95.

123 Girinsky, T., Bernheim, A., Lubin, R., Tavakoli Razavi, T., Baker, F., Janot, F., Wibault, P., Cosset, J.M., Duvillard, P., Duverger, A. and et al., 1994, In vitro parameters and treatment outcome in head and neck cancers treated with surgery and/or radiation: cell characterization and correlations with local control and overall survival. *International Journal of Radiation Oncology Biology Physics*, **30,** 789-94.

124 Gleason, D.F., 1966, Classification of prostatic carcinomas. *Cancer Chemother Rep*, **50,** 125-8.

125 Gleason, D.F., 1992, Histologic grading of prostate cancer: a perspective. *Hum Pathol*, **23,** 273-9.

126 Goodhead, D.T., 1982, An assessment of the role of microdosimetry in radiobiology. *Radiation Research*, **91,** 45-76.

127 Grant, W.B., 1999, An ecologic study of dietary links to prostate cancer. *Altern Med Rev*, **4,** 162-9.

128 Gray, L.H. and Scholes, M.E., 1951, The effect of ionising radiations on the broad bean root. Part VIII; Growth rate studies and histological analysis. *Br. J. Radiol.*, **24,** 285–291.

129 Gu, Y., Jin, S., Gao, Y., Weaver, D.T. and Alt, F.W., 1997, Ku70-deficient embryonic stem cells have increased ionizing radiosensitivity, defective DNA end-binding activity, and inability to support V(D)J recombination. *Proceedings of the National Academy of Sciences USA*, **94,** 8076-8081.

130 Guillouf, C., Rosselli, F., Krishnaraju, K., Moustacchi, E., Hoffman, B. and Liebermann, D.A., 1995, p53 involvement in control of G2 exit of the cell cycle: role in DNA damage-induced apoptosis. *Oncogene*, **10,** 2263-70.

131 Hahnfeldt, P. and Hlatky, L., 1996, Resensitization due to redistribution of cells in the phases of the cell cycle during arbitrary radiation protocols. *Radiation Research*, **145,** 134-43.

132 Hahnfeldt, P. and Hlatky, L., 1998, Cell resensitization during protracted dosing of heterogeneous cell populations. *Radiation Research*, **150,** 681-7.

133 Hall, E.J., Bedford J.S.,, 1964, Dose Rate: Its Effect on the Survival of HeLa Cells Irradiated with Gamma Rays. *Radiat. Res.*, **22,** 305–315.

134 Hall, E.J., 1994, Radiobiology for the Radiologist. *Philadelphia*, **4 ed.,**

135 Hall, E.J. and Brenner, D.J., 1992, The dose-rate effect in interstitial brachytherapy: a controversy resolved. *Br J Radiol*, **65,** 242-7.

136 Hall, E.J., Miller, R.C. and Brenner, D.J., 1991, Neoplastic transformation and the inverse dose-rate effect for neutrons. *Radiation Research*, **128,** S75-80.

137 Han, A., Hill, C.K. and Elkind, M.M., 1980, Repair of cell killing and neoplastic transformation at reduced dose rates of 60Co gamma-rays. *Cancer Research*, **40,** 3328-32.

138 Harris, E.E.R., Kao, G.D., Muschel, R.J. and McKenna, W.G., 1998, Potential applications of cell-cycle manipulation to clinical response. *Cancer Treat. Res.*, **93,** 169—190.

139 Hartwell, L.H. and Kastan, M.B., 1994, Cell cycle control and cancer. *Science*, **266,** 1821-8.

140 Haynes, R.H., Eckardt, F. and Kunz, B.A., 1984, The DNA damage-repair hypothesis in radiation biology: comparison with classical hit theory. *British Journal of Cancer*, **6,** 81-90.

141 Heiskanen, M., Karhu, R., Hellsten, E., Peltonen, L., Kallioniemi, O.P. and Palotie, A., 1994, High resolution mapping using fluorescence in situ hybridisation to extended DNA fibers prepared from agarose-embedded cells. *Biotechniques*, **17,** 928-933.

142 Hendrickson, E.A., 1997, Cell-cycle regulation of mammalian DNA double-strand-break repair. *American Journal of Human Genetics*, **61,** 795-800.

143 Hendry, J.H., 1986, Radioresistance induced in fern spores by prior irradiation. *Radiat. Res.*, **106,** 396–400.

144 Henkelman, R.M., Lam, G.K., Kornelsen, R.O. and Eaves, C.J., 1980, Explanation of dose-rate and split-dose effects on mouse foot reactions using the same time factor. *Radiation Research*, **84,** 276-89.

145 Henshaw, P.S., Henshaw, C.T. and Francis, D.T., 1933, Action of X-rays on *Arbacia* eggs. *Radiology*, **21,** 533.

146 Herring, C.J., West, C.M., Wilks, D.P., Davidson, S.E., Hunter, R.D., Berry, P., Forster, G., MacKinnon, J., Rafferty, J.A., Elder, R.H., Hendry, J.H. and Margison, G.P., 1998, Levels of the DNA repair enzyme human apurinic/apyrimidinic endonuclease (APE1, APEX, Ref-1) are associated with the intrinsic radiosensitivity of cervical cancers. *British Journal of Cancer*, **78,** 1128-33.

147 Higashikubo, R., Ragouzis, M. and Roti Roti, J.L., 1996, Flow cytometric BrdUrd-pulse-chase study of X-ray-induced alterations in cell cycle progression. *Cell Proliferation*, **29,** 43-57.

148 Hill, C.K., Buonaguro, F.M., Myers, C.P., Han, A. and Elkind, M.M., 1982, Fission-spectrum neutrons at reduced dose rates enhance neoplastic transformation. *Nature*, **298,** 67-9.

149 Hill, C.K., Carnes, B.A., Han, A. and Elkind, M.M., 1985, Neoplastic transformation is enhanced by multiple low doses of fission-spectrum neutrons. *Radiation Research*, **102,** 404-10.

150 Hill, C.K., Han, A. and Elkind, M.M., 1984, Fission-spectrum neutrons at a low dose rate enhance neoplastic transformation in the linear, low dose region (0-10 cGy). *International Journal of Radiation Biology*, **46,** 11-5.

151 Hillova, J. and Drasil, V., 1967, The inhibitory effect of iodoacetamide on recovery from sub-lethal damage in Chlamydomonas reinhardti. *International Journal of Radiation Biology*, **12,** 201-8.

152 Hlatky, L., Van Buren, T. and Hahnfeldt, P., 1995, Quantifying intracellular radioresponse diversity in irradiated sandwich cultures via micronucleus expression. *International Journal of Radiation Biology*, **67,** 541-8.

153 Hlatky, L.R., Hahnfeldt, P. and Sachs, R.K., 1994, Influence of time-dependent stochastic heterogeneity on the radiation response of a cell population. *Math Biosci*, **122,** 201-20.

154 Holm, H.H., Juul, N., Pedersen, J.F., Hansen, H. and Stroyer, I., 1983, Transperineal 125iodine seed implantation in prostatic cancer guided by transrectal ultrasonography. *J Urol*, **130,** 283-6.

155 Hornung, R.W. and Meinhardt, T.J., 1987, Quantitative risk assessment of lung cancer in U.S. uranium miners. *Health Physics*, **52,** 417-30.

156 Horsley, R.J. and Laszlo, A., 1971, Unexpected additional recovery following a first x-ray dose to a synchronous cell culture. *International Journal of Radiation Biology*, **20,** 593-6.

157 Horsley, R.J. and Pujara, C.M., 1969, Study of the inflexion of x-radiation survival curves for synchronized cell populations of the green alga (Oedogonium cardiacum). *Radiation Research*, **40,** 440-9.

158 Howard, A. and Cowie, F.G., 1976, Induced resistance in a desmid Closterium moniliferum. *Radiation Research*, **65,** 540-9 Issn: 0033-7587.

159 Howard, A. and Cowie, F.G., 1978, Induced resistance in Closterium: indirect evidence for the induction of repair enzyme. *Radiation Research*, **75,** 607-16 Issn: 0033-7587.

160 Howard, A. and Pelc, S.R., 1953, Nuclear incorporation of ^{32}P as demonstrated by autoradiographs. *Exp. Cell. Res.*, **2,** 178—187.

161 Hu, Q. and Hill, R.P., 1996, Radiosensitivity, apoptosis and repair of DNA double-strand breaks in radiation-sensitive Chinese hamster ovary cell mutants treated at different dose rates. *Radiation Research*, **146,** 636-45.

162 Huang, H. and Claycamp, H.G., 1993, DNA excision repair as a component of adaptation to low doses of ionizing radiation in Escherichia coli. *International Journal of Radiation Biology*, **64,** 613-9.

163 Ikushima, T., 1987, Chromosomal responses to ionizing radiation reminiscent of an adaptive response in cultured Chinese hamster cells. *Mutation Research*, **180,** 215-21.

164 Iliakis, G., 1991, The role of DNA double strand breaks in ionizing radiation-induced killing of eukaryotic cells. *Bioessays*, **13,** 641-8 issn: 0265-9247.

165 Iliakis, G., 1997, Cell cycle regulation in irradiated and nonirradiated cells. *Seminars in Oncology*, **24,** 602-15.

166 Iliakis, G., Okayasu, R., Varlotto, J., Shernoff, C. and Wang, Y., 1993, Hypertonic treatment during premature chromosome condensation allows visualization of interphase chromosome breaks repaired with fast kinetics in irradiated CHO cells. *Radiation Research*, **135,** 160-170.

167 Inoue, T., Inoue, T., Yoshida, K., Yoshinoka, Y., Shgimamoto, S. and Yamazaki, H., 2000, Phase III trial of HDR versus LDR interstitial brachytherapy as monotherapy for early carcinoma of the mobile tongue. *Radiotherapy Oncology*, **55,** 19.

168 Inoue, T., Teshima, T., Murayama, S., Shimizutani, K., Fuchihata, H. and Furukawa, S., 1996, Phase III trial of high and low dose rate interstitial radiotherapy for early oral tongue cancer. *Int J Radiat Oncol Biol Phys*, **36,** 1201-4.

169 Inoue, T., Yamazaki, H., Koizumi, M., Kagawa, K., Yoshida, K., Shiomi, H., Imai, A., Shimizutani, K., Tanaka, E., Nose, T., Teshima, T., Furukawa, S. and Fuchihata, H., 1998, High dose rate versus low dose rate interstitial radiotherapy for carcinoma of the floor of mouth. *Int J Radiat Oncol Biol Phys*, **41,** 53-8.

170 Isaacs, W.B., Carter, B.S. and Ewing, C.M., 1991, Wild-type p53 suppresses growth of human prostate cancer cells containing mutant p53 alleles. *Cancer Research*, **51,** 4716-20.

171 Israel, K., Sanders, B.G. and Kline, K., 1995, RRR-alpha-tocopheryl succinate inhibits the proliferation of human prostatic tumor cells with defective cell cycle/differentiation pathways. *Nutr Cancer*, **24,** 161-9.

172 Jackson, S.P. and Jeggo, P.A., 1995, DNA double-strand break repair and V(D)J recombination: involvement of DNA-PK. *Trends-Biochem-Sci*, **20,** 412-5 issn: 0167-7640.

173 Jeggo, P.A., 1997, DNA-PK: at the cross-roads of biochemistry and genetics. *Mutation Research*, **384,** 1-14.

174 Jeggo, P.A., 1998, Identification of genes involved in repair of DNA double-strand breaks in mammalian cells. *Radiation Research*, **150,** S80-91.

175 Joiner, M.C., Denekamp, J. and Maughan, R.L., 1986, The use of 'top-up' experiments to investigate the effect of very small doses per fraction in mouse skin. *International Journal of Radiation Biology*, **49,** 565-80.

176 Joiner, M.C. and Johns, H., 1988, Renal damage in the mouse: the response to very small doses per fraction. *Radiation Research*, **114,** 385-98.

177 Joiner, M.C., Lambin, P., Malaise, E.P., Robson, T., Arrand, J.E., Skov, K.A. and Marples, B., 1996, Hypersensitivity to very-low single radiation doses: its relationship to the adaptive response and induced radioresistance. *Mutation Research*, **358,** 171-83.

178 Joiner, M.C. and Marples, B., 1992, Does induced repair determine the lethal effects of very low radiation doses? *BJR Suppl*, **24,** 74-8.

179 Jones, C.A., Sedita, B.A., Hill, C.K. and Elkind, M.M., 1989, Influence of dose rate on the transformation of Syrian hamster embryo cells by fission-spectrum neutrons. In: *Low Dose Radiation, Biological Bases of Risk Assessment.* Edited by: K. F. Baverstock and J. W. Stather. (Taylor & Francis, London), pp. 539–546.

180 Jones, L.A., Scott, D., Cowan, R. and Roberts, S.A., 1995, Abnormal radiosensitivity of lymphocytes from breast cancer patients with excessive normal tissue damage after radiotherapy: chromosome aberrations after low dose-rate irradiation. *International Journal of Radiation Biology*, **67,** 519-28.

181 Jostes, R.F., Bushnell, K.M. and Dewey, W.C., 1980, X-ray induction of 8-azaguanine-resistant mutants in synchronous Chinese hamster ovary cells. *Radiation Research*, **83,** 146-61.

182 Kal, H.B., Barendsen, G.W., Hauwe, R.B. and Roelse, H., 1975, Increased radiosensitivity of rat rhabdomyosarcoma cells induced by protracted irradiation. *Radiation Research*, **63,** 521-30.

183 Kamiya, K., Yasukawa Barnes, J., Mitchen, J.M., Gould, M.N. and Clifton, K.H., 1995, Evidence that carcinogenesis involves an imbalance between epigenetic high-frequency initiation and suppression of promotion. *Proceedings of the National Academy of Sciences USA*, **92,** 1332-6.

184 Karn, J., Watson, J.V., Lowe, A.D., Green, S.M. and Vedeckis, W., 1989, Regulation of cell cycle duration by c-myc levels. *Oncogene*, **4,** 773-87.

185 Kastan, M.B. and Kuerbitz, S.J., 1993, Control of G1 arrest after DNA damage. *Environ Health Perspect*, **101 Suppl 5,** 55-8.

186 Kastan, M.B., Onyekwere, O., Sidransky, D., Vogelstein, B. and Craig, R.W., 1991, Participation of p53 protein in the cellular response to DNA damage. *Cancer Research*, **51,** 6304-11.

187 Kastan, M.B., Zhan, Q., el Deiry, W.S., Carrier, F., Jacks, T., Walsh, W.V., Plunkett, B.S., Vogelstein, B. and Fornace, A.J., Jr., 1992, A mammalian cell cycle checkpoint pathway utilizing p53 and GADD45 is defective in ataxia-telangiectasia. *Cell*, **71,** 587-97.

188 Kasten, U., Borgmann, K., Burgmann, P., Li, G. and Dikomey, E., 1999, Overexpression of human Ku70/Ku80 in rat cells resulting in reduced DSB repair capacity with appropriate increase in cell radiosensitivity but with no effect on cell recovery. *Radiation Research*, **151,** 532-9.

189 Kaufmann, W.K. and Paules, R.S., 1996, DNA damage and cell cycle checkpoints. *Faseb J*, **10,** 238-47.

190 Kaye, S.B., Lewis, C.R., Paul, J., Duncan, I.D., Gordon, H.K., Kitchener, H.C., Cruickshank, D.J., Atkinson, R.J., Soukop, M., Rankin, E.M. and et al., 1992, Randomised study of two doses of cisplatin with cyclophosphamide in epithelial ovarian cancer [see comments]. *Lancet*, **340,** 329-33.

191 Kelland, L.R., Burgess, L. and Steel, G.G., 1988a, Differential radiosensitization by the poly(ADP-ribose) transferase inhibitor 3-aminobenzamide in human tumor cells of varying radiosensitivity. *International Journal of Radiation Oncology Biology Physics*, **14,** 1239-46.

192 Kelland, L.R., Burgess, L. and Steel, G.G., 1988b, Inhibition of radiation dose-rate-sparing effects in human tumor cells by 3-aminobenzamide. *NCI Monographs*, **6,** 167-71.

193 Kelland, L.R., Edwards, S.M. and Steel, G.G., 1988c, Induction and rejoining of DNA double-strand breaks in human cervix carcinoma cell lines of differing radiosensitivity. *Radiation Research*, **116,** 526-38.

194 Kelland, L.R. and Steel, G.G., 1988a, Differences in radiation response among human cervix carcinoma cell lines. *Radiotherapy and Oncology*, **13,** 225-32.

195 Kelland, L.R. and Steel, G.G., 1988b, Inhibition of recovery from damage induced by ionizing radiation in mammalian cells. *Radiotherapy and Oncology*, **13,** 285-99.

196 Kelland, L.R. and Steel, G.G., 1988c, Modification of radiation dose-rate sparing effects in a human carcinoma of the cervix cell line by inhibitors of DNA repair. *International Journal of Radiation Biology*, **54,** 229-44.

197 Kelland, L.R. and Steel, G.G., 1989, Recovery from radiation damage in human squamous carcinoma of the cervix. *International Journal of Radiation Biology*, **55,** 119-27.

198 Kelland, L.R. and Tonkin, K.S., 1989, The effect of 3-aminobenzamide in the radiation response of three human cervix carcinoma xenografts. *Radiotherapy and Oncology*, **15,** 363-9.

199 Kellerer, A. and Rossi, H.H., 1972, A generalised formulation of dual radiation action. *Radiat. Res.*, **75,** 471-488.

200 Kellerer, A.M. and Rossi, H.H., 1978, A generalized formulation of dual radiation action. **75,** 471-488.

201 Kemp, L.M., Sedgwick, S.G. and Jeggo, P.A., 1984, X-ray sensitive mutants of Chinese hamster ovary cells defective in double-strand break rejoining. *Mutation Research*, **132,** 189-96.

202 Kennedy, A.R., 1985, Evidence that the first step leading to carcinogen-induced malignant transformation is a high frequency, common event. *Carcinog Compr Surv*, **9,** 355-64.

203 Kiltie, A.E., Orton, C.J., Ryan, A.J., Roberts, S.A., Marples, B., Davidson, S.E., Hunter, R.D., Margison, G.P., West, C.M. and Hendry, J.H., 1997, A correlation between residual DNA double-strand breaks and clonogenic measurements of radiosensitivity in fibroblasts from preradiotherapy cervix cancer patients. *International Journal of Radiation Oncology Biology Physics*, **39,** 1137-44.

204 Kiser, G.L. and Weinert, T.A., 1996, Distinct roles of yeast MEC and RAD checkpoint genes in transcriptional induction after DNA damage and implications for function. *Mol Biol Cell*, **7,** 703-18.

205 Knox, S.J., Sutherland, W. and Goris, M.L., 1993, Correlation of tumor sensitivity to low-dose-rate irradiation with G2/M-phase block and other radiobiological parameters [published erratum appears in Radiat Res 1993 Dec;136(3):439]. *Radiation Research*, **135,** 24-31.

206 Kolman, A. and Harms Ringdahl, M., 1996, Radiation-induced neoplastic transformation of stationary phase C3H/10T1/2 cells in response to different dose rates and to post-irradiation treatment with tumor promoter. *Chem Biol Interact*, **101,** 59-69.

207 Komatsu, K., Sawada, S., Takeoka, S., Kodama, S. and Okumura, Y., 1993, Dose-rate effects of neutrons and gamma-rays on the induction of mutation and

oncogenic transformation in plateau-phase mouse m5S cells. *International Journal of Radiation Biology*, **63,** 469-74.

208 Koval, T.M., 1984, Multiphasic survival response of a radioresistant lepidopteran insect cell line. *Radiation Research*, **98,** 642-8.

209 Koval, T.M., 1988, Enhanced recovery from ionizing radiation damage in a lepidopteran insect cell line. *Radiation Research*, **115,** 413-20.

210 Kruszewski, M., Wojewodzka, M., Iwanenko, T., Szumiel, I. and Okuyama, A., 1998, Differential inhibitory effect of OK-1035 on DNA repair in L5178Y murine lymphoma sublines with functional or defective repair of double strand breaks. *Mutation Research*, **409,** 31-36.

211 Kubota, N. and Hill, C.K., 1989, Dose rate effect of fission-spectrum neutrons on mutation induction in chinese hamster cells and human diploid fibroblasts. *Sci. Pap. Inst. Phys. Chem. Res.*, **83,** 25–30.

212 Kuerbitz, S.J., Plunkett, B.S., Walsh, W.V. and Kastan, M.B., 1992, Wild-type p53 is a cell cycle checkpoint determinant following irradiation. *Proceedings of the National Academy of Sciences USA*, **89,** 7491-5.

213 Kumaravel, T.S., Bharathy, K., Kudoh, S., Tanaka, K. and Kamada, N., 1998, Expression, localization and functional interactions of Ku70 subunit of DNA-PK in peripheral lymphocytes and Nalm-19 cells after irradiation. *Int-J-Radiat-Biol*, **74,** 481-9 issn: 0955-3002.

214 Kunz, B.A., Eckardt, F. and Haynes, R.H., 1985, Analysis of non-linearities in frequency curves for UV-induced mitotic recombination in wild-type and excision-repair-deficient strains of yeast. *Mutation Research*, **151,** 235-42.

215 Kysela, B.P., Michael, B.D. and Arrand, J.E., 1993, Relative contributions of levels of initial DNA damage and repair of double strand breaks to the ionizing radiation-sensitive phenotype of the Chinese hamster cell mutant, XR-V15B. Part I. X-rays. *International Journal of Radiation Biology*, **63,** 609-16.

216 Labhart, P., 1999, Nonhomologous DNA end joining in cell-free systems. *European Journal of Biochemistry*, **265,** 849-61.

217 Lajtha, L.G., Oliver, R., 1961, Some radiobiological considerations in radiotherapy. *Br. J. Radiol.*, **34,** 252–257.

218 Lambin, P., Cederval, B., Chavaudra, N., Badie, C., Joiner, M.C. and Malaise, E.P., 1992, Initial and residual number of X-ray induced DNA double-strand breaks in radiosensitive and radioresistant human tumour cell lines. *Radiother. Oncol.*, **25,** S51.

219 Lambin, P., Gerbaulet, A., Kramar, A., Scalliet, P., Haie Meder, C., Michel, G., Prade, M., Bouzy, J., Malaise, E.P. and Chassagne, D., 1994a, A comparison of

early effects with two dose rates in brachytherapy of cervix carcinoma in a prospective randomised trial. *European Journal of Cancer*, **30a,** 312-20.

220 Lambin, P., Malaise, E.P. and Joiner, M.C., 1994b, The effect of very low radiation doses on the human bladder carcinoma cell line RT112. *Radiotherapy and Oncology*, **32,** 63-72.

221 Lambin, P., Malaise, E.P. and Joiner, M.C., 1996, Might intrinsic radioresistance of human tumour cells be induced by radiation? *International Journal of Radiation Biology*, **69,** 279-90 Issn: 0955-3002.

222 Lambin, P., Marples, B., Fertil, B., Malaise, E.P. and Joiner, M.C., 1993, Hypersensitivity of a human tumour cell line to very low radiation doses. *International Journal of Radiation Biology*, **63,** 639-50.

223 Lau, H.Y., Hay, J.H., Flores, A.D. and Threlfall, W.J., 1996, Seven fractions of twice daily high dose-rate brachytherapy for node-negative carcinoma of the mobile tongue results in loss of therapeutic ratio. *Radiother Oncol*, **39,** 15-8.

224 Lavey, R.S., Taylor, J.M., Tward, J.D., Li, L.T., Nguyen, A.A., Chon, Y. and McBride, W.H., 1994, The extent, time course, and fraction size dependence of mouse spinal cord recovery from radiation injury. *Int-J-Radiat-Oncol-Biol-Phys*, **30,** 609-17 issn: 0360-3016.

225 Lee, J.M. and Bernstein, A., 1993, p53 mutations increase resistance to ionizing radiation. *Proceedings of the National Academy of Sciences USA*, **90,** 5742-6.

226 Lee, S.E., Mitchell, R.A., Cheng, A. and Hendrickson, E.A., 1997, Evidence for DNA-PK-dependent and -independent DNA double-strand break repair pathways in mammalian cells as a function of the cell cycle. *Molecular and Cellular Biology*, **17,** 1425-33.

227 Leeper, D.B., Schneiderman, M.H. and Dewey, W.C., 1973, Radiation-induced cycle delay in synchronized Chinese hamster cells: comparison between DNA synthesis and division. *Radiation Research*, **53,** 326-37.

228 Lehmann, A.R., 1995, Nucleotide excision repair and the link with transcription. *Trends Biochem Sci*, **20,** 402-5.

229 Lehmann, A.R., Kirk Bell, S., Arlett, C.F., Harcourt, S.A., de Weerd Kastelein, E.A., Keijzer, W. and Hall Smith, P., 1977, Repair of ultraviolet light damage in a variety of human fibroblast cell strains. *Cancer Research*, **37,** 904-10.

230 Leirdal, M. and Sioud, M., 1999, Ribozyme inhibition of the protein kinase C alpha triggers apoptosis in glioma cells. *British Journal of Cancer*, **80,** 1558-64.

231 Leith, J.T., 1994, In vitro radiation sensitivity of the LNCaP prostatic tumor cell line. *Prostate*, **24,** 119-24.

232 Leith, J.T., Quaranto, L., Padfield, G., Michelson, S. and Hercbergs, A., 1993, Radiobiological studies of PC-3 and DU-145 human prostate cancer cells: x-ray sensitivity in vitro and hypoxic fractions of xenografted tumors in vivo. *International Journal of Radiation Oncology Biology Physics*, **25,** 283-7.

233 Levendag, P.C., Schmitz, P.I., Jansen, P.P., Senan, S., Eijkenboom, W.M., Sipkema, D., Meeuwis, C.A., Kolkman Deurloo, I.K. and Visser, A.G., 1997, Fractionated high-dose-rate and pulsed-dose-rate brachytherapy: first clinical experience in squamous cell carcinoma of the tonsillar fossa and soft palate. *Int J Radiat Oncol Biol Phys*, **38,** 497-506.

234 Lewis, L.K. and Resnick, M.A., 2000, Tying up loose ends: nonhomologous end-joining in Saccharomyces cerevisiae. *Mutation Research*, **451,** 71-89.

235 Li, C., Nagasawa, H., Tsang, N.M. and Little, J.B., 1995, Radiation-induced irreversible G(0)/G(1) block is abolished in human diploid fibroblasts transfected with the human papilloma virus E6 gene: implications of the p53-Cip1/WAF1 pathway. *Int. J. Oncol.*, **6,** 233—236.

236 Lieber, M.R., Grawunder, U., Wu, X. and Yaneva, M., 1997, Tying loose ends: roles of Ku and DNA-dependent protein kinase in the repair of double-strand breaks. *Curr Opin Genet Dev*, **7,** 99-104.

237 Little, J.B., 1990, Low-dose radiation effects: interactions and synergism. *Health Physics*, **59,** 49-55.

238 Little, J.B., Kennedy, A.R. and McGandy, R.B., 1985, Effect of dose rate on the induction of experimental lung cancer in hamsters by alpha radiation. *Radiation Research*, **103,** 293-9.

239 Little, J.B. and Nove, J., 1990, Sensitivity of human diploid fibroblast cell strains from various genetic disorders to acute and protracted radiation exposure. *Radiation Research*, **123,** 87-92.

240 Little, M.P. and Muirhead, C.R., 2000, Derivation of low-dose extrapolation factors from analysis of curvature in the cancer incidence dose response in Japanese atomic bomb survivors. *International Journal of Radiation Biology*, **76,** 939-53.

241 Liversage, W.E., 1969, A general formula for equating protracted and acute regimes of radiation. *British Journal of Radiology*, **42,** 432-40.

242 Lorenz, R., Leuner, K., Deubel, W., Gollner, T. and Hempel, K., 1993, Normal and reverse dose-rate effect for the induction of mutants in somatic cells by ionizing radiation. *Toxicol Lett*, **67,** 353-63.

243 Lubin, J.H., Qiao, Y.L., Taylor, P.R., Yao, S.X., Schatzkin, A., Mao, B.L., Rao, J.Y., Xuan, X.Z. and Li, J.Y., 1990, Quantitative evaluation of the radon and lung

cancer association in a case control study of Chinese tin miners. *Cancer Research*, **50,** 174-80.

244 Lundell, M., Mattsson, A., Karlsson, P., Holmberg, E., Gustafsson, A. and Holm, L.E., 1999, Breast cancer risk after radiotherapy in infancy: a pooled analysis of two Swedish cohorts of 17,202 infants. *Radiation Research*, **151,** 626-32.

245 Macklis, R.M., Beresford, B.A. and Humm, J.L., 1994, Radiobiologic studies of low-dose-rate 90Y-lymphoma therapy. *Cancer*, **73,** 966-73.

246 Malaise, E.P., Fertil, B., Chavaudra, N. and Guichard, M., 1996, Distribution of radiation sensitivites for human tumour cells of specific histological types: comparison of in vitro and in vivo data. *Int. J. Rad. Oncol. Biol. Phys.*, **12,** 617.

247 Malaise, E.P., Fertil, B., Deschavanne, P.J., Chavaudra, N. and Brock, W.A., 1987, Initial slope of radiation survival curves is characteristic of the origin of primary and established cultures of human tumor cells and fibroblasts. *Radiation Research*, **111,** 319-33.

248 Malyapa, R.S., Wright, W.D. and Roti Roti, J.L., 1994, Radiation sensitivity correlates with changes in DNA supercoiling and nucleoid protein content in cells of three Chinese hamster cell lines. *Radiation Research*, **140,** 312-320.

249 Marchese, M.J., Zaider, M. and Hall, E.J., 1987, Dose-rate effects in normal and malignant cells of human origin. *British Journal of Radiology*, **60,** 573-6.

250 Marin, L.A., Smith, C.E., Langston, M.Y., Quashie, D. and Dillehay, L.E., 1991, Response of glioblastoma cell lines to low dose rate irradiation. *International Journal of Radiation Oncology Biology Physics*, **21,** 397-402.

251 Marples, B. and Joiner, M.C., 1993, The response of Chinese hamster V79 cells to low radiation doses: evidence of enhanced sensitivity of the whole cell population. *Radiat-Res*, **133,** 41-51 issn: 0033-7587.

252 Marples, B. and Joiner, M.C., 1995, The elimination of low-dose hypersensitivity in Chinese hamster V79-379A cells by pretreatment with X rays or hydrogen peroxide. *Radiation Research*, **141,** 160-9 Issn: 0033-7587.

253 Marples, B., Joiner, M.C. and Skov, K.A., 1994, The effect of oxygen on low-dose hypersensitivity and increased radioresistance in Chinese hamster V79-379A cells. *Radiation Research*, **138,** S17-20 Issn: 0033-7587.

254 Marples, B., Lambin, P., Skov, K.A. and Joiner, M.C., 1997, Low dose hyper-radiosensitivity and increased radioresistance in mammalian cells. *International Journal of Radiation Biology*, **71,** 721-35 Issn: 0955-3002.

255 Marples, B., Longhurst, D., Eastham, A.M. and West, C.M., 1998, The ratio of initial/residual DNA damage predicts intrinsic radiosensitivity in seven cervix carcinoma cell lines. *British Journal of Cancer*, **77,** 1108-14.

256 Mason, K.A., Thames, H.D., Ochran, T.G., Ruifrok, A.C. and Janjan, N., 1994, Comparison of continuous and pulsed low dose rate brachytherapy: biological equivalence in vivo [see comments]. *Int J Radiat Oncol Biol Phys*, **28,** 667-71.

257 Matthews, R.W., 1973, Effect of solute concentration and temperature on the ceric-cerous dosimeter. *Radiation Research*, **55,** 242-55.

258 Matthews, R.W., Barker, N.T. and Sangster, D.F., 1978, A comparison of some aqueous chemical dosimeters for absorbed doses of less than 1000 rads. *Int J Appl Radiat Isot*, **29,** 1-8.

259 Mazeron, J.J., Simon, J.M., Crook, J., Calitchi, E., Otmezguine, Y., Le Bourgeois, J.P. and Pierquin, B., 1991a, Influence of dose rate on local control of breast carcinoma treated by external beam irradiation plus iridium 192 implant. *Int J Radiat Oncol Biol Phys*, **21,** 1173-7.

260 Mazeron, J.J., Simon, J.M., Le Pechoux, C., Crook, J.M., Grimard, L., Piedbois, P., Le Bourgeois, J.P. and Pierquin, B., 1991b, Effect of dose rate on local control and complications in definitive irradiation of T1-2 squamous cell carcinomas of mobile tongue and floor of mouth with interstitial iridium-192 [see comments]. *Radiother Oncol*, **21,** 39-47.

261 McKelvey-Martin, V.J., Ho, E.T., McKeown, S.R., Johnston, S.R., McCarthy, P.J., Rajab, N.F. and Downes, C.S., 1998, Emerging applications of the single cell gel electrophoresis (Comet) assay. I. Management of invasive transitional cell human bladder carcinoma. II. Fluorescent in situ hybridization Comets for the identification of damaged and repaired DNA sequences in individual cells. *Mutagenesis*, **13,** 1-8.

262 McKenna, W.G., Bernhard, E.J., Markiewicz, D.A., Rudoltz, M.S., Maity, A. and Muschel, R.J., 1996, Regulation of radiation-induced apoptosis in oncogene-transfected fibroblasts: influence of H-ras on the G2 delay. *Oncogene*, **12,** 237-45.

263 McLean, M., 1994, Initial PDR brachytherapy experience at Toronto, Canada. *Activity (Int. Nucletron Radiother. J.)*, **Report no. 5,** 6–10.

264 Meredith, W.S.E., 1967, Radium dosage; The Manchester System,. **2nd edn,** 42.

265 Metzger, L. and Iliakis, G., 1991, Kinetics of DNA double-strand break repair throughout the cell cycle as assayed by pulsed field gel electrophoresis in CHO cells. *International Journal of Radiation Biology*, **59,** 1325-1339.

266 Micheletti, E., La Face, B., Bianchi, E., Cagna, E. and Sartori, E., 1996, [Locally advanced carcinoma of the cervix uteri (stage IIB-IIIB TNM-UICC): radiotherapy combined with simultaneous daily low-dose platinum. Phase II study]. *Radiol Med Torino*, **91,** 628-34.

267 Millar, W.T. and Canney, P.A., 1993a, Derivation and application of equations describing the effects of fractionated protracted irradiation, based on multiple and incomplete repair processes. Part 2. Analysis of mouse lung data. *International Journal of Radiation Biology*, **64,** 293-303.

268 Millar, W.T. and Canney, P.A., 1993b, Derivation and application of equations describing the effects of fractionated protracted irradiation, based on multiple and incomplete repair processes. Part I. Derivation of equations. *International Journal of Radiation Biology*, **64,** 275-91.

269 Miller, R.C., Brenner, D.J., Geard, C.R., Komatsu, K., Marino, S.A. and Hall, E.J., 1988, Oncogenic transformation by fractionated doses of neutrons [published erratum appears in Radiat Res 1988 Dec;116(3):550]. *Radiation Research*, **114,** 589-98.

270 Miller, R.C., Brenner, D.J., Randers Pehrson, G., Marino, S.A. and Hall, E.J., 1990, The effects of the temporal distribution of dose on oncogenic transformation by neutrons and charged particles of intermediate LET. *Radiation Research*, **124,** S62-8.

271 Miller, R.C., Geard, C.R., Brenner, D.J., Komatsu, K., Marino, S.A. and Hall, E.J., 1989, Neutron-energy-dependent oncogenic transformation of C3H 10T1/2 mouse cells. *Radiation Research*, **117,** 114-27.

272 Miller, R.C., Geard, C.R., Geard, M.J. and Hall, E.J., 1992, Cell-cycle-dependent radiation-induced oncogenic transformation of C3H 10T1/2 cells. *Radiation Research*, **130,** 129-33.

273 Miller, R.C., Geard, C.R., Martin, S.G., Marino, S.A. and Hall, E.J., 1995, Neutron-induced cell cycle-dependent oncogenic transformation of C3H 10T1/2 cells. *Radiation Research*, **142,** 270-5.

274 Miller, R.C. and Hall, E.J., 1991, Oncogenic transformation of C3H 10T1/2 cells by acute and protracted exposures to monoenergetic neutrons. *Radiation Research*, **128,** S60-4.

275 Mitchell, J.B., Bedford, J.S., Bailey S.M., 1979, Dose-Rate Effects on the Cell Cycle and Survival of S3 Hela and V79 Cells. *Radiat. Res.*, **79,** 520–536.

276 Mitchell, J.B. and Bedford, J.S., 1977, Dose-rate effects in synchronous mammalian cells in culture. II. A comparison of the life cycle of HeLa cells during continuous irradiation or multiple-dose fractionation. *Radiation Research*, **71,** 547-60.

277 Mitchell, J.B., Bedford, J.S. and Bailey, S.M., 1979a, Dose-rate effects in mammalian cells in culture III. Comparison of cell killing and cell proliferation during continuous irradiation for six different cell lines. *Radiation Research*, **79,** 537-51.

278 Mitchell, J.B., Bedford, J.S. and Bailey, S.M., 1979b, Dose-rate effects in plateau-phase cultures of S3 HeLa and V79 cells. *Radiation Research*, **79,** 552-67.

279 Mitchell, J.B., Russo, A., Cook, J.A., Straus, K.L. and Glatstein, E., 1989, Radiobiology and clinical application of halogenated pyrimidine radiosensitizers. *International Journal of Radiation Biology*, **56,** 827-36.

280 Mitchell, S.A. 1999, The radiation response of human dermal fibroblasts. University of London.

281 Mitchell, S.A., Joiner, M.C., Wilson, G.D. and Lawton, P.A., 2000, Measurement of DNA damage in comparison with clonogenic survival in fibroblasts from control and clinically radiosensitive individuals. *Radiother. Oncol. (in press)*,

282 Morstyn, G., Miller, R., Russo, A. and Mitchell, J., 1984, 131-iodine conjugated antibody cell kill enhanced by bromodeoxyuridine. *International Journal of Radiation Oncology Biology Physics*, **10,** 1437-40.

283 Musk, S.R. and Steel, G.G., 1990, The inhibition of cellular recovery in human tumour cells by inhibitors of topoisomerase. *British Journal of Cancer*, **62,** 364-7.

284 Nackerdien, Z., Michie, J. and Bohm, L., 1989, Chromatin decondensed by acetylation shows an elevated radiation response. *Radiation Research*, **117,** 234-244.

285 Nagasawa, H., Chen, D.J. and Strniste, G.F., 1989, Response of X-ray-sensitive CHO mutant cells to gamma radiation. I. Effects of low dose rates and the process of repair of potentially lethal damage in G1 phase. *Radiation Research*, **118,** 559-67.

286 Nagasawa, H., Keng, P., Harley, R., Dahlberg, W. and Little, J.B., 1994, Relationship between gamma-ray-induced G2/M delay and cellular radiosensitivity. *International Journal of Radiation Biology*, **66,** 373-9.

287 Nagasawa, H., Li, C.Y., Maki, C.G., Imrich, A.C. and Little, J.B., 1995, Relationship between radiation-induced G1 phase arrest and p53 function in human tumor cells. *Cancer Research*, **55,** 1842-6.

288 Natarajan, N., Murphy, G.P. and Mettlin, C., 1989, Prostate cancer in blacks: an update from the American College of Surgeons' patterns of care studies. *J Surg Oncol*, **40,** 232-6.

289 Nias, A.H.W. and Lajtha, L.G., 1964, Continuous irradiation with tritiated water in mammalian cells in a monolayer. *Nature*, **202,** 613–614.

290 Nilsson, P., Thames, H.D. and Joiner, M.C., 1990, A generalized formulation of the 'incomplete-repair' model for cell survival and tissue response to fractionated low dose-rate irradiation. *International Journal of Radiation Biology*, **57,** 127-42.

291 Ning, S. and Knox, S.J., 1999, G2/M-phase arrest and death by apoptosis of HL60 cells irradiated with exponentially decreasing low-dose-rate gamma radiation. *Radiation Research*, **151,** 659-69.

292 Odegaard, E., Yang, C.R. and Boothman, D.A., 1998, DNA-dependent protein kinase does not play a role in adaptive survival responses to ionizing radiation. *Environ Health Perspect*, **1,** 301-5.

293 Okayasu, R., Varlotto, J. and Iliakis, G., 1993, Hypertonic treatment does not affect the radiation yield of interphase chromosome breaks in DNA double-strand break repair-deficient xrs-5 cells. *Radiation Research*, **135,** 171-177.

294 Olive, P.L. and Banath, J.P., 1995, Radiation-induced DNA double-strand breaks produced in histone-depleted tumor cell nuclei measured using the neutral comet assay. *Radiation Research*, **142,** 144-152.

295 Olive, P.L., Banath, J.P. and MacPhail, H.S., 1994, Lack of a correlation between radiosensitivity and DNA double-strand break induction or rejoining in six human tumor cell lines. *Cancer Research*, **54,** 3939-46.

296 Oliver, R., 1964, A comparison of the effects of acute and protracted gamma-radiation on the growth of seedlings of Vicia faba. II. Theoretical Calculations. *International Journal of Radiation Biology*, **8,** 475–488.

297 Olivieri, G., Bodycote, J. and Wolff, S., 1984, Adaptive response of human lymphocytes to low concentrations of radioactive thymidine. *Science*, **223,** 594-7 Issn: 0036-8075.

298 Omura, M., Torigoe, S., Kurihara, H., Matsubara, S. and Kubota, N., 1998, Comparison between fractionated high dose rate irradiation and continuous low dose rate irradiation in spheroids. *Acta Oncol*, **37,** 681-6.

299 Orton, C.G., 1998, High and low dose-rate brachytherapy for cervical carcinoma [see comments]. *Acta Oncol*, **37,** 117-25.

300 Palayoor, S.T., Macklis, R.M., Bump, E.A. and Coleman, C.N., 1995, Modulation of radiation-induced apoptosis and G2/M block in murine T-lymphoma cells. *Radiation Research*, **141,** 235-43.

301 Palcic, B. and Jaggi, B., 1986, The use of solid-state image sensor technology to detect and characterize live mammalian cells growing in tissue culture. *International Journal of Radiation Biology*, **50,** 345-52.

302 Parkin, D.M., Pisani, P. and Ferlay, J., 1999, Global cancer statistics. *CA Cancer J Clin*, **49,** 33-64, 2.

303 Parkins, C.S. and Fowler, J.F., 1986, The linear quadratic fit for lung function after irradiation with X-rays at smaller doses per fraction than 2 Gy. *British Journal of Cancer*, **7,** 320-323.

304 Paterson, M.C., Smith, B.P., Lohman, P.H., Anderson, A.K. and Fishman, L., 1976, Defective excision repair of gamma-ray-damaged DNA in human (ataxia telangiectasia) fibroblasts. *Nature*, **260,** 444-7.

305 Paterson, R., Parker, H.M., 1934, A dosage system for gamma-ray therapy. *Br. J. Radiol.*, **7,** 592–600.

306 Paulovich, A.G., Toczyski, D.P. and Hartwell, L.H., 1997, When checkpoints fail. *Cell*, **88,** 315-21.

307 Pazzaglia, S., Saran, A., Pariset, L., Rebessi, S., Di Majo, V., Coppola, M. and Covelli, V., 1996, Sensitivity of C3H 10T1/2 cells to radiation-induced killing and neoplastic transformation as a function of cell cycle. *International Journal of Radiation Biology*, **69,** 57-65.

308 Peacock, J.H., Shipley, W.U., Steel, G.G. and Stephens, T.C., 1985, Adriamycin sensitivity following "ultra" low dose rate irradiation of Lewis lung carcinoma in vivo. *International Journal of Radiation Oncology Biology Physics*, **11,** 2099-104.

309 Pernot, M., Malissard, L., Hoffstetter, S., Luporsi, E., Aletti, P., Peiffert, D., Allavena, C., Kozminski, P. and Bey, P., 1994, Influence of tumoral, radiobiological, and general factors on local control and survival of a series of 361 tumors of the velotonsillar area treated by exclusive irradiation (external beam irradiation+brachytherapy or brachytherapy alone) [see comments]. *Int J Radiat Oncol Biol Phys*, **30,** 1051-7.

310 Pienta, K.J., Demers, R., Hoff, M., Kau, T.Y., Montie, J.E. and Severson, R.K., 1995, Effect of age and race on the survival of men with prostate cancer in the Metropolitan Detroit tricounty area, 1973 to 1987. *Urology*, **45,** 93-101.

311 Pinilla, J., 1998, Cost minimization analysis of high-dose-rate versus low-dose-rate brachytherapy in endometrial cancer. Gynecology Tumor Group. *Int J Radiat Oncol Biol Phys*, **42,** 87-90.

312 Pizzi, G.B. and Marchetti, C., 1997, [Brachytherapy with pulsed dosage. General considerations. Radiobiological considerations. First clinical experience in Mestre (Venice)]. *Radiol Med Torino*, **93,** 260-6.

313 Pogozelski, W.K., Xapsos, M.A. and Blakely, W.F., 1999, Quantitative assessment of the contribution of clustered damage to DNA double-strand breaks induced by 60Co gamma rays and fission neutrons. *Radiation Research*, **151,** 442-8.

314 Pohlit, W. and Heyder, I.R., 1981, The shape of dose - survival curves for mammalian cells and repair of potentially lethal damage analyzed by hypertonic treatment. **87,** 613-634.

315 Pollard, E.C. and Achey, P.M., 1975, Induction of radioresistance in Escherichia coli. *Biophysics Journal*, **15,** 1141-54.

316 Pollycove, M., 1998, Nonlinearity of radiation health effects. *Environ Health Perspect*, **1,** 363-8.

317 Pomp, J., Wike, J.L., Ouwerkerk, I.J., Hoogstraten, C., Davelaar, J., Schrier, P.I., Leer, J.W., Thames, H.D. and Brock, W.A., 1996, Cell density dependent plating efficiency affects outcome and interpretation of colony forming assays. *Radiother-Oncol*, **40,** 121-5 issn: 0167-8140.

318 Pomp, J., Woudstra, E.C. and Kampinga, H.H., 1999, Pulsed-dose-rate and low-dose-rate brachytherapy: comparison of sparing effects in cells of a radiosensitive and a radioresistant cell line. *Radiat Res*, **151,** 449-53.

319 Pop, L.A., van den Broek, J.F., Visser, A.G. and van der Kogel, A.J., 1996, Constraints in the use of repair half times and mathematical modelling for the clinical application of HDR and PDR treatment schedules as an alternative for LDR brachytherapy. *Radiother Oncol*, **38,** 153-62.

320 Powell, 1996, *Molecular Biology for Oncologists*. Edited (Chapman Hall)

321 Powell, S.N., Whitaker, S.J., Edwards, S.M. and McMillan, T.J., 1992, A DNA repair defect in a radiation-sensitive clone of a human bladder carcinoma cell line. *British Journal of Cancer*, **65,** 798-802.

322 Power, O.M. 1998, Cellular and molecular mechanisms affecting tumour radiosensitivity: An *in vitro* study. University of London.

323 Puck, T.T. and Marcus, P.I., 1956, Action of X rays on mammalian cells. **103,** 653-666.

324 Quimby, E.H., Castro, V., 1953, The calculation of dosage in interstitial radium therapy. *American Journal of Roentgenology*, **70,** 739–749.

325 Quimby, E.H., 1963, Dosage calculations with radioactive material. *Physical Foundations of Radiobiology*, **3rd edn,** 336–381 Harper and Row New York.

326 Raaphorst, G.P., 1993, Prediction of radiotherapy response using SF2: is it methodology or mythology? [see comments]. *Radiotherapy and Oncology*, **28,** 187-8.

327 Raaphorst, G.P. and Azzam, E.I., 1981, Fixation of potentially lethal radiation damage in Chinese hamster cells by anisotonic solutions, polyamines and DMSO. *Radiation Research*, **86,** 52-66.

328 Raaphorst, G.P., Maio, J., Ng, C.E. and Stewart, D.J., 1998, Concomitant treatment with mild hyperthermia, cisplatin and low dose-rate irradiation in

human ovarian cancer cells sensitive and resistant to cisplatin. *Oncol Rep*, **5,** 971-7.

329 Raaphorst, G.P., Miao, J. and Ng, C.E., 1997, Cisplatin and mild hyperthermia in radiosensitization to low dose rate irradiation in human ovarian carcinoma cells. *Anticancer Research*, **17,** 3469-72.

330 Raaphorst, G.P., Wang, G., Stewart, D. and Ng, C.E., 1996a, Concomitant low dose-rate irradiation and cisplatin treatment in ovarian carcinoma cell lines sensitive and resistant to cisplatin treatment. *International Journal of Radiation Biology*, **69,** 623-31.

331 Raaphorst, G.P., Yang, H., Wilkins, D.E. and Ng, C.E., 1996b, Cisplatin, hyperthermia and radiation treatment in human cisplatin-sensitive and resistant glioma cell lines. *International Journal of Hyperthermia*, **12,** 801-12.

332 Radford, I.R., 1985, The level of induced DNA double-strand breakage correlates with cell killing after X-irradiation. *Int-J-Radiat-Biol-Relat-Stud-Phys-Chem-Med*, **48,** 45-54 issn: 0020-7616.

333 Raju, M.R., Carpenter, S.G., Chmielewski, J.J., Schillaci, M.E., Wilder, M.E., Freyer, J.P., Johnson, N.F., Schor, P.L., Sebring, R.J. and Goodhead, D.T., 1987, Radiobiology of ultrasoft X rays. I. Cultured hamster cells (V79). *Radiation Research*, **110,** 396-412.

334 Redpath, J.L., Antoniono, R.J., Sun, C., Gerstenberg, H.M. and Blakely, W.F., 1995, Late mitosis/early G1 phase and mid-G1 phase are not hypersensitive cell cycle phases for neoplastic transformation of HeLa x skin fibroblast human hybrid cells induced by fission-spectrum neutrons. *Radiation Research*, **141,** 37-43.

335 Redpath, J.L., Hill, C.K., Jones, C.A. and Sun, C., 1990, Fission-neutron-induced expression of a tumour-associated antigen in human cell hybrids (HeLa x skin fibroblasts): evidence for increased expression at low dose rate. *International Journal of Radiation Biology*, **58,** 673-80.

336 Redpath, J.L. and Sun, C., 1990, Sensitivity of a human hybrid cell line (HeLa X skin fibroblast) to radiation-induced neoplastic transformation in G2, M, and mid-G1 phases of the cell cycle. *Radiation Research*, **121,** 206-11.

337 Revesz, L. and Palcic, B., 1985, Radiation dose dependence of the sensitization by oxygen and oxygen mimic sensitizers. *Acta Radiol Oncol*, **24,** 209-217.

338 Rigaud, O. and Moustacchi, E., 1996, Radioadaptation for gene mutation and the possible molecular mechanisms of the adaptive response. *Mutation Research*, **358,** 127-34.

339 Robson, T., Joiner, M.C., Wilson, G.D., McCullough, W., Price, M.E., Logan, I., Jones, H., McKeown, S.R. and Hirst, D.G., 1999, A novel human stress response-

related gene with a potential role in induced radioresistance. *Radiation Research*, **152,** 451-61.

340 Robson, T., Price, M.E., Moore, M.L., Joiner, M.C., McKelvey-Martin, V.J., McKeown, S.R. and Hirst, D.G., 2000, Increased repair and cell survival in cells treated with DIR1 antisense oligonucleotides: implications for induced radioresistance. *International Journal of Radiation Biology*, **76,** 617-623.

341 Roed, H., Engelholm, S.A., Svendsen, L.B., Rosendal, F. and Olsen, K.J., 1996, Pulsed dose rate (PDR) brachytherapy of anal carcinoma [see comments]. *Radiother Oncol*, **41,** 131-4.

342 Rojas, A. and Joiner, M.C., 1989, The influence of dose per fraction on repair kinetics. *Radiotherapy and Oncology*, **14,** 329-36.

343 Rossi, H.H. and Kellerer, A.M., 1986, The dose rate dependence of oncogenic transformation by neutrons may be due to variation of response during the cell cycle. *International Journal of Radiation Biology*, **50,** 353-61.

344 Roush, A.A., Suarez, M., Friedberg, E.C., Radman, M. and Siede, W., 1998, Deletion of the Saccharomyces cerevisiae gene RAD30 encoding an Escherichia coli DinB homolog confers UV radiation sensitivity and altered mutability. *Molecular and General Genetics*, **257,** 686-92.

345 Rowan, S. and Fisher, D.E., 1997, Mechanisms of apoptotic cell death. *Leukemia*, **11,** 457-65.

346 Ruiz de Almodovar, J.M., Bush, C., Peacock, J.H., Steel, G.G., Whitaker, S.J. and McMillan, T.J., 1994, Dose-rate effect for DNA damage induced by ionizing radiation in human tumor cells. *Radiat-Res*, **138,** S93-6 issn: 0033-7587.

347 Russell, W.L., Russell, L.B. and Kelly, E.M., 1958, Radiation dose rate and mutation frequency. *Science*, **128,** 1546–1550.

348 Russo, T., Zambrano, N., Esposito, F., Ammendola, R., Cimino, F., Fiscella, M., Jackman, J., O'Connor, P.M., Anderson, C.W. and Appella, E., 1995, A p53-independent pathway for activation of WAF1/CIP1 expression following oxidative stress. *J-Biol-Chem*, **270,** 29386-91 issn: 0021-9258.

349 Rutgers, D.H., 1988, A Cs-137 afterloading device. Preliminary results of cell kinetic effects of low dose-rate irradiation in an experimental tumour. *Strahlenther Onkol*, **164,** 105-7.

350 Rutgers, D.H., van Oostrum, I.E., Noorman van der Dussen, M.F. and Wils, I.S., 1989, Relationship between cell kinetics and radiation-induced arrest of proliferating cells in G2: relevance to efficacy of radiotherapy. *Anal Cell Pathol*, **1,** 53-62.

351 Sakr, W.A., Grignon, D.J., Crissman, J.D., heillbrun, L.K., Cassin, B.J., Pontes, J.J., Haas, G.P., 1994, High grade prostatic intraepithelial neoplasis (HGPIN) and protatic adenocarcinoma between the ages 20–69; An autopsy study of 249 cases. *In Vivo*, **8,** 439–443.

352 Sakr, W.A., Grignon, D.J., Crissman, J.D., Heilbrun, L.K., Cassin, B.J., Pontes, J.J. and Haas, G.P., 1994, High grade prostatic intraepithelial neoplasia (HGPIN) and prostatic adenocarcinoma between the ages of 20-69: an autopsy study of 249 cases. *In Vivo*, **8,** 439-43.

353 Sakurai, H., Mitsuhashi, N., Tamaki, Y., Akimoto, T., Murata, O., Kitamoto, Y., Maebayashi, K., Ishikawa, H., Hayakawa, K. and Niibe, H., 1999, Interaction between low dose-rate irradiation, mild hyperthermia and low-dose caffeine in a human lung cancer cell line. *International Journal of Radiation Biology*, **75,** 739-45.

354 Santier, S., Gilet, R. and Malaise, E.P., 1985, Induced radiation resistance during low-dose-rate gamma irradiation in plateau-phase *Chlorella* cells. *Radiat. Res.*, **104,** 224–233.

355 Santos, S.J., Singh, N.P. and Natarajan, A.T., 1997, Fluorescence in situ hybridization with comets. *Experimental Cell Research*, **232,** 407-411.

356 Saran, A., Pazzaglia, S., Pariset, L., Rebessi, S., Broerse, J.J., Zoetelief, J., Di Majo, V., Coppola, M. and Covelli, V., 1994, Neoplastic transformation of C3H 10T1/2 cells: a study with fractionated doses of monoenergetic neutrons. *Radiation Research*, **138,** 246-51.

357 Sarkaria, J.N., Tibbetts, R.S., Busby, E.C., Kennedy, A.P., Hill, D.E. and Abraham, R.T., 1998, Inhibition of phosphoinositide 3-kinase related kinases by the radiosensitizing agent wortmannin. *Cancer Research*, **58,** 4375-4382.

358 Sasaki, M.S., 1995, On the reaction kinetics of the radioadaptive response in cultured mouse cells. *International Journal of Radiation Biology*, **68,** 281-91.

359 Saunders, M.I. and Dische, S., 1992, Continuous, hyperfractionated accelerated radiation therapy (CHART). In: *Radiation research: a 20th century perspective.* Edited by: W. C. Dewey, M. Eddington, R. J. M. Fry, E. J. Hall, and G. F. Whitmore. (Academic Press, San Diego), pp. 561-566.

360 Saunders, M.I., Hoskin, P.J., Pigott, K., Powell, M.E., Goodchild, K., Dische, S., Denekamp, J., Stratford, M.R., Dennis, M.F. and Rojas, A.M., 1997, Accelerated radiotherapy, carbogen and nicotinamide (ARCON) in locally advanced head and neck cancer: a feasibility study. *Radiotherapy and Oncology*, **45,** 159-166.

361 Sax, K., 1939, Time factor in X-ray production of chromosome aberrations. *Proc. Natl. Acad. Sci. U.S.*, **25,** 225.

362 Schwartz, D. and Rotter, V., 1998, p53-dependent cell cycle control: response to genotoxic stress. *Semin Cancer Biol*, **8,** 325-36.

363 Schwartz, J.L., Shadley, J., Jaffe, D.R., Whitlock, J., Rotmensch, J., Cowan, J.M., Gordon, D.J. and Vaughan, A.T.M., 1990, Association between radiation sensitivity, DNA repair, and chromosome organisation in the Chinese hamster ovary cell line xrs 5. In: *Mutation and the Environment Part A: Basic mechanisms*. Edited by: M. L. Mendelsohn and R. J. Albertini. (Wiley-Liss, New York), pp. 255-264.

364 Schwartz, J.L. and Vaughan, A.T.M., 1989, Association among DNA/chromosome break rejoining rates, chromatin structure alterations, and radiation sensitivity in human tumour cell lines. *Cancer Research*, **49,** 5054-5057.

365 Scott, A.D. and Waters, R., 1997, Inducible nucleotide excision repair (NER) of UV-induced cyclobutane pyrimidine dimers in the cell cycle of the budding yeast Saccharomyces cerevisiae: evidence that inducible NER is confined to the G1 phase of the mitotic cell cycle. *Molecular and General Genetics*, **254,** 43-53.

366 Seeberg, E., Eide, L. and Bjoras, M., 1995, The base excision repair pathway. *Trends Biochem Sci*, **20,** 391-7.

367 Selvanayagam, C.S., Davis, C.M., Cornforth, M.N. and Ullrich, R.L., 1995, Latent expression of p53 mutations and radiation-induced mammary cancer. *Cancer Research*, **55,** 3310-7.

368 Seong, J. and Kim, G.E., 1994, Adaptive response to ionizing radiation induced by low dose of gamma ray in human hepatoma cell lines. *Yonsei Med J*, **35,** 77-83.

369 Shadley, J.D., 1994, Chromosomal adaptive response in human lymphocytes. *Radiation Research*, **138,** S9-12.

370 Shadley, J.D. and Dai, G., 1993, Effect of low dose X-ray pretreatment on X-ray and drug induced abberations in human lymphocytes. *Environ. Mol. Mutag.*, **21,** i-iv.

371 Shadley, J.D. and Wiencke, J.K., 1989, Induction of the adaptive response by X-rays is dependent on radiation intensity. *International Journal of Radiation Biology*, **56,** 107-18.

372 Sherman, D.M., Carabell, S.C., Belli, J.A. and Hellman, S., 1982, The effect of dose rate and adriamycin on the tolerance of thoracic radiation in mice. *International Journal of Radiation Oncology Biology Physics*, **8,** 45-51.

373 Sherr, C.J., 1996, Cancer cell cycles. *Science*, **274,** 1672-7.

374 Shimizu, H., Ross, R.K., Bernstein, L., Yatani, R., Henderson, B.E. and Mack, T.M., 1991, Cancers of the prostate and breast among Japanese and white immigrants in Los Angeles County. *Br J Cancer*, **63,** 963-6.

375 Shinohara, A. and Ogawa, T., 1995, Homologous recombination and the roles of double-strand breaks. *Trends-Biochem-Sci*, **20,** 387-91 issn: 0167-7640.

376 Short, S., Mayes, C., Woodcock, M., Johns, H. and Joiner, M.C., 1999a, Low dose hypersensitivity in the T98G human glioblastoma cell line. *International Journal of Radiation Biology*, **75,** 847-55.

377 Short, S.C. 1999, New methods to overcome radioresistance. University of London.

378 Short, S.C., Mitchell, S.A., Boulton, P., Woodcock, M. and Joiner, M.C., 1999b, The response of human glioma cell lines to low-dose radiation exposure. *International Journal of Radiation Biology*, **75,** 1341-8.

379 Siede, W. and Eckardt, F., 1984, Indications for an inducible component of error-prone DNA repair in yeast. *British Journal of Cancer*, **6,** 103-6.

380 Siede, W. and Eckardt Schupp, F., 1986, A mismatch repair-based model can explain some features of u.v. mutagenesis in yeast. *Mutagenesis*, **1,** 471-4.

381 Siede, W., Friedl, A.A., Dianova, I., Eckardt Schupp, F. and Friedberg, E.C., 1996, The Saccharomyces cerevisiae Ku autoantigen homologue affects radiosensitivity only in the absence of homologous recombination. *Genetics*, **142,** 91-102.

382 Siede, W., Obermaier, S. and Eckardt, F., 1985, Influence of different inhibitors on the activity of the RAD54 dependent step of DNA repair in Saccharomyces cerevisiae. *Radiation and Environmental Biophysics*, **24,** 1-7.

383 Sinclair, W.K., 1968, Cyclic x-ray responses in mammalian cells in vitro. *Radiation Research*, **33,** 620-43.

384 Sinclair, W.K. and Morton, R.A., 1965, X-ray and ultraviolet sensitivity of synchronised Chinese hamster cells at variuos stages of the cell cycle. *Biophysics Journal*, **5,** 1–25.

385 Sinclair, W.K. and Morton, R.A., 1966, X-ray sensitivity during the cell generation cycle of cultured Chinese hamster cells. *Radiation Research*, **29,** 450-74.

386 Singh, B., Arrand, J.E. and Joiner, M.C., 1994, Hypersensitive response of normal human lung epithelial cells at low radiation doses. *International Journal of Radiation Biology*, **65,** 457-64.

387 Sionov, R.V. and Haupt, Y., 1999, The cellular response to p53: the decision between life and death. *Oncogene*, **18,** 6145-57.

388 Skarsgard, L.D., Harrison, I. and Durand, R.E., 1991, The radiation response of asynchronous cells at low dose: evidence of substructure. *Radiation Research*, **127,** 248-56.

389 Skarsgard, L.D., Skwarchuk, M.W., Wouters, B.G. and Durand, R.E., 1996, Substructure in the radiation survival response at low dose in cells of human tumor cell lines. *Radiation Research*, **146,** 388-98.

390 Skarsgard, L.D., Wilson, D.J. and Durand, R.E., 1993, Survival at low dose in asynchronous and partially synchronized Chinese hamster V79-171 cells. *Radiation Research*, **133,** 102-7.

391 Skladowski, K., McMillan, T.J., Peacock, J., Titley, J. and Steel, G.G., 1993, Cell-cycle progression during continuous low dose rate irradiation of a human bladder carcinoma cell line. *Radiotherapy and Oncology*, **28,** 219-27.

392 Skov, K., Marples, B., Matthews, J.B., Joiner, M.C. and Zhou, H., 1994, A preliminary investigation into the extent of increased radioresistance or hyper-radiosensitivity in cells of hamster cell lines known to be deficient in DNA repair. *Radiation Research*, **138,** S126-9.

393 Smeets, M.F., Mooren, E.H., Abdel Wahab, A.H., Bartelink, H. and Begg, A.C., 1994a, Differential repair of radiation-induced DNA damage in cells of human squamous cell carcinoma and the effect of caffeine and cysteamine on induction and repair of DNA double-strand breaks. *Radiation Research*, **140,** 153-60.

394 Smeets, M.F., Mooren, E.H. and Begg, A.C., 1994b, The effect of radiation on G2 blocks, cyclin B expression and cdc2 expression in human squamous carcinoma cell lines with different radiosensitivities. *Radiotherapy and Oncology*, **33,** 217-27.

395 Society, A.C., 1996, Cancer Facts and Figures. *American Cancer Society, Atlanta*,
396 Somasundaram, K., 2000, Tumor suppressor p53: regulation and function. *Front Biosci*, **5,** D424-37.

397 Spadinger, I. and Palcic, B., 1993, Cell survival measurements at low doses using an automated image cytometry device. *Int-J-Radiat-Biol*, **63,** 183-9 issn: 0955-3002.

398 Spadinger, I., Poon, S.S. and Palcic, B., 1989, Automated detection and recognition of live cells in tissue culture using image cytometry. *Cytometry*, **10,** 375-81.

399 Spinks, J.W.T. and Woods, R.J., 1990, Chemical dosimetry. In: *An introduction to radiation chemistry*. Edited (John Wiley & Sons, Inc., New York), pp. 97–101.

400 Spivak, I. and Kolman, A., 1998, Alteration of p53 protein in C3H/10T1/2 cells morphologically transformed by gamma-rays in stationary phase. *Mutation Research*, **397,** 345-52.

401 Sproston, A.R., Boyle, J.M., Heighway, J., Birch, J.M. and Scott, D., 1996, Fibroblasts from Li-Fraumeni patients are resistant to low dose-rate irradiation. *International Journal of Radiation Biology*, **70,** 145-50.

402 Stackhouse, M.A. and Bedford, J.S., 1993, An ionizing radiation-sensitive mutant of CHO cells: irs-20. II. Dose-rate effects and cellular recovery processes. *Radiation Research*, **136,** 250-4.

403 Stapper, N.J., Stuschke, M., Sak, A. and Stuben, G., 1995, Radiation-induced apoptosis in human sarcoma and glioma cell lines. *International Journal of Cancer*, **62,** 58-62.

404 Stecca, C. and Gerber, G.B., 1998, Adaptive response to DNA-damaging agents: a review of potential mechanisms. *Biochemical Pharmacology*, **55,** 941-51.

405 Steel, G.G., 1991, The ESTRO Breur lecture. Cellular sensitivity to low dose-rate irradiation focuses the problem of tumour radioresistance. *Radiotherapy and Oncology*, **20,** 71-83.

406 Steel, G.G., Deacon, J.M., Duchesne, G.M., Horwich, A., Kelland, L.R. and Peacock, J.H., 1987, The dose-rate effect in human tumour cells. *Radiotherapy and Oncology*, **9,** 299-310.

407 Stein, G.H., 1979, T98G: An Anchorage-independent Human Tumor Cell Line that Exhibits Stationary Phase G1 Arrest In Vitro. *J. Cell. Physiol.*, **99,** 43-54.

408 Stemmerman, G.N., Nomura, A.G., Choyou, P.H., Yatani R., 1992, A prospective comparison of prostate cancer at autopsy and as a clinical event: The Hawaii Japanese experience. *Cancer Epidemiol. Biomarkers Prevent.*, **1,** 189–193.

409 Stewart, N., Hicks, G.G., Paraskevas, F. and Mowat, M., 1995, Evidence for a second cell cycle block at G2/M by p53. *Oncogene*, **10,** 109-15.

410 Storey, M.R., Landgren, R.C., Cottone, J.L., Stallings, J.W., Logan, C.W., Fraiser, L.P., Ross, C.S., Kock, R.J., Berkley, L.W. and Hauer Jensen, M., 1999, Transperineal 125iodine implantation for treatment of clinically localized prostate cancer: 5-year tumor control and morbidity. *Int J Radiat Oncol Biol Phys*, **43,** 565-70.

411 Strebel, H., 1903, Vorsclaege zur radiumtherapie. *Deuche med. Zeitung*, **24,** 11–45.

412 Stuben, G., van der Kogel, A.J. and van der Schueren, E., 1997, Biological equivalance of low dose rate to multifractionated high dose rate irradiations: investigations in mouse lip mucosa. *Radiother Oncol*, **42,** 189-96.

413 Swift, P.S., Purser, P., Roberts, L.W., Pickett, B., Powell, C.B. and Phillips, T.L., 1997, Pulsed low dose rate brachytherapy for pelvic malignancies. *Int J Radiat Oncol Biol Phys*, **37,** 811-7.

414 Szumiel, I., 1998, Monitoring and signaling of radiation-induced damage in mammalian cells. *Radiation Research*, **150,** S92-101.

415 Take, Y., Kumano, M., Hamano, Y., Fukatsu, H., Teraoka, H., Nishimura, S. and Okuyama, A., 1995, OK-1035, a selective inhibitor of DNA-dependent protein kinase. *Biochemical and Biophysical Research Communications*, **215,** 41-47.

416 Teng, Y., Longhese, M., McDonough, G. and Waters, R., 1998, Mutants with changes in different domains of yeast replication protein A exhibit differences in repairing the control region, the transcribed strand and the non-transcribed strand of the Saccharomyces cerevisiae MFA2 gene. *Journal of Molecular Biology*, **280,** 355-63.

417 Thacker, J., Wilkinson, R.E. and Goodhead, D.T., 1986, The induction of chromosome exchange aberrations by carbon ultrasoft X-rays in V79 hamster cells. *International Journal of Radiation Biology*, **49,** 645-56.

418 Thames, H.D., 1985, An 'incomplete-repair' model for survival after fractionated and continuous irradiations. *International Journal of Radiation Biology*, **47,** 319-39.

419 Thames, H.D., 1989, Repair kinetics in tissues: alternative models. *Radiotherapy and Oncology*, **14,** 321-7.

420 Thames, H.D. and Hendry, J.H., 1987, *Fractionation in Radiotherapy.* (Taylor & Francis, London).

421 Thompson, L.H. and Schild, D., 1999, The contribution of homologous recombination in preserving genome integrity in mammalian cells. *Biochimie*, **81,** 87-105.

422 Tobias, C.A., Blakely, E.A., Ngo, F.Q.H. and Yang, T.C.H., 1980, The repair-misrepair model of cell survival. In: *Radiation Biology and Cancer Research.* Edited by: R. E. M. a. H. R. Withers. (Raven, New York), pp. 195–230.

423 Tolmach, L.J., Jones, R.W. and Busse, P.M., 1977, The action of caffeine on X-irradiated HeLa cells. I. Delayed inhibition of DNA synthesis. *Radiation Research*, **71,** 653-65.

424 Tonkin, K.S., Kelland, L.R. and Steel, G.G., 1989, A comparison of the in vivo and in vitro radiation response of three human cervix carcinomas [published erratum appears in Radiother Oncol 1989 Oct;16(2):157]. *Radiotherapy and Oncology*, **16,** 55-63.

425 Toyoshima, F., Moriguchi, T., Wada, A., Fukuda, M. and Nishida, E., 1998, Nuclear export of cyclin B1 and its possible role in the DNA damage-induced G2 checkpoint. *Embo Journal*, **17,** 2728-35.

426 Travis, E.L., Thames, H.D., Watkins, T.L. and Kiss, I., 1987, The kinetics of repair in mouse lung after fractionated irradiation. *International Journal of Radiation Biology*, **52,** 903-19.

427 Troelstra, C. and Jaspers, N.G., 1994, Recombination and repair. Ku starts at the end. *Curr-Biol*, **4,** 1149-51 issn: 0960-9822.

428 Tucker, S.L. and Thames, H.D., Jr., 1989, The effect of patient-to-patient variability on the accuracy of predictive assays of tumor response to radiotherapy: a theoretical evaluation. *International Journal of Radiation Oncology Biology Physics*, **17,** 145-57.

429 Ullrich, R.L., 1984, Tumor induction in BALB/c mice after fractionated or protracted exposures to fission-spectrum neutrons. *Radiation Research*, **97,** 587-97.

430 Vaganay-Juéry, S., Muller, C., Abdulkarim, B., Deutsch, E., Marangoni, E., Lambin, P., Calsou, P., Salles, B., Joiner, M. and Bourhis, J., 2000, Decreased DNA-PK activity in human cancer cells exhibiting hypersensitivity to low-dose irradiation. *Brit J Cancer*, in press.

431 Van Meir, E.G., Kikuchi, T., Tada, M., Li, H., Diserens, A.C., Wojcik, B.E., Huang, H.J., Friedmann, T., de Tribolet, N. and Cavenee, W.K., 1994, Analysis of the p53 gene and its expression in human glioblastoma cells. *Cancer Research*, **54,** 649-52.

432 van Oostrum, I.E., Erkens Schulze, S., Petterson, M., Wils, I.S. and Rutgers, D.H., 1990, The relationship between radiosensitivity and cell kinetic effects after low- and high-dose-rate irradiation in five human tumors in nude mice. *Radiation Research*, **122,** 252-61.

433 vanAnkeren, S.C., Murray, D. and Meyn, R.E., 1988, Induction and rejoining of gamma-ray-induced DNA single- and double-strand breaks in Chinese hamster AA8 cells and in two radiosensitive clones. *Radiation Research*, **116,** 511-25.

434 Vijayalaxmi and Burkart, W., 1989a, Effect of 3-aminobenzamide on chromosome damage in human blood lymphocytes adapted to bleomycin. *Mutagenesis*, **4,** 187-9.

435 Vijayalaxmi and Burkart, W., 1989b, Resistance and cross-resistance to chromosome damage in human blood lymphocytes adapted to bleomycin. *Mutation Research*, **211,** 1-5.

436 Vilenchik, M.M. and Knudson, A.G., Jr., 2000, Inverse radiation dose-rate effects on somatic and germ-line mutations and DNA damage rates. *Proceedings of the National Academy of Sciences USA*, **97,** 5381-6.

437 Visser, A.G., van den Aardweg, G.J. and Levendag, P.C., 1996, Pulsed dose rate and fractionated high dose rate brachytherapy: choice of brachytherapy schedules to replace low dose rate treatments [see comments]. *Int J Radiat Oncol Biol Phys*, **34,** 497-505.

438 Wachsberger, P.R., Li, W.H., Guo, M., Chen, D., Cheong, N., Ling, C.C., Li, G. and Iliakis, G., 1999, Rejoining of DNA double-strand breaks in Ku80-deficient mouse fibroblasts. *Radiation Research*, **151,** 398-407.

439 Wallace, S.S., 1998, Enzymatic processing of radiation-induced free radical damage in DNA. *Radiation Research*, **150,** S60-79.

440 Ward, J.F., 1986, Mechanisms of DNA repair and their potential modification for radiotherapy. *International Journal of Radiation Oncology Biology Physics*, **12,** 1027-32.

441 Ward, J.F., 1988, DNA damage produced by ionizing radiation in mammalian cells: identities, mechanisms of formation, and reparability. *Prog Nucleic Acid Res Mol Biol*, **35,** 95-125.

442 Ward, J.F., 1990, The yield of DNA double-strand breaks produced intracellularly by ionizing radiation: a review. *International Journal of Radiation Biology*, **57,** 1141-50.

443 Ward, T.H. and Marples, B., 2000, Technical report: SYBR Green I and the improved sensitivity of the single-cell electrophoresis assay. *International Journal of Radiation Biology*, **76,** 61-5.

444 Watanabe, H., Igari, D., Tanahashi, Y., Harada, K. and Saitoh, M., 1975, Transrectal ultrasonotomography of the prostate. *J Urol*, **114,** 734-9.

445 Watanabe, M. and Horikawa, M., 1980, Analyses of differential sensitivities of synchronized HeLa S3 cells to radiations and chemical carcinogens during the cell cycle. Par V. Radiation- and chemical carcinogen-induced mutagenesis. *Mutation Research*, **71,** 219-31.

446 Waters, R., Zhang, R. and Jones, N.J., 1993, Inducible removal of UV-induced pyrimidine dimers from transcriptionally active and inactive genes of Saccharomyces cerevisiae. *Molecular and General Genetics*, **239,** 28-32.

447 Watson, J.V. and Taylor, I.W., 1977, Cell cycle analysis in vitro using flow cytofluorimetry after synchronization. *British Journal of Cancer*, **36,** 281-7.

448 Wells, R.L., Cao, J., Xing, Y., He, L. and Elkind, M.M., 1993, Transformation-sensitive cells in G2/M-phase are not promoted by TPA following 137Cs gamma-rays. *International Journal of Radiation Biology*, **64,** 727-30.

449 West, C.M., 1995, Invited review: intrinsic radiosensitivity as a predictor of patient response to radiotherapy. *British Journal of Radiology*, **68,** 827-37.

450 West, C.M., Davidson, S.E., Roberts, S.A. and Hunter, R.D., 1993, Intrinsic radiosensitivity and prediction of patient response to radiotherapy for carcinoma of the cervix. *British Journal of Cancer*, **68,** 819-23.

451 West, C.M., Davidson, S.E., Roberts, S.A. and Hunter, R.D., 1997, The independence of intrinsic radiosensitivity as a prognostic factor for patient response to radiotherapy of carcinoma of the cervix. *British Journal of Cancer*, **76,** 1184-90.

452 Whitaker, S.J., Ung, Y.C. and McMillan, T.J., 1995, DNA double-strand break induction and rejoining as determinants of human tumour cell radiosensitivity. A pulsed-field gel electrophoresis study. *International Journal of Radiation Biology*, **67,** 7-18.

453 Whitmore, W.F., Jr., Hilaris, B. and Grabstald, H., 1972, Retropubic implantation to iodine 125 in the treatment of prostatic cancer. *J Urol*, **108,** 918-20.

454 Whittemore, A.S., Kolonel, L.N., Wu, A.H., John, E.M., Gallagher, R.P., Howe, G.R., Burch, J.D., Hankin, J., Dreon, D.M., West, D.W. and et al., 1995, Prostate cancer in relation to diet, physical activity, and body size in blacks, whites, and Asians in the United States and Canada [see comments]. *Journal of the National Cancer Institute*, **87,** 652-61.

455 Wilkins, D.E., Ng, C.E. and Raaphorst, G.P., 1996, Cisplatin and low dose rate irradiation in cisplatin resistant and sensitive human glioma cells. *International Journal of Radiation Oncology Biology Physics*, **36,** 105-11.

456 Williams, J.A., Williams, J.R., Yuan, X. and Dillehay, L.E., 1998, Protracted exposure radiosensitization of experimental human malignant glioma. *Radiat Oncol Investig*, **6,** 255-63.

457 Wlodek, D. and Hittelman, W.N., 1988, The relationship of DNA and chromosome damage to survival of synchronized X-irradiated L5178Y cells. I. Initial damage. *Radiation Research*, **115,** 550-65.

458 Wlodek, D. and Olive, P.L., 1992, Neutral filter elution detects differences in chromatin organization which can influence cellular radiosensitivity. *Radiation Research*, **132,** 242-247.

459 Wojcik, A., Shadley, J.D. and Szumiel, I., 1999, Adaptive response in lymphocytes: Is DNA repair involved? *Radiat. Res. Abstracts*, **2,** 434-437.

460 Wojewodzka, M., Walicka, M., Sochanowicz, B. and Szumiel, I., 1994, Calcium antagonist, TMB-8, prevents the induction of adaptive response by hydrogen peroxide or X-rays in human lymphocytes. *J. Radiat. Biol.*, **66,** 99-109.

461 Wolff, J.K., Wiencke, V., Afzal, J., Youngbloom and F., C., 1989, The adaptive response of human lymphocyes to very low doses of ionising radiation: a case of induced chromosomal repair with induction of specific proteins. In: *Low Dose Radiation: Biological Basis of Risk Assessment.* Edited by: K. F. Baverstock and J. W. Stather. (Taylor and Francis, London), pp. 446-454.

462 Wong, C.S., Minkin, S. and Hill, R.P., 1992, Linear-quadratic model underestimates sparing effect of small doses per fraction in rat spinal cord. *Radiother-Oncol*, **23,** 176-84 issn: 0167-8140.

463 Wong, C.S., Minkin, S. and Hill, R.P., 1993, Effect of small doses per fraction in rat spinal cord: influence of initial vs. final top-up doses. *Radiotherapy and Oncology*, **28,** 52-6.

464 Woudstra, E.C., Brunsting, J.F., Roesink, J.M., Konings, A.W. and Kampinga, H.H., 1996a, Radiation induced DNA damage and damage repair in three human tumour cell lines. *Mutat-Res*, **362,** 51-9 issn: 0027-5107.

465 Woudstra, E.C., Roesink, J.M., Rosemann, M., Brunsting, J.F., Driessen, C., Orta, T., Konings, A.W., Peacock, J.H. and Kampinga, H.H., 1996b, Chromatin structure and cellular radiosensitivity: a comparison of two human tumour cell lines. *International Journal of Radiation Biology*, **70,** 693-703.

466 Wouters, B.G. and Skarsgard, L.D., 1997, Low-dose radiation sensitivity and induced radioresistance to cell killing in HT-29 cells is distinct from the "adaptive response" and cannot be explained by a subpopulation of sensitive cells. *Radiation Research*, **148,** 435-42 Issn: 0033-7587.

467 Wouters, B.G., Sy, A.M. and Skarsgard, L.D., 1996, Low-dose hypersensitivity and increased radioresistance in a panel of human tumor cell lines with different radiosensitivity. *Radiation Research*, **146,** 399-413.

468 Wuarin, J. and Nurse, P., 1996, Regulating S phase: CDKs, licensing and proteolysis. *Cell*, **85,** 785-7.

469 Wurm, R., Burnet, N.G., Duggal, N., Yarnold, J.R. and Peacock, J.H., 1994, Cellular radiosensitivity and DNA damage in primary human fibroblasts [see comments]. *International Journal of Radiation Oncology Biology Physics*, **30,** 625-33.

470 Yasui, L.S., Ling-Indeck, L., Johnson-Wint, B., Fink, T.J. and Molsen, D., 1991, Changes in the nuclear structure in the radiation-sensitive CHO mutant, xrs-5. *Radiation Research*, **127,** 269-277.

471 Yount, G.L., Haas-Kogan, D.A., Vidair, C.A., Haas, M., W.C., D. and Israel, M.A., 1996, Cell-cycle synchrony unmasks the influence of p53 function on radiosensitivity of human glioblastoma cells. *Cancer Res.*, **56,** 500-506.

472 Zaffaroni, N., Orlandi, L., Villa, R., Bearzatto, A., Rofstad, E.K. and Silvestrini, R., 1994, DNA double-strand break repair and radiation response in human tumour primary cultures. *International Journal of Radiation Biology*, **66,** 279-85.

473 Zamorano, L., Yakar, D., Dujovny, M., Sheehan, M. and Kim, J., 1992, Permanent iodine-125 implant and external beam radiation therapy for the treatment of malignant brain tumors. *Stereotact Funct Neurosurg*, **59,** 183-92.

474 Zuckerman, S., 1936, The endocrine control of the prostate. *Proc. Roy. Soc. Med.*, **29,** 1557.